

Dissertation zur Erlangung des Doktorgrades  
der Fakultät für Chemie und Pharmazie  
der Ludwig-Maximilians-Universität München

**Tertiary structures, self-sorting behavior, and formation of an  
eight helix bundle of helical aromatic  $\delta$ -amino acid abiotic  
foldamers in organic solvents**

Friedericke Sonja Menke

aus

Tübingen, Deutschland

2023

## Erklärung

Diese Dissertation wurde im Sinne von § 7 der Promotionsordnung vom 28. November 2011 von Herrn Prof. Dr. Ivan Huc betreut.

## Eidesstattliche Versicherung

Diese Dissertation wurde eigenständig und ohne unerlaubte Hilfe erarbeitet.

München, den 23.01.2023

---

Friedericke S. Menke

Dissertation eingereicht am 23.01.2023

1. Gutachter: Prof. Dr. Ivan Huc

2. Gutachter: Prof. Dr. Oliver Trapp

Mündliche Prüfung am 07.03.2023

## Table of Contents

1	Abstract .....	5
2	Introduction .....	6
2.1	Introduction to foldamer research .....	8
2.2	Folding principles, monomer design and handedness control .....	10
2.3	Design of tertiary folding .....	12
2.4	Self-assembly and potential applications .....	16
2.5	Guiding Objective: design of helix bundles .....	21
2.6	References for chapter 2 .....	24
3	Relation between hydrogen bonds and their effects on the stability of a tertiary structure.....	32
3.1	Publication (published) .....	34
3.2	Supplementary Information .....	50
4	Effect of a linear array of hydrogen bond donors in a single helix on its self-assembly behavior	85
4.1	Publication (published) .....	87
4.2	Supporting Informations .....	97
5	Effects on self-organization when introducing a flexible linker to a helix-assembly .....	178
5.1	Publication (accepted).....	180
5.2	Supplementary Information .....	197
6	Summary and Perspective .....	299
6.1	References for Chapter 6.....	305
7	Supplementary Information (non-published) .....	307
8	Acknowledgements .....	328

## List of publications

Chapter 3-5 are generated from the publication below. For formatting convenience, the figure numbering has been kept consistent with the publication. For example, the numbering in sub-chapter 3.1 starts from Figure 1 and the numbering in sub-chapter 3.2 (SI) starts from Figure S1. Furthermore, each sub-chapter (for example 3.1 and 3.2) has its own references which start from 1. Thus chapter 2, 6 and 7 also have their own references which start from 1.

### Published:

F. S. Menke, D. Mazzier, B. Wicher, B. Kauffmann, V. Maurizot and I. Huc, Molecular torsion springs: alteration of helix curvature in frustrated tertiary folds. *Org. Biomol. Chem.* **2023**, 21, 1275-1283. (<https://doi.org/10.1039/D2OB02109A>)

(See chapter 3)

F. S. Menke, B. Wicher, V. Maurizot and I. Huc, Homochiral versus Heterochiral Dimeric Helical Foldamer Bundles: Chlorinated Solvent-Dependent Self-Sorting. *Angew. Chem. Int. Ed.* **2023**, 62, e202217325; *Angew. Chem.* **2023**, 135, e202217325.  
(<https://doi.org/10.1002/anie.202217325>, DOI numbers 0.1002/anie.202217325 and 10.1002/ange.202217325)

(See chapter 4)

### Accepted:

F. S. Menke, B. Wicher, L. Allmendinger, V. Maurizot and I. Huc, An abiotic, tetrameric, eight-helix bundle. *Chem. Sci.* **2023** (accepted, DOI: [10.1039/D3SC00267E](https://doi.org/10.1039/D3SC00267E))

(See chapter 5)

# 1 Abstract

The structure-function relationship of biopolymers inspired the field of foldamers, synthetic oligomers that adopt well-defined three-dimensional structures. In the pursuit of accessing unnatural shapes and functions, different from peptides, research led to the field of *abiotic* foldamers. In this context, side chain positioning and thereby functional design have been greatly simplified by using oligo-quinolinecarboxamides, known to adopt predictable helical structures. Thus, the formation and shape of a tertiary structure has been successfully predicted by computational modelling and verified by X-ray crystallography. The structure consisted of a helix-turn-helix-motif stabilized by inter-helical hydrogen bonds. In this work the correlation between the conformational preference inherent to each helix and the stability of the tertiary structure was investigated. Therefore, helix-turn-helix sequences were synthesized in which some hydrogen bonds have been removed. Unexpectedly, no strong destabilization of the tertiary fold has been observed. Examination of a new crystal structure revealed that helices adopt their natural curvature when some hydrogen bonds are missing. Otherwise, these hydrogen bonds enforce a spring torsion on the helices, thus causing a conformational frustration as it exists in proteins. This observation also helped increase the understanding of aggregational patterns formed in self-assemblies in which helices were no longer bound to one another by a turn unit. In this case, different kinds of intermolecular hydrogen bonding interfaces in solution have been observed involving two linear arrays of hydrogen bond donors and acceptors at the surface of the helices. In the aim to simplify aggregational behavior, sequences containing only one linear array of hydrogen bond donors and acceptors at their surface have been synthesized. Sequences were synthesized on solid phase and their aggregational behavior examined via solution  $^1\text{H}$  NMR spectroscopic studies and solid state crystallographic structures. These showed the formation of stable hydrogen bond-mediated dimeric helix bundles that could be either heterochiral (with a *P* and an *M* helix) or homochiral (with two *P* or two *M* helices). Thus, these foldamers displayed either a social or narcissistic chiral self-sorting behavior. This behavior could be influenced by using different chlorinated solvents, thereby causing quantitative formation of the hetero- or homochiral dimers. Another way to influence aggregation behavior is to forbid *PM* species by imposing absolute handedness to the helices. Summing up, in this kind of self-assembly a new hydrogen bonding interface imposing some sort of parallelism on the helices has been discovered. However, to access more diverse complex structures, the formation of non-parallel motifs such as tilted dimers, should become more predictable. Therefore, a flexible linker to stabilize a tilted dimer was designed using a crystal structure of such a dimer as starting point. The design was validated. However, the flexible linker also allowed for the discovery of an abiotic, tetrameric, eight-helix bundle. This large (>12 kDa) discrete aggregate is stabilized via inter- and intra-molecular hydrogen bonds, featuring several hydrogen bonding interfaces, including some that had not yet been reported. The discovery of this complex structure provides insights into future designs and enables the prediction of more diverse and sophisticated self-organizations.

## 2 Introduction

In nature, shape complementarity between two entities is required to bring functions such as enzyme catalysis, signal transduction, and pathogen recognition.<sup>1,2</sup> Nature, can afford such diversity of functions by the use of oligomeric biopolymers, particularly proteins, using only a surprisingly small set of building blocks: 20 canonical amino acids. The diversity of protein functions results from the diversity of folding, which organizes functional groups in specific spatial orientations. The important features are the precise arrangement of secondary structures such as alpha-helices and beta-sheets, turns, loops and intrinsically disordered stretches of amino acid sequences.<sup>3-7</sup> Alpha-helical structures are often found at protein-protein-interfaces, thereby they represent an interesting target for drug-development. However, these structures often show poor conformational stability when removed from the context of the folded protein structures.<sup>6, 8</sup> A smaller, simplified and thus synthetically accessible version of a protein is a mini-protein. These have potential use in providing templates for functional domains, such as catalysis and biomolecular binding, and thus have significant applications in biotechnology and medicine.<sup>9</sup> A mini-protein is defined as a short protein of  $\leq 40$  amino acids with well-defined folds consisting of two or more secondary structure elements, sequestered hydrophobic cores, and cooperative folding.<sup>9</sup> However, when imitating natural shapes, functions are limited to those already occurring in nature. Research towards unnatural shapes and functions, different from natural biopolymers led to the field of *abiotic* foldamers.<sup>7</sup> Such foldamers consist of units not seen in the natural world, that fold into conformationally ordered states, stabilized by noncovalent interactions (Figure 2.1).<sup>10</sup>

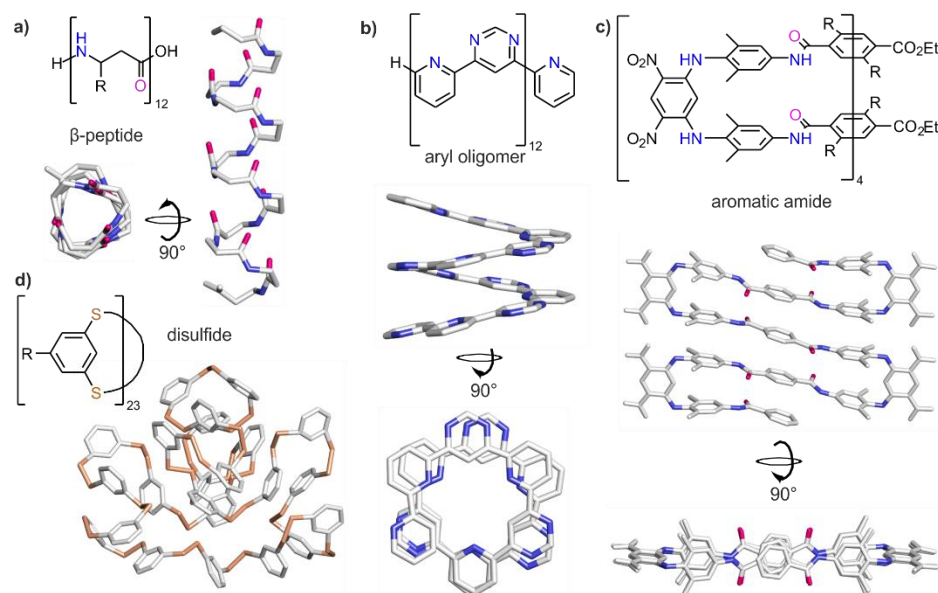


**Figure 2.1.**<sup>10</sup> Crystal structure of a  $\beta$ -peptide 12-mer (a).<sup>11</sup> Crystal structure of a helical aryl oligomer (b).<sup>12</sup> Crystal structure of a sheet-forming aromatic oligoamide (c).<sup>13</sup> Crystal structure of an aryl disulfide macrocycle (d).<sup>14</sup> Disulfide bonds are highlighted in orange. Oxygen and nitrogen atoms are highlighted in purple and blue, respectively. In all structures hydrogen atoms and side chains are omitted for clarity.<sup>10</sup>

To achieve similar complexity as biological architectures, more sophisticated, higher-order structures (tertiary and quaternary folding) are needed. In this work, research in the field of abiotic folding is focused on oligomers mainly consisting of aromatic  $\delta$ -amino acids. These are accessed easily by synthesis, are amenable to solid phase synthetic methods and show a high folding propensity. Quinoline based foldamers adopt a helical shape in the solid as well as in the solution state.<sup>15</sup> Helical shapes are far more abundant in the literature than sheets are. This could be related to aggregation properties of sheets, which drastically reduce their solubility and thus complicate their analysis in solution. Other patterns observed in foldamers that, are uncommon in nature include cyclic topologies,<sup>16</sup> sheet-like stacks,<sup>17</sup> knots,<sup>18</sup> tail-biters,<sup>19</sup> and non-canonical helices.<sup>20</sup> The high preference of quinoline based  $\delta$ -amino acid oligomers to fold into very stable helical structures makes them highly predictability. In consequence, side chain positioning and geometry are equally straight-forward to predict, simplifying functional designs. Taking advantage of this characteristic,<sup>3</sup> a tertiary arrangement of helices has been designed and stabilized by inter-helical hydrogen bonds in a helix-turn-helix motif.<sup>3</sup> However, further investigations on stability of a tertiary fold, manipulation of a self-assembly and potential access to more sophisticated structures are needed. In this thesis, steps towards this goal are taken while exclusively focusing on organic solutions. In organic solvents interactions, such as hydrogen bonds, are more predictable, which possibly leads to the formation of specific intra- and intermolecular hydrogen bonding interfaces. Therefore, folding behavior and aggregation in such a solvent is easier to manipulate, which might lead to easily accessible new functions not seen in nature. This section provides a general introduction into the field of foldamer science based on aromatic amides as building blocks.

## 2.1 Introduction to foldamer research

First attempts to propose structural mimics of proteins and thereby accessing their biological functions involved molecules that are still closely related to their natural models.<sup>21, 22</sup> Indeed these molecules, peptoids, only differ in the location of the amino acids' side chains in the oligomeric backbone. These side chains are located on the amide nitrogen instead of the  $\alpha$ -carbon (Figure 2.2a&b). In contrast to proteins, structural complexity in peptoids is not derived from chirality and intramolecular hydrogen bonds of the backbone, but through *cis/trans* tertiary amide bond isomerism that is influenced by the nature of the side chains. Peptoids adopt structures similar to  $\alpha$ -peptides such as helices, sheets, loops, and ribbons, while being more membrane permeable and displaying a higher resistance to enzymatic degradation.<sup>2</sup> Later, another family of mimics,  $\beta$ -Peptides, which are composed of amino acids bearing one more carbon between the carbonyl and the amine functions (Figure 2.2c&d), were also predicted to adopt well-folded conformations stabilized through hydrogen bonding between backbone amide functions. This was firstly investigated by Seebach *et al.*, who found a hexamer, consisting of solely  $\beta$ -peptides which not only formed a stable enantiomeric helical structure (Figure 2.1a),<sup>11, 23</sup> but were also resistant towards actions of proteases.<sup>23, 24</sup>

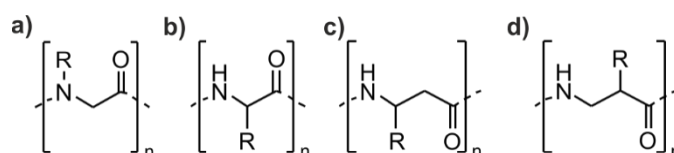


**Figure 2.2.** Structures of Peptoid (a),  $\alpha$ -Peptide (b),  $\beta^2$ -Peptide (c) and  $\beta^3$ -Peptide (d).

In order to limit the internal dynamics of such  $\beta$ -Peptides, Gellman and coworkers examined the effects of introducing small carbocycles within their backbones thus restricting the flexibility without blocking hydrogen bonding sites using computational models.<sup>25</sup> They found that the use of *trans*-2-aminocyclohexanecarboxylic acid (ACHC) as a rigid building block enhances the stability of a 14-helical conformation.<sup>25</sup>

These results showed that the known biopolymers are not the only oligomers with the ability to adopt well-folded conformations, essentially extending the research field of foldamers to other backbone types chemically more remote from those of biopolymers. Thus, research in *biotic* foldamers was extended to the investigation on homologues with larger units such as ( $\gamma$ - and  $\delta$ -peptides-) and the possibility of exchanging the amide functions with ureas, hydrazides and sulfonamides (Figure 2.3).<sup>26-34</sup> However, these structures are still very similar to their natural model ( $\alpha$ -peptides). To access unnatural shapes and functions, different from peptides, the field was extended to more diverse, *abiotic* backbone types. Particularly, backbones containing aromatic units were of particular interest. Throughout the years, several systems have been developed, such as oligo-phenylene-ethynylenes,<sup>35</sup> aromatic electron donor and acceptor systems,<sup>17</sup> aryl oligomers,<sup>12, 36-40</sup> and aromatic oligoamides,<sup>34, 41, 42</sup> which often bring unique properties and stability.



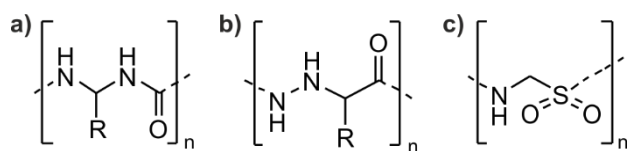


**Figure 2.3.** Structures of urea-bond (a), hydrazide-bond (b) and  $\alpha$ -sulfonamide (c).

Today's available foldamers can be categorized by different criteria. One of which is the type of linkage between units, which can be amide, hydrazide, urea, or alkyne groups (Figure 2.3). The other is the nature of the backbone units themselves. These can consist of aromatic, a mixture of aromatic and aliphatic parts or purely aliphatic components. Additionally, foldamers may consist of only a single building block<sup>14</sup> or may be a combination of two or more different building blocks, which can be arranged in an alternating<sup>43</sup> or a block-like fashion.<sup>44</sup> Another classification may be the way the monomers are connected: linear, cyclic,<sup>45</sup> branched,<sup>46</sup> or polymeric.<sup>47</sup>

Extensive research in the area of aromatic oligoamide foldamers using different heterocyclic as well as multicyclic systems bearing a variety of substituents was conducted. It was found that their structure is strongly influenced by the positioning of the amide linkages on the aromatic rings of their monomers. Thus oligomers of *ortho*-substituted amino benzoic acid form a zigzag-shaped linear strand,<sup>39</sup> *meta*-substitution usually leads to formation of crescent or helical structures,<sup>48</sup> while *para*-substitution again favors linear strands.<sup>49</sup> Huc and coworkers showed that oligomers consisting of the quasi *ortho*-substituted 8-amino-2-quinolinecarboxylic acid (Q) fold into stable helical structures with a high curvature.<sup>34</sup> Other folds such as sheets may be generated through the combination of different building blocks acting as strands and turns.<sup>13</sup>

Since this work will focus mainly on quinoline based oligoamides, the following will represent the state of the art for this class of foldamers. Such compounds can either be synthesized using solution or solid phase assisted strategies. Previously, solely solution phase methods were used for the synthesis of aromatic oligoamides. Acid chloride activation has been preferred over peptide coupling reagents or reactive ester activation due the low reactivity of aromatic amines (Figure 2.4). Additionally, for synthesis of longer oligomers, harsher conditions such as increased temperature may be required.<sup>10</sup>

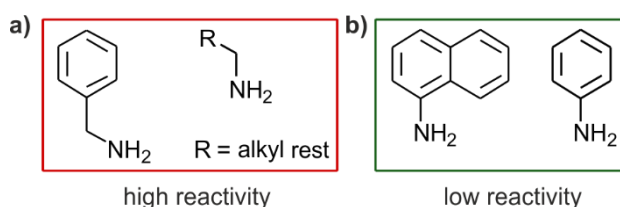


**Figure 2.4.** Examples of aliphatic (a) and aromatic (b) amines.

The synthesis of an oligomer consists of several activation, deprotection and coupling steps with purification after each step. These tedious efforts severely limit the scope of accessible oligomers. Therefore, convergent synthetic schemes with segment doubling condensation strategies were used, leading to successful synthesis of long oligomers consisting of 96 quinoline units (25.7 kDa).<sup>50, 51</sup> However, such strategies avoid the

preparation of sequences bearing a variety of different side chains in arbitrary orders.<sup>52</sup> On the other hand, solid phase assisted synthesis has been developed for peptides, consisting of  $\alpha$ -amino acids whose amine function is more reactive compared to most aromatic amines (Figure 2.4b). Thus, transferring this kind of chemistry to aromatic amino acids is not trivial but has been achieved<sup>52-54</sup> by using *in situ* conditions to convert Fmoc-protected amino acids to their respective acid chlorides. These reactive derivatives were then coupled with the free amine on solid support (Figure 2.5).<sup>10</sup>

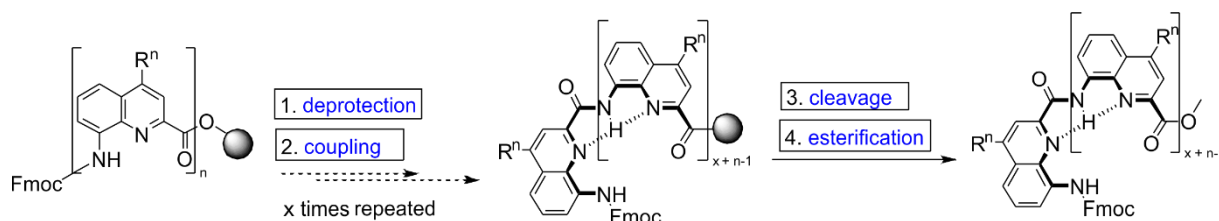


**Figure 2.5.** Synthetic solid phase strategy for the synthesis of quinoline based aromatic oligoamides.

In general, the final shape of a molecule is determined by the sum of multiple factors. More easily predictable driving forces of folding are the internal constraints, the shape and the rigidity of the monomers. Others, are attractive and repulsive local and non-local intramolecular interactions between monomers. Hydrogen bonding, donor–acceptor interactions,<sup>17</sup> and aromatic stacking are counted among possible attractive forces, whereas steric and electrostatic (dipole–dipole) repulsion<sup>12</sup> is among the repulsive forces. Other, external factors that may influence folding behavior are solvent effects (hydrophobic effect), aggregation phenomena, host-guest complexation<sup>55</sup> and surface interactions.<sup>56</sup> In aromatic oligoamides hydrogen bonding typically occurs between neighboring units.<sup>57</sup> In an 8-aminoquinoline based oligoamide all amido protons are involved in hydrogen bonds with the adjacent quinoline moieties (Figure 2.6) thus filling the helix cavity completely and preventing a penetration of solvent molecules in solid phase.<sup>34</sup> These adjacent hydrogen bonds lead to higher stability and thus predictability of their secondary structure patterns. In the design of new functional foldamers a certain structural stability and predictability is useful.

## 2.2 Folding principles, monomer design and handedness control

In a quinoline-based oligoamide the helical shape is stabilized by aromatic stacking within the helix, while the curvature in a helical shape is dictated by hydrogen bonds between the amide-NH and the neighboring endocyclic quinoline nitrogens<sup>33</sup>. Thereby inducing a contraction at the inner rim resulting in a helical fold. In such a helix a turn is complete after 2.5 units instead of the expected 3 units per turn.<sup>34</sup> Thus, a quinoline trimer (Q<sub>3</sub>), which is expected to be planar, already folds into a helical shape (Figure 2.6). Helices are chiral objects that can exist in a right-handed (*P*) or left-handed (*M*) conformation. When a helical oligomer consists of chiral monomers, a strong preference for one helix sense occurs.<sup>23</sup> However, quinoline-based units are achiral, therefore oligomers thereof are obtained as a racemic mixture of *P*- and *M*-helices (Figure 2.6). Handedness inversion occurs via partial unfolding of these helices in solution and the rate at which it takes place is an indication of helix stability in a certain solvent. The inversion half-life of an octamer is 6 minutes in chloroform

as well as 40 minutes and 900 minutes in more polar solvents such as dimethylformamide and methanol, respectively.<sup>41</sup> Length also has an impact.<sup>41</sup> In water, on the one hand, pentamers or smaller still invert with a half-life of hours.<sup>58</sup> On the other hand, longer sequences are kinetically locked and do not interconvert their handedness on a practical timescale. Moreover, this equilibrium may be biased towards one handedness through external factors such as binding to chiral surfaces<sup>58</sup> or guests.<sup>59</sup> In general, most chiral functionalizations in proximity to the helix backbone will create a preference, since little energy difference between the diastereomers is necessary to infer a small handedness bias.<sup>60-62</sup> Thus, covalent attachment of chiral moieties to side-chains, at the N- or C-terminus of the helix or within the sequence is sufficient to do so. Handedness control by incorporation of  $\alpha$ -amino acids into a quinoline-based oligomer, however, can lead to a distortion of the usual curvature.<sup>63</sup> Hereby nearly quantitative bias is achieved by introducing bulky groups that engage in hydrogen bonding interactions with the quinoline-backbone.<sup>64, 65</sup> Groups installed either at the C- or N-terminus, do not alter the curvature but their placement prevents further functionalizing or engagement in binding/recognition events at the effected locations.

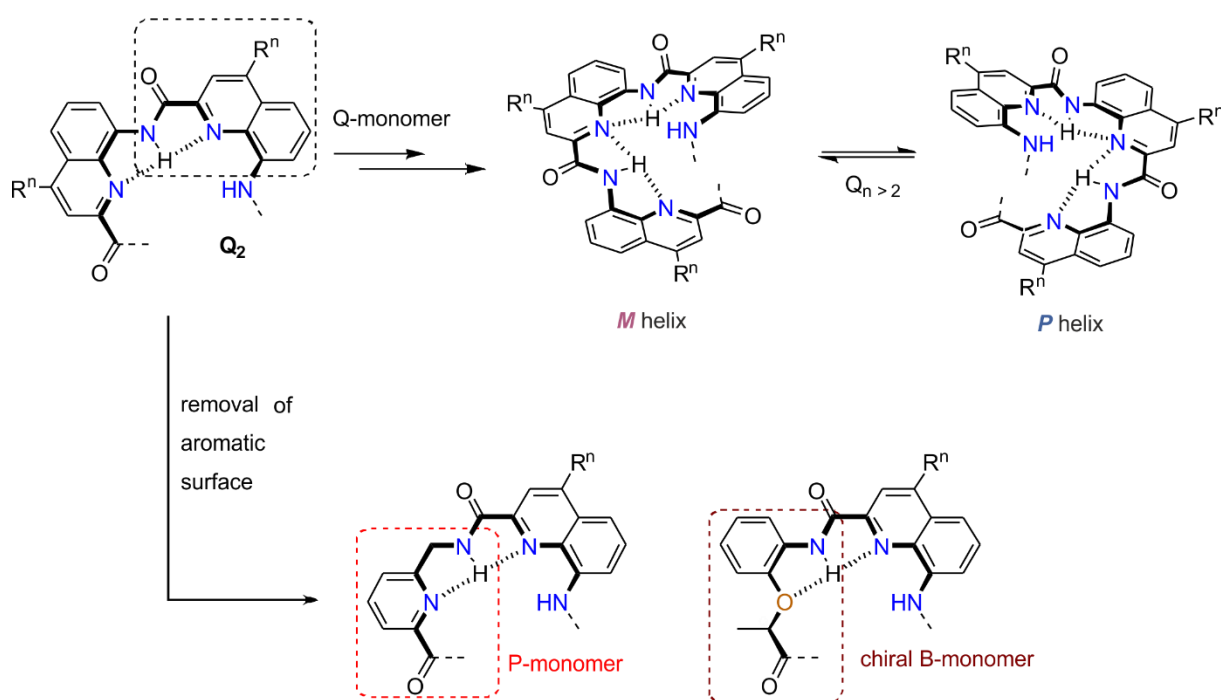


**Figure 2.6.** Monomer structures of aromatic  $\delta$ -amino acid oligomers. Hydrogen bonds are indicated by dashed lines and atoms involved in hydrogen bonding are highlighted in color (oxygen: orange, nitrogen: blue). Steric repulsion in the trimer leads to helical structures with left-handed (M) or right-handed (P) helicity.<sup>34</sup> The inner rim of the helix is indicated with bold bonds. Q-monomers may be replaced by P- or B-monomers that are able to form a similar hydrogen bonding pattern.<sup>34, 41, 42, 66, 67</sup>

Handedness-induction can be promoted by combining Q-monomers with other chiral building blocks such as (*S*)-3-(2-(methylamino)phenoxy)butan-2-one 2-(2-aminophenoxy)-acetic acid (B) units, which act as a surrogate for the Q-unit (Figure 2.6). In B, the endocyclic nitrogen is replaced by an ether oxygen to preserve the hydrogen bonding pattern and the quinoline ring is replaced by a smaller phenyl ring. Thereby, handedness

is induced within a helix while preserving helix curvature. Such a handedness-induction has been shown to be more efficient than a (*1S*)-Camphanic-group at the *N*-terminus of a helix in a medium such as water.<sup>67</sup>

In the same vein Q-monomers may be replaced by 5-methylaminopyridine-2-carboxylic acid (P) units,<sup>20, 66, 68, 69</sup> which differ from Q only by the removal of one aromatic ring (Figure 2.6). Both impose the same curvature on the helix, thus the overall structure is preserved. P monomers participate in similar hydrogen bonding patterns as Q, however, the increased flexibility resulting from the aliphatic methylene group and reduced aromatic surface of P leads to a reduction in the stability of the helix. Therefore, pure P oligomers do not fold into well-defined structures in aqueous media.<sup>68</sup> In oligomers consisting of Q and P units, it is possible to tune the conformational dynamics of the architecture in a medium such as chloroform, depending on the amount and the position of a P unit in a sequence. A crystal structure analysis of this sequence shows that this molecule is indeed not completely helical, instead it is partially folded into a helix and partially unfolded.<sup>70</sup> Thus, handedness inversion kinetics might be increased.<sup>69</sup>

## 2.3 Design of tertiary folding

A protein consists of strictly hierarchical structure motifs, such as primary, secondary, tertiary and quaternary structures. Its primary structure is defined as a precise sequence or order of monomeric units<sup>71</sup>, while its secondary structure refers to the regular, local structure of the protein backbone, stabilized by intramolecular and sometimes intermolecular hydrogen bonding of amide groups.<sup>72</sup> The tertiary fold is stabilized by intramolecular interaction forces between its secondary folds.<sup>72</sup> Lastly, the quaternary structure consists of several tertiary structures forming intermolecular interactions with one another.<sup>73</sup> Protein structure formation occurs by self-organization, which depends on the shape of its unity and also various kinds of non-covalent interactions such as salt-bridges, dipole-dipole interaction and hydrogen bonding.<sup>74, 75</sup> Usually, most functions only arise at the level of tertiary and quaternary structure. Accordingly, new functions of foldamers should arise at the tertiary and quaternary level<sup>76</sup> in addition to the already reported applications that only rely on secondary structures. These include biological activity, and even potential as therapeutic agents.<sup>6, 77-84</sup> This is anticipated due to their ability to cross cell membranes efficiently, while having a low toxicity and immunogenicity and a high stability against proteolytic degradation.<sup>85-89</sup> So far  $\alpha$ -helix stabilization,<sup>90</sup>  $\alpha$ -helix mimicry,<sup>91</sup> DNA mimicry,<sup>79</sup> and protein surface recognition<sup>92</sup> have been used as potential strategies for drug discovery. Additionally, hybrid macrocyclic structures in which an aromatic helix forces the  $\alpha$ -peptide to adopt a stretched conformation is stable against proteolytic degradation.<sup>44, 93</sup>

Eliciting folding of secondary motifs such as single helices or sheets in a great variety of synthetic oligomers is now well mastered,<sup>5, 7, 37, 94-96</sup> however, increasing the complexity of molecular architectures to the level of tertiary or quaternary structures is far more challenging, making the *ab initio* design an area needing optimization where literature is rare. In the past, progress has been made in protein design<sup>9, 97-103</sup> and programming binding interfaces between peptidic structures.<sup>98, 99, 104-115</sup> This led to the successful design of a mini-protein with a hydrophobic core and a quaternary structure.<sup>116</sup> In the top-down approach specific natural

amino acids are replaced by non-natural moieties in an already tertiary folded protein. These non-natural moieties have a similar structure and should thus retain the overall fold. Applying such a strategy to proteins such as that of the zinc finger domain SP1-3 at which around 20 % was replaced by non-natural units resulted in an increase of the overall folding stability of the tertiary structure.<sup>117</sup> However, the majority of the molecule is still constituted of  $\alpha$ -amino acids. A fully artificial protein, which would be designed by the bottom-up approach where design is started from scratch has not yet been reported. When designing tertiary structures using solely abiotic units the kind of intramolecular interaction, and thus the formed shape, could be hard to predict. This might be simplified by using a foldamer that forms a very stable and thus predictable secondary fold, which would reduce the number of possible shapes to be taken. So far, quinoline based oligomers showed a high structural predictability.<sup>34, 41, 42</sup> Furthermore, within a Qn oligoamide helix fold a large number of flexible 6-aminomethyl-2-pyridinecarboxylic acid units (P in Figure 2.6) can be tolerated.<sup>20, 66, 68, 69</sup> Moreover, quinoline and pyridine based monomers are easily synthesized and their oligomers are straight-forwardly accessible by solid phase synthesis.<sup>68</sup> These foldamers are easier to analyze and showed good crystallization properties. So far they have been used in circularly polarized luminescence,<sup>118, 119</sup> charge transport and metal coordination,<sup>120</sup> as well as protein surface recognition.<sup>79, 84, 121-123</sup> This supports the assumption that many more accessible functions will be possible at the stage of a quinoline based tertiary structure.

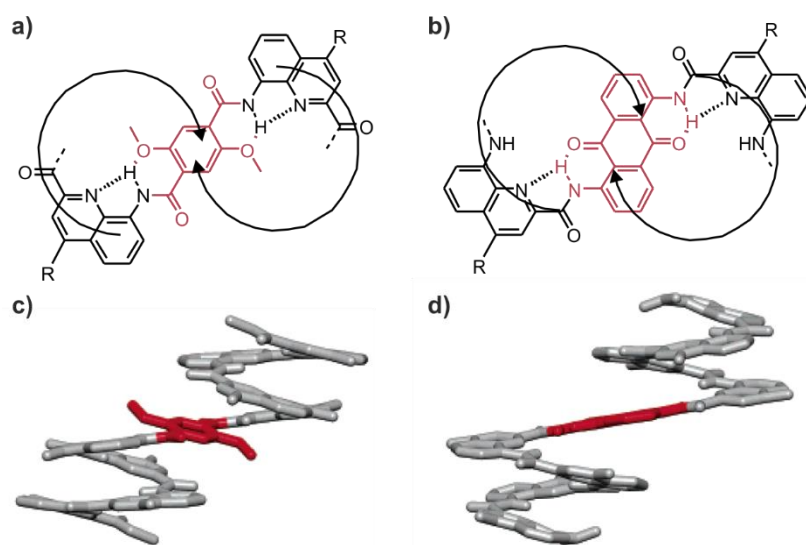


**Figure 2.7.** Part of a foldamer structure featuring a dimethoxyterephthaloyl (a) and a diaminoanthraquinone (b) spacer, respectively. R replaces *i*OBu-groups. Side view of a crystal structure of a foldamer containing a dimethoxyterephthaloyl (c) and a diaminoanthraquinone (d) spacer, respectively. The spacer units are shown in red. Included solvent molecules, isobutyl groups, and carbon hydrogens have been omitted for clarity.<sup>124</sup>

In early linker designs, helices were tied to one another by a turn unit and thus oriented exclusively in one direction. Here, steric hindrance within the molecule was used to enforce opposite handedness in both helices, thus the two helices were pointing away from one another (Figure 2.7).<sup>124</sup> The relative orientation of the helices relied only on steric hindrance. In further designs tertiary structure was formed by intermolecular attractive driving forces such as salt bridges, hydrophobic effects and hydrogen bonds.<sup>125-129</sup> So far, hydrogen bonds

which are directional and strong in chlorinated solvents have been the easiest to predict. Thus, in order to give two helices, the possibility to interact through the formation of such bonds, hydroxyl groups have been introduced at certain positions on their backbone (Figure 2.8a, b, d). In order to force these two helices to be at close proximity, a linker (T1-unit, Figure 2.8c) has been introduced to connect them at each C-terminus (Figure 2.9a & 2.10a,c).

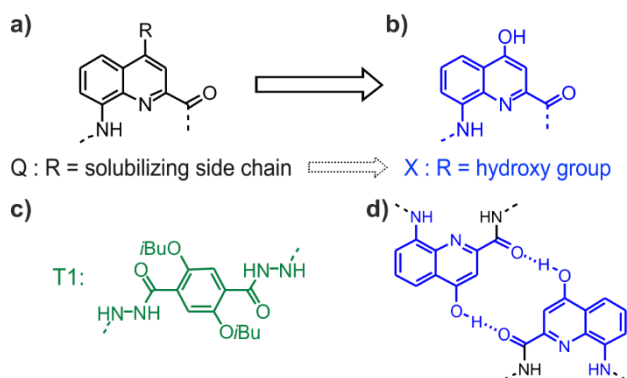


**Figure 2.8.** Structure of Q unit with solubilizing side chains such as isobutoxy groups (a) and of X unit (b). Here a hydroxyl group replaces a solubilizing side-chain. Structure of T1 linker (c). Hydrogen bonding patterns involving X units (d).<sup>3</sup>

This turn unit is a rigid linker with enough flexibility to slightly bend, allowing for the helices to interact via hydrogen bonds. Such bonds are formed between the hydroxyl groups placed on some units and the carbonyl function of the amide bond, which points outwards from the helices. Two types of hydrogen donor-units were used, one was a quinoline-based X-Unit (Figure 2.8d) and the other was the pyridine-based Y-unit (Figure 2.9e). The Y-Unit was introduced to prevent a steric clash, which could occur between the aromatic region of quinoline units between the two helices (Figure 2.9a, b, d).<sup>3</sup> Hydrogen bonds of the X-units are formed by bonding to the carbonyl-function of the amide bond of the opposite X-unit (Figure 2.8d). In the case of the Y-Unit, the carbonyl-function of the neighboring Q-unit of the opposite Y-Unit is involved in the hydrogen bond (Figure 2.9e).<sup>3</sup>

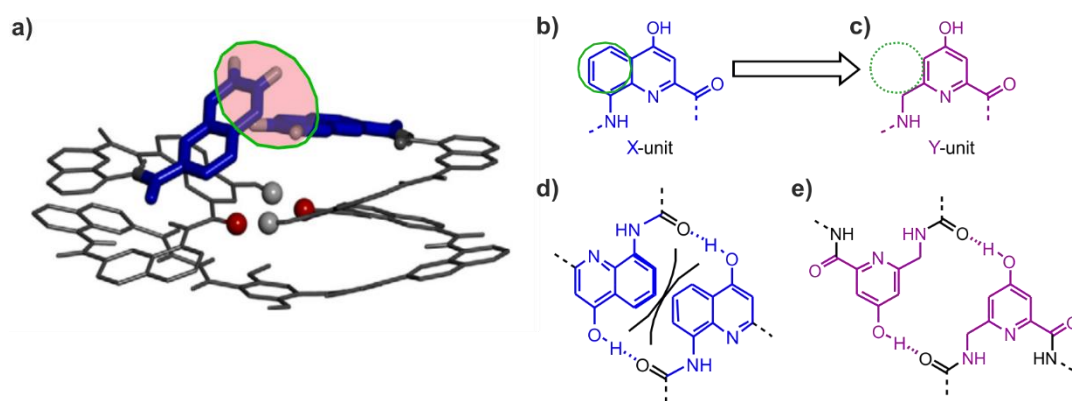


**Figure 2.9.** Energy-minimized model of a hypothetical foldamer at which helices are connected by a T1 unit, the isobutoxy groups of the linker were replaced by methoxy groups. The units of interest are shown as thick blue tubes. The occurrence of a sterical clash between those two is indicated by a pink surface, circled in green. Protons and oxygen atoms involved in hydrogen bonds are shown as white and red balls, respectively. (a). Structure of X-unit (b) and Y-unit (c). Steric hindrance in case of hydrogen bonding patterns involving X and Q units (d). Hydrogen bonding patterns involving Y and Q units (e). The green circle indicates the sterical clash inducing aromatic part.<sup>3</sup>

In this way, a stable homochiral head-to-head dimer was synthesized (Figure 2.10c). This tertiary structure showed a high stability in chloroform.<sup>3</sup> When applying such a design of helix-helix bundle to helices that do not fold into stable helical structures, the helical fold is induced by the tertiary fold. This behavior is similar to cooperative protein tertiary structure folding.<sup>70</sup>

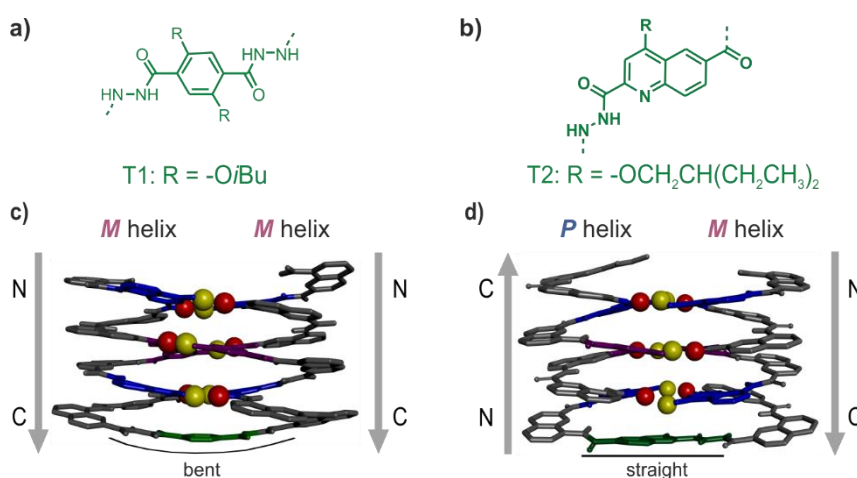


**Figure 2.10.** Structures of T1- (a) and T2-unit (b). Side-views of crystal structures of a parallel head-to-head homochiral dimer stabilized by a T1-Unit (c)<sup>3</sup> and of a parallel head-to-tail heterochiral dimer stabilized by a T2-Unit (d).<sup>130</sup> The hydroxy protons and carbonyl oxygen atoms of the hydrogen-bonding arrays are shown as yellow and red balls, respectively. The X-units are shown in blue, the Y-units in violet, and the turn units in green tubes. Included solvent molecules, non-polar hydrogen atoms and side-chains are omitted for clarity.

The T1-unit was designed to link two helices of the same handedness together at their C-terminus (Figure 2.10a&c). In search to connect two helices of opposite handedness, another linker, the T2-unit, was developed (Figure 2.10b). This linker stabilizes the formation of a heterochiral head-to-tail parallel dimer (Figure 2.10d). The stability of this assembly is comparable to the previous homochiral head-to-head parallel

dimer. Combining these two patterns in one sequence led to the formation of the largest tertiary abiotic structure so far.<sup>130</sup> In conclusion, previous work in the field of *abiotic* foldamers regarding abiotic tertiary folding stabilized by hydrogen bonds has led to the successful synthesis of a helix-turn-helix foldamer with the expected shape.<sup>3, 70, 130</sup> However, prognosis on how many intramolecular hydrogen bonds are necessary to stabilize a tertiary fold and if all hydrogen bonds cause the same stabilizing effects warranted further investigations. Work regarding this subject is described in chapter 3.

The design of a quaternary fold could become possible when implementing intermolecular driving forces to a stable tertiary fold. However, as of yet the formation of a true abiotic quaternary structure has not been reported.

## 2.4 Self-assembly and potential applications

As mentioned above, complex folding can be achieved through self-organization of a single oligomer, with intramolecular driving forces leading to the formation of a tertiary structure. Another way to reach higher folding states could be the self-assembly of secondary structures, which occurs due to intermolecular driving forces. In general, the final shape of a molecule is determined by the sum of several factors, the nature of the units that make up a foldamer and its driving forces of folding – intramolecular and intermolecular forces. Therefore, research in the field of self-assembly is as vast and diverse as the diversity of foldamers and their potential intermolecular interactions. The functions derived from it are as varied as the field of self-assembly. Furthermore, self-assemblies can be divided into those that occur by themselves and those that only occur upon introduction of another reactant. Examples of reactant induced self-assembly include metal-<sup>131, 132</sup>, halogens-<sup>133, 134</sup>, and ion-pair-bonding-directed self-assemblies.<sup>135</sup> Others are the self-assemblies of aromatic foldamers to double helices or other duplexes, as well as fiber formation. Here their formation is triggered by either metals<sup>136</sup> or fullerenes.<sup>137</sup> A metal-directed self-assembly of peptoid foldamers has also been reported.<sup>138</sup> In addition, foldamers can also mediate self-assembly of nanostructures (e.g., nanoparticle formation mediated by peptoid foldamers<sup>139</sup>). Self-assemblies that occur spontaneously often take place in protic solvents. Driving forces are usually hydrophobic effects, hydrogen bonds, salt bonds and conformational preferences of individual units.<sup>140</sup> To access similar driving forces as in a peptide, the top-down approach in which natural amino acids are replaced by non-natural units has been used as well. However, the effects of the exchanged units on a self-assembly can be drastic. Thus, replacing some  $\alpha$ -peptides with sugar derivatives resulted in the formation of well-defined, microscale, homogeneous, and finite structures with unique morphologies such as windmill, tooth, and trigonal bipyramid shapes (Figure 2.11a&b). This crystalline peptidic material is called foldecture.<sup>141</sup> Another way to access driving forces similar to those present in a peptide is to introduce proteinaceous side chains into an oligo-urea based  $\alpha$ -helicomimetic foldamer. Here, the final self-assembly can be controlled at the sequence level, allowing the programmed formation of either discrete helical bundles that either contain isolated cavities or pH-responsive water-filled channels with controllable pore diameters (Figure 2.11c).<sup>142</sup> In a similar approach proteinaceous side chains have been introduced to a helical oligo-



urea.<sup>113</sup> This helical oligo-urea forms a very stable secondary fold, whose shape is not disturbed by intermolecular interactions.<sup>142, 143</sup> In this self-assembly, the formation of a hexameric bundle was observed.<sup>113</sup>

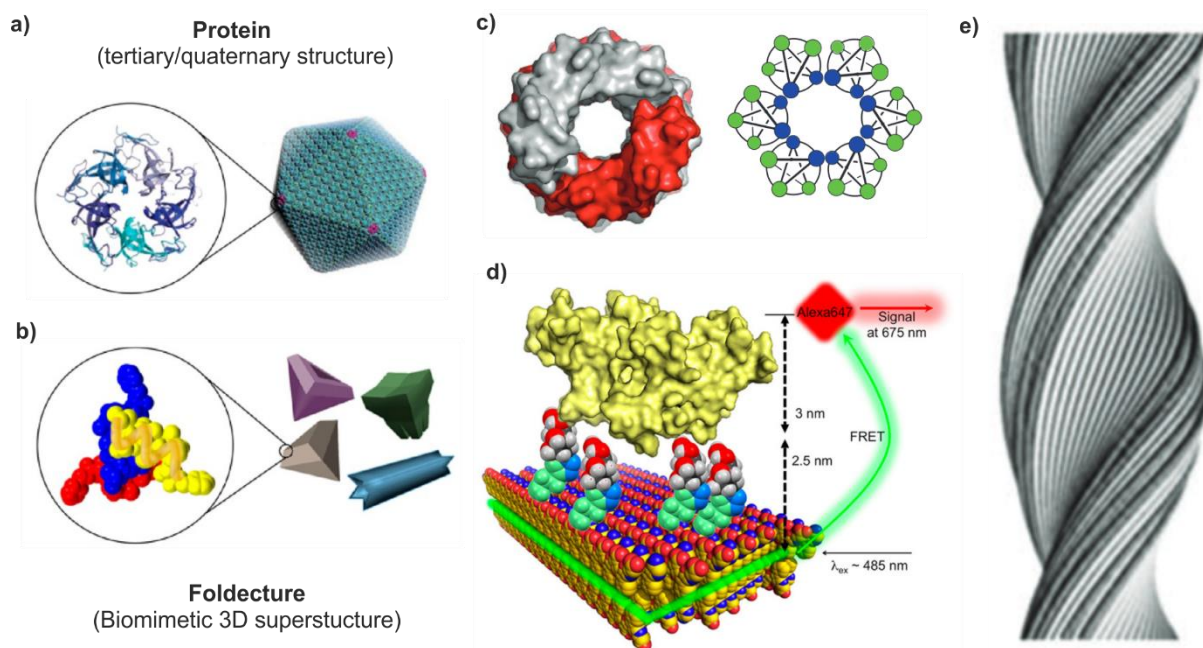


**Figure 2.11.** Examples of self-assembly in protic solvents.<sup>140</sup> Controlled self-assembly of Foldectures of peptidic foldamers mimic 3D biological architecture (a&b).<sup>141</sup> Crystal structure of the channel-type assembly formed from an oligoureia capable of contracting a single mobile water molecule. The two individual superhelix chains of the channel are coloured separately (c).<sup>142</sup> Molecular model of lectins (yellow molecular surface) binding to peptoid nanosheets displaying carbohydrate-ligands and FRET-based assay—BODIPY-FL C16 forms a layer between the two peptoids layers, which are arranged in parallel rows and display carbohydrates on the surface (unnecessary hydrogens are omitted for clarity, carbons are in yellow, oxygens in red, and nitrogens in blue; lectin represented as yellow molecular surface d); binding of lectins is detected by the emission of Alexa647 after FRET between BODIPY-FL C16 and Alexa647 (d).<sup>144</sup> Twisted fiber formation of base-pair stabilized self-assembly (e).<sup>145</sup>

Some research of self-assembly was focused on the conformational preference of each unit as the driving force of folding. In the group of Fülöp, the controlled self-assembly of  $\beta$ -peptide foldamers, inducing either the formation of helix bundles or pleated sheets, were obtained by accurate choice of structure and configuration of  $\beta$ -peptide backbones, and ultimately led to the formation of vesicles or fibrils, respectively.<sup>146</sup> After addition of nucleobase to the backbone of the  $\beta$ -peptides<sup>147, 148</sup> its self-assembly became highly dependent on environmental conditions such as temperature, pH and ionic strength. This led to the formation of macroscopic fibers<sup>149-159</sup> which then lead to the development of nanofiber networks that could entrap water and form hydrogels<sup>152</sup> and when injected to transgenic mice showed a possible integration in neurons.<sup>159</sup> However, this was only possible with lapidated analogues.<sup>158</sup> In a  $\beta$ -homoalanine foldamer, nucleobase guided pairing led to the formation of beta-sheet-like antiparallel double strand structures.<sup>147, 148</sup> When introducing nucleobase guided pairing to  $\alpha$ -peptides the formation of a twisted fiber was observed (Figure 2.11 e). In this case,  $\pi$ - $\pi$ -stacking as a hydrophobic driving force was also observed.<sup>145</sup> Other self-assemblies in which hydrophobic forces were used as the main driving force were stack formations of polymeric foldamers of para-

aryl-triazole which preferably adopt a cisoid conformation. Here the stacking increased with increased water content.<sup>160</sup> A peptoid, in which sidechains of an  $\alpha$ -amino acid based peptide have been replaced by sugar derivatives irreversibly formed nano sheets while the sugar-bearing monomers pointed outward on the exterior surface. Due to these outward pointing carbohydrates, the self-assembly was also able to interact with lectins (Figure 2.11d) and acted similarly to a cell-membrane, since it consisted of a hydrophobic core and a zwitterionic hydrophilic surface.<sup>144</sup>

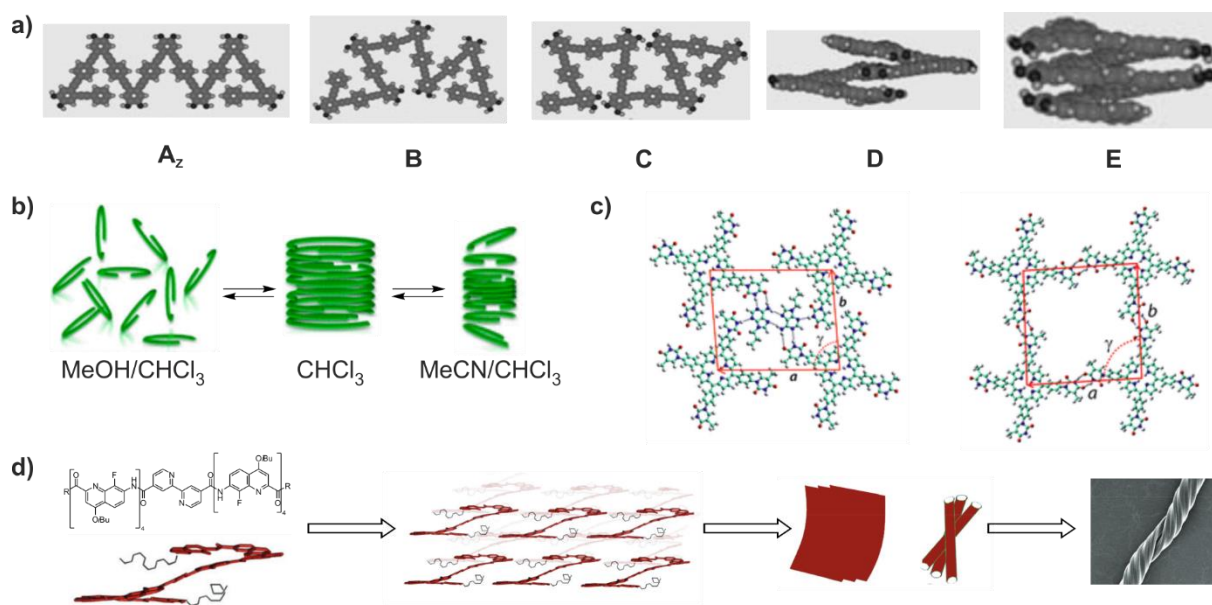


**Figure 2.12.** Examples of self-assembly in non-protic solvents.<sup>140</sup> Molecular models of the five conformations of a self-assembly stabilized by  $\pi$ - $\pi$ -stacking on a solid phase (a).<sup>161</sup> Aromatic  $\pi$ - $\pi$ -stacking of stable short aromatic oligoamide (b).<sup>162</sup> Lattice formation through thymine/thymine hydrogen-bonding of a thymine functionalised porphyrins (c).<sup>163</sup> Fiber formation of 8-fluoro amino-quinoline carboxyl acid based foldamers, R replaces amine alkyl chain. Here alkyl chains can be of different length (d).<sup>164</sup>

So far, there have been only a few examples of self-organization in non-protic solvents.<sup>140</sup> Driving forces of them are usually  $\pi$ - $\pi$ -stacking and hydrogen bonds. Nevertheless, self-assemblies in organic solvents are as diverse as self-assemblies occurring in protic solvents. Driven by  $\pi$ - $\pi$ -stacking foldamers with an aromatic backbone were shown to adapt five different conformations on solid phase (Figure 2.12a).<sup>161</sup> Stacking of stable short aromatic oligoamide stabilized by  $\pi$ - $\pi$ -interaction was observed in pure chloroform. In contrast to typical aromatic stacking, here stacking is enhanced in solvents of low polarity, and weakened in solvents of high polarity, especially those with hydrogen bond donor capacity (Figure 2.12b).<sup>162</sup> Formation of well-defined twisted helical microfibers can be observed when using a quinolinecarboxamide-derivative bound to a bipyridyl segment. Here, intermolecular  $\pi$ - $\pi$ -stacking as well as van-der-Waals forces are driving forces of the folding (Figure 2.12d).<sup>164</sup> Self-assembly using base-pairing in chloroform is also known. This intermolecular interaction leads to the formation of an almost perfectly squared self-assembled lattice through thymine/thymine hydrogen-bonding of a thymine functionalised porphyrins (Figure 2.12c).<sup>163</sup> Intermolecular hydrogen bonds are also the driving force for the folding of foldamers consisting of a mixture of aliphatic and

aromatic backbones. Hereby, quadruply and sixtuply intermolecularly hydrogen bonded dimers are formed.<sup>165-</sup>  
169

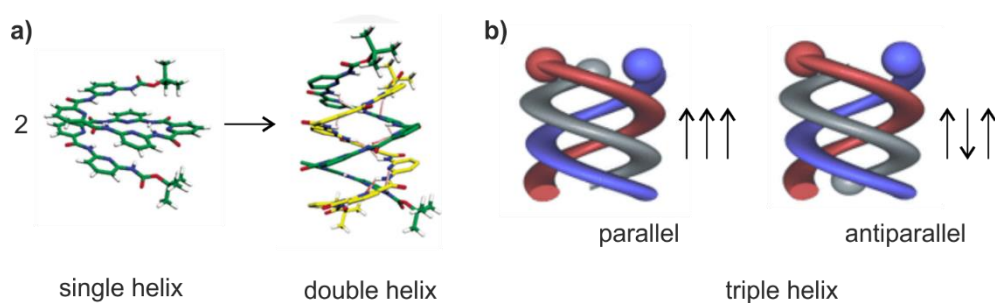


**Figure 2.13.** Intertwining process of two strands of oligo-pyridinecarboxamides to form a antiparallel double helix in chloroform (a).<sup>170</sup> Formation of parallel and antiparallel triple helices in chloroform and acetonitrile, respectively. Here naphthyridine based foldamers are used (b).<sup>171</sup>

An example of the combination of intermolecular hydrogen bonding and  $\pi$ - $\pi$ -stacking is the intertwining process of two strands of oligo-pyridinecarboxamide oligomers, between which an antiparallel double helix is formed (Figure 2.13a).<sup>170</sup> However, when using naphthyridine based oligoamides interstrand interactions consist only of extensive  $\pi$ - $\pi$ -contacts, leading to the formation of either parallel or antiparallel triple helices (Figure 2.13b). Here, parallel triple helices are preferably formed in chloroform, whereas the antiparallel triple helix is predominantly formed in acetonitrile.<sup>171</sup> Generally, the design of a self-assembly would be simplified if the intermolecular driving force as well as the secondary fold were easily predictable. In the design of quinoline-based tertiary structures, the interaction of foldamers via hydrogen bond formation proved easiest to predict. The same approach has been used for self-assemblies.<sup>3</sup>

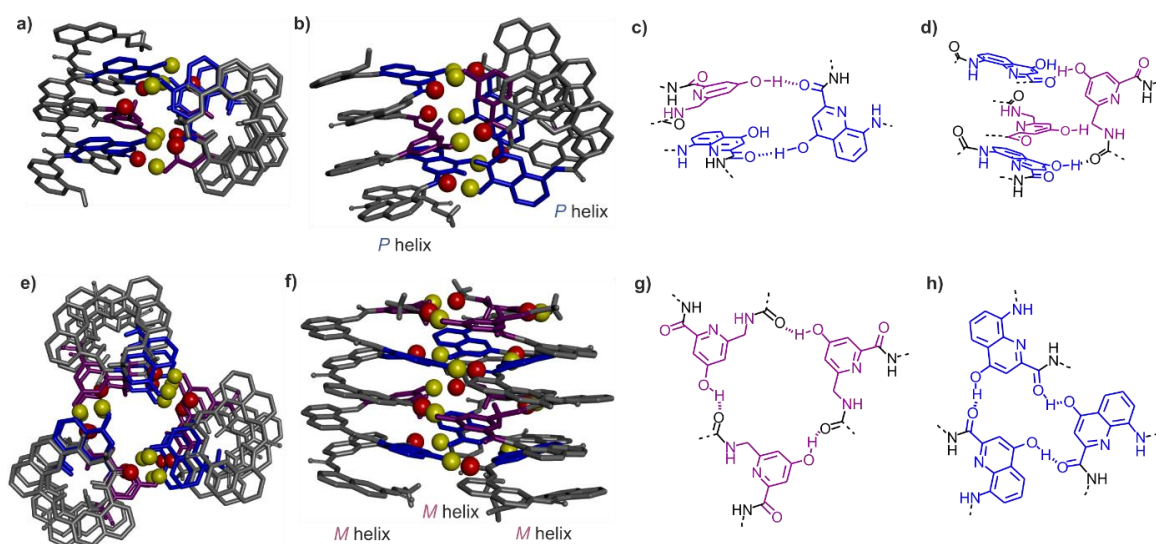


**Figure 2.14.** Top- (a) and side-view (b) of crystal structure of a tilted dimer. Top- (e) and side-view (f) of crystal structure of a trimer. The hydroxyl protons and carbonyl oxygen atoms of the hydrogen-bonding arrays are shown as yellow and red balls, respectively. The X-units are shown in blue and the Y units in violet tubes. Included solvent molecules, hydrogens and other side-chains are omitted for clarity. Hydrogen bonding pattern found in a tilted dimer (c & d) and a trimer (g&h).<sup>3</sup>

As reported earlier, quinoline-based foldamers form very stable helical structures.<sup>15, 33</sup> Point introduction of hydroxyl-bearing residues such as X and Y units to such a helix gives access to inter-chain hydrogen bonds with the exposed oxygen atoms of the carbonyl function of the amide groups. Introduction of a turn unit leads to the formation of a stable, parallel homochiral<sup>3</sup> or antiparallel heterochiral<sup>70</sup> dimer. However, when removing these units, a higher degree of freedom allows for another kind of aggregation to take place, leading to formation of a trimeric helix bundle and a tilted dimer (Figure 2.14).<sup>3</sup> This indicates that the head-to-head parallel dimer observed as a tertiary fold is not the most preferred aggregation mode. Furthermore, a tilted dimer and a trimer are very different from one another. In a trimer, three helices are assembled in a head-to-head parallel arrangement. Whereas in a tilted dimer two helices are hydrogen bonded to one another in a non-parallel way. In the case of the trimer, only two types of hydrogen bonds are formed. In this type of aggregate three hydrogen bond donor units are involved in one type of hydrogen bond each. The hydroxyl group of the Y-units bind to the carbonyl function of the Q-units of the neighboring helix (Figure 2.14h) and the hydroxyl group of the X-Units bind to the carbonyl function of the X-unit of the neighboring helix (Figure 2.14g). In case of the tilted dimer, three different types of hydrogen bonds are formed. One type being the hydroxyl group of the Y-unit binding to the carbonyl function of the X-unit on the opposing helix, whose hydroxyl group is then binding to the carbonyl function of the first helix for the second type (Figure 2.14c). Lastly one hydroxyl group of an X-unit within the first helix binds to the carbonyl function of a Y-unit of the second (Figure 2.14d). Thus, the hydrogen bonding pair involving a Y unit bridges over two helix turns. All this shows how many possibilities of different hydrogen bonds there are. The diversity of the aggregates observed leaves too many options for the helices to self-assemble. Investigation on how the hydrogen bonding interface might be manipulated to create new assemblies by precise changes of the number of hydroxyl groups within one foldamer will be discussed in chapter 4. Research on how a tilted dimer might be stabilized and therefore selectively forms will be discussed in chapter 5.

In a protein, most functions emerge at the level of tertiary or quaternary structure. Predictions of quaternary structures are more complicated due to the increased level of complexity. Additionally, in aprotic organic solvents solvation and desolvation phenomena would be completely different. Therefore, it is expected that protein-like behavior in aprotic organic solvents may differ from that of proteins in water. In chapter 5 the discovery of an abiotic eight helix bundle featuring protein-like features is reported.

## 2.5 Guiding Objective: design of helix bundles

Research in the field of *abiotic* foldamers has led to the successful synthesis of a tertiary folding stabilized by hydrogen bonds.<sup>3</sup> In such a structure, two quinoline-based helices are connected by a turn-unit, preventing unwanted aggregates from forming. If such a turn unit is removed, different finite aggregates are formed. These aggregates feature a different relative orientation of the involved helices towards each other as well as differences in molecularity.<sup>3</sup> To restrict the diversity of self-assemblies and allow for more precise predictions, the interactive surface of monomers was to be altered. The front-view of a single helix revealed (Figure 2.15d) two arrays of hydrogen donors and acceptors at their surface.<sup>3</sup> Put differently, a helix containing X- and Y-units had two active interaction interfaces (Figure 2.15d). Hydroxy groups of the two hydrogen donor units were located on two neighboring columns on the same side of a helix backbone. To restrict aggregation to only one side of the helix and thereby reduce the amount of possible assemblies, hydroxyl groups were to be removed from one column of the helix backbone, essentially removing the hydroxyl groups of one donor unit. As a replacement for the hydroxy groups of pyridine based Y-units, protons were to be introduced (Figure 2.15a). A removal of these hydroxy groups also meant the removal of hydrogen bonds in a helix-turn-helix tertiary fold, which was thought to destabilize such a fold. In this work, the stability of a helix-turn-helix tertiary fold in which certain hydrogen bonds were removed will be estimated (chapter 3, Figure 2.15b&c).

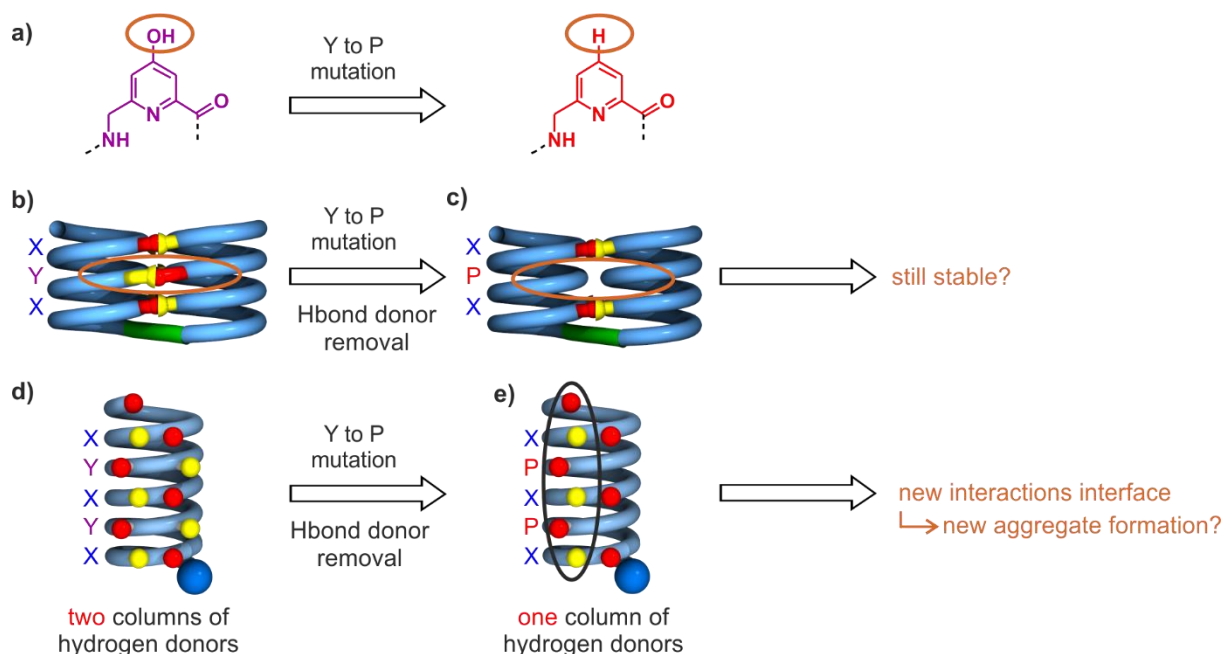


**Figure 2.15.** Y to P mutation, replacing a hydroxy group by a proton (a). Schematic representation of helix-turn-helix tertiary motifs before (b) and after (c) hydrogen donor removal. Schematic representation of the front view of a single helix before (d) and after (e) precise point removal of hydroxy groups. Hydrogen donor and acceptors are shown as yellow and red balls, respectively. The turn unit is represented in green in b&c. The N-terminus is represented as a blue ball in d&e.

As mentioned before a helix containing X- and Y-units has two columns of hydrogen donors on one side of a helix. Self-assemblies of such sequences have led to tilted dimer and trimer formation. However, when

restricting aggregation to only one column side of the helix, the formation of those structures could be destabilized. Which could lead to the formation of a new hydrogen bonding interface during a helix self-assembly. In this work self-assembly of such helices will be observed and analyzed (chapter 4, Figure 2.15d&e).

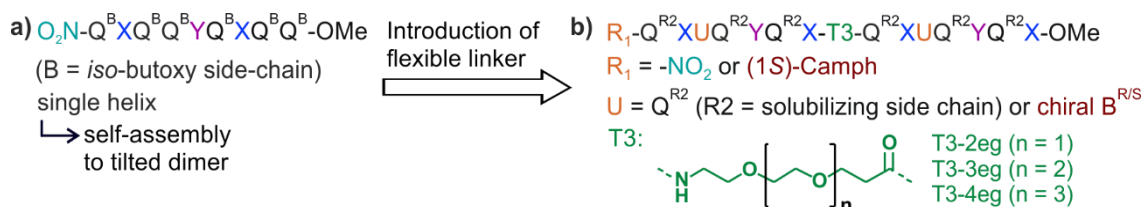


**Figure 2.16.** Foldamer sequence of a single helix self-assembling to a tilted dimer in solution (a). Introduction of a flexible linker into a foldamer sequence which prefers to form tilted dimers. Here handedness control is introduced either as a N-terminal chiral (1*S*)-Camph unit or a chiral B unit from within the helix (marked in brown). Furthermore, achiral sequences are synthesized by replacing a terminal amine by a nitro group (marked in turquoise). As linker polyethylene based units containing a 2eg, 3eg and 4eg backbone, respectively are used (marked in green). Hydrogen donor units X and Y are shown in blue and violet, respectively.

So far, only tertiary structures in which a turn unit enforces the formation of a parallel assembly of two helices have been established.<sup>3, 130</sup> However, natural biopolymers, such as protein structures, do not always contain parallel assemblies.<sup>172</sup> Finding turn units that could stabilize non-parallel aggregate formation, such as a tilted dimer formation, could therefore be rewarding (Figure 2.16). The observation of a non-parallel tilted dimer as seen in Figure 2.14a gave inspiration for a new design where a flexible linker would connect two helices, whose self-assembly showed tilted dimer formation. Here the linker is flexible enough to allow for a non-parallel arrangement (Figure 2.17).

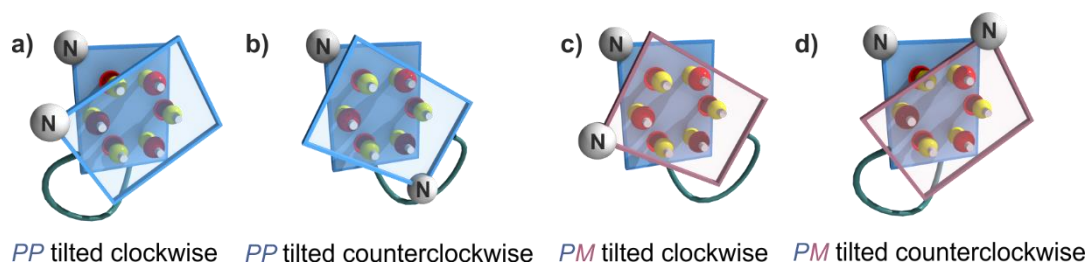


**Figure 2.17.** Schematic representation of possible tilted dimers stabilized by a flexible turn unit.

Linkers with differing levels of flexibility were to be introduced to observe their effects on the self-organization. Even though the tilted dimer observed in the crystal structure is a homochiral aggregate,<sup>3</sup> computational modelling has shown that PM helix-to-helix interactions are also possible (Figure 2.17c&d). Thusly, to prevent formation of PM aggregates, handedness control has to be introduced. There are several approaches to this. One option was to introduce chiral B units (see chapter 2.2, Figure 2.6) into both helices, enforcing the formation of a homochiral aggregate. Previously, the effect of chiral B units had only been demonstrated in water, methanol and DMSO<sup>67</sup>, thus their influence on handedness control in organic solvent

such as dichloromethane and chloroform was to be investigated before introducing them. A second option was to enforce handedness control in one helix via an N-terminal (1*S*)-Camphanic group (Figure 2.16). Here PM aggregates were thought to be possible in principle. If the use of such a group was to be complicit with the formation of a tilted dimer, achiral sequences might be synthesized as well. Progress on this topic will be reported in chapter 5.

## 2.6 References for chapter 2

1. B. Frolund, B. Ebert, U. Kristiansen, T. Liljefors and P. Krogsgaard-Larsen, *Curr. Top. Med. Chem.*, 2002, **2**, 817-832.
2. A. S. Culf, *Biopolymers*, 2019, **110**.
3. S. De, B. Chi, T. Granier, T. Qi, V. Maurizot and I. Huc, *Nat. Chem.*, 2018, **10**, 51-57.
4. I. Arrata, A. Barnard, D. C. Tomlinson and A. J. Wilson, *Chem. Commun.*, 2017, **53**, 2834-2837.
5. G. Guichard and I. Huc, *Chem. Commun.*, 2011, **47**, 5933.
6. J. W. Checco and S. H. Gellman, *Curr. Opin. Struct. Biol.*, 2016, **39**, 96-105.
7. S. H. Gellman, *Acc. Chem. Res.*, 1998, **31**, 173-180.
8. T.-K. Lee and J.-M. Ahn, *ACS Combinatorial Science*, 2011, **13**, 107-111.
9. E. G. Baker, G. J. Bartlett, K. L. Porter Goff and D. N. Woolfson, *Acc. Chem. Res.*, 2017, **50**, 2085-2092.
10. D. Bindl. Folding properties, handedness control and aggregation behavior of helical aromatic  $\delta$ -amino acid foldamers in water (Fakultät für Chemie und Pharmazie der Ludwig-Maximilian-Universität München, 2022).
11. D. S. Daniels, E. J. Petersson, J. X. Qiu and A. Schepartz, *J. Am. Chem. Soc.*, 2007, **129**, 1532-1533.
12. D. M. Bassani, J.-M. Lehn, G. Baum and D. Fenske, *Angew. Chem. Int. Ed.*, 1997, **36**, 1845-1847.
13. L. Sebaoun, V. Maurizot, T. Granier, B. Kauffmann and I. Huc, *J. Am. Chem. Soc.*, 2014, **136**, 2168-2174.
14. C. G. Pappas, P. K. Mandal, B. Liu, B. Kauffmann, X. Miao, D. Komáromy, W. Hoffmann, C. Manz, R. Chang, K. Liu, K. Pagel, I. Huc and S. Otto, *Nat. Chem.*, 2020, **12**, 1180-1186.
15. C. Dolain, A. Grélard, M. Laguerre, H. Jiang, V. Maurizot and I. Huc, *Chem. Eur. J.*, 2005, **11**, 6135-6144.
16. K. Yoshida, S.-I. Kawamura, T. Morita and S. Kimura, *J. Am. Chem. Soc.*, 2006, **128**, 8034-8041.
17. R. Scott Lokey and B. L. Iverson, *Nature*, 1995, **375**, 303-305.
18. J. Brüggemann, S. Bitter, S. Müller, W. M. Müller, U. Müller, N. M. Maier, W. Lindner and F. Vögtle, *Angew. Chem. Int. Ed.*, 2007, **46**, 254-259.
19. C. A. Hunter, A. Spitaleri and S. Tomas, *Chem. Commun.*, 2005, DOI: 10.1039/b506093a, 3691.
20. N. Delsuc, F. Godde, B. Kauffmann, J.-M. Léger and I. Huc, *J. Am. Chem. Soc.*, 2007, **129**, 11348-11349.
21. P. E. Nielsen, M. Egholm, R. H. Berg and O. Buchardt, *Science*, 1991, **254**, 1497-1500.
22. R. J. Simon, R. S. Kania, R. N. Zuckermann, V. D. Huebner, D. A. Jewell, S. Banville, S. Ng, L. Wang, S. Rosenberg and C. K. Marlowe, *Proc. Natl. Acad. Sci. U.S.A.*, 1992, **89**, 9367-9371.
23. D. Seebach, M. Overhand, F. N. M. Kühnle, B. Martinoni, L. Oberer, U. Hommel and H. Widmer, *Helvetica Chimica Acta*, 1996, **79**, 913-941.



24. D. Seebach and J. L. Matthews, *Chem. Commun.*, 1997, DOI: 10.1039/a704933a, 2015-2022.
25. D. H. Appella, L. A. Christianson, I. L. Karle, D. R. Powell and S. H. Gellman, *J. Am. Chem. Soc.*, 1996, **118**, 13071-13072.
26. D. Seebach, D. F. Hook and A. Glättli, *Biopolymers*, 2006, **84**, 23-37.
27. M. D. Smith, D. D. Long, T. D. W. Claridge, G. W. J. Fleet, D. G. Marquess and D. G. Marquess, *Chem. Commun.*, 1998, DOI: 10.1039/a805364b, 2039-2040.
28. H.-D. Arndt, B. Ziemer and U. Koert, *Org. Lett.*, 2004, **6**, 3269-3272.
29. V. Semetey, D. Rognan, C. Hemmerlin, R. Graff, J.-P. Briand, M. Marraud and G. Guichard, *Angew. Chem. Int. Ed.*, 2002, **41**, 1893-1895.
30. A. Salaün, M. Potel, T. Roisnel, P. Gall and P. Le Grel, *J. Am. Chem. Soc.*, 2005, **70**, 6499-6502.
31. X. Li and D. Yang, *Chem. Commun.*, 2006, DOI: 10.1039/b602230h, 3367.
32. M. Gude, U. Piarulli, D. Potenza, B. Salom and C. Gennari, *Tetrahedron Lett.*, 1996, **37**, 8589-8592.
33. H. Jiang, J.-M. Léger, C. Dolain, P. Guionneau and I. Huc, *Tetrahedron Lett.*, 2003, **59**, 8365.
34. H. Jiang, J.-M. Léger and I. Huc, *J. Am. Chem. Soc.*, 2003, **125**, 3448-3449.
35. J. C. Nelson, J. G. Saven, J. S. Moore and P. G. Wolynes, *Science*, 1997, **277**, 1793-1796.
36. I. Huc, *Eur. J. Org. Chem.*, 2004, **2004**, 17-29.
37. D.-W. Zhang, X. Zhao, J.-L. Hou and Z.-T. Li, *Chem. Rev.*, 2012, **112**, 5271-5316.
38. V. Berl, I. Huc, R. G. Khoury, M. J. Krische and J.-M. Lehn, *Nature*, 2000, **407**, 720-723.
39. Y. Hamuro, S. J. Geib and A. D. Hamilton, *J. Am. Chem. Soc.*, 1996, **118**, 7529-7541.
40. J. Zhu, R. D. Parra, H. Zeng, E. Skrzypczak-Jankun, X. C. Zeng and B. Gong, *J. Am. Chem. Soc.*, 2000, **122**, 4219-4220.
41. T. Qi, V. Maurizot, H. Noguchi, T. Charoenraks, B. Kauffmann, M. Takafuji, H. Ihara and I. Huc, *Chem. Commun.*, 2012, **48**, 6337.
42. F. Devaux, X. Li, D. Sluysmans, V. Maurizot, E. Bakalis, F. Zerbetto, I. Huc and A.-S. Duwez, *Chem*, 2021, **7**, 1333-1346.
43. X. Hu, P. K. Mandal, B. Kauffmann and I. Huc, *ChemPlusChem*, 2020, **85**, 1580-1586.
44. J. M. Rogers, S. Kwon, S. J. Dawson, P. K. Mandal, H. Suga and I. Huc, *Nat. Chem.*, 2018, **10**, 405-412.
45. K. Urushibara, Y. Ferrand, Z. Liu, K. Katagiri, M. Kawahata, E. Morvan, R. D'Elia, V. Pophristic, A. Tanatani and I. Huc, *Chem. Eur. J.*, 2021, **27**, 11205-11215.
46. B. Huang, M. A. Prantil, T. L. Gustafson and J. R. Parquette, *J. Am. Chem. Soc.*, 2003, **125**, 14518-14530.
47. E. Yashima, K. Maeda, H. Iida, Y. Furusho and K. Nagai, *Chem. Rev.*, 2009, **109**, 6102-6211.
48. Y. Yan, B. Qin, Y. Shu, X. Chen, Y. K. Yip, D. Zhang, H. Su and H. Zeng, *Org. Lett.*, 2009, **11**, 1201-1204.
49. J. T. Ernst, J. Becerril, H. S. Park, H. Yin and A. D. Hamilton, *Angew. Chem. Int. Ed.*, 2003, **42**, 535-539.

50. X. Li, T. Qi, K. Srinivas, S. Massip, V. Maurizot and I. Huc, *Org. Lett.*, 2016, **18**, 1044-1047.
51. D. Sánchez-García, B. Kauffmann, T. Kawanami, H. Ihara, M. Takafuji, M.-H. I. n. Delville and I. Huc, *J. Am. Chem. Soc.*, 2009, **131**, 8642–8648.
52. C. D. Tsiamantas, Simon J. and I. Huc, *C. R. Chimie* **19**, 2016, 132-142.
53. B. t. Baptiste, C. l. Douat-Casassus, K. Laxmi-Reddy, F. d. r. Godde and I. Huc, *J. Org. Chem.*, 2010, **75**, 7175–7185.
54. X. Hu, S. J. Dawson, Y. Nagaoka, A. Tanatani and I. Huc, *J. Org. Chem.*, 2016, **81**, 1137–1150.
55. Y.-X. Xu, G.-T. Wang, X. Zhao, X.-K. Jiang and Z.-T. Li, *J. Org. Chem.*, 2009, **74**, 7267-7273.
56. D. H. Appella, L. A. Christianson, D. A. Klein, D. R. Powell, X. Huang, J. J. Barchi and S. H. Gellman, *Nature*, 1997, **387**, 381-384.
57. H. S. Chan and K. A. Dill, *Annu. Rev. Biophys. Biophys. Chem.* , 1991, **20**, 447-490.
58. M. Jewginski, L. Fischer, C. Colombo, I. Huc and C. D. Mackereth, *ChemBioChem*, 2016, **17**, 727-736.
59. Y. Ferrand, A. M. Kendhale, B. Kauffmann, A. Grélard, C. Marie, V. Blot, M. Pipelier, D. Dubreuil and I. Huc, *J. Am. Chem. Soc.*, 2010, **132**, 7858-7859.
60. Z. Liu, X. Hu, A. M. Abramyan, Á. Mészáros, M. Csékei, A. Kotschy, I. Huc and V. Pophristic, *Chem. Eur. J.*, 2017, **23**, 3605-3615.
61. E. Yashima, N. Ousaka, D. Taura, K. Shimomura, T. Ikai and K. Maeda, *Chem. Rev.*, 2016, **116**, 13752-13990.
62. L. Zheng, Y. Zhan, C. Yu, F. Huang, Y. Wang and H. Jiang, *Org. Lett.*, 2017, **19**, 1482-1485.
63. X. Hu, S. J. Dawson, Y. Nagaoka, A. Tanatani and I. Huc, *J. Org. Chem.*, 2016, **81**, 1137-1150.
64. A. M. Kendhale, L. Poniman, Z. Dong, K. Laxmi-Reddy, B. Kauffmann, Y. Ferrand and I. Huc, *J. Org. Chem.*, 2011, **76**, 195-200.
65. L. Yang, C. Ma, B. Kauffmann, D. Li and Q. Gan, *Org. Biomol. Chem.*, 2020, **18**, 6643-6650.
66. D. Sánchez-García, B. Kauffmann, T. Kawanami, H. Ihara, M. Takafuji, M.-H. Delville and I. Huc, *J. Am. Chem. Soc.*, 2009, **131**, 8642-8648.
67. D. Bindl, E. Heinemann, P. K. Mandal and I. Huc, *Chem. Commun.*, 2021, **57**, 5662-5665.
68. B. Baptiste, C. Douat-Casassus, K. Laxmi-Reddy, F. Godde and I. Huc, *J. Org. Chem.*, 2010, **75**, 7175-7185.
69. M. Vallade, P. Sai Reddy, L. Fischer and I. Huc, *Eur. J. Org. Chem.*, 2018, **2018**, 5489-5498.
70. D. Mazzier, S. De, B. Wicher, V. Maurizot and I. Huc, *Chem. Sci.*, 2019, **10**, 6984-6991.
71. F. Sanger, *Adv. Protein Chem.*, 1952, **7**, 1-67.
72. C. B. a. J. Tooze, *Introduction to Protein Structure*, Garland Publishing, New York, 1990 and 1991.
73. J. Kyte, *Structure in Protein Chemistry*, Garland Publishing, New York, 1995.
74. H.-D. Jakubke and H. Jeschkeit, *Aminosäuren, Peptide, Proteine*, Verlag Chemie, Weinheim, 1982.
75. H. Rehm and T. Letzel, *Der Experimentator: Proteinbiochemie/Proteomics.*, Spektrum Akademischer Verlag, Heidelberg, 2009.

76. W. S. Horne and T. N. Grossmann, *Nat. Chem.*, 2020, **12**, 331-337.
77. J. P. Saludes, J. B. Ames and J. Gervay-Hague, *J. Am. Chem. Soc.*, 2009, **131**, 5495-5505.
78. J. W. Checco, E. F. Lee, M. Evangelista, N. J. Sleebs, K. Rogers, A. Pettikiriarachchi, N. J. Kershaw, G. A. Eddinger, D. G. Belair, J. L. Wilson, C. H. Eller, R. T. Raines, W. L. Murphy, B. J. Smith, S. H. Gellman and W. D. Fairlie, *J. Am. Chem. Soc.*, 2015, **137**, 11365-11375.
79. K. Ziach, C. Chollet, V. Parissi, P. Prabhakaran, M. Marchivie, V. Corvaglia, P. P. Bose, K. Laxmi-Reddy, F. Godde, J.-M. Schmitter, S. Chaignepain, P. Pourquier and I. Huc, *Nat. Chem.*, 2018, **10**, 511-518.
80. G. N. Tew, R. W. Scott, M. L. Klein and W. F. DeGrado, *Acc. Chem. Res.*, 2010, **43**, 30-39.
81. S. Abdulkadir, C. Li, W. Jiang, X. Zhao, P. Sang, L. Wei, Y. Hu, Q. Li and J. Cai, *J. Am. Chem. Soc.*, 2022, **144**, 270-281.
82. J. Niu, A. J. Cederstrand, G. A. Eddinger, B. Yin, J. W. Checco, C. A. Bingman, V. K. Outlaw and S. H. Gellman, *J. Am. Chem. Soc.*, 2022, **144**, 9610-9617.
83. R. Gopalakrishnan, A. I. Frolov, L. Knerr, W. J. Drury and E. Valeur, *J. Med. Chem.*, 2016, **59**, 9599-9621.
84. J. Ahmed, T. C. Fitch, C. M. Donnelly, J. A. Joseph, T. D. Ball, M. M. Bassil, A. Son, C. Zhang, A. Ledreux, S. Horowitz, Y. Qin, D. Paredes and S. Kumar, *Nat. Commun.*, 2022, **13**.
85. M. Rueping, Y. Mahajan, M. Sauer and D. Seebach, *ChemBioChem*, 2002, **3**, 257-259.
86. J. Iriondo-Alberdi, K. Laxmi-Reddy, B. Bouguerne, C. Staedel and I. Huc, *ChemBioChem*, 2010, **11**, 1679-1685.
87. T. B. Potocky, A. K. Menon and S. H. Gellman, *J. Am. Chem. Soc.*, 2005, **127**, 3686-3687.
88. M. Oba, *ChemBioChem*, 2019, **20**, 2041-2045.
89. M. Pasco, C. Dolain and G. Guichard, *Comprehensive supramolecular chemistry II*, Elsevier, Amsterdam, Netherlands, 2017.
90. J. Fremaux, L. Mauran, K. Pulka-Ziach, B. Kauffmann, B. Odaert and G. Guichard, *Angew. Chem. Int. Ed.*, 2015, **54**, 9816-9820.
91. M. Zwillinger, P. S. Reddy, B. Wicher, P. K. Mandal, M. Csékei, L. Fischer, A. Kotschy and I. Huc, *Chem. Eur. J.*, 2020, **26**, 17366-17370.
92. M. Vallade, M. Jewginski, L. Fischer, J. Buratto, K. Bathany, J.-M. Schmitter, M. Stupfel, F. Godde, C. D. Mackereth and I. Huc, *Bioconjugate Chem.*, 2019, **30**, 54-62.
93. S. Dengler, P. K. Mandal, L. Allmendinger, C. Douat and I. Huc, *Chem. Sci.*, 2021, **12**, 11004-11012.
94. C. M. Goodman, S. Choi, S. Shandler and W. F. DeGrado, *Nat. Chem. Biol.*, 2007, **3**, 252-262.
95. R. V. Nair, K. N. Vijayadas, A. Roy and G. J. Sanjayan, *Eur. J. Org. Chem.*, 2014, **2014**, 7763-7780.
96. I. Saraogi and A. D. Hamilton, *Chem. Soc. Rev.*, 2009, **38**, 1726.
97. D. Hilvert, *Annu. Rev. Biochem.*, 2013, **82**, 447-470.
98. N. H. Joh, T. Wang, M. P. Bhate, R. Acharya, Y. Wu, M. Grabe, M. Hong, G. Grigoryan and W. F. DeGrado, *Science*, 2014, **346**, 1520-1524.

99. S. E. Boyken, Z. Chen, B. Groves, R. A. Langan, G. Oberdorfer, A. Ford, J. M. Gilmore, C. Xu, F. DiMaio, J. Henrique Pereira, B. Sankaran, G. Seelig, P. H. Zwart and D. Baker, *Science*, 2016, **352**, 680-687.
100. P.-S. Huang, S. E. Boyken and D. Baker, *Nature*, 2016, **537**, 320-327.
101. B. Dang, H. Wu, V. K. Mulligan, M. Mravic, Y. Wu, T. Lemmin, A. Ford, D.-A. Silva, D. Baker and W. F. DeGrado, *Proc. Natl. Acad. Sci.*, 2017, **114**, 10852-10857.
102. W. M. Dawson, G. G. Rhys and D. N. Woolfson, *Curr. Opin. Chem. Biol.*, 2019, **52**, 102-111.
103. J. Dou, A. A. Vorobieva, W. Sheffler, L. A. Doyle, H. Park, M. J. Bick, B. Mao, G. W. Foight, M. Y. Lee, L. A. Gagnon, L. Carter, B. Sankaran, S. Ovchinnikov, E. Marcos, P.-S. Huang, J. C. Vaughan, B. L. Stoddard and D. Baker, *Nature*, 2018, **561**, 485-491.
104. W. S. Horne, J. L. Price, J. L. Keck and S. H. Gellman, *J. Am. Chem. Soc.*, 2007, **129**, 4178-4180.
105. J. L. Price, E. B. Hadley, J. D. Steinkruger and S. H. Gellman, *Angew. Chem. Int. Ed.*, 2010, **49**, 368-371.
106. G. Grigoryan and W. F. DeGrado, *J. Mol. Biol.*, 2011, **405**, 1079-1100.
107. H. Gradišar, S. Božič, T. Doles, D. Vengust, I. Hafner-Bratkovič, A. Mertelj, B. Webb, A. Šali, S. Klavžar and J. Roman, *Nat. Chem. Biol.*, 2013, **9**, 362-366.
108. J. L. Beesley and D. N. Woolfson, *Curr. Opin. Biotechnol.*, 2019, **58**, 175-182.
109. G. G. Rhys, C. W. Wood, J. L. Beesley, N. R. Zaccai, A. J. Burton, R. L. Brady, A. R. Thomson and D. N. Woolfson, *J. Am. Chem. Soc.*, 2019, **141**, 8787-8797.
110. E. J. Petersson, C. J. Craig, D. S. Daniels, J. X. Qiu and A. Schepartz, *J. Am. Chem. Soc.*, 2007, **129**, 5344-5345.
111. D. S. Daniels, E. J. Petersson, J. X. Qiu and A. Schepartz, *J. Am. Chem. Soc.*, 2007, **129**, 1532-1533.
112. G. W. Collie, K. Pulka-Ziach, C. M. Lombardo, J. Fremaux, F. Rosu, M. Decossas, L. Mauran, O. Lambert, V. Gabelica, C. D. Mackereth and G. Guichard, *Nat. Chem.*, 2015, **7**, 871-878.
113. G. W. Collie, R. Bailly, K. Pulka-Ziach, C. M. Lombardo, L. Mauran, N. Taib-Maamar, J. Dessolin, C. D. Mackereth and G. Guichard, *Am. Chem. Soc.*, 2017, **139**, 6128-6137.
114. K. Ożga, M. Drewniak-Świtalska, E. Rudzińska-Szostak and Ł. Berlicki, *ChemPlusChem*, 2021, **86**, 646-649.
115. M. Drewniak-Świtalska, B. Barycza, E. Rudzińska-Szostak, P. Morawiak and Ł. Berlicki, *Org. Biomol. Chem.*, 2021, **19**, 4272-4278.
116. M. Bejger, P. Fortuna, M. Drewniak-Świtalska, J. Plewka, W. Rypniewski and Ł. Berlicki, *Chem. Commun.*, 2021, **57**, 6015-6018.
117. K. L. George and W. S. Horne, *J. Am. Chem. Soc.*, 2017, **139**, 7931-7938.
118. D. Zheng, L. Zheng, C. Yu, Y. Zhan, Y. Wang and H. Jiang, *Org. Lett.*, 2019, **21**, 2555-2559.
119. E. Merlet, K. Moreno, A. Tron, N. Mcclenaghan, B. Kauffmann, Y. Ferrand and C. Olivier, *Chem. Commun.*, 2019, **55**, 9825-9828.

120. J. Wang, B. Wicher, A. Méndez-Ardoy, X. Li, G. Pecastaings, T. Buffeteau, D. M. Bassani, V. Maurizot and I. Huc, *Angew. Chem. Int. Ed.*, 2021, **133**, 18609-18614.
121. S. Kumar, M. Birol, D. E. Schlamadinger, S. P. Wojcik, E. Rhoades and A. D. Miranker, *Nat. Commun.*, 2016, **7**, 11412.
122. S. Kumar, A. Henning-Knechtel, I. Chehade, M. Magzoub and A. D. Hamilton, *J. Am. Chem. Soc.*, 2017, **139**, 17098-17108.
123. J. Buratto, C. Colombo, M. Stupfel, S. J. Dawson, C. Dolain, B. Langlois D'Estaintot, L. Fischer, T. Granier, M. Laguerre, B. Gallois and I. Huc, *Angew. Chem. Int. Ed.*, 2014, **53**, 883-887.
124. V. Maurizot, C. Dolain, Y. Leydet, J.-M. Léger, P. Guionneau and I. Huc, *J. Am. Chem. Soc.*, 2004, **126**, 10049-10052.
125. F. H. C. Crick, *Acta Crystallogr.*, 1953, **6**, 689-697.
126. L. Pauling and R. B. Corey, *Nature*, 1953, **171**, 59-61.
127. J. Jumper, R. Evans, A. Pritzel, T. Green, M. Figurnov, O. Ronneberger, K. Tunyasuvunakool, R. Bates, A. Žídek, A. Potapenko, A. Bridgland, C. Meyer, S. A. A. Kohl, A. J. Ballard, A. Cowie, B. Romera-Paredes, S. Nikolov, R. Jain, J. Adler, T. Back, S. Petersen, D. Reiman, E. Clancy, M. Zielinski, M. Steinegger, M. Pacholska, T. Berghammer, S. Bodenstein, D. Silver, O. Vinyals, A. W. Senior, K. Kavukcuoglu, P. Kohli and D. Hassabis, *Nature*, 2021, **596**, 583-589.
128. P. B. Harbury, T. Zhang, P. S. Kim and T. Alber, *Science*, 1993, **262**, 1401-1407.
129. L. Stryer, *New York*, 2005, 596.
130. D. Mazzier, S. De, B. Wicher, V. Maurizot and I. Huc, *Angew. Chem. Int. Ed.*, 2020, **59**, 1606-1610.
131. H.-G. Jeon, H. K. Lee, S. Lee and K.-S. Jeong, *Chem. Commun.*, 2018, **54**, 5740-5743.
132. V. E. Campbell, X. De Hatten, N. Delsuc, B. Kauffmann, I. Huc and J. R. Nitschke, *Nat. Chem.*, 2010, **2**, 684-687.
133. Y. Liu, F. C. Parks, W. Zhao and A. H. Flood, *J. Am. Chem. Soc.*, 2018, **140**, 15477-15486.
134. C.-Z. Liu, S. Koppireddi, H. Wang, D.-W. Zhang and Z.-T. Li, *Angew. Chem.*, 2019, **131**, 232-236.
135. Z.-M. Shi, C.-F. Wu, T.-Y. Zhou, D.-W. Zhang, X. Zhao and Z.-T. Li, *Chem. Commun.*, 2013, **49**, 2673.
136. M. H.-Y. Chan, M. Ng, S. Y.-L. Leung, W. H. Lam and V. W.-W. Yam, *J. Am. Chem. Soc.*, 2017, **139**, 8639-8645.
137. C. Li, Y.-Y. Zhu, H.-P. Yi, C.-Z. Li, X.-K. Jiang, Z.-T. Li and Y.-H. Yu, *Chem. Eur. J.*, 2007, **13**, 9990-9998.
138. T. Ghosh, N. Fridman, M. Kosa and G. Maayan, *Angew. Chem.*, 2018, **130**, 7829-7834.
139. H. Tigger-Zaborov and G. Maayan, *Organic & Biomolecular Chemistry*, 2015, **13**, 8978-8992.
140. S. Rinaldi, *Molecules*, 2020, **25**, 3276.
141. S. H. Yoo and H.-S. Lee, *Acc. Chem. Res.*, 2017, **50**, 832-841.
142. G. W. Collie, K. Pulka-Ziach, C. M. Lombardo, J. Fremaux, F. Rosu, M. Decossas, L. Mauran, O. Lambert, V. Gabelica, C. D. Mackereth and G. Guichard, *Nat. Chem.*, 2015, **7**, 871-878.

143. G. W. Collie, K. Pulka-Ziach and G. Guichard, *Chem. Commun.*, 2016, **52**, 1202-1205.
144. A. Battigelli, J. H. Kim, D. C. Dehigaspitiya, C. Proulx, E. J. Robertson, D. J. Murray, B. Rad, K. Kirshenbaum and R. N. Zuckermann, *ACS Nano*, 2018, **12**, 2455-2465.
145. G. Marafon, I. Menegazzo, M. De Zotti, M. Crisma, C. Toniolo and A. Moretto, *Soft Matter*, 2017, **13**, 4231-4240.
146. T. A. Martinek, I. M. Mándity, L. Fülöp, G. K. Tóth, E. Vass, M. Hollósi, E. Forró and F. Fülöp, *J. Am. Chem. Soc.*, 2006, **128**, 13539-13544.
147. U. Diederichsen and H. W. Schmitt, *Angew. Chem. Int. Ed.*, 1998, **37**, 302-305.
148. U. Diederichsen and H. W. Schmitt, *Eur. J. Org. Chem.*, 1998, 827-835.
149. M. P. Del Borgo, A. I. Mechler, D. Traore, C. Forsyth, J. A. Wilce, M. C. J. Wilce, M.-I. Aguilar and P. Perlmutter, *Angew. Chem.*, 2013, **125**, 8424-8428.
150. R. S. Seoudi, A. Dowd, M. Del Borgo, K. Kulkarni, P. Perlmutter and M.-I. M. Aguilar, *Pure Appl. Chem.*, 2015, **87**, 1021-1028.
151. R. S. Seoudi, M. P. Del Borgo, K. Kulkarni, P. Perlmutter, M.-I. Aguilar and A. Mechler, *New J. Chem.*, 2015, **39**, 3280-3287.
152. S. Motamed, M. P. Del Borgo, K. Kulkarni, N. Habila, K. Zhou, P. Perlmutter, J. S. Forsythe and M. I. Aguilar, *Soft Matter*, 2016, **12**, 2243-2246.
153. K. Luder, K. Kulkarni, H. W. Lee, R. E. Widdop, M. P. Del Borgo and M.-I. Aguilar, *Chem. Commun.*, 2016, **52**, 4549-4552.
154. K. Kulkarni, S. Motamed, N. Habila, P. Perlmutter, J. S. Forsythe, M.-I. Aguilar and M. P. Del Borgo, *Chem. Commun.*, 2016, **52**, 5844-5847.
155. R. S. Seoudi, M. G. Hinds, D. J. D. Wilson, C. G. Adda, M. Del Borgo, M.-I. Aguilar, P. Perlmutter and A. Mechler, *Nanotechnology*, 2016, **27**, 13560.
156. M. P. Del Borgo, K. Kulkarni, M. A. Tonta, J. L. Ratcliffe, R. Seoudi, A. I. Mechler, P. Perlmutter, H. C. Parkington and M.-I. Aguilar, *APL Bioengineering*, 2018, **2**, 026104.
157. A. J. Christofferson, Z. S. Al-Garawi, N. Todorova, J. Turner, M. P. Del Borgo, L. C. Serpell, M.-I. Aguilar and I. Yarovsky, *ACS Nano*, 2018, **12**, 9101-9109.
158. K. Kulkarni, J. Hung, A. J. Fulcher, A. H. P. Chan, A. Hong, J. S. Forsythe, M.-I. Aguilar, S. G. Wise and M. P. Del Borgo, *ACS Biomaterials Science & Engineering*, 2018, **4**, 3843-3847.
159. S. Motamed, M. P. Del Borgo, K. Zhou, K. Kulkarni, P. J. Crack, T. D. Merson, M.-I. Aguilar, D. I. Finkelstein and J. S. Forsythe, *Front. Bioeng. Biotechnol.*, 2019, **7**, 315.
160. R. Pfulkwa, P. H. J. Kouwer, A. E. Rowan and B. Klumperman, *Angew. Chem. Int. Ed.*, 2013, **52**, 11040-11044.
161. Y.-T. Shen, N. Zhu, X.-M. Zhang, K. Deng, W. Feng, Q. Yan, S. Lei, D. Zhao, Q.-D. Zeng and C. Wang, *Chem. Eur. J.*, 2011, **17**, 7061-7068.
162. Y. Zhao, A. L. Connor, T. A. Sobiech and B. Gong, *Org. Lett.*, 2018, **20**, 5486-5489.

163. A. G. Slater, Y. Hu, L. Yang, S. P. Argent, W. Lewis, M. O. Blunt and N. R. Champness, *Chemical Science*, 2015, **6**, 1562-1569.
164. Y. W. a. H. J. Q. Gan, *Chin. J. Chem.*, 2013, **31**, 651-656.
165. B. Gong, Y. Yan, H. Zeng, E. Skrzypczak-Jankunn, Y. W. Kim, J. Zhu and H. Ickes, *J. Am. Chem. Soc.*, 1999, **121**, 5607-5608.
166. H. Zeng, R. S. Miller, R. A. Flowers and B. Gong, *J. Am. Chem. Soc.*, 2000, **122**, 2635-2644.
167. H. Zeng, H. Ickes, R. A. Flowers and B. Gong, *J. Org. Chem.*, 2001, **66**, 3574-3583.
168. Y. Zhang, R. Cao, J. Shen, C. S. F. Detchou, Y. Zhong, H. Wang, S. Zou, Q. Huang, C. Lian, Q. Wang, J. Zhu and B. Gong, *Org. Lett.*, 2018, **20**, 1555-1558.
169. H. Zeng, X. Yang, R. A. Flowers and B. Gong, *J. Am. Chem. Soc.*, 2002, **124**, 2903-2910.
170. A. Acocella, A. Venturini and F. Zerbetto, *J. Am. Chem. Soc.*, 2004, **126**, 2362-2367.
171. Y. Ferrand, A. M. Kendhale, J. Garric, B. Kauffmann and I. Huc, *Angew. Chem. Int. Ed.*, 2010, **49**, 1778-1781.
172. P. D. Sun, C. E. Foster and J. C. Boyington, *Curr. Protoc. Protein Sci.*, 2004, **35**.

### 3 Relation between hydrogen bonds and their effects on the stability of a tertiary structure

Previous work regarding abiotic tertiary folding stabilized by hydrogen bonds has led to the successful synthesis of a helix-turn-helix foldamer with the expected shape. In such a tertiary fold hydroxy groups have been introduced to the helices at every turn in order to form hydrogen bonds with carbonyl groups of the opposite helix within. The resulting tertiary structure is stable and only disrupted by addition of polar solvents such as DMF and DMSO. Its formation, however, is reliant on the rigid turn unit connecting the helices. Without it, other aggregates are formed. This suggests that this variant of a tertiary fold is not preferred and only forms due to the presence of a rigid linker. Here we want to test how many and what kind of hydrogen bonds are needed to stabilize the tertiary structure. Therefore, hydroxy groups within a helix were replaced by protons, every other turn. This led to a decreased total amount of hydrogen bonds formed within the resulting tertiary structure, which should, in theory, destabilize the fold.

Our findings, which are summarized in a manuscript that has been accepted in *Organic and Biomolecular Chemistry*, showed surprising results. X-ray and  $^1\text{H}$  NMR analysis of the new compounds revealed a similar helix-turn-helix structure as previously reported. Stability of these new tertiary structures was assessed via various polar solvent dependencies. A comparison of their stability with the originals yielded surprising results. Tertiary structures in which hydrogen bonds are formed every other helix turn featured stability comparable to those with hydrogen bonds at every turn. A closer look at the X-ray structure of the latter revealed a curvature change in its helices. This twisting strain was found to be enforced by certain hydrogen bonds. In a tertiary fold in which these hydrogen bonds had been removed no such curvature change was observed (Figure 3.1).

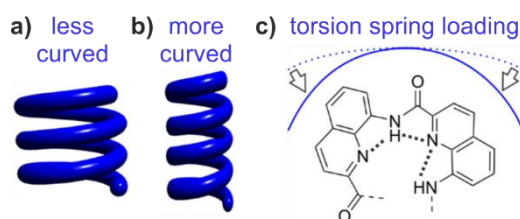


**Figure 3.1.** Helix curvature in a helix-turn-helix motif with hydrogen bonds at every (a) and every 2<sup>nd</sup> (b) helix turn. Exemplification of the molecular torsion spring.

This observation also shed light on the question why tilted dimers and trimers are being formed in a self-assembly of helix monomers in solution instead of parallel homochiral aggregates. In both aggregational variants, stable hydrogen bonds are formed respecting the curvature and therefore without introducing a strain. It was concluded that, hydrogen bonds would not always have a strong stabilizing effect on a tertiary fold, but could instead cause a conformational frustration similar to those found in proteins as well. In enzymes, similar local destabilizations may promote conformational changes and mediate catalysis. With regard to the future



development of abiotic tertiary folds with enzyme-like function, the conscious introduction of tension and destabilization is a worthwhile undertaking.

**Contributions:** The project was planned in collaboration with D. Mazzier, V. Maurizot and I. Huc. Synthetic monomer precursors have been provided by M. Palchyk. Monomer synthesis have been performed by me and S. Kwon. Foldamer synthesis was performed by me and D. Mazzier. Solution studies were performed by me and L. Allmendinger. MALDI measurements have been carried out by A. Schmidt. C. Glas and L. Allmendinger carried out NMR measurements. Crystallographic studies and structure refinement were performed by B. Wicher and B. Kauffmann. Me, I. Huc, L. Allmendinger, V. Maurizot, D. Mazzier, B. Wicher and B. Kauffmann contributed to experiment design and interpretation. The research was supervised by I. Huc. The manuscript was written by me and I. Huc. Me, I. Huc, V. Maurizot, L. Allmendinger, B. Wicher, S. Wang and D. Mazzier proofread and improved the manuscript. This work was supported by the DFG (Excellence Cluster 114, CIPSM). Furthermore, F. Borel facilitated collection on the FIP beamline at ESRF (Grenoble).

## 3.1 Publication (published)

### Molecular torsion springs: alteration of helix curvature in frustrated tertiary folds

Authors: Friedericke S. Menke,<sup>a</sup> Daniela Mazzier,<sup>a</sup> Barbara Wicher,<sup>b</sup> Lars Allmendinger,<sup>a</sup> Brice Kauffmann,<sup>c</sup> Victor Maurizot<sup>d</sup> and Ivan Huc<sup>\*a</sup>

Published: *Org. Biomol. Chem.* **2023**, 21, 1275-1283. (<https://doi.org/10.1039/D2OB02109A>)

**Abstract:** The first abiotic foldamer tertiary structures have been recently reported in the form of aromatic helix-turn-helix motifs based on oligo-quinolinecarboxamides held together by intramolecular hydrogen bonds. Tertiary folds were predicted by computational modelling of the hydrogen-bonding interfaces between helices and later verified by X-ray crystallography. However, the prognosis of how the conformational preference inherent to each helix influences the tertiary structure warranted further investigations. Several new helix-turn-helix sequences were synthesised in which some hydrogen bonds have been removed. Contrary to expectations, this change did not strongly destabilise the tertiary folds. On closer inspection, a new crystal structure revealed that helices adopt their natural curvature when some hydrogen bonds are missing and undergo some spring torsion upon forming the said hydrogen bonds, thus potentially giving rise to a conformational frustration. This phenomenon sheds light on the aggregation behaviour of the helices when they are not linked by a turn unit

### Introduction

The functions of biopolymers are enabled by their shapes and folded structures. This structure-function relationship has inspired chemists to design foldamers, synthetic oligomers also able to adopt folded conformations.<sup>1-7</sup> Eliciting secondary structures such as single helices or sheets in a great variety of synthetic oligomers has been successful when using aliphatic, aliphatic–aromatic, or aromatic amino acid building blocks. Useful properties of these secondary structures have been reported, including biological activity, and even potential as therapeutic agents.<sup>8-16</sup> Thus, short foldamers may be able to cross cell membranes efficiently while having low toxicity and immunogenicity.<sup>17-21</sup> They may also resist proteolytic degradation.

In biopolymers, numerous functions emerge only in tertiary and quaternary structures. Accordingly, many more functions of foldamers may be expected by reaching similar size and structural complexity.<sup>22</sup> However, predicting folding conducive to tertiary structure formation is far more challenging. Two aspects that make tertiary structure prediction difficult are cooperativity and frustration. Cooperativity refers to the fact that individual secondary modules of a tertiary structure need not be inherently stable:  $\alpha$ -helices found in proteins are more often than not unstable when isolated but are stabilised within the full sequence tertiary fold. Frustration refers to the fact that the overall stability gained in the tertiary fold allows non-ideal – energetically costly – conformations to be present: strain is acceptable to a certain extent and may be beneficial to functions.<sup>23</sup> Despite the fact that the energy terms associated with cooperativity and frustration are difficult to estimate – they usually reflect multiple contributions that partly compensate for each other – the *ab initio*

design of proteins has made great progress.<sup>24-31</sup> Synthetically accessible mini-proteins have also attracted interest due to their potential applications in biotechnology and medicine.<sup>32</sup> Using various approaches, steps were made away from purely  $\alpha$ -peptidic backbones, and  $\beta$ -amino acids were introduced in tertiary structures.<sup>33-39</sup> Some helix bundles from  $\beta$ -peptides<sup>40, 41</sup> and oligoureas<sup>42, 43</sup> have also been reported.

To access shapes and functions remote from (and beyond) those achieved by biopolymers, research in the field of *abiotic* foldamers is conducted. Such foldamers consist of units not seen in the natural world that nevertheless fold into conformationally ordered states stabilised by non-covalent interactions. A major class of abiotic foldamers are aromatic oligomers, *i.e.* oligomers that possess aryl rings in their main chain.<sup>6, 7, 44-46</sup> A prototypical family of aromatic foldamers are the oligoamides of 8-amino-2-quinolinecarboxylic acid (Q in Figure 1a), which adopt particularly stable helical conformations in essentially any solvent.<sup>47-49</sup>

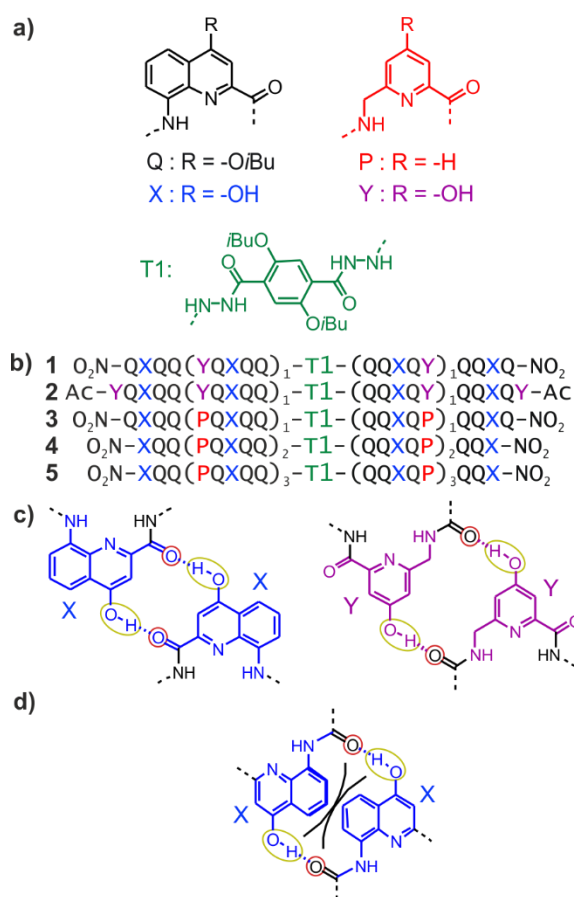


**Figure 1.** a) Structures of units Q, X, Y, P, and T1. b) Foldamer sequences. Note the inversion of C $\rightarrow$ N polarity on each side of the central T1 unit. In sequences ending with an 8-nitro group, "NO<sub>2</sub>" replaces the terminal amine. c) Hydrogen-bonding patterns involving X and Y units as observed in the structures of **1** and **2**. The yellow and red circles around the hydrogen bond donors and acceptors correspond to the yellow cups and red knobs in Figure 2d) Expected steric clash (black lines) if Y units were replaced by X units.<sup>50</sup>

Q<sub>n</sub> oligoamide helices are so stable that they tolerate a large proportion of more flexible 6-aminomethyl-2-pyridinecarboxylic acid units (P in Figure 1a).<sup>51-54</sup> Oligomers consisting of Q and P units are easily accessible by solid phase synthesis,<sup>53</sup> and show a high propensity to crystallise. They may find applications in diverse

areas, including circularly polarised luminescence,<sup>55, 56</sup> charge transport and metal coordination,<sup>57</sup> and protein surface recognition.<sup>11, 16, 58-60</sup>

Early steps were made towards abiotic tertiary structures by connecting several  $Q_n$  helices to various types of linkers.<sup>61-63</sup> Recently, the first true abiotic tertiary foldamers were designed and characterised in the form of helix-turn-helix motifs composed of two helical oligomers connected at their C-terminus by a T1 turn unit (Figure 1a) and in which inter-helix hydrogen bonds were mediated by units X and Y, the 4-hydroxy substituted analogues of Q and P, respectively.<sup>50, 64, 65</sup> This design exploits the fact that all amide carbonyl groups, that is, good hydrogen bond acceptors, diverge from  $Q_n$  helices. X and Y units were introduced so that each hydroxy group forms a hydrogen bond with a carbonyl group of the other helix as, for example, in sequences **1** and **2** (Figure 1b). The outcome was inter-helix hydrogen bonding patterns involving pairs of X monomers and pairs of Y monomers (Figure 1c). One may note that the hydrogen bonding pattern involving two Y units could not be achieved with X units because the benzenic rings of the latter would sterically hamper a short X-to-X distance (Figure 1d).

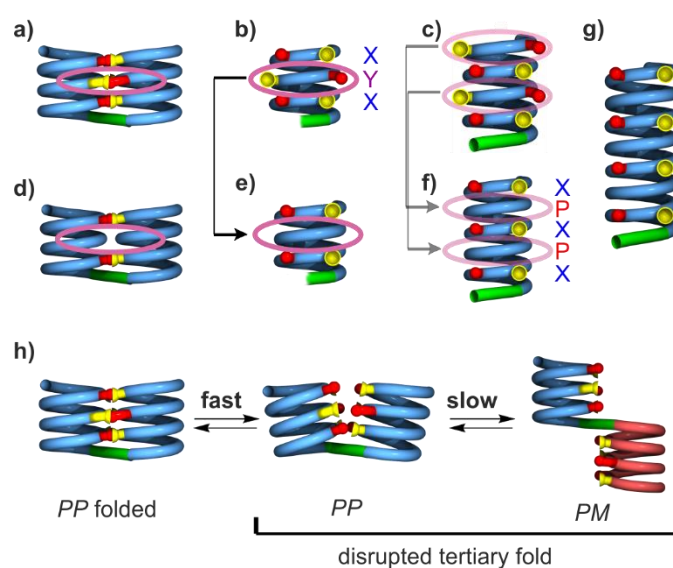


**Figure 2.** Schematic representation of helix-turn-helix tertiary motifs of different lengths with and without Y units. a) Side view of a helix-turn-helix-motif with six hydrogen bonds formed by sequence **1**. b) Front view of the hydrogen-bonding interface involved in the structure shown in a). c) Front view of a hydrogen-bonding interface one turn longer than that of b), *i.e.* with eight hydrogen bonding sites (two X and two Y units per helix), as it occurs in **2**. d-f) Structures analogous to those of a-c), respectively, in which Y units have been replaced by P. Hydrogen bonding sites associated with X units are present at every other helix turn. g) Hydrogen-bonding interface two turns longer than that shown in f) with eight hydrogen bonding sites (four X units). h) Schematic representation of the conformational equilibria involved when polar solvents disrupt a helix–turn–helix fold. The arrays of hydroxy protons and carbonyl oxygen atoms involved in hydrogen bonding are shown in yellow and red, respectively. Blue, red and green tubes represent *P*- and *M*-helical segments and turn units, respectively. Pink ovals indicate hydrogen bonding sites associated with Y units or the equivalent areas where Y units have been replaced by P.

As a consequence of inter-helix hydrogen bonding, the two helices are held parallel to each other at a close distance and with the same N-to-C orientation.<sup>‡,50, 65</sup> In addition, the hydrogen bonds only form when the two helices have the same handedness. Schematic representations in Figure 2a-2c depict the resulting architectures, including the fact that a pair of hydrogen bonds form at every helix turn, involving alternatively X and Y units. Thus, six inter-helix hydrogen bonds formed in sequence **1** (Figure 2a, b) and eight in sequence **2** (Figure 2c). The resulting helix-turn-helix motifs are very stable in chlorinated solvents and may be disrupted upon adding DMSO, a hydrogen bonding competitor, leading to the emergence of a conformer with one *P* and one *M* helix (Figure 2h).<sup>50</sup> However, earlier investigations also revealed that, in the absence of turn units, independent helices aggregate through modes other than the parallel *PP* or *MM* head-to-head motif found in helix-turn-helix structures. Instead, trimeric parallel aggregates and tilted dimers were characterised.<sup>50</sup> This outcome points non-ideal interactions or conformations within the tertiary motifs that are constrained by the geometry of the turn unit.

Here we show that, contrary to expectations, removing some hydrogen bonds within the helix-turn-helix structures, namely replacing Y by P (sequences **3-5**, Figure 1b), does not result in a strong destabilisation. A crystallographic structure of **3** showed that the missing hydrogen bonds permit a relaxation of the helix curvature, which must be somewhat spring-loaded by the Y-to-Y hydrogen bonding. These results thus shed light on subtle aspects of the interactions and tensions within abiotic tertiary folds that resemble those observed in proteins<sup>23</sup> and provide guidelines to elaborate these designs further.

## Results and discussion

### Design, synthesis, and helix-turn-helix folding

Sequences **3**, **4** and **5** were conceived as analogues of **1** and **2** containing P units instead of Y (Figure 1b). In **3-5**, inter-helix hydrogen bonding is mediated only by X units. It may occur at every other helix turn and not at every turn as in **1** or **2**. Sequence **3** is identical to **1** but for the replacement of the two Y units by P. With a total of four X units, up to four inter-helix hydrogen bonds may form within a tertiary helix-turn-helix fold of **3** (Figure 2d, 2e). Exploiting the fact that helices of Q/P sequences span two full turns every five units,<sup>47</sup> compound **4** is composed of helical segments that have both been extended by one QQXQP pentad with respect to the helices of **3**. Compound **4** thus has the potential for six inter-helix hydrogen bonds (Figure 2f), as in **1**, though its helices are two turns longer. Similarly, the helical segments of **5** have each been extended by one more QQXQP pentad with respect to the helices of **4**. Compound **5** has the potential for eight inter-helix hydrogen bonds (Figure 2g), as in **2**, though the helices of **5** span over seven turns and are almost twice as long as the helices of **2**.

Compounds **3-5** were synthesised following the same approach (see Supplementary Information). Helical segments spanning from the N-terminus to the unit before the linker were prepared on solid phase using Q, P, and X monomers with an Fmoc-amine protection, a free carboxylic acid, and a *t*Bu-ether protection of the hydroxy group of X.<sup>53</sup> Coupling was mediated by acid chloride activation, and Fmoc was removed after each

coupling with piperidine. The last monomer introduced at the N-terminus was either X or Q with a nitro group in position 8. Synthesis was performed on an acid labile Sasrin® resin so that mild acid (hexafluoroisopropanol) allowed for resin cleavage while preserving *t*Bu-ether protection of X units. Sequences were then purified by crystallisation in CH<sub>2</sub>Cl<sub>2</sub>/methanol before being coupled in solution to T1 units using PyBOP as a coupling agent. Finally, the protected precursors of **3**, **4** and **5** were purified by crystallisation from CH<sub>2</sub>Cl<sub>2</sub>/methanol (for **3**), or by recycling GPC (for **4** and **5**).

Before *t*Bu-ether cleavage at X units, helices cannot form hydrogen bonds. All *PP/MM* and *PM* conformers of these precursors are thus populated (Figure 2h). Equilibrium between *PP/MM* and *PM* conformers is slow on the NMR time scale and NMR spectra show two sets of signals in different proportions, typically around 10:1 (Figure S1<sup>†</sup>), as was previously observed for the precursors of **1** and **2**.<sup>50</sup> A crystal structure of the protected precursor of **3** in its *PM* conformation is shown Figure S2a<sup>†</sup>, which presumably corresponds to the major species in solution. The final products **3-5** were obtained after TFA deprotection of the X units without further purification.

The <sup>1</sup>H NMR spectra of **1-5** all show a single set of signals (Figure 3), indicating conformational equilibria are no longer at play and that a single species is present in solution, thus hinting at the formation of helix-turn-helix motifs. This also applied to the longest sequence **5**, even though it could not be isolated in a very pure form. Also, further investigations of **5** were not conducted because of its low solubility.

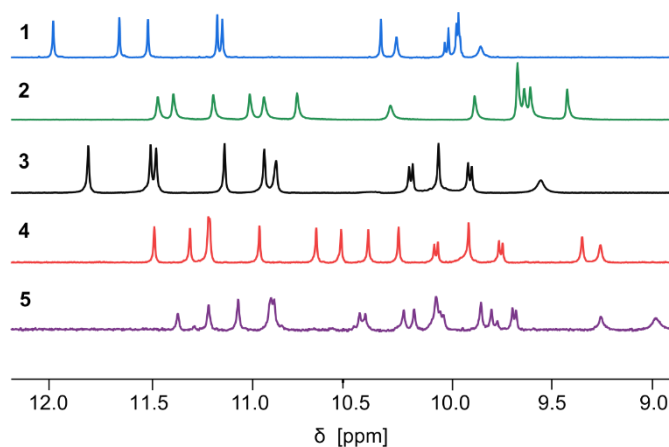


**Figure 3.** Part of the 500 MHz <sup>1</sup>H NMR spectra of sequences **1-5** in CDCl<sub>3</sub> at 25 °C showing the resonances of amide protons and hydrogen-bonded hydroxy protons. The spectra of **1** and **2** are from ref.<sup>50</sup>

Helix-turn-helix folding was confirmed by a solid state structure of **3** (Figure 4b,d) that closely resembles that of **1** (Figure 4a,c). The molecular structure of **3** shows the expected head-to-head parallel arrangement and the same handedness of the two helices. The structure admits a pseudo-C<sub>2</sub> symmetry axis pointed through the aromatic ring of the turn unit. The crystal lattice is centrosymmetric and contains both the *PP* and the *MM* conformers. Four inter-helix hydrogen bonds between X units form according to the expected pattern (Figure 1c). As for the Y units of **1**, the P units of **3** face each other but no hydrogen bonding, not even a C-H...O

contact, is observed. In **1**, the shortest  $C=O \cdots C_{Ar}$  distance is around 3.3 Å, while it is 3.9 Å in **3**. The molecular structures **1** and **3** both show the same slight bending of the turn unit (Figure 4a, 4b).

The side views of **1** and **3** (Figure 4a, 4b) display a minor difference: at a given helix turn, all four hydrogen bond donors and acceptors (yellow and red spheres belonging to a pair of hydrogen-bonded X or Y units) are in the same plane in the structure of **1** whereas they are slightly out of plane in the structure of **3**. Furthermore, top views (Figure 4c, 4d) showed an alignment of the hydrogen bond donors and acceptors of X units in the structure of **3**, but not in the structure of **1**. In summary, NMR and crystallographic data concur to show that, for P-containing sequence **3**, four hydrogen bonds are sufficient to stabilise the tertiary fold.

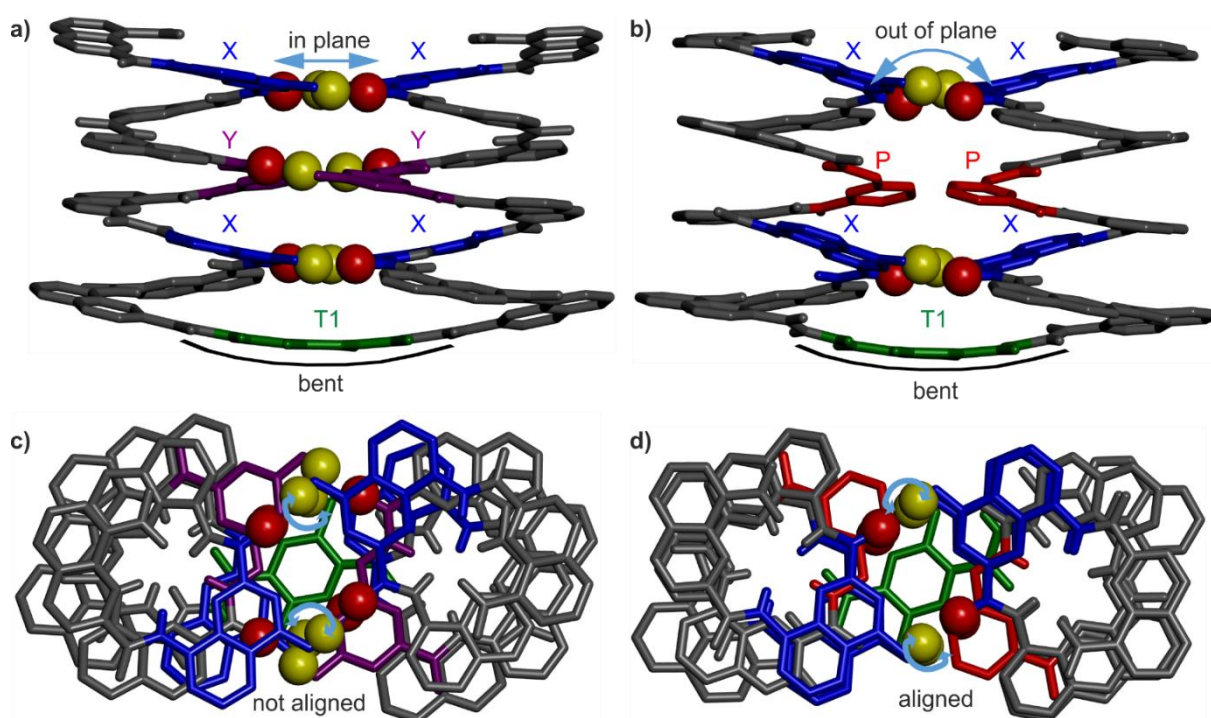


**Figure 4.** a) And b) show the side views of the crystal structures of **1** and **3**, respectively. c) And d) show the top views of the crystal structures of **1** and **3**, respectively. The hydroxy protons and carbonyl oxygen atoms of the hydrogen-bonding arrays are shown as yellow and red balls, respectively. The X units are shown in blue, the Y units in violet, the P-units in red and the turn units in green. Blue arrows point to notable differences between the two structures. Included solvent molecules, non-polar hydrogen atoms and side chains are omitted for clarity.

### Solution state studies reveal unexpected stability patterns

Polar solvents such as DMSO and DMF compete for hydrogen bonding and have the capacity to disrupt the hydrogen-bonded interface of helix-turn-helix motifs, giving rise to structures as those shown in Figure 2h. For example, adding DMSO- $d_6$  to a  $CDCl_3$  solution of **2** resulted in shifts of  $^1H$  NMR signals associated with a fast equilibrium between folded and disrupted conformations without helix handedness inversion, leading to an averaging of the  $^1H$  NMR signals.<sup>50</sup> Adding DMSO to the protected precursor of **2**, which is unable to fold, did not result in such changes. The chemical shift variations occur over a narrow range of solvent compositions suggesting a cooperative, all-or-nothing, disruption of the hydrogen-bonding interface. Concomitantly to the chemical shift variations,  $^1H$  NMR spectra show the emergence of a new species assigned to the disrupted *PM*

conformers, in slow exchange with the *PP* and *MM* conformers. In the case of **2**, a solid state structure of the disrupted *PP/MM* conformers was obtained from crystals grown from DMF.<sup>50</sup>

Similar experiments, that is, <sup>1</sup>H NMR monitoring of polar solvent-induced disruption of the tertiary fold, were carried out with compound **3**, a priori the least stable helix-turn-helix motif of all since it contains only four inter-helix hydrogen bonds (Figure 4b). Deuterated DMSO, pyridine, DMF, methanol, acetonitrile, acetone and tetrahydrofuran were tested to compare their ability to disrupt the four hydrogen bonds (Figures S3-S12<sup>†</sup>). These experiments were important not only to assess the robustness of the tertiary folds but also for practical reasons, for example, to guide the choice of crystallisation solvents. Remarkably, relatively small chemical shift variations and no second set of <sup>1</sup>H NMR signals, meaning no disruption of the tertiary turn, was observed even in pure acetone-*d*<sub>6</sub> or tetrahydrofuran-*d*<sub>8</sub>. Similarly, up to 70% [vol/vol] of acetonitrile-*d*<sub>3</sub> or 50% of methanol-*d*<sub>3</sub> could be added to a chloroform solution of **3** without any disruption. For these two solvents, higher volume fractions could not be reached due to the precipitation of the sample. Precipitation also occurred upon adding 30% of DMF-*d*<sub>7</sub>. Nevertheless, chemical shift changes and the emergence of a new set of signals were observed in the course of solvent additions, indicating a certain level of helix-turn-helix disruption, with a transition above 30% of DMF-*d*<sub>7</sub>. In the case of DMSO-*d*<sub>6</sub> and pyridine-*d*<sub>5</sub>, complete disruption was achieved without any precipitation. Chemical shift variations showed sharp cooperative transitions near 18.5% of DMSO-*d*<sub>6</sub> and 27.5% of pyridine-*d*<sub>5</sub>, indicating the stronger ability of DMSO to interfere with intramolecular hydrogen bonding among all tested polar solvents. Conversely, a comparison of the <sup>1</sup>H NMR spectra of **3** in CDCl<sub>3</sub> containing 16% of either DMSO-*d*<sub>6</sub>, pyridine-*d*<sub>5</sub> or DMF-*d*<sub>7</sub> revealed different proportions of the *PM* conformer in these three solvents: 30%, 20% and <10%, respectively (Figure 5a). Altogether, these results establish a clear ranking of the disrupting ability of these three solvents, alongside the other polar solvents in which non disruption was observed. As a final control experiment, the addition of pyridine and DMF to the protected precursor of **3**, which is unable to fold, did not result in significant changes of the chemical shifts (Figures S13-S15<sup>†</sup>).



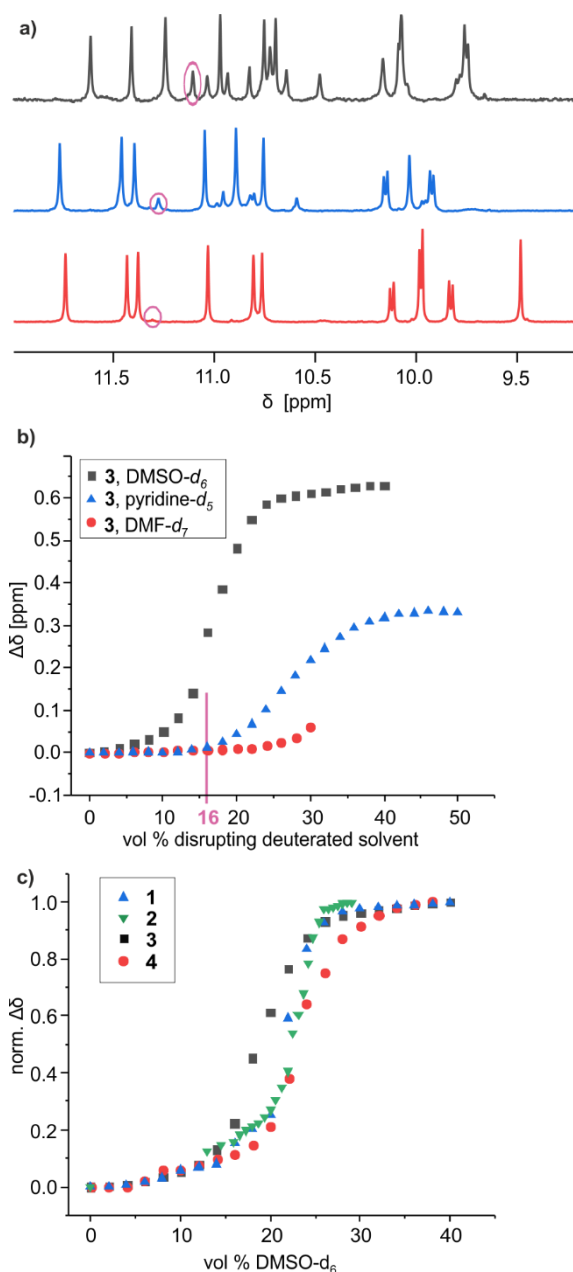


**Figure 5.** a) Part of the <sup>1</sup>H NMR spectra (500 MHz, 25 °C) of **3** in a 84:16 [vol/vol] mixture of CDCl<sub>3</sub> and a disrupting solvent like DMF-*d*<sub>7</sub> (red), pyridine-*d*<sub>5</sub> (blue) and DMSO-*d*<sub>6</sub> (black), showing the amide and hydrogen-bonded hydroxy proton resonances. Signals encircled in pink belong to the disrupted structures. b) Variations of the chemical shift of selected <sup>1</sup>H NMR signals of **3** upon adding disruptive solvents to CDCl<sub>3</sub> solutions (see ESI). Precipitation occurred above 32% of DMF-*d*<sub>7</sub>. c) Normalised variations ( $\Delta\delta/\Delta\delta_{\max}$ ) of the chemical shift of selected <sup>1</sup>H NMR signals of **1**, **2**, **3**, and **4** upon adding DMSO-*d*<sub>6</sub> to CDCl<sub>3</sub> solutions. Normalisation facilitates comparison even when the amplitude and sign of the chemical shift variation vary.

In order to assess the stability of the tertiary folds as a function of the number and nature of the hydrogen bonds involved, we next compared the ability of DMSO to disrupt the folds of **1**, **2**, **3** and **4** (Figures S16-S19<sup>†</sup>). Chemical shift variations ( $\Delta\delta$ ) of a representative proton of these species upon adding DMSO-*d*<sub>6</sub> to a solution in CDCl<sub>3</sub> are shown in Figure 5c. As explained above, these variations reflect the rapid equilibrium between the folded and disrupted helix-turn-helix without inversion of helix handedness. Unsurprisingly, the transition

between the folded and disrupted conformations of **3** occurred with the smallest amount of DMSO (inflexion near 18.5%), since this compound involves only four hydrogen bonds at its helix-helix interface. However, the trend for the other compounds turned out to deviate from what could be expected. For instance, the transition between folded and disrupted states occurs at similar amounts of DMSO for **1** (21.5%) and **2** (22.5%), as if the additional two hydrogen bonds associated with the peripheral Y units in the structure of **2** had no significant effects on the tertiary structure stability. Furthermore, compound **4** proved the most stable of all: about 24% of DMSO is required to reach the transition. Compound **4** has six hydrogen bonds at its helix-helix interface, that is, as many as **1** and two less than **2**, but hydrogen bonds in **4** only involve X units. To enhance the stability of **3**, it is thus more beneficial to add two X units (as in **4**) than to replace two P with two Y units (as in **1**). These results suggest that the hydrogen bonds involving Y units provide less stabilisation to the tertiary folds than those involving the X units.

### The solid state structures point to helix curvature strain

That pairs of hydrogen-bonded X units and pairs of hydrogen-bonded Y do not contribute to the same extent to the stability of helix-turn-helix motifs invited a closer look at the solid state structures. As mentioned above,  $Q_n$  helices span exactly five units per two turns.<sup>47</sup> The same applies when Q and P units are mixed.<sup>52</sup> Thus, when looking at a helix from the top, down the helix axis, the inner rim of the backbone typically has the shape of a 15-crown-5. For the solid state structures of **1** and **3**, the helix inner rim of **3** does show a 15-crown-5-ether shape (Figure 6b), whereas the helix inner rim of **1** does not (Figure 6a).

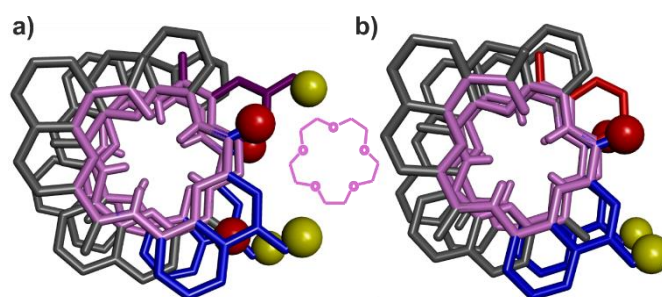


**Figure 6.** Top view of one helix of the crystal structures of **1** (a) and of **3** (b). The inner rim of each helix is highlighted in pink. The hydroxy protons and carbonyl oxygen atoms involved in helix-to-helix hydrogen bonding are shown as yellow and red balls, respectively. The X units are shown in blue, the Y units in violet and the P units in red. Included solvent molecules, non-polar hydrogen atoms and side chains are omitted for clarity. For comparison to the inner rims, a 15-crown-5 is drawn between a) and b).

This means that, in the case of **1**, helix curvature deviates from its preferred form. To identify where this deviation occurs, the structures of **1** and **3** were overlaid so that the turn units and the C-terminal Q units perfectly match. Then, the extent of their overlap was compared at every helix turn (Figure 7). It was found that the hydrogen-bonded pairs of X units closest to T1 overlap almost perfectly (Figure 7d). One turn further away from T1, the Y units (in **1**) and the P units (in **3**) also overlap well. However, the subsequent Q units that are hydrogen bonded to Y in **1** and not to P in **3** are significantly offset in the two structures (Figure 7c). Removing the hydroxy groups of Y thus results in a change of curvature, allowing the conformation to match

more closely five units per two turns. In other words, hydrogen bonding between Y units is acceptable but it proceeds at the cost of a certain strain (spring loading) of helix curvature. The differences between the structures of **1** and **3** extend beyond Y (or P) units all the way to the next helix turn. Thus, the peripheral pair of X units form hydrogen bonds in the same manner in the two structures, but their position as well as the position of the N-terminal Q units differ (Figure 7b).

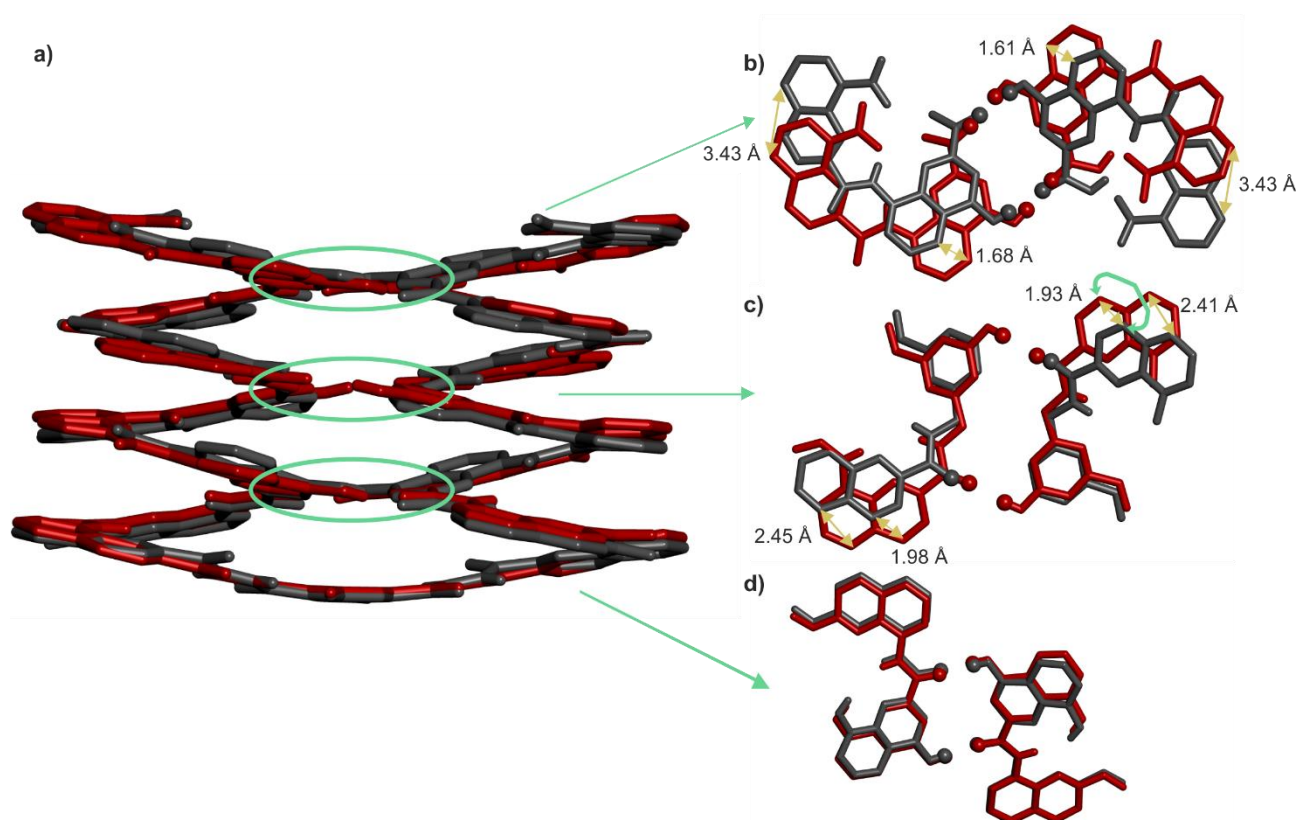


**Figure 7.** a) Side view of the overlay of the crystal structures of **1** (red) and **3** (grey) in tube representation. The turn units and C-terminal Q units of the two structures have been overlaid and match almost perfectly. b)-d) Slices of the overlaid helix-turn-helix structures at different helix-helix contacts (marked with green circles and arrows) showing poor overlap in areas closer to the N-termini. Included solvent molecules, non-polar hydrogen atoms and side chains are omitted for clarity.

We thus theorise that inter-helix hydrogen bonding involving the hydroxy groups of Y units requires a deviation of helix curvature from its preferred conformation. Put simply, a disfavoured secondary fold was induced by tertiary folding. This interpretation was further validated by the crystal structures of the *PM* conformers of the synthetic precursors of **2** and **3**, in which X and Y units are protected as *t*Bu-ethers and within which no hydrogen bond can form (Figure S2<sup>†</sup>). In both cases, the inner rims of the helices have the preferred 15-crown-5 shape, indicating that no strain in helix curvature occurred in the absence of inter-helix hydrogen bonds.

These insights also shed light on previous, not-well explained observations, namely the self-assembly behaviour of the X- and Y-containing individual helical segments of **1** and **2** when they are not connected by a T1 unit.<sup>60</sup> We reported before that for such helices, X and Y units mediate intermolecular inter-helix hydrogen

bonding, that is, a sort of helix bundling. However, the intramolecular hydrogen-bonding interface characteristic of **1** and **2** is never observed within aggregates: no head-to-head parallel *PP* or *MM* dimer form. Instead, tilted dimers and parallel trimers were characterised (Figure 8).<sup>50</sup> In a tilted dimer, the helix axes are oriented at an angle of  $+120^\circ$  or  $-120^\circ$ . In a trimer, the helix axes are parallel but the relative orientation of X and Y units differ from those of the helix-turn-helix motif. Both the tilted dimer and trimer configurations cannot occur intramolecularly within **1** and **2** due to the rigidity and geometry of T1. In all motifs, all X and Y hydroxy groups are involved in hydrogen bonding to an amide carbonyl group. We previously assigned the formation of tilted dimers and parallel trimers to potentially stronger, *e.g.* better oriented or shorter, hydrogen bonds. Now we might connect this behaviour to the fact that all helices adopt their preferred curvature in the aggregates. The views down the helix axis in Figure 8 clearly show the 15-crown-5 shape of the inner rim. Tilted dimer and parallel trimer formation might thus also be guided by the absence of curvature strain. Parallel dimer formation is disfavoured in this respect.

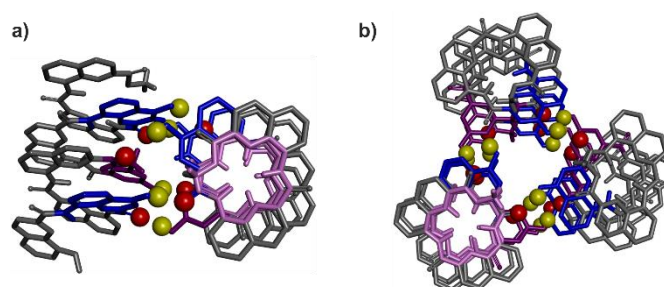


**Figure 8.** Previously reported crystal structures of a tilted dimer (a) and a parallel trimer (b).<sup>50</sup> Views have been oriented to see one helix down its axis. The corresponding inner rim is highlighted in pink, showing a 15-crown-5 shape. The other helices all have the same conformation. The hydroxy protons and carbonyl oxygen atoms involved in helix-helix hydrogen bonding are shown as yellow and red balls, respectively. The X units are shown in blue and the Y units in violet tubes. Included solvent molecules, non-polar hydrogen atoms and side-chains are omitted for clarity.

Conformational frustration is ubiquitous in tertiary protein structures.<sup>23</sup> For example, burying a hydrophobic residue in the hydrophobic core of a protein will generate frustration if the adjacent residue is polar and not involved in hydrogen bonding or salt bridging. Conversely, bringing this polar residue to the protein surface will generate frustration if it leads to exposure of the adjacent hydrophobic residue to water. The consequences, including the benefits, of frustration in protein folding, have been extensively investigated. For instance, the co-existence of multiple conflicting conformations and sub-optimal energetic state shapes the energy landscape and facilitates protein folding, *i.e.* it makes it more likely to reach a conformation close to the ground state.<sup>66</sup> In addition, redistributing local frustration facilitates conformational transitions as they occur, for example, during enzyme catalysis.<sup>67-70</sup> In short, if a tertiary protein fold would be deprived of conformational frustration, it would turn into a rigid body lacking functionality.<sup>71, 72</sup> The discovery of non-ideal folding in abiotic tertiary folds thus represents an important step towards the future design not only of structures, but also of functions associated to dynamics.

## Conclusions

The design and synthesis of large and complex abiotic folded tertiary structures similar to proteins represent ambitious and exciting challenges for chemistry. Developing structures that fold like biological macromolecules in media other than water is intriguing and will undoubtedly enable us to explore functions that would be unthinkable in living organisms. The successful prediction and synthesis of aromatic oligoamide helix-turn-helix motifs stabilised by hydrogen bonds is a first step towards this goal. We have presented a detailed analysis of the solid state structures of such tertiary folds stabilised by hydrogen-bonded interfaces based on X units only, or on both X and Y units, as well as a solution study of the susceptibility of these interfaces towards disruption in the presence of polar solvents. This, together with the structures of aggregated helices not linked by turn units highlighted possible deviations of the helices from their preferred curvature upon interacting with one another. Such deviations amount to a sort of torsional spring loading. They occur only under the constraint of relatively rigid T1 turn units in the absence of which helices generally find different ways to interact that do not impair their curvature. It is thus the tertiary folding that alters the secondary fold. In this respect it would be interesting to explore the folding behaviour of sequences in which other, less rigid, turns replace T1 unit.

The conformational frustration associated with non-ideal helix curvature is analogous to frustration as it occurs in protein tertiary folds. In enzymes, local conformational destabilisation may promote conformational changes and mediate catalysis.<sup>67-69</sup> In view of the future development of abiotic tertiary folds with enzyme-like function, the deliberate introduction of tensions and destabilisation is a worthy endeavour.

Finally, X- and Y-containing helices have been shown to form hydrogen-bonded assemblies that differ from the helix-turn-helix structures mediated by turn T1 in part because helices are able to adopt their preferred curvature in these assemblies and not in the tertiary structures. The self-assembly behaviour of helices in which Y has been replaced by P warrants further investigation. Tertiary structures are less strained in this case, as we have shown here, but this does not prevent individual helices from finding yet other ways to interact than that imposed by rigid T1 units. Research along these lines is currently conducted in our laboratory and will be reported in due course.

## Author contributions

FM and DM performed syntheses. FM and LA performed solution studies. BW and BK performed crystallographic studies. All authors contributed to experiment design and interpretation. IH supervised the research. FM and IH wrote the manuscript. All authors proofread and improved the manuscript.

## Conflicts of interest

There are no conflicts to declare

## Acknowledgements

This work was supported by the DFG (Excellence Cluster 114, CIPSM). M. Palchyk is gratefully acknowledged for contributing synthetic precursors, S. Kwon for monomer synthesis, A. Schmidt for mass measurement and C. Glas for assistance with NMR measurements. We are grateful to F. Borel for beam time and technical assistance during data collection on the FIP beamline at ESRF (Grenoble).

## Notes and references

† <https://doi.org/10.1039/d2ob02109a>

‡ Helix-turn-helix motifs with opposite N-to-C orientation of the helices, *i.e.* head-to-tail, were also produced. See reference 65.

1. G. Guichard and I. Huc, *Chem. Commun.*, 2011, **47**, 5933-5941.
2. S. H. Gellman, *Acc. Chem. Res.*, 1998, **31**, 173-180.
3. C. M. Goodman, S. Choi, S. Shandler and W. F. DeGrado, *Nat. Chem. Biol.*, 2007, **3**, 252-262.
4. R. V. Nair, K. N. Vijayadas, A. Roy and G. J. Sanjayan, *Eur. J. Org. Chem.*, 2014, **2014**, 7763-7780.
5. I. Saraogi and A. D. Hamilton, *Chem. Soc. Rev.*, 2009, **38**, 1726-1743.
6. I. Huc, *Eur. J. Org. Chem.*, 2004, **2004**, 17-29.
7. D.-W. Zhang, X. Zhao, J.-L. Hou and Z.-T. Li, *Chem. Rev.*, 2012, **112**, 5271-5316.
8. J. W. Checco and S. H. Gellman, *Curr. Opin. Struct. Biol.*, 2016, **39**, 96-105.
9. J. P. Saludes, J. B. Ames and J. Gervay-Hague, *J. Am. Chem. Soc.*, 2009, **131**, 5495-5505.
10. J. W. Checco, E. F. Lee, M. Evangelista, N. J. Sleebs, K. Rogers, A. Pettikiriarachchi, N. J. Kershaw, G. A. Eddinger, D. G. Belair, J. L. Wilson, C. H. Eller, R. T. Raines, W. L. Murphy, B. J. Smith, S. H. Gellman and W. D. Fairlie, *J. Am. Chem. Soc.*, 2015, **137**, 11365-11375.
11. K. Ziach, C. Chollet, V. Parissi, P. Prabhakaran, M. Marchivie, V. Corvaglia, P. P. Bose, K. Laxmi-Reddy, F. Godde, J.-M. Schmitter, S. Chaignepain, P. Pourquier and I. Huc, *Nat. Chem.*, 2018, **10**, 511-518.
12. G. N. Tew, R. W. Scott, M. L. Klein and W. F. DeGrado, *Acc. Chem. Res.*, 2010, **43**, 30-39.
13. S. Abdulkadir, C. Li, W. Jiang, X. Zhao, P. Sang, L. Wei, Y. Hu, Q. Li and J. Cai, *J. Am. Chem. Soc.*, 2022, **144**, 270-281.
14. J. Niu, A. J. Cederstrand, G. A. Eddinger, B. Yin, J. W. Checco, C. A. Bingman, V. K. Outlaw and S. H. Gellman, *J. Am. Chem. Soc.*, 2022, **144**, 9610-9617.
15. R. Gopalakrishnan, A. I. Frolov, L. Knerr, W. J. Drury and E. Valeur, *J. Med. Chem.*, 2016, **59**, 9599-9621.
16. J. Ahmed, T. C. Fitch, C. M. Donnelly, J. A. Joseph, T. D. Ball, M. M. Bassil, A. Son, C. Zhang, A. Ledreux, S. Horowitz, Y. Qin, D. Paredes and S. Kumar, *Nat. Commun.*, 2022, **13**, 2273, DOI: 10.1038/s41467-022-29724-4.
17. M. Rueping, Y. Mahajan, M. Sauer and D. Seebach, *ChemBioChem*, 2002, **3**, 257-259.

18. J. Iriondo-Alberdi, K. Laxmi-Reddy, B. Bouguerne, C. Staedel and I. Huc, *ChemBioChem*, 2010, **11**, 1679-1685.
19. T. B. Potocky, A. K. Menon and S. H. Gellman, *J. Am. Chem. Soc.*, 2005, **127**, 3686-3687.
20. M. Oba, *ChemBioChem*, 2019, **20**, 2041-2045.
21. M. Pasco, C. Dolain and G. Guichard, in *Comprehensive supramolecular chemistry II*, ed. J. L. Atwood, G. W. Gokel, L. J. Barbour, Elsevier, Amsterdam, Netherlands, 2017, pp. 89-125.
22. W. S. Horne and T. N. Grossmann, *Nat. Chem.*, 2020, **12**, 331-337.
23. D. U. Ferreira, E. A. Komives and P. G. Wolynes, *Q. Rev. Biophys.*, 2014, **47**, 285-363.
24. D. Hilvert, *Annu. Rev. Biochem*, 2013, **82**, 447-470.
25. N. H. Joh, T. Wang, M. P. Bhate, R. Acharya, Y. Wu, M. Grabe, M. Hong, G. Grigoryan and W. F. DeGrado, *Science*, 2014, **346**, 1520-1524.
26. S. E. Boyken, Z. Chen, B. Groves, R. A. Langan, G. Oberdorfer, A. Ford, J. M. Gilmore, C. Xu, F. DiMaio, J. Henrique Pereira, B. Sankaran, G. Seelig, P. H. Zwart and D. Baker, *Science*, 2016, **352**, 680-687.
27. P.-S. Huang, S. E. Boyken and D. Baker, *Nature*, 2016, **537**, 320-327.
28. B. Dang, H. Wu, V. K. Mulligan, M. Mravic, Y. Wu, T. Lemmin, A. Ford, D.-A. Silva, D. Baker and W. F. DeGrado, *Proc. Natl. Acad. Sci.*, 2017, **114**, 10852-10857.
29. W. M. Dawson, G. G. Rhys and D. N. Woolfson, *Curr. Opin. Chem. Biol.*, 2019, **52**, 102-111.
30. J. Dou, A. A. Vorobieva, W. Sheffler, L. A. Doyle, H. Park, M. J. Bick, B. Mao, G. W. Foight, M. Y. Lee, L. A. Gagnon, L. Carter, B. Sankaran, S. Ovchinnikov, E. Marcos, P.-S. Huang, J. C. Vaughan, B. L. Stoddard and D. Baker, *Nature*, 2018, **561**, 485-491.
31. J. Jumper, R. Evans, A. Pritzel, T. Green, M. Figurnov, O. Ronneberger, K. Tunyasuvunakool, R. Bates, A. Žídek, A. Potapenko, A. Bridgland, C. Meyer, S. A. A. Kohl, A. J. Ballard, A. Cowie, B. Romera-Paredes, S. Nikolov, R. Jain, J. Adler, T. Back, S. Petersen, D. Reiman, E. Clancy, M. Zielinski, M. Steinegger, M. Pacholska, T. Berghammer, S. Bodenstein, D. Silver, O. Vinyals, A. W. Senior, K. Kavukcuoglu, P. Kohli and D. Hassabis, *Nature*, 2021, **596**, 583-589.
32. E. G. Baker, G. J. Bartlett, K. L. Porter Goff and D. N. Woolfson, *Acc. Chem. Res.*, 2017, **50**, 2085-2092.
33. K. Ożga, M. Drewniak-Świtalska, E. Rudzińska-Szostak and Ł. Berlicki, *ChemPlusChem*, 2021, **86**, 646-649.
34. M. Drewniak-Świtalska, B. Barycza, E. Rudzińska-Szostak, P. Morawiak and Ł. Berlicki, *Org. Biomol. Chem.*, 2021, **19**, 4272-4278.
35. M. Bejger, P. Fortuna, M. Drewniak-Świtalska, J. Plewka, W. Rypniewski and Ł. Berlicki, *Chem. Commun.*, 2021, **57**, 6015-6018.
36. Z. E. Reinert and W. S. Horne, *Org. Biomol. Chem.*, 2014, **12**, 8796-8802.
37. K. L. George and W. S. Horne, *Acc. Chem. Res.*, 2018, **51**, 1220-1228.

38. T. L. Raguse, J. R. Lai, P. R. Leplae and S. H. Gellman, *Org. Lett.*, 2001, **3**, 3963-3966.
39. J. W. Checco and S. H. Gellman, *ChemBioChem*, 2017, **18**, 291-299.
40. E. J. Petersson, C. J. Craig, D. S. Daniels, J. X. Qiu and A. Schepartz, *J. Am. Chem. Soc.*, 2007, **129**, 5344-5345.
41. D. S. Daniels, E. J. Petersson, J. X. Qiu and A. Schepartz, *J. Am. Chem. Soc.*, 2007, **129**, 1532-1533.
42. G. W. Collie, K. Pulka-Ziach, C. M. Lombardo, J. Fremaux, F. Rosu, M. Decossas, L. Mauran, O. Lambert, V. Gabelica, C. D. Mackereth and G. Guichard, *Nat. Chem.*, 2015, **7**, 871-878.
43. G. W. Collie, R. Bailly, K. Pulka-Ziach, C. M. Lombardo, L. Mauran, N. Taib-Maamar, J. Dessolin, C. D. Mackereth and G. Guichard, *J. Am. Chem. Soc.*, 2017, **139**, 6128-6137.
44. V. Berl, I. Huc, R. G. Khoury, M. J. Krische and J.-M. Lehn, *Nature*, 2000, **407**, 720-723.
45. Y. Hamuro, S. J. Geib and A. D. Hamilton, *J. Am. Chem. Soc.*, 1996, **118**, 7529-7541.
46. J. Zhu, R. D. Parra, H. Zeng, E. Skrzypczak-Jankun, X. C. Zeng and B. Gong, *J. Am. Chem. Soc.*, 2000, **122**, 4219-4220.
47. H. Jiang, J.-M. Léger and I. Huc, *J. Am. Chem. Soc.*, 2003, **125**, 3448-3449.
48. T. Qi, V. Maurizot, H. Noguchi, T. Charoenraks, B. Kauffmann, M. Takafuji, H. Ihara and I. Huc, *Chem. Commun.*, 2012, **48**, 6337-6339.
49. F. Devaux, X. Li, D. Sluysmans, V. Maurizot, E. Bakalis, F. Zerbetto, I. Huc and A.-S. Duwez, *Chem*, 2021, **7**, 1333-1346.
50. S. De, B. Chi, T. Granier, T. Qi, V. Maurizot and I. Huc, *Nat. Chem.*, 2018, **10**, 51-57.
51. N. Delsuc, F. Godde, B. Kauffmann, J.-M. Léger and I. Huc, *J. Am. Chem. Soc.*, 2007, **129**, 11348-11349.
52. D. Sánchez-García, B. Kauffmann, T. Kawanami, H. Ihara, M. Takafuji, M.-H. Delville and I. Huc, *J. Am. Chem. Soc.*, 2009, **131**, 8642-8648.
53. B. Baptiste, C. Douat-Casassus, K. Laxmi-Reddy, F. Godde and I. Huc, *J. Org. Chem.*, 2010, **75**, 7175-7185.
54. M. Vallade, P. Sai Reddy, L. Fischer and I. Huc, *Eur. J. Org. Chem.*, 2018, **2018**, 5489-5498.
55. D. Zheng, L. Zheng, C. Yu, Y. Zhan, Y. Wang and H. Jiang, *Org. Lett.*, 2019, **21**, 2555-2559.
56. E. Merlet, K. Moreno, A. Tron, N. D. McClenaghan, B. Kauffmann, Y. Ferrand and C. Olivier, *Chem. Commun.*, 2019, **55**, 9825-9828.
57. J. Wang, B. Wicher, A. Méndez-Ardoy, X. Li, G. Pecastaings, T. Buffeteau, D. M. Bassani, V. Maurizot and I. Huc, *Angew. Chem. Int. Ed.*, 2021, **133**, 18609-18614.
58. S. Kumar, M. Birol, D. E. Schlamadinger, S. P. Wojcik, E. Rhoades and A. D. Miranker, *Nat. Commun.*, 2016, **7**, 11412.
59. S. Kumar, A. Henning-Knechtel, I. Chehade, M. Magzoub and A. D. Hamilton, *J. Am. Chem. Soc.*, 2017, **139**, 17098-17108.
60. J. Buratto, C. Colombo, M. Stupfel, S. J. Dawson, C. Dolain, B. Langlois D'Estaintot, L. Fischer, T. Granier, M. Laguerre, B. Gallois and I. Huc, *Angew. Chem. Int. Ed.*, 2014, **53**, 883-887.



61. V. Maurizot, C. Dolain, Y. Leydet, J.-M. Léger, P. Guionneau and I. Huc, *J. Am. Chem. Soc.*, 2004, **126**, 10049-10052.
62. N. Delsuc, S. Massip, J.-M. Léger, B. Kauffmann and I. Huc, *J. Am. Chem. Soc.*, 2011, **133**, 3165-3172.
63. C. Dolain, J.-M. Léger, N. Delsuc, H. Gornitzka and I. Huc, *Proc. Natl. Acad. Sci.*, 2005, **102**, 16146-16151.
64. D. Mazzier, S. De, B. Wicher, V. Maurizot and I. Huc, *Chem. Sci.*, 2019, **10**, 6984-6991.
65. D. Mazzier, S. De, B. Wicher, V. Maurizot and I. Huc, *Angew. Chem. Int. Ed.*, 2020, **59**, 1606-1610.
66. C. Clementi, H. Nymeyer and J. N. Onuchic, *J. Mol. Biol.*, 2000, **298**, 937-953.
67. B. K. Shoichet, W. A. Baase, R. Kuroki and B. W. Matthews, *Proc. Natl. Acad. Sci. U.S.A.*, 1995, **92**, 452-456.
68. E. M. Meiering, L. Serrano and A. R. Fersht, *J. Mol. Biol.*, 1992, **225**, 585-589.
69. N. Tokuriki and D. S. Tawfik, *Curr. Opin. Struct. Biol.*, 2009, **19**, 596-604.
70. H. Im, H.-Y. Ahn and M.-H. Yu, *Protein Sci.*, 2000, **9**, 1497-1502.
71. A. M. Figueiredo, S. B.-M. Whittaker, S. E. Knowling, S. E. Radford and G. R. Moore, *Protein Sci.*, 2013, **22**, 1722-1738.
72. S. B.-M. Whittaker, N. J. Clayden and G. R. Moore, *J. Mol. Biol.*, 2011, **414**, 511-529.

## 3.2 Supplementary Information

for:

Molecular torsion springs: alteration of helix curvature in frustrated tertiary folds

Friedericke S. Menke, Daniela Mazzier, Barbara Wicher, Lars Allmendinger, Brice Kauffmann, Victor Maurizot and Ivan Huc

### Table of contents

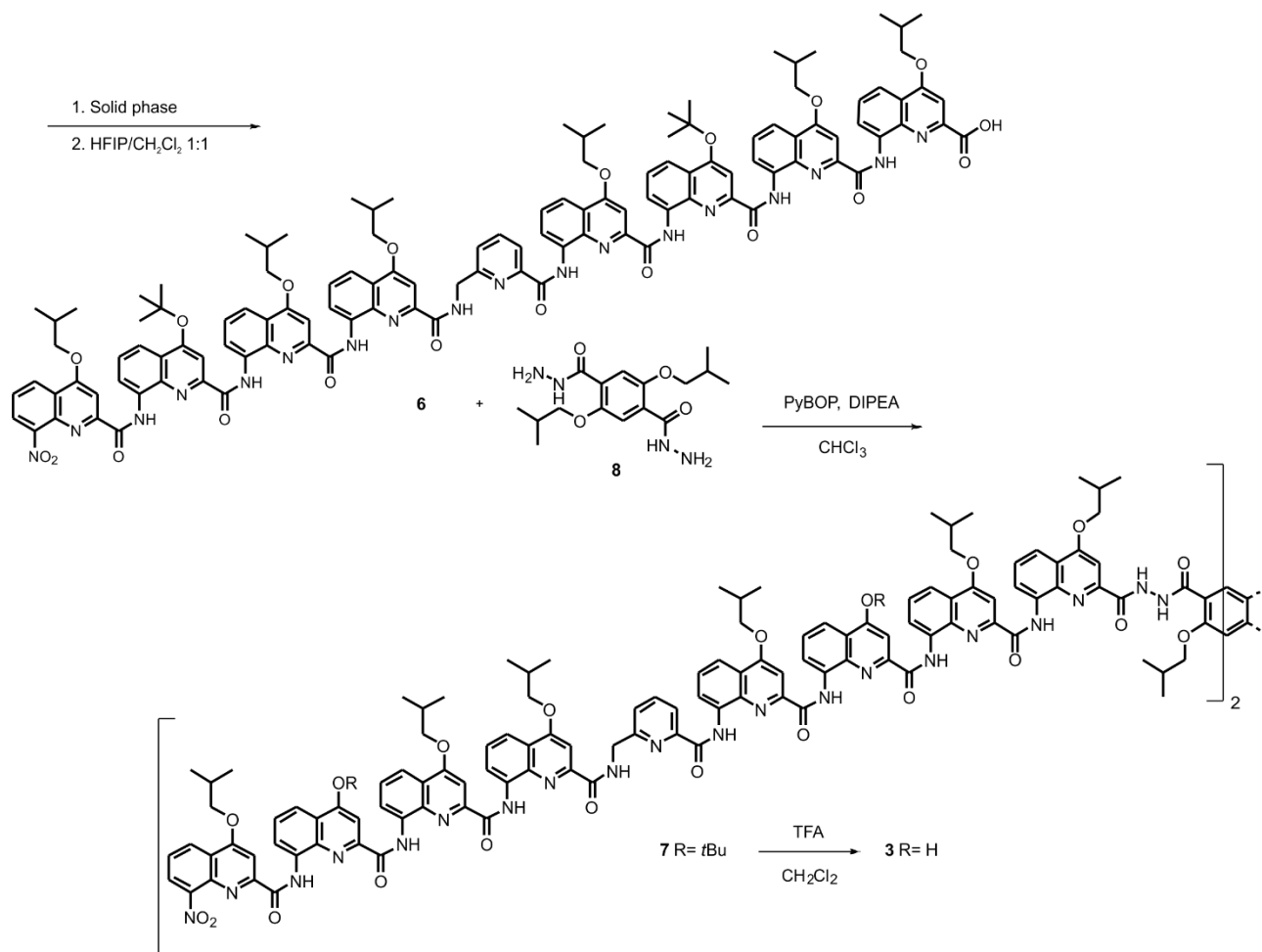
3.2.1	List of Abbreviations	51
3.2.2	Synthetic Schemes	52
	3.2.2.1 Synthesis of foldamers	52
3.2.3	Supplementary figures	55
3.2.4	Supplementary methods	65
	3.2.4.1 Nuclear magnetic resonance spectroscopy	65
	3.2.4.2 Solution state <sup>1</sup> H NMR studies	65
	3.2.4.3 X-ray crystallography	65
3.2.5	Experimental Procedures	70
	3.2.5.1 General methods	70
	3.2.5.2 Solid phase synthesis general protocol	70
	3.2.5.3 Synthesis of oligomers	71
3.2.6	References	75
3.2.7	<sup>1</sup> H NMR spectra of new compounds	76

### 3.2.1 List of Abbreviations

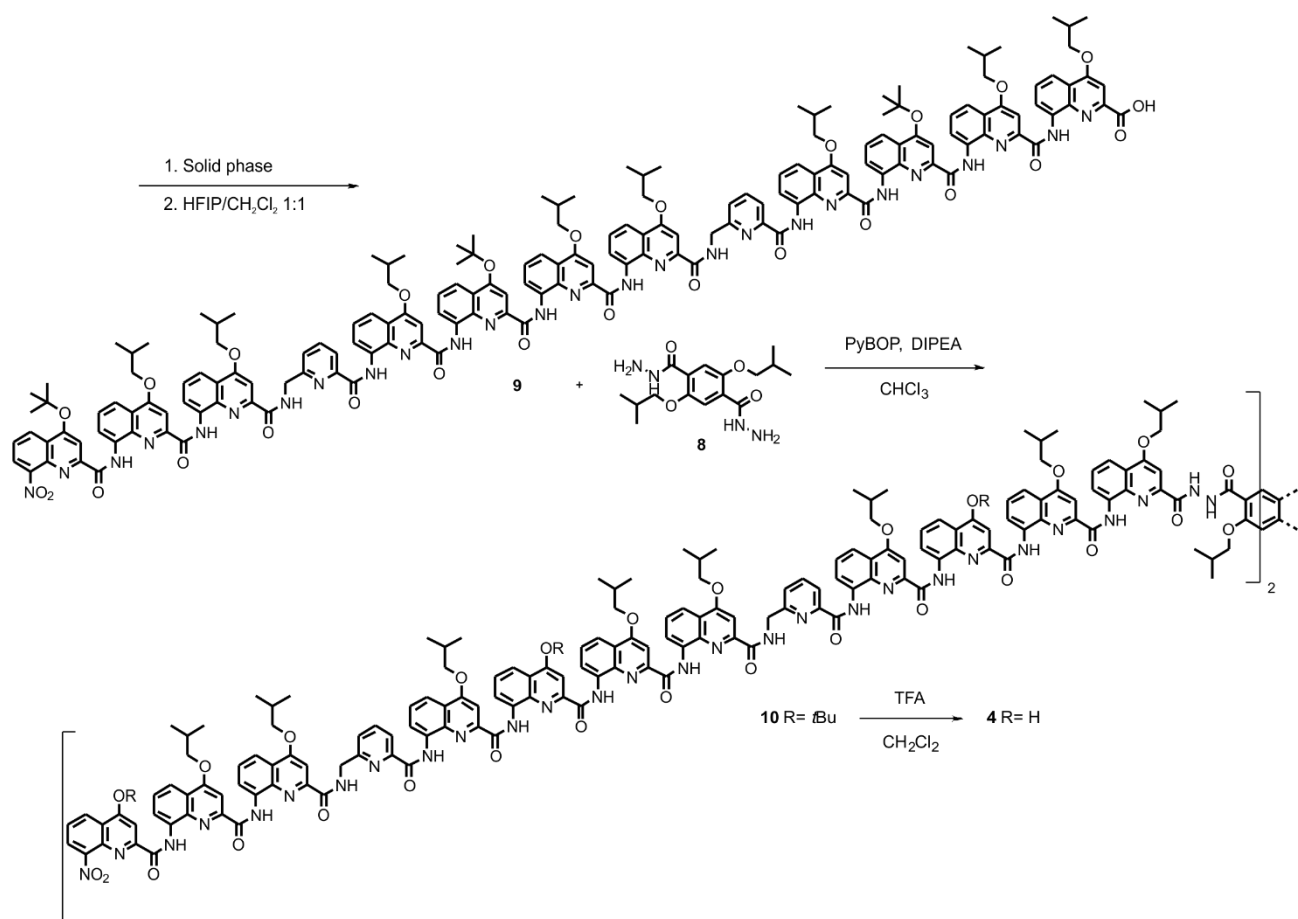
<b>DCM</b>	dichloromethane
<b>DIPEA</b>	<i>N,N</i> -diisopropylethylamine
<b>DMF</b>	<i>N,N</i> -dimethylformamide
<b>DMSO</b>	dimethyl sulfoxide
<b>eq.</b>	equivalent
<b>Fmoc</b>	fluorenylmethoxycarbonyl
<b>MS</b>	mass spectrometry
<b>HFIP</b>	hexafluoroisopropanol
<b>HR-ESI</b>	high resolution electrospray ionization
<b>HR-MALDI</b>	high resolution matrix-assisted laser desorption/ionization
<b>MeOH</b>	methanol
<b>MW</b>	microwave
<b>NMP</b>	<i>N</i> -Methyl-2-pyrrolidone
<b>NMR</b>	nuclear magnetic resonance
<b>r. t.</b>	room temperature
<b>SPS</b>	solid phase synthesis
<b>TEA</b>	triethylamine
<b>TFA</b>	trifluoroacetic acid
<b>THAP</b>	trihydroxy acetophenone
<b>THF</b>	tetrahydrofuran
<b>TMS</b>	tetramethylsilane
<b>UV/Vis</b>	ultraviolet–visible

## 3.2.2 Synthetic Schemes

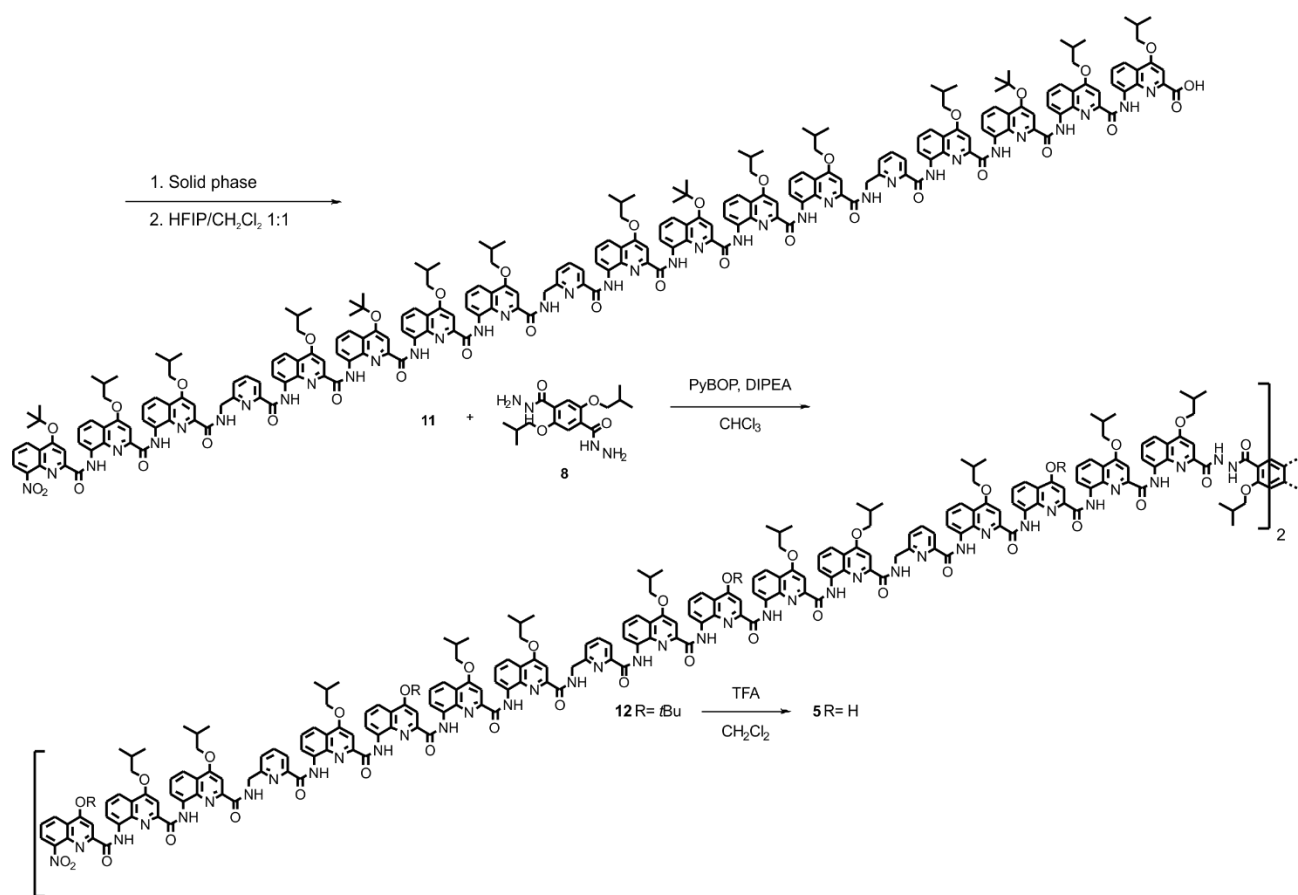
### 3.2.2.1 Synthesis of foldamers



**Scheme 1.** Synthesis of **3**.



**Scheme 2.** Synthesis of **4**.



**Scheme 3.** Synthesis of **5**.

### 3.2.3 Supplementary figures

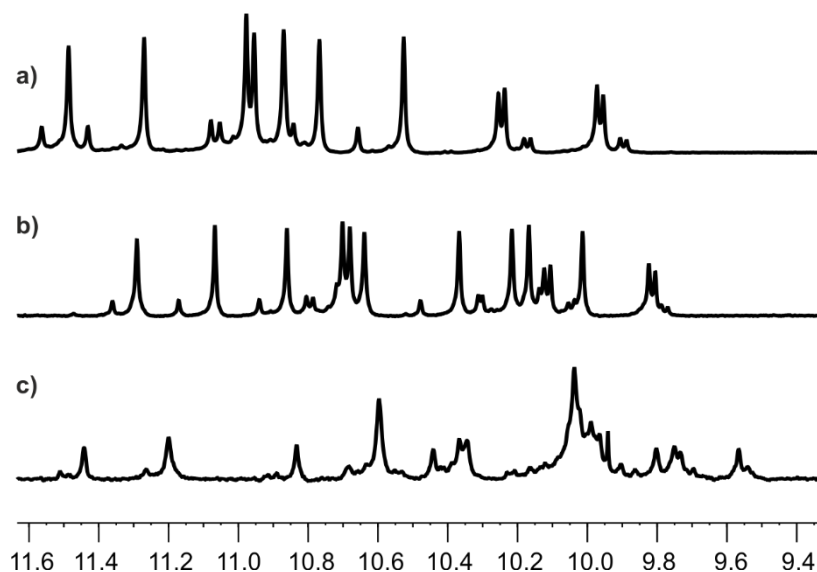


**Figure S1.** Part of the 500 MHz  $^1\text{H}$  NMR-spectra of a) 7, b) 10 and c) 12 at 25 °C in  $\text{CDCl}_3$  showing the amide proton resonances.

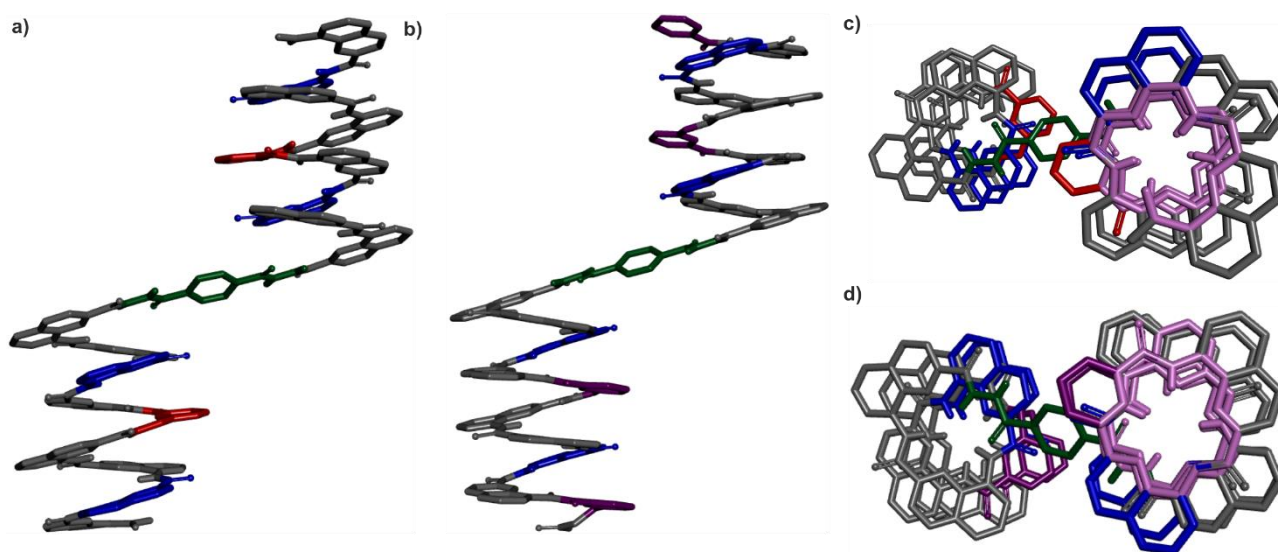


**Figure S2.** Side-views a) of the crystal structures of protected sequence 7 (new data) and b) of the protected precursor of 2 (from reference 1). The corresponding top-views are shown in c) and d), respectively, where the inner rim of one helix is highlighted in pink. The curvature adopted in these structure corresponds to the preferred curvature, as highlighted by the 15-crown-5 shape of the inner rim. The X units are shown in blue, the Y units in violet and the P units in red tubes. Included solvent molecules, hydrogen atoms and side-chains are omitted for clarity.

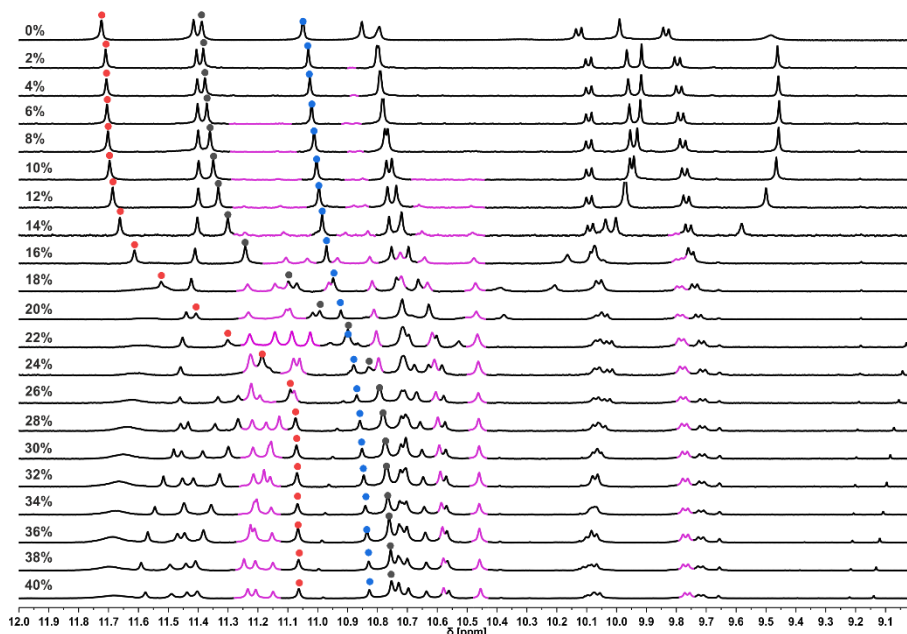


**Figure S3.** Amide region of the  $^1\text{H}$  NMR spectra (500 MHz, 25  $^\circ\text{C}$ ) of **3** in  $\text{CDCl}_3/\text{DMSO-}d_6$ . The corresponding volume percentages of  $\text{DMSO-}d_6$  in  $\text{CDCl}_3$  are indicated at left. All  $^1\text{H}$  NMR spectra containing  $\text{DMSO}$  have been calibrated on the signal corresponding to  $\text{DMSO}$  at  $\delta = 2.5$  ppm. The one containing no  $\text{DMSO}$  has been calibrated on the signal corresponding to  $\text{TMS}$  at  $\delta = 0.0$  ppm. Minimal changes in some chemical shift variations can be assigned to calibration. The chemical shift variations of the signal marked with a red, black and blue dot are shown in Figure S4; those with a black dot are also shown in Figures 5b & c. The emergence of the disrupted PM conformer is highlighted in pink.

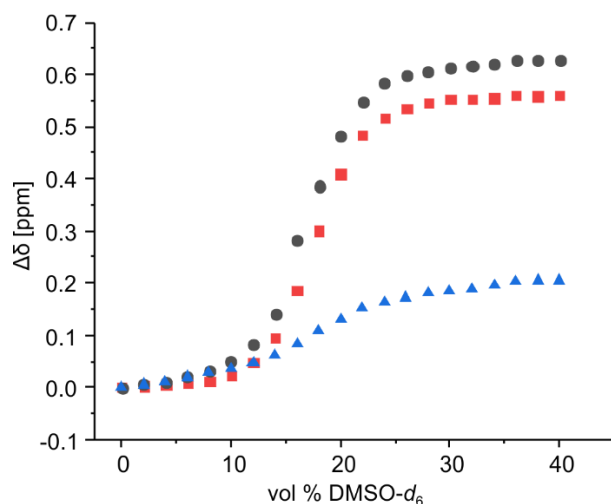


**Figure S4.** Variation of the chemical shift value of selected  $^1\text{H}$  NMR signals of **3** upon addition of  $\text{DMSO-}d_6$  (signals marked with dots of the same color in Figure S3). The data in black is also shown in Figures 5b & 5c. The inflection occurs near 18.5% of  $\text{DMSO-}d_6$ .



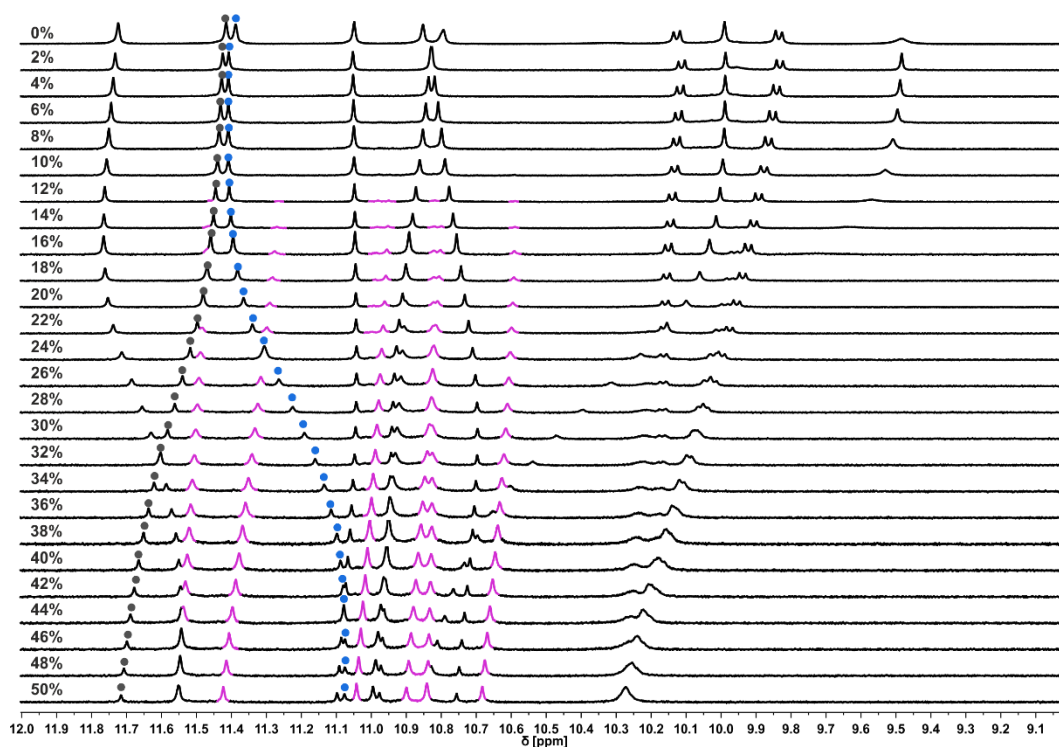


**Figure S5.** Amide region of the  $^1\text{H}$  NMR spectra (500 MHz, 25 °C) of **3** in  $\text{CDCl}_3/\text{pyridine-}d_5$ . The volume percentages of pyridine- $d_5$  in  $\text{CDCl}_3$  are indicated at left. All  $^1\text{H}$  NMR spectra have been calibrated on the signal corresponding to TMS at  $\delta = 0.0$  ppm. Minimal changes in some chemical shift variations may be assigned to calibration. The chemical shift variations of the signals marked with a black and blue dot are shown in Figure S6, those with a blue dot are also shown in Figure 5b. The emergence of the disrupted PM conformer is highlighted in pink.

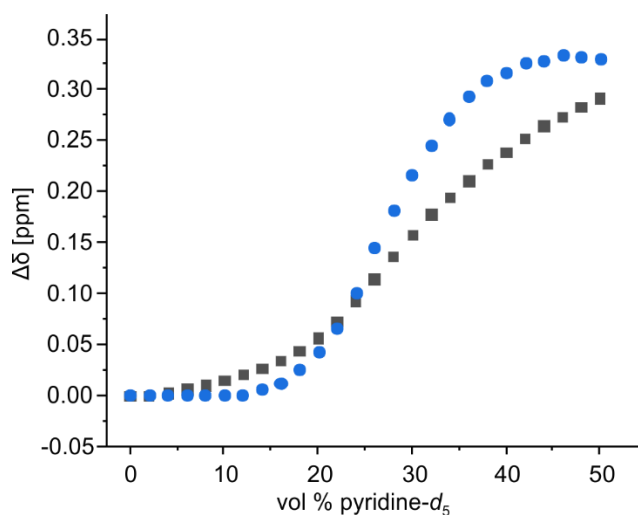


**Figure S6.** Variations of the chemical shift value of selected  $^1\text{H}$  NMR signals of sequence **3** upon addition of pyridine- $d_5$  (signals marked with dots of the same color in Figure S5). The data in blue is also shown in Figure 5b. The inflection occurs near 27.5% of pyridine- $d_5$ .

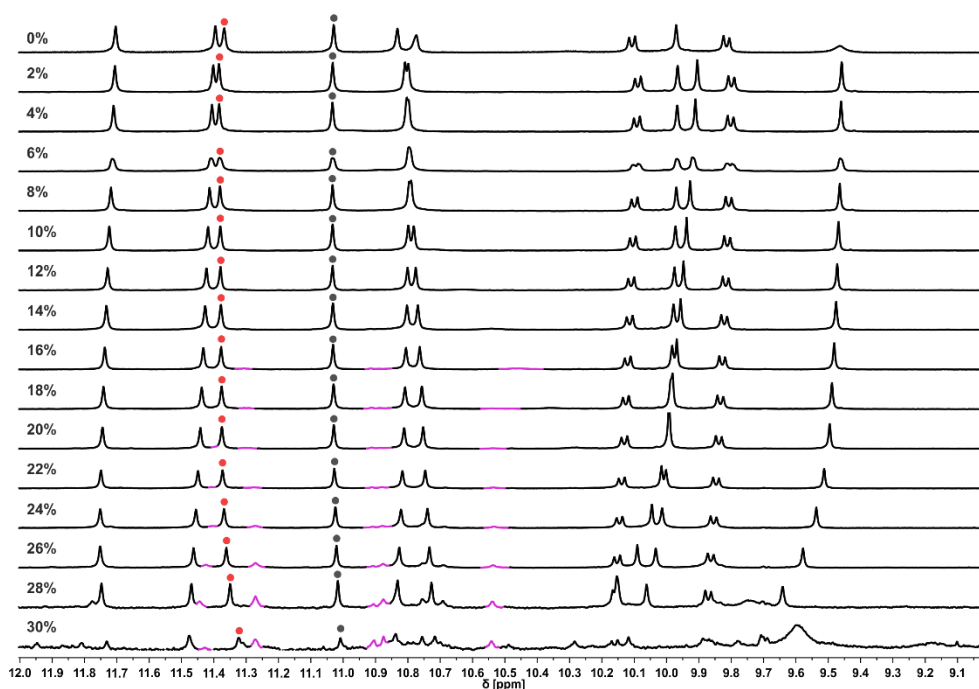


**Figure S7.** Amide region of the  $^1\text{H}$  NMR spectra (500 MHz, 25  $^\circ\text{C}$ ) resonances of **3** in  $\text{CDCl}_3/\text{DMF-}d_7$ . The volume percentages of  $\text{DMF-}d_7$  in  $\text{CDCl}_3$  are written at left. All  $^1\text{H}$  NMR spectra have been calibrated on the signal corresponding to TMS at  $\delta = 0.0$  ppm. Minimal changes in some chemical shift variations may be assigned to calibration. The chemical shift variations of the signals marked with a red and black dot are shown in Figure S8, those with a red dot are also shown in Figure 5b. The emergence of the disrupted PM conformer is highlighted in pink. The sample precipitated at 32%  $\text{DMF-}d_7$ .

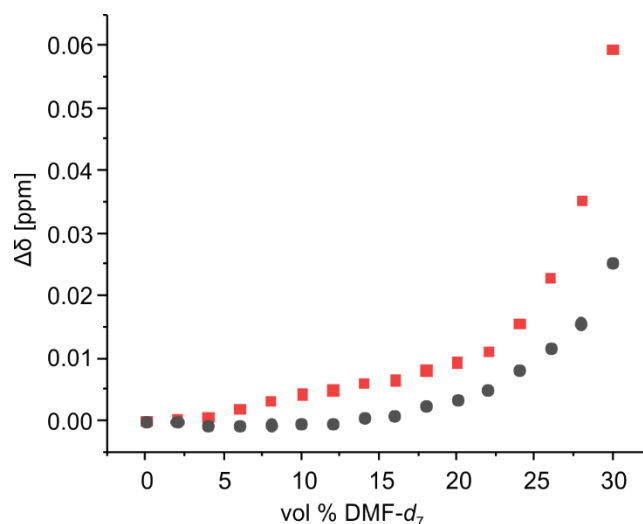


**Figure S8.** Variations of the chemical shift value of selected  $^1\text{H}$  NMR signals of **3** on the addition of  $\text{DMF-}d_7$  (signals marked with dots of the same color in Figure S7). The curve in red is also shown in Figure 5b. The inflection occurs at  $> 30\%$  of  $\text{DMF-}d_7$ .

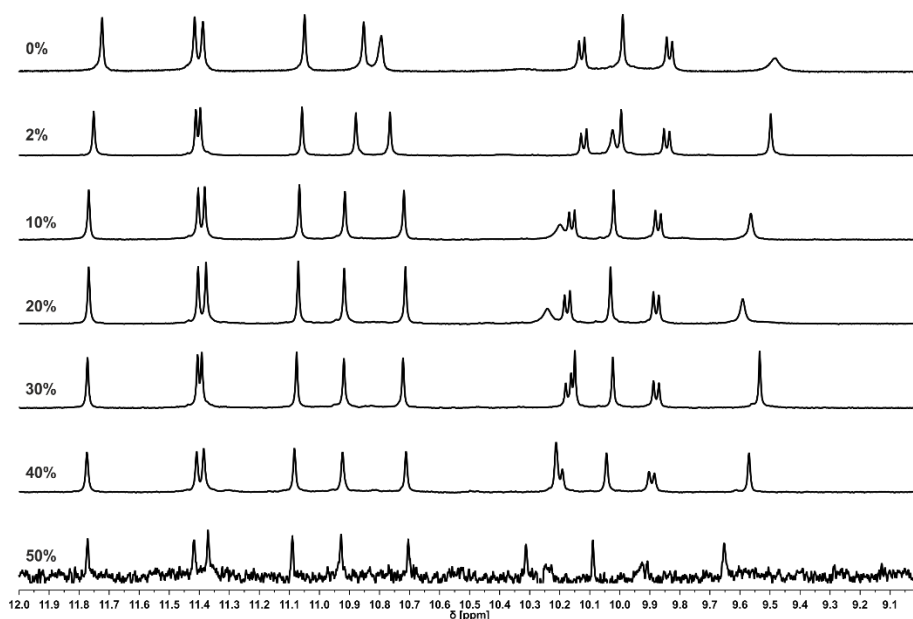


**Figure S9.** Amide region of the  $^1\text{H}$  NMR spectra (500 MHz, 25  $^\circ\text{C}$ ) of **3** in  $\text{CDCl}_3/\text{methanol-}d_3$ . The volume percentages of methanol- $d_3$  in  $\text{CDCl}_3$  are written on the left side of each  $^1\text{H}$  NMR spectra. All  $^1\text{H}$  NMR spectra have been calibrated on the signal corresponding to TMS at  $\delta = 0.0$  ppm. Minimal changes in some chemical shift variations may be assigned to calibration. No formation of a second species has been observed. The sample precipitated at 60% methanol- $d_3$ .

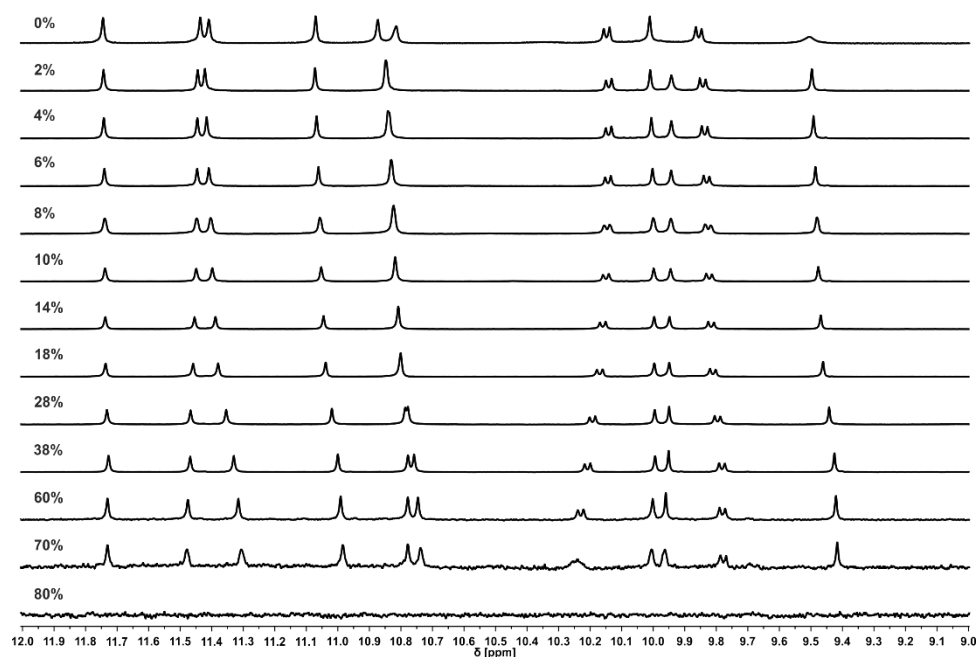


**Figure S10.** Amide region of the  $^1\text{H}$  NMR spectra (500 MHz, 25  $^\circ\text{C}$ ) of **3** in  $\text{CDCl}_3/\text{acetonitrile-}d_3$ . The volume percentages of acetonitrile- $d_3$  in  $\text{CDCl}_3$  are written at left. All  $^1\text{H}$  NMR spectra have been calibrated on the signal corresponding to TMS at  $\delta = 0.0$  ppm. Minimal changes in some chemical shift variations may be assigned. No formation of a second species has been observed. The sample precipitated at 80% acetonitrile- $d_3$ .

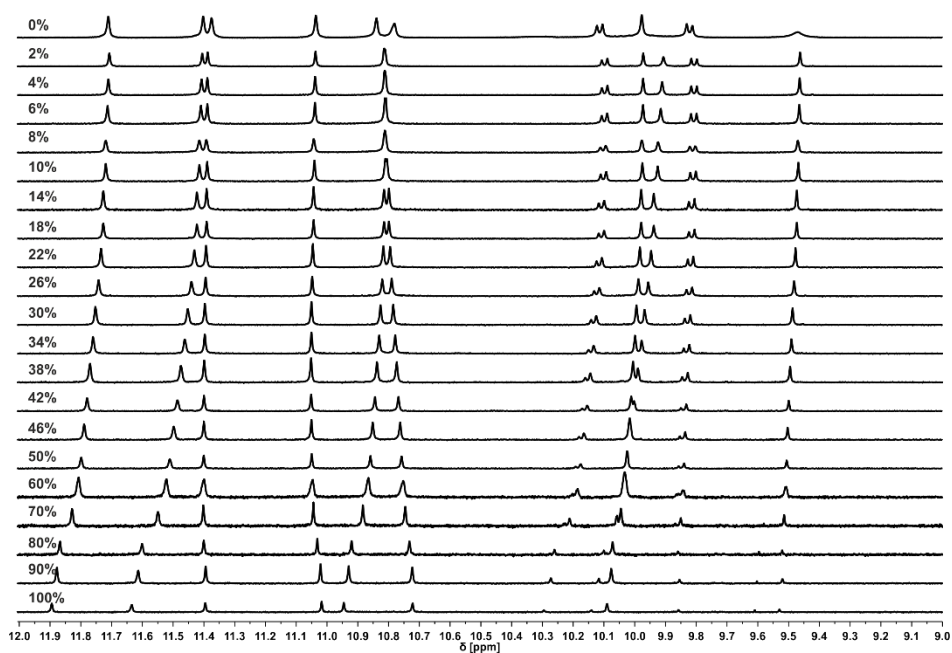


**Figure S11.** Amide region of the  $^1\text{H}$  NMR spectra (500 MHz, 25 °C) of **3** in  $\text{CDCl}_3/\text{acetone-}d_6$ . The volume percentages of acetone- $d_6$  in  $\text{CDCl}_3$  are indicated at left. All  $^1\text{H}$  NMR spectra have been calibrated on the signal corresponding to TMS at  $\delta = 0.0$  ppm. Minimal changes in some chemical shift variations can be assigned to calibration. No formation of a second species has been observed.

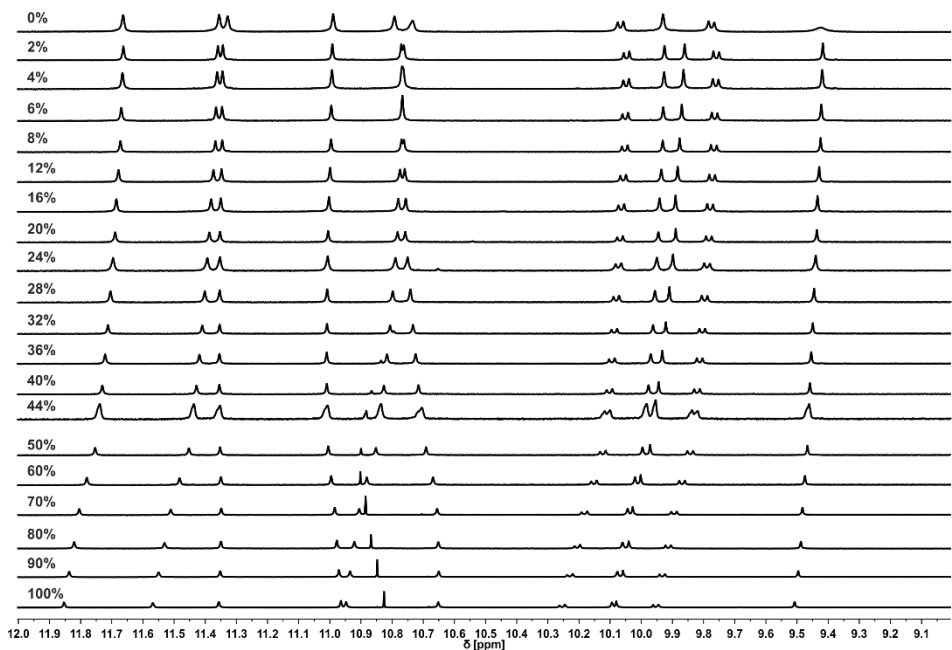


**Figure S12.** Amide region of the  $^1\text{H}$  NMR spectra (500 MHz, 25 °C) of **3** in  $\text{CDCl}_3/\text{tetrahydrofuran-}d_8$ . The volume percentages of tetrahydrofuran- $d_8$  in  $\text{CDCl}_3$  are indicated at the left. All spectra have been calibrated on the signal corresponding to TMS at  $\delta = 0.0$  ppm. Minimal changes in some chemical shift variations may be assigned to calibration. No formation of a second species has been observed.

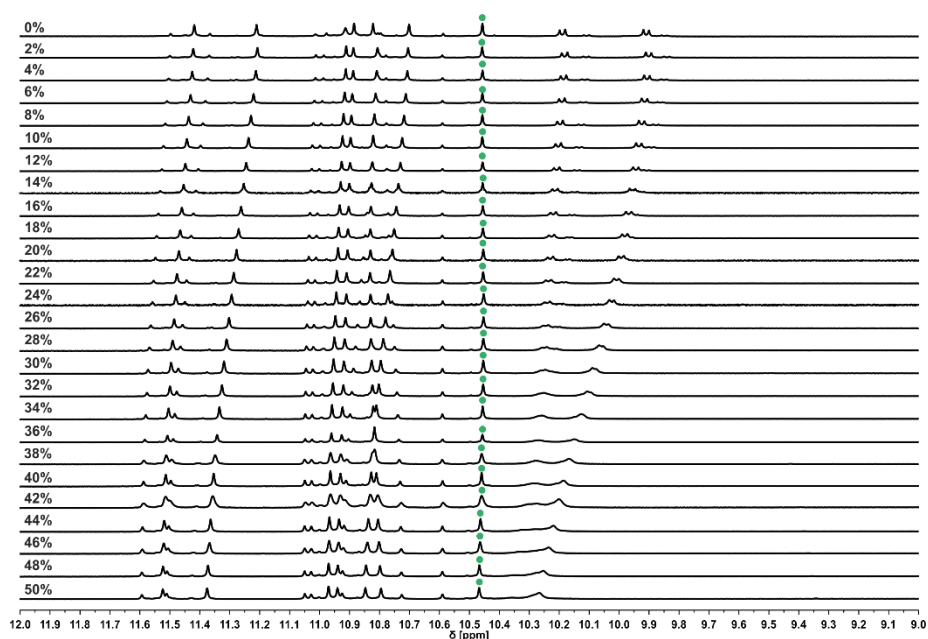


**Figure S13.** Amide region of the <sup>1</sup>H NMR spectra (500 MHz, 25 °C) of **7** in CDCl<sub>3</sub>/pyridine-*d*<sub>5</sub>. The volume percentages of pyridine-*d*<sub>5</sub> in CDCl<sub>3</sub> are indicated at left. All spectra have been calibrated on the signal corresponding to TMS at  $\delta = 0.0$  ppm. Minimal changes of some chemical shift variations may be assigned to calibration. The chemical shift variations of the signal marked with a green dot are shown in Figure S15.

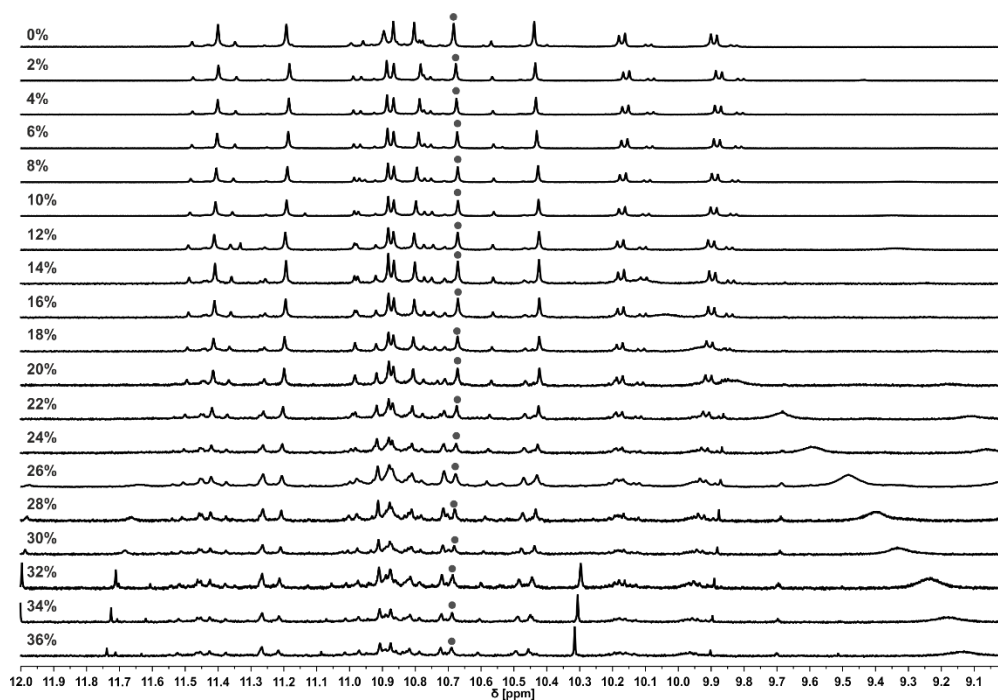


**Figure S14.** Amide region of the <sup>1</sup>H NMR spectra (500 MHz, 25 °C) of **7** in CDCl<sub>3</sub>/DMF-*d*<sub>7</sub>. The volume percentages of DMF-*d*<sub>7</sub> in CDCl<sub>3</sub> are indicated at left. All <sup>1</sup>H NMR have been calibrated on the signal corresponding to TMS at  $\delta = 0.0$  ppm. Minimal changes in some chemical shift variations may be assigned to calibration. No formation of a second species has been observed. The chemical shift variations of the signal marked with a black dot are shown in Figure S15. The sample precipitated at 38% DMF-*d*<sub>7</sub> in solution.

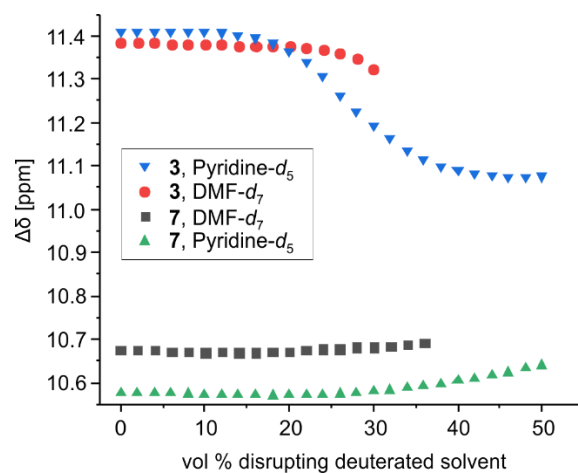


**Figure S15.** Variation of the chemical shift of selected  $^1\text{H}$  NMR signals of **3** and its protected precursor **7** in  $\text{CDCl}_3$  on the addition of disruptive solvents like  $\text{DMF-}d_7$  (red and black) and pyridine- $d_5$  (green and blue). The colors of the data matches those of the dots marked in Figure S5, Figure S7, Figure S13 and Figure S14. The experiment with  $\text{DMF-}d_7$  was ended due to precipitation of the sample at 32% (in case of **3**) and 38% (in case of **7**).

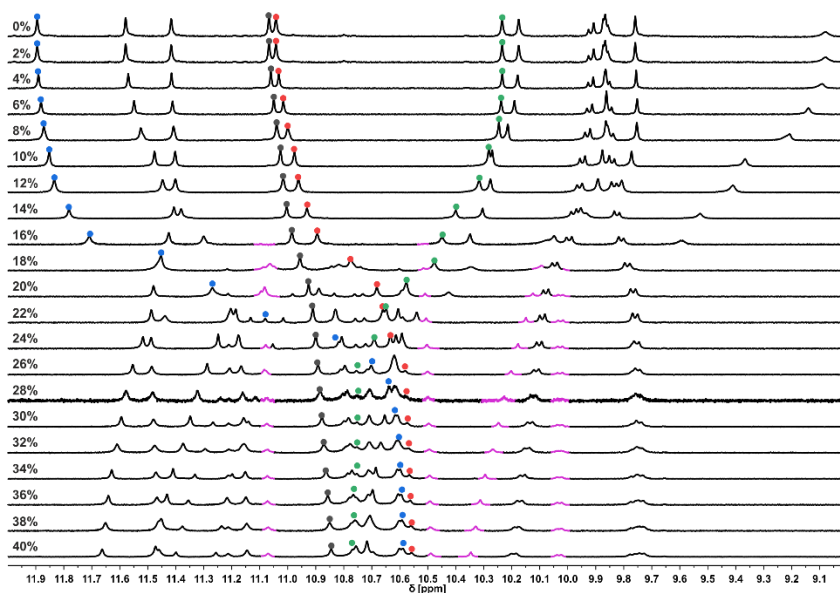


**Figure S16.** Amide region of the  $^1\text{H}$  NMR spectra (500 MHz, 25  $^\circ\text{C}$ ) of **1** in  $\text{CDCl}_3/\text{DMSO-}d_6$ . The volume percentages of  $\text{DMSO-}d_6$  in  $\text{CDCl}_3$  are indicated at left. All  $^1\text{H}$  NMR spectra containing  $\text{DMSO}$  have been calibrated on the signal corresponding to  $\text{DMSO}$  at  $\delta = 2.5$  ppm. The one containing no  $\text{DMSO}$  has been calibrated on the signal corresponding to  $\text{TMS}$  at  $\delta = 0.0$  ppm. Minimal changes in some chemical shift variations may be assigned to calibration. The chemical shift variations of the signal marked with a blue, black, red and green dot are shown in Figure S17, those with a blue dot are also shown in Figure 5c. The emergence of the disrupted *PM* conformer is highlighted in pink.

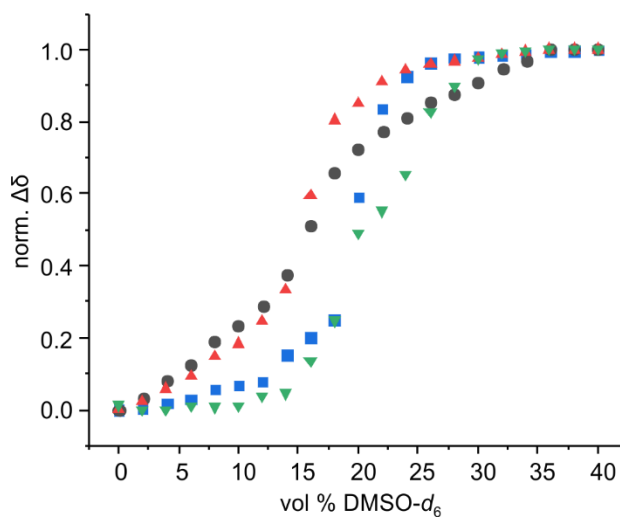


**Figure S17.** Normalized variation of the chemical shift value of selected  $^1\text{H}$  NMR signals of **1** upon the addition of  $\text{DMSO-}d_6$  (signals marked with dots of the same color in Figure S16). The curve in blue is also shown in Figure 5c. The inflection occurs near 21.5% of  $\text{DMSO-}d_6$ .

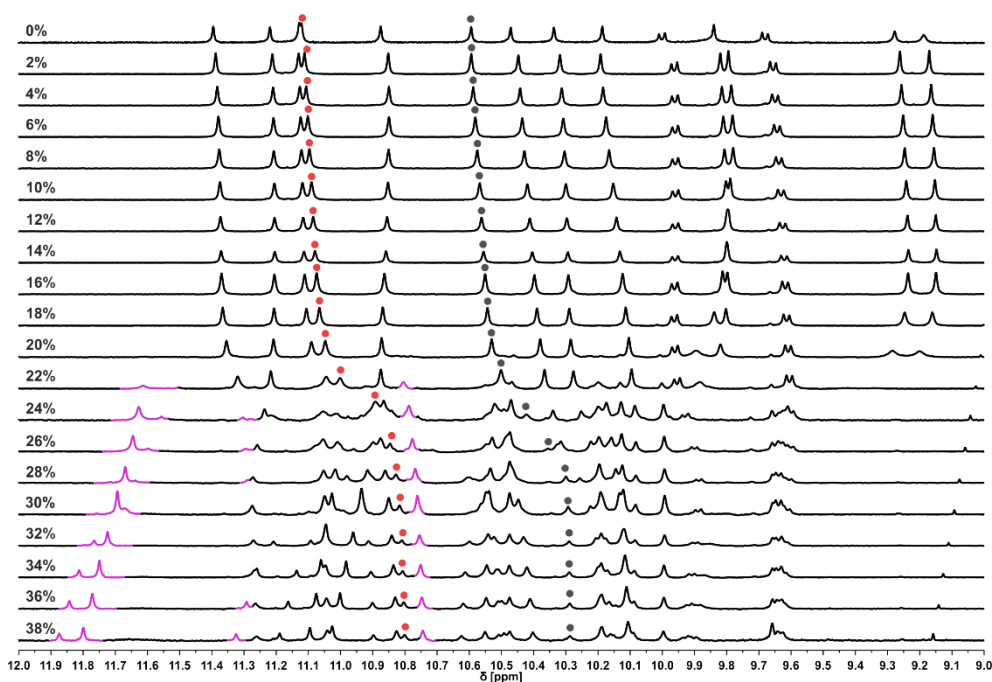


**Figure S18.** Amide region of the  $^1\text{H}$  NMR spectra (500 MHz, 25  $^\circ\text{C}$ ) of **4** in  $\text{CDCl}_3/\text{DMSO-}d_6$ . The volume percentages of  $\text{DMSO-}d_6$  in  $\text{CDCl}_3$  are indicated at left. All  $^1\text{H}$  NMR spectra containing  $\text{DMSO}$  have been calibrated on the signal corresponding to  $\text{DMSO}$  at  $\delta = 2.5$  ppm. The one containing no  $\text{DMSO}$  has been calibrated on the signal corresponding to  $\text{TMS}$  at  $\delta = 0.0$  ppm. Minimal changes in some chemical shift variations may be assigned to calibration. The chemical shift variations of the signals marked with a black and red dot are shown in Figure S19, those with a red dot are also shown in Figure 5c. The emergence of the disrupted PM conformer is highlighted in pink.

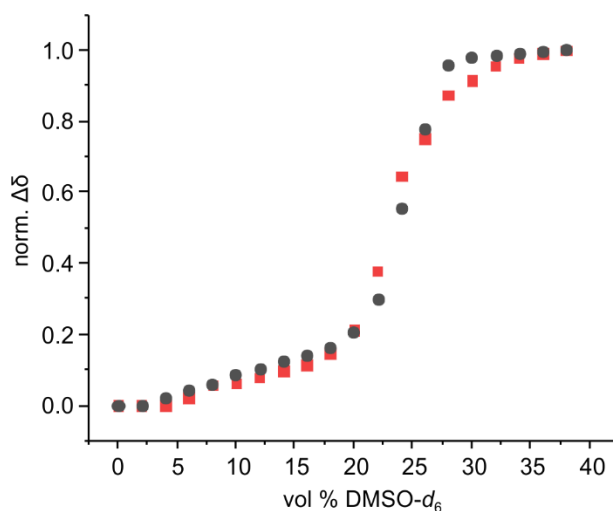


**Figure S19.** Normalized variation of the chemical shift value of selected  $^1\text{H}$  NMR signals of **4** on the addition of  $\text{DMSO-}d_6$  (signals marked with dots of the same color in Figure S18). The curve in red is also shown in Figure 5c. The inflection occurs near 24.0% of  $\text{DMSO-}d_6$ .



## 3.2.4 Supplementary methods

### 3.2.4.1 Nuclear magnetic resonance spectroscopy

NMR spectra were recorded on different NMR spectrometers: (I) an Avance II NMR spectrometer (Bruker BioSpin) with a vertical 7.05 T narrow-bore/ultrashield magnet operating at 300 MHz by means of a 5-mm direct BBO H/X probe with Z gradient capabilities; (II) an Avance III HD 400 MHz Bruker BioSpin spectrometer or an Avance III HD 500 MHz Bruker BioSpin spectrometer equipped with a broad band observe 5-mm BB-H&FD CryProbe™ Prodigy. Measurements were performed at 25 °C unless stated otherwise.

Chemical shifts are described in part per million (ppm,  $\delta$ ) relative to the  $^1\text{H}$  residual signal of the deuterated solvent used unless otherwise noted. Processing was done with MestReNovax64 NMR processing software from Mestrelab Research.  $^1\text{H}$  NMR splitting patterns with observed first-order coupling are entitled as singlet (s), doublet (d), triplet (t), or broad singlet (bs).

### 3.2.4.2 Solution state $^1\text{H}$ NMR studies

For the solvent concentration dependency study a sample was dissolved in  $\text{CDCl}_3$  ( $c = 1.2 \text{ mM}$ ) and the amount of polar solvent in solution was increased stepwise. After an equilibration time of two hours the  $^1\text{H}$  NMR was recorded after each increase. If a solvent is disruptive a significant change of the chemical shift in the amide region and the formation of a second species is observed, which reflects a conformational transition. The amount of polar solvent in the sample is increased until no further change of the chemical shifts in the amide region and no increase in the formation of a second species is observed.

This experiment has been carried out until 100% or precipitation of the sample in case of solvent at which no formation of a second species has been observed.

The solvents  $\text{CDCl}_3$  (quality: 99.8 atom % D, containing 0.03vol.% TMS),  $\text{DMSO-}d_6$  (quality: 99.9 atom % D),  $\text{DMF-}d_7$  (quality: 99.5 atom % D),  $\text{pyridine-}d_5$  (quality:  $\geq 99.5$  atom % D),  $\text{methanol-}d_3$  (quality: 99.8 atom % D),  $\text{acetonitrile-}d_3$  (quality:  $\geq 99.8$  atom % D),  $\text{acetone-}d_6$  (quality: 99.9 atom % D),  $\text{THF-}d_8$  (quality:  $\geq 99.5$  atom % D, containing 0.03vol.% TMS) have been used.

### 3.2.4.3 X-ray crystallography

The diffraction data for **3** were collected at the FIP (ESRF) beamline using 0.81 Å wavelength and were processed with the XDS package.<sup>2</sup> X-ray diffraction experiments for **7** were performed at the IECB x-ray facility (CNCR UMS 3033 – INSERM US001) with a Rigaku FRX rotating anode (2.9 kW) diffractometer.  $\text{CuK}\alpha$  radiation was monochromated with high flux Osmic Varimax HF mirrors for data

collection. The x-ray source was equipped with a Dectris Pilatus 200K detector and partial chi goniometer. The data were processed with CrysAlis PRO software<sup>3</sup> with a multiscan absorption correction. All crystals were kept at 100(2) K during data collection. Structures were solved with the ShelXT<sup>4</sup> structure solution program using a dual-space algorithm. Crystal model refinement was performed with ShelXL<sup>5</sup> package using Least Squares minimization implemented in Olex2.<sup>6</sup>

During refinement, anisotropic displacement parameters were used for backbones, some solvent molecules and side chains. The C- and N-bound hydrogen atoms were placed in an idealized position. In **3**, the positions of hydroxy H atoms were established based on hydrogen bond interactions. All H atoms were refined in the riding-model approximation, with  $U_{\text{iso}}(\text{H})=1.2U_{\text{eq}}(\text{CH}, \text{CH}_2, \text{NH})$ ,  $U_{\text{iso}}(\text{H})=1.5U_{\text{eq}}(\text{OH}, \text{CH}_3)$ . EADP, DELU and RIGU instructions were employed to model temperature parameters. The geometry of the molecules was improved with DFIX and AFIX commands.

The solvent masking procedure implemented in Olex2<sup>6</sup> was employed to remove severely disordered solvent molecules. The solvent radius was set to 1.2 Å, and the calculated total potential solvent-accessible void volume and electron counts per unit cell were 4656 Å<sup>3</sup> and 1132, 2518 Å<sup>3</sup> and 849 for **3** and **7**, respectively.

The final cif files were checked using IUCR's check cif algorithm. Due to the characteristics of the crystal, *i.e.* large volume fractions of disordered solvent molecules, weak diffraction intensity, incompleteness of the data and moderate resolution, A - level and B - level alerts remain in the check cif file. These alerts are inherent to the data and refinement procedures and do not reflect errors. They are explicitly listed below and have been divided into two groups. The first group illustrates the poor quality of the data and refinement statistics compared to that expected for small molecule structures from highly diffracting crystals. The second group is connected to decisions made during refinement and explained below.

#### **Group 1:**

PLAT029\_ALERT\_3\_B \_diffn\_measured\_fraction\_theta\_full value Low . 0.930

PLAT084\_ALERT\_3\_A High wR2 Value (*i.e.* > 0.25)

PLAT934\_ALERT\_3\_A Number of (Iobs-Icalc)/Sigma(W) > 10 Outliers

THETM01\_ALERT\_3\_A The value of sine(theta\_max)/wavelength is less than 0.550

PLAT023\_ALERT\_3\_A, B Resolution (too) Low [ $\sin(\theta)/\lambda < 0.6$ ].

PLAT082\_ALERT\_2\_B High R1 Value

PLAT098\_ALERT\_2\_B Large Reported Min. (Negative) Residual Density

PLAT220\_ALERT\_2\_B NonSolvent Resd 1 C Ueq(max)/Ueq(min) Range

PLAT230\_ALERT\_2\_B Hirshfeld Test Diff for

PLAT241\_ALERT\_2\_B High 'MainMol' Ueq as Compared to Neighbors

PLAT242\_ALERT\_2\_B Low 'MainMol' Ueq as Compared to Neighbors

PLAT340\_ALERT\_3\_B Low Bond Precision on C-C Bonds

**Group 2:**

PLAT201\_ALERT\_2\_A Isotropic non-H Atoms in Main Residue(s)

Not all atoms were refined with ADPs

DIFMN02\_ALERT\_2\_B The minimum difference density is  $< -0.1 * ZMAX * 1.00$

The solvent masking was used to remove severely disordered solvent molecules

PLAT315\_ALERT\_2\_B Singly Bonded Carbon Detected (H-atoms Missing)

Not all H-atoms were localized, but they were used in SFAC calculation

**Table S1.** Crystal data and refinement details for **3** and **7**.

<b>Identification code</b>	<b>3</b>	<b>7</b>
<b>Chemical formula</b>	C <sub>238</sub> H <sub>226</sub> N <sub>40</sub> O <sub>42</sub> ·7.7(CHCl <sub>3</sub> ) solvent*	C <sub>254</sub> H <sub>258</sub> N <sub>40</sub> O <sub>42</sub> ·8(CHCl <sub>3</sub> ) solvent*
<b>Formula weight</b>	5258.53	5497.93
<b>Crystal system</b>	Orthorhombic	Triclinic
<b>Space group</b>	<i>P</i> bcn	<i>P</i> -1
<b>Unit cell dimensions (Å, °)</b>	a=25.120 (5) α=90 b=27.450 (6) β=90 c=40.020 (8) γ=90	a=18.2180 (6) α=105.871 (3) b=18.4206 (6) β=95.140 (3) c=29.4522 (10) γ=114.061 (3)
<b>Volume (Å<sup>3</sup>)</b>	27596 (10)	8450.4 (5)
<b>Z</b>	4	1
<b>Density (calculated) (Mg m<sup>-3</sup>)</b>	1.27	1.080
<b>Absorption coefficient (mm<sup>-1</sup>)</b>	0.44	2.29
<b>Crystal size (mm)</b>	0.20 × 0.07 × 0.03	0.20 × 0.07 × 0.03
<b>Completeness</b>	94.1 (up to 25.23°)	99.3 (up to 57.90°)
<b>Reflections collected</b>	233506	85666
<b>Reflections observed [<i>I</i> &gt; 2σ(<i>I</i>)]</b>	15547	16731
<b>R<sub>int</sub></b>	0.049	0.133
<b>Data/parameters/restraints</b>	15863/1343/109	23289/1511/64
<b>Goodness-of-fit on F<sup>2</sup></b>	3.21	1.81
<b>Final R indices [<i>I</i> &gt; 2σ(<i>I</i>)]</b>	0.1596, 0.5440	0.1624, 0.4515
<b>R indices (all data)</b>	0.1606, 0.5480	0.1777, 0.4671
<b>Largest diff. peak and hole</b>	1.46, -2.24	0.95, -0.58
<b>CCDC #</b>	2213461	2213460

Experiments were carried out at 100 K with Cu *K*α radiation. Absorption was corrected by multi-scan

\* Solvent mask was used to remove severely disordered solvent molecules

**Table S2.** Hydrogen bonds geometry in the crystal structure of **3**. Atom numbers are those of the cif file.

$D-H\cdots A$	$D-H$ (Å)	$H\cdots A$ (Å)	$D\cdots A$ (Å)	$D-H\cdots A$ (°)
O2C-H2C $\cdots$ O7B <sup>i</sup>	0.84	1.87	2.704 (8)	169
O1C-H1C $\cdots$ O32B <sup>i</sup>	0.84	1.91	2.742 (7)	173

## 3.2.5 Experimental Procedures

### 3.2.5.1 General methods

Commercial reagents were purchased from Sigma-Aldrich, Alfa-Aesar or TCI and were used without further purification unless otherwise specified. SASRIN resin (100-200 mesh, loading 0.7-1.0 mmol/g) was purchased from Bachem. THF, DCM and toluene were dried over alumina columns (MBRAUN SPS-800 solvent purification system); diisopropylethylamine (DIPEA) was distilled over ninhydrin and then over potassium hydroxide (KOH); chloroform was distilled over calcium hydride ( $\text{CaH}_2$ ) prior to use. Preparative recycling GPC (gel permeation chromatography) was carried out on JAIGEL 20\*600 mm columns (Japan Analytical Industry) in chloroform containing 1% ethanol and 0.5% TEA as mobile phase, with a flow rate of 7.5 mL/min. Monitoring by UV detection was carried out at 254 nm, 280 nm, 300 nm and 360 nm. SPS was performed manually under MW irradiation on a CEM Discover (Liberty Bio) oven using an open reaction vessel and an internal optic fiber probe for temperature control. High-resolution electrospray mass spectra were recorded on a Thermo Exactive orbitrap instrument. High-resolution MALDI-TOF mass spectra have been recorded 4800 MALDI-TOF/TOF instrument.

### 3.2.5.2 Solid phase synthesis general protocol

The oligomers **9** & **11** were synthesized using SPS on SASRIN resin using previously reported.<sup>7</sup> Quinoline monomers (Fmoc-Q-OH,<sup>7</sup> Fmoc-X-OH,<sup>8</sup> Fmoc-P-OH<sup>9</sup>) were activated as acid chlorides. X refers to the *t*Bu-protected precursors of X.

Oligomer **6** was prepared using in situ coupling conditions as follows.<sup>10</sup> Loading of the resin was performed according to previously reported procedures.<sup>7</sup> After swelling of the SASRIN resin (100 mg, 100-200 mesh, loading 0.4616 mmol/g, 46.16  $\mu\text{mol}$ ) in DMF for 1 h, the resin was transferred into the MW vessel and washed three times with DMF. For deprotection a 8:2 mixture of DMF/piperidine (2 mL) was added to the resin, and nitrogen was bubbled through the suspension for 3 min. The solution was removed under vacuum, the resin was washed five times with DMF and an 8:2 mixture of DMF/piperidine (2 mL) was added again. After bubbling nitrogen through the suspension for 7 min, the resin was washed five times with DMF and five times with THF. For coupling dry THF (1 mL) and 2,3,5-collidine (5 eq. with respect to the resin-loading) were added to the resin. A mixture of the monomer (2 eq. with respect to the resin-loading) and  $\text{PPh}_3$  (4 eq. with respect to the resin-loading) in distilled  $\text{CHCl}_3$  (1 mL) or dry NMP (1 mL) was prepared. All monomers except Fmoc-P-OH were dissolved in distilled  $\text{CHCl}_3$ , Fmoc-P-OH was dissolved in dry NMP. After the addition of trichloroacetonitrile (4 eq. with respect to the resin-loading), this mixture was added to the resin. Then the reaction mixture was subjected to MW treatment (50 °C, 5 min, 25 W). Then the resin was washed five times with dry THF, then dry THF (4 mL) and 2,3,5-collidine (5 eq. with respect to the resin-loading) were added to the resin. Again, a mixture of monomer (2 eq. with respect to the resin-loading) and  $\text{PPh}_3$  (4 eq. with respect to the resin-loading) in distilled  $\text{CHCl}_3$  (4 mL) or dry NMP (4 mL) with trichloroacetonitrile was prepared and added to the resin. The reaction mixture was again subjected to MW

treatment (50 °C, 5 min, 50 W). After washing with DCM, THF, DMF and DCM, in that order, the resin was kept in a swollen state at 10 °C.

After complete solid phase synthesis, the sequence was cleaved from the resin. Thus, the SASRIN resin (~50 mg) was swelled in DCM for 15 min, HFIP/DCM 1:1 (vol/vol) (6 mL) was added and the mixture was stirred at r.t. for 12 h. The resin was filtered off, and then the solvent was evaporated. The process was repeated until no more foldamer was left on the resin (up to twenty times 12 h).

### 3.2.5.3 Synthesis of oligomers

**O<sub>2</sub>N-QXQQPQXQQ-OH (6)** Compound **6** was synthesized using the SPS procedures reported in 5.2 on SASRIN resin (scale: 46.3 μmol). The crude product was purified via precipitation in DCM/MeOH, and the product was obtained as a yellow solid (33%, 15.1 μmol, 30.3 mg). **<sup>1</sup>H NMR** (300 MHz, CDCl<sub>3</sub>) δ [ppm] 11.38 (s, 1H), 11.35 (s, 1H), 11.03 (s, 2H), 10.91 (s, 1H), 10.84 (s, 1H), 10.76 (s, 1H), 10.50 (s, 2H), 8.30 (dd, *J* = 8.3, 1.5 Hz, 1H), 8.16 (dd, *J* = 7.7, 1.2 Hz, 1H), 8.13 – 8.07 (m, 2H), 8.01 (dd, *J* = 8.3, 1.2 Hz, 2H), 7.92 – 7.85 (m, 2H), 7.82 (dd, *J* = 8.4, 1.2 Hz, 2H), 7.79-7.74 (m, 3H), 7.69 (d, *J* = 8.4 Hz, 1H), 7.61 (s, 1H), 7.60-7.59 (m, 1H), 7.46-7.40 (m, 4H), 7.38 (d, *J* = 2.3 Hz, 1H), 7.35 (s, 1H), 7.33-7.24 (m, overlap with residual solvent peak), 7.18 – 7.11 (m, 4H), 7.10 (s, 1H), 7.09-7.05 (m, 1H), 7.04 – 6.96 (m, 2H), 6.91 – 6.84 (m, 1H), 6.63 (s, 1H), 6.49 (s, 1H), 6.45 (s, 1H), 5.99 (s, 1H), 5.76 (s, 1H), 4.68 (s, 2H), 4.14-4.05 (m, 2H), 4.04 – 3.90 (m, 2H), 3.83-3.75 (m, 3H), 3.74-3.65 (m, 2H), 3.56 – 3.47 (m, 2H), 2.55 – 2.14 (m, 5H), 1.79 (s, 9H), 1.73 (s, 9H), 1.31 (d, *J* = 6.7 Hz, 6H), 1.26 (m, 6H), 1.23 – 1.18 (m, 12H), 1.17 (d, *J* = 3.9 Hz, 3H), 1.15 (d, *J* = 5.6 Hz, 6H), 1.11 (d, *J* = 7.1 Hz, 3H), 1.09 (d, *J* = 6.7 Hz, 3H). **HRMS** calcd for C<sub>119</sub>H<sub>119</sub>N<sub>18</sub>O<sub>20</sub> [M+H]<sup>+</sup> 2119.8848, found (HR-ESI) 2119.8798.

**(O<sub>2</sub>N-QXQQPQXQQ)<sub>2</sub>-T (7)** Compound **6** (30.3 mg, 14.3 μmol, 1 eq.), 2,6-diisobutoxyterephthalohydrazide (**8**)<sup>1</sup> (2.4 mg, 7.0 μmol, 0.5 eq.) and PyBOP (22.3 mg, 22.8 μmol, 3 eq.) were dissolved in dry CHCl<sub>3</sub> under N<sub>2</sub>. Then DIPEA (7.3 μL, 22.5 μmol, 3 eq.) was added, and the solution was stirred at r.t. for 1 week. The solvent was removed under vacuum, and the crude was purified via precipitation in DCM/MeOH. The product was recovered as a yellow solid (30.53 mg, 49% yield). **<sup>1</sup>H NMR** (400 MHz, CDCl<sub>3</sub>) δ [ppm] 11.49 (s, 2H), 11.27 (s, 2H), 10.98 (s, 2H), 10.95 (s, 2H), 10.87 (s, 2H), 10.77 (s, 2H), 10.53 (s, 2H), 10.25 (d, *J* = 9.3 Hz, 2H), 9.97 (d, *J* = 9.3 Hz, 2H), 8.28 (dd, *J* = 7.9, 1.5 Hz, 2H), 8.13 (d, *J* = 7.5 Hz, 2H), 8.07 – 8.02 (m, 6H), 8.00 (d, *J* = 8.0 Hz, 2H), 7.91-7.85 (m, 8H), 7.80 – 7.73 (m, 6H), 7.71 (d, *J* = 7.9 Hz, 2H), 7.63 – 7.51 (m, 8H), 7.44 – 7.27 (m, 10H), 7.24-7.19 (m, 4H), 7.14 – 6.96 (m, 18H), 6.90 (t, *J* = 7.8 Hz, 2H), 6.69 (s, 2H), 6.58 (s, 2H), 6.41 (s, 2H), 5.95 (s, 2H), 5.76 (s, 2H), 4.13-4.01 (m, 4H), 3.98-3.89 (m, 4H), 3.89 – 3.74 (m, 10H), 3.69 – 3.61 (m, 4H), 3.57 (t, *J* = 8.4 Hz, 2H), 3.50 (t, *J* = 7.6 Hz, 2H), 3.37 – 3.29 (m, 2H), 2.51-2.41 (m, 2H), 2.39 – 2.17 (m, 10H), 1.86 (d, *J* = 5.2 Hz, 6H), 1.61 (s, 18H), 1.47 (s, 18H), 1.32 (d, *J* = 6.7 Hz, 18H), 1.29 – 1.14 (m, 30H), 1.12 (d, *J* = 6.8 Hz, 6H), 1.07 (d, *J* = 6.7 Hz, 12H), 1.01 (d, *J* = 6.6 Hz, 12H), (mixture of two diastereomers *PP* and *PM* and their ratio is 10:1, only the major peaks are reported). **HRMS** calcd for C<sub>254</sub>H<sub>261</sub>N<sub>40</sub>O<sub>42</sub> [M+3H]<sup>3+</sup> 1514.3167, found (HR-ESI) 1514.3261.

**(O<sub>2</sub>N-QXQQPQXQQ)<sub>2</sub>-T (3)** Compound **7** (27.4 mg, 5.9 μmol) was treated with a 50% solution of TFA in CH<sub>2</sub>Cl<sub>2</sub> (2 mL) at r.t. for 2 h. The solvent was then removed under vacuum, yielding the product as a yellow solid (24.7 mg,

5.5  $\mu\text{mol}$ , 95%).  **$^1\text{H NMR}$**  (500 MHz,  $\text{CDCl}_3$ )  $\delta$  [ppm] 11.80 (s, 2H), 11.49 (s, 2H), 11.47 (s, 2H), 11.12 (s, 2H), 10.90 (s, 4H), 10.18 (d,  $J = 9.0$  Hz, 2H), 10.06 (s, 2H), 10.01 (s, 2H), 9.89 (d,  $J = 9.2$  Hz, 2H), 9.55 (s, 2H), 8.52 (s, 2H), 8.48 (d,  $J = 7.4$  Hz, 2H), 8.45 (d,  $J = 7.5$  Hz, 2H), 8.33 (dd,  $J = 7.9, 1.4$  Hz, 2H), 8.28 – 8.23 (m, 2H), 8.20 (dd,  $J = 6.8, 2.4$  Hz, 2H), 8.18 (dd,  $J = 7.9, 1.1$  Hz, 2H), 8.13 – 8.08 (m, 8H), 8.06 (d,  $J = 7.2$  Hz, 2H), 7.98 (d,  $J = 7.3$  Hz, 2H), 7.96 – 7.93 (m, 6H), 7.91 (dd,  $J = 7.9, 1.2$  Hz, 2H), 7.90 (dd,  $J = 7.9, 1.2$  Hz, 2H), 7.70- 7.67 (m, 4H), 7.65 – 7.61 (m, 2H), 7.49 – 7.44 (m, 8H), 7.42 – 7.29 (m, 12H), 7.24 (s, 2H), 7.19 – 7.13 (m, 8H), 7.07 -7.04 (m, 2H), 7.03 (s, 2H), 6.34 (s, 2H), 6.02 (s, 2H), 5.77 (s, 2H), 4.68 (s, 4H), 4.14 (t,  $J = 6.6$  Hz, 2H), 4.08 – 3.96 (m, 8H), 3.95 – 3.78 (m, 8H), 3.64 (t,  $J = 6.6$  Hz, 2H), 3.54 (t,  $J = 7.3$  Hz, 2H), 3.47 (t,  $J = 7.4$  Hz, 2H), 2.62 (d,  $J = 15.8$  Hz, 2H), 2.52 – 2.44 (m, 2H), 2.43 – 2.27 (m, 16H), 1.38 (d,  $J = 6.7$  Hz, 16H), 1.36 – 1.32 (m, 16H), 1.24 – 1.19 (m, 30H), 1.19 – 1.17 (m, 6H), 1.15 (d,  $J = 6.8$  Hz, 6H). **HRMS** calcd for  $\text{C}_{238}\text{H}_{228}\text{N}_{40}\text{O}_{42}$   $[\text{M}+2\text{H}]^{2+}$  2158.8462, found (HR-ESI) 2158.8540.

**$\text{O}_2\text{N-XQQPQXQQPQXQQ-OH}$  (9)** Compound **9** was synthesized using the SPS procedures previously reported<sup>7</sup> on SASRIN resin (scale: 15  $\mu\text{mol}$ ). The crude product was purified via precipitation in DCM/MeOH, and the product was obtained as a yellow solid (14.7 mg, 5.1  $\mu\text{mol}$ , 34%).  **$^1\text{H NMR}$**  (500 MHz,  $\text{CDCl}_3$ )  $\delta$  [ppm] 11.11 (s, 1H), 11.05 (s, 1H), 10.83 (s, 1H), 10.66 (s, 1H), 10.61 (s, 1H), 10.60 (s, 1H), 10.51 (s, 1H), 10.36 (s, 1H), 10.22 (s, 1H), 10.08 (s, 1H), 10.01 (s, 1H), 8.05 (dd,  $J = 8.1, 1.4$  Hz, 1H), 7.97 (dd,  $J = 7.3, 1.3$  Hz, 1H), 7.95 (s, 2H), 7.90 (dd,  $J = 7.5, 1.3$  Hz, 2H), 7.88 – 7.85 (m, 2H), 7.79 (dd,  $J = 7.4, 1.2$  Hz, 1H), 7.74 (ddd,  $J = 8.2, 5.1, 1.3$  Hz, 2H), 7.69 (ddd,  $J = 8.1, 4.6, 1.4$  Hz, 2H), 7.65 (ddd,  $J = 8.1, 4.3, 1.3$  Hz, 2H), 7.62 – 7.59 (m, 2H), 7.58 – 7.55 (m, 2H), 7.51 – 7.46 (m, 4H), 7.44 – 7.40 (m, 2H), 7.36 (dd,  $J = 7.4, 1.3$  Hz, 1H), 7.24 – 7.21 (m, 2H), 7.19 – 7.15 (m, 6H), 7.09 (dd,  $J = 7.2, 1.4$  Hz, 1H), 7.06 – 7.02 (m, 1H), 7.02 – 6.99 (m, 2H), 6.97 – 6.89 (m, 6H), 6.83 (t,  $J = 7.8$  Hz, 1H), 6.80 (ddd,  $J = 7.8, 4.8, 3.5$  Hz, 2H), 6.75 (d,  $J = 7.4$  Hz, 1H), 6.69 (dd,  $J = 7.4, 1.5$  Hz, 1H), 6.69 – 6.62 (m, 2H), 6.51 (s, 1H), 6.48 (s, 1H), 6.32 (s, 1H), 6.23 (s, 1H), 6.17 (s, 1H), 5.64 (s, 1H), 5.39 (s, 1H), 4.07-4.03 (q,  $J = 7.2$  Hz, 1H), 3.86 – 3.82 (m, 3H), 3.78 – 3.74 (m, 2H), 3.71 – 3.63 (m, 4H), 3.61 – 3.53 (m, 6H), 3.44 – 3.40 (m, 2H), 3.36 (t,  $J = 7.6$  Hz, 1H), 3.16 – 3.09 (m, 2H), 2.88 (s, 6H), 2.81 (s, 6H), 2.36 – 2.28 (m, 2H), 2.25 – 2.20 (m, 2H), 2.19 – 2.09 (m, 3H), 2.08 – 2.01 (m, 1H), 1.97 (s, 1H), 1.95 – 1.90 (m, 1H), 1.64 (s, 10H), 1.62 (s, 10H), 1.58 (s, 10H), 1.22 – 1.14 (m, 7H), 1.10 – 1.02 (m, 13H), 0.99 – 0.94 (m, 4H). **HRMS** calcd for  $\text{C}_{168}\text{H}_{168}\text{N}_{26}\text{O}_{27}$   $[\text{M}+2\text{H}]^{2+}$  1490.6281, found (HR-ESI) 1491.6532.

**$(\text{O}_2\text{N-XQQPQXQQPQXQQ})_2\text{-T}$  (10)** Compound **9** (7.7 mg, 2.6  $\mu\text{mol}$ , 1 eq.), 2,6-diisobutoxyterephthalohydrazide (**8**)<sup>1</sup> (0.4 mg, 1.3  $\mu\text{mol}$ , 0.5 eq.) and PyBOP (0.7 mg, 1.4  $\mu\text{mol}$ , 3 eq.) were dissolved in dry  $\text{CHCl}_3$  under  $\text{N}_2$ . Then DIPEA (0.2  $\mu\text{L}$ , 1.4  $\mu\text{mol}$ , 3 eq.) was added, and the solution was stirred at r.t. for 1 week. The solvent was removed under vacuum, and the crude was purified via GPC. The product was recovered after washing with a 5% citric acid solution, drying over  $\text{MgSO}_4$  and removal of solvent as a yellow solid (3.75 mg, 23% yield).  **$^1\text{H NMR}$**  (500 MHz,  $\text{CDCl}_3$ )  $\delta$  [ppm] 11.22 (s, 2H), 11.00 (s, 2H), 10.79 (s, 2H), 10.63 (s, 2H), 10.61 (s, 2H), 10.57 (s, 2H), 10.30 (s, 2H), 10.15 (s, 2H), 10.10 (s, 2H), 10.05 (d,  $J = 9.1$  Hz, 2H), 9.94 (s, 2H), 9.75 (d,  $J = 9.0$  Hz, 2H), 8.01 (dd,  $J = 7.9, 1.4$  Hz, 2H), 7.94 (t,  $J = 6.3$  Hz, 4H), 7.79 (s, 2H), 7.75 – 7.67 (m, 10H), 7.65 – 7.60 (m, 10H), 7.57 (dd,  $J = 8.0, 1.3$  Hz, 4H), 7.50 – 7.48 (m, 2H), 7.44 (s, 2H), 7.42 (s, 2H), 7.40 – 7.38 (m, 3H), 7.35-7.31 (t,  $J = 7.3$  Hz, 4H), 7.24 (q,  $J = 7.0$  Hz, 2H), 7.18 – 7.10 (m, 8H), 7.09 – 7.05 (m, 4H), 7.03



– 6.99 (m, 4H), 6.96 (dd,  $J = 14.4, 7.0$  Hz, 4H), 6.91 – 6.82 (m, 6H), 6.82 (s, 2H), 6.79 (q,  $J = 7.3, 6.5$  Hz, 4H), 6.73 (dd,  $J = 12.4, 7.0$  Hz, 4H), 6.67 (dd,  $J = 12.1, 6.5$  Hz, 4H), 6.64–6.59 (m, 2H), 6.54 (s, 2H), 6.46 (s, 2H), 6.41 (s, 2H), 6.19 (s, 2H), 6.15 (s, 2H), 5.63 (s, 2H), 5.59 (s, 2H), 5.39 (s, 2H), 5.21 – 5.16 (m, 4H), 4.25 – 4.19 (m, 10H), 4.11 – 4.06 (m, 10H), 3.88 – 3.79 (m, 6H), 3.77 – 3.70 (m, 4H), 3.69 – 3.65 (m, 14H), 3.64 – 3.51 (m, 14H), 3.48 – 3.45 (m, 2H), 3.39 (s, 8H), 3.35 – 3.31 (m, 2H), 3.11 – 3.08 (m, 2H), 3.06 – 3.01 (m, 2H), 2.95 – 2.90 (m, 2H), 2.35 – 2.29 (m, 4H), 2.28 – 2.23 (m, 12H), 2.17 – 2.11 (m, 4H), 2.10 (s, 2H), 2.01 (s, 10H), 2.01 (s, 10H), 2.00 (s, 10H), 1.97 (s, 12H), 1.75 (s, 4H), 1.65 – 1.64 (m, 8H), 1.53 (s, 18H), 1.28 (s, 12H), 1.17 – 1.12 (m, 6H), 1.09 – 0.98 (m, 18H), 0.91 (s, 2H), 0.83 – 0.74 (m, 13H). (mixture of two diastereomers *PP* and *PM* and their ratio is 10:1, only the major peaks are reported). **HRMS** calcd for  $C_{352}H_{356}N_{56}O_{58}$   $[M+2H]^{2+}$  3131.3360, found (HR-ESI) 3132.0238.

**(O<sub>2</sub>N-XQQPQXQQPQXQQ)<sub>2</sub>-T (4)** Compound **10** (0.6 mg, 0.1  $\mu$ mol) was treated with a 50% solution of TFA in  $CH_2Cl_2$  (2 mL) at r.t. for 2 h. The solvent was then removed under vacuum, yielding the product as a yellow solid (quant.). **<sup>1</sup>H NMR** (500 MHz,  $CDCl_3$ )  $\delta$  [ppm] 11.40 (s, 2H), 11.22 (s, 2H), 11.13 (s, 2H), 11.12 (s, 2H), 10.88 (s, 2H), 10.60 (s, 2H), 10.47 (s, 2H), 10.34 (s, 2H), 10.19 (s, 2H), 10.00 (d,  $J = 9.0$  Hz, 2H), 9.84 (s, 2H), 9.68 (d,  $J = 9.0$  Hz, 2H), 9.28 (s, 2H), 9.19 (s, 2H), 8.27 (d,  $J = 7.1$  Hz, 2H), 8.21 (d,  $J = 7.2$  Hz, 2H), 8.13 (d,  $J = 7.8$  Hz, 2H), 8.08 (s, 2H), 8.04 – 8.02 (m, 2H), 8.01 (s, 1H), 7.98 (d,  $J = 6.9$  Hz, 2H), 7.94 (d,  $J = 7.4$  Hz, 2H), 7.85 (d,  $J = 7.8$  Hz, 2H), 7.82 (d,  $J = 7.8$  Hz, 2H), 7.79 – 7.76 (m,  $J = 7.78$ , 12H), 7.76 – 7.72 (m,  $J = 7.74$ , 10H), 7.71 – 7.67 (m, 4H), 7.57 (d,  $J = 7.1$  Hz, 2H), 7.43 (t,  $J = 7.4$  Hz, 2H), 7.40 (s, 1H), 7.37 (d,  $J = 6.9$  Hz, 2H), 7.26 – 7.20 (m, 20H), 7.18 (s, 6H), 7.17 – 7.12 (m, 10H), 7.12 – 7.06 (m, 10H), 6.99 (s, 2H), 6.98 (s, 2H), 6.97 – 6.94 (m, 6H), 6.92 – 6.87 (m, 8H), 6.86 – 6.83 (m,  $J = 6.85$ , 8H), 6.76 (s, 2H), 6.50 (s, 2H), 6.28 (s, 2H), 5.97 (s, 2H), 5.91 (s, 2H), 5.78 (s, 2H), 5.49 (s, 2H), 3.96 – 3.91 (m, 6H), 3.90 – 3.85 (m, 6H), 3.84 – 3.79 (m, 10H), 3.76 – 3.68 (m, 14H), 3.68 – 3.61 (m, 10H), 3.60 – 3.55 (m, 3H), 3.51 – 3.46 (m, 6H), 3.44 (s, 1H), 3.32 – 3.30 (m, 2H), 2.39 – 2.29 (m, 14H), 2.27 – 2.20 (m, 14H), 2.19 – 2.13 (m, 8H), 2.12 – 2.07 (m, 6H), 2.02 (s, 1H), 2.01 – 2.00 (m, 2H), 1.97 – 1.93 (m, 6H), 1.59 – 1.56 (m, 2H), 1.53 – 1.47 (m, 3H), 1.45 – 1.38 (m, 2H), 1.10 – 1.06 (m, 2H), 1.05 – 1.02 (m, 6H), 0.98 – 0.92 (m, 6H), 0.67 – 0.63 (m, 8H). **HRMS** calcd for  $C_{328}H_{306}N_{56}O_{56}$   $[M+2H]^{2+}$  2963.14, found (HR-ESI) 2963.14; calcd for  $C_{328}H_{307}N_{56}O_{56}$   $[M+3H]^{3+}$  1975.7679, found (HR-ESI) 1975.7618.

**O<sub>2</sub>N-XQQPQXQQPQXQQPQXQQ-OH (11)** Compound **11** was synthesized using the SPS procedures previously reported<sup>7</sup> on SASRIN resin (scale: 58  $\mu$ mol). The crude product was purified via precipitation in DCM/MeOH, and the product was obtained as a yellow solid (33.4 mg, 8.2  $\mu$ mol, 14.1%). **<sup>1</sup>H NMR** (500 MHz,  $CDCl_3$ )  $\delta$  [ppm] 11.04 (s, 1H), 10.98 (s, 1H), 10.74 (s, 1H), 10.51 (s, 1H), 10.44 (s, 1H), 10.42 (s, 1H), 10.38 (s, 1H), 10.16 (s, 1H), 10.01 (s, 1H), 10.00 (s, 1H), 9.96 (s, 1H), 9.89 (s, 1H), 9.86 (s, 1H), 9.57 (s, 1H), 8.02 – 8.00 (m, 1H), 7.91 – 7.89 (m, 2H), 7.83 (ddd,  $J = 14.1, 7.3, 1.2$  Hz, 3H), 7.76 (s, 1H), 7.73 (dd,  $J = 7.2, 1.1$  Hz, 1H), 7.69 (dd,  $J = 8.1, 1.2$  Hz, 1H), 7.66 – 7.63 (m, 2H), 7.61 – 7.49 (m, 11H), 7.45 (s, 1H), 7.42 – 7.39 (m, 3H), 7.38 – 7.31 (m, 6H), 7.23 – 7.20 (m, 1H), 7.18 – 7.15 (m, 4H), 7.15 – 7.10 (m, 4H), 7.09–7.05 (qd,  $J = 7.3, 1.3$  Hz, 4H), 7.00 (d,  $J = 4.6$  Hz, 2H), 6.96 (dd,  $J = 14.9, 7.4$  Hz, 2H), 6.90 – 6.90 (m, 1H), 6.89 – 6.88 (m, 1H), 6.88 – 6.78 (m, 9H), 6.77 – 6.70 (m, 4H), 6.69 – 6.63 (m, 4H), 6.63–6.56 (m, 3H), 6.56 – 6.49 (m, 5H), 6.28 (s, 1H), 6.15 (s, 1H), 6.05 (s, 1H), 5.85 (s, 1H), 5.60 (s, 1H), 5.53 (s, 1H), 5.46 (s, 1H), 5.27 (s, 1H), 5.21 (s, 1H), 4.32 (s, 1H), 3.96

(s, 1H), 3.82 – 3.59 (m, 12H), 3.55 – 3.43 (m, 12H), 3.36 – 3.26 (m, 6H), 3.04 – 3.00 (m, 3H), 2.81 – 2.77 (m, 2H), 2.30 – 2.22 (m, 4H), 2.20 – 1.98 (m, 14H), 1.14 – 1.05 (m, 32H), 1.04 – 0.99 (m, 32H), 0.98 (s, 2H), 0.96 – 0.92 (m, 8H). **HRMS** calcd for  $C_{231}H_{230}N_{36}O_{36} [M+2H]^{2+}$  2041.8631, found (HR-ESI) 2041.8769.

**(O<sub>2</sub>N-XQQPQXQQPQXQQPQXQQ)<sub>2</sub>-T (12)** Compound **11** (11.0 mg, 2.6 μmol, 1 eq.), 2,6-diisobutoxyterephthalohydrazide (**8**)<sup>1</sup> (0.5 mg, 1.3 μmol, 0.5 eq.) and PyBOP (4.2 mg, 8.1 μmol, 3 eq.) were dissolved in dry CHCl<sub>3</sub> under N<sub>2</sub>. Then DIPEA (1.4 μL, 1.0 μmol, 3 eq.) was added, and the solution was stirred at r.t. for 2 weeks. The solvent was removed under vacuum, and the crude was purified via GPC. The product was recovered after washing with a 5% citric acid solution, drying over MgSO<sub>4</sub> and removal of solvent as a yellow solid (2 mg, 0.2 μmol, 9% yield). **<sup>1</sup>H NMR** (500 MHz, CDCl<sub>3</sub>) δ [ppm] 11.13 (s, 2H), 10.95 (s, 2H), 10.72 (s, 2H), 10.52 (s, 4H), 10.37 (s, 2H), 10.28 (s, 2H), 10.12 (s, 2H), 9.99 – 9.90 (m, 8H), 9.84 (s, 2H), 9.82 (s, 2H), 9.67 (d, *J* = 8.9 Hz, 2H), 9.49 (s, 2H), 7.98 (d, *J* = 7.5 Hz, 2H), 7.87 (dd, *J* = 11.5, 6.7 Hz, 4H), 7.73 – 7.69 (m, 4H), 7.67 – 7.61 (m, 8H), 7.59 – 7.52 (m, 12H), 7.51 – 7.46 (m, 9H), 7.43 – 7.41 (m, 5H), 7.40 – 7.37 (m, 5H), 7.32 – 7.31 (m, 3H), 7.28 – 7.26 (m, 4H), 7.25 – 7.22 (m, 4H), 7.16 – 7.06 (m, 12H), 7.05 – 6.99 (m, 5H), 6.94 – 6.90 (m, 6H), 6.87 – 6.81 (m, 6H), 6.77 – 6.67 (m, 18H), 6.66 – 6.64 (m, 3H), 6.62 – 6.60 (m, 5H), 6.59 – 6.52 (m, 5H), 6.49 – 6.44 (m, 4H), 6.42 – 6.35 (m, 4H), 6.10 (s, 2H), 6.03 (s, 2H), 5.84 (s, 2H), 5.58 (s, 2H), 5.46 (s, 2H), 5.41 (s, 2H), 5.22 (s, 2H), 5.20 (s, 2H), 3.79 – 3.75 (m, 5H), 3.70 – 3.49 (m, 34H), 3.46 – 3.39 (m, 12H), 3.37 – 3.22 (m, 15H), 3.13–3.05 (m, 5H), 2.30 – 2.20 (m, 10H), 2.10 – 2.02 (m, 14H), 1.98 – 1.92 (m, 4H), 1.82 – 1.73 (m, 8H), 1.67 (s, 4H), 1.63 (s, 5H), 1.59 (s, 8H), 1.51 (s, 22H), 1.48 (s, 20H), 1.41 (s, 18H), 1.37 (s, 5H), 1.18 – 1.08 (m, 26H), 1.06 – 1.03 (m, 25H), 1.02 – 0.93 (m, 40H), 0.84 – 0.72 (m, 22H). (mixture of two diastereomers *PP* and *PM* and their ratio is 10:1, only the major peaks are reported). **HRMS** calcd for  $C_{478}H_{481}N_{76}O_{74} [M+3H]^{3+}$  2822.8732, found (HR-ESI) 2823.2296; calcd for  $C_{478}H_{482}N_{76}O_{74} [M+4H]^{4+}$  2117.4067, found (HR-ESI) 2117.6679.

**(O<sub>2</sub>N-XQQPQXQQPQXQQPQXQQ)<sub>2</sub>-T (5)**. Compound **12** (2 mg, 0.2 μmol) was treated with a 50% solution of TFA in CH<sub>2</sub>Cl<sub>2</sub> (2 mL) at r.t. for 2 h. The solvent was then removed under vacuum, yielding the product as a yellow solid (quant.). **<sup>1</sup>H NMR** (500 MHz, CDCl<sub>3</sub>) δ [ppm] 11.28 (s, 1H), 11.13 (s, 2H), 10.98 (s, 2H), 10.82 (s, 3H), 10.80 (s, 2H), 10.37 (d, *J* = 14.0 Hz, 2H), 10.16 (s, 2H), 10.11 (s, 2H), 10.00 (s, 4H), 9.98 (s, 2H), 9.97 (s, 2H), 9.78 (s, 2H), 9.73 (s, 2H), 9.62 (d, *J* = 8.9 Hz, 2H), 9.18 (s, 2H), 8.91 (s, 4H), 8.27 (s, 1H), 8.18 (d, *J* = 6.7 Hz, 2H), 8.12 (d, *J* = 6.9 Hz, 2H), 8.06 – 7.94 (m, 4H), 8.00 – 7.97 (m, 1H), 7.94 (d, *J* = 7.5 Hz, 2H), 7.75 – 7.64 (m, 9H), 7.63 – 7.49 (m, 10H), 7.48 – 7.41 (m, 8H), 7.39 – 7.34 (m, 7H), 7.31 – 7.24 (m, overlap with residual solvent peak), 7.16 – 7.09 (m, 11H), 7.08 – 7.01 (m, 10H), 6.95 – 6.89 (m, 8H), 6.87 – 6.84 (m, 10H), 6.81 – 6.78 (m, 10H), 6.76 – 6.70 (m, 9H), 6.66 – 6.60 (m, 10H), 6.45 (s, 2H), 6.41 – 6.37 (m, 2H), 5.93 (s, 2H), 5.86 (s, 2H), 5.83 (s, 2H), 5.71 (s, 2H), 5.66 (s, 2H), 5.57 – 5.49 (m, 4H), 5.42 (s, 2H), 5.33 – 5.26 (m, 10H), 3.96 (d, *J* = 9.5 Hz, 12H), 3.76 – 3.48 (m, 28H), 3.45 – 3.41 (m, 5H), 3.34 (s, 2H), 3.26 (s, 3H), 2.30 – 2.27 (m, 21H), 2.25 – 2.17 (m, 19H), 1.60 – 1.55 (m, 21H), 1.53 – 1.48 (m, 39H), 1.44 – 1.38 (m, 23H), 1.08 – 0.98 (m, 22H), 0.97 – 0.89 (m, 11H), 0.70 – 0.62 (m, 28H). **HRMS** calcd for  $C_{446}H_{414}N_{76}O_{76} [M]$  8017.0969, found (HR-MALDI-TOF, THAP) 8017.1500.

### 3.2.6 References

1. S. De, B. Chi, T. Granier, T. Qi, V. Maurizot and I. Huc, *Nat. Chem.*, 2018, **10**, 51-57.
2. W. Kabsch, *Acta Cryst.*, 2010, **D66**, 125.
3. Rigaku-Oxford-Diffraction, *CrysAlisPro Software System, Version 171.41*, 2020, Rigaku Corporation: Wrocław, Poland.
4. G. M. Sheldrick, *Acta Cryst.*, 2015, **A71**, 3–8.
5. G. M. Sheldrick, *Acta Cryst.*, 2015, **C71**, 3-8.
6. O. V. Dolomanov, L. J. Bourhis, R. J. Gildea, J. A. K. Howard and H. Puschmann, *J. Appl. Cryst.*, 2009, **42**, 339-341.
7. B. Baptiste, C. Douat-Casassus, K. Laxmi-Reddy, F. Godde and I. Huc, *J. Org. Chem.*, 2010, **75**, 7175-7185.
8. D. Mazzier, S. De, B. Wicher, V. Maurizot and I. Huc, *Chem. Sci.*, 2019, **10**, 6984-6991.
9. M. Vallade, P. Sai Reddy, L. Fischer and I. Huc, *Eur. J. Org. Chem.*, 2018, **2018**, 5489-5498.
10. X. Hu, S. J. Dawson, Y. Nagaoka, A. Tanatani and I. Huc, *J. Org. Chem.*, 2016, **81**, 1137-1150.

### 3.2.7 $^1\text{H}$ NMR spectra of new compounds

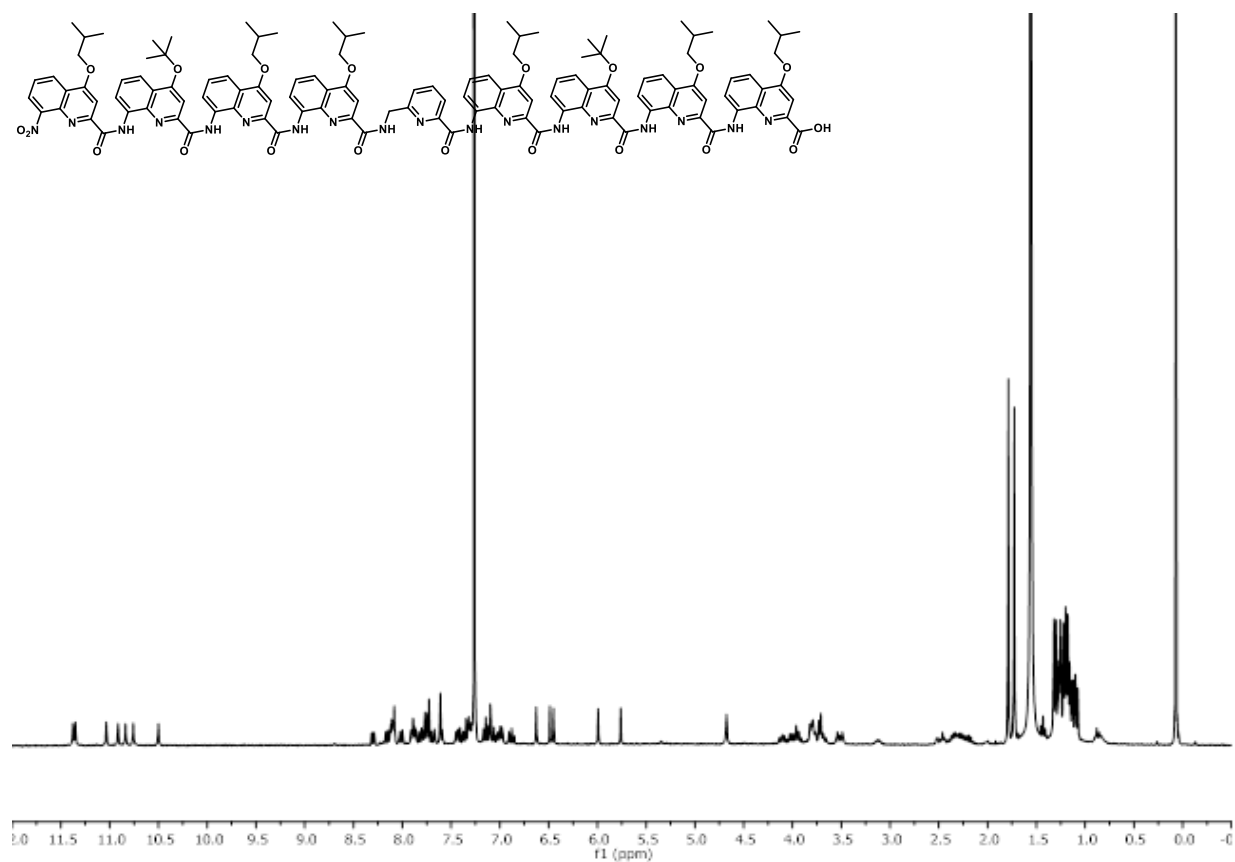


**Figure S20.**  $^1\text{H}$  NMR spectrum (300 MHz,  $\text{CDCl}_3$ ) of **6**.

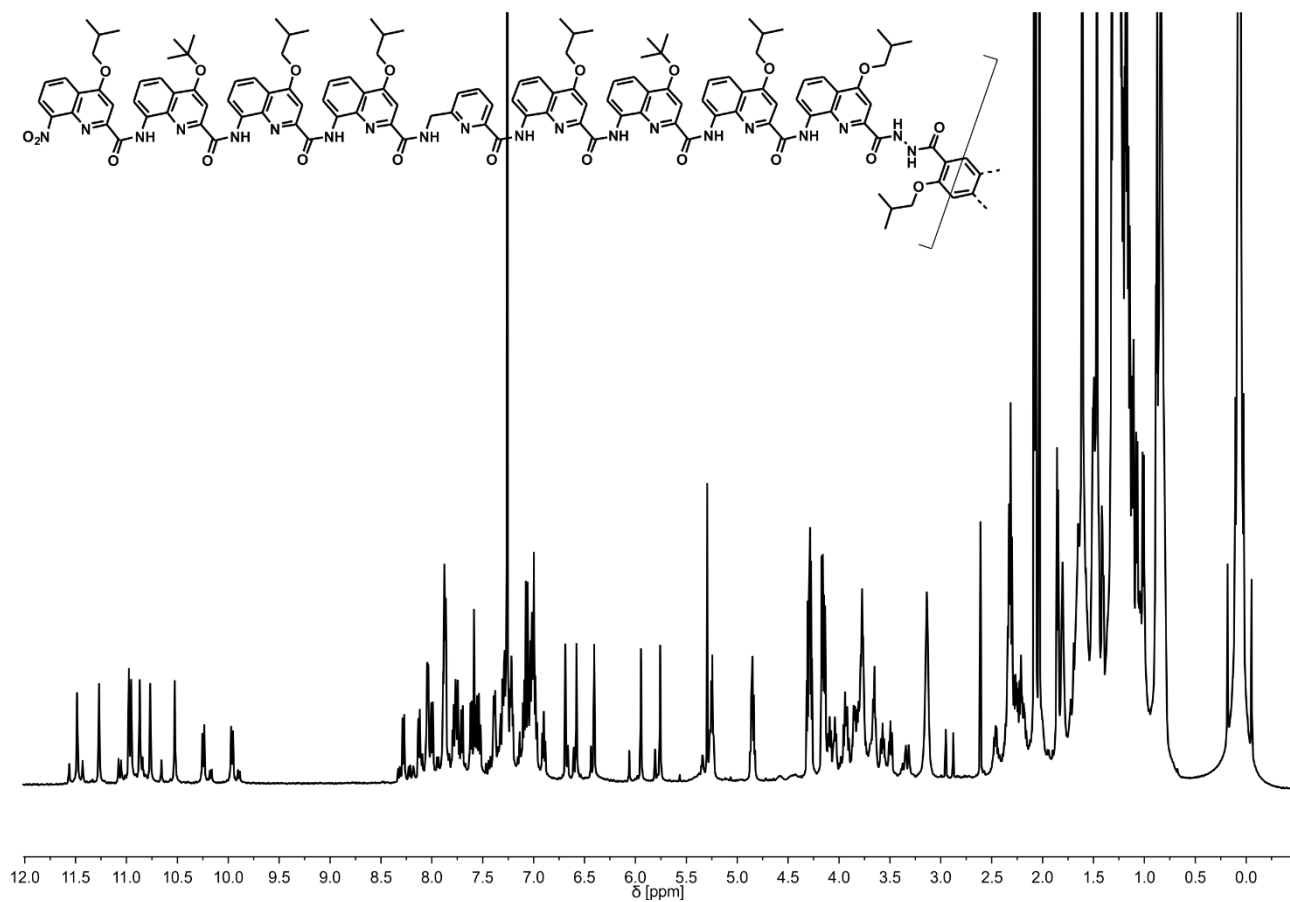


**Figure S21.** <sup>1</sup>H NMR spectrum (400 MHz, CDCl<sub>3</sub>) of 7.

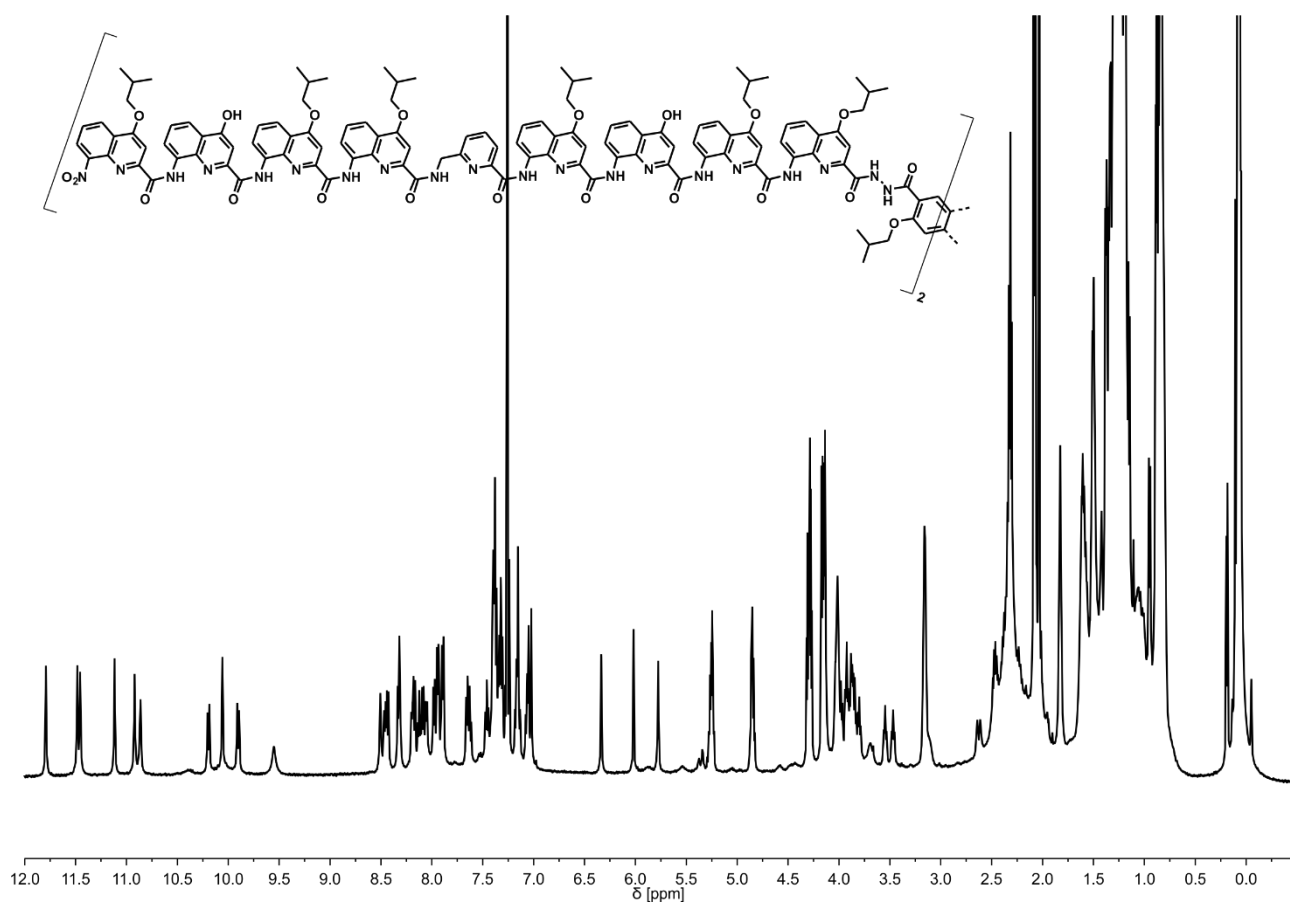


**Figure S22.** <sup>1</sup>H NMR spectrum (500 MHz, CDCl<sub>3</sub>) of **3**.

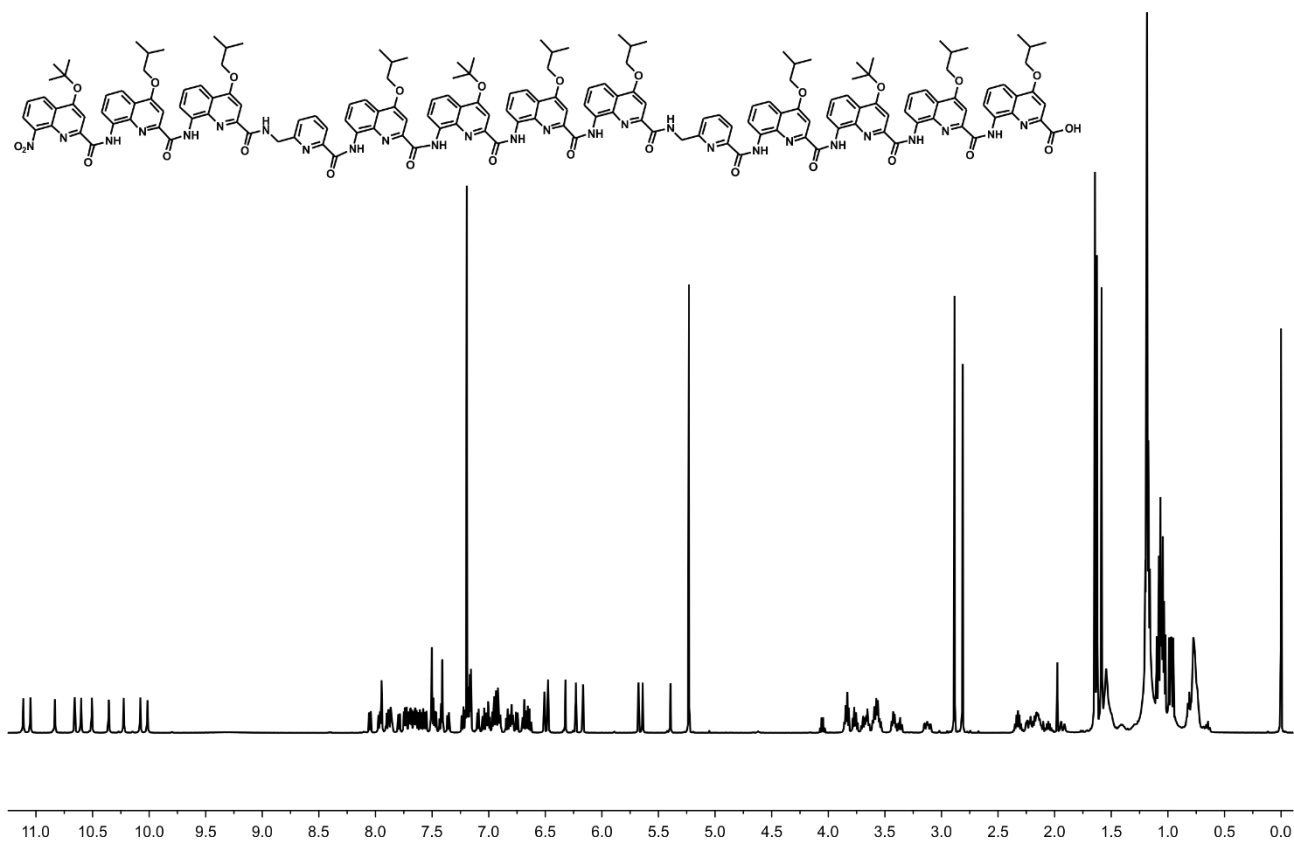


**Figure S23.**  $^1\text{H}$  NMR spectrum (500 MHz,  $\text{CDCl}_3$ ) of **9**.

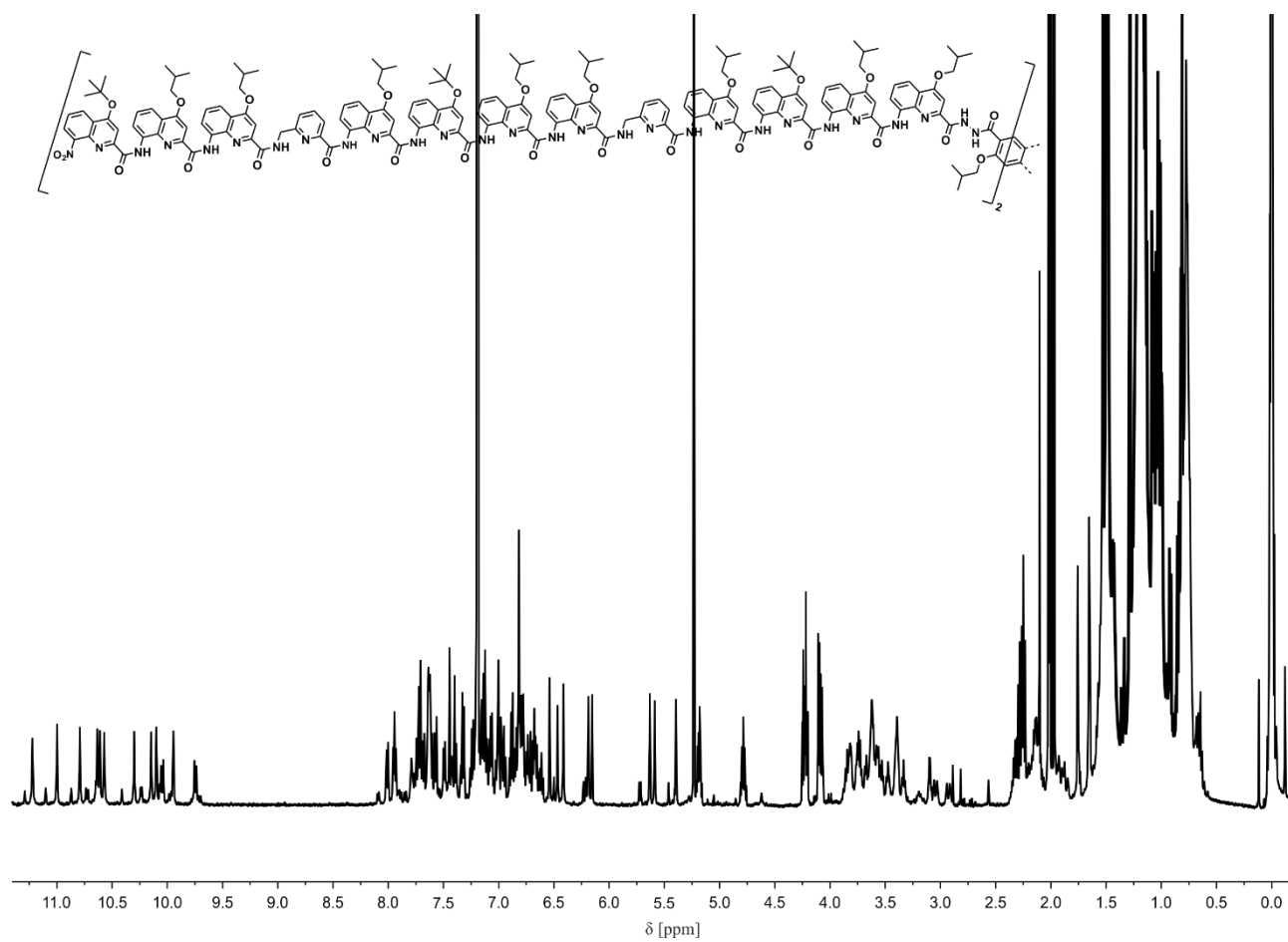


**Figure S24.** <sup>1</sup>H NMR spectrum (500 MHz, CDCl<sub>3</sub>) of **10**.



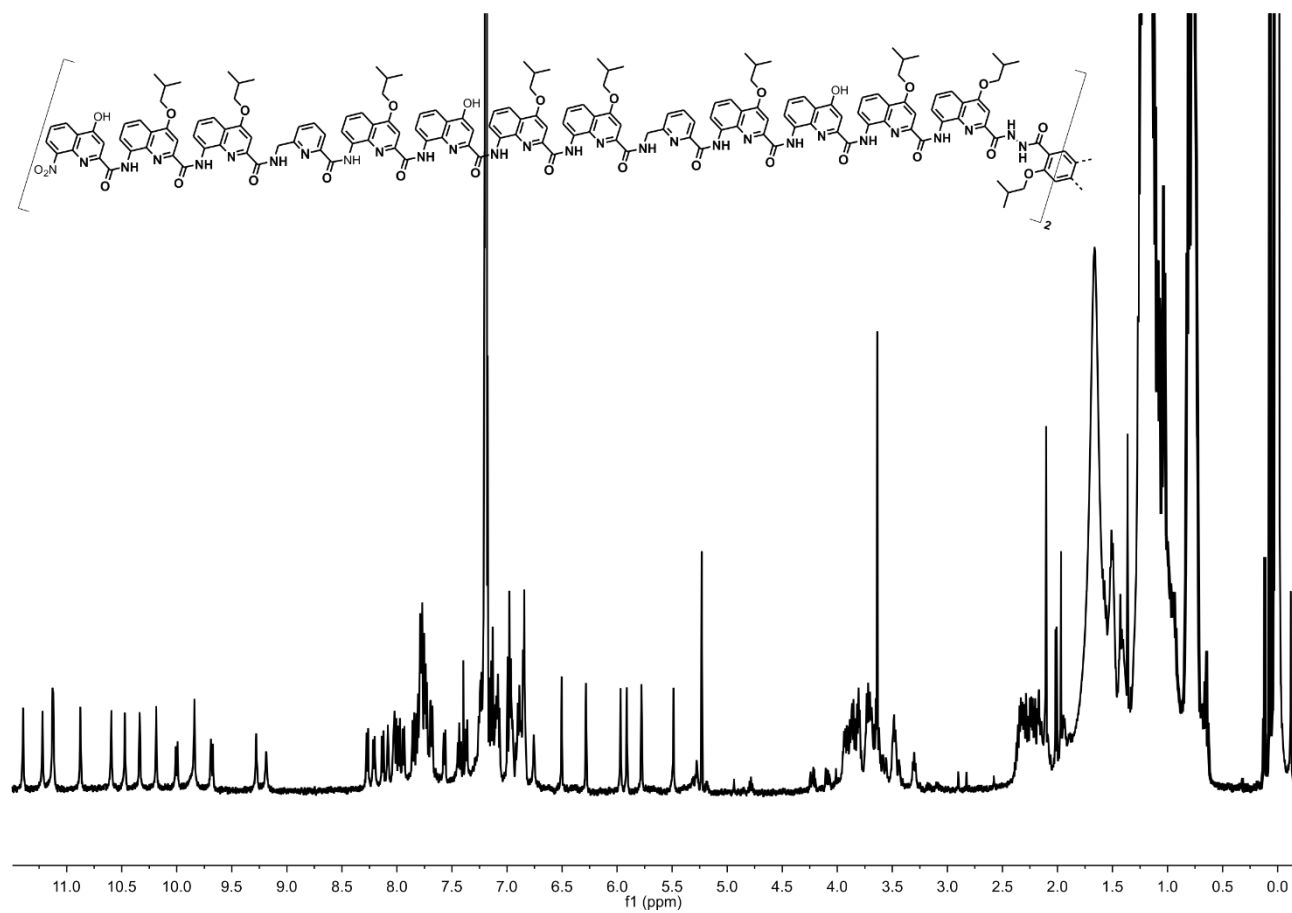


**Figure S25.** <sup>1</sup>H NMR spectrum (500 MHz, CDCl<sub>3</sub>) of **4**.

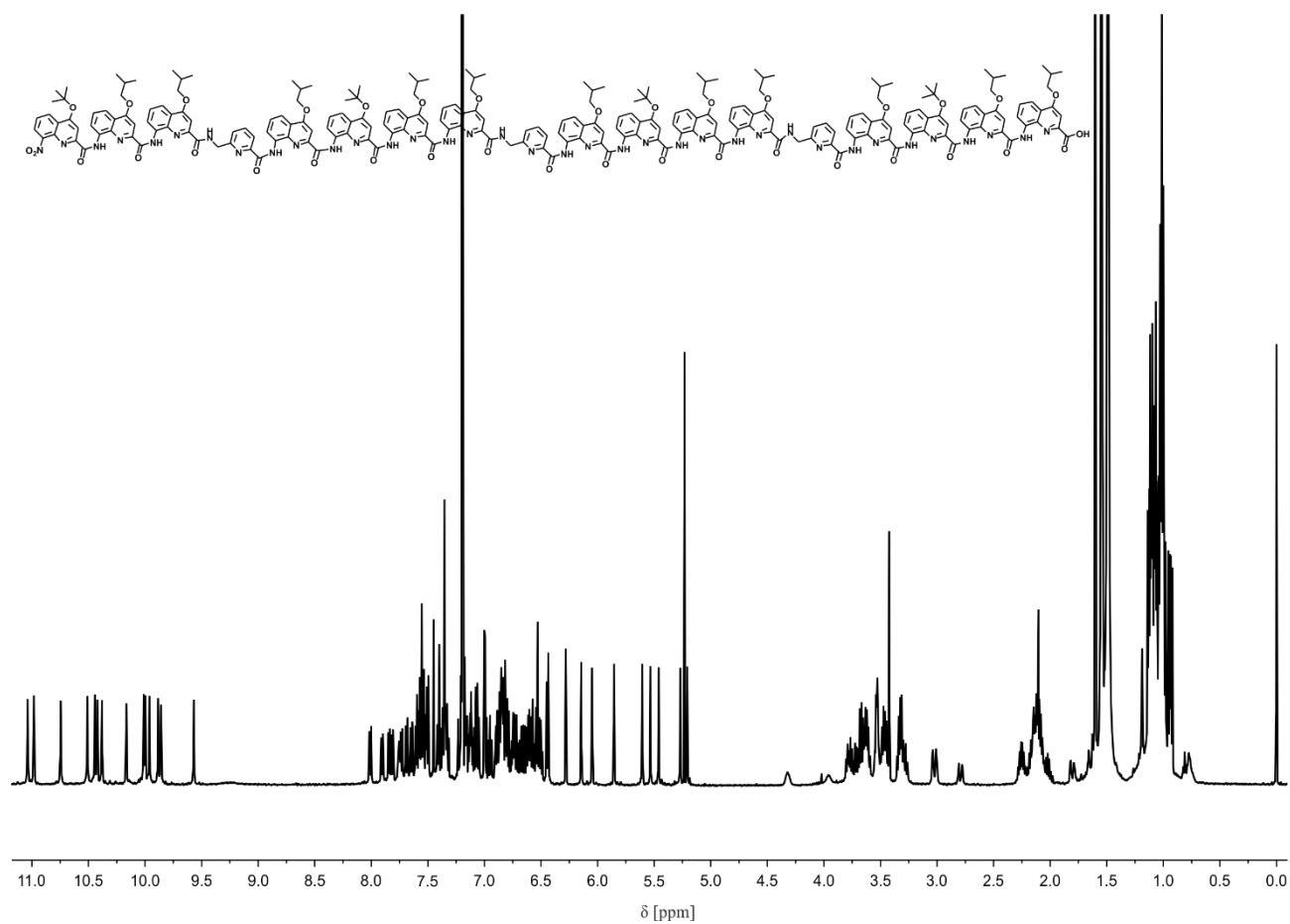


**Figure S26.** <sup>1</sup>H NMR spectrum (500 MHz, CDCl<sub>3</sub>) of **11**.

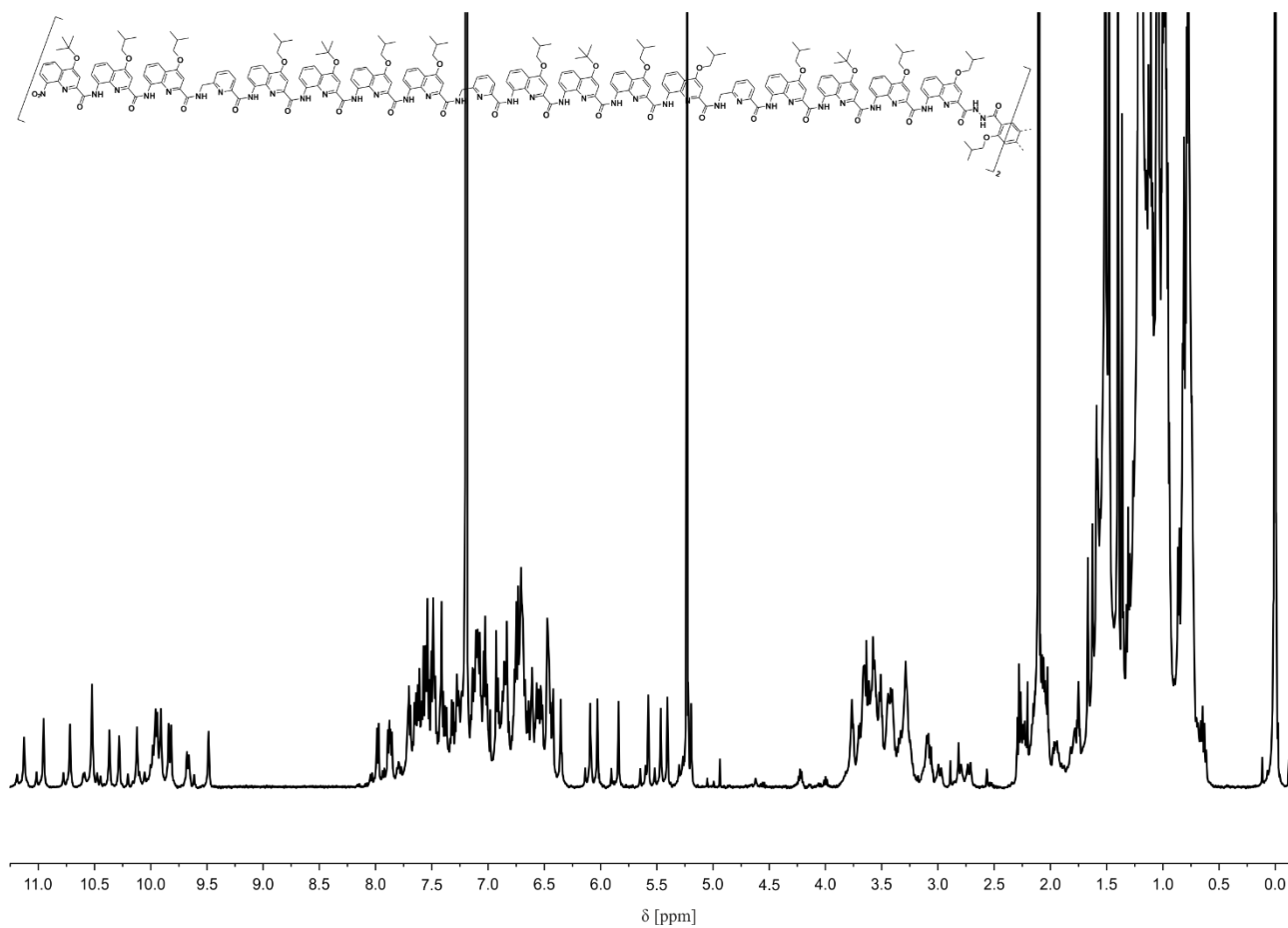


**Figure S27.** <sup>1</sup>H NMR spectrum (500 MHz, CDCl<sub>3</sub>) of **12**.

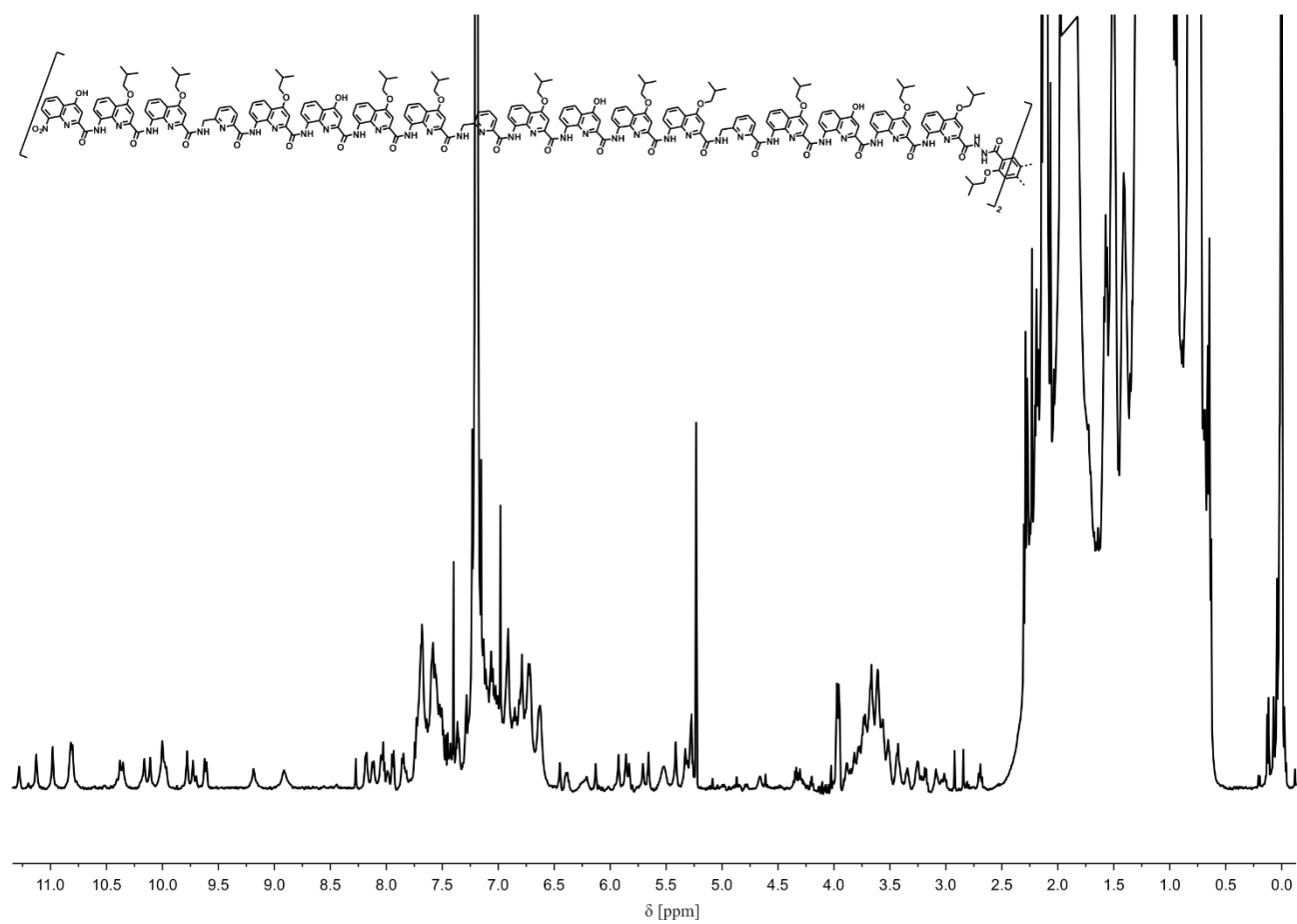


**Figure S28.** <sup>1</sup>H NMR spectrum (500 MHz, CDCl<sub>3</sub>) of 5.

## 4 Effect of a linear array of hydrogen bond donors in a single helix on its self-assembly behavior

Previous work in the field of *abiotic* foldamers takes advantage of the very stable helical folding of quinoline based foldamers. Stabilized by key hydrogen bonds, these foldamers formed the first true *abiotic* tertiary structure with a helix-turn-helix motif. In this tertiary folding the helices are parallel to one another, thus this structure is referred to as a parallel dimer. Here, computational modelling has successfully been used to predict its shape and structure. The molecular shape in such a tertiary fold is not only supported by intramolecular hydrogen bonding but also by a rigid turn unit that links the two helices together. This stabilizes the formation of a parallel dimer while preventing the formation of other aggregates. So far, self-assemblies without support of such a stabilizing turn unit created a diversity of unpredicted aggregates, such as tilted dimer and trimer formation (Figure 4.1a). These two aggregates are very different from one another. While the helices in a trimeric aggregate are head-to-head parallel to one another, the helices are tilted by 60 °clockwise or 120 °anti-clockwise, respectively, in a tilted dimer. If the initial helices are comparably short in length, a tilted dimer is observed as a major species, whereas trimeric aggregates remain a minor one. When prolonging these helices, however, trimer formation becomes more dominant. Suggesting that with increased helix length, aggregates which display some kind of parallelism are favored. Yet, different aggregates were found to coexist in solution, in most cases. When looking at the front view of a single helix two columns of hydroxy groups can be seen. In other words, hydrogen bonds can start off on two sides at one helix simultaneously. In an attempt to reduce the amount of conformational variations between helices, one such column of hydroxy groups was removed from helix monomers. Furthermore, their length was increased to ensure the formation of parallel aggregates thereby excluding tilted dimer formation. As described in chapter three, the deleted hydroxy groups did not provide a strong stabilizing effect on the formation of a parallel dimer in the first place, but caused a twisting strain in its tertiary fold instead. Thus, single helices from which these hydroxy groups were removed might as well be able to form parallel dimers in solution. Another possible aggregate could be a parallel trimer formation (Figure 4.1a). Nevertheless, the possible formation of new, previously unseen, hydrogen bonding interfaces cannot be ignored.

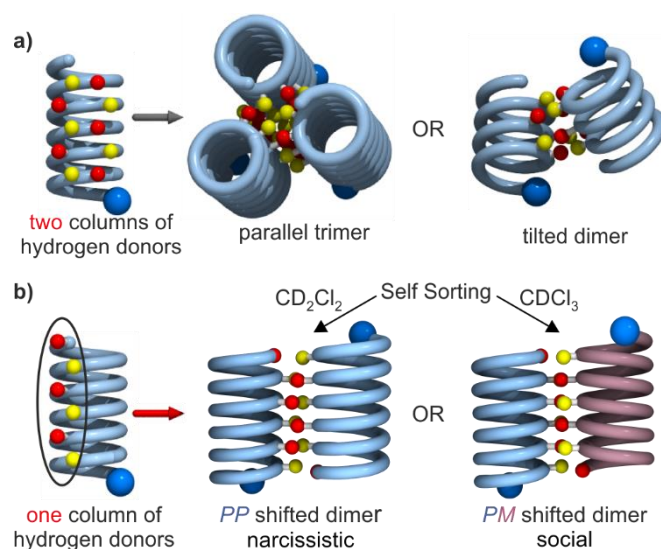


**Figure 4.1.** Self-assembly behavior of helices with two (a) and one (b) columns of hydrogen donors.

The results are summarized in a manuscript that has been accepted in *Angewandte Chemie International Edition*. Here, we show how precise point changes to the number of hydrogen bond donors within one foldamer can manipulate its hydrogen bonding interface. This did not only reduce the aggregational variance in favor of selective dimerization but also led to the discovery of chiral *self-sorting* behavior in solution. Such self-sorting behavior could be influenced by the chlorinated solvent chosen and by inducing complete handedness control. Thus either hetero- or homochiral shifted dimers formed or – in other words – either social or narcissistic chiral self-sorting occurred (Figure 4.1b).

**Contributions:** The project was planned in collaboration with V. Maurizot and I. Huc. Synthetic monomer precursors have been provided by M. Palchyk and D. Gill. Monomer synthesis has been performed by me, D. Gill and D. Bindl. Foldamer synthesis and solution state studies were carried out by me. NMR measurements have been conducted by L. Allmendinger and C. Glas. Crystals have been obtained by V. Maurizot. Crystallographic data collection was performed by B. Kauffmann at the Biophysical and Structural Chemistry platform (BPCS) at IECB, CNRS UMS3033, Inserm US001, and Bordeaux University. Crystallographic structure refinement was performed by B. Wicher. Me, V. Maurizot, I. Huc and B. Wicher contributed to experiment design and interpretation. The research was supervised by I. Huc. The manuscript was written by me and I. Huc. Me, B. Wicher, L. Allmendinger, S. Wang and I. Huc proofread and improved the manuscript.

## 4.1 Publication (published)

### Homochiral versus Heterochiral Dimeric Helical Foldamer Bundles: Chlorinated Solvent-Dependent Self-Sorting

Authors: Friedericke S. Menke,<sup>[a]</sup> Barbara Wicher,<sup>[b]</sup> Victor Maurizot,<sup>[c]</sup> and Ivan Huc\*<sup>[a]</sup>

Published: *Angew. Chem. Int. Ed.*, **2023**, 62, e202217325; *Angew. Chem.* **2023**, 135, e202217325.

(<https://doi.org/10.1002/anie.202217325>, DOI numbers 0.1002/anie.202217325 and 10.1002/ange.202217325)

**Abstract:** Aromatic oligoamide sequences programmed to fold into stable helical conformations were designed to display a linear array of hydrogen bond donors and acceptors at their surface. Sequences were synthesized on solid phase synthesis. Solution <sup>1</sup>H NMR spectroscopic studies and solid state crystallographic structures demonstrated the formation of stable hydrogen bond-mediated dimeric helix bundles that could be either heterochiral (with a *P* and an *M* helix) or homochiral (with two *P* or two *M* helices). Formation of the hetero- or homochiral dimers could be driven quantitatively using different chlorinated solvents – exemplifying a remarkable case of either social or narcissistic chiral self-sorting or upon imposing absolute handedness to the helices to forbid *PM* species.

The bundling of  $\alpha$ -helices mediated by hydrophobic residues, charge reinforced hydrogen bonds, or metal ion coordination in water is the best understood assembly mode of protein secondary structural motifs. It is amenable to design and has found applications in multiple contexts.<sup>[1]</sup> It has, for example, been extended to  $\alpha$ -peptide <sub>310</sub> helices,<sup>[2]</sup>  $\alpha/\beta$ -peptides,<sup>[3]</sup>  $\beta$ -peptides<sup>[4]</sup> and oligoureia foldamers.<sup>[5]</sup> A general feature of peptide helix bundling is the homochiral nature of the helices, which eventually gives rise to coil-coiling, that is, the winding of helices around one another. Certain amino-acid patterns have also been found to allow for bundling between L- and D-peptide helices.<sup>[6]</sup> The opposite handedness of the helices then leads to strictly parallel<sup>[7]</sup> arrangements, *i.e.* without coiling of the coils.

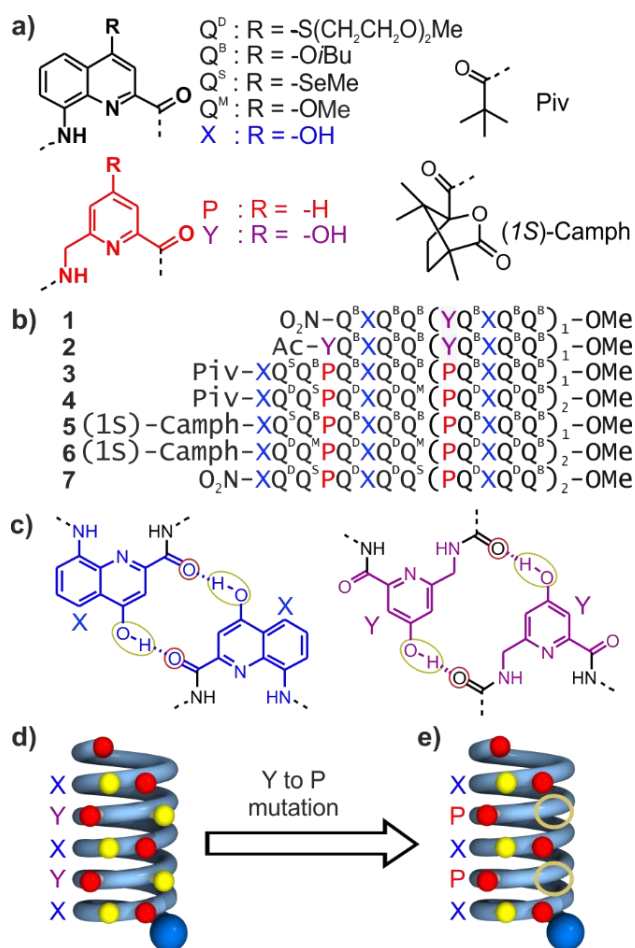


**Figure 1.** a) Structures of units Q, X, P and Y, amino acid monomers as well as N-terminal piv- and (1S)-camph groups.  $Q^D$  and  $Q^B$  carry organic solubilizing side chains.  $Q^S$  was introduced in some sequences to assist crystallographic structure elucidation using the anomalous scattering of Se, though it turned out to be unneeded.  $Q^M$  is isosteric to  $Q^S$ . b) Oligoamide foldamer sequences. In sequences ending with an 8-nitro group, this group replaces the terminal amine. c) Hydrogen-bonding patterns involving X and Y units as observed in tertiary structures in which sequences **1** or **2** are connected by a linker at their C-terminus.<sup>[9a,9c]</sup> d,e) Schematic representation of the positioning of hydrogen bond donors (yellow balls) and acceptors (red balls) at the surface of a helix containing X and Y (d) or X and P (e). The N-terminus is marked with a blue ball.

In the context of a program aiming at producing abiotic protein-like tertiary structures, we have explored the extension of helix bundling to organic solvents using aromatic foldamer helices. Starting from the structurally well-defined 2.5 helices formed by oligoamides of  $\delta$ -amino acids Q and P (Figure 1a),<sup>[8]</sup> we have introduced analogous hydroxy-functionalized X and Y monomers to create arrays of helix-to-helix hydrogen bonds between hydroxy donors and amide carbonyl acceptors. For example, when connected by a rigid linker at their C-terminus, sequences **1** and **2** form homochiral head-to-head helix-turn-helix structures stabilized by X...X and Y...Y hydrogen bonding (Figure 1c).<sup>[9]</sup> Using N-to-C helix connection with another linker, a similar, albeit heterochiral and head-to-tail, helix-turn-helix structure was generated.<sup>[9c]</sup> However, in the absence of linker, helical **1** and **2** assemble into several types of aggregates including tilted dimers in which helix axes form an angle of  $\sim 60^\circ$ , as well as trimers with all helices parallel<sup>[7]</sup> with a head-to-head arrangement of the oligomers (Figure S1).<sup>[9a]</sup> In most cases, different aggregates were found to coexist in solution. In search for better-behaved helix bundling by self-assembly, *i.e.* not guided by a rigid linker, we have now explored and report on the aggregation behavior of sequences **3-7** where Y



units have been replaced by P. These helices thus only contain X hydrogen bond donors located every five units, that is, every other helix turn, so as to form a linear array (Figure 1d). This design was motivated by the key role played by Y units in the above-mentioned aggregates (Figure S1): it was expected that removing them would change the aggregation behavior and also that long helices would favor parallel,<sup>[7]</sup> as opposed to tilted, arrangements of helix axes. Besides, helix-turn-helix folding has been shown to occur without any Y units.<sup>[10]</sup> Here, we report that the new sequences may form homo- or heterochiral helix dimers mediated by a new array of hydrogen bonds. Furthermore, we found that dimer formation was found to strongly depend on the chlorinated solvent used, namely chloroform [CDCl<sub>3</sub>], tetrachloroethane [(C<sub>2</sub>Cl<sub>4</sub>)<sub>2</sub>], dichloromethane [CD<sub>2</sub>Cl<sub>2</sub>], and dichloroethane [(C<sub>2</sub>H<sub>4</sub>Cl)<sub>2</sub>]. Thus, hetero- vs. homochiral helix association can be quantitatively reverted by changes in the solvent nature as small as going from CDCl<sub>3</sub> to CD<sub>2</sub>Cl<sub>2</sub>. Our results thus not only delivered new robust aggregation modes that can serve for future abiotic tertiary and quaternary structure design, but also the possibility to switch them. They also highlight large amplitude chlorinated solvent effects that raise questions about their generality.

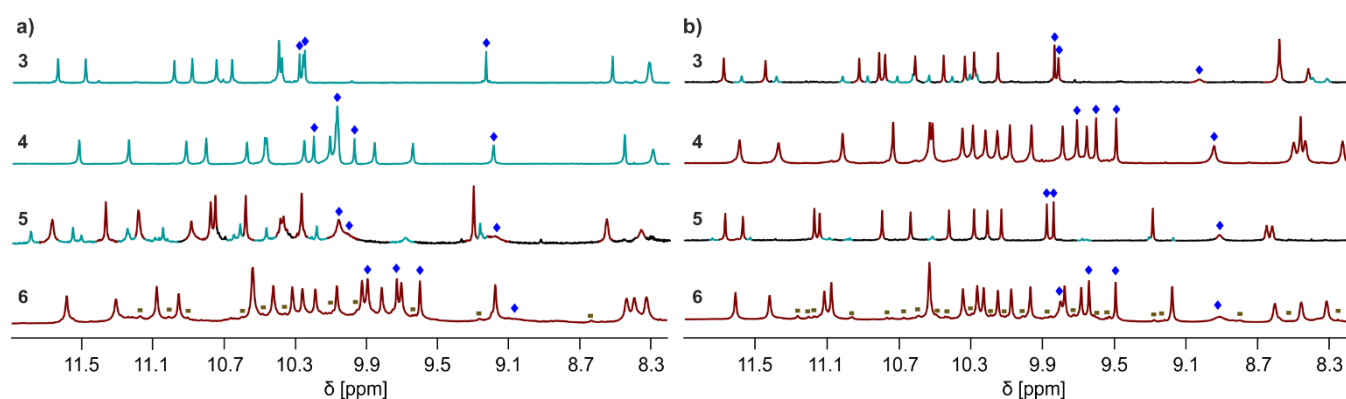


**Figure 2.** Extracts of 500 MHz <sup>1</sup>H NMR-spectra of **3-6** at 2.4 mM in CDCl<sub>3</sub> (a) and CD<sub>2</sub>Cl<sub>2</sub> (b) at 25 °C showing the amide and hydrogen-bonded OH proton resonances. Signals assigned to OH protons are marked with a blue diamond. Signals assigned to the *PM* shifted dimer and to the chiral shifted dimer are shown in turquoise and in brown, respectively. Impurities in spectra of **6** are marked with brown squares.

Sequence **3** and its extended version **4** were synthesized (see Supporting Information for details). Their <sup>1</sup>H NMR spectra in CDCl<sub>3</sub> show a single set of sharp resonances (Figure 2a). The signals of OH protons could be identified as being exchangeable with deuterium and not correlated to nitrogen in <sup>1</sup>H<sup>15</sup>N-HSQC spectra (Figures S2, S3). The chemical shift values >9 ppm of the OH protons indicated their involvement in hydrogen bonding, *i.e.* the formation of aggregates. The multiplicity of NMR signals showed that all the helices within the aggregate are in an identical environment, implying that the aggregate must be symmetrical. A solid state structure of **3** was then obtained<sup>[11]</sup> that revealed a new head-to-tail dimeric arrangement held together by six very similar intermolecular hydrogen bonds arranged in a linear array (Figure S4). Attempts to crystallize **4** were unsuccessful, but its nitro-terminated analogue **7** crystallized, and its solid state structure revealed the very same pattern as **3** extended to eight intermolecular hydrogen bonds (Figure 3a, b).<sup>[11]</sup> The conservation of the pattern for different helix lengths indicates it is robust. In both cases, the helices axes are parallel,<sup>[7]</sup> and the dimer is heterochiral (*meso*) – it involves

a *P* helix and an *M* helix – and is nearly (not crystallographically) centrosymmetric and thus, in those cases, achiral. Hydrogen bonds occur between hydroxy groups of *X* units of one helix and amide carbonyl groups preceding *P* units of the other helix or the ester carbonyl at the C-terminus (Figure 3c). This contrast with earlier parallel aggregates involving *X*...*X* and *Y*...*Y* hydrogen bonding (Figure 1c). Because the helices are now shifted (or out of register) by one helix turn with respect to earlier parallel aggregates, and the *X*-units no longer face each other, we called this new aggregates *PM* (or heterochiral) *shifted* dimers. Using molecular models, we could build alternate plausible hydrogen bond arrays between *P* and *M* helices, including one non-shifted dimer involving *X*...*X* hydrogen bonding, but these must be less stable (Figure S5, see Supporting Information for details). Dilution studies (down to 0.15 mM) led to no visible change in the <sup>1</sup>H NMR spectra of **3** and **4** suggesting a tight association in CDCl<sub>3</sub>. However, *PM* shifted dimers can be dissociated upon adding DMSO-*d*<sub>6</sub> (Figures S6, S7). Slow exchange on the NMR time scale between monomer and dimer is then observed. A dilution study in 9:1 CDCl<sub>3</sub>/DMSO-*d*<sub>6</sub> gave a *K*<sub>d</sub> of 62 μM at 25 °C in this solvent. *PM* shifted dimers thus represent a novel and robust form of heterochiral social self-sorting.<sup>[12]</sup> The *PM* shifted dimers were replaced by another species in slow exchange on the NMR timescale upon adding CD<sub>2</sub>Cl<sub>2</sub> (Figure 2b, S8, S9). In pure CD<sub>2</sub>Cl<sub>2</sub>, the replacement is quantitative for **4**. The replacement by the same species was quantitative for both **3** and **4** in (CD<sub>2</sub>Cl)<sub>2</sub> or toluene-*d*<sub>8</sub> (Figures S10-S12). In (CDCl<sub>2</sub>)<sub>2</sub>, both species coexisted for **3** (Figure S13). Upon changing solvent, equilibration sometimes took multiple days and care was taken to ascertain that samples had reached thermodynamic equilibrium (Figures S14, S15, see Supporting Information for details). The proportions between the two species in solvent where they coexist did not depend on concentration, suggesting that both are dimers (from 2.4 to 0.1 mM, Figure S16). They did not change upon heating up to 110 °C either (Figure S17). Consistently, a DOSY spectrum of **3** in CD<sub>2</sub>Cl<sub>2</sub> showed that the new aggregate has the same hydrodynamic radius as the *PM* shifted dimers (Figure S18). Signal multiplicity again indicated that the new dimer must have some sort of symmetry and <sup>1</sup>H<sup>15</sup>N-HSQC spectra in several solvents confirmed that, in all cases, hydroxy protons resonances were downfield-shifted, indicating their involvement in hydrogen bonds (Figures S19-21). We also noted that the chemical shift values of OH protons had similar patterns in the two dimers, with one signal at a slightly higher field (near 9.2 ppm in CDCl<sub>3</sub> and 8.9 ppm in CD<sub>2</sub>Cl<sub>2</sub>, see below for a tentative assignment) and other signals clustered above 9.5 ppm, hinting at some structural similarity. Dilution studies (down to 0.1 mM) showed no sign of dissociation of the new dimer. Measuring an association constant in CD<sub>2</sub>Cl<sub>2</sub>/DMSO-*d*<sub>6</sub> mixtures was hampered by the fact that DMSO-*d*<sub>6</sub> also promoted the formation of the *PM* shifted dimer.

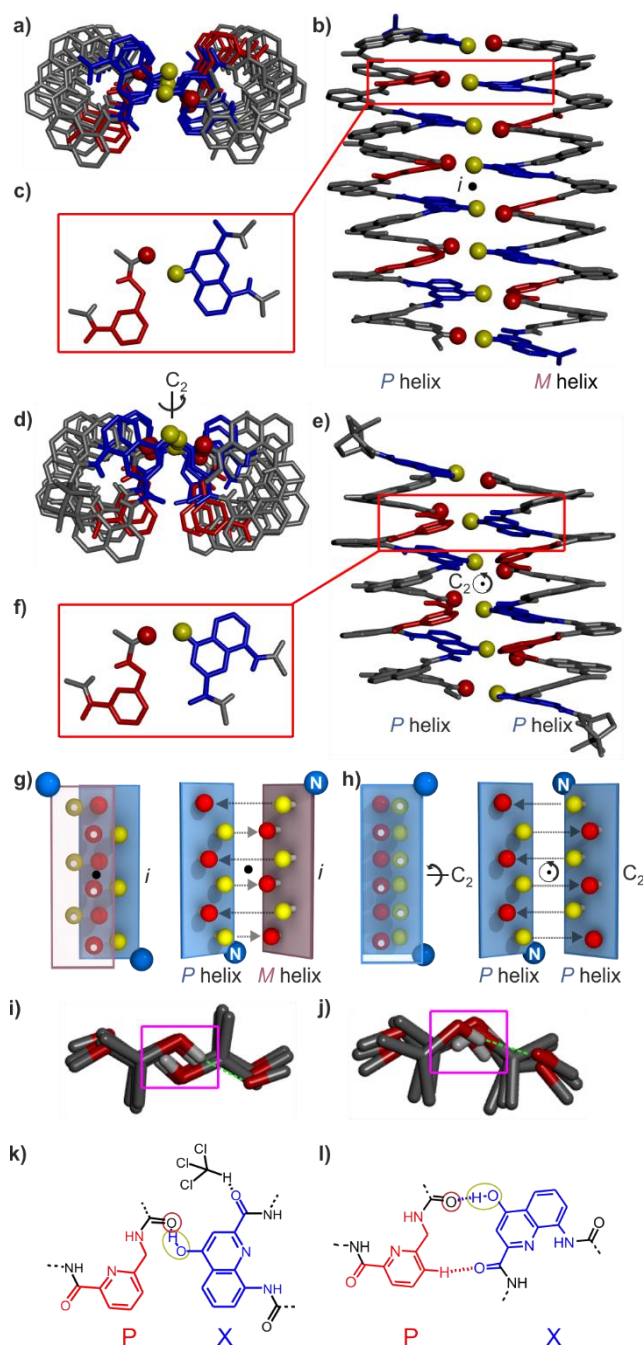


**Figure 3.** Top-view (a), side-view (b), and hydrogen bonding pattern (c) of the crystal structure of *PM* shifted dimer of **7** that prevails in  $\text{CHCl}_3$ . Top-view (d), side-view (e) and hydrogen-bonding pattern (f) of the crystal structure of the *PP* shifted dimer of **5** that prevails in  $\text{CH}_2\text{Cl}_2$ . The pseudo inversion center is indicated by  $i$ , pseudo-two-fold axis by  $C_2$ . In (a-f) hydroxy and carbonyl oxygen atoms of the hydrogen-bonding arrays are shown as yellow and red balls, respectively. The X and P units are shown in blue and red tubes, respectively. Included solvent molecules, hydrogen atoms and side-chains are omitted for clarity. g) Schematic representations of the hydrogen-bonding array of the structure shown in a-c): overlaid view (left) and open-book view (right) (see Figure S23 for details). h) Schematic representations of the hydrogen-bonding array of the structure shown in d-f): overlaid view (left) and open-book view (right). i) Top-view of the hydrogen bond array of the structure shown in a). The pink box highlights that local dipoles associated with OH groups are anti-parallel. j) Top-view of the hydrogen bond array of the structure shown in d). The pink box highlights that local dipoles associated with OH groups are not cancelling each other. k) Typical solvation by  $\text{CHCl}_3$  molecules of the structure shown in a-d). l)  $\text{CH}\dots\text{O}=\text{C}$  contact of the structure shown in d-f) that prevents solvation as in k).

Attempts to crystallize the new dimers of **3** and **4** were unsuccessful, but their nature could be unraveled by studying **5** and **6**, the analogues of **3** and **4** bearing a (1*S*)-camphanyl group at their N-terminus. This modification has been shown to quantitatively (as far as an NMR can detect) bias the handedness of Q<sub>n</sub> helices to right-handed (*P*).<sup>[13]</sup> Sequences **5** and **6** were thus expected to be unable to form *PM* shifted dimers. Indeed, a solid state structure of **5** was elucidated from a single crystal grown from CH<sub>2</sub>Cl<sub>2</sub>,<sup>[11]</sup> showing a nearly C<sub>2</sub>-symmetrical parallel<sup>[7]</sup> head-to-tail homochiral (*PP*) dimer (Figure 3d-f). As in the *PM* shifted dimer, a linear and regular array of six hydrogen bonds is formed between hydroxy protons on one helix and the carbonyl preceding a P unit on the other helix. By analogy, we called this type of dimer a *PP* (or *MM*, homochiral) shifted dimer. Again, we could build energy-minimized models of plausible alternate hydrogen bond-mediated homochiral helix bundles, but these must be less stable (Figure S22). Differences between the *PM* and *PP/MM* shifted dimers are highlighted in Figures 3a-3h, S23 and in Tables S1-S4. The main differences concern symmetry and the orientation of the hydrogen bonds, but the two types of dimers are overall similar. Compounds **3** and **4** exist as racemic mixtures of *P*- and *M*-helical conformers and thus may also form *PP/MM* shifted dimers. Their social self-sorting behavior in CDCl<sub>3</sub> is all the more remarkable.

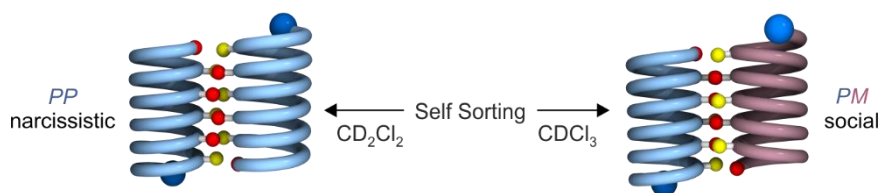
The <sup>1</sup>H NMR spectra of **5** and **6** in CD<sub>2</sub>Cl<sub>2</sub> are quite similar to those of **3** and **4** (Figures 2b, S24, and S25). In the case of **5**, a second species is present in small amounts similar to the *PM* shifted dimer found in the spectrum of **3**. The proportion of this minor species increases in CDCl<sub>3</sub> (Figures 2a,2b, S26) and the species is absent in (CD<sub>2</sub>Cl)<sub>2</sub> and toluene-*d*<sub>8</sub> (Figures S27-S29). In contrast, the spectra of **6** in CD<sub>2</sub>Cl<sub>2</sub> shows one species only, which we presume to be a *PP* shifted dimer, and the same species is present in CDCl<sub>3</sub> or any CDCl<sub>3</sub>/CD<sub>2</sub>Cl<sub>2</sub> mixture (Figure S30). The (1*S*)-camphanyl group of **6** thus plays its role and *PM* shifted dimer formation is prevented in the absence of *M* helix. We surmised that the second set of signals in the spectra of **5** in CDCl<sub>3</sub> and CD<sub>2</sub>Cl<sub>2</sub> could be a *PM* shifted dimer that would counteract the effect of the camphanyl group in a sort of mismatched stereochemical pairing.<sup>[14]</sup> We then measured the circular dichroism (CD) spectra of **5** in these two solvents and observed a reduced intensity in CDCl<sub>3</sub> (Figure S31). The change in intensity matched with the change of proportion measured by NMR. No change in CD intensity was observed with the helical precursor of **5** in which X units are protected as *t*Bu ethers. Furthermore, a second solid state structure of **5** could be obtained from a single crystal grown from CHCl<sub>3</sub> that showed a *PM* shifted dimer extremely similar to that of **3** (Figure S4).<sup>[11]</sup> This dimer has a *P* and an *M* helix but is not centrosymmetrical: since both helices carry the same (1*S*)-camphanyl group, it is an overall chiral species. In short, the *PM* shifted dimer has such a considerable stability in CHCl<sub>3</sub> that, at least in the case of **5**, it partly counteracts the handedness control of the (1*S*)-camphanyl group. Given the behavior of **5** and **6**, we think it reasonable to assign the dimers of **3** and **4** that prevail in CD<sub>2</sub>Cl<sub>2</sub>, (CDCl<sub>2</sub>)<sub>2</sub>, and toluene-*d*<sub>8</sub> to *PP/MM* shifted dimers, exemplifying strong chiral narcissistic self-sorting in these solvents.<sup>[12]</sup>

The quantitative reversal of self-sorting of the *P* and *M* helices of **3** and **4** in solution at thermodynamic equilibrium in solvents as similar as CDCl<sub>3</sub>, which favors social self-sorting, and, for example, (CD<sub>2</sub>Cl)<sub>2</sub>, which favors narcissistic self-sorting, is, to the best of our knowledge, unprecedented.<sup>[12f,12g]</sup> We carefully examined the structural parameters of the two types of shifted dimers in the solid state structures of **3** and **5** (Tables S1-S4) and found no major differences. In both cases, top views of the structure show that helix curvature does not significantly deviate from the preferred 2.5 units per turn (Figure S32). Helix bundling does not generate any apparent strain.<sup>[10]</sup>

In both cases also, a certain degree of steric complementarity is observed like the knobs-into-hole complementarity of peptide helix bundles. Specifically, steric clashes would result from replacing the P units by Q monomers because of the additional benzenic ring of the latter. In both cases again, the hydrogen bond involving the N-terminal. X unit of one helix and the C-terminal ester carbonyl of the other unit is a little longer than other hydrogen bonds, in agreement with one OH resonance being a little less downfield-shifted than the others (Figure 2). The angles formed by C and O atoms in the COH $\cdots$ O=C hydrogen bonds are not the same in the *PM* and chiral dimers, reflecting a different orientation of OH and carbonyl groups (Figure 3i-3l). In the *PM* dimers, the center of symmetry leads to a better cancellation (anti-parallel arrangement) of local dipoles than in the  $C_2$ -symmetrical chiral dimer in which an additive parallel component of the OH dipoles along the  $C_2$  axis can be noted. We thus considered that solvent polarity could influence the relative stability of the two dimers. However, no descriptor of solvent polarity provided a trend that would match with proportions observed experimentally. For example, relative permittivities increase from CDCl<sub>3</sub>, to (CD<sub>2</sub>Cl)<sub>2</sub>, CD<sub>2</sub>Cl<sub>2</sub> and (CDCl<sub>2</sub>)<sub>2</sub> ( $\epsilon_r = 4.81, 8.42, 8.93$  and  $10.36$ , respectively),<sup>[15]</sup> which would fit our observations, but toluene-*d*<sub>8</sub> would then be an outlier ( $\epsilon_r = 2.38$ ).<sup>[16]</sup> A possible source of the effect may be solvent acidity, *i.e.* hydrogen bonding ability, in particular to the multiple amide carbonyl groups at the surface of helices. Indeed, the solid structures of the *PM* shifted dimers of **3**, **5** and **7** contain numerous CHCl<sub>3</sub> molecules almost all of which establish Cl<sub>3</sub>CH $\cdots$ O=C contacts (Figures 3k, S33). In contrast, the CH<sub>2</sub>Cl<sub>2</sub> molecules in the structure of the *PP* dimer of **5** do not play this role (Figure S33). Instead, some amide carbonyl groups are involved in CH $\cdots$ O=C contacts in the chiral dimer structure and are thus unavailable to interact with the solvent (Figure 3d,3l). This does not occur in the *PM* dimers in which all carbonyl groups, not hydrogen bonded to hydroxy groups are available for interactions with an acidic proton of the solvent. Such different roles of CHCl<sub>3</sub> and CH<sub>2</sub>Cl<sub>2</sub> in solvation have been documented for when these solvent molecules are included in solid state structures.<sup>[17]</sup> However, the effects in solution and their potential amplitude remain unclear. It is also unclear how these effects may vary as a function of helix length. For the shorter helices **3** and **5**, the *PM* shifted dimer shows such stability that it does not completely disappear in CD<sub>2</sub>Cl<sub>2</sub> (it does in (CD<sub>2</sub>Cl)<sub>2</sub>), and it partly counteracts the effect of the camphanyl group, whereas the longer helices **4** and **6** are better behaved. Solvent effects as strong as those we report may also influence some of the innumerable hydrogen bonded assemblies in chlorinated solvents described in the literature. Yet we found no such report.

In conclusion, we have described the formation of stable and well-defined helix bundles of aromatic foldamer helices mediated by new linear arrays of hydrogen bonds, adding to the rich literature on helical molecules and their properties.<sup>[18]</sup> The spatial organization of the hydrogen bond donors and acceptors in the helix bundles much contrast with tape-like or flat rigid structures presented in other contexts.<sup>[19]</sup> Helix bundling was shown to undergo a quantitative reversal of self-sorting from social heterochiral (*meso*) to narcissistic homochiral depending on the chlorinated solvent used. The reason why similar solvents may give rise to such large effects will warrant further investigations. Nevertheless, the new bundles as well as their amenability to solvent-induced reconstitution can already serve as building blocks to further elaborate tertiary and quaternary abiotic foldamers. Work along these lines is in progress in our laboratories and will be reported in due course.

## Entry for the Table of Contents



Insert text for Table of Contents here. Aromatic foldamer helices form stable head-to-tail dimers in solution and in the solid state mediated by linear arrays of hydrogen bonds. The preference for dimerization between helices with opposite or identical handedness can be quantitatively reversed by the choice of chlorinated solvent.

Institute and/or researcher Twitter usernames: @ak\_huc

## Acknowledgements

This work was supported by the DFG (Excellence Cluster 114, CIPSM). M. Palchyk and D. Gill are gratefully acknowledged for contributing synthetic precursors. We also thank D. Gill and D. Bindl for monomer synthesis, L. Allmendinger and C. Glas for assistance with NMR measurements, and B. Kauffmann for crystallographic data collection. This work has benefited from the facilities and expertise of the Biophysical and Structural Chemistry platform (BPCS) at IECB, CNRS UMS3033, Inserm US001, and Bordeaux University.

**Keywords:** helix bundling • foldamer • self-sorting • hydrogen bonding • chlorinated solvents

- [1] a) C. W. Wood, D. N. Woolfson, *Protein Sci.* **2018**, *27*, 103-111; b) F. Thomas, W. M. Dawson, E. J. M. Lang, A. J. Burton, G. J. Bartlett, G. G. Rhys, A. J. Mulholland, D. N. Woolfson, *ACS Synth. Biol.* **2018**, *7*, 1808-1816; c) G. G. Rhys, J. A. Cross, W. M. Dawson, H. F. Thompson, S. Shanmugaratnam, N. J. Savery, M. P. Dodding, B. Höcker, D. N. Woolfson, *Nat. Chem. Biol.* **2022**, *18*, 999-1004; d) A. J. Scott, A. Niitsu, H. T. Kratochvil, E. J. M. Lang, J. T. Sengel, W. M. Dawson, K. R. Mahendran, M. Mravic, A. R. Thomson, R. L. Brady, L. Liu, A. J. Mulholland, H. Bayley, W. F. Degrado, M. I. Wallace, D. N. Woolfson, *Nat. Chem.* **2021**, *13*, 643-650; e) M. J. Chalkley, S. I. Mann, W. F. Degrado, *Nat. Rev. Chem.* **2022**, *6*, 31-50; f) M. Mravic, J. L. Thomaston, M. Tucker, P. E. S. Lijun Liu, W. F. Degrado, *Science* **2019**, *363*, 1418-1423; g) F. Pirro, N. Schmidt, J. Lincoff, Z. X. Widell, N. F. Polizzi, L. Liu, M. J. Therien, M. Grabe, M. Chino, A. Lombardi, W. F. Degrado, *Proc. Natl. Acad. Sci.* **2020**, *117*, 33246-33253; h) T. Lebar, D. Lainšček, E. Merljak, J. Aupič, R. Jerala, *Nat. Chem. Biol.* **2020**, *16*, 513-519; i) F. Lapenta, J. Aupič, M. Vezzoli, Ž. Strmšek, S. Da Vela, D. I. Svergun, J. M. Carazo, R. Melero, R. Jerala, *Nat. Commun.* **2021**, *12*; j) F. Lapenta, J. Aupič, Ž. Strmšek, R. Jerala, *Chem. Soc. Rev.* **2018**, *47*, 3530-3542.
- [2] P. Kumar, N. G. Paterson, J. Clayden, D. N. Woolfson, *Nature* **2022**, *607*, 387-392.
- [3] W. S. Horne, J. L. Price, J. L. Keck, S. H. Gellman, *J. Am. Chem. Soc.* **2007**, *129*, 4178-4180.

- [4] a) E. J. Petersson, C. J. Craig, D. S. Daniels, J. X. Qiu, A. Schepartz, *J. Am. Chem. Soc.* **2007**, *129*, 5344-5345; b) D. S. Daniels, E. J. Petersson, J. X. Qiu, A. Schepartz, *J. Am. Chem. Soc.* **2007**, *129*, 1532-1533.
- [5] a) G. W. Collie, K. Pulka-Ziach, C. M. Lombardo, J. Fremaux, F. Rosu, M. Decossas, L. Mauran, O. Lambert, V. Gabelica, C. D. Mackereth, G. Guichard, *Nat. Chem.* **2015**, *7*, 871-878; b) G. W. Collie, R. Bailly, K. Pulka-Ziach, C. M. Lombardo, L. Mauran, N. Taib-Maamar, J. Dessolin, C. D. Mackereth, G. Guichard, *J. Am. Chem. Soc.* **2017**, *139*, 6128-6137.
- [6] a) D. E. Mortenson, J. D. Steinkruger, D. F. Kreitler, D. V. Perroni, G. P. Sorenson, L. Huang, R. Mittal, H. G. Yun, B. R. Travis, M. K. Mahanthappa, K. T. Forest, S. H. Gellman, *Proc. Natl. Acad. Sci.* **2015**, *112*, 13144-13149; b) D. F. Kreitler, Z. Yao, J. D. Steinkruger, D. E. Mortenson, L. Huang, R. Mittal, B. R. Travis, K. T. Forest, S. H. Gellman, *J. Am. Chem. Soc.* **2019**, *141*, 1583-1592.
- [7] Throughout the manuscript, the term "parallel" refers to helical axes having a parallel orientation without prejudice of the head-to-head or head-to-tail relative arrangement of the oligoamide chains. The term "anti-parallel" is avoided.
- [8] a) H. Jiang, J.-M. Léger, I. Huc, *J. Am. Chem. Soc.* **2003**, *125*, 3448-3449; b) D. Sánchez-García, B. Kauffmann, T. Kawanami, H. Ihara, M. Takafuji, M.-H. Delville, I. Huc, *J. Am. Chem. Soc.* **2009**, *131*, 8642-8648; c) T. Qi, V. Maurizot, H. Noguchi, T. Charoenraks, B. Kauffmann, M. Takafuji, H. Ihara, I. Huc, *Chem. Commun.* **2012**, *48*, 6337; d) F. Devaux, X. Li, D. Sluysmans, V. Maurizot, E. Bakalis, F. Zerbetto, I. Huc, A.-S. Duwez, *Chem* **2021**, *7*, 1333-1346.
- [9] a) S. De, B. Chi, T. Granier, T. Qi, V. Maurizot, I. Huc, *Nat. Chem.* **2018**, *10*, 51-57; b) D. Mazzier, S. De, B. Wicher, V. Maurizot, I. Huc, *Chem. Sci.* **2019**, *10*, 6984-6991; c) D. Mazzier, S. De, B. Wicher, V. Maurizot, I. Huc, *Angew. Chem. Int. Ed.* **2020**, *59*, 1606-1610; *Angew. Chem.* **2020**, *132*, 1623-1627.
- [10] F. S. Menke, D. Mazzier, B. Wicher, L. Allmendinger, B. Kauffmann, V. Maurizot, I. Huc, *Org. Biomol. Chem.* **2023**, accepted, doi.org/10.1039/D2OB02109A.
- [11] Crystallographic data that support the findings of this study are openly available at the Cambridge Crystallographic Data Centre at <https://ccdc.cam.ac.uk>, reference numbers: 2209189 (**3**, racemic); 2209187 (**5**, homochiral); 2209188 (**7**, racemic); 2209186 (**5**, pseudo-racemic).
- [12] a) Y. Z. C. Li, Y.-Q. Zhao and S. Zhang, *Chem. Lett.* **2020**, *49*, 1356-1366; b) H. Jędrzejewska, A. Szumna, *Chem. Rev.* **2017**, *117*, 4863-4899; c) T. Koga, M. Matsuoka, N. Higashi, *J. Am. Chem. Soc.* **2005**, *127*, 17596-17597; d) A. Wu, L. Isaacs, *J. Am. Chem. Soc.* **2003**, *125*, 4831-4835; *Angew. Chem.* **2002**, *114*, 4200-4203; e) A. Wu, A. Chakraborty, J. C. Fettinger, R. A. Flowers II, L. Isaacs, *Angew. Chem. Int. Ed.* **2002**, *41*, 4028-4031; f) D. Beaudoin, F. Rominger, M. Mastalerz, *Angew. Chem. Int. Ed.* **2017**, *56*, 1244-1248; *Angew. Chem.* **2017**, *129*, 1264-1268; g) P. Wagner, F. Rominger, W. S. Zhang, J. H. Gross, S. M. Elbert, R. R. Schröder, M. Mastalerz, *Angew. Chem. Int. Ed.* **2021**, *60*, 8896-8904; *Angew. Chem.* **2021**, *133*, 8978-8986.

- [13] A. M. Kendhale, L. Poniman, Z. Dong, K. Laxmi-Reddy, B. Kauffmann, Y. Ferrand, I. Huc, *J. Org. Chem.* **2011**, *76*, 195-200.
- [14] a) X. Sun, W. Li, L. Zhou, X. Zhang, *Chem. Eur. J.* **2009**, *15*, 7302–7305. b) H. B. Jang, Y. R. Choi, K.-S. Jeong, *J. Org. Chem.* **2018**, *83*, 5123–5131.
- [15] a) I. G. Tironi, W. F. Van Gunsteren, *Mol. Phy.* **1994**, *83*, 381–403; b) C. Wohlfarth, M. D. Lechner (ed), *Vol. 17*, Springer-Verlag, Berlin Heidelberg, **2008**; c) J. Nath, S. K. Chaudhary, *J. Chem. Eng. Data* **1992**, *37*, 387–390.
- [16] U. V. Mardolcar, C. A. Nieto de Castro, F. J. V. Santos, *Fluid Phase Equilibria; Dielectric constant measurements of toluene and benzene, Vol. 79*, Elsevier, Aubiere, France, **1992**.
- [17] F. H. Allen, P. A. Wood, P. T. A. Galek, *Acta Cryst.* **2013**, *B69*, 379-388.
- [18] E. Yashima, N. Ousaka, D. Taura, K. Shimomura, T. Ikai, K. Maeda, *Chem. Rev.* **2016**, *116*, 13752–13990.
- [19] a) B. Gong, *Acc. Chem. Res.* **2012**, *45*, 2077-2087; b) D. A. Leigh, C. C. Robertson, A. M. Z. Slawin, P. I. T. Thomson, *J. Am. Chem. Soc.* **2013**, *135*, 9939-9943; c) J. Liu, Y. Wang, G. Lei, J. Peng, Y. Huang, Y. Cao, M. Xie, X. Pu, Z. Lu, *J. Mater. Chem.* **2009**, *19*, 7753; d) P. Troselj, P. Bolgar, P. Ballester, C. A. Hunter, *J. Am. Chem. Soc.* **2021**, *143*, 8669-8678.



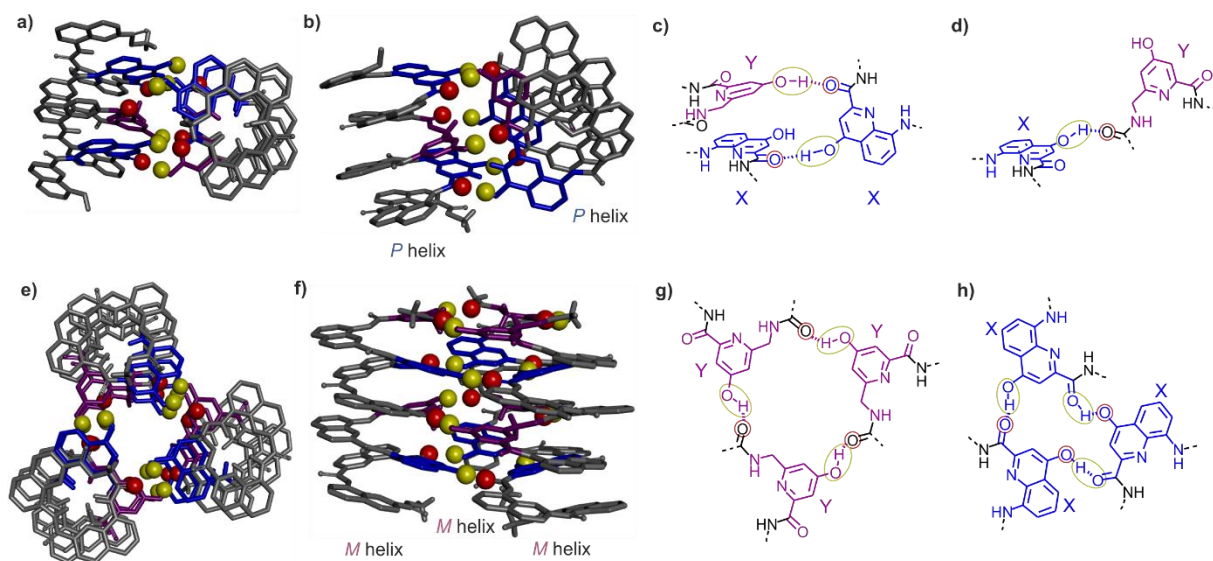
## 4.2 Supporting Informations

4.2.1	List of Abbreviations	98
4.2.2	Supplementary figures	99
4.2.3	Supplementary tables	126
4.2.4	Supplementary methods	129
4.2.4.1	MS analyses	129
4.2.4.2	Molecular modeling	129
4.2.4.3	Nuclear magnetic resonance spectroscopy	129
4.2.4.4	CD studies	131
4.2.4.5	X-ray crystallography	131
4.2.5	Synthetic Schemes	138
4.2.5.1	Synthesis of monomers	138
4.2.5.2	Synthesis of foldamers	138
4.2.6	Experimental Procedures	141
4.2.6.1	General methods	141
4.2.6.2	Synthesis of small units	141
4.2.6.3	Solid phase synthesis general methods	145
4.2.6.3.1	Loading of the resin via HBTU-coupling	145
4.2.6.3.2	Estimation of the loading	145
4.2.6.3.3	Solid Phase Synthesis via in-situ-activation	145
4.2.6.3.4	Mini Cleavage	146
4.2.6.3.5	Full Cleavage	146
4.2.6.4	Synthesis of oligomers	147
4.2.7	References	154
4.2.8	NMR spectra of new compounds	155
4.2.8.1	$^1\text{H}$ NMR and $^{13}\text{C}$ NMR spectra of new small compounds	155
4.2.8.2	$^1\text{H}$ NMR of new oligomers	163

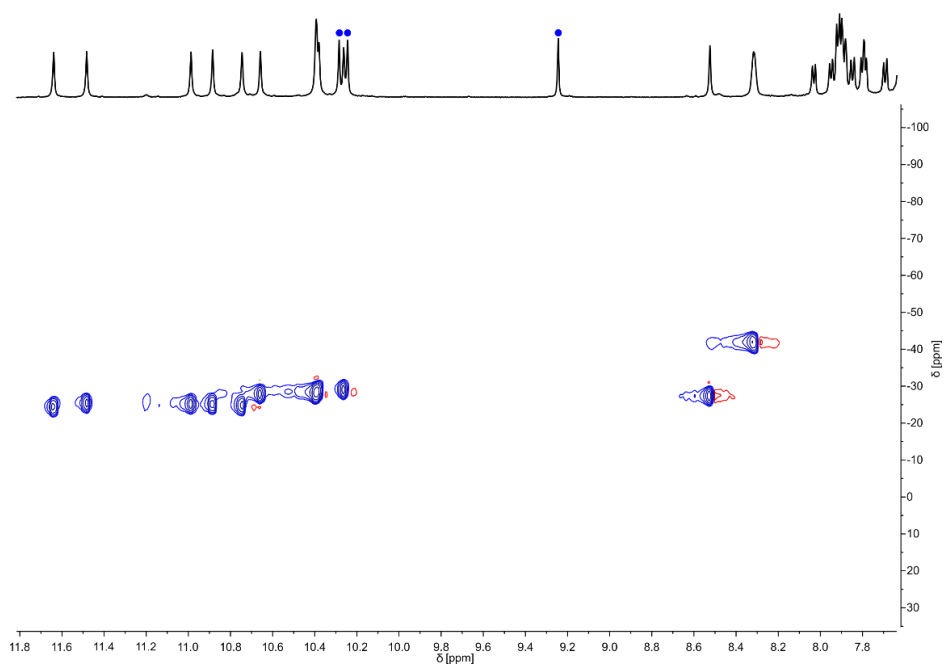
## 4.2.1 List of Abbreviations

<b>CD</b>	circular dichroism
<b>DCM</b>	dichloromethane
<b>DCE</b>	dichloroethane
<b>DIPEA</b>	<i>N,N</i> -diisopropylethylamine
<b>DMF</b>	<i>N,N</i> -dimethylformamide
<b>DMSO</b>	dimethyl sulfoxide
<b>DOSY</b>	diffusion ordered spectroscopy
<b>HR-ESI</b>	high resolution electrospray ionization
<b>EtOAc</b>	ethylacetate
<b>Eq</b>	equivalent
<b>Fmoc</b>	fluorenylmethoxycarbonyl
<b>HBTU</b>	hexafluorophosphate benzotriazole tetramethyl uronium
<b>HFIP</b>	hexafluoroisopropanol
<b>HSQC</b>	heteronuclear single quantum correlation
<b>Me</b>	methyl
<b>MeOH</b>	methanol
<b>Min</b>	minutes
<b>MPLC</b>	Medium pressure liquid chromatography
<b>MS</b>	mass spectrometry
<b>MW</b>	microwave
<b>hex</b>	hexane
<b>NMP</b>	<i>N</i> -Methyl-2-pyrrolidone
<b>NMR</b>	nuclear magnetic resonance
<b>Pd/C</b>	palladium on carbon
<b>r. t.</b>	room temperature
<b>SPS</b>	solid phase synthesis
<b><i>t</i>Bu</b>	<i>tert</i> -butyl
<b>TFA</b>	trifluoroacetic acid
<b>THF</b>	tetrahydrofuran
<b>TLC</b>	thin layer chromatography
<b>UV/Vis</b>	ultraviolet–visible

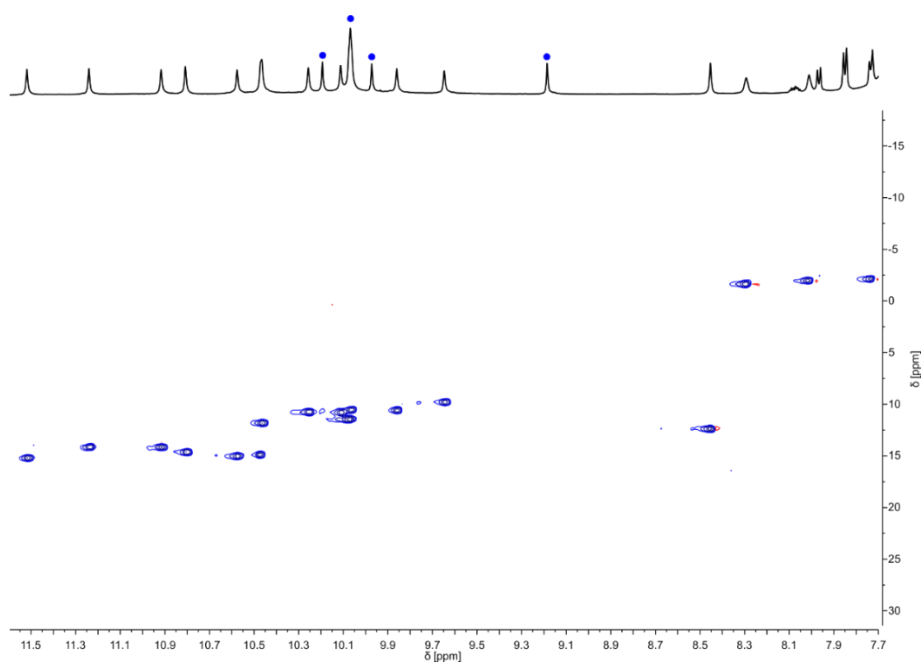
## 4.2.2 Supplementary figures



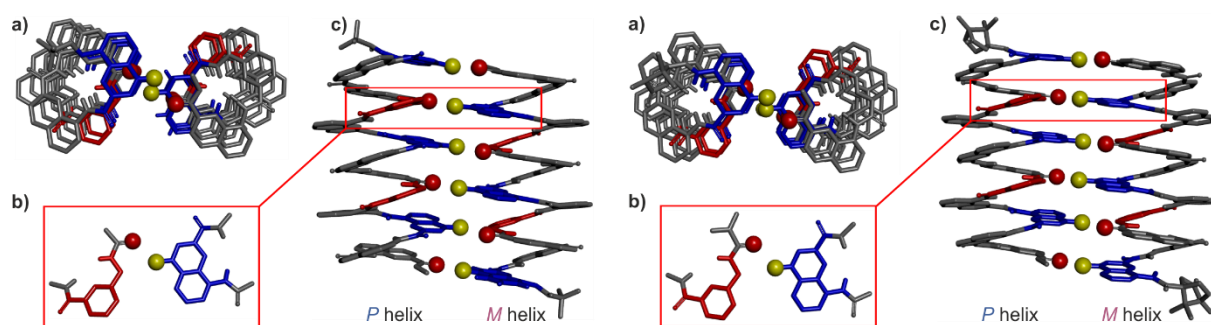
**Figure S1. Previously described aggregates and corresponding hydrogen bonding motifs.** Top (a) and side view (b) of a crystal structure of a tilted dimer of **1**.<sup>[1]</sup> Top- (e) and side view (f) of a crystal structure of a trimer of **2**.<sup>[1]</sup> The hydroxy protons and carbonyl oxygen atoms of the arrays of hydrogen bonds are shown as yellow and red balls, respectively. The X units are shown in blue and the P units in red tubes. Included solvent molecules, nonpolar hydrogen atoms and side-chains are omitted for clarity. The patterns of hydrogen bonds in the tilted dimer of **1** are shown in (c) and (d) and those in the trimer of **2** are shown in (g) and (h).



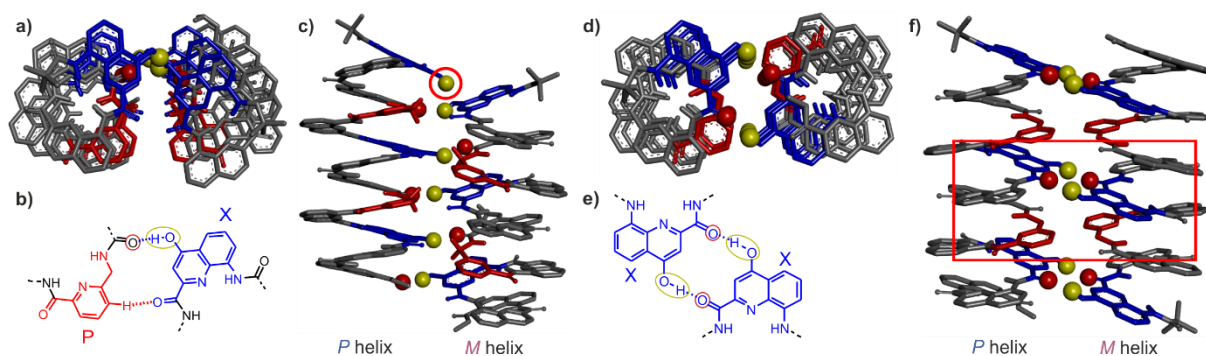
**Figure S2. Identification of hydrogen bonded OH signals of 3 in CDCl<sub>3</sub>.** Part of the <sup>15</sup>N,<sup>1</sup>H HSQC NMR spectrum of **3** (500 MHz, 8 mM in CDCl<sub>3</sub>) at 25 °C showing the amide and hydroxy proton resonances. Only NH resonances correlate, blue dots indicate the signals of OH protons. The spectrum was measured after 2 h equilibration.



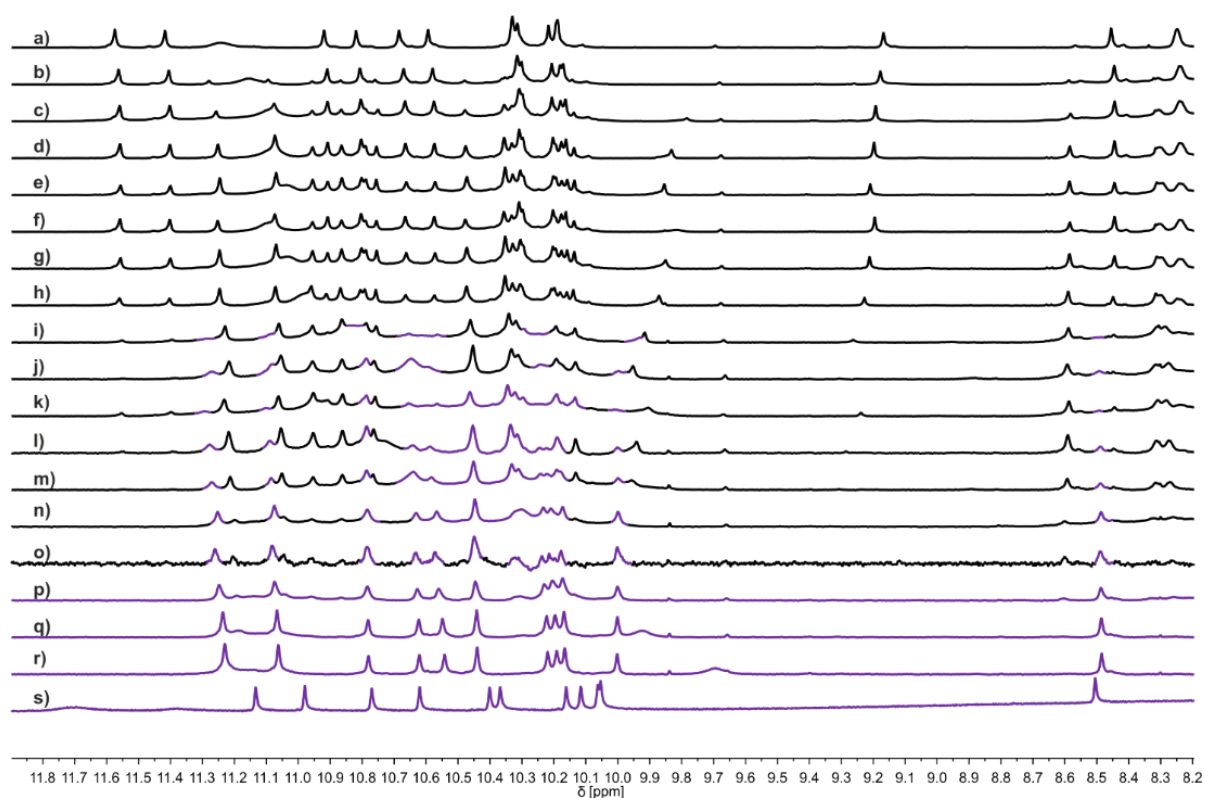
**Figure S3. Identification of hydrogen bonded OH signals of 4 in CDCl<sub>3</sub>.** Part of the 500 MHz <sup>15</sup>N,<sup>1</sup>H HSQC NMR spectrum of **4** (6.9 mM in CDCl<sub>3</sub>) at 25 °C showing the amide and hydroxy proton resonances. Only NH resonances correlate, blue dots indicate the signals of OH protons. A pyridine solution of **4** was evaporated, dried and the solid was dissolved in CDCl<sub>3</sub> and incubated for four weeks prior to measuring the spectrum.



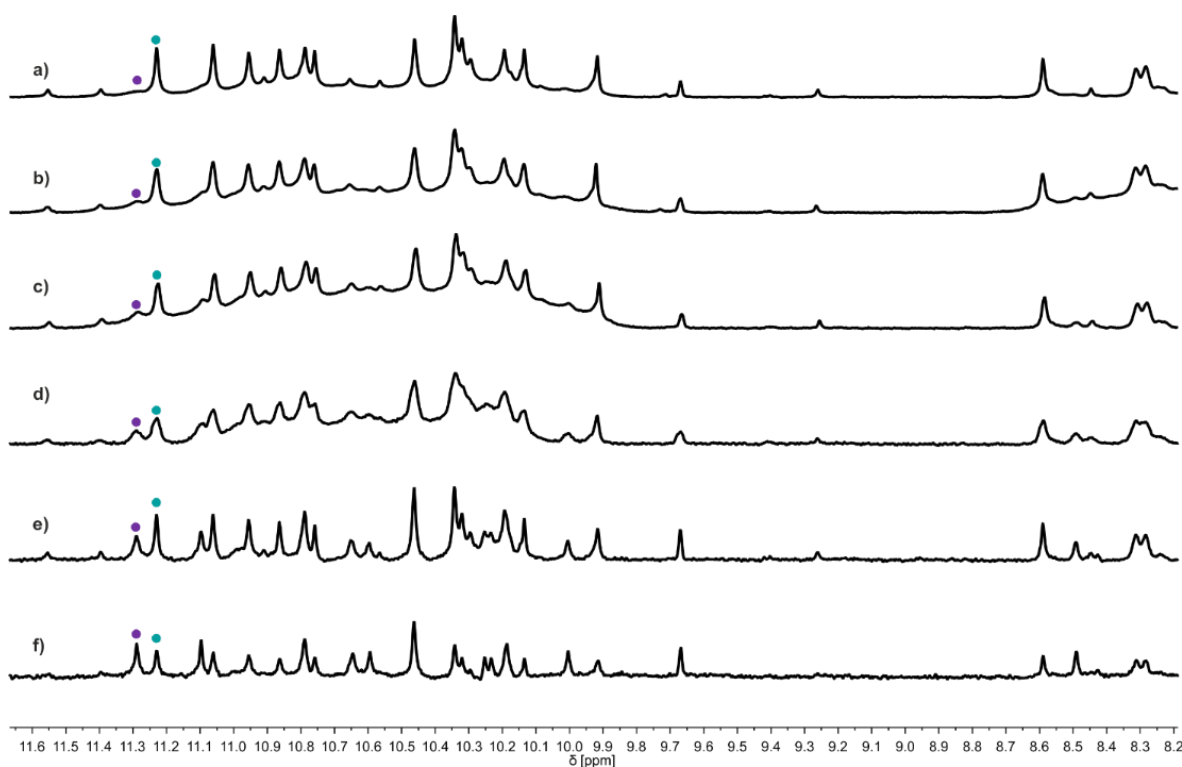
**Figure S4. Crystal structure of 3 and 5 from chloroform.** Top view (a) and side view (c) of the solid state structure of **3** obtained from crystals grown from  $\text{CHCl}_3$ . The prevalent hydrogen-bonding pattern is shown in (b). Top view (a) and side view (c) of the pseudo-racemic solid state structure of **5** obtained from crystals grown from  $\text{CHCl}_3$  (a pseudo center of inversion applies to the helices but not to the camphanyl groups). The prevalent hydrogen-bonding pattern is shown in (b). Both structures show a PM shifted dimer. The hydrogen-bonding donor and acceptors are shown as yellow and red balls, respectively. The X units are shown in blue and the P Units in red tubes. Included solvent molecules, hydrogen atoms and side-chains are omitted for clarity.



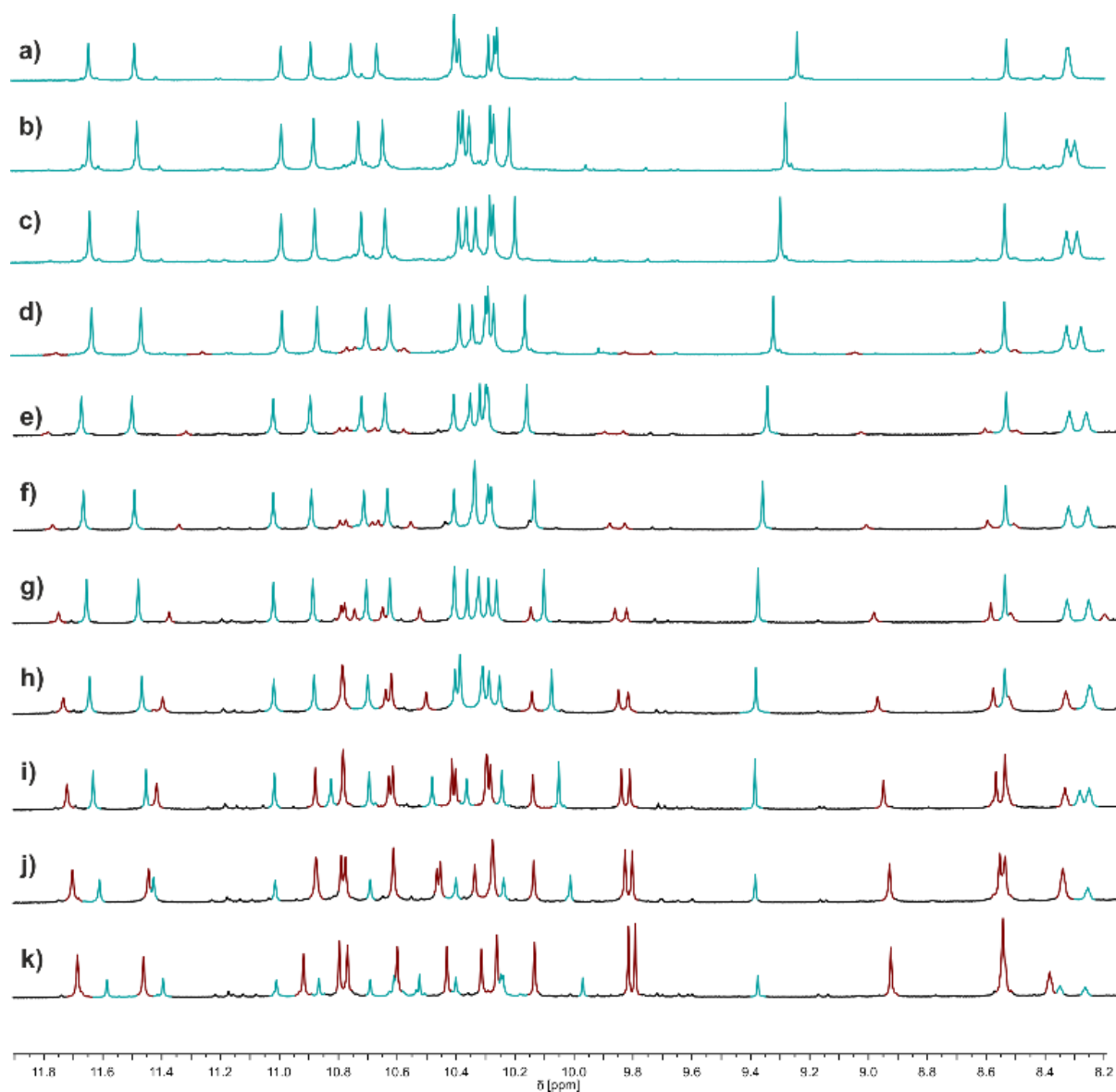
**Figure S5. Energy minimized models of alternate, not experimentally observed hydrogen-bonded PM dimers.** Top view (a) and side view (c) of an energy-minimized computational model<sup>[2]</sup> of **3** in a head-to-head PM shifted dimer arrangement (as opposed to the head-to-tail observed in the crystal). The prevalent hydrogen-bonding pattern is shown in (b). Here, one hydroxy group is not involved in hydrogen-bonding (encircled in red in c). Top view (d), side view (f) and hydrogen-bonding pattern (e) of an energy-minimized computational model<sup>[2]</sup> of a PM head-to-tail (not shifted) parallel arrangement of **3** as observed in a helix-turn-helix tertiary structure.<sup>[3]</sup> Here, two hydrogen bonds form every other helix turn, instead of one every helix turn in the shifted dimer. The hydrogen-bonding donors and acceptors are shown as yellow and red balls, respectively. The X units are shown in blue and the P Units in red tubes. Included solvent molecules, hydrogen atoms and side-chains are omitted for clarity.



**Figure S6. Solution NMR observation of the DMSO-induced dissociation of  $3_2$ .** Part of the 500 MHz  $^1\text{H}$  NMR spectra of **3** (2.4 mM in  $\text{CDCl}_3/\text{DMSO-d}_6$ ) at 25 °C showing the amide and hydroxy proton resonances. The volume percentages of  $\text{DMSO-d}_6$  are 2 (a), 4 (b), 6 (c), 8 (d), 10 (e), 12 (f), 14 (g), 16 (h), 18 (i), 20 (j), 22 (k), 24 (l), 26 (m), 28 (n), 30 (o), 32 (p), 34 (q), 36 (r) and 100 (s), respectively. Signals marked in violet color indicate the monomer. All spectra were measured after a 2h incubation time to reach equilibrium.

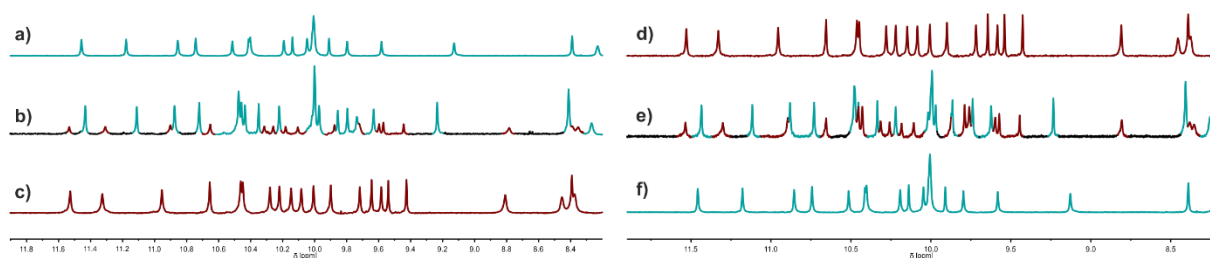


**Figure S7. Solution NMR estimation of the dissociation constant of **3**.** Part of the 500 MHz  $^1\text{H}$  NMR spectra of **3** (in 10:90  $\text{DMSO-d}_6/\text{CDCl}_3$ ) at 25 °C showing the amide and hydroxy proton resonances. The total concentration of the sample was 2.44 mM (a), 1.22 mM (b), 0.61 mM (c), 0.30 mM (d), 0.15 mM (e), and 0.076 mM (f). The signals whose integration was used for the determination of the dissociation constant are marked in turquoise and violet. The ratio of monomer to dimer is 10:100 (a), 22:100 (b), 42:100 (c), 92:100 (d), 140:100 (e), 260:100 (f). Thus, the concentration of monomer in solution is 0.12 mM (a), 0.12 mM (b), 0.11 mM (c), 0.095 mM (d), 0.062 mM (e) and 0.043 mM (f). The concentration of dimer in solution is 1.16 mM (a), 0.55 mM (b), 0.25 mM (c), 0.103 mM (d), 0.044 mM (e), 0.017 mM (f). The dissociation constant was calculated using the following equation:  $K = \frac{[\text{Monomer}]^2}{[\text{Dimer}]}$ . The value of the dissociation constant equals  $1.24 \times 10^{-5}$  (a),  $2.62 \times 10^{-5}$  (b),  $4.84 \times 10^{-5}$  (c),  $8.76 \times 10^{-5}$  (d),  $8.73 \times 10^{-5}$  (e) and  $1.09 \times 10^{-4}$  M (f) leading to an average dissociation constant  $K_d$  of 62  $\mu\text{M}$ . All spectra were measured after a two-week incubation time to reach equilibrium.

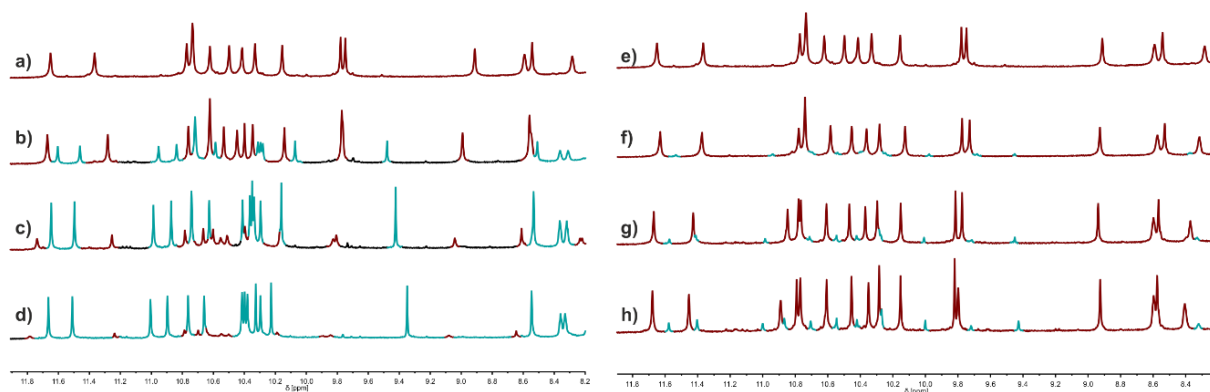


**Figure S8. Conversion of the PM into the PP/MM shifted dimer of 3 upon increasing the proportion of  $\text{CD}_2\text{Cl}_2$  in  $\text{CDCl}_3$ .** Part of the 500 MHz  $^1\text{H}$  NMR spectra of **3** (2.4 mM in  $\text{CDCl}_3/\text{CD}_2\text{Cl}_2$ ) at 25 °C showing the amide and hydroxy proton resonances. The volume percentages of  $\text{CD}_2\text{Cl}_2$  are 0 (a), 10 (b), 20 (c), 30 (d), 40 (e), 50 (f), 60 (g), 70 (h), 80 (i), 90 (j) and 100 (k). The signals of two different species are marked with different colors. Signals of the species dominant in  $\text{CHCl}_3$  (PM shifted dimer) are marked in turquoise, those of the species dominant in  $\text{CH}_2\text{Cl}_2$  (PP/MM shifted dimer) are marked in brown. All spectra were measured after a 2h incubation time to reach equilibrium.

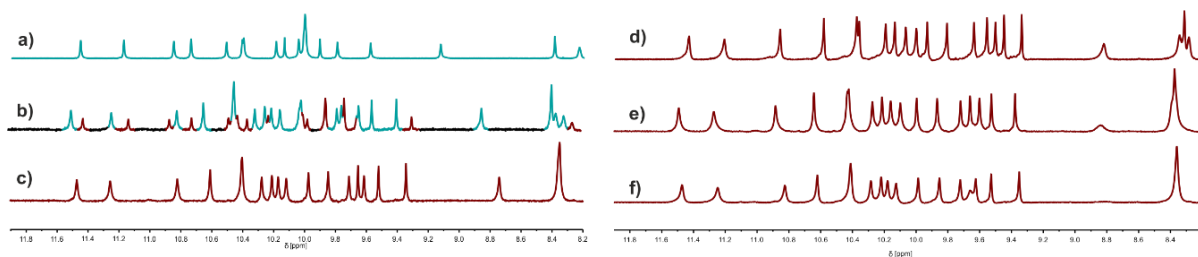




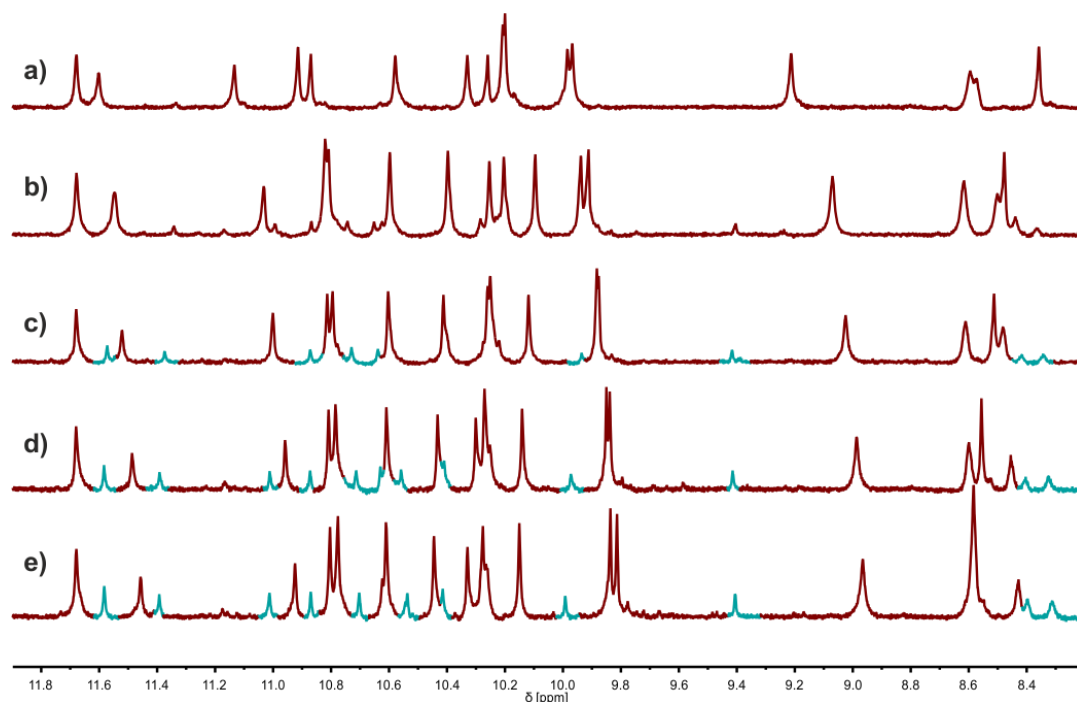
**Figure S9. Interconversion of the PM and PP/MM shifted dimers of 4 upon changing  $\text{CDCl}_3/\text{CD}_2\text{Cl}_2$  solvent mixtures.** Part of the 500 MHz  $^1\text{H}$  NMR spectra of **4** (2.4 mM in various solvents) at 25 °C showing the amide and hydroxy proton resonances. a) In  $\text{CDCl}_3$ . b) In 1:1  $\text{CDCl}_3/\text{CD}_2\text{Cl}_2$  after evaporating and re-dissolving sample a). c) In  $\text{CD}_2\text{Cl}_2$  after evaporating and re-dissolving sample b). d) same as c). e) In 1:1  $\text{CDCl}_3/\text{CD}_2\text{Cl}_2$  after evaporating and re-dissolving sample e). f) In  $\text{CDCl}_3$  after evaporating and re-dissolving sample e). The slight differences between b) and e) suggest that one sample (probably b) had not fully reached equilibrium. The signals of two different species are marked with different colors. Signals of the species dominant in  $\text{CHCl}_3$  (PM shifted dimer) are marked in turquoise, those of the species dominant in  $\text{CH}_2\text{Cl}_2$  (PP/MM shifted dimer) are marked in brown. Samples were incubated at least three weeks prior to measurement.



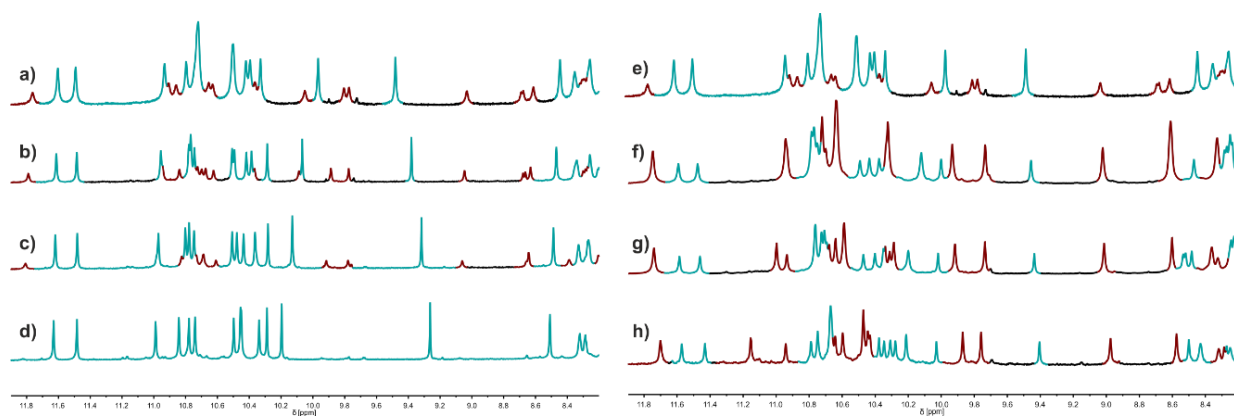
**Figure S10. Interconversion of the PM and PP/MM shifted dimers of 3 upon changing  $\text{CDCl}_3/(\text{CD}_2\text{Cl})_2/\text{CD}_2\text{Cl}_2$  solvent mixtures.** a)-d) Part of the 500 MHz  $^1\text{H}$  NMR spectra of **3** (2.4 mM in  $\text{CDCl}_3/(\text{CD}_2\text{Cl})_2$  mixtures) at 25 °C showing the amide and hydroxy proton resonances. The volume percentages of  $(\text{CD}_2\text{Cl})_2$  are 100 (a), 75 (b), 50 (c), 25 (d). e)-f) Part of the  $^1\text{H}$  NMR spectra (500 MHz, 25 °C) showing the amide and hydroxy proton resonances of **3**, 2.4 mM in  $\text{CD}_2\text{Cl}_2/(\text{CD}_2\text{Cl})_2$ . The volume percentages of  $(\text{CD}_2\text{Cl})_2$  are 100 (e), 75 (f), 50 (g), and 25 (h). The signals of two different species are marked with different colors. Signals of the species dominant in  $\text{CHCl}_3$  (PM shifted dimer) are marked in turquoise, those of the species dominant in  $\text{CH}_2\text{Cl}_2$  (PP/MM shifted dimer) are marked in brown. All spectra were measured after a 2h incubation time to reach equilibrium.



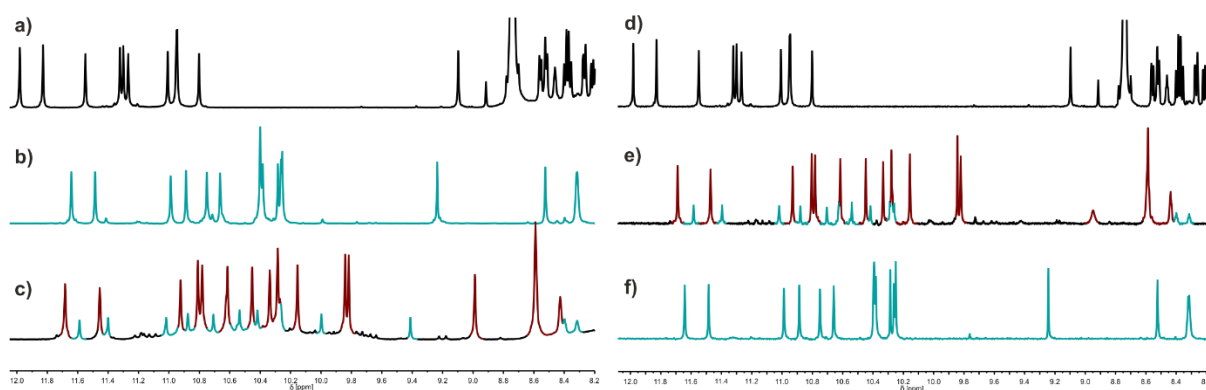
**Figure S11. Interconversion of the PM and PP/MM shifted dimers of 4 upon changing  $\text{CDCl}_3/(\text{CD}_2\text{Cl})_2/\text{CD}_2\text{Cl}_2$  solvent mixtures.** Part of the 500  $^1\text{H}$  NMR spectra of **4** (2.4 mM in various solvent mixtures) at 25 °C showing the amide and hydroxy proton resonances. a) In  $\text{CDCl}_3$ . b) In 1:1  $\text{CDCl}_3/(\text{CD}_2\text{Cl})_2$ . c) In  $(\text{CDCl}_2)_2$  (sample from b)). d) In  $\text{CD}_2\text{Cl}_2$ . e) In 1:1  $\text{CD}_2\text{Cl}_2/(\text{CD}_2\text{Cl})_2$ . f) In  $(\text{CD}_2\text{Cl})_2$  (sample from e)). The signals of two different species are marked with different colors. Signals of the species dominant in  $\text{CHCl}_3$  (PM shifted dimer) are marked in turquoise, those of the species dominant in  $\text{CH}_2\text{Cl}_2$  (PP/MM shifted dimer) are marked in brown. Samples were incubated at least three weeks prior to measurement.



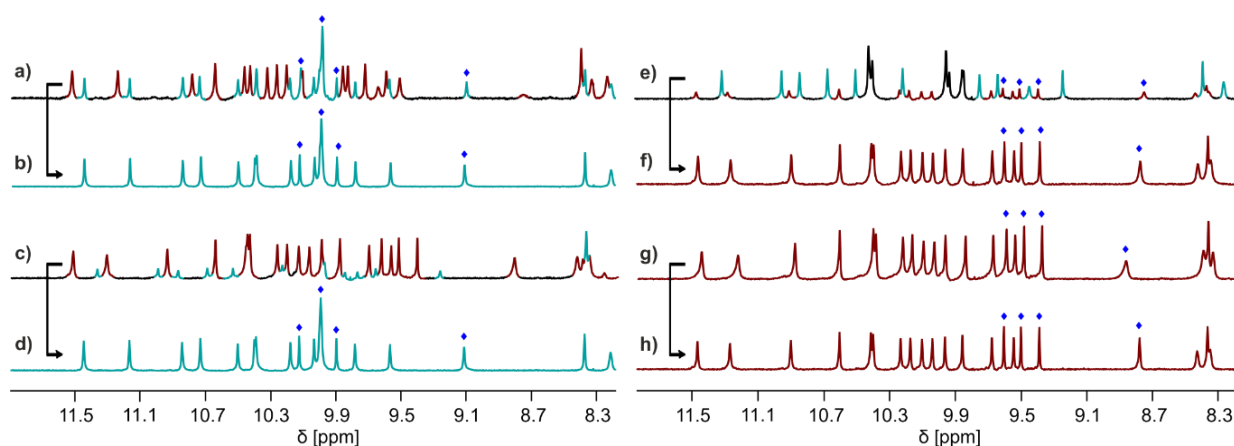
**Figure S12. Interconversion of the PM and PP/MM shifted dimers of 3 upon changing toluene- $d_8/\text{CD}_2\text{Cl}_2$  solvent mixtures.** Part of the 500 MHz  $^1\text{H}$  NMR spectra of **3** (2.4 mM in  $\text{CD}_2\text{Cl}_2/\text{toluene-}d_8$  mixtures) at 25 °C showing the amide and hydroxy proton resonances. The volume percentages of  $\text{CD}_2\text{Cl}_2$  are 0 (a), 25 (b), 50 (c), 75 (d) and 100 (e). The signals of two different species are marked with different colors. The signals of two different species are marked with different colors. Signals of the species dominant in  $\text{CHCl}_3$  (PM shifted dimer) are marked in turquoise, those of the species dominant in  $\text{CH}_2\text{Cl}_2$  (PP/MM shifted dimer) are marked in brown. All spectra were measured after a 12h incubation time to reach equilibrium.



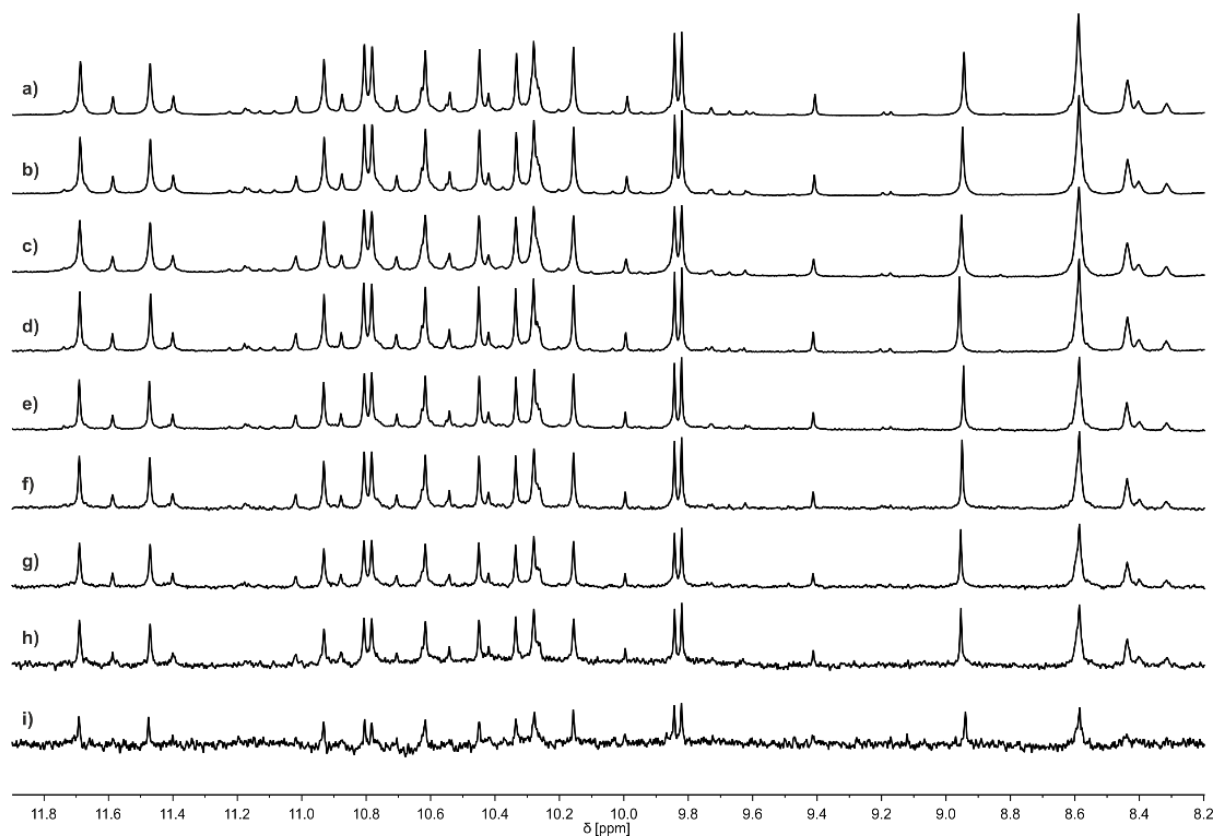
**Figure S13. Interconversion of the *PM* and *PP/MM* shifted dimers of **4** upon changing  $\text{CDCl}_3/(\text{CDCl}_2)_2/\text{CD}_2\text{Cl}_2$  solvent mixtures.** a-d) Part of the 500 MHz  $^1\text{H}$  NMR spectra of **3** (2.4 mM in  $\text{CDCl}_3/(\text{CDCl}_2)_2$  mixtures) at 25 °C showing the amide and hydroxy proton resonances. The volume percentages of  $(\text{CDCl}_2)_2$  are 100 (a), 75 (b), 50 (c), and 25 (d). e-f) Part of the  $^1\text{H}$  NMR spectra (500 MHz, 25 °C) showing the amide and hydroxy proton resonances of **3** at 2.4 mM in  $\text{CD}_2\text{Cl}_2/(\text{CDCl}_2)_2$  mixtures. The volume percentages of  $(\text{CDCl}_2)_2$  are 100 (e), 75 (f), 50 (g), and 25 (h). The signals of two different species are marked with different colors. Signals of the species dominant in  $\text{CHCl}_3$  (*PM* shifted dimer) are marked in turquoise, those of the species dominant in  $\text{CH}_2\text{Cl}_2$  (*PP/MM* shifted dimer) are marked in brown. All spectra were measured after a 2h incubation time to reach equilibrium.



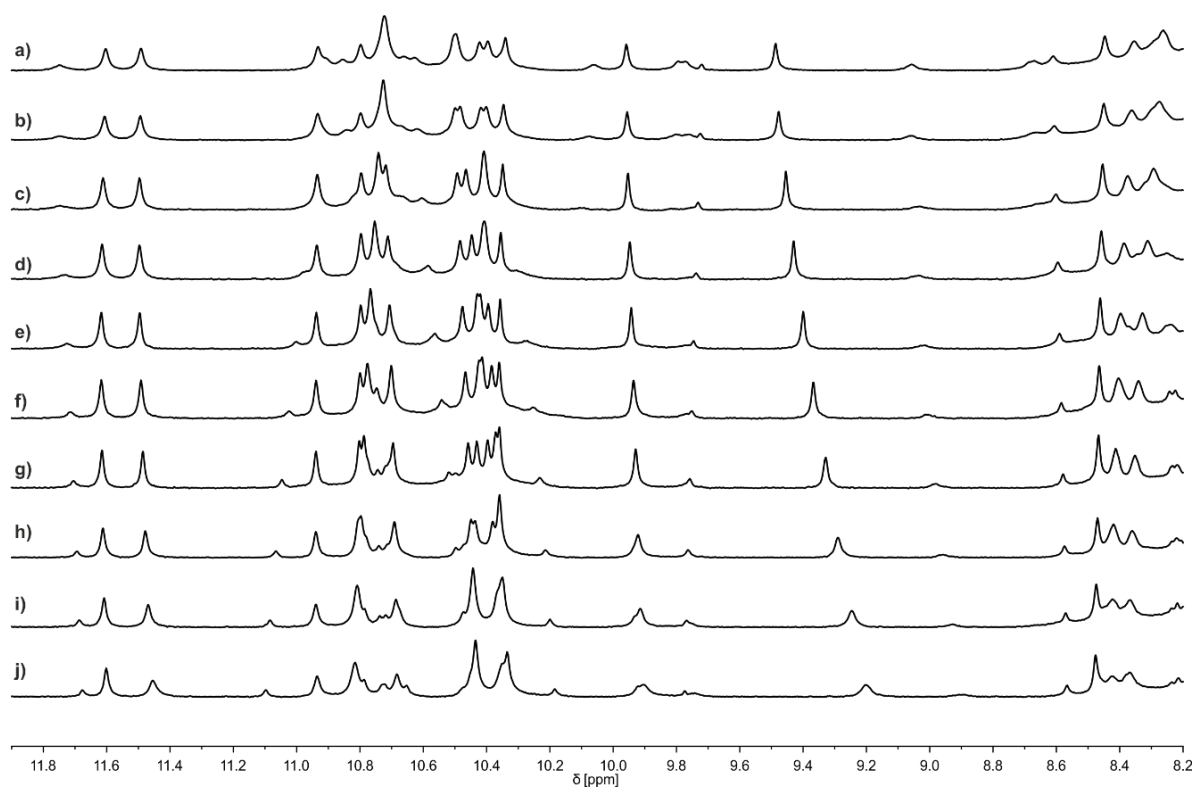
**Figure S14. Control experiment to verify thermodynamic equilibrium is reached between the *PM* and *PP/MM* shifted dimers of **3**.** Part of the 500  $^1\text{H}$  NMR spectra of **3** (2.4 mM in various solvents) at 25 °C showing the amide and hydroxy proton resonances. a) in pyridine- $d_5$ . b) in  $\text{CDCl}_3$  after evaporating and re-dissolving the pyridine- $d_5$  sample. c) in  $\text{CD}_2\text{Cl}_2$  after evaporating and re-dissolving the  $\text{CDCl}_3$  sample. d) in pyridine- $d_5$ . e) in  $\text{CD}_2\text{Cl}_2$  after evaporating and re-dissolving the pyridine- $d_5$  sample. f) in  $\text{CDCl}_3$  after evaporating and re-dissolving the  $\text{CD}_2\text{Cl}_2$  sample. The signals of two different species are marked with different colors. Signals of the species dominant in  $\text{CHCl}_3$  are marked in turquoise, those of the species dominant in  $\text{CH}_2\text{Cl}_2$  are marked in brown. The spectrum in pyridine- $d_5$  in black shows the monomer. All spectra were measured after a 2h incubation time to reach equilibrium.



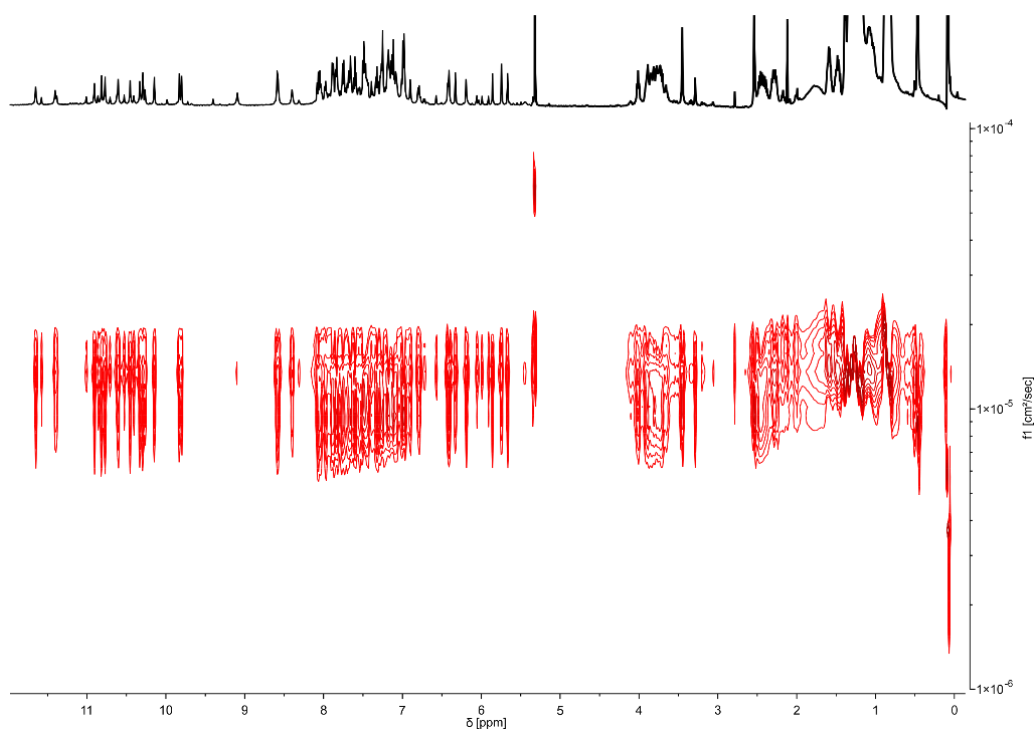
**Figure S15. Control experiment to verify thermodynamic equilibrium is reached between the PM and PP/MM shifted dimers of 4.** Extracts of 500 MHz  $^1\text{H}$  NMR-spectra of **4** (2.4 mM) at 25 °C in various solvents and after various equilibration times. a) Sample evaporated from an equilibrated  $\text{CD}_2\text{Cl}_2$  solution, re-dissolved in  $\text{CDCl}_3$ , and incubated for 2 days. b) Same sample after a three-week incubation. c) Sample evaporated from an equilibrated pyridine solution, re-dissolved in  $\text{CDCl}_3$ , and incubated for 2 days. d) Same sample after a three-week incubation. e) Sample evaporated from an equilibrated  $\text{CDCl}_3$  solution, re-dissolved in  $\text{CD}_2\text{Cl}_2$ , and incubated for 1 day. f) same sample after a six-week incubation. g) sample evaporated from an equilibrated pyridine solution, re-dissolved in  $\text{CD}_2\text{Cl}_2$ , and incubated for 2h. h) Same sample after a three-week incubation. The signals of two different species are marked with different colors.



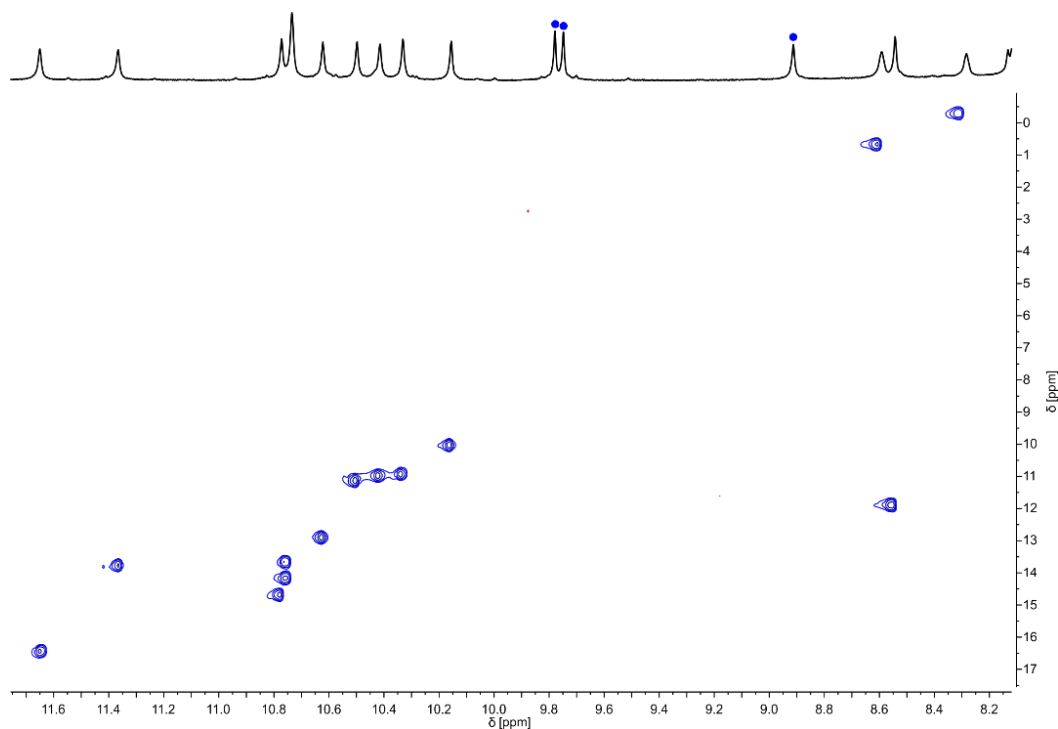
**Figure S16. The proportions of the PM and PP/MM shifted dimers of 3 do not depend on concentration.** Part of the 500 MHz <sup>1</sup>H NMR spectra of 3 (CD<sub>2</sub>Cl<sub>2</sub>, 25 °C) showing the amide and hydroxy proton resonances at 2.2 mM (a), 1.1 mM (b), 0.55 mM (c), 0.28 mM (d), 0.14 mM (e), 0.7 mM (f), 0.035 mM (g), 0.017 mM (h) and 0.009 mM (i). All spectra were measured after a two-week incubation time to reach equilibrium.



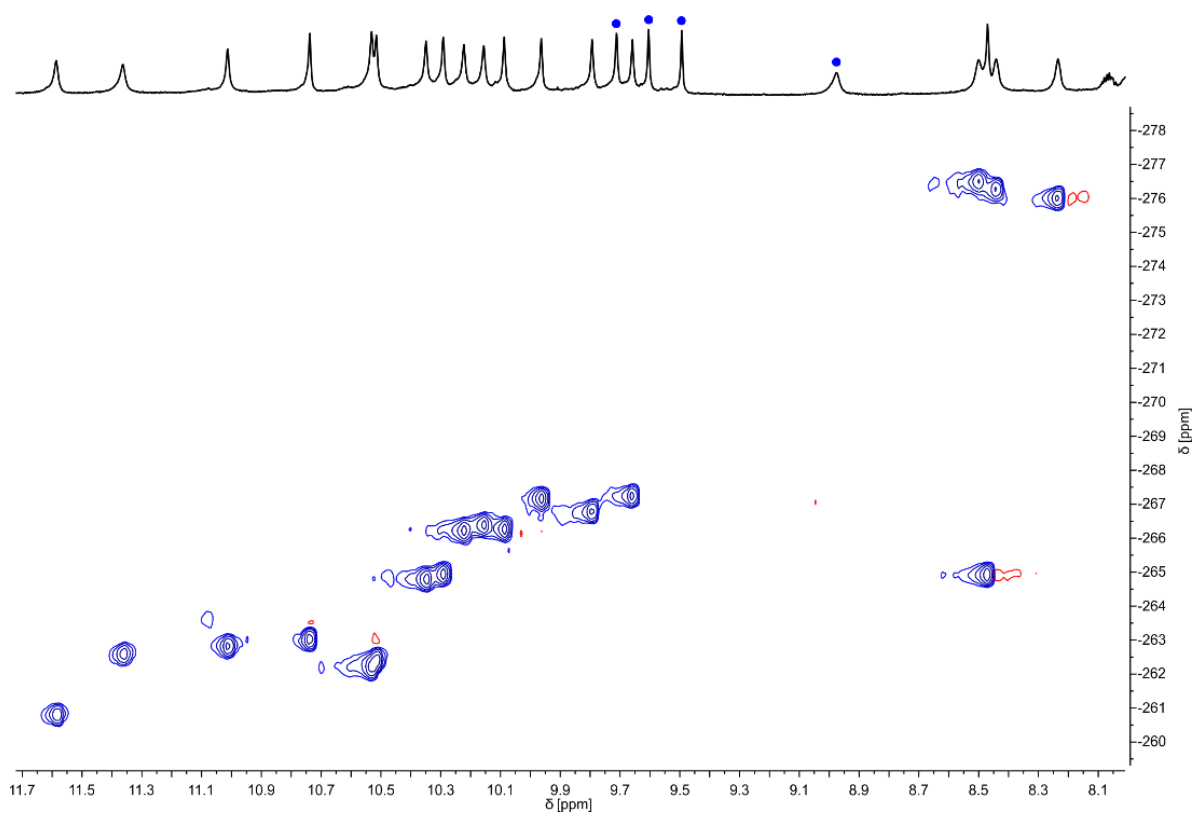
**Figure S17. The proportions of the PM and PP/MM shifted dimers of 3 do not depend on temperature.** Part of the 400 MHz <sup>1</sup>H NMR spectra of **3** (2.5 mM in (CDCl<sub>2</sub>)<sub>2</sub>) showing the amide and hydroxy proton resonances at 25 °C (a), 30 °C (b), 40 °C (c), 50 °C (d), 60 °C (e), 70 °C (f), 80 °C (g), 90 °C (h), 100 °C (i), and 110 °C (j). The initial spectrum was measured after a two-week incubation time to reach equilibrium. Between each other measurement the sample was equilibrated for 15 min.



**Figure S18.** The *PM* and *PP/MM* shifted dimers of **3** have the same hydrodynamic radius. 500 MHz  $^1\text{H}$  DOSY spectrum of **3** (5 mM in  $\text{CD}_2\text{Cl}_2$ ) at 25 °C. The spectrum was measured after a two-hour incubation time to reach equilibrium.

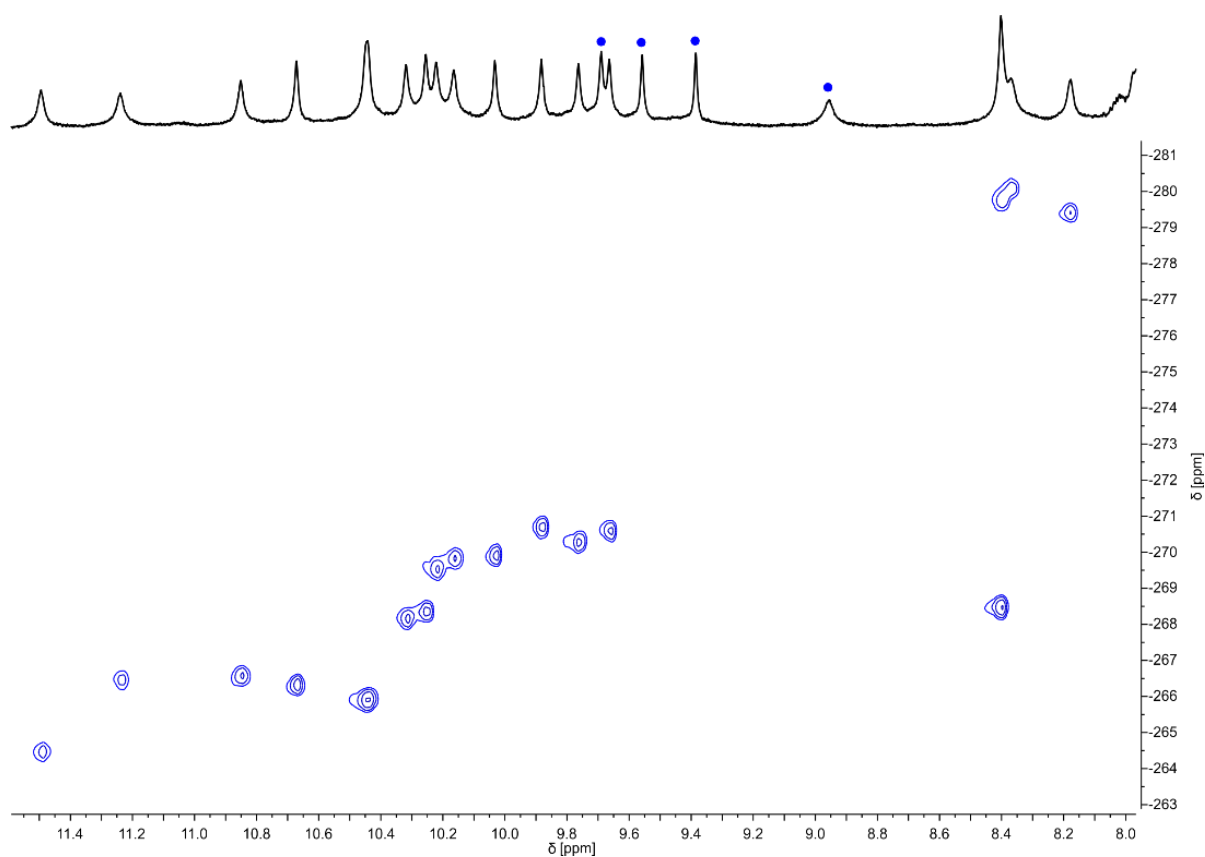


**Figure S19.** Identification of hydrogen bonded OH signals of **3** in  $(\text{CD}_2\text{Cl})_2$ . Part of the 500 MHz  $^{15}\text{N}$ ,  $^1\text{H}$  HSQC NMR spectrum of **3** (4.4 mM in  $(\text{CD}_2\text{Cl})_2$ ) at 25 °C showing the amide and hydroxy proton resonances. Only NH resonances correlate, blue dots indicate the signals of OH protons. The spectrum was measured after a two-hour incubation time to reach equilibrium.

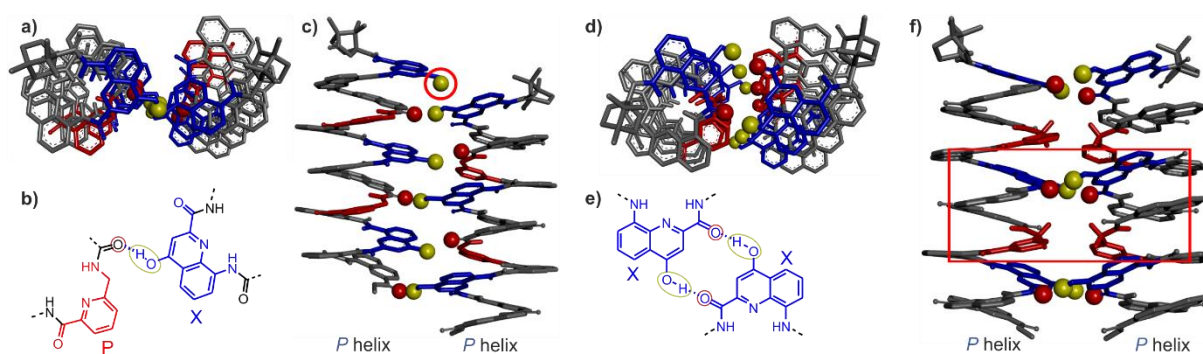


**Figure S20. Identification of hydrogen bonded OH signals of 4 in CD<sub>2</sub>Cl<sub>2</sub>.** Part of the 500 MHz <sup>15</sup>N, <sup>1</sup>H HSQC NMR spectrum of 4 (7.02 mM in CD<sub>2</sub>Cl<sub>2</sub>) 25 °C showing the amide and hydroxy proton resonances. Only NH resonances correlate, blue dots indicate the signals of OH protons. A pyridine solution of 4 was evaporated, dried and the solid was dissolved in CD<sub>2</sub>Cl<sub>2</sub> and incubated for four weeks prior to measuring the spectrum.

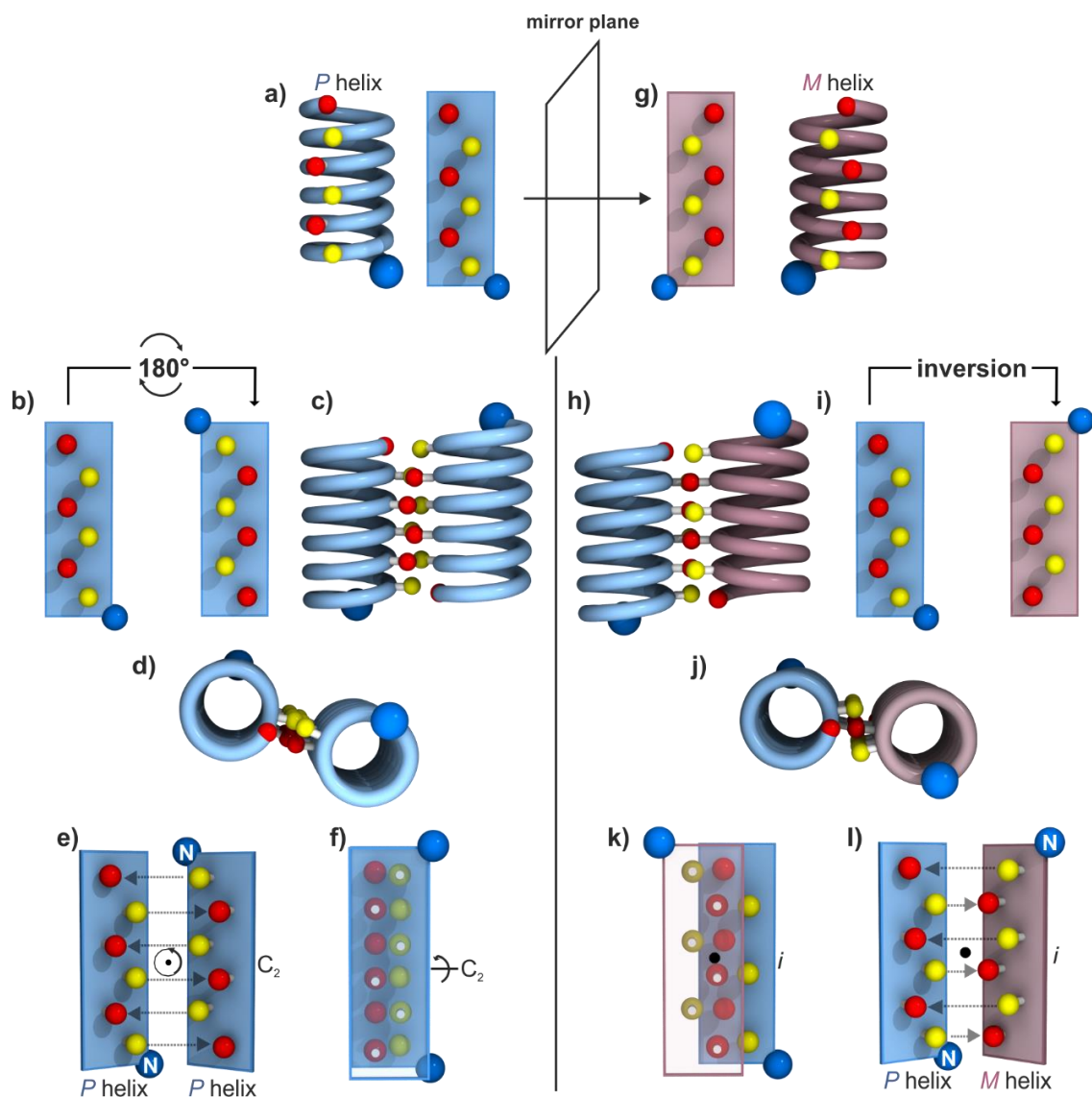




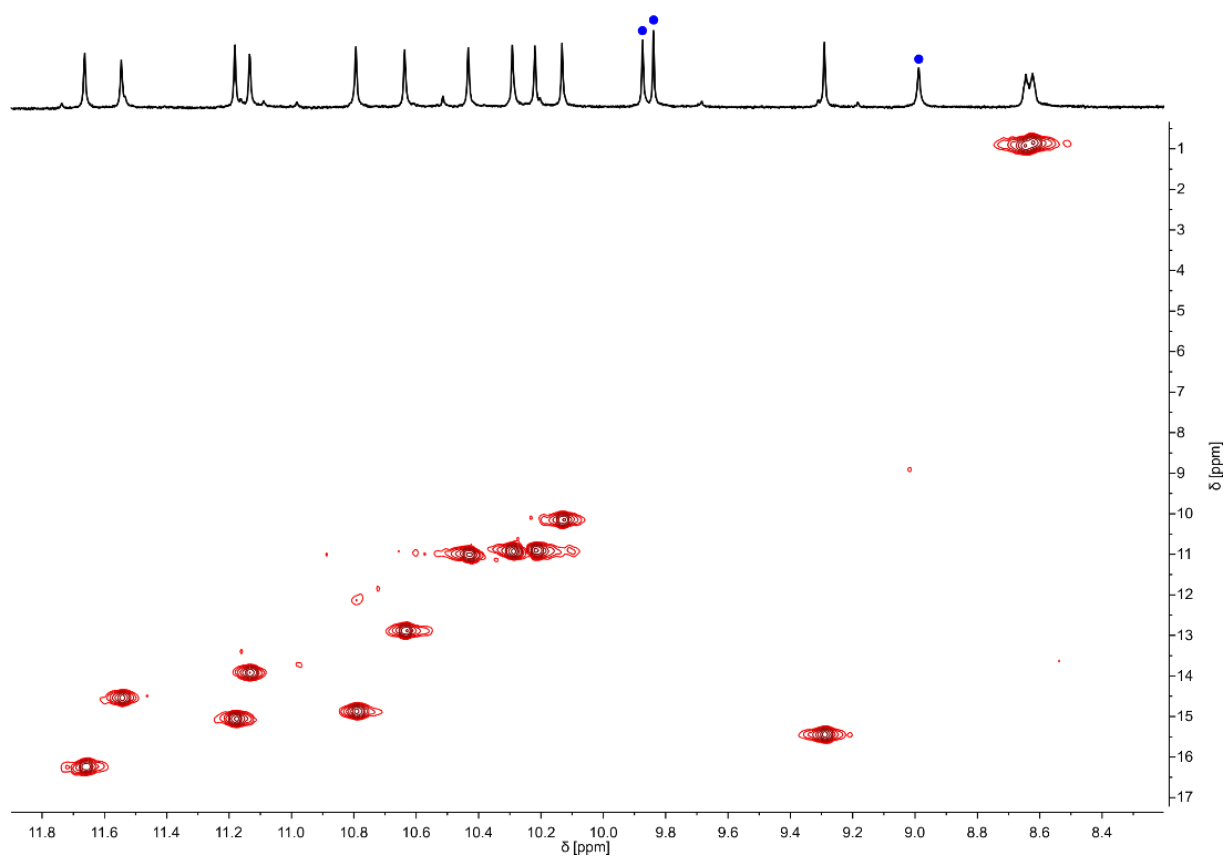
**Figure S21. Identification of hydrogen bonded OH signals of **4** in  $(\text{CD}_2\text{Cl}_2)_2$ .** Part of the 500 MHz  $^{15}\text{N}, ^1\text{H}$  HSQC NMR spectrum of **4** (6.92 mM in  $(\text{CD}_2\text{Cl}_2)_2$ ) at 25 °C showing the amide and hydroxy proton resonances. Only NH resonances correlate, blue dots indicate the signals of OH protons. A pyridine solution of **4** was evaporated, dried and the solid was dissolved in  $(\text{CDCl}_2)_2$  and incubated for four weeks prior to measuring the spectrum.



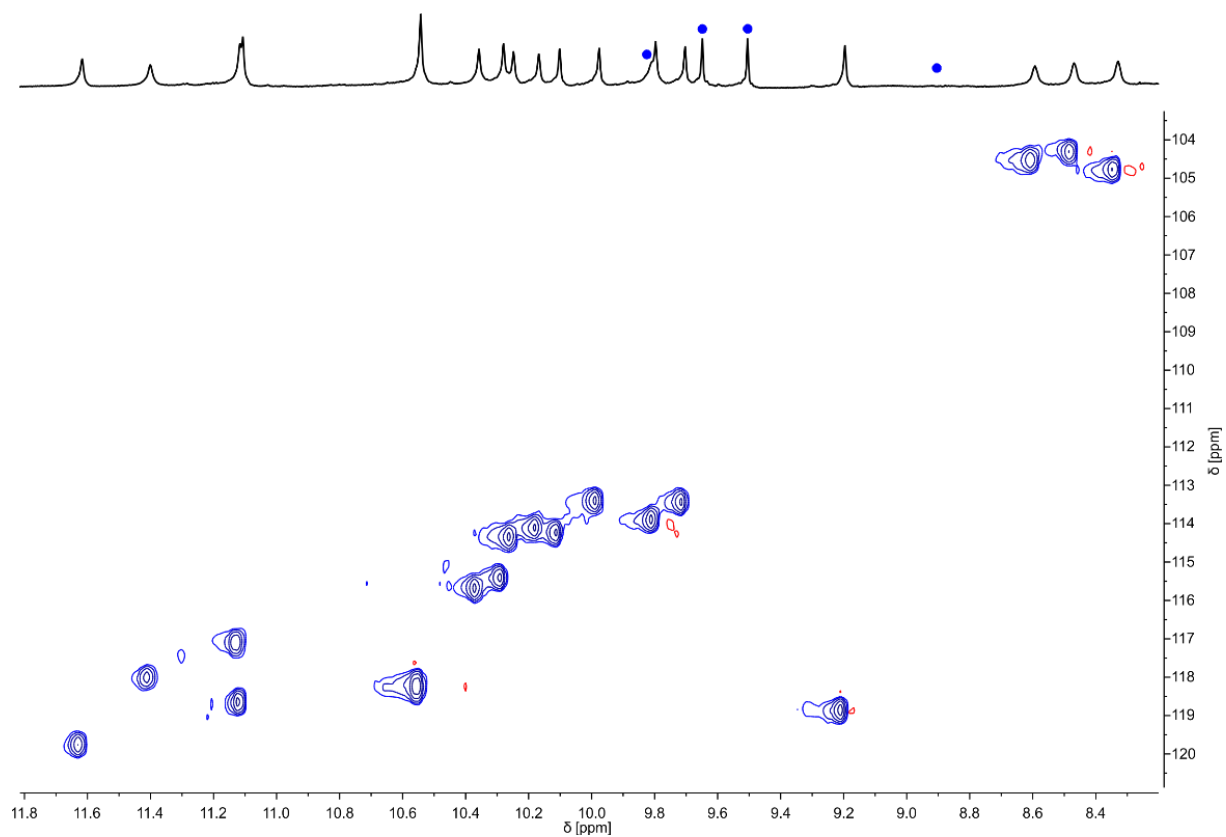
**Figure S22. Energy minimized models of alternate, not experimentally observed hydrogen-bonded PP dimers.** Top view (a) and side view (c) of an energy-minimized computational model<sup>[2]</sup> of **5** in a head-to-head PP shifted dimer arrangement (as opposed to the head-to-tail observed in the crystal). The prevalent hydrogen-bonding pattern is shown in (b). Here, one hydroxy group is not involved in hydrogen-bonding (encircled in red in c). Top view (d), side view (f) and hydrogen-bonding pattern (e) of an energy-minimized computational model<sup>[2]</sup> of a PP head-to-head (not shifted) parallel arrangement of **5** as observed in a helix-turn-helix tertiary structure.<sup>[1,3,4]</sup> Here, two hydrogen bonds form every other helix turn, instead of one every helix turn in the shifted dimer. The hydrogen-bonding donors and acceptors are shown as yellow and red balls, respectively. The X units are shown in blue and the P Units in red tubes. Included solvent molecules, hydrogen atoms and side-chains are omitted for clarity.



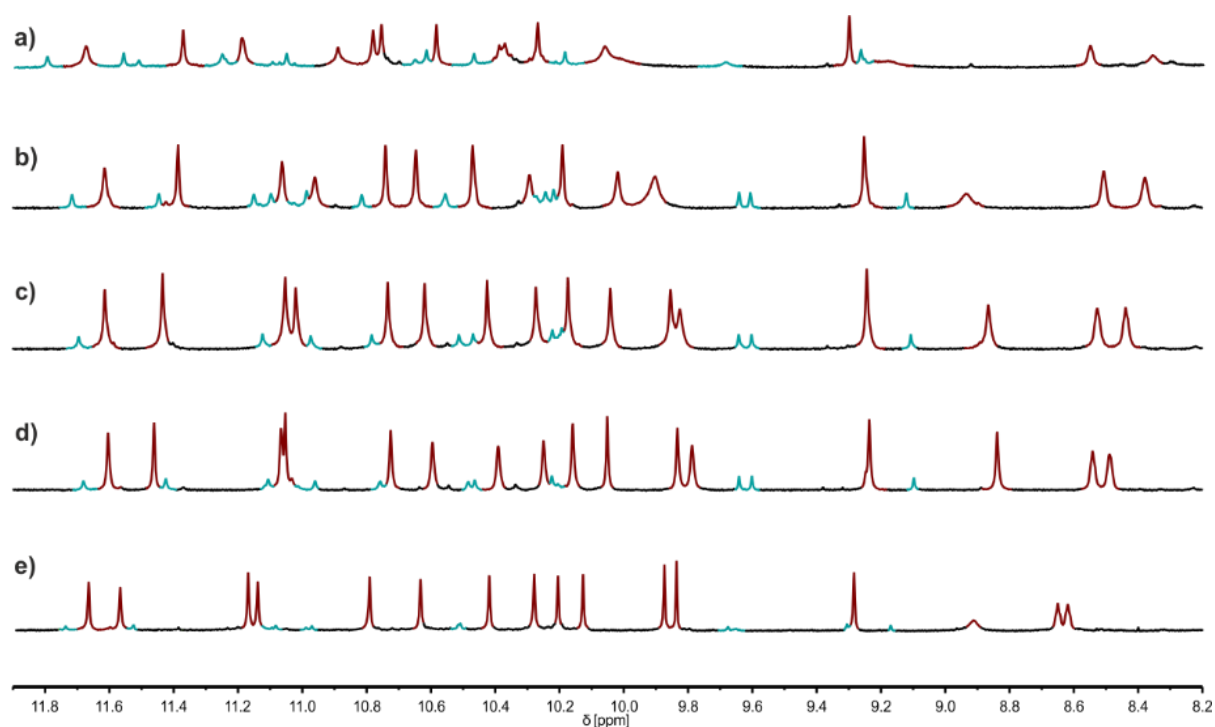
**Figure S23. Schematic representation of foldamer helix assembly into shifted dimers.** a) Front view of the hydrogen array of hydrogen bond donors and acceptors on a P helix (in blue) and its simplified representation on a plane. Hydroxy hydrogen bond donors are shown as yellow spheres. Amide carbonyl oxygen atoms that act as hydrogen bond acceptors (and only those) are shown as red spheres. Blue spheres indicate the N-terminus of the helix. b)-f) Views of the formation of a head-to-tail chiral (PP) shifted dimer, including the  $180^\circ$  rotation of the array of hydrogen bond donors and acceptors (b); a side-view (c) and a top-view (d) of the chiral dimer; an “open-book” view with arrows linking each hydrogen bond donor to the corresponding acceptor (e); and a transparent view showing the two hydrogen-bonding array above each other (f). g) Mirror image of the views in a) showing the enantiomeric M helix (in purple). h)-l) Views of the formation of a head-to-tail PM (meso) shifted dimer, including the inversion of the array of hydrogen bond donors and acceptors (i); a side-view (g) and a top-view (j) of the PM dimer; an “open-book” view with arrows linking each hydrogen bond donor to the corresponding acceptor (l); and a transparent view showing the two hydrogen-bonding array above each other (k).



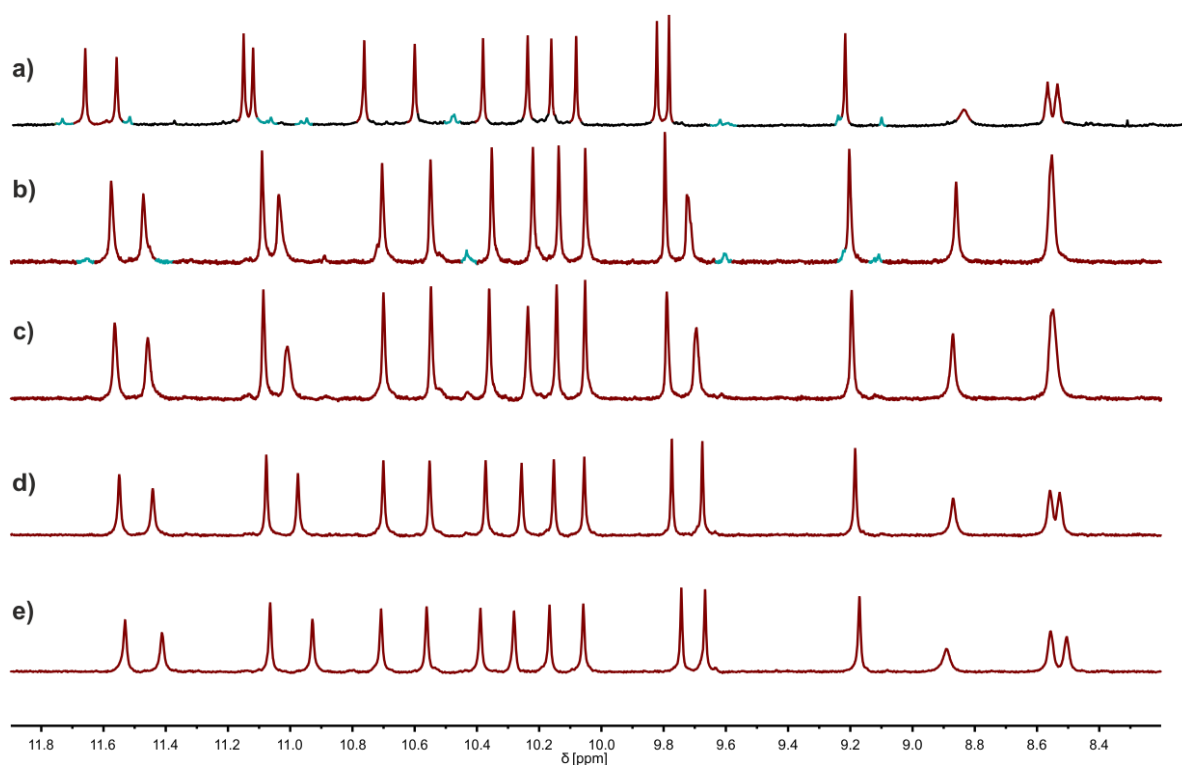
**Figure S24. Identification of hydrogen bonded OH signals of **5** in CD<sub>2</sub>Cl<sub>2</sub>.** Part of the 500 MHz <sup>15</sup>N, <sup>1</sup>H HSQC NMR spectrum of **5** (8.0 mM in CD<sub>2</sub>Cl<sub>2</sub>) at 25 °C showing the amide and hydroxy proton resonances. Only NH resonances correlate, blue dots indicate the signals of OH protons. The spectrum was measured after a two-hour incubation time to reach equilibrium.



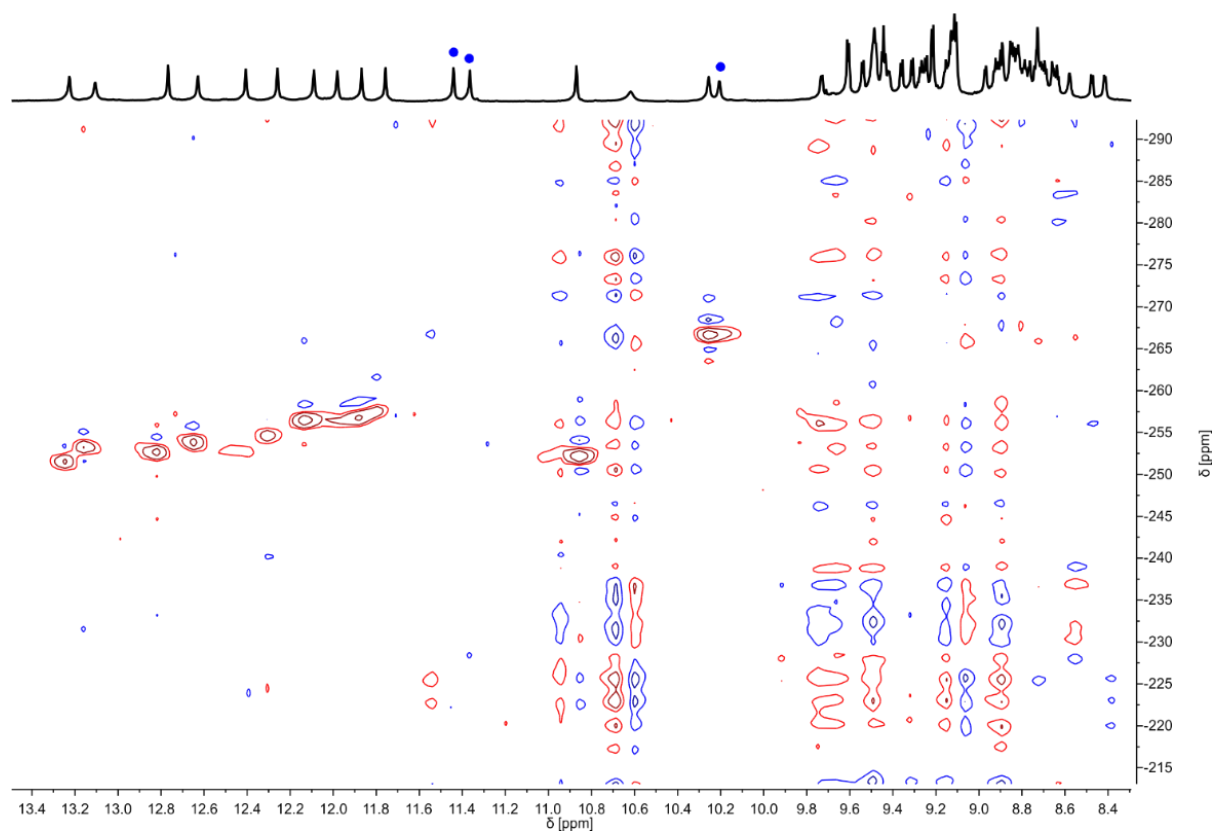
**Figure S25. Identification of hydrogen bonded OH signals of **6** in  $\text{CD}_2\text{Cl}_2$ .** Part of the 500 MHz  $^{15}\text{N}, ^1\text{H}$  HSQC NMR spectra (11.1 mM in  $\text{CD}_2\text{Cl}_2$ ) at 25 °C showing the amide and hydroxy proton resonances of **6** after 2 h after pyridine-treatment. A pyridine solution of **6** was evaporated, dried and the solid was dissolved in  $\text{CD}_2\text{Cl}_2$  and incubated for 2h prior to measuring the spectrum. Only NH resonances correlate, blue dots indicate the signals of OH protons.



**Figure S26. Interconversion of the PM and PP/MM shifted dimers of 5 upon changing CDCl<sub>3</sub>/CD<sub>2</sub>Cl<sub>2</sub> solvent mixtures.** Part of the 500 MHz <sup>1</sup>H NMR spectra of **5** (2.4 mM in CDCl<sub>3</sub>/CD<sub>2</sub>Cl<sub>2</sub> mixtures) at 25 °C showing the amide and hydroxy proton resonances. The volume percentages of CD<sub>2</sub>Cl<sub>2</sub> are 0 (a), 25 (b), 50 (c), 75 (d), and 100 (e). The signals of two different species are marked with different colors. Signals of the PP/MM shifted dimer are marked in turquoise, those of the PP shifted dimer dominant in CH<sub>2</sub>Cl<sub>2</sub> are marked in brown. The spectra were measured after a two-hour incubation time to reach equilibrium.

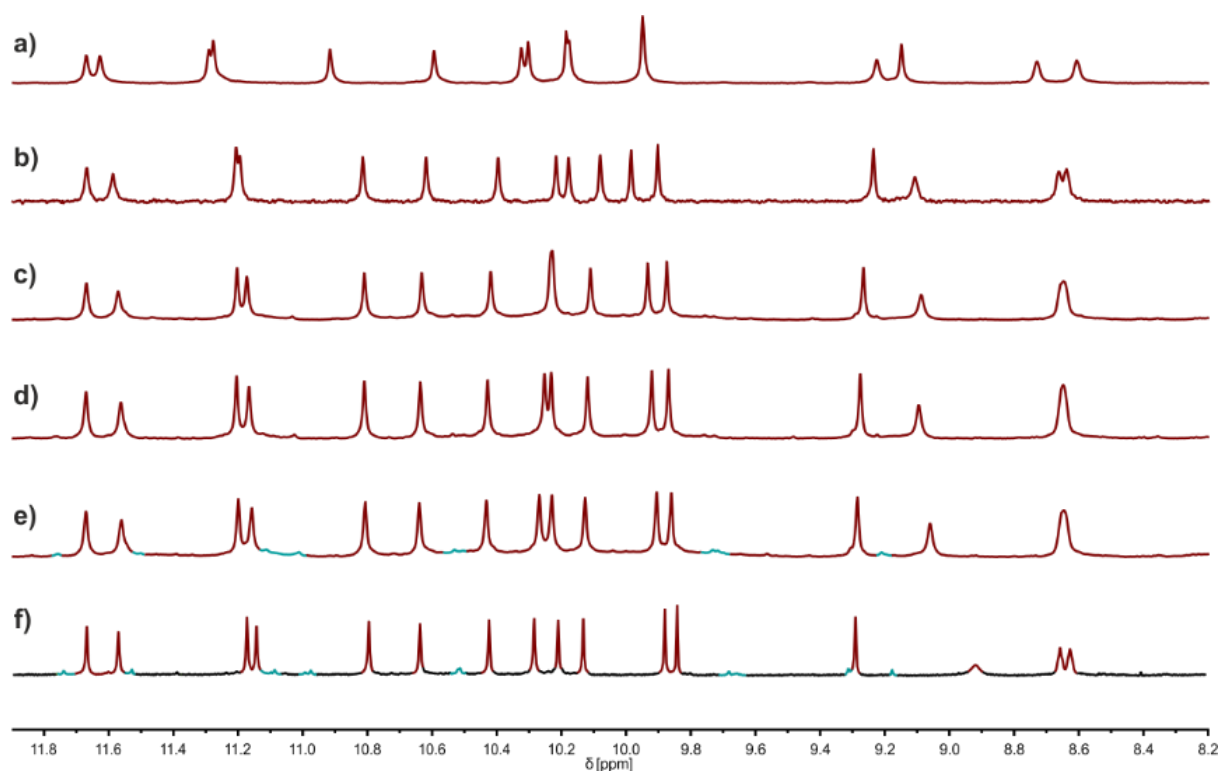


**Figure S27. The *PP* shifted dimer of **5** prevails in  $\text{CD}_2\text{Cl}_2/(\text{CD}_2\text{Cl})_2$  solvent mixtures.** Part of the 500 MHz  $^1\text{H}$  NMR spectra of **5** (2.4 mM in  $\text{CD}_2\text{Cl}_2/(\text{CD}_2\text{Cl})_2$  mixtures) at 25 °C showing the amide and hydroxy proton resonances. The volume percentages of  $(\text{CD}_2\text{Cl})_2$  are 0 (a), 25 (b), 50 (c), 75 (d) and 100 (e). The signals of two different species are marked with different colors. Signals of *PM* shifted dimer are marked in turquoise, those of the *PP* shifted dimer are marked in brown. The spectra were measured after a two-hour incubation time to reach equilibrium.

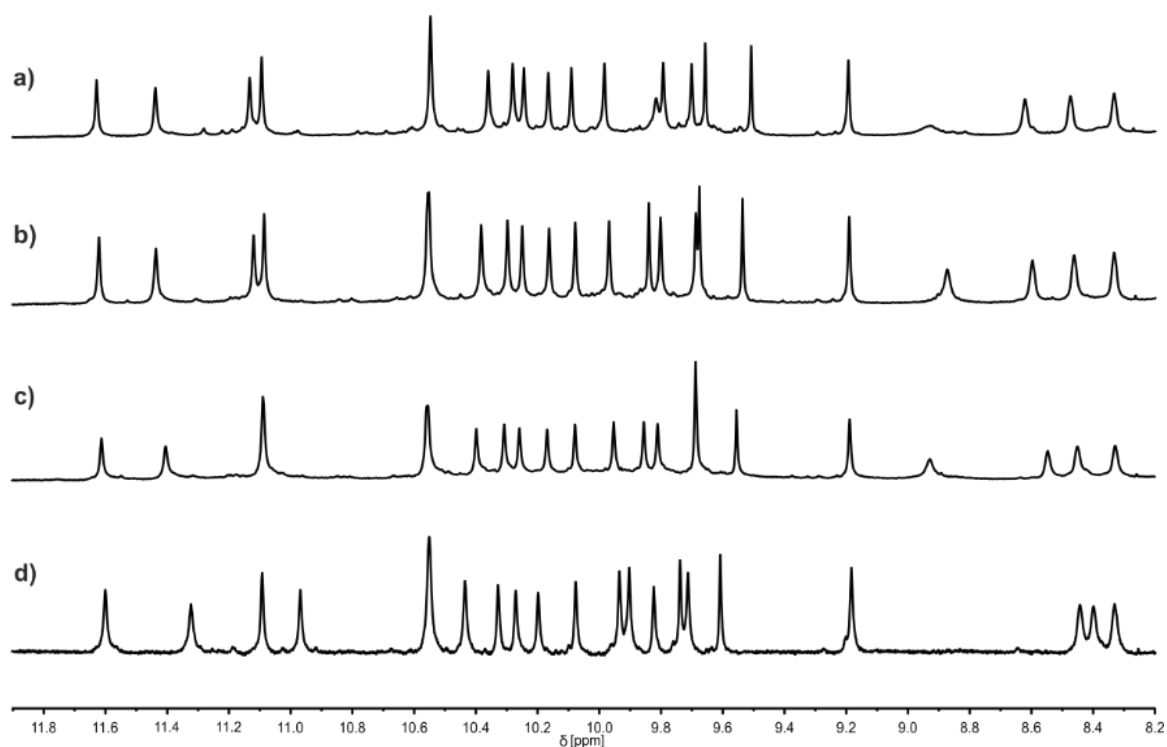


**Figure S28. Identification of hydrogen bonded OH signals of **5** in  $(\text{CD}_2\text{Cl})_2$ .** Part of the 500 MHz  $^{15}\text{N}, ^1\text{H}$  HSQC NMR spectrum of **5** (2.31 mM in  $(\text{CD}_2\text{Cl})_2$ ) at 25 °C showing the amide and hydroxy proton resonances. Only NH resonances correlate, blue dots indicate the signals of OH protons. The spectrum was measured after a two-hour incubation time to reach equilibrium.

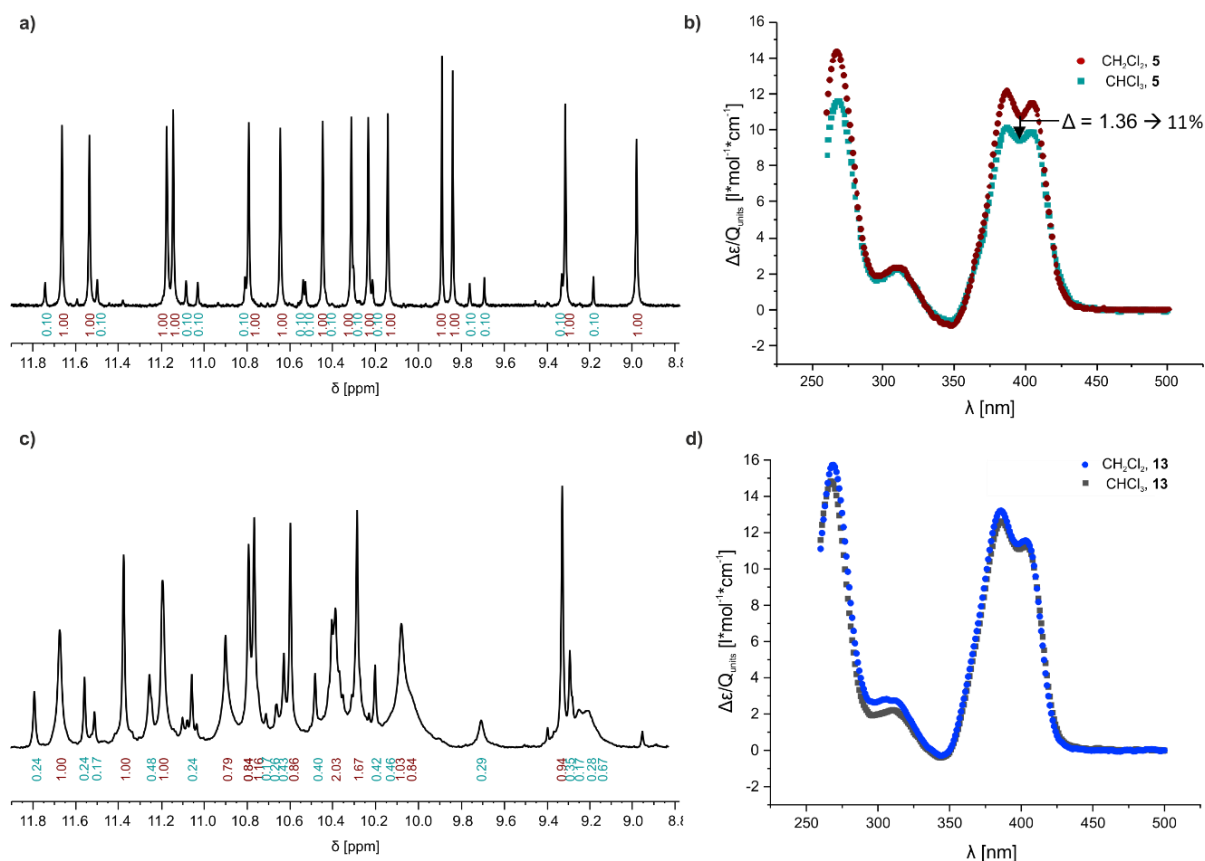




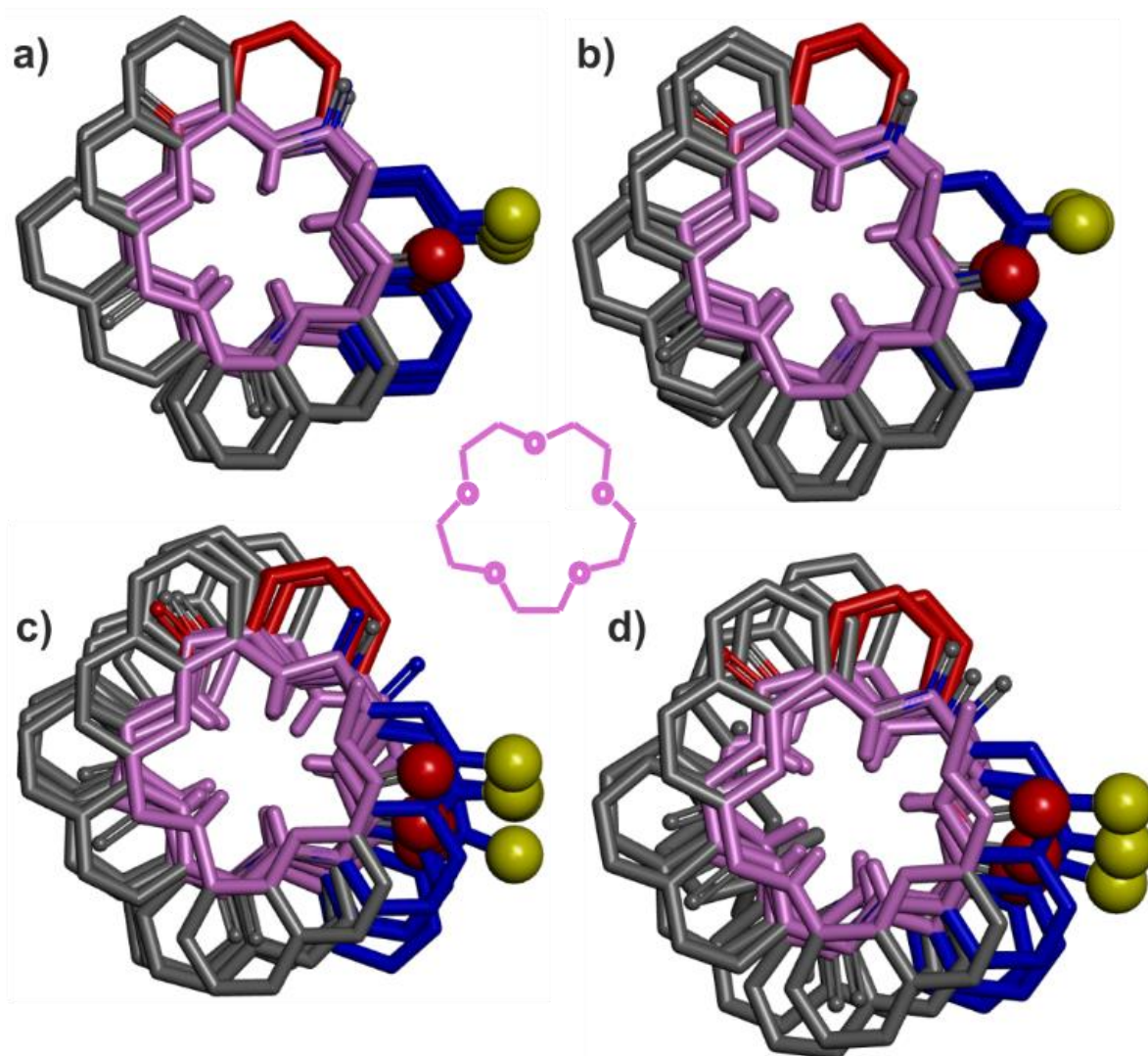
**Figure S29.** The *PP* shifted dimer of **5** prevails in CD<sub>2</sub>Cl<sub>2</sub>/ toluene-*d*<sub>8</sub> solvent mixtures. Part of the 500 MHz <sup>1</sup>H NMR spectra of **5** (2.4 mM in CD<sub>2</sub>Cl<sub>2</sub>/toluene-*d*<sub>8</sub> mixtures) at 25 °C showing the amide and hydroxy proton resonances. The volume percentages of CD<sub>2</sub>Cl<sub>2</sub> are 0 (a), 25 (b), 50 (c), 75 (d) and 100 (e). The signals of two different species are marked with different colors. Signals of the species dominant in CHCl<sub>3</sub> are marked in turquoise, those of the species dominant in CH<sub>2</sub>Cl<sub>2</sub> are marked in brown. The spectra were measured after a two-hour incubation time to reach equilibrium.



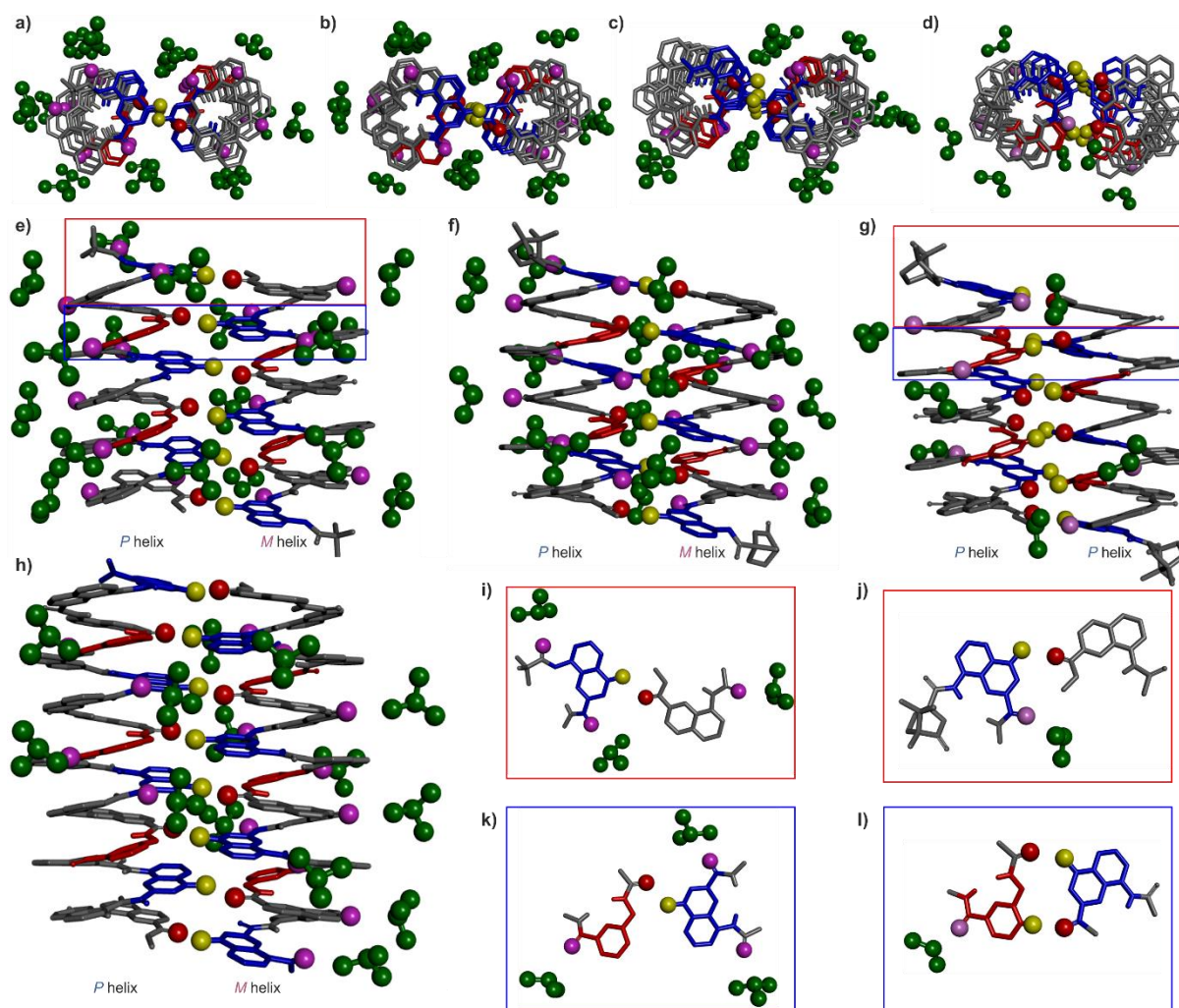
**Figure S30. The *PP* shifted dimer of **6** prevails in various solvents** Part of the 500 MHz  $^1\text{H}$  NMR spectra of **6** (2.4 mM in various solvents) at 25 °C showing the amide and hydroxy proton resonances. A pyridine solution of **6** was evaporated, dried and the solid was dissolved in  $\text{CD}_2\text{Cl}_2$  and incubated for six weeks prior to measuring the spectrum in (a). The sample in a) was evaporated, dried and the solid was dissolved in 1:1  $\text{CDCl}_3/\text{CD}_2\text{Cl}_2$  and incubated for one week (b) and six weeks (c) prior to measuring the spectra. The sample in c) was evaporated, dried and the solid was dissolved in  $\text{CDCl}_3$  and incubated for six weeks prior to measuring the spectrum (d).



**Figure S31.** Assignment of the PM and PP/MM shifted dimers of **5** in  $\text{CDCl}_3$  and  $\text{CD}_2\text{Cl}_2$ . Part of the 500 MHz  $^1\text{H}$  NMR spectra of **5** in  $\text{CD}_2\text{Cl}_2$  (a) and  $\text{CDCl}_3$  (c) at 25 °C and 2.4 mM showing the integration of amide and hydroxy proton resonances. CD spectra of **5** in  $\text{CD}_2\text{Cl}_2$  and  $\text{CDCl}_3$  at 25 °C (b). CD spectra of **13** (protected precursor of **5**, see Scheme S5 for its formula) in  $\text{CD}_2\text{Cl}_2$  and  $\text{CDCl}_3$  at 25 °C (d). At these wavelengths, CD bands are mostly due to quinoline rings. The molar extinction ( $\Delta\epsilon$ ) is thus normalized to the number of Q units for better comparability.

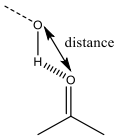


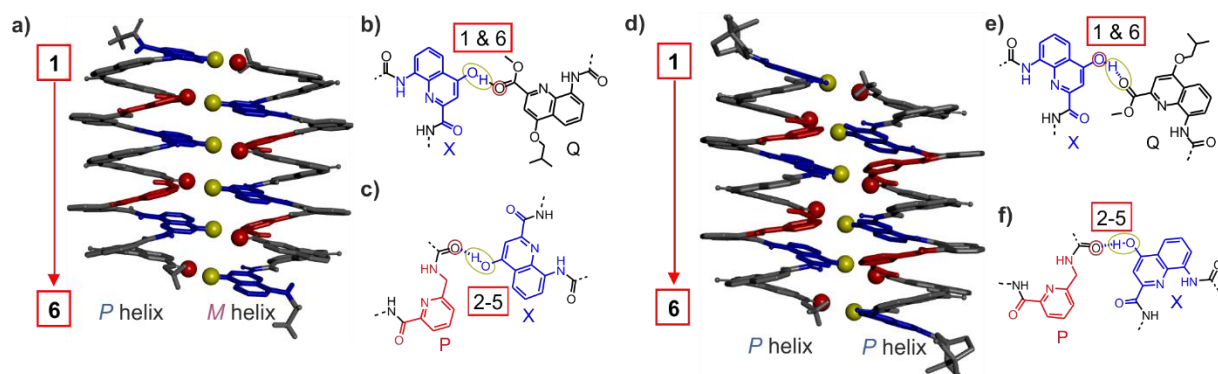
**Figure S32. The shapes of the helix inner rims suggest there is no helix torsional strain.** Top views of one helix of the crystal structures of the *PM* shifted dimers of **3** (a), **5** (b) and **7** (c) and of the *PP* shifted dimer of **5** (d). The inner rim of the helix is highlighted in pink. The preferred curvature of  $Q_n$  oligomers typically shows a 15-crown-5 shape of the inner rim (a 15-crown-5 is shown in the middle of the Figure for comparison). There is little (c, d) or no (a, b) deviation from this pattern in the four cases. The X units are shown in blue, the Y units in violet and the P units in red tubes. Carbonyl and hydroxy oxygen atoms involved in intermolecular hydrogen bonds are shown as red and yellow spheres, respectively. Included solvent molecules, hydrogen atoms and side-chains are omitted for clarity.



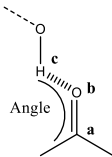
### 4.2.3 Supplementary tables

**Table S1.** Distances between hydrogen-bonded carbonyl and hydroxy oxygen atoms in the solid state structures of **3** and **5**. Entries are numbered from 1 to 6, as in the structures below. Remarkable values are shown in red.

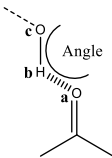
Entry	Distance	<i>PM</i> dimer of <b>3</b>	<i>PP</i> dimer of <b>5</b>
1		2.782 Å	2.766 Å
2		2.646 Å	2.680 Å
3		2.710 Å	2.610 Å
4		2.710 Å	2.608 Å
5		2.646 Å	2.645 Å
6		2.782 Å	2.699 Å



**Table S2.** C=O...H angles within the hydrogen-bonded carbonyl and hydroxy groups in the solid state structures of **3** and **5**. Entries are numbered as in Table 1. Remarkable values are shown in red.

Entry	Angle	<i>PM</i> dimer of <b>3</b>	<i>PP</i> dimer of <b>5</b>
			
1		137.57°	165.07°
2		135.88°	145.86°
3		135.24°	143.79°
4		135.24°	148.79°
5		135.88°	139.18°
6		137.57°	167.38°

**Table S3.** O-H...O angles within the hydrogen-bonded carbonyl and hydroxy groups in the solid state structures of **3** and **5**. Entries are numbered as in Table 1. Remarkable values are shown in red.

Entry	Angle	<i>PM</i> dimer of <b>3</b>	<i>PP</i> dimer of <b>5</b>
			
1		162.19°	163.07°
2		146.92°	149.97°
3		152.62°	154.05°
4		152.62°	148.29°
5		146.92°	138.32°
6		162.19°	165.04°

**Table S4.** Hydrogen bonds geometry in the crystal structures. Atom numbers are those of the cif file.

D—H...A	D—H	H...A	D...A	D—H...A
<b>7</b>				
O1D-H1D...O3E	0.84	1.81	2.63 (2)	163
O6H-H6H...O3C	0.84	2.06	2.70 (2)	133
O2D-H2D...O13G	0.84	1.98	2.77 (2)	155
O4H-H4H...O21	0.84	1.89	2.59 (3)	139
O3D-H3D...O8G	0.84	1.99	2.79 (2)	159
O2H-H2H...O13C	0.84	1.92	2.65 (2)	145
O5D-H5D...O3G	0.84	1.90	2.56 (3)	134
O1H-H1H...O3A	0.84	2.12	2.84 (3)	143
<b>3</b>				
O1C-H1C...O2A <sup>i</sup>	0.84	1.97	2.77 (2)	159
O3C-H3C...O3B <sup>i</sup>	0.84	1.88	2.64 (2)	150
O2C-H2C...O8B <sup>i</sup>	0.84	1.97	2.74 (1)	153
O1H-H1H...O2G <sup>ii</sup>	0.84	1.98	2.80 (2)	165
O3H-H3H...O3F <sup>ii</sup>	0.84	1.93	2.65 (2)	144
O2H-H2H...O8F <sup>ii</sup>	0.84	1.91	2.68 (2)	152
<b>5 (chiral aggregate)</b>				
O1C-H1C...O1	0.84	1.88	2.70 (2)	165
O3F-H3F...O3B	0.84	1.96	2.65 (2)	139
O2C-H2C...O8E	0.84	1.86	2.60 (2)	148
O2F-H2F...O8B	0.84	1.83	2.61 (2)	154
O3C-H3C...O3E	0.84	1.92	2.68 (3)	150
O1F-H1F...O2A	0.84	1.95	2.76 (2)	163
<b>5 (pseudo-racemic aggregate)</b>				
O1C-H1C...O16B	0.84	1.94	2.40 (3)	114
O3A-H3A...O6D	0.84	1.93	2.72 (3)	158
O2C-H2C...O11B	0.84	1.90	2.58 (2)	138
O2A-H2A...O11D	0.84	1.80	2.59 (2)	155
O3C-H3C...O6B	0.84	1.89	2.61 (2)	143
O1A-H1A...O16D	0.84	1.97	2.75 (3)	154



Symmetry codes: (i)-x, -1-y, 1-z, (ii) 1-x, -y, 1-z

*See the section on crystallography below for Tables S5 and S6.*

## 4.2.4 Supplementary methods

### 4.2.4.1 MS analyses

HR-MS spectra were recorded on a Bruker microTOF II by direct infusion from acetonitrile in positive ionization mode. The instrument was calibrated in positive mode by direct infusion of a calibration solution (Agilent Technologies ESI-L Low Concentration Tuning Mix). The mass sample was prepared by adding 10  $\mu$ L of a solution of the sample in DCM (0.1 mg/mL) to 1 mL of a solution of 0.1% formic acid in acetonitrile.

### 4.2.4.2 Molecular modeling

Models were simulated by using Maestro version 11.5 (Schrödinger Inc.). Energy minimized structures were obtained using MacroModel energy minimization with the following parameters: force field: MMFFs; solvent: none; electrostatic treatment: constant dielectric; dielectric constant: 1.0; charges from: force field; cutoff: normal; Van der Waals: 7.0; electrostatic: 12.0; H-bond: 4.0; mini method: TNCG; maximum iterations: 2500; converge on: gradient; convergence threshold: 0.05; constraints: distances. As a starting point, the coordinates of the crystal structure of **3** (CCDC entry # 2209189) and **5** (CCDC entry # 2209187) were used. A single helix was first energy-minimized. In a second round, two helices were placed in a plausible arrangement, and distance constraints between plausible hydrogen-bonding partners were set on purpose to 2.5. While setting the constraints, it was important to match the hydroxy group to their correct hydrogen-bonding carbonyl partner. The energy-minimized model was fixed was possible unlikely conformations and energy-minimized again. Then all constraints were removed, and energy minimization was repeated. Typically, only minimal changes occurred at this stage, and the structure was exported as a mol2 file.

### 4.2.4.3 Nuclear magnetic resonance spectroscopy

NMR spectra were recorded on different NMR spectrometers: (I) an Avance III HD NMR spectrometer 400 MHz (Bruker BioSpin) for  $^1\text{H}$  NMR and  $^{13}\text{C}$  NMR spectra of small units. (II) an Avance III HD NMR spectrometer 500 MHz (Bruker BioSpin) with CryoProbe<sup>TM</sup> Prodigy for  $^1\text{H}$  NMR,  $^1\text{H}$ ,  $^{15}\text{N}$ -HSQC, and DOSY spectra of foldamers. (III) a Bruker HD NMR spectrometer 400 MHz (Bruker BioSpin) for variable temperature measurements. Chemical shifts are described in part per million (ppm,  $\delta$ ) relative to the  $^1\text{H}$  residual signal of the deuterated solvent used. Meaning DMSO- $d_6$  ( $\delta$  2.50 ppm), pyridine- $d_5$  ( $\delta$  8.74 ppm),  $\text{CD}_2\text{Cl}_2$  ( $\delta$  5.32 ppm) and  $\text{CDCl}_3$  ( $\delta$  7.16 ppm).  $^1\text{H}$  NMR splitting patterns with observed

first-order coupling are entitled as singlet (s), doublet (d), triplet (t), quartet (q), multiplet (m) or broad singlet (bs). Coupling constants ( $J$ ) are ported in Hertz.

Sample preparation and incubation times to reach equilibrium required attention. The required equilibration times of sequences **3-6** were estimated by equilibrating each sample in  $\text{CDCl}_3$  and  $\text{CD}_2\text{Cl}_2$  after complete disruption of the aggregates. Complete disruption was achieved by dissolving the sample in pyridine and then evaporating the solvent. Spectra were measured at different time intervals from 2h to 9 weeks until no further change was observed. Additionally, samples were dissolved and incubated in  $\text{CDCl}_3$  and  $\text{CD}_2\text{Cl}_2$  after being brought to equilibrium in the other solvent. At equilibrium, the same spectra were obtained regardless of the solvent history of the sample. However, the required incubation times were found to depend on the previous solvent in which the sample was equilibrated. For example, **4** is monomeric in pyridine and forms a *PM* shifted dimer in  $\text{CDCl}_3$ . When these solutions are evaporated and re-dissolved in  $\text{CD}_2\text{Cl}_2$  the starting species are not the same and the equilibrium to produce the homochiral shifted is reached faster with the sample coming from pyridine than with the sample coming from  $\text{CDCl}_3$ .

In the case of shorter sequences **3** and **5**, equilibration times were generally fast (around 5 min). Samples were typically incubated for 2h which gave a large margin. In the case of **4** and **6**, equilibration times are considerably longer and incubation of three to six weeks is indicated.

Solvent-dependency studies of **3** and **5** were carried out by adding *e.g.*  $\text{CD}_2\text{Cl}_2$  to a solution in *e.g.*  $\text{CDCl}_3$  stepwise up to 50:50 and by making the reverse experiment, that is adding  $\text{CDCl}_3$  to a  $\text{CD}_2\text{Cl}_2$  solution stepwise up to 50:50. Because of the faster equilibration, the same sample could be used and spectra were measured 2h after every addition. In the case of **4** and **6**, equilibration times are much longer and a minimum of two weeks is recommended between each addition. Alternatively, individual samples for each solvent mixture may be prepared and incubated concomitantly.

$^1\text{H}$ ,  $^{15}\text{N}$ -HSQC spectra were recorded with a phase-sensitive pulse sequence with sensitivity enhancement using trim pulses in inept transfer (hsqcetgpsi2) from the Bruker pulse program library. Data acquisition was performed utilizing non-uniform sampling (NUS; NUS amount: 50% with an automatically created NUSList) yielding 1024 (F2) x 128 (F1) data points in Echo/Antiecho gradient selection mode. The recycling delay was 2.0 s and 64 transients per increment were applied at a sweep width of 2.5 kHz in F2 and 7 kHz in F1 resulting in an acquisition time of 0.1462 s. NUS processing was performed using the fully automated NUS processing tool provided by MestReNova. Zero filling in F1 has been used to yield a final matrix of 1K x 1K real points.

The DOSY spectrum was recorded applying a pulse sequence with stimulated echo using bipolar gradient pulses for diffusion from the Bruker pulse program library (stebpgp1s). The diffusion delay  $\Delta$  (big delta) was set to 120 ms and the diffusion gradient pulse length  $\delta$  (little delta) was set to 1.2 ms. The number of gradient steps were set to 32 with linear spacing starting from 2% reaching 95% of the

full gradient strength in the final step. For each of the 32 gradient amplitudes, 16 transients of 65k complex data points were acquired. DOSY processing was performed with the DOSY processing tool from MestReNova (v.12.x64) employing the Peak Heights Fit algorithm including the overlapped peaks analysis” with 128 points in diffusion dimension and a window of  $1.00 \times 10^{-16}$  to  $1.00 \times 10^{+03}$   $\text{cm}^2 \text{ s}^{-1}$ .

#### 4.2.4.4 CD studies

All CD spectra were recorded on a Jasco J-810 spectrometer with 10 mm quartz cuvette. The following parameters were used: wavelength range from 500 to 250 nm. Scan speed: 200 nm/min; accumulation: 3; response time: 1.0 s; bandwidth: 2; temperature: 25 °C; sensitivity: standard (100 mdeg); data pitch: 1 nm; nitrogen gas flow rate: 500L/h. The sample solution was prepared in distilled chloroform or DCM filtered over alumina before use.  $\Delta\epsilon$  values (in  $\text{cm}^2 \cdot \text{mmol}^{-1}$ ) were obtained by using the formula:  $\Delta\epsilon = m^\circ / (C \cdot l \cdot 32980)$  where  $m^\circ$  = CD value in millidegrees;  $l$  = cuvette pathlength in cm;  $C$  = sample concentration in mol/L. The CD spectra of **5** and its protected precursor **13** were carried out at 0.01 mM in chloroform and DCM. Thus, a solution of **5** or **13** in pyridine was prepared and the same volume was taken, respectively. After removal of the solvent, the samples were dissolved and incubated in chloroform or DCM.

#### 4.2.4.5 X-ray crystallography

The diffraction data for selected single crystals were collected at the IECB x-ray facility (CNRS UMS 3033 – INSERM US001) with a Rigaku FRX rotating anode (2.9 kW) diffractometer.  $\text{CuK}\alpha$  radiation monochromated with high flux Osmic Varimax HF mirrors was used for data collection. The x-ray source is equipped with a Dectris Pilatus 200K detector and partial chi goniometer. All crystals were kept at 100(2) K during data collection. The data were processed with the CrysAlis PRO software<sup>[5]</sup> with a multiscan absorption correction. Structures were solved with the ShelXT<sup>[6]</sup> structure solution program using a dual-space algorithm. Crystal model refinement was performed with ShelXL<sup>[7]</sup> package using Least Squares minimization implemented in Olex2.<sup>[8]</sup>

For some side chains, not all C or O atoms were found. During refinement, anisotropic displacement parameters were used for backbones, some solvent molecules and side chains. The C- and N-bound hydrogen atoms were placed at an idealized position. The positions of hydrogen atoms of O-H groups were found based on possible hydrogen bonds. All H atoms were refined in the riding-model approximation, with  $U_{\text{iso}}(\text{H}) = 1.2U_{\text{eq}}(\text{CH}, \text{CH}_2, \text{NH})$  and  $U_{\text{iso}}(\text{H}) = 1.5U_{\text{eq}}(\text{OH})$ . EADP, DELU, SIMU and RIGU instructions were employed to model temperature parameters. The geometry of the molecules was improved with DFIX, FLAT or AFIX commands.

The structure of **7** was refined as a racemic twin in a P1 space group. Attempts to perform refinement in a centrosymmetric space group (P-1) were made, but the model was unstable.

The electron density maps were carefully inspected to localize the position of solvent molecules. The unrecognized residual electron density peaks close to chloroform molecules were introduced to the refinement as dummy Cl atoms, in other areas as dummy O atoms. However, some solvent molecules were severely disordered, and their introduction to the model caused significant deterioration of the refinement parameters. Thus, the solvent masking procedure implemented in Olex2<sup>[8]</sup> was employed to remove them. The solvent radius was set to 1.2 Å, calculated total potential solvent-accessible void volume and electron counts per unit-cell 2689 Å<sup>3</sup> and 791, 802 Å<sup>3</sup> and 148, 8894 Å<sup>3</sup> and 1914, 5921 Å<sup>3</sup> and 1301, for racemic crystal structure of **3** and **7**, as well as homochiral and pseudo-racemic crystal structure of **5**, respectively.

The final cif files were checked using IUCR's checkcif algorithm. Due to the characteristics of the crystals, *i.e.* large volume fractions of disordered solvent molecules, weak diffraction intensity, incompleteness of the data and moderate resolution, and twinning, a number of A - level and B - level alerts remain in the check cif file. These alerts are inherent to the data and refinement procedures and do not reflect errors. They are explicitly listed below and have been divided into two groups. The first group illustrates the poor quality of the data and refinement statistics compared to that expected for small molecule structures from highly diffracting crystals. The second group is connected to decisions made during refinement and explained below.

#### **Group 1:**

THETM01\_ALERT\_3\_A The value of sine(theta\_max)/wavelength is less than 0.550

PLAT023\_ALERT\_3\_A, B Resolution (too) Low [sin(theta)/Lambda < 0.6].

PLAT082\_ALERT\_2\_A, B High R1 Value

PLAT084\_ALERT\_3\_A, B High wR2 Value (*i.e.* > 0.25)

PLAT934\_ALERT\_3\_A, B Number of (Iobs-Icalc)/Sigma(W) > 10 Outliers

PLAT971\_ALERT\_2\_B Check Calcd Positive Resid. Density

PLAT090\_ALERT\_3\_B Poor Data / Parameter Ratio (Zmax > 18)

PLAT220\_ALERT\_2\_B NonSolvent Resd 1 C Ueq(max)/Ueq(min) Range

PLAT241\_ALERT\_2\_B High 'MainMol' Ueq as Compared to Neighbors

PLAT242\_ALERT\_2\_B Low 'MainMol' Ueq as Compared to Neighbors

PLAT340\_ALERT\_3\_B Low Bond Precision on C-C Bonds

#### **Group 2:**

PLAT201\_ALERT\_2\_A Isotropic non-H Atoms in Main Residue(s)

As mentioned above, not all atoms were refined with ADPs

PLAT315\_ALERT\_2\_B Singly Bonded Carbon Detected (H-atoms Missing)

Not all H-atoms were localized, but they were used in SFAC calculation

PLAT306\_ALERT\_2\_B Isolated Oxygen Atom (H-atoms Missing ?)

Unrecognized electron density was introduced to the refinement as dummy oxygen atoms.

PLAT430\_ALERT\_2\_A Short Inter D...A Contact

Contacts between dummy O atoms.

**Table S5** Crystal data and refinement details for racemic crystal structure of **3** and **7**, as well as homochiral of **5**.

Identification code	<b>3</b> (racemic)	<b>5</b> (homochiral)	<b>7</b> (racemic)
Chemical formula	2(C <sub>159</sub> H <sub>148</sub> N <sub>26</sub> O <sub>25</sub> Se)· 23.74(CHCl <sub>3</sub> ) solvent**	C <sub>164</sub> H <sub>152</sub> N <sub>26</sub> O <sub>27</sub> Se·4 (CH <sub>2</sub> Cl <sub>2</sub> )·solvent**	2(C <sub>217</sub> H <sub>200</sub> N <sub>36</sub> O <sub>41</sub> S <sub>7</sub> S e <sub>2</sub> )·21(O)*·1.7(Cl)*· 23.6(CHCl <sub>3</sub> ) solvent**
Formula weight	8637.59	3337.77	11918.87
Crystal system	Triclinic	Orthorhombic	Triclinic
Space group	P-1	P2 <sub>1</sub> 2 <sub>1</sub> 2	P1
Unit cell dimensions (Å, °)	a=26.6435 (7), α=87.193 (2)	a=34.7079 (1), α=90	a=19.2663 (6) α=107.926 (2)
	b=27.0228 (7), β=68.158 (2)	b=52.844 (2), β=90	b=27.5957 (6) β=92.018 (3)
	c=30.0865 (7), γ=84.410 (2)	c=20.0658 (4), γ=90	c=29.3722 (10) γ=100.461 (2)
Volume (Å <sup>3</sup> )	20009.2 (9)	36802 (2)	14541.8 (8)
Z	2	8	1
Density (calculated) (Mg m <sup>-3</sup> )	1.434	1.205	1.36
Absorption coefficient (mm <sup>-1</sup> )	5.20	1.92	4.47
Crystal size (mm)	0.10 × 0.07 × 0.03	0.20 × 0.06 × 0.02	0.10 × 0.08 × 0.03
Completeness	98.5 (up to 50.43°)	100 (up to 44.48°)	99.4 (up to 50.43°)
Reflections collected	127174	83736	120984
Reflections observed [I > 2σ(I)]	25187	17095	28821
R <sub>int</sub>	0.078	0.043	0.058
Data/parameters/re strains	41251/3074/657	28971/2767/2491	49594/1812/2979
Goodness-of-fit on F <sup>2</sup>	2.35	1.19	1.70
Final R indices [I > 2σ(I)]	0.2341, 0.5699	0.1130, 0.2959	0.1993, 0.4590

<b>R indices (all data)</b>	0.2765, 0.6040	0.1536, 0.3343	0.2396, 0.4962
<b>Largest diff. peak and hole</b>	3.30, -1.57	0.46, -0.44	1.88, -0.70
<b>CCDC #</b>	2209189	2209187	2209188

Experiments were carried out at 100 K with Cu K $\alpha$  radiation. Absorption was corrected by multi-scan

\* Unrecognized electron density was introduced to the refinement as dummy oxygen or as chlorine atoms

\*\* Solvent mask was used to remove severely disordered solvent molecules

**Table S6.** Crystal data and refinement details for pseudo-racemic crystal structure of **5**.

<b>Identification code</b>	<b>5</b> (pseudo-racemic)
<b>Chemical formula</b>	C <sub>164</sub> H <sub>152</sub> N <sub>26</sub> O <sub>27</sub> Se·18(CHCl <sub>3</sub> )·solvent* *
<b>Formula weight</b>	8144.76
<b>Crystal system</b>	Monoclinic
<b>Space group</b>	P2
<b>Unit cell dimensions</b> (Å, °)	a=26.2355 (5), α=90 b=20.3023 (6), β=94.254 (2) c=41.8226 (8), γ=90
<b>Volume (Å<sup>3</sup>)</b>	22215.1 (9)
<b>Z</b>	2
<b>Density (calculated)</b> (Mg m <sup>-3</sup> )	1.218
<b>Absorption coefficient</b> (mm <sup>-1</sup> )	3.73
<b>Crystal size</b> (mm)	0.20 × 0.07 × 0.03
<b>Completeness</b>	91.2 (up to 47.53°)
<b>Reflections collected</b>	76330
<b>Reflections observed</b> [I > 2σ(I)]	22119
<b>R<sub>int</sub></b>	0.060
<b>Data/parameters/restraints</b>	37171/2090/3147
<b>Goodness-of-fit on F<sup>2</sup></b>	1.72
<b>Final R indices</b> [I > 2σ(I)]	0.1790, 0.4450
<b>R indices (all data)</b>	0.2162, 0.4794
<b>Largest diff. peak and hole</b>	1.29, -0.56



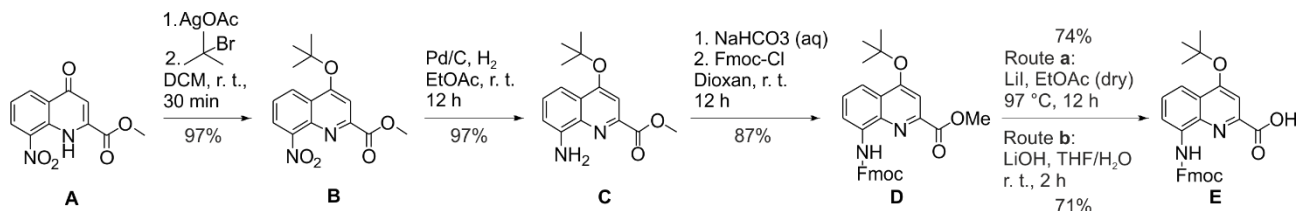
CCDC #	2209186
--------	---------

Experiments were carried out at 100 K with Cu K $\alpha$  radiation. Absorption was corrected by multi-scan

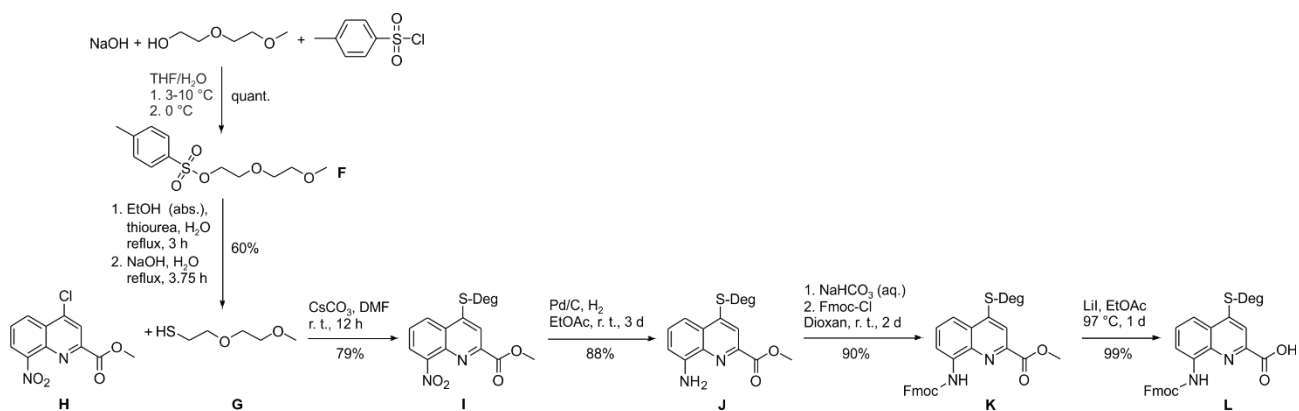
\*\* Solvent mask was used to remove severely disordered solvent molecules

## 4.2.5 Synthetic Schemes

### 4.2.5.1 Synthesis of monomers

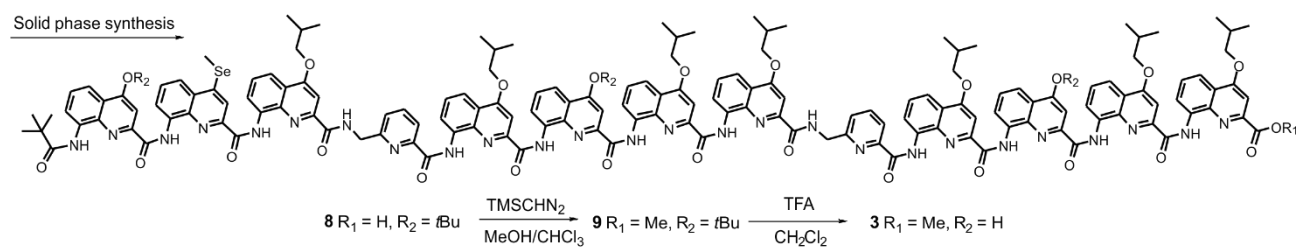


**Scheme 1. Synthesis of Fmoc-X-OH E. (X denotes tBu-protected X)**

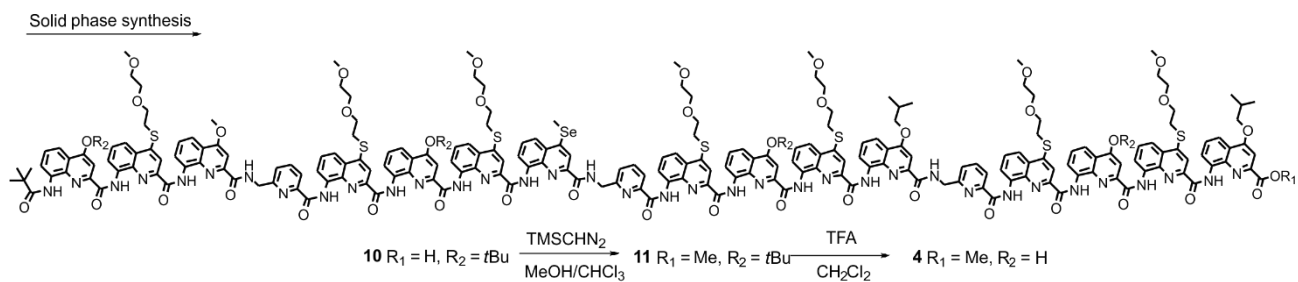


**Scheme 2. Synthesis of Fmoc-Q<sup>D</sup>-OH L.**

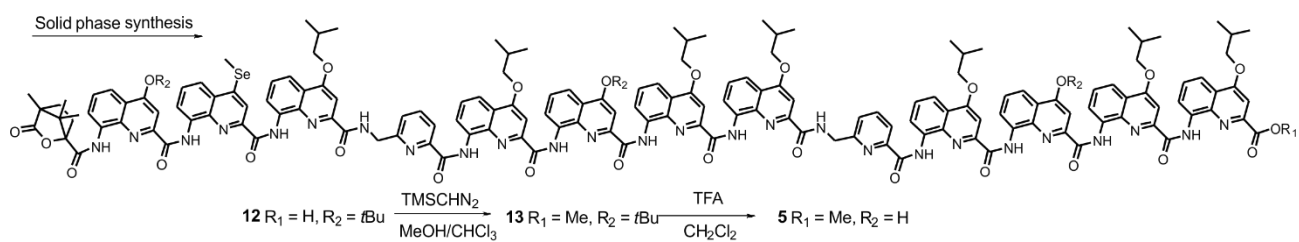
### 4.2.5.2 Synthesis of foldamers



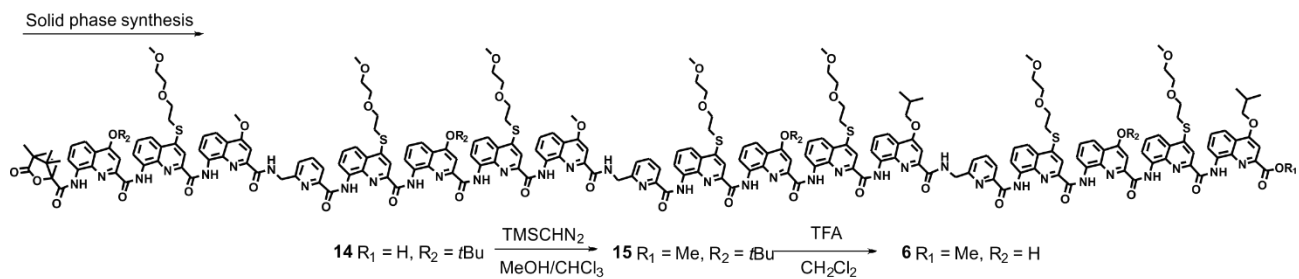
**Scheme 3. Synthesis of 3.**



**Scheme 4.** Synthesis of **4**.

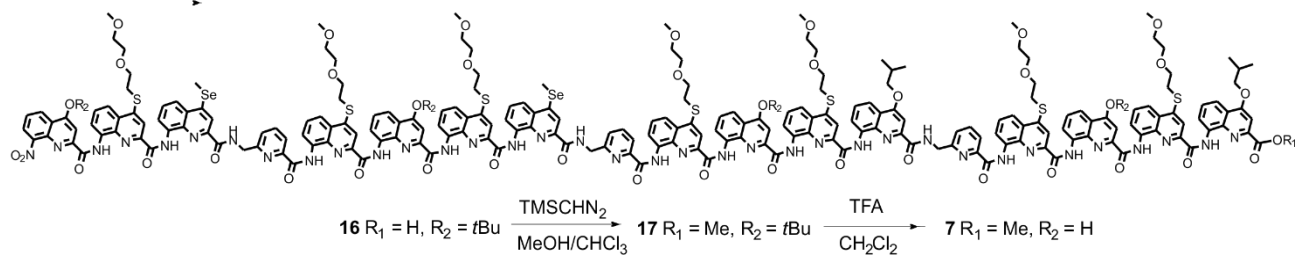


**Scheme 5.** Synthesis of **5**.



**Scheme 6.** Synthesis of **6**.

Solid phase synthesis



**Scheme 7.** Synthesis of **7**.

## 4.2.6 Experimental Procedures

### 4.2.6.1 General methods

Commercial available reagents were purchased from Sigma-Aldrich, Alfa-Aesar or TCI and were used without further purification unless otherwise specified. SASRIN resin (100-200 mesh, loading 0.7-1.0 mmol/g) was purchased from Bachem. Tetrahydrofuran (THF), dichloromethane (DCM) and toluene were dried over alumina columns (MBRAUN SPS-800 solvent purification system); diisopropylethylamine (DIPEA) was distilled over ninhydrin and then over potassium hydroxide (KOH); chloroform was distilled over calcium hydride ( $\text{CaH}_2$ ) prior to use. Reactions were monitored by thin layer chromatography (TLC) on Merck silica gel 60-F254 plates and observed under UV light. Column chromatography purifications were carried out on Merck GEDURAN Si60 (40-63  $\mu\text{m}$ ). MPLC was carried out on puriFlash® XS520Plus (interchim) using a PF-15C18HQ-F0080 column (3.5 x 19 cm, 15 $\mu\text{m}$ , 20 bar, interchim). The mobile phase was composed of  $\text{H}_2\text{O}$  (solvent A) and  $\text{CH}_3\text{CN}$  (solvent B). Solid phase synthesis (SPS) was performed manually under MW-irradiation on a CEM Discover (Liberty Bio) microwave oven using an open reaction vessel and an internal fibre optic probe for temperature control. High-resolution electrospray mass spectra were recorded on a Thermo Exactive orbitrap instrument.

### 4.2.6.2 Synthesis of small units

The monomers Fmoc- $\text{Q}^{\text{B}}\text{-OH}$ ,<sup>[9]</sup> Fmoc- $\text{Q}^{\text{M}}\text{-OH}$ <sup>[10]</sup> and Fmoc- $\text{P-OH}$ <sup>[11]</sup> have been synthesized according to the literature. The synthesis of Fmoc- $\text{Q}^{\text{S}}\text{-OH}$  will be published elsewhere. The syntheses of Fmoc- $\text{X-OH}$  ( $\text{X}$  denotes *t*Bu-protected X) and Fmoc- $\text{Q}^{\text{D}}\text{-OH}$  were previously reported.<sup>[4, 12]</sup> Improved/modified protocols are presented below. Final Fmoc-protected amino acid had to have a purity of  $\geq 97\%$ .

**Methyl 4-(*tert*-butoxy)-8-nitroquinoline-2-carboxylate (B).** Methyl 8-nitro-4-oxo-1,4-dihydroquinoline-2-carboxylate (**A**)<sup>[9]</sup> (88.8 g, 0.36 mol, 1 eq.) and silver acetate (246 g, 1.47 mol, 4.15 eq.) were suspended in DCM (3.8 L) under nitrogen atmosphere and protected from the exposure to light. After stirring for 5 min, *tert*-Butyl bromide (162 mL, 197.6 g, 1.44 mol, 4 eq.) was added dropwise over the course of 5 min. After vigorous stirring of the suspension at r. t for 30 min it was filtered over a pad of celite into a saturated solution of  $\text{NaHCO}_3$  in water. The residue was washed with DCM until the yellow filtrate remained colorless. The layers of the filtrate were separated, and the DCM phase was washed with water, and then with brine. The organic layer was dried over  $\text{Na}_2\text{SO}_4$ , and the solvent was removed under reduced pressure. The residue purified via filtration over a pad of silica, the residue was washed with 5% EtOAc in DCM (2 L) until the yellow filtrate remained almost colorless. The filtrate was evaporated in vacuo at 50 °C to give the product as a yellow solid (105.1 g, 0.35 mol, 97%). <sup>1</sup>H NMR (400 MHz,  $\text{CD}_2\text{Cl}_2$ , 25 °C)  $\delta$  [ppm] 8.44 (dd,  $J = 8.5, 1.4$  Hz, 1H), 7.99 (dd,  $J = 7.4, 1.4$  Hz, 1H), 7.81 (s, 1H), 7.62 (dd,  $J = 8.5, 7.4$  Hz, 1H), 4.03 (s, 3H), 1.69 (s, 9H). <sup>13</sup>C NMR (101 MHz,  $\text{CD}_2\text{Cl}_2$ )  $\delta$  [ppm] 166.0, 161.1, 151.2, 149.2, 140.6, 127.2, 126.1, 125.9, 124.5, 107.2,

83.2, 28.7. **MS** calcd for C<sub>15</sub>H<sub>16</sub>N<sub>2</sub>NaO<sub>2</sub> [M+Na]<sup>+</sup> 327.0951, found (HR-ESI) 327.0952. The data obtained are in agreement with the literature values.<sup>[4]</sup>

**Methyl 8-amino-4-(tert-butoxy)quinoline-2-carboxylate (C).** Compound **B** (105.1 g, 0.35 mol, 1 eq.) was dissolved in EtOAc (2.21 L) and N<sub>2</sub> was bubbled through for 5 min. After addition of the Pd/C-catalyst (10.5 g, 10wt%) vacuum was pulled shortly prior to establishing H<sub>2</sub> atmosphere. The suspension was stirred for 12 h under H<sub>2</sub> atmosphere at r. t., then the mixture was filtered over a pad of celite, the residue was washed with EtOAc until the yellow filtrate remained colorless. The filtrate was evaporated removed in vacuo at 50 °C water bath to give the product as a yellow solid (93.3 g, 0.34 mol, 99%). <sup>1</sup>H NMR (400 MHz, CD<sub>2</sub>Cl<sub>2</sub>, 25 °C) δ [ppm] 7.67 (s, 1H), 7.47 (dd, *J* = 8.4, 1.3 Hz, 1H), 7.34 (dd, *J* = 8.4, 7.5 Hz, 1H), 6.91 (dd, *J* = 7.5, 1.3 Hz, 1H), 5.09 (s, 2H), 4.00 (s, 3H), 1.64 (s, 9H), <sup>13</sup>C NMR (101 MHz, CD<sub>2</sub>Cl<sub>2</sub>) δ [ppm] 166.6, 160.8, 145.9, 145.4, 139.2, 128.7, 126.0, 110.7, 110.7, 107.0, 81.6, 28.8. **MS** calcd for C<sub>11</sub>H<sub>11</sub>N<sub>2</sub>O<sub>3</sub> [M-<sup>t</sup>Bu+H]<sup>+</sup> 219.0764, found (HR-ESI) 219.0763.

**Methyl 8-(((9H-fluoren-9-yl)methoxy)carbonyl)amino)-4-(tert-butoxy)quinoline-2-carboxylate (D).** Compound **C** (93.3 g, 0.34 mol, 1 eq.) was dissolved in dioxane (1.0 L), then a solution of NaHCO<sub>3</sub> (143.0 g, 1.70 mol, 5 eq.) in water (1.4 L, 10wt%-solution) was added and the reaction mixture was cooled down to 0 °C. At this temperature a solution of Fmoc-chloride (114 g, 0.44 mol, 1.3 eq.) in dioxane (357.0 mL) was added dropwise over the course of an hour. After complete addition, the reaction mixture was stirred 1 h at 0 °C, followed by 12 h at r.t.. The reaction mixture was brought to pH 3-4 using a 5% citric acid-solution in water. The precipitate was filtered off, dissolved in DCM, the water-phase separated and the organic layer dried over MgSO<sub>4</sub>. The solvent was then removed under reduced pressure at 50 °C water bath and precipitated from Et<sub>2</sub>O. The product was obtained as white solid (147.4 g, 0.30 mol, 87%). <sup>1</sup>H NMR (400 MHz, CD<sub>2</sub>Cl<sub>2</sub>, 25 °C) δ [ppm] 9.31 (s, 1 H), 8.41 (s, 1 H), 7.88 (td, *J* = 8.5, 1.2 Hz, 3 H), 7.79 (s, 1 H), 7.77 (dt, *J* = 7.4, 0.9 Hz, 2H), 7.57 (t, *J* = 8.1 Hz, 1 H), 7.50 – 7.45 (m, 2 H), 7.40 (td, *J* = 7.5, 1.2 Hz, 2 H), 4.61 (d, *J* = 7.0 Hz, 2 H), 4.45 (t, *J* = 7.1 Hz, 1 H), 4.09 (s, 3 H), 1.72 (s, 9 H). <sup>13</sup>C NMR (101 MHz, CD<sub>2</sub>Cl<sub>2</sub>) δ [ppm] 166.3, 161.3, 153.6, 147.0, 144.4, 141.7, 139.2, 135.7, 128.2, 128.2, 127.5, 125.6, 125.0, 120.4, 116.0, 115.7, 107.0, 82.2, 67.6, 47.6, 28.8. **MS** calcd for C<sub>30</sub>H<sub>29</sub>N<sub>2</sub>O<sub>5</sub> [M+H]<sup>+</sup> 497.2071, found (HR-ESI) 497.2069.

**8-(((9H-fluoren-9-yl)methoxy)carbonyl)amino)-4-(tert-butoxy)quinoline-2-carboxylic acid (E).**

**Synthesis Route a:** Compound **D** (79.2 g, 0.16 mol, 1 eq.) was dissolved in EtOAc (1.0 L) and three times degassed with N<sub>2</sub>. The mixture was heated to 97 °C and LiI (82.3 g, 0.61 mol, 3.8 eq.) was added in portions. The reaction mixture refluxed for 12 h, then allowed to cool down to r. t. prior to diluting with EtOAc. The solution was washed once with a Na<sub>2</sub>S<sub>2</sub>O<sub>3</sub> solution (5% in water), twice with a solution of citric acid (5% in water), and finally once with water. The organic layer was then dried over Na<sub>2</sub>SO<sub>4</sub> and, after filtration, the solvent was removed under reduced pressure at 50 °C water bath. The product was obtained as a yellow solid (57.0 g, 0.12 mol, 74%) with a purity of 97%. **Synthesis Route b:** Compound **D** (2.15 g, 4.33 mmol, 1 eq.) was dissolved in THF (100 mL). A solution of LiOH (waterfree) (104 mg, 4.3 mmol, 1 eq.) in water (10 mL) was added dropwise. The reaction mixture was stirred at r.t. for 2 h, then it was brought to pH 5-6 using a 5%

citric acid-solution in water. The mixture was extracted with DCM. The combined organic layers were washed with brine and dried over MgSO<sub>4</sub>. The solvent was then removed under reduced pressure at 50 °C water bath and the crude purified by MPLC (50-100 CH<sub>3</sub>CN in water). The product was obtained as a white solid (1.48 g, 3.07 mmol, 71 %) with a purity of 99 %. <sup>1</sup>H NMR (500 MHz, DMSO-*d*<sub>6</sub>, 25 °C) δ [ppm] 13.52 (s, 1H), 10.42 (s, 1H), 8.33 (s, 1H), 7.93 (d, *J* = 7.5 Hz, 2H), 7.80–7.77 (m, 3H), 7.71 (s, 1H), 7.63 – 7.55 (m, 1H), 7.44 (t, *J* = 7.4 Hz, 2H), 7.36 (t, *J* = 7.4 Hz, 2H), 4.61 (d, *J* = 6.4 Hz, 1H), 4.45 (t, *J* = 6.7 Hz, 1H), 1.63 (s, 9H). MS calcd for C<sub>29</sub>H<sub>27</sub>N<sub>2</sub>O<sub>5</sub> [M+H]<sup>+</sup> 483.1914 found (HR-ESI) 483.1912. The data obtained are in agreement with the literature values.<sup>[4]</sup>

**1-(*p*-Tolylsulfonyl)-3,6-dioxoheptane (F).** To a solution of diethylene monomethyl alcohol (150.0 g, 1.25 mol) in dry THF (312.0 mL) was added a solution of NaOH (70.9 g, 1.78 mol) in water (375.0 mL). The mixture was cooled to 0 °C internal temperature, then a solution of *p*-toluenesulfonylchloride (226 g, 0.94 mol) was added dropwise while keeping the internal temperature at 4-10 °C. After complete addition the reaction mixture was stirred at 2°C for 4 h. Before being extracted with with Et<sub>2</sub>O (100 mL) five times. The combined organic layers were washed with water until the aqueous phase was neutral. Then the organic layer was dried over Na<sub>2</sub>SO<sub>4</sub>, filtered and the solvent removed under reduced pressure without heating. The product was obtained as a colorless oil that solidifies over time (280.0 g, quant.). <sup>1</sup>H NMR (500 MHz, CDCl<sub>3</sub>, 25 °C) δ [ppm] 7.81 – 7.78 (m, 2H), 7.35 – 7.32 (m, 2H), 4.18 – 4.15 (m, 2H), 3.75 – 3.72 (m, 4H), 3.70 – 3.67 (m, 2H), 3.59 – 3.56 (m, 2H), 3.49 – 3.47 (m, 2H), 3.34 (s, 3H), 2.44 (s, 3H). The data obtained are in agreement with the literature values.<sup>[13]</sup>

**1-Mercapto-3,6-dioxoheptane (G).** To a solution of F (33.6 g, 0.13 mol) in ethanol (67.0 mL) was added a solution of thiourea (9.2 g, 0.12 mol) in water (4.9 mL). The reaction mixture was refluxed for 3 h, after what a solution of NaOH (6.7 g, 0.17 mol) in water (28.0 mL) was added and the reaction mixture was heated to reflux for 3.75 h. After cooling down to r. t., the crude was acidified with HCl (conc.), extracted with DCM and dried over MgSO<sub>4</sub>. The residue was purified via distillation at 80 °C oil bath under 20 mbar of pressure to afford the product as a colorless oil (24.5 g, 0.08 mol, 60%). <sup>1</sup>H NMR (500 MHz, CDCl<sub>3</sub>, 25 °C) δ [ppm] 3.65 – 3.60 (m, 4H), 3.57 – 3.54 (m, 2H), 3.39 (s, 3H), 2.71 (dt, *J* = 8.2, 6.6 Hz, 2H), 1.59-1.55 (t, *J* = 8.2 Hz, 1H). The data obtained are in agreement with the literature values.<sup>[13]</sup>

**Methyl 4-((2-(2-methoxyethoxy)ethyl)thio)-8-nitroquinoline-2-carboxylate (I).** Methyl-4-chloro-8-nitroquinoline-2-carboxylate (**H**) (41.0 g, 0.15 mol, 1.0 eq.) and CsCO<sub>3</sub> (75.0 g, 0.23 mol, 1.5 eq.) were dissolved in dry DMF (1.3L) under N<sub>2</sub> atmosphere. Compound **G** (20.0 g, 0.15 mol, 0.94 eq.) was then added and the suspension was stirred overnight at r. t. under N<sub>2</sub> atmosphere. The reaction mixture was then filtered over a small pad of silica and washed with a 1:1 mixture of EtOAc and *n*-hex until the filtrate came of colourless. Some colour remained on the pad, which is assumed to be by-product. The solvent was removed under reduced pressure and the residue was precipitated in DCM/MeOH to obtain a first batch of pure product as a yellow solid (20.063 g). The mother solution was evaporated under reduced pressure and the residue purified via column chromatography on silica gel with cyclohexane/EtOAc (9:1 to 4:6) as eluent. After

evaporation at 50 °C water bath the two batches were combined to give the product as a yellow solid (43.6 g, 0.12 mol, 79%). <sup>1</sup>H NMR (500 MHz, CDCl<sub>3</sub>, 25 °C) δ [ppm] 8.38 (dd, *J* = 8.5, 1.4, 1H), 8.12 (1H, s), 8.06 (dd, *J* = 7.5, 1.2, 1H), 7.69 (dd, *J* = 8.5, 7.5, 1H), 4.03 (s, 3H), 3.89 (t, *J* = 6.3, 2H), 3.69 – 3.67 (m, 2H), 3.57 – 3.55 (m, 2H), 3.46 (t, *J* = 6.3, 2H), and 3.37 (s, 3H). <sup>13</sup>C NMR (126 MHz, CDCl<sub>3</sub>) δ [ppm] 165.6, 150.7, 149.3, 148.9, 138.7, 128.2, 127.7, 126.9, 124.8, 117.1, 72.1, 70.9, 68.9, 59.3, 53.6, 31.7. MS calcd for C<sub>16</sub>H<sub>19</sub>N<sub>2</sub>O<sub>6</sub>S [M+H]<sup>+</sup> 367.0958, found (HR-ES) 367.1002. The data obtained are in agreement with the literature values.<sup>[12]</sup>

**Methyl 8-amino-4-((2-(2-methoxyethoxy)ethyl)thio)quinoline-2-carboxylate (J).** Compound **I** (43.6 g, 0.12 mol, 1 eq.) was suspended in EtOAc (1.0 L) and N<sub>2</sub> was bubbled through for 5 min. After addition of the Pd/C-catalyst (6.5 g, 15wt%), vacuum was pulled shortly prior to establishing H<sub>2</sub> atmosphere. The suspension was stirred for 3 d under H<sub>2</sub> atmosphere, then the mixture was filtered over a pad of celite, the residue was washed with EtOAc until the yellow filtrate remained colorless. Some brown color remained on the pad which is assumed to be by-product. The filtrate was evaporated removed in vacuo at 50 °C water bath to give the product as a yellow solid (35.3 g, 0.105 mol, 88 %). <sup>1</sup>H NMR (500 MHz, CDCl<sub>3</sub>, 25 °C) δ [ppm] 7.98 (s, 1H), 7.43 (d, *J* = 2.8 Hz, 1H), 7.39 (s, 1H), 6.96 (dd, *J* = 5.7, 3.0 Hz, 1H), 5.25 (d, *J* = 73.0 Hz, 2H), 4.05 (s, 3H), 3.88 (t, *J* = 6.6 Hz, 2H), 3.74 – 3.68 (m, 2H), 3.62 – 3.57 (m, 2H), 3.39 – 3.41 (m, 5H). <sup>13</sup>C NMR (126 MHz, CDCl<sub>3</sub>) δ [ppm] 166.2, 148.4, 145.8, 143.6, 136.5, 129.7, 128.1, 115.8, 111.4, 110.8, 72.0, 70.7, 69.1, 60.6, 59.2, 53.0, 31.0. MS calcd for C<sub>16</sub>H<sub>20</sub>N<sub>2</sub>NaO<sub>4</sub>S [M+Na]<sup>+</sup> 359.1036, found (HR-ESI) 359.1037.

**Methyl 8-(((9H-fluoren-9-yl)methoxy)carbonyl)amino)-4-((2-(2-methoxyethoxy)ethyl)thio)quinoline-2-carboxylate (K).** Compound **J** (35.3 g, 0.10 mol, 1 eq.) was dissolved in dioxane (1.0 L), then a solution of NaHCO<sub>3</sub> (139.0 g, 1.65 mol, 15 eq.) in water (1.4 L, 10wt%-solution) was added and the reaction mixture was cooled down to 0 °C. At this temperature a solution of Fmoc-chloride (35.3 g, 0.14 mol, 1.3 eq.) in dioxane (350.0 mL) was added dropwise over the course of an hour. After complete addition, the reaction mixture was stirred 1 h at 0 °C, followed by 2 d at r.t.. The reaction mixture was brought to pH 3-4 using a 20% HCl-solution in water. The precipitate was filtered off, dissolved in DCM, the water-phase separated and the organic layer dried over MgSO<sub>4</sub>. The solvent was then removed under reduced pressure at 50 °C water bath to give the product as a brown solid (50.8 g, 0.09 mol, 90%). <sup>1</sup>H NMR (400 MHz, CD<sub>2</sub>Cl<sub>2</sub>, 25 °C) δ [ppm] 9.30 (s, 1H), 8.40 (s, 1H), 8.05 (s, 1H), 7.96 (d, *J* = 2.0 Hz, 1H), 7.85 – 7.76 (m, 2H), 7.76 – 7.69 (m, 2H), 7.60 (t, *J* = 8.1 Hz, 1H), 7.44 (ddt, *J* = 8.4, 7.5, 1.0 Hz, 2H), 7.39 – 7.30 (m, 2H), 4.58 (d, *J* = 7.0 Hz, 2H), 4.40 (t, *J* = 7.0 Hz, 1H), 4.06 (s, 3H), 3.90 – 3.83 (m, 2H), 3.69 – 3.62 (m, 2H), 3.57 – 3.50 (m, 2H), 3.43 (t, *J* = 6.3 Hz, 2H), 3.34 (s, 3H). <sup>13</sup>C NMR (101 MHz, CD<sub>2</sub>Cl<sub>2</sub>) δ [ppm] 166.1, 153.8, 150.4, 145.4, 144.5, 141.9, 137.1, 136.6, 129.6, 129.3, 128.3, 127.7, 127.7, 125.7, 121.5, 120.6, 116.9, 116.6, 116.2, 72.4, 71.1, 69.3, 67.9, 59.3, 47.7, 36.9, 31.9, 31.7. MS calcd for C<sub>31</sub>H<sub>31</sub>N<sub>2</sub>O<sub>6</sub>S [M+H]<sup>+</sup> 559.1897, found (HR-ESI) 559.1896.

**8-(((9H-fluoren-9-yl)methoxy)carbonyl)amino)-4-((2-(2-methoxyethoxy)ethyl)thio)quinoline-2-carboxylic acid (L).** Compound **K** (50.8 g, 0.09 mol, 1 eq.) was suspended in EtOAc (0.8 L) and three times degassed with N<sub>2</sub>. The mixture was heated to 97 °C and LiI (96.7 g, 0.72 mol, 7.9 eq.) was added in portions.



The reaction mixture refluxed for 1 d, then allowed to cool down to r. t. prior to recovering the precipitate via filtration. The solid was dissolved in DCM, washed once with a Na<sub>2</sub>S<sub>2</sub>O<sub>3</sub> (5% in water), twice with a solution of citric acid (5% in water), and finally once with water. The organic layer was then dried over Na<sub>2</sub>SO<sub>4</sub> and, after filtration, the solvent was removed under reduced pressure at 50 °C water bath. The residue was precipitated in a mixture of EtOAc and Et<sub>2</sub>O to give the product as a yellow solid (49.4 g, 0.09 mol, 99%) with a purity of 97%. <sup>1</sup>H NMR (500 MHz, DMSO-*d*<sub>6</sub>, 25 °C) δ [ppm] 13.58 (s, 1H), 10.44 (s, 1H), 8.36 (s, 1H), 8.08 (s, 1H), 7.94 (dt, *J* = 7.6, 1.1 Hz, 2H), 7.78 (dt, *J* = 7.5, 1.1 Hz, 2H), 7.75 (dd, *J* = 8.5, 1.3 Hz, 1H), 7.68 (d, *J* = 7.3 Hz, 1H), 7.47 – 7.42 (m, 2H), 7.37 (td, *J* = 7.5, 1.2 Hz, 2H), 4.62 (d, *J* = 7.0 Hz, 2H), 4.45 (t, *J* = 6.7 Hz, 1H), 3.80 (t, *J* = 6.1 Hz, 2H), 3.62 – 3.58 (m, 2H), 3.50 (t, *J* = 6.1 Hz, 2H), 3.47 – 3.44 (m, 2H), 3.24 (s, 3H). The data obtained are in agreement with the literature values.<sup>[12]</sup>

### 4.2.6.3 Solid phase synthesis general methods

#### 4.2.6.3.1 Loading of the resin via HBTU-coupling

SASRIN resin (800 mg, 100-200 mesh, loading 0.7-1.0 mmol/g) was swollen in DMF for 1 h, transferred to the microwave vessel and washed three times with dry DMF (purchased as ‘extra-dry’ solvent from Acros Organics). DIPEA (272 μL, 2 eq.) was added to a mixture of Q<sup>B</sup> (232 mg; 0.6 eq.) and HBTU (456 mg, 1.5 eq.) in dry DMF (5 mL), then the mixture was added to the resin. The reaction mixture was subjected to treatment in the microwave (50 °C, 20 min, 25 W), then the resin was washed five times with DMF until the washing solution was colourless, then it was washed ten times with DCM. If the loading was sufficient a capping was performed, otherwise the resin re-loaded. Capping was performed by adding a mixture of DCM/pyridine/benzoyl chloride (v/v/v, 3:1:1) and the resin left for 30 min, then it was rinsed 20x times with DCM.

#### 4.2.6.3.2 Estimation of the loading

After drying a small part of the resin under vacuum for 5 h, the loading of the resin was determined. To a small amount of resin (1-2 mg), a freshly prepared of DMF/piperidine (v/v, 8:2, 3 mL) was added. The mixture was shaken and incubated for 5 min. Then the absorption was measured at 290 nm using a NanoDrop One Microvolume UV-Vis Spectrophotometer and a Hellma quartz glass cuvette 104 (path length 10 mm). Three replicates were measured, then the loading was calculated with the following equation:

$$\text{loading (in } \frac{\text{mmol}}{\text{g}}) = \frac{A_{290 \text{ nm}}}{1.65 * m_{\text{resin}} \text{ (in mg)}} \quad (1)$$

#### 4.2.6.3.3 Solid Phase Synthesis via in-situ-activation

After swelling of the SASRIN resin (800 mg, 100-200 mesh, loading 0.388 mmol/g, 0.310 μmol) in DMF for 1 h, the resin was transferred into the microwave vessel and washed three times with DMF. For deprotection

a 8:2 mixture of DMF/piperidine (6 mL) was added to the resin and nitrogen was bubbled through the suspension for 3 min. The solution was removed, the resin washed five times with DMF and an 8:2 mixture of DMF/piperidine (6 mL) was added again. After bubbling nitrogen through the suspension for 7 min, the resin was washed five times with DMF and five times with THF. For coupling dry THF (4 mL) and 2,3,5-collidine (5 eq. with regards to the resin-loading) were added to the resin. A mixture of the monomer (2 eq. with regards to the resin-loading) and PPh<sub>3</sub> (4 eq. with regards to the resin-loading) in dest. CHCl<sub>3</sub> (4 mL) or dry NMP (4 mL) was prepared. All monomers except for Fmoc-P-OH were dissolved in dest. chloroform. Fmoc-P-OH was dissolved in dry NMP. After the addition of trichloroacetonitrile (4 eq. with regards to the resin-loading), this mixture was added to the resin. Then the reaction mixture was subjected to treatment in the microwave (50 °C, 5 min, 50 W) Then the resin was washed five times with dry THF, then dry THF (4 mL) and 2,3,5-collidine (5 eq. with regards to the resin-loading) were added to the resin. Again, a mixture of monomer (2 eq. with regards to the resin-loading) and PPh<sub>3</sub> (4 eq. with regards to the resin-loading) in dest. CHCl<sub>3</sub> (4 mL) or dry NMP (4 mL) with trichloroacetonitrile was prepared and added to the resin. The reaction mixture was again subjected to microwave vessel treatment (50 °C, 5 min, 25 W). After washing with DCM, THF, DMF and DCM, in that order, the resin was kept in a swollen state at 10 °C.

For installation of the pivaloyl- and (1*S*)-camphanic amide the resin (0.030 mmol) was Fmoc deprotected (20% piperidine in DMF, 1 x 3 min and 1 x 7 min), washed with DMF and dry THF, then a solution of DIPEA (31.1 µL, 10 eq.) in dry THF (0.5 mL) was added to the resin. To this suspension a solution of pivaloylchloride or (1*S*)-camphanic acid chloride (3 eq.) in dry THF (0.5 mL) was added and rests on the reaction vessel were rinsed down with dry THF (0.5 mL). The reaction was carried out under MW irradiation (25 W) at 50°C for 5 min. The resin was washed briefly with dry THF, and the process repeated. Successively the resin was washed with DMF and DCM.

#### 4.2.6.3.4 Mini Cleavage

To perform a mini cleavage, SASRIN resin (~5 mg) was swelled in DCM for 15 min, then either HFIP [DCM (2.8 mL) and HFIP (1.2 mL)] or TFA [(TFA/DCM 3:7)] were added and the mixture was stirred at r. t. for 1 h (in case of HFIP) or 10 min (in case of TFA). If the mini cleavage was executed with HFIP, the solvent was evaporated. If TFA was used, the reaction mixture was filtered into a saturated sodium carbonate solution. After extraction with DCM, the combined organic layers were dried over magnesium sulfate, and then the solvent was evaporated.

#### 4.2.6.3.5 Full Cleavage

To perform the full cleavage, SASRIN resin (~50 mg) was swelled in DCM for 15 min, HFIP [DCM/HFIP, v/v, 1:1 (6 mL in total)] was added, and the mixture was stirred at r. t. for 12 h. Then the solvent was evaporated. The process was repeated until no more foldamer is left on the resin (up to ten times).

#### 4.2.6.4 Synthesis of oligomers

**Piv-X<sup>S</sup>Q<sup>B</sup>PQ<sup>B</sup>X<sup>S</sup>Q<sup>B</sup>PQ<sup>B</sup>X<sup>S</sup>Q<sup>B</sup>-OH (8)** Compound **8** was synthesized using the SPS procedures reported in 0 on SASRIN resin loaded via HBTU-coupling described in 0 (scale: 60.40  $\mu$ mol). The crude product was obtained after full cleavage and used without further purification (184.5 mg, quant). <sup>1</sup>H NMR (500 MHz, CDCl<sub>3</sub>, 25 °C)  $\delta$  [ppm] 11.18 (s, 1H), 10.81 (s, 1H), 10.80 (s, 1H), 10.74 (s, 1H), 10.68 (s, 1H), 10.60 (s, 1H), 10.51 (s, 1H), 10.28 (s, 1H), 10.21 (s, 1H), 10.12 (s, 1H), 8.52 (s, 1H), 7.96 (d,  $J$  = 4.3 Hz, 1H), 7.94 – 7.93 (m, 1H), 7.90-7.88 (dd,  $J$  = 7.5, 1.1 Hz, 1H), 7.82 – 7.73 (m,  $J$  = 7.78, 4H), 7.72 (d,  $J$  = 1.2 Hz, 1H), 7.70 – 7.65 (m, 2H), 7.60 (ddt,  $J$  = 8.7, 7.1, 1.3 Hz, 5H), 7.57 – 7.49 (m,  $J$  = 7.53, 3H), 7.45 – 7.43 (m, 2H), 7.33 (t,  $J$  = 7.8 Hz, 3H), 7.23 – 7.19 (m, 5H), 7.13 (d,  $J$  = 7.5 Hz, 2H), 7.09 – 7.04 (m, 2H), 6.99 – 6.92 (m, 7H), 6.91 – 6.85 (m, 2H), 6.78 – 6.73 (m, 3H), 6.69 (dd,  $J$  = 7.3, 1.4 Hz, 1H), 6.53 (s, 1H), 6.39 (s, 1H), 6.20 (s, 1H), 6.18 (s, 1H), 5.79 (s, 1H), 5.75 (s, 1H), 5.55 (s, 1H), 2.98 (s, 3H), 2.89 (s, 3H), 2.41 (s, 3H), 2.30 (s, 6H), 1.71 (s, 9H), 1.70 (s, 9H), 1.60 (s, 9H), 1.17 – 1.10 (m, 10H), 1.09 – 1.03 (m, 20H), 0.90 – 0.86 (m, 15H), 0.85 – 0.78 (m, 11H), 0.43 (s, 9H). MS calcd for C<sub>170</sub>H<sub>171</sub>N<sub>26</sub>O<sub>25</sub>Se [M+H]<sup>+</sup> 3056.2068, found (HR-ESI) 3056.8976.

**Piv-X<sup>S</sup>Q<sup>B</sup>PQ<sup>B</sup>X<sup>S</sup>Q<sup>B</sup>PQ<sup>B</sup>X<sup>S</sup>Q<sup>B</sup>-OMe (9)** Compound **8** (184.5 mg, 60.40  $\mu$ mol, 1 eq.) was dissolved in a mixture of dry chloroform/MeOH 3:2 (10 mL) under N<sub>2</sub>. TMSCHN<sub>2</sub> (2 M in hex, 106.0  $\mu$ L, 0.17 mmol, 2 eq.) was added dropwise, and the solution was stirred at r.t. for 2 h. A few drops of acetic acid were added, and the solution stirred for 5 min at r.t. Then the solution was diluted with DCM, washed with NaHCO<sub>3</sub>, dried MgSO<sub>4</sub>, filtered and concentrated. The crude product was purified via precipitation in DCM/MeOH (90.0 mg, 50% yield). <sup>1</sup>H NMR (500 MHz, CDCl<sub>3</sub>, 25 °C)  $\delta$  [ppm] 11.38 (s, 1H), 11.15 (s, 1H), 10.89 (s, 1H), 10.79 (s, 1H), 10.74 (s, 1H), 10.65 (s, 1H), 10.45 (s, 1H), 10.27 (s, 1H), 10.18 (s, 1H), 10.00 (s, 1H), 8.49 (s, 1H), 7.95 (ddd,  $J$  = 12.7, 7.4, 1.2 Hz, 1H), 7.91 – 7.89 (m, 1H), 7.85 (dd,  $J$  = 7.6, 1.2 Hz, 1H), 7.78 (dddd,  $J$  = 9.8, 7.2, 6.2, 1.3 Hz, 2H), 7.74 – 7.69 (m, 1H), 7.66 (t,  $J$  = 3.5 Hz, 1H), 7.60 – 7.50 (m, 8H), 7.43 – 7.40 (m, 5H), 7.33 (dd,  $J$  = 7.4, 1.3 Hz, 1H), 7.30 – 7.27 (m, 1H), 7.24 – 7.19 (m, 4H), 7.17 – 7.13 (m, 1H), 7.07 (d,  $J$  = 7.7 Hz, 1H), 7.07 (d,  $J$  = 4.3 Hz, 1H), 7.05 (d,  $J$  = 1.4 Hz, 1H), 7.03 – 6.97 (m, 5H), 6.95 – 6.92 (m, 2H), 6.91 (s, 1H), 6.87 (td,  $J$  = 7.4, 4.5 Hz, 3H), 6.81 (dd,  $J$  = 7.4, 1.3 Hz, 1H), 6.74 (d,  $J$  = 7.8 Hz, 1H), 6.70 – 6.66 (m, 2H), 6.50 (s, 1H), 6.34 (s, 2H), 6.33 (s, 1H), 5.73 (s, 1H), 5.69 (s, 1H), 5.50 (s, 1H), 3.96 (s, 1H), 3.94 – 3.90 (m, 2H), 3.87 – 3.83 (m, 2H), 3.74 (t,  $J$  = 6.0 Hz, 2H), 3.68 (dd,  $J$  = 8.0, 6.2 Hz, 1H), 3.63 – 3.55 (m, 5H), 3.53 – 3.49 (m, 3H), 3.34 – 3.30 (m, 1H), 3.18 (dd,  $J$  = 17.0, 3.8 Hz, 1H), 3.08 (s, 3H), 2.43 – 2.36 (m, 6H), 2.32 (dt,  $J$  = 13.4, 6.7 Hz, 1H), 2.25 – 2.17 (m, 5H), 2.09 (ddd,  $J$  = 16.7, 10.0, 4.7 Hz, 2H), 1.63 (s, 1H), 1.27 – 1.22 (m, 21H), 1.17 – 1.13 (m, 18H), 1.13 – 1.10 (m, 8H), 1.04 (dd,  $J$  = 12.8, 6.7 Hz, 8H), 0.90 – 0.78 (m, 9H), 0.44 (s, 9H). MS calcd for C<sub>171</sub>H<sub>173</sub>N<sub>26</sub>O<sub>25</sub>Se [M+H]<sup>+</sup> 3070.2225, found (HR-ESI) 3070.9091.

**Piv-XQ<sup>S</sup>Q<sup>B</sup>PQ<sup>B</sup>XQ<sup>B</sup>PQ<sup>B</sup>XQ<sup>B</sup>-OMe (3)** Compound **9** (13.2 mg, 4.32  $\mu$ mol) was treated with a 50% solution of TFA in DCM (2 mL) at r.t. for 2 h. Then the solvent was removed under vacuum, obtaining the product as a yellow solid (12.9 mg, quant.). <sup>1</sup>H NMR (500 MHz, DMSO-*d*<sub>6</sub>, 25 °C)  $\delta$  [ppm] 11.71 (s, 1H), 11.69 (s, 1H), 11.37 (s, 1H), 11.13 (s, 1H), 10.98 (s, 1H), 10.77 (s, 1H), 10.62 (s, 1H), 10.40 (s, 1H), 10.37 (s, 1H), 10.16 (s, 1H), 10.11 (s, 1H), 10.06 (s, 1H), 10.05 (s, 1H), 8.50 (s, 1H), 7.90 – 7.86 (m, 1H), 7.81 (d,  $J$  =

7.5 Hz, 1H), 7.74 (d,  $J = 7.6$  Hz, 2H), 7.65 (dt,  $J = 7.3, 1.4$  Hz, 4H), 7.59 (td,  $J = 8.2, 2.1$  Hz, 3H), 7.55 – 7.44 (m, 5H), 7.44 – 7.38 (m, 4H), 7.37 – 7.30 (m, 3H), 7.24 – 7.17 (m, 3H), 7.11 (dd,  $J = 7.4, 1.4$  Hz, 2H), 7.08 – 6.94 (m, 6H), 6.93 – 6.87 (m, 5H), 6.79 (t,  $J = 7.9$  Hz, 2H), 6.76 – 6.74 (m, 1H), 6.68 – 6.65 (m, 1H), 6.58 (d,  $J = 7.5$  Hz, 1H), 6.52 (d,  $J = 7.6$  Hz, 1H), 6.40 (s, 1H), 6.24 (s, 1H), 5.85 (s, 1H), 5.84 (s, 1H), 5.63 (s, 1H), 5.51 (s, 1H), 5.38 (s, 1H), 3.95 (t,  $J = 7.5$  Hz, 2H), 3.92 – 3.88 (m, 2H), 3.83 (t,  $J = 7.6$  Hz, 2H), 3.78 – 3.70 (m, 6H), 3.69 – 3.62 (m, 5H), 3.58 (q,  $J = 8.4$  Hz, 3H), 3.50 (t,  $J = 7.7$  Hz, 2H), 3.20 (s, 2H), 3.06 (s, 3H), 3.01 (d,  $J = 13.9$  Hz, 2H), 2.29 (dq,  $J = 13.7, 6.9$  Hz, 2H), 2.25 – 2.16 (m, 2H), 2.14 – 2.06 (m, 2H), 2.03 – 1.96 (m, 3H), 1.68 (t,  $J = 13.9$  Hz, 3H), 1.30 – 1.11 (m, 20H), 1.06 (dd,  $J = 14.8, 6.7$  Hz, 8H), 0.85 (t,  $J = 6.9$  Hz, 4H), 0.36 (s, 9H). **MS** calcd for  $C_{159}H_{149}N_{26}O_{25}Se$   $[M+H]^+$  2902.0347, found (HR-ESI) 2902.9310, calcd for  $C_{159}H_{150}N_{26}O_{25}Se$   $[M+2H]^{2+}$  1451.5210, found (HR-ESI) 1451.9640.

**Piv-XQ<sup>D</sup>Q<sup>M</sup>PQ<sup>D</sup>XQ<sup>D</sup>Q<sup>S</sup>PQ<sup>D</sup>XQ<sup>D</sup>Q<sup>D</sup>PQ<sup>D</sup>XQ<sup>D</sup>Q<sup>D</sup>-OH (10)** Compound **10** was synthesized using the SPS procedures reported in 0 on SASRIN resin loaded via HBTU-coupling described in 0 (scale: 81.3  $\mu$ mol). The crude product was obtained after precipitation in EtOAc/*n*-hex, and the product was obtained as a yellow solid (270.0 mg, 73%). **<sup>1</sup>H NMR** (500 MHz, CD<sub>2</sub>Cl<sub>2</sub>, 25 °C)  $\delta$  [ppm] 11.14 (s, 1H), 10.81 (s, 1H), 10.68 (s, 1H), 10.47 (s, 1H), 10.47 (s, 1H), 10.37 (s, 1H), 10.34 (s, 1H), 10.22 (s, 1H), 10.12 (s, 1H), 10.07 (s, 1H), 9.97 (s, 1H), 9.94 (s, 1H), 9.90 (s, 1H), 9.74 (s, 1H), 8.46 (s, 1H), 8.03 – 8.00 (m, 2H), 7.95 (dd,  $J = 14.6, 7.1$  Hz, 4H), 7.77 (s, 1H), 7.70 (d,  $J = 8.0$  Hz, 1H), 7.68 – 7.61 (m, 4H), 7.55 – 7.44 (m, 6H), 7.44 – 7.28 (m, 7H), 7.23 (d,  $J = 7.3$  Hz, 1H), 7.18 – 7.09 (m, 5H), 7.07 – 7.02 (m, 6H), 7.00 (d,  $J = 11.6$  Hz, 4H), 6.98 – 6.91 (m, 6H), 6.91 – 6.83 (m, 5H), 6.83 – 6.80 (m, 3H), 6.75 (t,  $J = 8.1$  Hz, 2H), 6.68 (dd,  $J = 13.7, 7.3$  Hz, 2H), 6.62 (d,  $J = 7.3$  Hz, 1H), 6.58 (dd,  $J = 7.4, 3.2$  Hz, 2H), 6.37 (t,  $J = 3.5$  Hz, 2H), 6.33 (s, 1H), 6.20 (s, 1H), 6.03 (s, 1H), 5.99 (s, 1H), 5.84 (s, 1H), 5.81 (s, 1H), 5.67 (s, 1H), 5.60 (s, 1H), 3.94 – 3.90 (m, 5H), 3.90 – 3.87 (m, 5H), 3.85 (d,  $J = 6.7$  Hz, 5H), 3.82 (dd,  $J = 6.1, 3.6$  Hz, 10H), 3.80 – 3.76 (m, 9H), 3.74 (d,  $J = 4.7$  Hz, 11H), 3.71 (dd,  $J = 9.3, 5.0$  Hz, 9H), 3.69 – 3.64 (m, 7H), 3.60 – 3.55 (m, 6H), 3.55 (s, 3H), 3.54 (s, 3H), 3.53 (s, 3H), 3.53 – 3.51 (m, 3H), 3.50 (s, 3H), 3.45 (s, 3H), 3.38 (s, 3H), 3.33 (d,  $J = 7.2$  Hz, 1H), 3.31 (s, 3H), 3.26 (q,  $J = 6.3$  Hz, 1H), 3.17 – 3.07 (m, 8H), 3.05 – 2.99 (m, 8H), 2.89 – 2.92 (m, 2H), 2.91 (s, 2H), 2.82 (s, 2H), 2.56 (s, 2H), 2.22 (s, 2H), 1.18 – 1.14 (m, 8H), 1.09 – 1.04 (m, 8H), 0.86 – 0.80 (m, 9H), 0.38 (s, 9H). **MS** calcd for  $C_{237}H_{240}N_{36}Na_2O_{41}S_7Se$   $[M+2Na]^{2+}$  2297.73982, found (HR-ESI) 2298.5187.

**Piv-XQ<sup>D</sup>Q<sup>M</sup>PQ<sup>D</sup>XQ<sup>D</sup>Q<sup>S</sup>PQ<sup>D</sup>XQ<sup>D</sup>Q<sup>D</sup>PQ<sup>D</sup>XQ<sup>D</sup>Q<sup>D</sup>-OMe (11)** Compound **10** (175.0 mg, 52  $\mu$ mol, 1 eq.) was dissolved in a mixture of dry chloroform/MeOH 3:2 (5 mL) under N<sub>2</sub>. TMSCHN<sub>2</sub> (2 M in hex, 92  $\mu$ L, 0.10 mmol, 2 eq.) was added dropwise, and the solution was stirred at r.t. for 2 h. A few drops of acetic acid were added, and the solution was stirred for 5 min at r.t. Then the solution was diluted with DCM, washed with NaHCO<sub>3</sub>, dried MgSO<sub>4</sub>, filtered and concentrated. The crude product was obtained as a yellow solid (165.0 mg, 94% yield). **<sup>1</sup>H NMR** (500 MHz, CD<sub>2</sub>Cl<sub>2</sub>, 25 °C)  $\delta$  [ppm] 11.27 (s, 1H), 10.99 (s, 1H), 10.81 (s, 1H), 10.68 (s, 1H), 10.46 (s, 1H), 10.37 (s, 1H), 10.32 (s, 1H), 10.20 (s, 1H), 10.12 (s, 1H), 10.08 (s, 1H), 9.94 (s, 1H), 9.93 (s, 1H), 9.90 (s, 1H), 9.73 (s, 1H), 8.45 (s, 1H), 8.03 – 8.01 (m, 1H), 7.97 (dd,  $J = 7.3, 1.1$  Hz, 1H), 7.93 (dd,  $J = 7.4, 1.1$  Hz, 1H), 7.82 (dd,  $J = 7.3, 1.2$  Hz, 1H), 7.77 (t,  $J = 3.5$  Hz, 1H), 7.67 – 7.59 (m, 5H),

7.59 – 7.43 (m, 12H), 7.43 – 7.38 (m, 3H), 7.36-7.31 (m, 4H), 7.23 (ddd,  $J = 8.1, 4.4, 3.1$  Hz, 3H), 7.18 – 7.09 (m, 5H), 7.07 – 7.02 (m, 6H), 7.02 – 6.98 (m, 4H), 6.97 – 6.81 (m, 8H), 6.76 – 6.72 (m, 2H), 6.70 (dd,  $J = 7.3, 1.3$  Hz, 1H), 6.65 (d,  $J = 7.3$  Hz, 1H), 6.61 (dd,  $J = 7.4, 1.3$  Hz, 1H), 6.59 – 6.55 (m, 2H), 6.38 – 6.34 (m, 2H), 6.29 (s, 1H), 6.19 (s, 1H), 6.03 (s, 1H), 5.98 (s, 1H), 5.84 (s, 1H), 5.81 (s, 1H), 5.67 (s, 1H), 5.57 (s, 1H), 3.93 – 3.86 (m, 5H), 3.85 – 3.79 (m, 5H), 3.78 – 3.76 (m, 4H), 3.75 – 3.69 (m, 10H), 3.68 – 3.64 (m, 4H), 3.63 – 3.58 (m, 4H), 3.58 (t,  $J = 1.6$  Hz, 2H), 3.57-3.55 (m, 3H), 3.55 (s, 2H), 3.54 (d,  $J = 3.4$  Hz, 6H), 3.53 (s, 2H), 3.53 – 3.51 (m, 1H), 3.50 (s, 3H), 3.49 (s, 1H), 3.49 – 3.47 (m, 2H), 3.45 (s, 3H), 3.44 (s, 1H), 3.38 (s, 2H), 3.31 (s, 2H), 3.29 – 3.22 (m, 3H), 3.21 – 3.09 (m, 8H), 3.06 (ddd,  $J = 8.2, 5.6, 2.1$  Hz, 4H), 3.03 (s, 4H), 3.03 – 2.95 (m, 5H), 2.95 – 2.92 (m, 1H), 2.91 – 2.82 (m, 2H), 2.72 – 2.67 (m, 1H), 2.22 (s, 2H), 2.12 (s, 3H), 1.69 – 1.67 (m, 2H), 1.65 (s, 6H), 1.61 (s, 12H), 1.58 (s, 6H), 1.25 (s, 4H), 1.16 (q,  $J = 6.9$  Hz, 4H), 1.08 (d,  $J = 6.7$  Hz, 4H), 1.05 (d,  $J = 6.7$  Hz, 4H), 0.90 – 0.81 (m, 9H), 0.39 (s, 9H). **MS** calcd for  $C_{238}H_{243}N_{36}NaO_{41}S_7Se$   $[M+H+Na]^{2+}$  2293.75667, found (HR-ESI) 2294.5324.

**Piv-XQ<sup>D</sup>Q<sup>M</sup>PQ<sup>D</sup>XQ<sup>D</sup>Q<sup>S</sup>PQ<sup>D</sup>XQ<sup>D</sup>Q<sup>D</sup>PQ<sup>D</sup>XQ<sup>D</sup>Q<sup>D</sup>-OMe (4)** Compound **11** (27.1 mg, 5.94  $\mu$ mol) was treated with a 50% solution of TFA in DCM (2 mL) at r.t. for 2 h. Then the solvent was removed under vacuum, obtaining the product as a yellow solid (23.1 mg, 90%). **<sup>1</sup>H NMR** (500 MHz, DMSO-*d*<sub>6</sub>, 25 °C)  $\delta$  [ppm] 11.72 (s, 1H), 11.66 (s, 1H), 11.37 (s, 1H), 11.29 (s, 1H), 11.09 (s, 1H), 10.85 (s, 1H), 10.71 (s, 1H), 10.56 (s, 1H), 10.28 (s, 1H), 10.23 (s, 1H), 10.19 (s, 1H), 10.10 (s, 1H), 9.99 (s, 1H), 9.97 (s, 1H), 9.86 (s, 2H), 9.75 (s, 1H), 9.57 (s, 1H), 8.44 (s, 1H), 7.85 (d,  $J = 6.3$  Hz, 1H), 7.79 (d,  $J = 7.3$  Hz, 1H), 7.76 – 7.72 (m, 1H), 7.69 (d,  $J = 6.9$  Hz, 1H), 7.67 – 7.59 (m, 3H), 7.57 – 7.53 (m, 4H), 7.52 – 7.46 (m, 3H), 7.39 (ddt,  $J = 17.5, 7.5, 4.0$  Hz, 4H), 7.34 – 7.22 (m, 3H), 7.19 (q,  $J = 5.8, 3.1$  Hz, 6H), 7.13 – 7.06 (m, 10H), 7.01 – 6.92 (m, 5H), 6.91 – 6.75 (m, 12H), 6.69 – 6.62 (m, 3H), 6.58 (d,  $J = 7.0$  Hz, 1H), 6.53 – 6.49 (m, 2H), 6.42 (dd,  $J = 13.7, 7.2$  Hz, 2H), 6.22 (d,  $J = 9.3$  Hz, 3H), 6.08 (s, 1H), 5.98 (s, 1H), 5.83 (s, 1H), 5.62 (s, 1H), 5.60 (s, 1H), 5.59 (s, 1H), 5.46 (s, 1H), 3.85 – 3.63 (m, 24H), 3.62 – 3.56 (m, 6H), 3.54 – 3.52 (m, 2H), 3.48 (s, 1H), 3.51 – 3.44 (m, 15H), 3.42 (s, 3H), 3.39 – 3.38 (m, 8H), 3.37 (s, 3H), 3.31 (s, 3H), 3.25 (s, 3H), 3.12 (tt,  $J = 16.9, 7.9$  Hz, 3H), 3.02 (s, 2H), 2.97 (t,  $J = 6.0$  Hz, 2H), 2.89 (dt,  $J = 12.2, 6.8$  Hz, 2H), 2.10 – 2.03 (m, 2H), 1.60 – 1.41 (m, 3H), 1.40 – 1.35 (m, 2H), 1.30 – 1.24 (m, 7H), 1.19 – 1.15 (m, 2H), 1.12 (dd,  $J = 6.7, 4.6$  Hz, 7H), 1.03 (dd,  $J = 13.9, 6.7$  Hz, 8H), 0.85 (t,  $J = 6.9$  Hz, 2H), 0.32 (s, 9H). **MS** calcd for  $C_{222}H_{211}N_{36}NaO_{41}S_7Se$   $[M+H+Na]^{2+}$  2181.6315, found (HR-ESI) 2182.1131.

**(1S)-Camph-XQ<sup>S</sup>Q<sup>B</sup>PQ<sup>B</sup>XQ<sup>B</sup>Q<sup>B</sup>PQ<sup>B</sup>XQ<sup>B</sup>Q<sup>B</sup>-OH (12)** Compound **12** was synthesized using the SPS procedures reported in 0 on SASRIN resin loaded via HBTU-coupling described in 0 (scale: 43.12  $\mu$ mol). The crude product was obtained after full cleavage and used without further purification (135.9 mg, quant). **<sup>1</sup>H NMR** (500 MHz, CDCl<sub>3</sub>, 25 °C)  $\delta$  [ppm] 11.20 (s, 1H), 11.18 (s, 1H), 10.95 (s, 1H), 10.71 (s, 1H), 10.69 (s, 1H), 10.58 (s, 1H), 10.42 (s, 1H), 10.26 (s, 1H), 10.19 (s, 1H), 10.05 (s, 1H), 9.20 (s, 1H), 7.98 – 7.94 (m, 3H), 7.84 (d,  $J = 3.5$  Hz, 1H), 7.82 – 7.76 (m, 5H), 7.76 (dd,  $J = 8.0, 1.3$  Hz, 1H), 7.72 (d,  $J = 1.5$  Hz, 1H), 7.70 (t,  $J = 1.5$  Hz, 1H), 7.67 – 7.63 (m, 1H), 7.63 – 7.58 (m, signal overlap with signals corresponding to benzoic acid), 7.57 – 7.54 (m, 2H), 7.54 – 7.52 (m, 1H), 7.51 (d,  $J = 2.8$  Hz, 1H), 7.50 – 7.45 (m, signal overlap with

signals corresponding to benzoic acid), 7.45 – 7.43 (m, 3H), 7.40 (d,  $J = 7.4$  Hz, 1H), 7.34 (s, 1H), 7.30 (s, 2H), 7.25-7.21 (m, 5H), 7.18 – 7.12 (m, 1H), 7.08 (td,  $J = 7.7, 5.3$  Hz, 3H), 7.04 – 6.94 (m, 3H), 6.93 (s, 1H), 6.88 (q,  $J = 7.4$  Hz, 2H), 6.83 (d,  $J = 7.5$  Hz, 1H), 6.81 – 6.76 (m, 2H), 6.75 – 6.70 (m, 2H), 6.55 (s, 1H), 6.39 (s, 1H), 6.27 (s, 1H), 6.23 (s, 1H), 5.72 (s, 1H), 5.71 (s, 1H), 5.58 (s, 1H), 5.49 (s, 1H), 5.35 (t,  $J = 4.7$  Hz, 2H), 4.73 (s, 1H), 4.63 (s, 1H), 4.16 – 4.11 (m, 1H), 3.91 – 3.86 (m, 2H), 3.84 – 3.79 (m, 4H), 3.78 – 3.73 (m, 2H), 3.66 – 3.60 (m, 3H), 3.52 – 3.48 (m, 3H), 3.28 – 3.16 (m, 1H), 1.76 – 0.99 (m, signal overlapping with water), 0.91-0.78 (m, signal overlapping with impurities), 0.52 (s, 3H), 0.48 (s, 3H), 0.01 (s, 3H). **MS** calcd for  $C_{175}H_{175}N_{26}O_{27}Se$   $[M+H]^+$  3152.2280, found (HR-ESI) 3152.9801.

**(1S)-Camph-XQ<sup>S</sup>Q<sup>B</sup>PQ<sup>B</sup>XQ<sup>B</sup>Q<sup>B</sup>PQ<sup>B</sup>XQ<sup>B</sup>Q<sup>B</sup>-OMe (13)** Compound **12** (135.9 mg, 43.12  $\mu$ mol, 1 eq.) was dissolved in a mixture of dry chloroform/MeOH 3:2 (5 mL) under  $N_2$ . TMSCHN<sub>2</sub> (2 M in hex, 76  $\mu$ L, 0.12 mmol, 2 eq.) was added dropwise, and the solution was stirred at r.t. for 2 h. A few drops of acetic acid were added, and the solution was stirred for 5 min at r.t. Then the solution was diluted with DCM, washed with NaHCO<sub>3</sub>, dried MgSO<sub>4</sub>, filtered and concentrated. The crude product was purified via precipitation in DCM/MeOH (56.6 mg, 46% yield). **<sup>1</sup>H NMR** (500 MHz, CDCl<sub>3</sub>, 25 °C)  $\delta$  [ppm] 11.37 (s, 1H), 11.19 (s, 1H), 11.15 (s, 1H), 10.95 (s, 1H), 10.71 (s, 1H), 10.65 (s, 1H), 10.37 (s, 1H), 10.25 (s, 1H), 10.17 (s, 1H), 9.99 (s, 1H), 9.20 (s, 1H), 7.93 (dd,  $J = 7.4, 3.6$  Hz, 2H), 7.83 (d,  $J = 7.3$  Hz, 1H), 7.77 (dtd,  $J = 14.1, 8.1, 3.6$  Hz, 6H), 7.69 (dt,  $J = 8.2, 1.5$  Hz, 2H), 7.57 (s, 1H), 7.57 – 7.49 (m, 6H), 7.49 – 7.44 (m, 1H), 7.44 – 7.40 (m, 3H), 7.39 – 7.32 (m, 2H), 7.31 – 7.27 (m, 1H), 7.25 – 7.14 (m, 5H), 7.11 – 7.05 (m, 3H), 7.04 – 6.92 (m, 7H), 6.89 – 6.67 (m, 8H), 6.48 (s, 1H), 6.30 (s, 1H), 6.28 (s, 1H), 6.25 (s, 1H), 5.68 (s, 2H), 5.47 (s, 1H), 3.93 – 3.86 (m, 3H), 3.83 – 3.79 (m, 3H), 3.74 – 3.70 (m, 2H), 3.63-3.53 (m, 9H), 3.29-3.23 (m, 5H), 3.06 (s, 3H), 2.30 (dq,  $J = 13.3, 6.5$  Hz, 2H), 2.26 – 2.15 (m, 5H), 2.15 – 2.08 (m, 3H), 2.08 – 1.88 (m, 15H), 1.86 – 1.73 (m, 5H), 1.16 – 1.12 (m, 11H), 1.09 (d,  $J = 6.8$  Hz, 9H), 1.02 (dd,  $J = 13.1, 6.7$  Hz, 16H), 0.89 – 0.76 (m, 10H), 0.50 (s, 3H), 0.46 (s, 3H), 0.00 (s, 3H). **MS** calcd for  $C_{176}H_{176}N_{26}NaO_{27}Se$   $[M+Na]^+$  3188.2256, found (HR-ESI) 3190.0299.

**(1S)-Camph-XQ<sup>S</sup>Q<sup>B</sup>PQ<sup>B</sup>XQ<sup>B</sup>Q<sup>B</sup>PQ<sup>B</sup>XQ<sup>B</sup>Q<sup>B</sup>-OMe (5)** Compound **13** (12.4 mg, 3.91  $\mu$ mol) was treated with a 50% solution of TFA in DCM (2 mL) at r.t. for 2 h. Then the solvent was removed under vacuum, obtaining the product as a yellow solid (11.7 mg, quant.). **<sup>1</sup>H NMR** (500 MHz, DMSO-*d*<sub>6</sub>, 25 °C)  $\delta$  [ppm] 11.76 (s, 1H), 11.74 (s, 1H), 11.38 (s, 1H), 11.13 (s, 1H), 10.99 (s, 1H), 10.97 (s, 1H), 10.83 (s, 1H), 10.39 (s, 1H), 10.36 (s, 1H), 10.15 (s, 1H), 10.07 (s, 1H), 10.05 (s, 2H), 9.13 (s, 1H), 7.88 (d,  $J = 7.3$  Hz, 1H), 7.74 (d,  $J = 7.3$  Hz, 2H), 7.71 (d,  $J = 7.3$  Hz, 1H), 7.64 (d,  $J = 7.9$  Hz, 2H), 7.56 (dt,  $J = 15.4, 7.3$  Hz, 4H), 7.49 (d,  $J = 8.1$  Hz, 5H), 7.47 – 7.42 (m, 2H), 7.41 – 7.35 (m, 4H), 7.35 – 7.30 (m, 3H), 7.19 – 7.09 (m, 5H), 6.99 (tt,  $J = 18.9, 6.7$  Hz, 5H), 6.88 (td,  $J = 14.4, 13.6, 9.2$  Hz, 5H), 6.80 (t,  $J = 7.7$  Hz, 2H), 6.75 (d,  $J = 7.3$  Hz, 1H), 6.71 (d,  $J = 7.5$  Hz, 1H), 6.58 (d,  $J = 7.3$  Hz, 1H), 6.48 (d,  $J = 7.5$  Hz, 1H), 6.39 (s, 1H), 6.24 (s, 1H), 5.85 (s, 1H), 5.81 (s, 1H), 5.59 (s, 1H), 5.51 (s, 1H), 5.37 (s, 1H), 3.96 – 3.93 (m, 1H), 3.91 – 3.88 (m, 2H), 3.82 – 3.79 (m, 2H), 3.77 – 3.70 (m, 5H), 3.69 – 3.55 (m, 4H), 3.53-3.44 (m, overlay with water peak), 3.19-3.14 (m, 2H), 3.05 (s, 3H), 3.01 – 2.98 (m, 2H), 2.42 (s, 3H), 2.33 – 2.26 (m, 4H), 2.24 – 2.16 (m, 4H), 2.13 – 2.04 (m, 2H), 2.00 (d,  $J = 7.8$  Hz, 1H), 1.72 – 1.66 (m, 4H), 1.56 – 1.43 (m, 4H), 1.42 – 1.32 (m, 4H), 1.28 – 1.21 (m, 4H), 1.21 –

1.13 (m, 4H), 1.13 – 1.09 (m, 4H), 1.07 (d,  $J = 6.7$  Hz, 4H), 1.04 (d,  $J = 6.7$  Hz, 6H), 0.84 (t,  $J = 6.9$  Hz, 8H), 0.47 (s, 3H), 0.40 (s, 3H), -0.07 (s, 3H). **MS** calcd for  $C_{164}H_{153}N_{26}O_{27}Se$   $[M+H]^+$  2998.0558, found (HR-ESI) 2998.8521, calcd for  $C_{164}H_{154}N_{26}O_{27}Se$   $[M+2H]^{2+}$  1499.5316, found (HR-ESI) 1499.9279.

**(1S)-Camph- $\underline{XQ^DQ^MPQ^D\underline{XQ^DQ^MPQ^D\underline{XQ^DQ^BPQ^D\underline{XQ^DQ^B-OH}}$  (14)** Compound **14** was synthesized using the SPS procedures reported in 0 on SASRIN resin loaded via HBTU-coupling described in 0 (scale: 82  $\mu$ mol). After full cleavage and precipitation in EtOAc/*n*-hex, the product was obtained as a yellow solid (192.2 mg, 51%).  **$^1H$  NMR** (500 MHz,  $CD_2Cl_2$ , 25  $^\circ C$ )  $\delta$  [ppm] 11.21 (s, 1H), 11.12 (s, 1H), 10.88 (s, 1H), 10.70 (s, 1H), 10.47 (s, 1H), 10.42 (s, 1H), 10.36 (s, 1H), 10.21 (s, 1H), 10.16 (s, 1H), 10.07 (s, 1H), 9.95 (s, 1H), 9.92 (s, 1H), 9.85 (s, 1H), 9.78 (s, 1H), 9.17 (s, 1H), 8.03 – 8.00 (m, 2H), 7.90 (d,  $J = 7.2$  Hz, 1H), 7.84 – 7.81 (m, 2H), 7.75 (ddd,  $J = 7.1, 5.8, 1.2$  Hz, 3H), 7.64 – 7.56 (m, 4H), 7.55 – 7.47 (m, 4H), 7.47 – 7.41 (m, 3H), 7.41 – 7.33 (m, 3H), 7.33 – 7.28 (m, 5H), 7.23 (t,  $J = 7.6$  Hz, 2H), 7.18 – 7.07 (m, 3H), 7.07 – 7.03 (m, 4H), 7.01 (d,  $J = 2.9$  Hz, 3H), 7.00 – 6.90 (m, 6H), 6.90 – 6.84 (m, 5H), 6.84 – 6.73 (m, 7H), 6.69 – 6.63 (m, 3H), 6.60 – 6.55 (m, 2H), 6.35 (s, 1H), 6.33 (d,  $J = 1.7$  Hz, 1H), 6.30 (s, 1H), 6.21 (s, 1H), 5.96 (s, 1H), 5.87 (s, 1H), 5.77 (s, 1H), 5.70 (s, 1H), 5.63 (s, 1H), 5.57 (s, 1H), 3.93 – 3.86 (m, 14H), 3.85 – 3.79 (m, 24H), 3.78 – 3.70 (m, 31H), 3.69 – 3.71 (m, 13H), 3.54 (s, 3H), 3.53 (s, 3H), 3.52 (s, 3H), 1.63 (s, 8H), 1.58 (s, 11H), 1.52 (s, 8H), 1.23 – 1.20 (m, 4H), 1.14 (dd,  $J = 14.7, 6.8$  Hz, 8H), 1.04 (dd,  $J = 14.6, 6.8$  Hz, 8H), 0.88 – 0.79 (m, 10H), 0.46 (s, 3H), 0.42 (s, 3H), -0.04 (s, 3H). **MS** calcd for  $C_{242}H_{244}N_{36}Na_2O_{44}S_7$   $[M+2Na]^{2+}$  2313.7896, found (HR-ESI) 2315.0568.

**(1S)-Camph- $\underline{XQ^DQ^MPQ^D\underline{XQ^DQ^MPQ^D\underline{XQ^DQ^BPQ^D\underline{XQ^DQ^B-OMe}}$  (15)** Compound **14** (192.2 mg, 41.95  $\mu$ mol, 1 eq.) was dissolved in a mixture of dry chloroform/MeOH 3:2 (5 mL) under  $N_2$ . TMSCHN<sub>2</sub> (2 M in *n*-hex, 24.8  $\mu$ L, 0.083 mmol, 2 eq.) was added dropwise, and the solution was stirred at r.t. for 2 h. A few drops of acetic acid were added, and the solution was stirred for 5 min at r.t. Then the solution was diluted with DCM, washed with  $NaHCO_3$ , dried  $MgSO_4$ , filtered and concentrated. The product was obtained as a yellow solid (146.7 mg, 76%).  **$^1H$  NMR** (500 MHz,  $CD_2Cl_2$ , 25  $^\circ C$ )  $\delta$  [ppm] 11.19 (s, 1H), 11.01 (s, 1H), 10.91 (s, 1H), 10.81 (s, 1H), 10.39 (s, 1H), 10.30 (s, 1H), 10.24 (s, 1H), 10.13 (s, 1H), 10.06 (s, 1H), 10.00 (s, 1H), 9.86 (s, 1H), 9.85 (s, 1H), 9.79 (s, 1H), 9.71 (s, 1H), 9.09 (s, 1H), 7.95 – 7.91 (m, 1H), 7.90 (dd,  $J = 7.4, 1.1$  Hz, 1H), 7.78 – 7.70 (m, 4H), 7.64 (dd,  $J = 7.4, 1.3$  Hz, 2H), 7.60 – 7.52 (m, 4H), 7.52 – 7.38 (m, 12H), 7.38 – 7.29 (m, 6H), 7.24 – 7.21 (m, 3H), 7.17 – 7.14 (m, 1H), 7.07 – 6.90 (m, 12H), 6.88 – 6.60 (m, 13H), 6.57 (d,  $J = 7.4$  Hz, 1H), 6.52 – 6.47 (m, 2H), 6.26 – 6.25 (m, 2H), 6.21 (s, 1H), 6.11 (s, 1H), 5.87 (s, 1H), 5.81 (s, 1H), 5.72 (s, 1H), 5.59 (s, 1H), 5.51 (s, 1H), 5.47 (s, 1H), 3.85 – 3.61 (m, 19H), 3.59 – 3.51 (m, 11H), 3.51 – 3.44 (m, 19H), 3.43 (s, 3H), 3.41 – 3.38 (m, 4H), 3.37 (s, 3H), 3.31 (s, 3H), 3.23 (s, 3H), 3.19 – 3.13 (m, 3H), 3.10 – 2.96 (m, 12H), 2.95 (s, 3H), 2.94 – 2.83 (m, 7H), 2.79 – 2.74 (d,  $J = 2.77$ , 1H), 2.63 – 2.58 (m, 1H), 1.59 (s, 8H), 1.52 (s, 8H), 1.51 (s, 8H), 1.49 (s, 8H), 1.11 (d,  $J = 6.8$  Hz, 4H), 1.07 (d,  $J = 6.7$  Hz, 4H), 1.00 (dd,  $J = 6.6, 3.5$  Hz, 8H), 0.81 – 0.73 (m, 10H), 0.40 (s, 3H), 0.37 (s, 3H), -0.09 (s, 3H). **MS** calcd for  $C_{243}H_{246}N_{36}Na_2O_{44}S_7$   $[M+2Na]^{2+}$  2320.7974 found (HR-ESI) 2321.5576.

**(1S)-Camph-XQ<sup>D</sup>Q<sup>M</sup>PQ<sup>D</sup>XQ<sup>D</sup>Q<sup>M</sup>PQ<sup>D</sup>XQ<sup>D</sup>Q<sup>B</sup>PQ<sup>D</sup>XQ<sup>D</sup>Q<sup>B</sup>-OMe (6)** Compound **15** (49.5 mg, 10.8  $\mu$ mol) was treated with a 50% solution of TFA in DCM (3 mL) at r.t. for 2 h. Then the solvent was removed under vacuum, obtaining the product as a yellow solid (47.2 mg, quant.). <sup>1</sup>H NMR (500 MHz, DMSO-*d*<sub>6</sub>, 25 °C)  $\delta$  [ppm] 11.72 (s, 2H), 11.33 (s, 1H), 11.29 (s, 1H), 11.09 (s, 1H), 10.96 (s, 1H), 10.85 (s, 1H), 10.77 (s, 1H), 10.28 (s, 1H), 10.24 (s, 1H), 10.18 (s, 1H), 10.10 (s, 1H), 10.01 (s, 1H), 9.98 (s, 1H), 9.85 (s, 1H), 9.80 (s, 1H), 9.78 (s, 1H), 9.67 (s, 1H), 9.07 (s, 1H), 7.85 (d, *J* = 7.6 Hz, 2H), 7.74 (d, *J* = 9.8 Hz, 2H), 7.69 (d, *J* = 7.0 Hz, 2H), 7.67 – 7.54 (m, 3H), 7.48 (ddd, *J* = 26.2, 12.7, 8.3 Hz, 6H), 7.42 – 7.27 (m, 11H), 7.27 – 7.16 (m, 7H), 7.16 – 7.02 (m, 6H), 7.01 – 6.72 (m, 15H), 6.69 (dd, *J* = 12.3, 6.6 Hz, 3H), 6.60 (dd, *J* = 7.8, 3.1 Hz, 2H), 6.56 (d, *J* = 6.9 Hz, 1H), 6.51 (d, *J* = 7.9 Hz, 1H), 6.39 (d, *J* = 7.9 Hz, 1H), 6.22 (d, *J* = 8.9 Hz, 2H), 6.16 (d, *J* = 7.2 Hz, 1H), 6.05 (s, 1H), 5.88 (s, 1H), 5.67 (s, 1H), 5.61 (s, 1H), 5.58 (s, 1H), 5.47 (s, 1H), 5.43 (s, 1H), 3.84 – 3.62 (m, 16H), 3.62 – 3.54 (m, 6H), 3.52 – 3.49 (m, 4H), 3.49 – 3.42 (m, 8H), 3.21 – 3.04 (m, 8H), 3.02 (s, 2H), 2.99 – 2.89 (m, 5H), 2.89 – 2.81 (m, 2H), 2.79 – 2.68 (m, 2H), 2.54 (s, 3H), 2.20 – 2.15 (m, 2H), 2.10–2.04 (m, 2H), 1.51 – 1.43 (m, 6H), 1.34 – 1.22 (m, 15H), 1.19–1.11 (m, 14H), 1.03 (dd, *J* = 14.0, 6.7 Hz, 8H), 0.84 (q, *J* = 5.4, 4.0 Hz, 4H), 0.77 (d, *J* = 9.6 Hz, 7H), 0.45 (s, 3H), 0.37 (s, 3H), -0.10 (s, 3H). MS calcd for C<sub>227</sub>H<sub>214</sub>N<sub>36</sub>Na<sub>2</sub>O<sub>44</sub>S<sub>7</sub> [M+2Na]<sup>2+</sup> 2208.6722, found (HR-ESI) 2209.1001.

**O<sub>2</sub>N-XQ<sup>D</sup>Q<sup>S</sup>PQ<sup>D</sup>XQ<sup>D</sup>Q<sup>S</sup>PQ<sup>D</sup>XQ<sup>D</sup>Q<sup>B</sup>PQ<sup>D</sup>XQ<sup>D</sup>Q<sup>B</sup>-OH (16)** Compound **16** was synthesized using the SPS procedures reported in 0 on SASRIN resin loaded via HBTU-coupling described in 0 (scale: 30.79  $\mu$ mol). After full cleavage, the crude product was purified via precipitation in DCM/MeOH, and the product was obtained as a yellow solid (71.0 mg, 51%). <sup>1</sup>H NMR (500 MHz, CDCl<sub>3</sub>, 25 °C)  $\delta$  [ppm] 11.14 (s, 1H), 11.08 (s, 1H), 10.83 (s, 1H), 10.54 (s, 1H), 10.53 (s, 1H), 10.44 (s, 1H), 10.40 (s, 1H), 10.16 (s, 1H), 10.10 (s, 1H), 9.96 (s, 1H), 9.94 (s, 1H), 9.91 (s, 1H), 9.78 (s, 1H), 9.48 (s, 1H), 8.08 – 8.04 (m, 4H), 7.93 (d, *J* = 7.2 Hz, 2H), 7.79 (d, *J* = 7.2 Hz, 1H), 7.64 (d, *J* = 13.4 Hz, 4H), 7.55 (t, *J* = 6.9 Hz, 4H), 7.44 – 7.41 (m, 4H), 7.40 – 7.36 (m, 4H), 7.35 – 7.30 (m, 11H), 7.14 – 7.12 (m, 2H), 7.08 – 7.04 (m, 4H), 7.04 – 6.98 (m, 5H), 6.97 – 6.94 (m, 2H), 6.92 – 6.88 (m, 4H), 6.87 – 6.85 (m, 2H), 6.81 – 6.74 (m, 2H), 6.70 – 6.67 (m, 3H), 6.66 – 6.61 (m, 4H), 6.57 – 6.54 (m, 2H), 6.46 (d, *J* = 7.0 Hz, 1H), 6.43 (s, 1H), 6.34 (s, 1H), 6.12 (s, 1H), 5.97 (s, 1H), 5.65 (s, 1H), 5.64 (s, 1H), 5.59 (s, 1H), 4.15 – 4.10 (m, 2H), 3.94 – 3.91 (m, 2H), 3.90 – 3.87 (m, 4H), 3.85 – 3.78 (m, 4H), 3.77 – 3.72 (m, 5H), 3.71 – 3.65 (m, 5H), 3.61 – 3.58 (m, 5H), 3.57 (s, 5H), 3.53 (s, 10H), 3.50 (s, 5H) 3.50 – 3.48 (m, 3H), 3.47 (s, 2H), 3.46 (s, 2H), 3.44 – 3.40 (m, 4H), 3.38 (s, 3H), 3.36 (s, 3H), 3.25 – 3.20 (m, 4H), 3.16 – 3.11 (m, 5H), 2.96 (s, 1H), 2.93 (s, 2H), 2.89 (s, 1H), 2.87 – 2.84 (m, 2H), 2.03–0.98 (m, signal overlapping with water). 0.91 – 0.80 (m, 18H). MS calcd for C<sub>232</sub>H<sub>232</sub>N<sub>36</sub>O<sub>41</sub>S<sub>7</sub>Se<sub>2</sub> [M+2H]<sup>2+</sup> 2280.6770, found (HR-ESI) 2283.5340, calcd for C<sub>232</sub>H<sub>231</sub>N<sub>36</sub>NaO<sub>41</sub>S<sub>7</sub>Se<sub>2</sub> [M+H+Na]<sup>2+</sup> 2291.6680, found (HR-ESI) 2294.1091.

**O<sub>2</sub>N-XQ<sup>D</sup>Q<sup>S</sup>PQ<sup>D</sup>XQ<sup>D</sup>Q<sup>S</sup>PQ<sup>D</sup>XQ<sup>D</sup>Q<sup>B</sup>PQ<sup>D</sup>XQ<sup>D</sup>Q<sup>B</sup>-OMe (17)** Compound **16** (67.0 mg, 15  $\mu$ mol, 1 eq.) was dissolved in a mixture of dry chloroform/MeOH 3:2 (5 mL) under N<sub>2</sub>. TMSCHN<sub>2</sub> (2 M in hex, 51  $\mu$ L, 70  $\mu$ mol, 2 eq.) was added dropwise, and the solution was stirred at r.t. for 2 h. A few drops of acetic acid were added, and the solution was stirred for 5 min at r.t. Then the solution was diluted with DCM, washed with NaHCO<sub>3</sub>, dried MgSO<sub>4</sub>, filtered and concentrated. The pure product was a yellow solid (68.0 mg, quant.). <sup>1</sup>H NMR



(500 MHz, CDCl<sub>3</sub>, 25 °C) δ [ppm] 11.32 (s, 1H), 11.08 (s, 1H), 10.99 (s, 1H), 10.83 (s, 1H), 10.52 (s, 2H), 10.45 (s, 1H), 10.16 (s, 1H), 10.11 (s, 1H), 9.96 (s, 1H), 9.94 (s, 1H), 9.89 (s, 1H), 9.77 (s, 1H), 9.46 (s, 1H), 8.07 (dt, *J* = 10.7, 3.9 Hz, 2H), 7.95 – 7.91 (m, 1H), 7.87 (d, *J* = 8.0 Hz, 1H), 7.81 – 7.75 (m, 2H), 7.70 – 7.66 (m, 3H), 7.66 – 7.62 (m, 2H), 7.60 (dt, *J* = 7.9, 1.2 Hz, 3H), 7.57 – 7.51 (m, 3H), 7.51 – 7.42 (m, 4H), 7.42 (d, *J* = 1.1 Hz, 1H), 7.39 (ddd, *J* = 8.0, 5.6, 1.4 Hz, 7H), 7.35 – 7.27 (m, 3H), 7.18 (t, *J* = 7.7 Hz, 1H), 7.14 – 7.09 (m, 1H), 7.09 – 7.03 (m, 5H), 7.03 – 6.97 (m, 5H), 6.97 – 6.91 (m, 3H), 6.90 (q, *J* = 4.7, 3.9 Hz, 4H), 6.86 (q, *J* = 5.4, 4.3 Hz, 4H), 6.79 (d, *J* = 6.1 Hz, 1H), 6.75 (t, *J* = 7.7 Hz, 1H), 6.71 – 6.62 (m, 6H), 6.57 – 6.52 (m, 2H), 6.47 – 6.45 (m, 1H), 6.25 (s, 1H), 6.12 (s, 1H), 5.96 (s, 1H), 5.64 (s, 1H), 5.63 (s, 1H), 5.58 (d, *J* = 3.7 Hz, 1H), 3.90 – 3.86 (m, 3H), 3.86 – 3.80 (m, 4H), 3.80 – 3.68 (m, 8H), 3.67 (s, 4H), 3.61 – 3.56 (m, 9H), 3.55 – 3.51 (m, 14H), 3.50 (s, 8H), 3.42 – 3.40 (m, 3H), 3.38 (s, 4H), 3.36 (s, 4H), 3.16 – 3.08 (m, 5H), 3.03 (s, 3H), 2.96 – 2.82 (m, 2H), 2.80 (s, 2H), 2.35 (t, *J* = 7.5 Hz, 4H), 2.30 (t, *J* = 7.6 Hz, 7H), 2.26 (d, *J* = 8.3 Hz, 4H), 2.17 (s, 3H), 2.15 (s, 3H), 2.09 – 0.99 (m, signal overlapping with water). **MS** calcd for C<sub>233</sub>H<sub>232</sub>N<sub>36</sub>Na<sub>2</sub>O<sub>41</sub>S<sub>7</sub>Se<sub>2</sub> [M+2Na]<sup>2+</sup> 2309.6668, found (HR-ESI) 2310.0220.

**O<sub>2</sub>N-XQ<sup>D</sup>PQ<sup>D</sup>XQ<sup>D</sup>Q<sup>S</sup>PQ<sup>D</sup>XQ<sup>D</sup>Q<sup>B</sup>PQ<sup>D</sup>XQ<sup>D</sup>Q<sup>B</sup>-OMe (7)** Compound **17** (15.0 mg, 3.28 μmol) was treated with a 50% solution of TFA in DCM (4 mL) at r.t. for 2 h. Then the solvent was removed under vacuum, obtaining the product as a yellow solid (14.3 mg, quant.). <sup>1</sup>H NMR (500 MHz, pyridine-*d*<sub>5</sub>, 25 °C) δ [ppm] 11.79 (s, 1H), 11.52 (s, 1H), 11.43 (s, 1H), 11.41 (s, 1H), 11.01 (s, 1H), 10.95 (s, 1H), 10.92 (s, 1H), 10.76 (s, 1H), 10.63 (s, 1H), 10.59 (s, 2H), 10.46 (s, 1H), 10.43 (s, 1H), 10.18 (s, 1H), 8.53 – 8.50 (m, 1H), 8.40 – 8.38 (m, 1H), 8.36 – 8.34 (m, 1H), 8.31 – 8.30 (m, 1H), 8.26 – 8.23 (m, 2H), 8.21 – 8.15 (m, 4H), 8.02 – 7.97 (m, 3H), 7.96 – 7.92 (m, 3H), 7.84 – 7.77 (m, 3H), 7.75 (s, 1H), 7.71 – 7.66 (m, 2H), 7.67 – 7.64 (m, 3H), 7.58 (s, 1H), 7.55 – 7.53 (m, 4H), 7.46 – 7.40 (m, 4H), 7.37 – 7.31 (m, 4H), 7.29 – 7.25 (m, 4H), 7.24 – 7.16 (m, 5H), 7.09 – 6.97 (m, 4H), 6.96 (s, 5H), 6.88 – 6.86 (m, 3H), 6.84 – 6.73 (m, 5H), 6.64 (s, 4H), 6.54 (s, 1H), 6.22 (s, 1H), 6.21 (s, 1H), 6.18 (s, 1H), 3.86 – 3.79 (m, 8H), 3.86 – 3.79 (m, 4H), 3.78 (s, 4H), 3.77 – 3.73 (m, 7H), 3.72 – 3.86 (m, 5H), 3.65 – 3.60 (m, 3H), 3.58 – 3.55 (m, 1H), 3.50 – 3.47 (m, 1H), 3.45 (s, 4H), 3.44 (s, 3H), 3.43 (s, 3H), 3.38 (s, 3H), 3.32 (s, 3H), 3.27 (s, 3H), 3.24 (s, 3H), 3.22 (s, 1H), 2.62 (s, 3H), 2.52 (s, 3H), 2.45 (t, *J* = 7.4 Hz, 10H), 2.37 – 2.33 (m, 5H), 2.06 – 0.63 (m, signal overlapping with water), 0.52–0.36 (m, 10H). **MS** calcd for C<sub>217</sub>H<sub>201</sub>N<sub>36</sub>NaO<sub>41</sub>S<sub>7</sub>Se<sub>2</sub> [M+H+Na]<sup>2+</sup> 2186.5506, found (HR-ESI) 2186.2298.

## 4.2.7 References

- [1] S. De, B. Chi, T. Granier, T. Qi, V. Maurizot, I. Huc, *Nat. Chem.* **2018**, *10*, 51-57.
- [2] *Maestro*, Schrödinger, LLC, New York, NY, **2021**.
- [3] D. Mazzier, S. De, B. Wicher, V. Maurizot, I. Huc, *Angew. Chem. Int. Ed.* **2020**, *59*, 1606-1610.
- [4] D. Mazzier, S. De, B. Wicher, V. Maurizot, I. Huc, *Chem. Sci.* **2019**, *10*, 6984-6991.
- [5] Rigaku-Oxford-Diffraction, *CrysAlisPro Software System, Version 171.41* **2020**, Rigaku Corporation: Wrocław, Poland.
- [6] G. M. Sheldrick, *Acta Cryst.* **2015**, *A71*, 3-8.
- [7] G. M. Sheldrick, *Acta Cryst.* **2015**, *C71*, 3-8.
- [8] O. V. Dolomanov, L. J. Bourhis, R. J. Gildea, J. A. K. Howard, H. Puschmann, *J. Appl. Cryst.* **2009**, *42*, 339-341.
- [9] B. Baptiste, C. Douat-Casassus, K. Laxmi-Reddy, F. Godde, I. Huc, *J. Org. Chem.* **2010**, *75*, 7175-7185.
- [10] J. Buratto, C. Colombo, M. Stupfel, S. J. Dawson, C. Dolain, B. Langlois D'Estaintot, L. Fischer, T. Granier, M. Laguerre, B. Gallois, I. Huc, *Angew. Chem. Int. Ed.* **2014**, *126*, 902-906.
- [11] M. Vallade, P. Sai Reddy, L. Fischer, I. Huc, *Eur. J. Org. Chem.* **2018**, *2018*, 5489-5498.
- [12] C. Tsiamantas, S. J. Dawson, I. Huc, *C. R. Chimie* **2016**, *19*, 132-142.
- [13] A. W. Snow, E. E. Foos, *Synthesis* **2003**, *2003*, 0509-0512.

## 4.2.8 NMR spectra of new compounds

### 4.2.8.1 <sup>1</sup>H NMR and <sup>13</sup>C NMR spectra of new small compounds

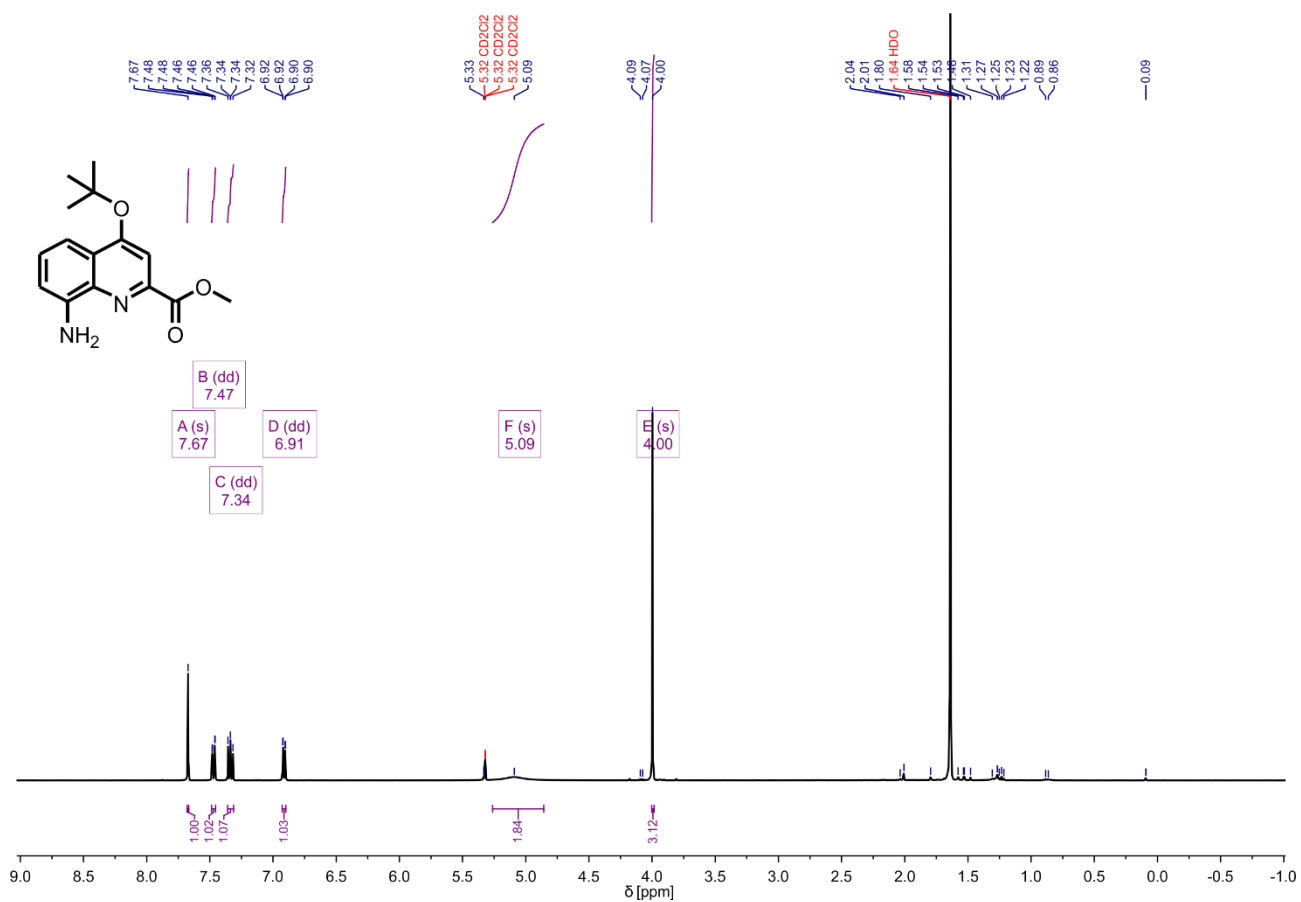


**Figure S34.** <sup>1</sup>H NMR spectrum (400 MHz, CD<sub>2</sub>Cl<sub>2</sub>) of C.

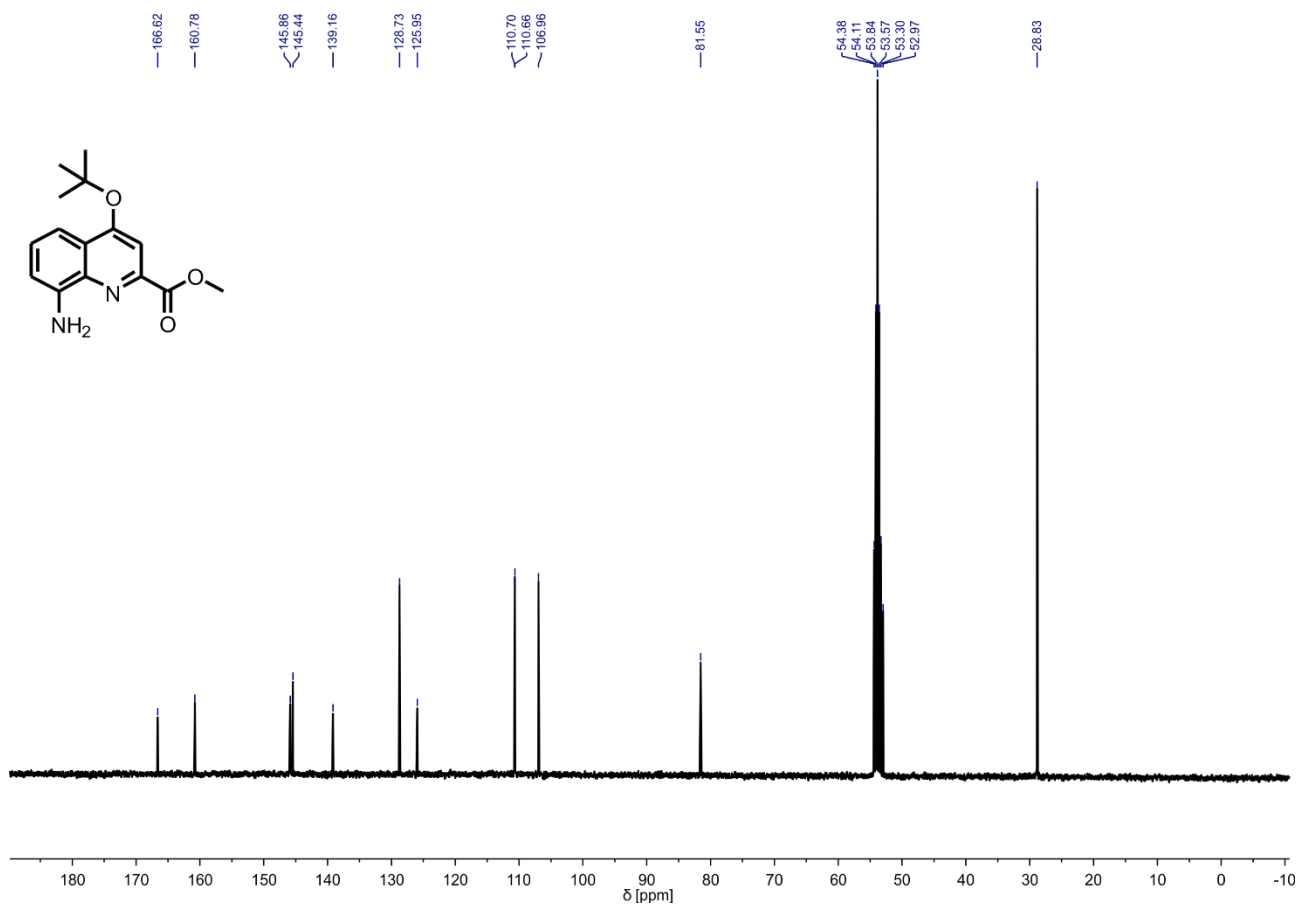


**Figure S35.**  $^{13}\text{C}$  NMR spectrum (101 MHz,  $\text{CD}_2\text{Cl}_2$ ) of C.

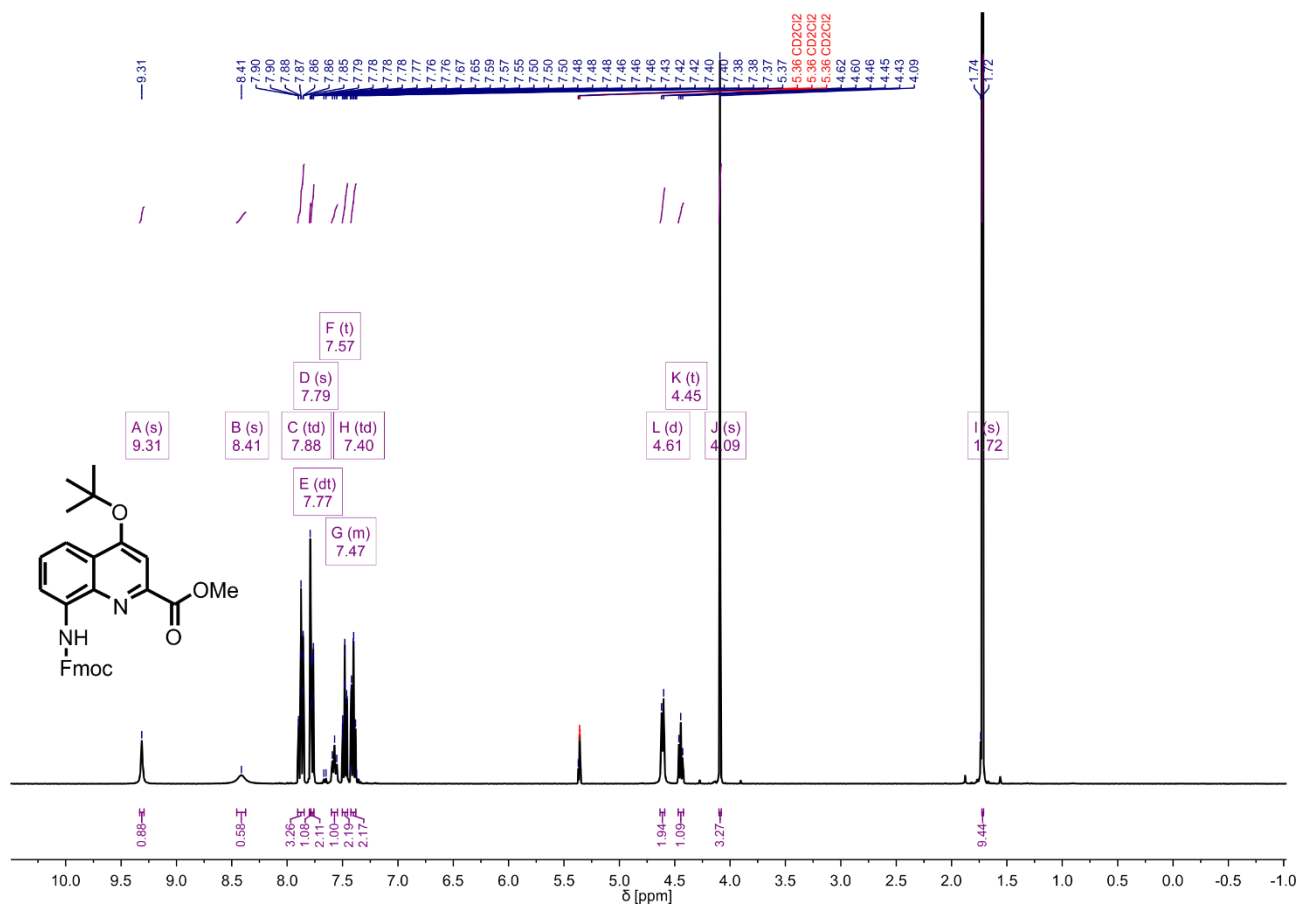


**Figure S36.**  $^1\text{H}$  NMR spectrum (400 MHz,  $\text{CD}_2\text{Cl}_2$ ) of **D**.

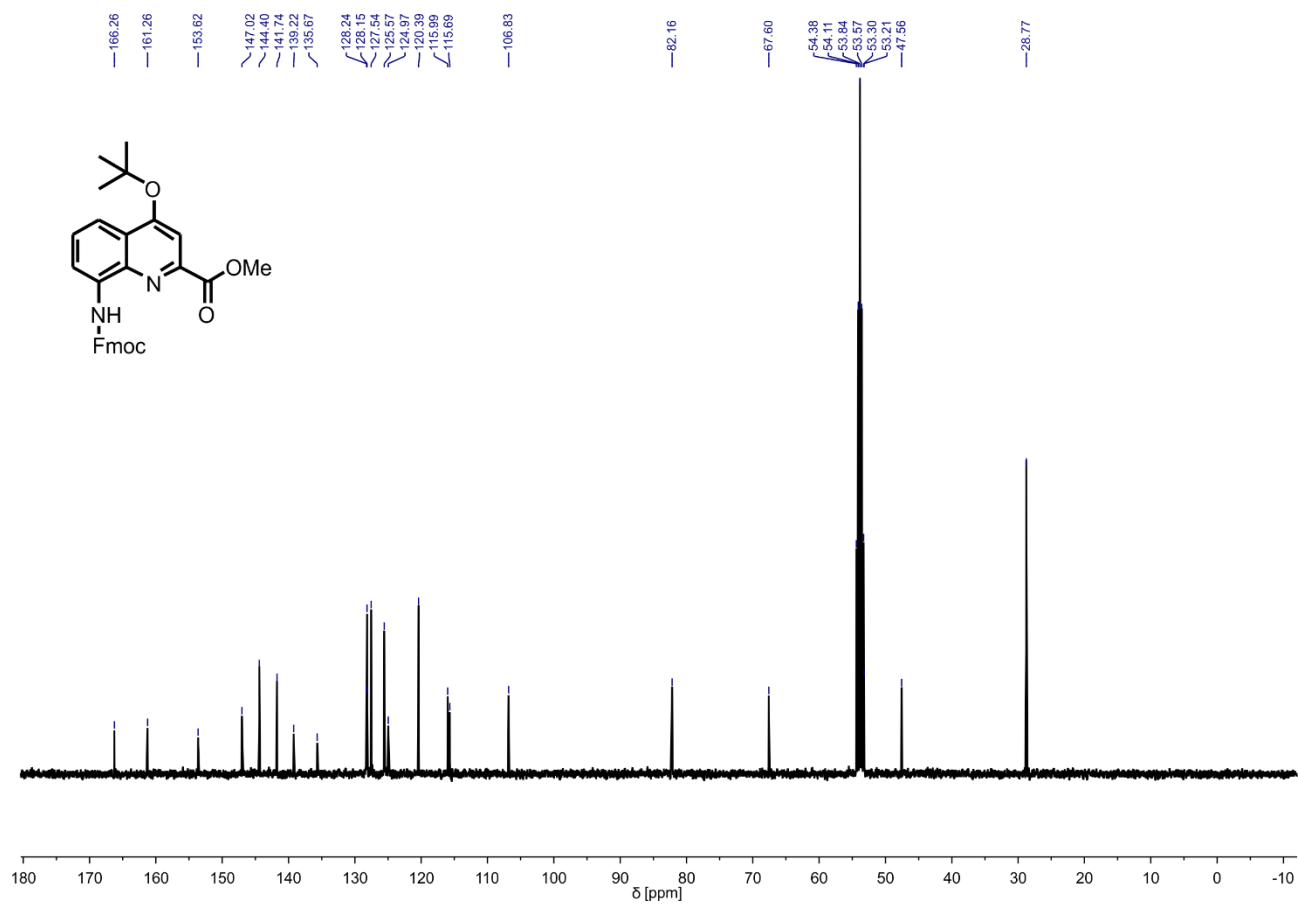


**Figure S37.**  $^{13}\text{C}$  NMR spectrum (101 MHz,  $\text{CD}_2\text{Cl}_2$ ) of D.

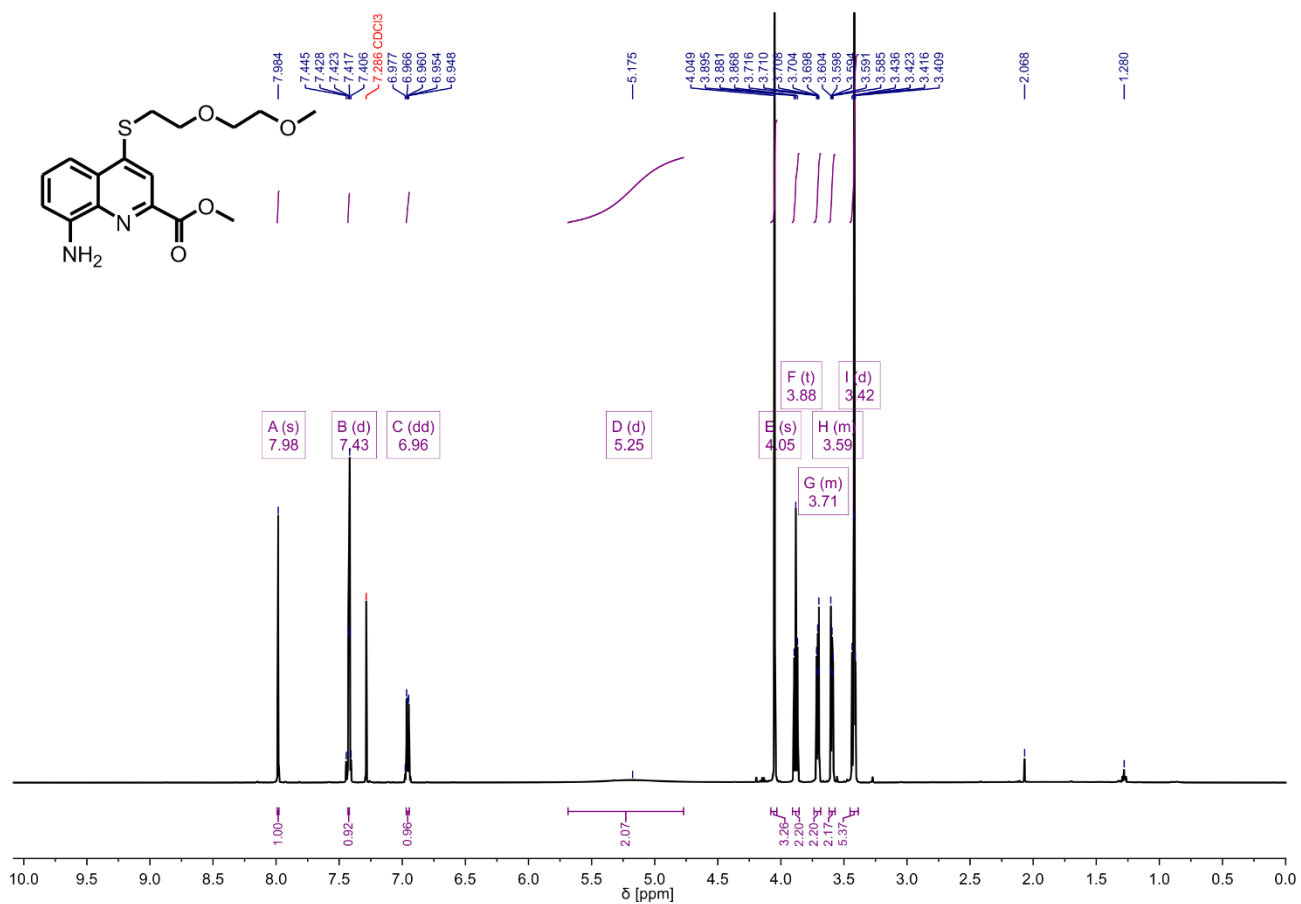
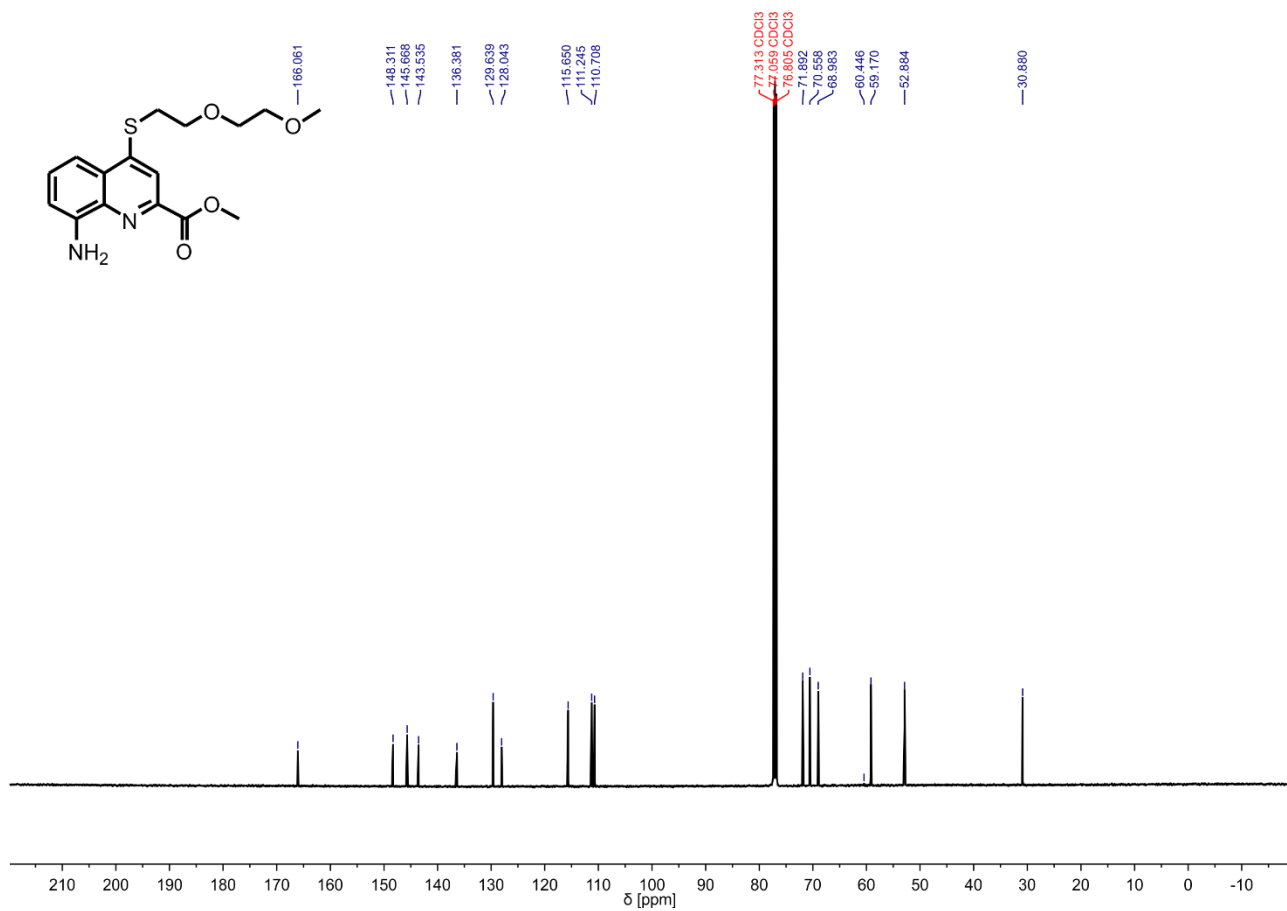
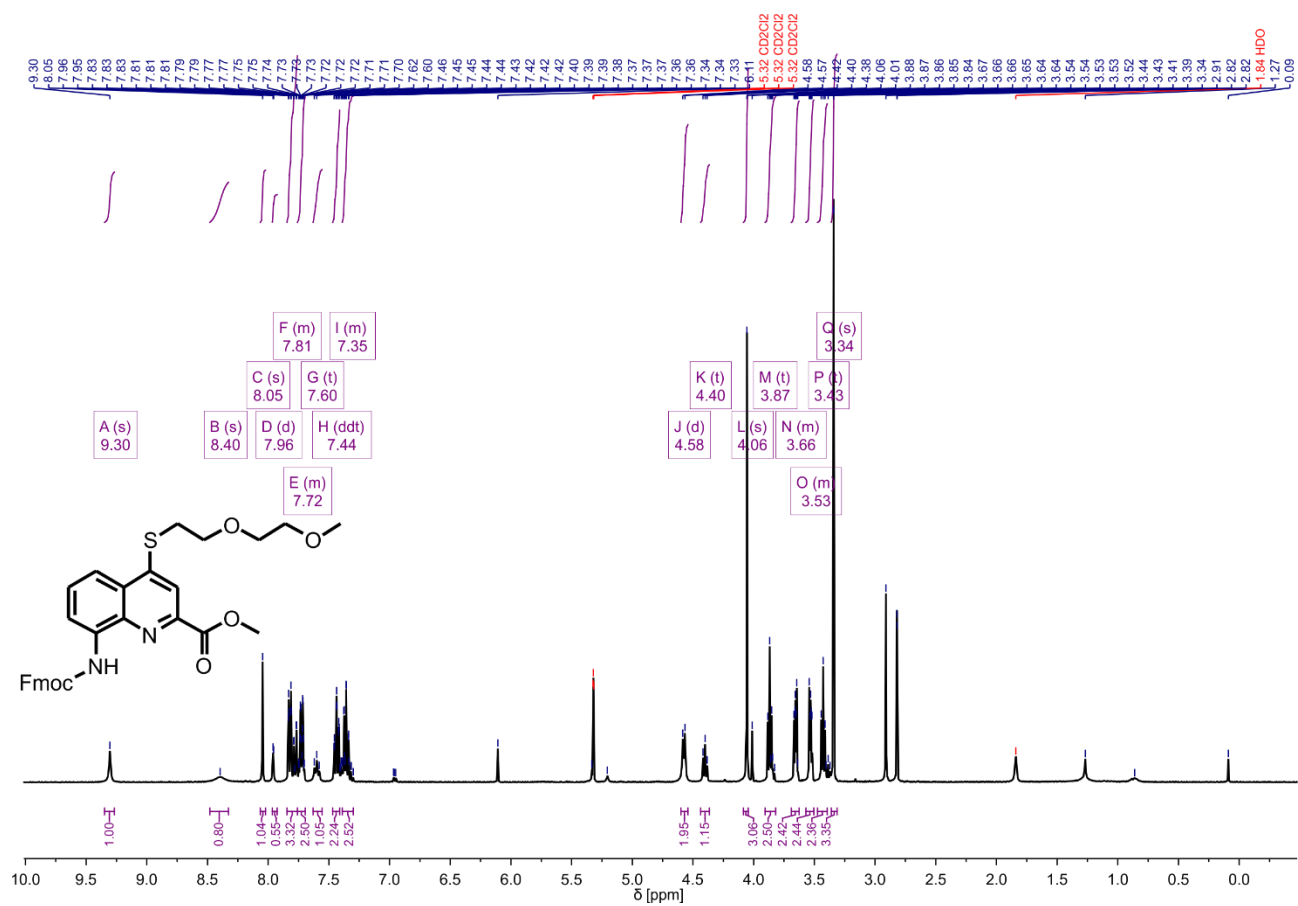


Figure S38. <sup>1</sup>H NMR spectrum (500 MHz, CDCl<sub>3</sub>) of J.



**Figure S39.** <sup>13</sup>C NMR spectrum (126 MHz, CDCl<sub>3</sub>) of **J**.





**Figure S40.** <sup>1</sup>H NMR spectrum (400 MHz, CD<sub>2</sub>Cl<sub>2</sub>) of K.

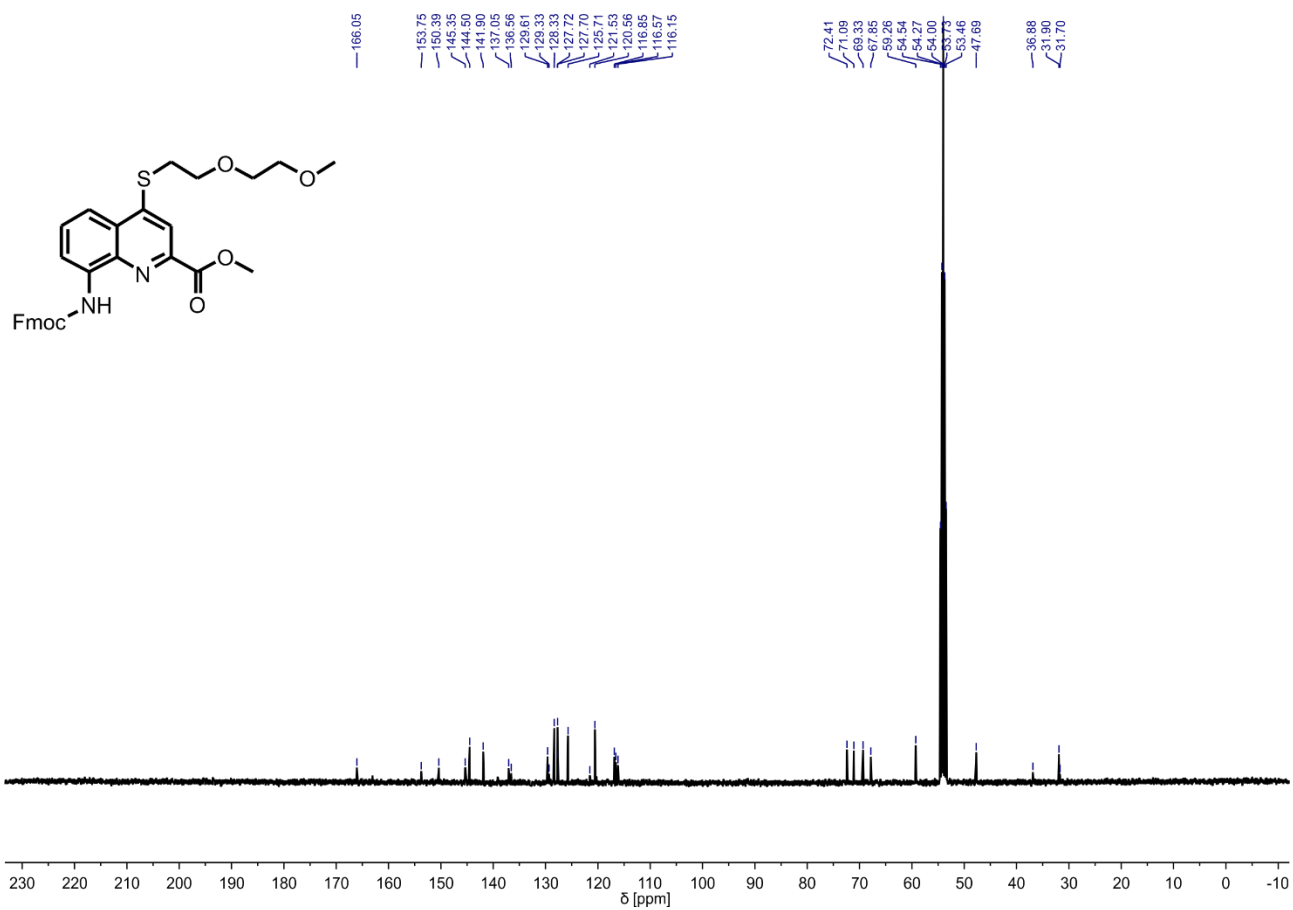


**Figure S41.**  $^{13}\text{C}$  NMR spectrum (101 MHz,  $\text{CD}_2\text{Cl}_2$ ) of **K**.

#### 4.2.8.2 $^1\text{H}$ NMR of new oligomers

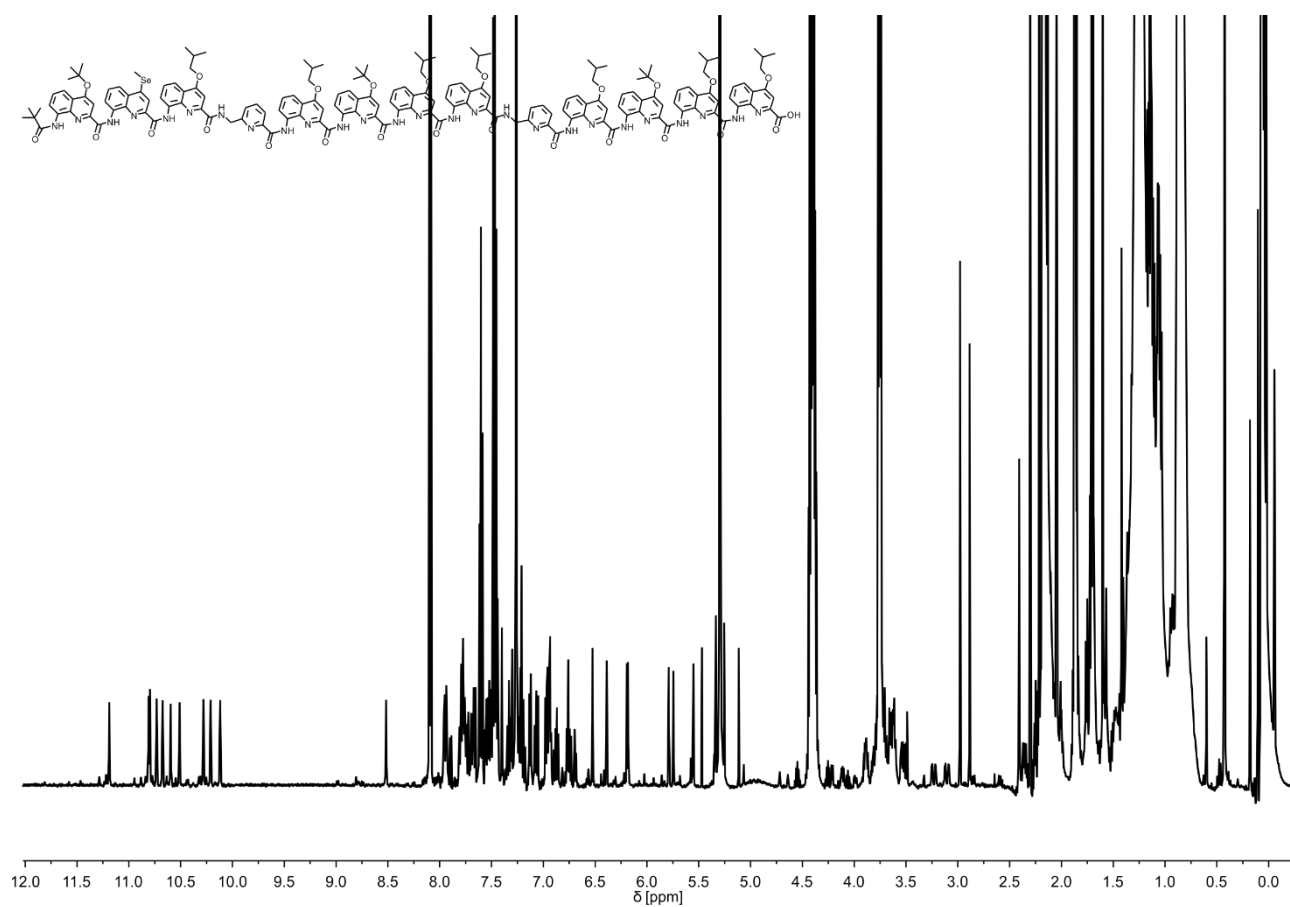


**Figure S42.**  $^1\text{H}$  NMR spectrum (500 MHz,  $\text{CDCl}_3$ ) of **8**.

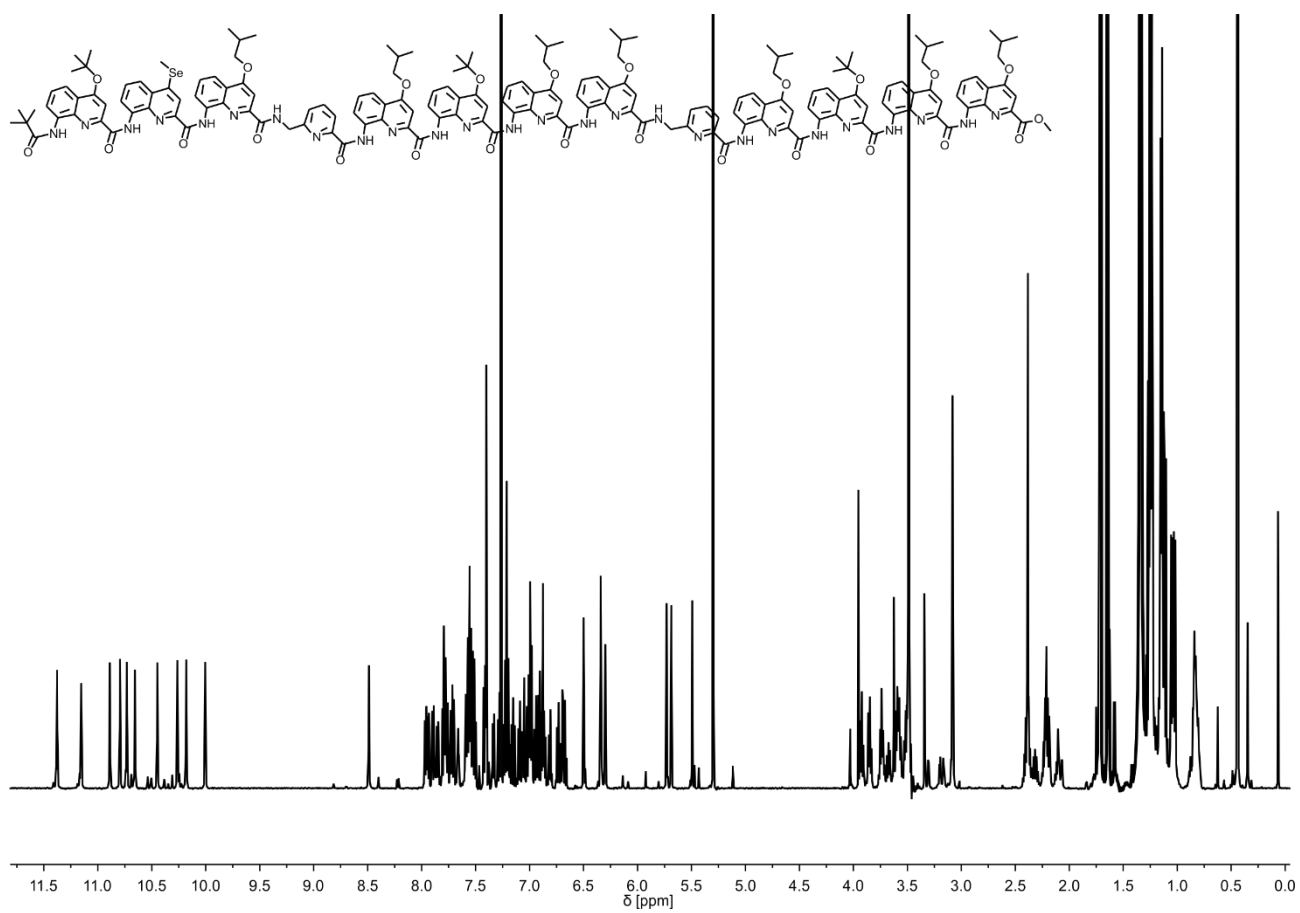


**Figure S43.** <sup>1</sup>H NMR spectrum (500 MHz, CDCl<sub>3</sub>) of **9**.

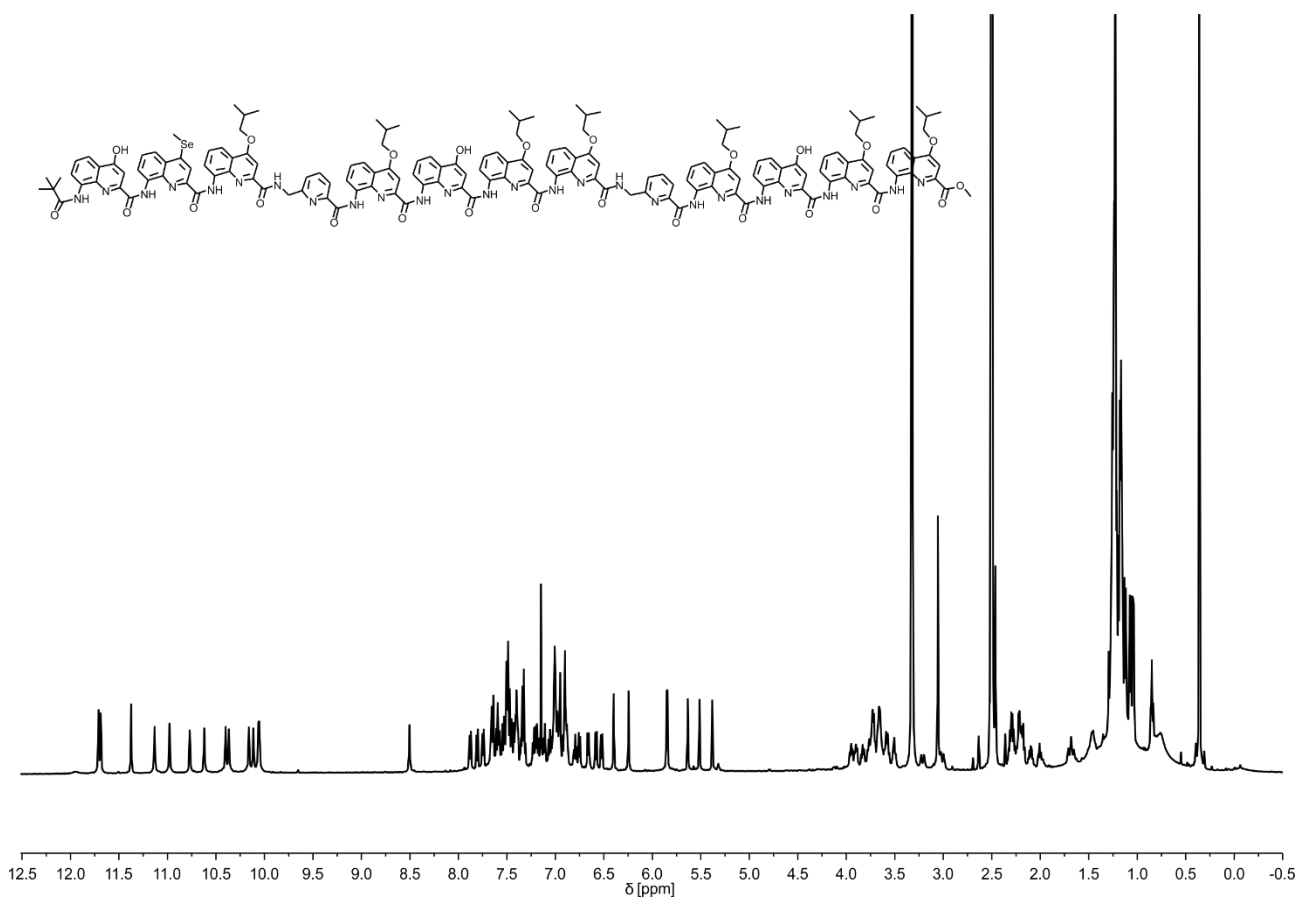


**Figure S44.** <sup>1</sup>H NMR spectrum (500 MHz, DMSO-*d*<sub>6</sub>) of **3**.

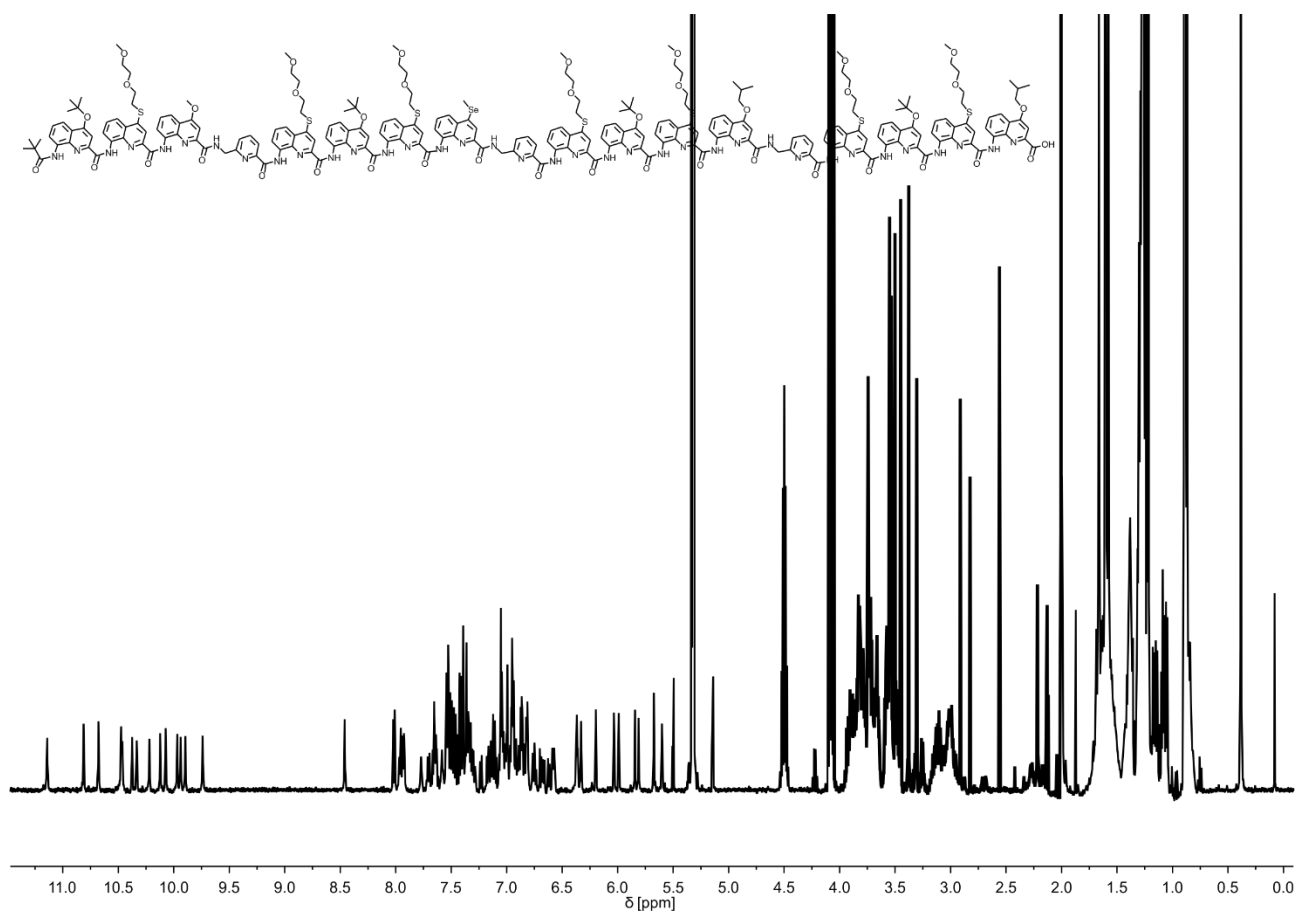


**Figure S45.**  $^1\text{H}$  NMR spectrum (500 MHz,  $\text{CD}_2\text{Cl}_2$ ) of **10**.

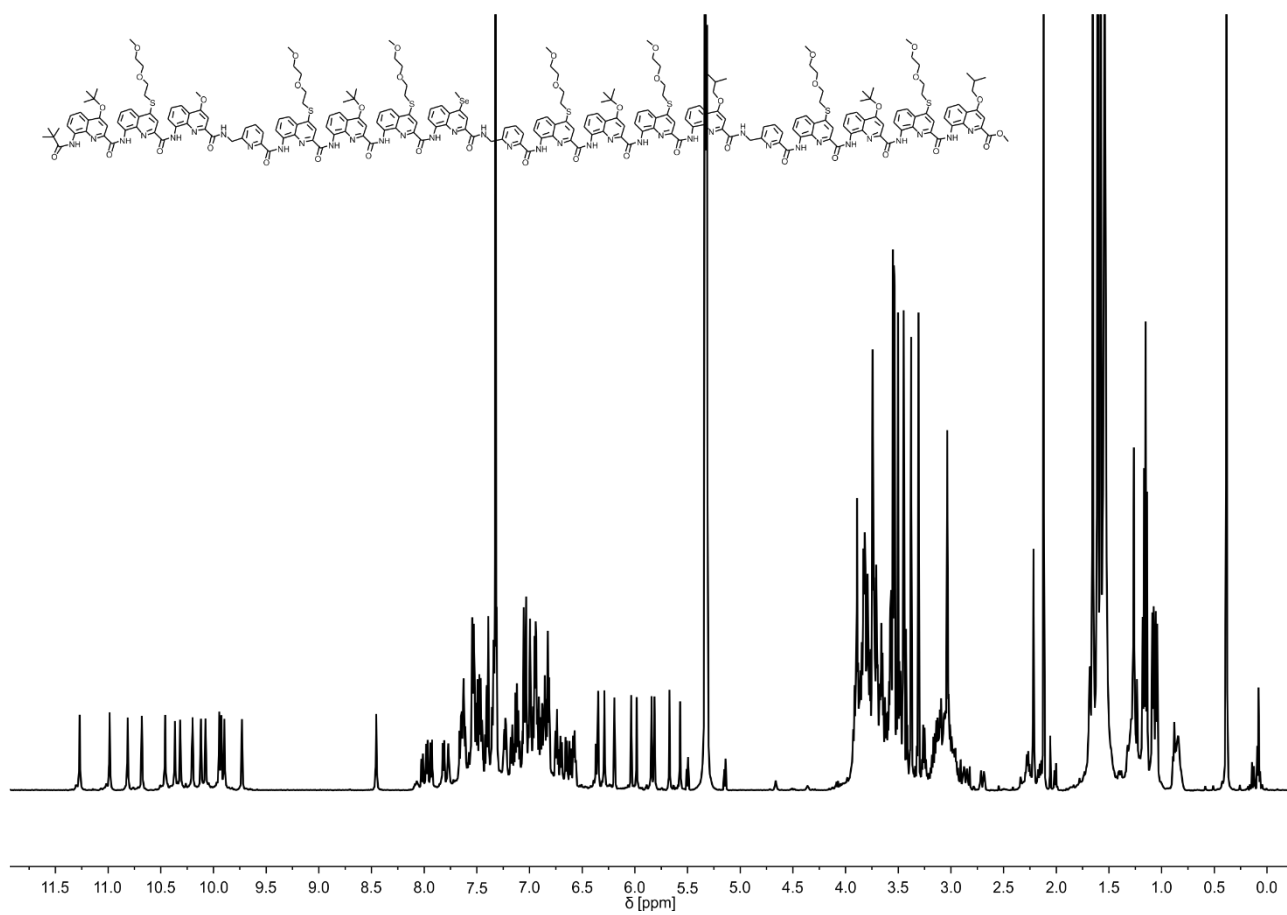


**Figure S46.**  $^1\text{H}$  NMR spectrum (500 MHz,  $\text{CD}_2\text{Cl}_2$ ) of **11**.

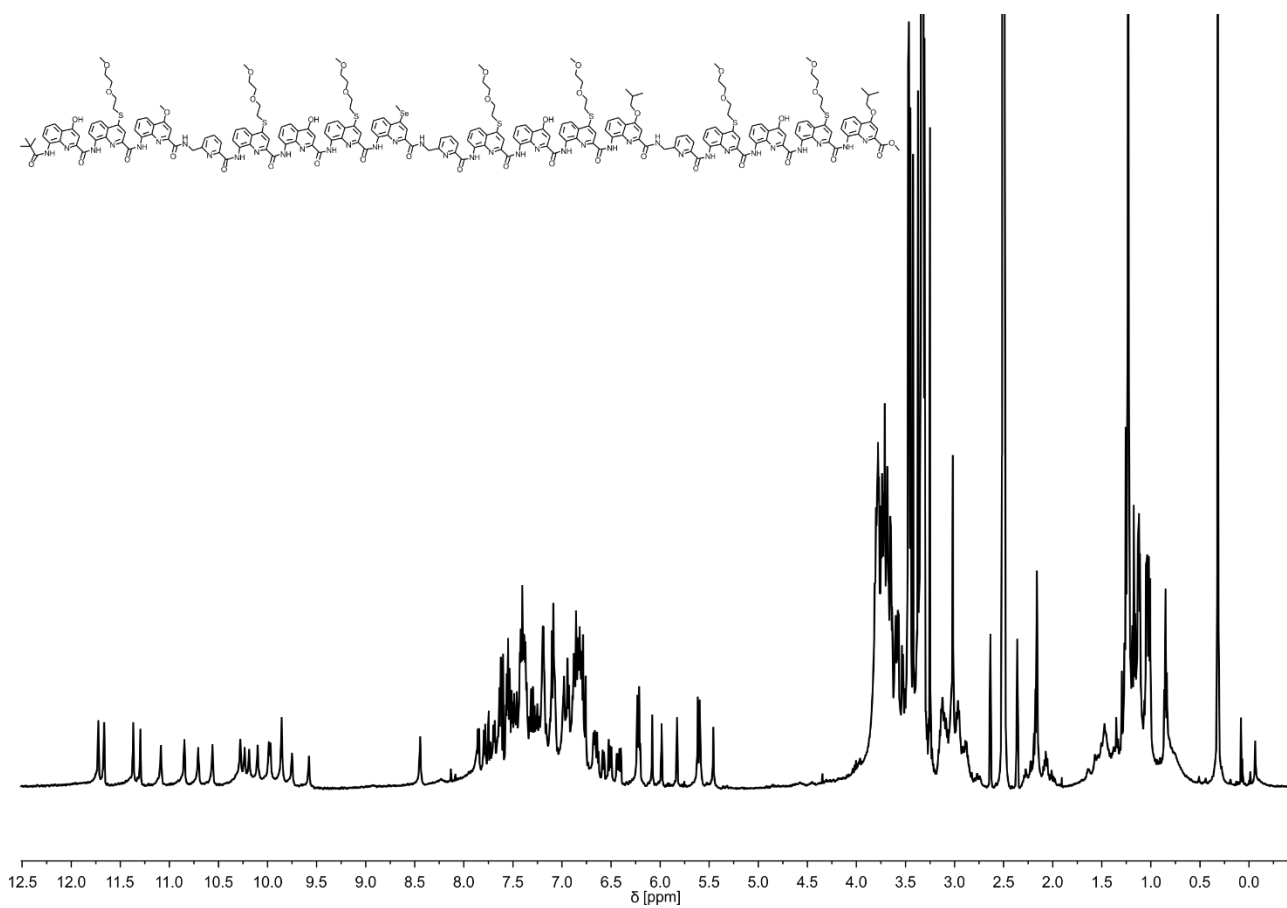


**Figure S47.** <sup>1</sup>H NMR spectrum (500 MHz, DMSO-*d*<sub>6</sub>) of **4**.



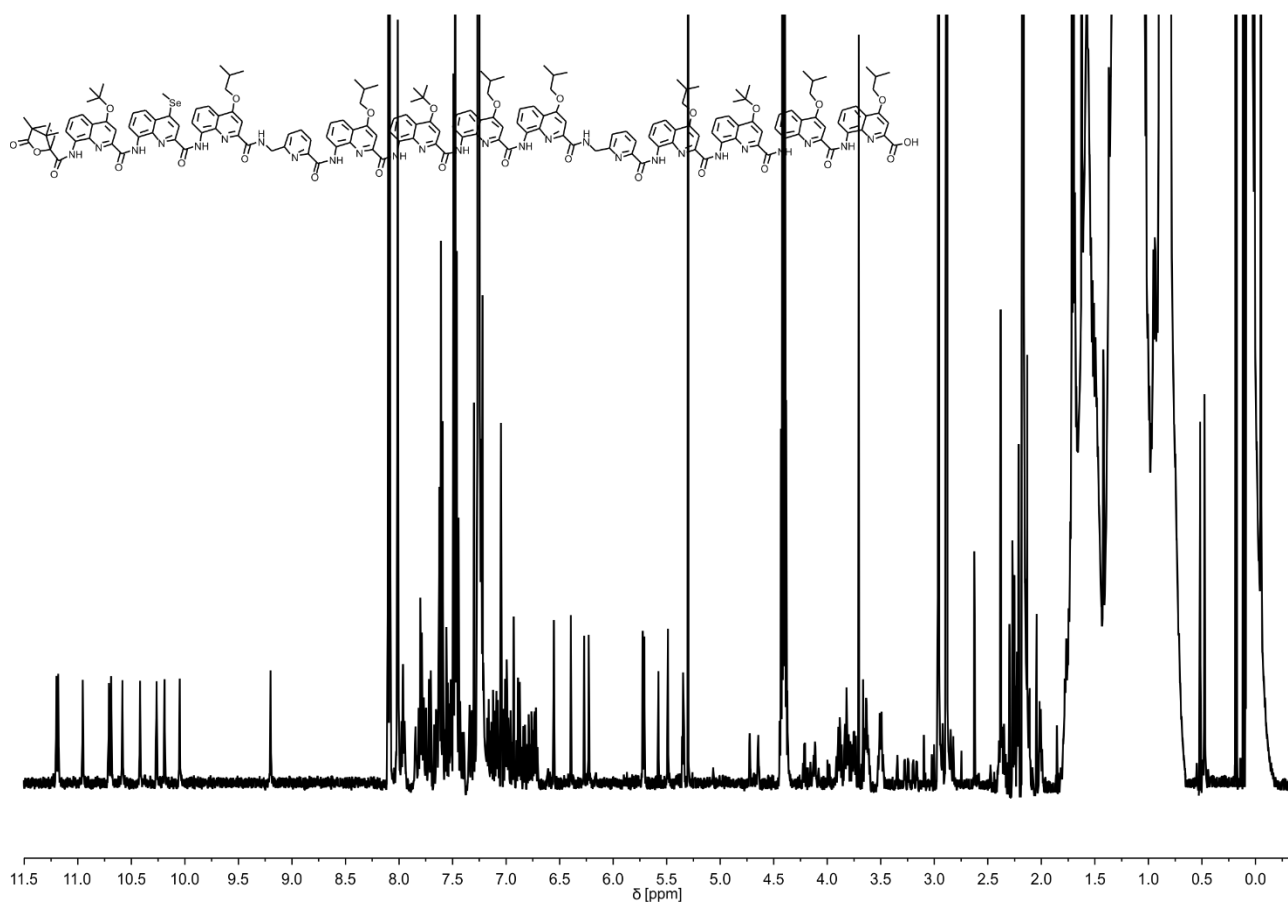


**Figure S48.** <sup>1</sup>H NMR spectrum (500 MHz, CDCl<sub>3</sub>) of **12**.

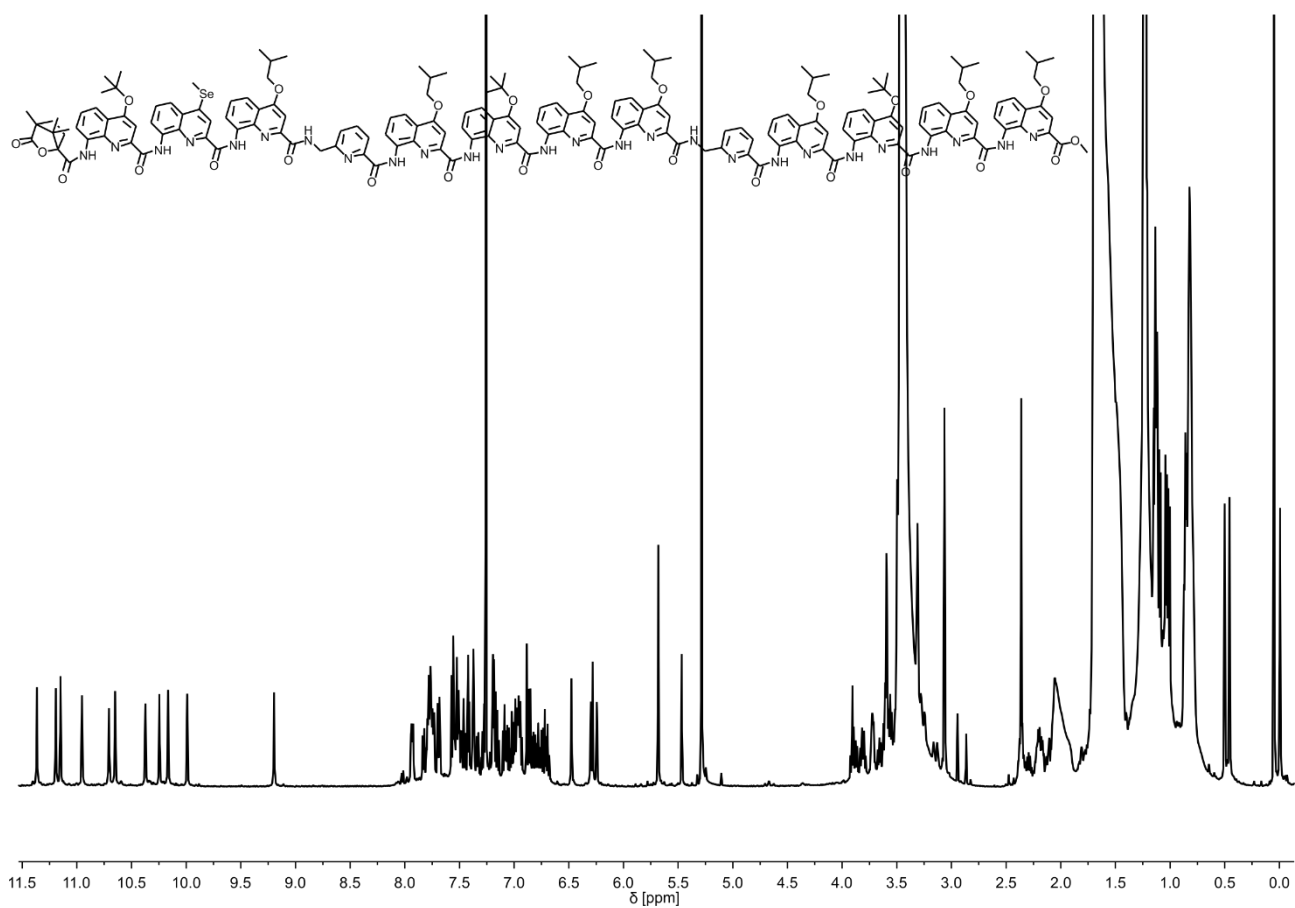


**Figure S49.** <sup>1</sup>H NMR spectrum (500 MHz, CDCl<sub>3</sub>) of **13**.

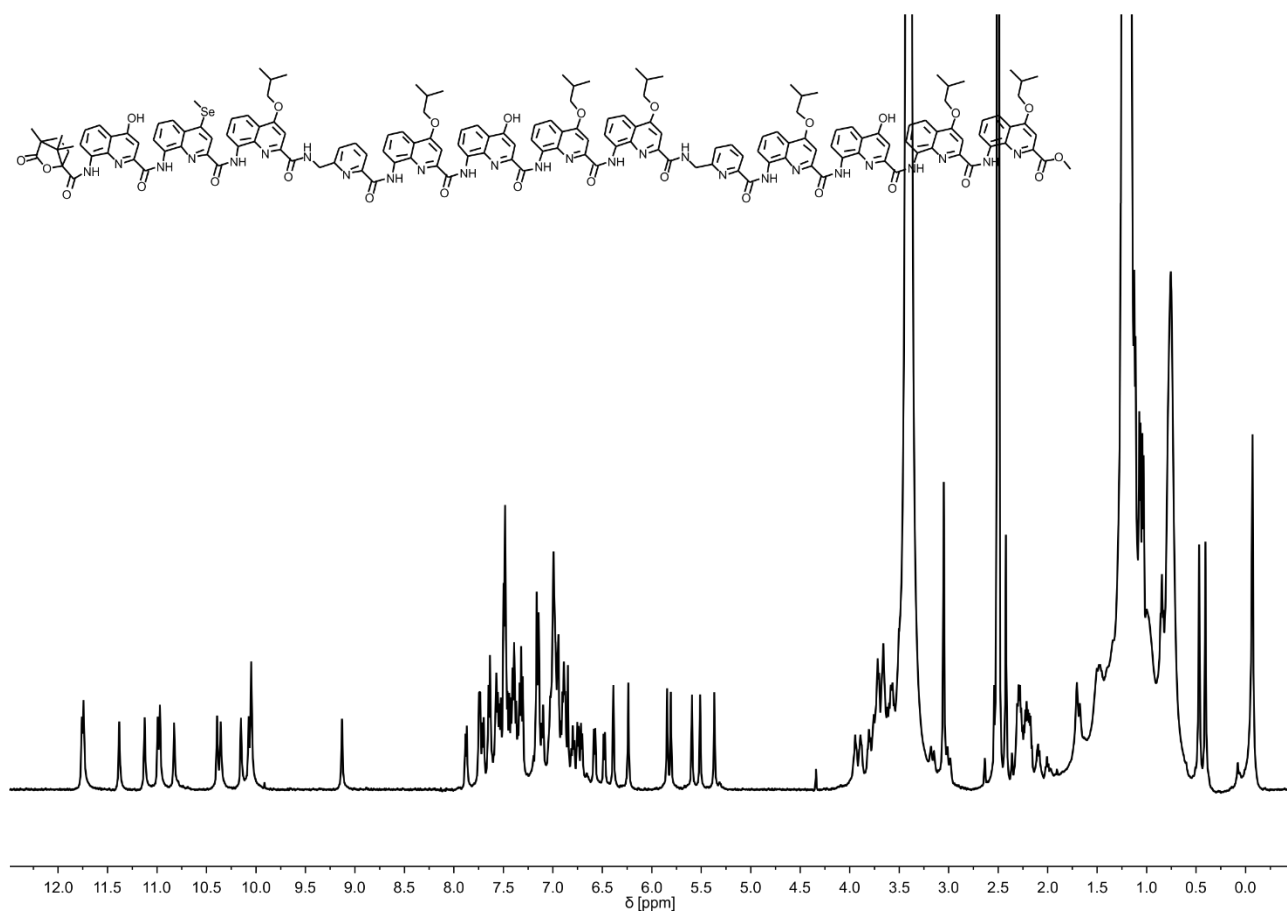


**Figure S50.** <sup>1</sup>H NMR spectrum (500 MHz, DMSO-*d*<sub>6</sub>) of **5**.

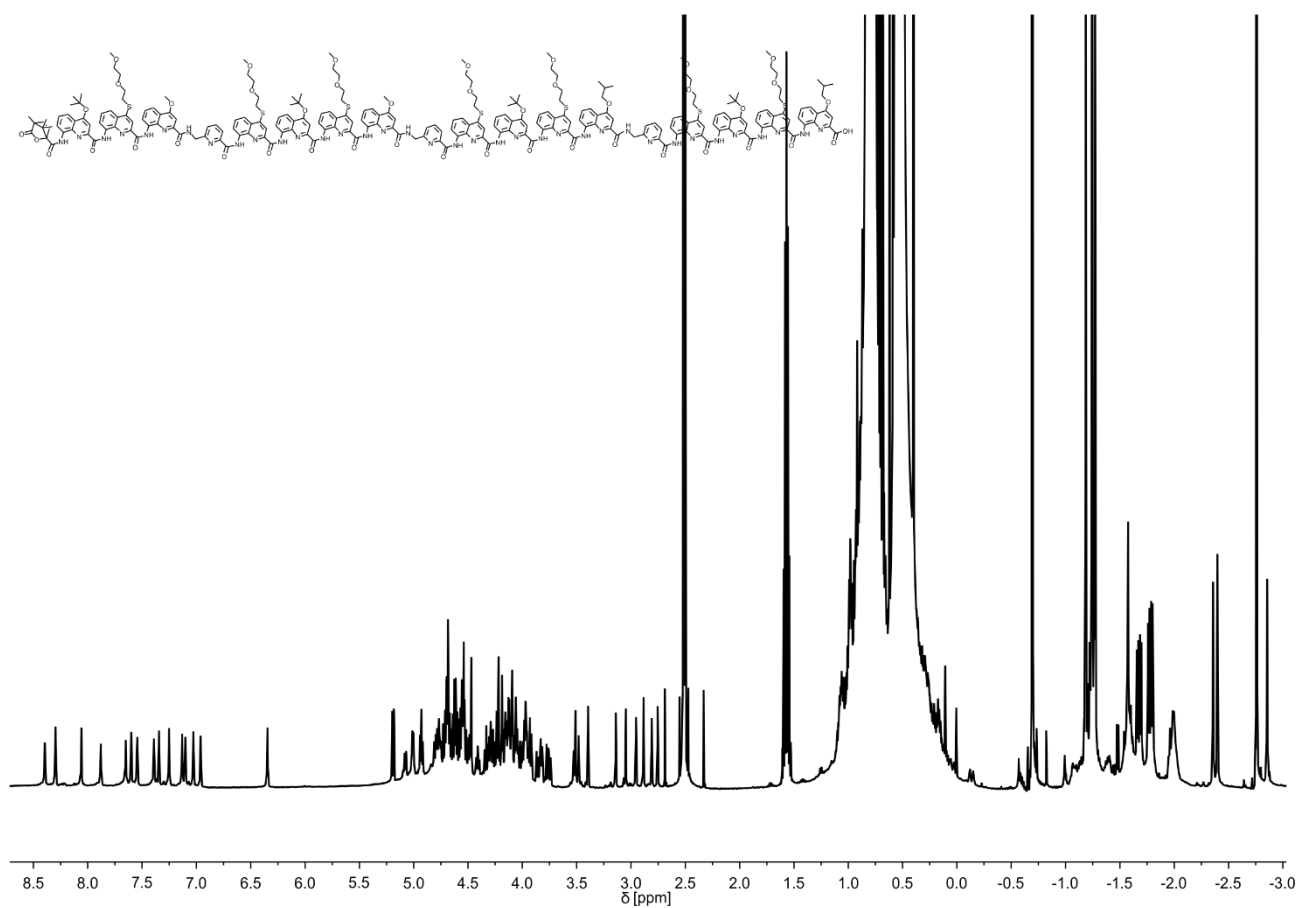


**Figure S51.** <sup>1</sup>H NMR spectrum (500 MHz, CD<sub>2</sub>Cl<sub>2</sub>) of **14**.

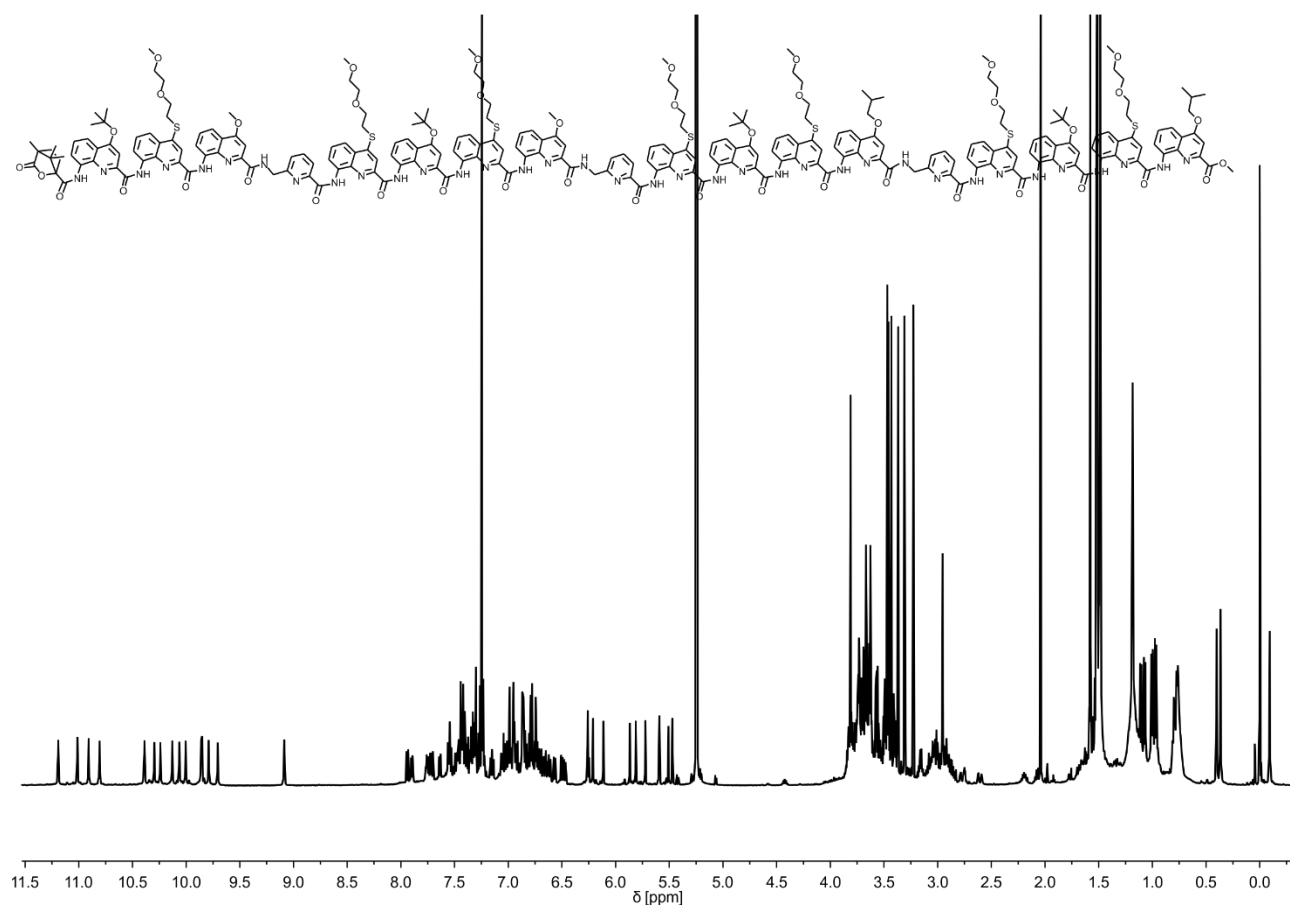


**Figure S52.**  $^1\text{H}$  NMR spectrum (500 MHz,  $\text{CD}_2\text{Cl}_2$ ) of **15**.

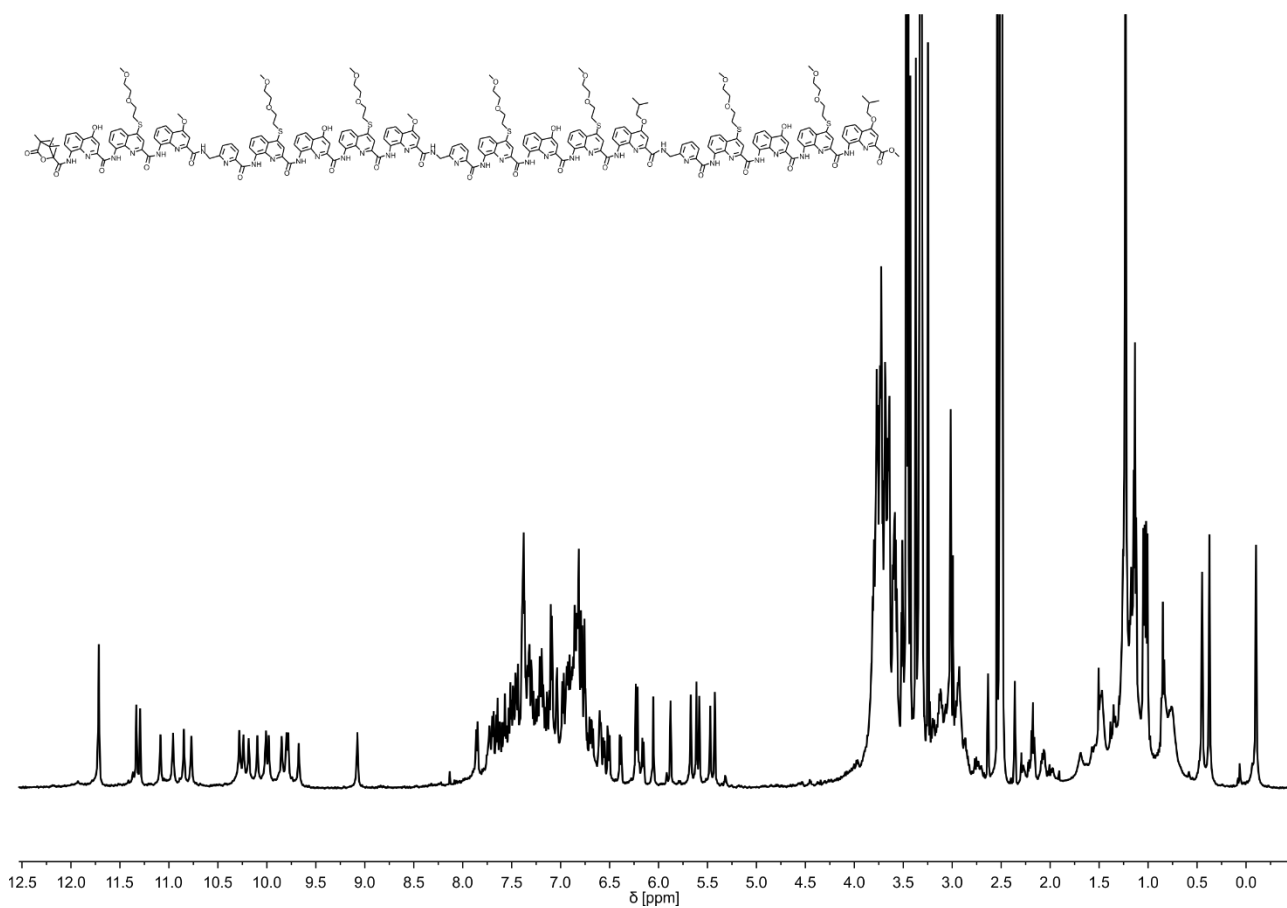


**Figure S53.** <sup>1</sup>H NMR spectrum (500 MHz, DMSO-*d*<sub>6</sub>) of **6**.

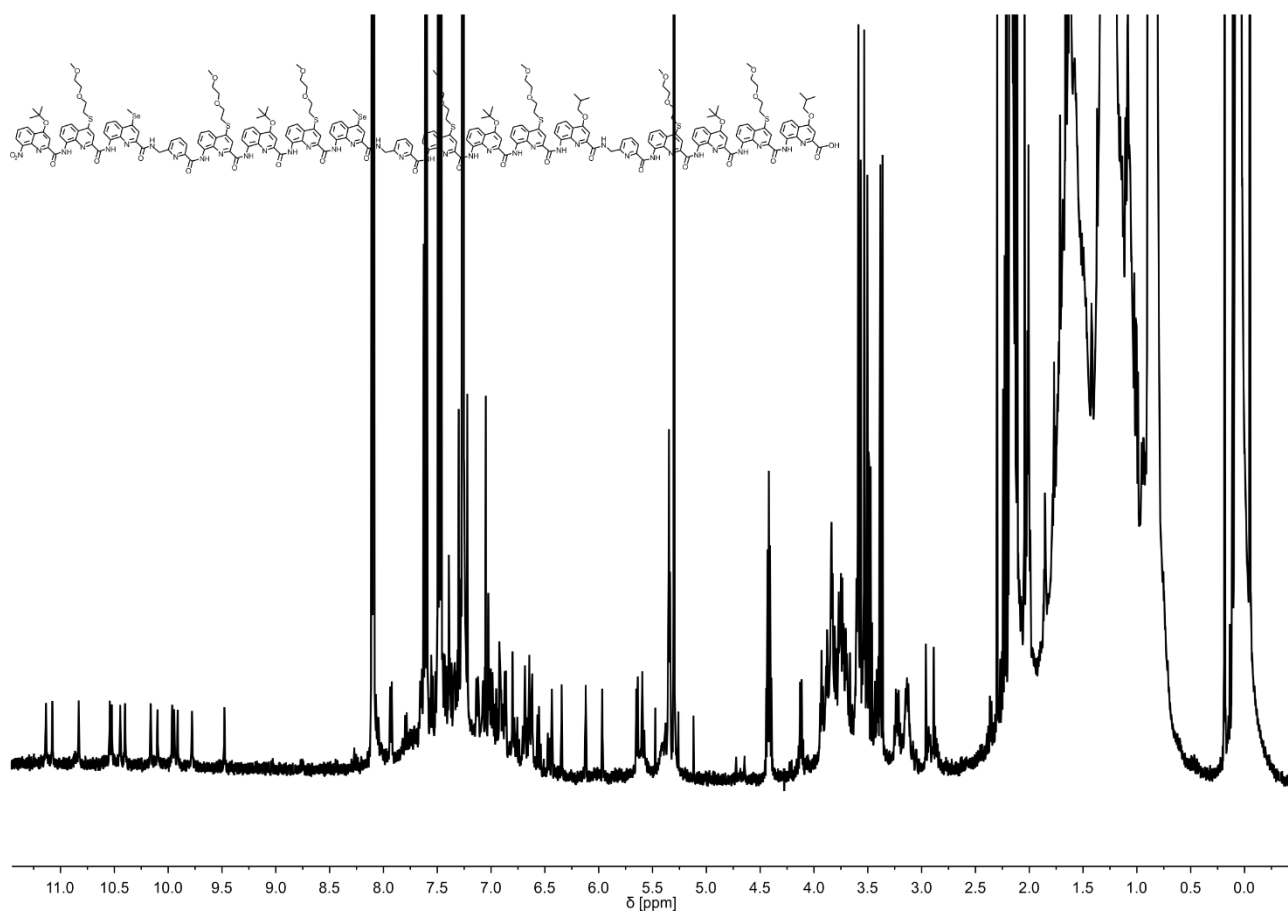


**Figure S54.** <sup>1</sup>H NMR spectrum (500 MHz, CDCl<sub>3</sub>) of **16**.

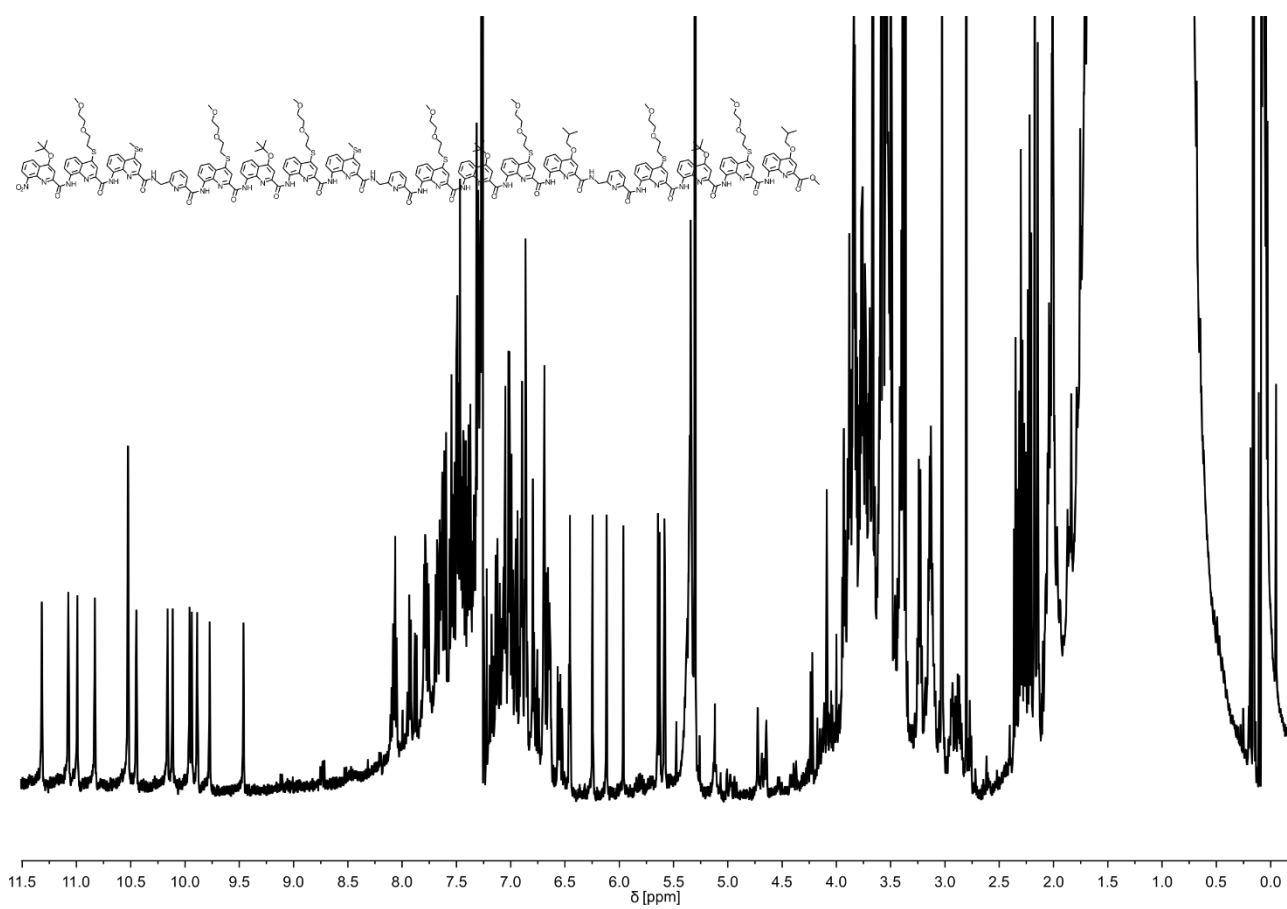


**Figure S55.** <sup>1</sup>H NMR spectrum (500 MHz, CDCl<sub>3</sub>) of **17**.



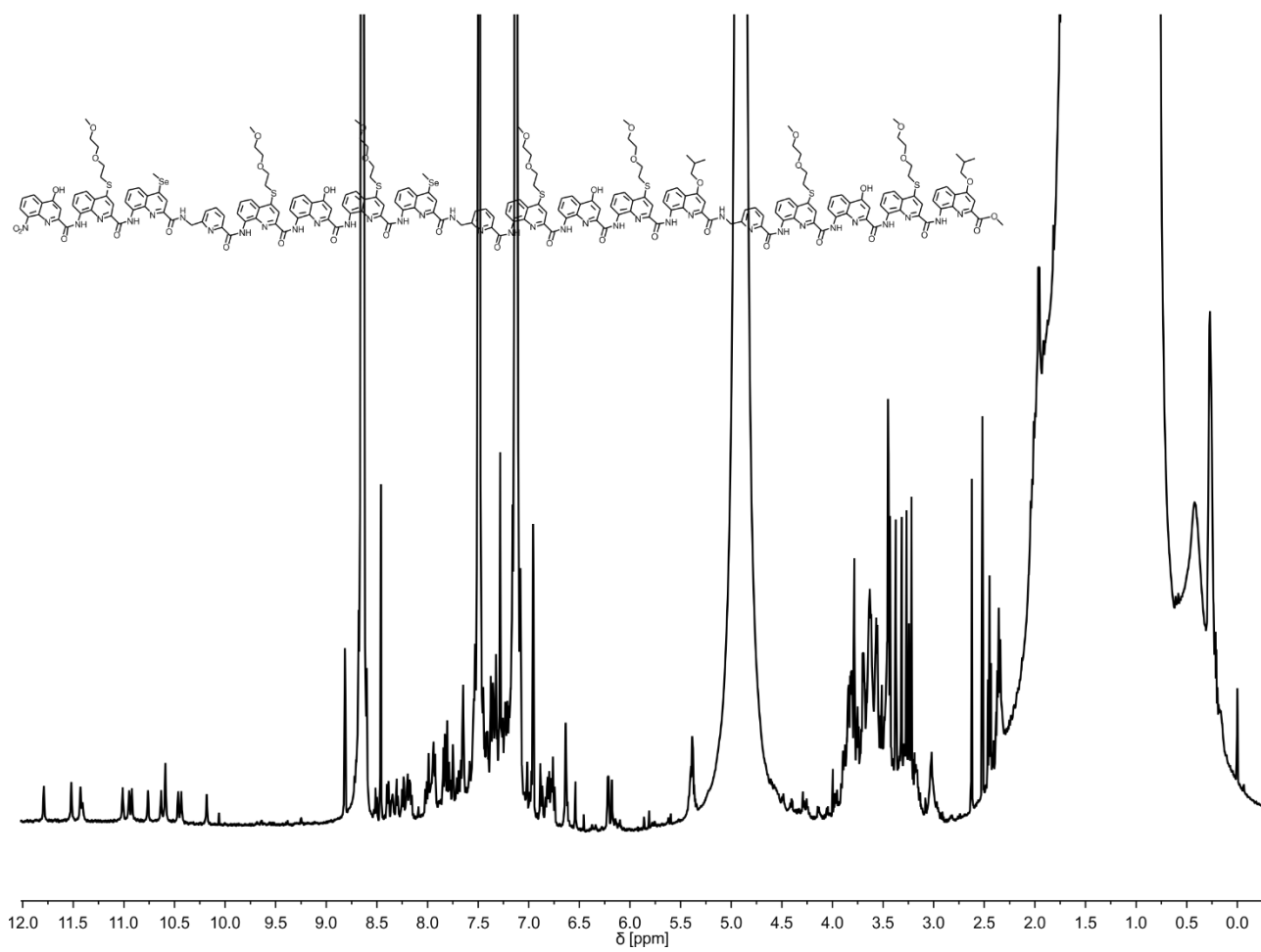


**Figure S56.** <sup>1</sup>H NMR spectrum (500 MHz, pyridine-*d*<sub>5</sub>) of 7.

## 5 Effects on self-organization when introducing a flexible linker to a helix-assembly

In the field of *abiotic* foldamers accurate computational modelling has led to the successful synthesis of a tertiary structure. Such a tertiary structure is based on a helix-turn-helix motif stabilized by intermolecular hydrogen bonds and a rigid linker in which helices are parallel to one another. In order to access more diverse and complex structures in the future, the formation of non-parallel motifs such as a tilted dimer, should become more predictable. In this work, flexible turn units of varying lengths and thus flexibility were introduced between two helices, which had previously formed tilted dimers when aggregating freely. Even though the crystal structure of the tilted dimer showed a homochiral aggregate computational modelling predicted that the formation of PM tilted dimers would be possible as well. Furthermore, a tilted dimer can either be tilted clockwise or counterclockwise (Figure 5.1a). In an unimolecular aggregate the formation of four different shapes is therefore possible. To avoid PM aggregates and thusly reduce the number of possible variations to two, handedness control was to be introduced via a chiral B unit (see chapter 2.2, Figure 2.6). Before doing so, their capacity to introduce full handedness control in organic solvents such as chloroform and dichloromethane needed to be validated.

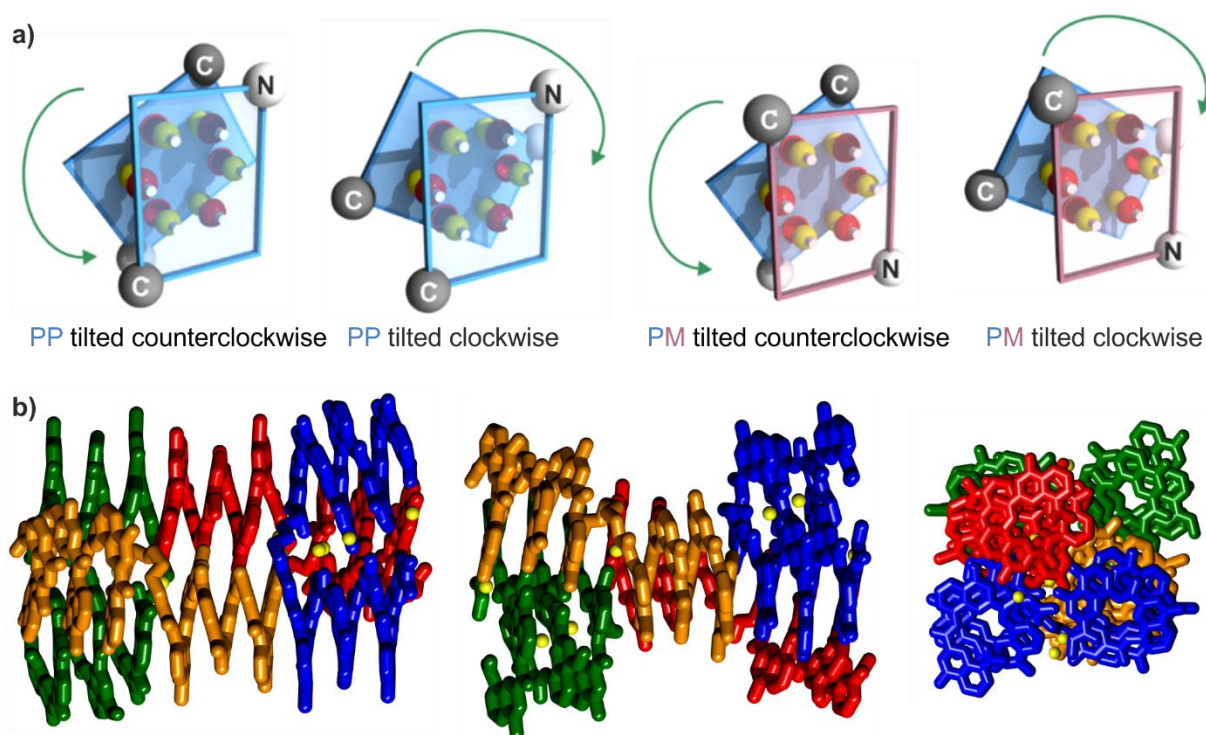


**Figure 5.1.** Schematic representation of PP and PM counter- and clockwise tilted dimers (a). Yellow and red balls represent hydrogen-bond donors and acceptors, respectively. Blue and red planes represent P and M helices, respectively. Black and white balls represent the C- and N-terminus, respectively. Different views of an *abiotic*, tetrameric, eight-helix bundle (b). The four molecules are shown in blue, red, gold and green. Water molecules are shown as yellow balls.

The results of our findings are summarized in a manuscript that has been submitted to *Chemical Science*. Here, we demonstrated that the chiral B unit biased helix handedness quantitatively in chloroform and dichloromethane. Furthermore, it quantitatively overcame an opposing effect of the camphanyl group and thus ensured reliable helix handedness control. Thus sequences in which handedness in both helices is induced via chiral B units were synthesized. To these, a di-, tri- or tetraethylene glycol linker was introduced, respectively. Additionally, sequences in which handedness was controlled in only one helix via an (*1S*)-camphanyl group were synthesized as well. NMR and CD spectroscopic studies showed that, in some cases, well-defined, stable, discrete abiotic helix-turn-helix tertiary folds form in organic solvents. Molecular modelling suggested that these correspond to structures in which the two helix axes are angled towards each other. In an attempt to receive supporting crystal structures, achiral sequences were synthesized. In one case this has led to the formation of a complex and large aggregate stabilized via inter- and intra-molecular hydrogen bonds. Here, four secondary structures, meaning eight helices, combined. The complex featured three subdomains: two hydrogen-bonded three-helix bundles and one two-helix-bundle. In this structure both right and left handedness was present. Furthermore, several helix-to-helix hydrogen bonds were mediated by bridging water molecules (Figure 5.1b). The discovery of this structure provides possible insights into future designs and synthesis of abiotic protein-like architectures.

**Contributions:** The project was planned in collaboration with V. Maurizot and I. Huc. Synthetic monomer precursors have been provided by D. Gill. Monomer synthesis has been performed by me, S. Wang, L. Wang, D. Gill and D. Bindl. Foldamer synthesis were carried out by me. Solution state studies were performed by me and L. Allmendinger. NMR measurements have been conducted by L. Allmendinger, C. Glas, and C. Ober. Modelling studies were performed by me and V-Maurizot. Crystals have been obtained by V. Maurizot. Crystallographic data collection data collection was performed by B. Kauffmann at the Biophysical and Structural Chemistry platform (BPCS) at IECB, CNRS UMS3033, Inserm US001, and Bordeaux University. Crystallographic structure refinement was performed by B. Wicher. Me, V. Maurizot, I. Huc, L. Allmendinger and B. Wicher contributed to experiment design and interpretation. The research was supervised by I. Huc. The manuscript was written by me and I. Huc. Me, B. Wicher, L. Allmendinger, S. Wang and I. Huc proofread and improved the manuscript.

## 5.1 Publication (accepted)

### An abiotic, tetrameric, eight-helix bundle

Authors: Friedericke S. Menke,<sup>a</sup> Barbara Wicher,<sup>b</sup> Lars Allmendinger,<sup>a</sup> Victor Maurizot<sup>c</sup> and Ivan Huc<sup>\*a</sup>

Accepted: *Chemical Science*, 2023 (accepted, DOI: [10.1039/D3SC00267E](https://doi.org/10.1039/D3SC00267E))

**Abstract:** Four helically folded aromatic oligoamide sequences containing either a chiral monomer based on 2-(2-aminophenoxy)-propionic acid, an N-terminal (1*H*)-camphanyl group, or both, were synthesized. Spectroscopic solution investigations using <sup>1</sup>H NMR and circular dichroism (CD) demonstrated that the 2-(2-aminophenoxy)-propionic acid unit biases helix handedness quantitatively in chloroform and dichloromethane. It even quantitatively overcomes an opposing effect of the camphanyl group and thus ensures reliable helix handedness control. A series of nine sequences comprised of two helically folded aromatic oligoamide segments separated by a flexible linker based on a di-, tri- or tetraethylene glycol unit were then synthesized. In these sequences, helix handedness was controlled by means of an N-terminal (1*S*)-camphanyl group or a 2-(2-aminophenoxy)-propionic acid units in either both helical segments, or only in the N-terminal segment, or in none of the segments. The helical segments all displayed hydroxy and carbonyl groups at their surface as hydrogen bond donors and acceptors so as to promote helix-to-helix hydrogen bonding. NMR and CD spectroscopic studies showed that, in some cases, well-defined, stable, discrete abiotic helix-turn-helix tertiary folds form in organic solvents. Molecular modelling suggests that these correspond to structures in which the two helix axes are at an angle. In one case, the absence of handedness control resulted in a complex and large aggregate. A solid state structure obtained by single crystal X-ray diffraction analysis revealed a tetrameric assembly composed of eight helices with both right and left handedness arranged in three subdomains consisting of two hydrogen-bonded three-helix bundles and one two-helix-bundle. Several helix-to-helix hydrogen bonds were mediated by bridging water molecules. This structure constitutes an important milestone in the construction of abiotic protein-like architectures.

### Introduction

We have engaged in a program aiming at eliciting protein-like folding in organic solvents using abiotic structures, that is, at the exclusion of  $\alpha$ -amino acids or analogous building blocks. This program is motivated by the prediction that sophisticated functions may emerge in abiotic tertiary or quaternary structures, just like this level of complexity is required for most protein functions. It is also expected that protein-like behaviour in aprotic organic solvents may differ from that of proteins in water because solvation and desolvation phenomena would be completely different. The field is essentially uncharted and caught our curiosity.

Foldamer research has produced numerous synthetic backbones that have an ability to fold into helices.<sup>1-7</sup> Furthermore, helix-helix interactions are among the best-understood protein structural patterns. Coiled-coiled

peptide helix bundles are amenable to design,<sup>8-17</sup> and have been extended to peptidomimetic structures that do not exist in nature, including  $3_{10}$   $\alpha$ -peptide helices,<sup>18</sup>  $\alpha/\beta$ -peptide helices,<sup>19</sup>  $\beta$ -peptide helices,<sup>20,21</sup> and oligourea helices.<sup>22, 23</sup> It was thus a logical step to consider abiotic tertiary folds using helices as a starting point. Oligoamides of 8-amino-2-quinoline carboxylic acid (Q in Figure 1a) constitute an attractive class of abiotic foldamers that adopt stable 2.5 helical conformations.<sup>24-26</sup> Structural stability is illustrated, for example, by the persistence of an octaamide helix at 120 °C in DMSO.<sup>24</sup> Extreme stability is not necessarily desirable when designing a protein-like object. In the case of  $Q_n$  oligomers, it can be mitigated by replacing some Q units with more flexible P units that possess additional rotatable bonds and have a smaller surface for aromatic stacking while coding for the same helix curvature (Figure 1a).<sup>27-29</sup>

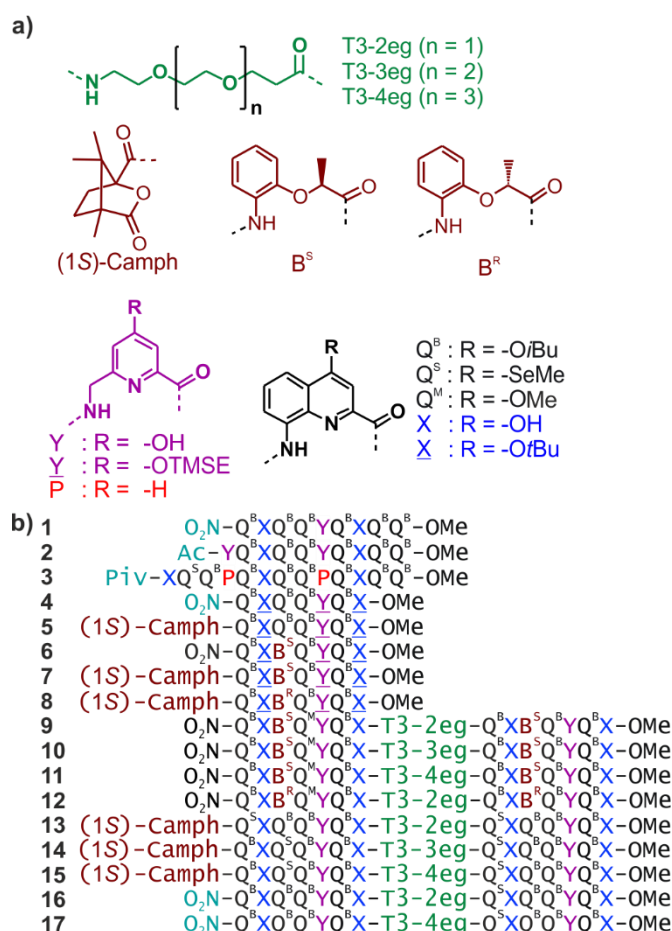


**Figure 1.** a) Structures of di-, tri- and tetraethyleneglycol T3 spacers, chiral (1S)-camph, B<sup>S</sup> and B<sup>R</sup> units, and Q, X, P and Y amino acid monomers. Q<sup>B</sup> carries organic solubilizing side chains. Q<sup>S</sup> was introduced in some sequences to assist crystallographic structure elucidation using the anomalous scattering of Se, though it turned out to be unneeded. Q<sup>M</sup> is isosteric to Q<sup>S</sup>. X and Y are the protected precursors of hydrogen-bonding monomers X and Y, respectively. TMSE = 2-trimethylsilylethyl. b) Oligoamide foldamer sequences. Piv = pivaloyl. In sequences ending with an 8-nitro group, this group replaces the terminal amine.

Thus, tertiary fold design was initially considered using P- and Q-containing oligomers as predictable construction modules. Preliminary work essentially involved connecting helices with short linkers.<sup>30-32</sup> This first generation did not qualify as true tertiary folds in that no defined helix-helix interactions occurred. Next,

we considered functionalizing Q and P monomers with 4-hydroxy substituents as hydrogen bond donors and produced analogous monomers X and Y (Figure 1).

Acidic phenols are excellent hydrogen bond donors<sup>33</sup> and the amide carbonyl groups diverge from  $Q_n$  helices, providing good hydrogen bond acceptors. We thus planned to mediate helix-to-helix hydrogen bonding in organic solvents using these donors and acceptors. During synthesis, hydroxy groups are protected. Protected monomers are referred to as  $\underline{X}$  and  $\underline{Y}$ .

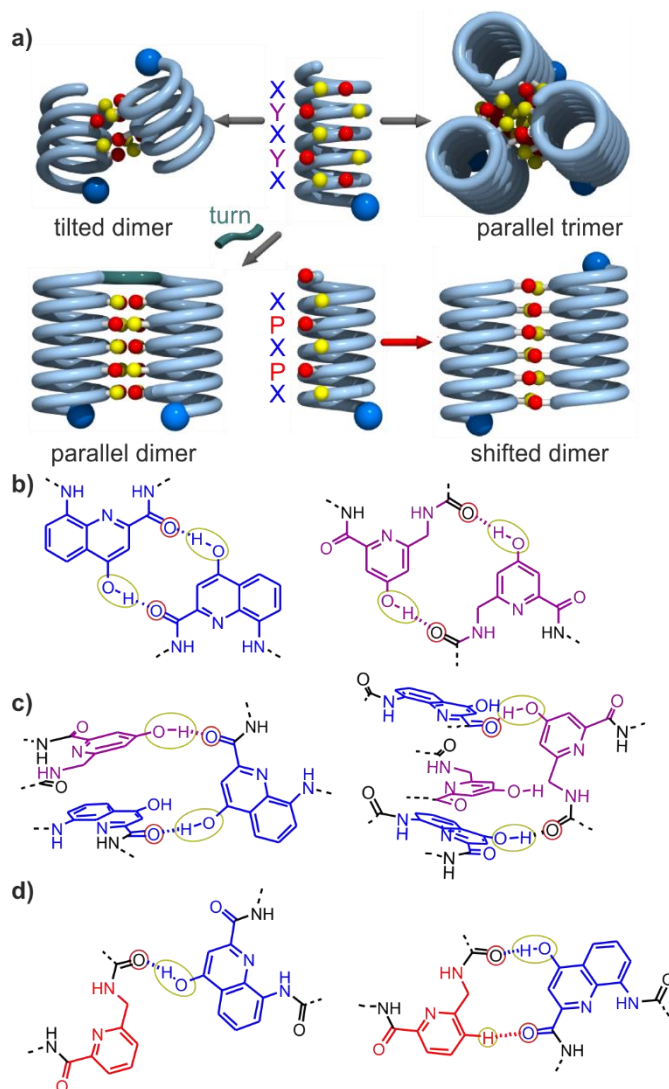


**Figure 2.** a) Cartoons representing identified assembly modes of aromatic helices displaying hydrogen bond acceptors and donors shown as red and yellow balls, respectively. The bottom left structure exists only when the helices are covalently linked. b) Hydrogen-bonding patterns involving X and Y units as observed in helix-turn-helix tertiary structures in which sequences **1** or **2** are connected by a rigid linker.<sup>34-36</sup> c) Hydrogen-bonding patterns involving X and Y units as observed in a tilted dimer of **1**.<sup>34</sup> d) Hydrogen-bonding patterns involving X and P units as observed in a *PM* (left) and in *PP* or *MM* (right) shifted dimers of **3**.<sup>38</sup> In a)-d), yellow and red circles around the hydrogen bond donors and acceptors correspond to the yellow cups and red knobs in a) and Figure 3, and to the yellow and red balls in Figure 7.

Progress towards abiotic folds has been paved by a mix of successful designs and serendipitous discoveries. For example, we rationally designed the first abiotic helix-turn-helix motifs based on careful modelling of the structures.<sup>34</sup> After choosing relatively rigid turn units of appropriate length as linkers, hydroxy groups were introduced at precise locations so as to mediate helix-to-helix hydrogen bonding between X and between Y units (Figures 2a,b, S1). Depending on the type of turn unit, a parallel† head-to-head homochiral arrangement (*i.e.* with both helices having the same handedness) or a parallel† head-to-tail heterochiral arrangement (*i.e.* with one *P* helix and one *M* helix) could be rationally produced (Figures 3a,b, S1).<sup>34-37</sup> In contrast, the self-assembly of the same or similar sequences not linked by a turn unit was full of surprises. Thus, sequence **2** (Figure 1) forms not a dimeric but a trimeric parallel† head-to-head homochiral bundle involving similar hydrogen bonding to that of the helix-turn-helix structures, as well as other species (Figure 2a).<sup>34</sup> Sequence **1** forms (again among other species) a homochiral tilted dimer where the two helix axes are not parallel but instead tilted at an angle of 120° (Figures 2a,c, 3, S1).<sup>34</sup> This is made possible by the fact that a stack of two X units and one Y at the surface of a helix create an array of three hydrogen bond donors and three acceptors arranged in a sort of hexagon: donors and acceptors may meet in three different configurations by rotating the array by  $\pm 120^\circ$ , potentially generating the parallel dimer, one clockwise and one counterclockwise tilted dimer (Figure 3, S1). Furthermore, removing some of the hydroxy groups through Y->P mutations, as in **3**, resulted in the formation of unexpected, shifted parallel† dimers (Figure 2a).<sup>38</sup> The term shifted was used because, in these structures, X units did not face X units of the other helices but were instead shifted by one helix turn and hydrogen-bonded to a P unit. Both *PM* heterochiral or *PP/MM* homochiral shifted dimers have been observed. These aggregates are similar and are stabilized by one type of helix-to-helix hydrogen bond (Figures 2d, S1). Eventually, we found that the arrangement of the rationally designed helix-turn-helix structures never forms in the absence of a rigid turn unit, indicating that the rigid turn mediates some sort of strain while simultaneously preventing other helix-helix interaction patterns.<sup>37</sup>

We now report on the folding and assembly of helix-turn-helix structures in which the turn unit possesses considerable flexibility. The initial intention was to identify links that would stabilize the tilted dimers in an intramolecular tertiary fold. While this objective was met with good confidence (albeit without crystallographic evidence), we also discovered one case where four helix-linker-helix modules assemble into a 12.9 kDa quaternary-like object composed of eight helices. The resulting eight-helix bundle involves some already identified helix-helix arrays of hydrogen bonds, such as a sort of parallel trimer and a shifted dimer. It also revealed new patterns involving multiple water molecule bridges. Altogether, these results represent an important milestone on the way to increasingly large and complex abiotic tertiary and quaternary folds.

## Results and discussion

### Absolute helix handedness control

New heptaamide **4** was derived from sequence **1** and used as the elementary helical building block in this study. It contains protected X and Y units at positions suitable to form, after deprotection, the hydrogen-bonded

parallel or tilted dimers mentioned in the introduction. With respect to **1**, sequence **4** has been shortened by two Q<sup>B</sup> units at the C-terminus and should thus span a little less than three helix turns. It does not contain any stereogenic center and must, therefore, fold as a racemic mixture of right-handed (*P*) or left-handed (*M*) helices. In order to explore the possible occurrence of well-defined intramolecular helix-to-helix hydrogen bonding patterns (as opposed to dimeric assemblies), we considered sequences that would comprise two segments analogous to the sequence of **4** linked by a flexible T3 linker containing two, three or four ethylene glycol units (see next section for design considerations). In such sequences, each helical segment can, in principle, be *P* or *M*. Therefore, *PP/MM* and *PM/MP* diastereomeric conformers may coexist.<sup>31, 39</sup> After deprotection of X and Y, we anticipated that different types of helix-to-helix hydrogen bonding may occur within each of the *PP/MM* and *PM/MP* conformers (not taking into account possible intermolecular hydrogen bonding) and that the overall behaviour may be difficult to analyse.

To reduce, at least at the start, the number of conformational degrees of freedom in these molecules, we decided to introduce an absolute handedness control of the helical segments. We have shown before that a (1*S*)-camphanyl group (Figure 1a) at the N-terminus biases helix handedness quantitatively (as far as NMR can detect) in favour of *P* helicity.<sup>40</sup> This bias is effective in any solvent that we tested from water to chlorinated solvents. We have also shown that a B<sup>S</sup> unit inserted within a Q<sub>n</sub> oligomer biases handedness quantitatively (as far as NMR can detect) in favour of *P* helicity.<sup>41</sup> Conversely, B<sup>R</sup> favours *M* helicity. However, the effect of B<sup>R</sup> or B<sup>S</sup> units had only been demonstrated in water, methanol and DMSO using Q<sub>n</sub> oligomers bearing polar side chains. It was unknown whether handedness bias would also be effective in chloroform. We thus prepared sequences **5-8** that contain a (1*S*)-camphanyl group, a chiral B unit, or both, while all having X and Y units in the same positions as **1** (see ESI for details). Note that the more flexible B unit was introduced between two Q units and not next to the also flexible Y because consecutive flexible units may result in a loss of helix stability.<sup>35</sup>

The <sup>1</sup>H NMR spectra of all these compounds in CDCl<sub>3</sub> and CD<sub>2</sub>Cl<sub>2</sub> show one single set of signals (Figures S2, S3). For such long sequences, helix handedness reversal is slow on the NMR timescale, as shown, for example, by anisochronous CH<sub>2</sub> protons of *i*Bu side chains.<sup>29</sup> The *P* and *M* diastereomeric helices of chiral compounds **5-8** would thus appear as distinct sets of signals, should they both exist in significant amounts. The presence of a single set of signals is, therefore, indicative of the prevalence of a single species. This was expected for **5**, with its terminal camphanyl group. The behaviour of **6** shows that a single chiral B<sup>S</sup> unit is also effective in biasing handedness quantitatively in chlorinated solvents. In **7**, the (1*S*)-camphanyl and B<sup>S</sup> groups favour the same handedness. That one species prevails is, therefore, unsurprising. In contrast, the prevalence of a single diastereomeric helix in **8**, in which the (1*S*)-camphanyl and B<sup>R</sup> groups compete to favour one handedness or the other, indicates that the effect of one of the two groups completely overtakes the effect of the other. CD spectra of **5-8** show bands of equal intensities consistent with quantitative handedness bias (Figure S4).<sup>‡</sup> The sign of the bands allows for the absolute assignment of helix handedness,<sup>40</sup> and indicates that **5-7** are *P*-helical



whereas **8** is *M*-helical. The latter result demonstrates that, in **8**, the effect of the B<sup>R</sup> unit overtakes the effect of the (1*S*)-camphanyl group, thus highlighting a particularly strong handedness bias effect.

## Linker design

The initial purpose of this work was to explore which linker could eventually promote an intramolecular helix-turn-helix structure with the two helices hydrogen-bonded in a tilted arrangement. The art of installing a linker between two entities without perturbing the interactions in which each of them is involved is a delicate one, whether it is between helices<sup>42-45</sup> or between smaller molecules bound to proteins, as in PROTACs.<sup>46</sup> Actually, when designing the first abiotic helix-turn-helix structures,<sup>34-37</sup> we did not adjust the linker according to the interactions but instead implemented interactions, that is, introduced X and Y units, after having chosen the linker. Within tilted dimers, the helix N- and C-termini are not located at positions obvious to connect by a linker (Figure 3). We thus decided to test a set of rather flexible loops possessing two, three or four ethylene glycol units, namely T3-2eg, T3-3eg and T3-4eg (Figure 1), that have the advantage of being commercially available as Fmoc-protected amino acids ready for solid phase synthesis. We first systematically evaluated molecular models of sequences composed of two heptameric segments analogous to that of **4** (in its deprotected form with free OH groups). For each linker, we considered parallel,<sup>†</sup> clockwise tilted, counterclockwise tilted, and shifted dimers, both when the helices have the same handedness (*e.g.* *PP*) or when they have opposite handedness. As explained below, few of these configurations were predicted to be realistic. In a first step, an energy-minimized model of two hydrogen-bonded helices in the desired configuration was produced using Maestro (see ESI for details).<sup>47</sup> Starting from one helix, the linker was then built in a plausible conformation, a step which ended with the creation of a single bond between the end of the linker and the other helix. In many cases, an energy minimization at this stage ended in a disruption of a helix structure or of the array of hydrogen bonds. In the latter case, energy minimization was repeated upon imposing hydrogen bonding through distance constraints. Typically, the consequence was a perturbation of the helical structure indicating the inadequacy of the linker for that particular arrangement. Upon repeating energy minimization after having removed the constraints, the perturbation persisted. Only in a few cases, the array of hydrogen bond appeared to be compatible with unaltered helix structures and a reasonable turn conformation.

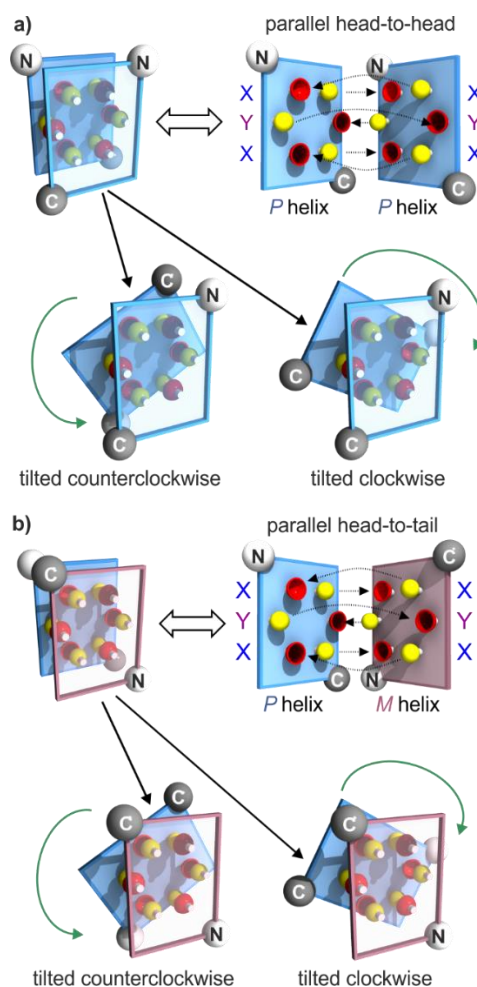


**Figure 3.** Schematic representations of helix-helix hydrogen bonding when three hydrogen bond donors (yellow knobs) and three acceptors (red cups) are arranged in a sort of hexagon at the surface of a helix, as in **1**.<sup>34</sup> The hexagonal arrangement stems from two X units flanking a Y unit at the surface of a helix, the hydrogen bond donor and acceptor being closer in X than in Y units (Figure 2b). The helix face is represented as a plane, with the N- and C-termini shown as white and grey balls, respectively. Planes with a blue and red frame correspond to *P* and *M* helices, respectively. a) “Open-book view” and stacked view of a hydrogen-bonded parallel† head-to-head arrangement of two *P* helices and of the related clockwise and counterclockwise dimers. Hydrogen bonds are shown as dashed lines in the open-book view. In the stacked view, the top plane is transparent so that one can see the six hydrogen bonds (knobs into cups) and the plane behind. The parallel head-to-head arrangement has been observed only when the two helices are linked by a rigid turn unit (Figures 2a, S1).<sup>34,35</sup> The *PP* clockwise tilted dimer of **1** has been characterized in the solid state.<sup>34</sup> b) Similar parallel arrangement, but this time head-to-tail, between a *P* and an *M* helix, as well as the clockwise and counterclockwise tilted dimers. The parallel arrangement has also been seen only when the helices are connected by a rigid linker.<sup>36</sup> There is no evidence for the existence of *PM* tilted dimers, but models show plausible structures (see ESI).

The results can be summarized as follows: (i) all shifted arrangements can be ruled out because they leave four out of six hydroxyl groups not involved in hydrogen bonds (Figures S5, S6); (ii) parallel *PP* arrangements were not considered since they must be head-to-head<sup>34,36</sup> putting the C-terminus of one helix too far from the N-terminus of the other helix (Figure 3a); (iii) parallel *PM* arrangements are head-to-tail<sup>36</sup> and in principle compatible with the T3 linker lengths with no or minute helix distortions (Figures 3b, S7). However, the fact that they do not occur in the absence of a linker makes them unlikely to happen with a flexible linker that does

not impose a particular geometry.<sup>34, 38</sup> Parallel *PM* arrangements were thus also dismissed; (*iv*) all linkers are too short for *PM* clockwise tilted arrangements (Figure S8); (*iv*) the two shorter linkers but not the longer T3-4eg perturb the arrangement of *PP* counterclockwise tilted arrangements (Figure S9); (*v*) all linkers seem compatible with *PM* counterclockwise tilted arrangements albeit in extended conformations unusual for oligoethylene glycols which normally prefer gauche conformations (Figure S10);<sup>48</sup> (*vi*) all linkers seem compatible with the *PP* clockwise tilted arrangements (Figure S11). Therefore, at best, two hydrogen-bonded helix-helix arrangements are compatible with the two shorter linkers (*PP* clockwise and *PM* counterclockwise tilted arrangements), and three with the longest linker (*PP* counterclockwise tilted arrangement on top of the former two). As representative example, a model of the *PP* clockwise tilted arrangement with a T3-2eg linker is shown in Figure 4.

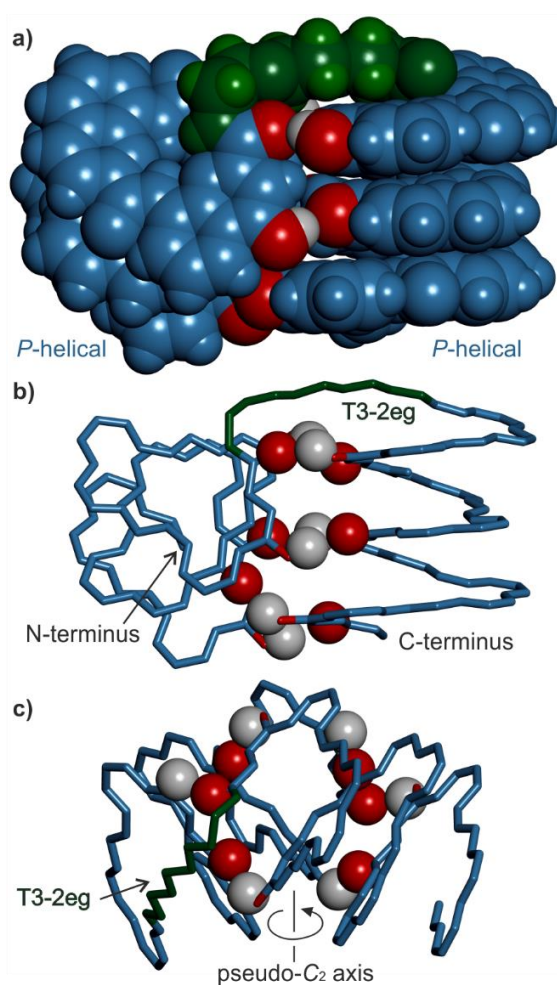


**Figure 4.** Energy minimized model of a *PP* clockwise tilted helix-T3-2eg-helix arrangement. The sequence is analogous to that of **16** using Q units without side chains. a) Space-filling representation with T3-2eg shown in green and the helices shown in blue. Amide carbonyl oxygen and hydroxy oxygen atoms involved in hydrogen bonding are shown in red. Hydroxy protons are shown in white. b) Same view as in a) showing only the outer rim of the backbone in tube representation. Hydrogen bond acceptors (carbonyl oxygen atoms) and donors (hydroxy protons) are shown as balls. c) Same representation as in b) but a different view showing the pseudo-symmetry of the structure (at the exclusion of the T3-2eg linker) and approximately hexagonal arrangement of the hydrogen bond donors and acceptors.

## Sequence design, synthesis and solution behaviour

Since the homochiral (*PP* or *MM*) tilted clockwise arrangements seem the most likely candidates, we first considered sequences **9-11**, which only differ through their linker length, and in which all helix segments contain a B<sup>S</sup> unit that should promote *P* helix handedness. Compounds **9-11** were assembled first with solid phase using Q<sup>B</sup>, Q<sup>M</sup>, B<sup>S</sup>, Y, X and T3 monomers having a main chain Fmoc-amine protection, a free carboxylic acid, and TMSE and *t*Bu-ether protections of the hydroxy group in Y and X, respectively (see Supplementary Information).<sup>49</sup> Coupling was mediated by acid chloride activation, and Fmoc was removed after each coupling using 20 % piperidine in DMF. The last monomer introduced at the N-terminus was Q<sup>B</sup>, with a nitro group in position 8. Synthesis was performed on an acid labile Sasrin® resin so that a mild acid (hexafluoroisopropanol) allowed for resin cleavage while preserving TMSE and *t*Bu-ether protections, yielding protected precursors of **9-11** having a C-terminal acid function. These precursors were purified by crystallization in ethyl acetate/*n*-hexane before being converted to methyl esters in solution using TMSCHN<sub>2</sub> in CHCl<sub>3</sub>/MeOH. If purity was insufficient, another crystallization using ethyl acetate/*n*-hexane was performed at this stage. Finally, treatment with TFA in CH<sub>2</sub>Cl<sub>2</sub> removed protecting groups from Y and X units. The deprotected sequences were used without further purification. All other sequences were prepared in a similar manner, with small modifications, *e.g.* to introduce a N-terminal (1*S*)-camphanic group (see ESI).

The CD spectra of **9-11** all showed a positive band near 375 nm, confirming that *P*-helicity was quantitatively preserved in all helical segments (Figure S12). The <sup>1</sup>H NMR spectra of **9** and **10** showed one set of signals (Figure 5), indicating the prevalence of one species in solution. § The prevalence of one species remained true at both higher (>5 mM) and lower (< 1mM) concentrations (Figures S13-15). The signals of the six OH protons could be identified as being exchangeable with deuterium and not correlated to nitrogen in <sup>1</sup>H,<sup>15</sup>N-HSQC spectra (Figures S16-18). The chemical shift values above 8.5 ppm of the OH protons indicated their involvement in hydrogen bonding.<sup>34</sup> A DOSY NMR spectrum of **9** mixed with its fully protected precursor showed that they have the same diffusion coefficient, *i.e.* that both species have the same size and thus that **9** is monomeric in solution (Figures S19, 20). A DOSY NMR spectrum of **10** measured in the similar conditions indicated a similar diffusion coefficient (Figure S21). This was confirmed by a DOSY NMR spectrum of **10** mixed with its fully protected precursor (Figure S22). Based on the molecular models discussed above, the single species observed in NMR spectra can be tentatively assigned to monomeric helix-turn-helix structures with a *PP* tilted clockwise arrangement (Figure 4). In contrast, the <sup>1</sup>H NMR spectrum of **11** showed two sets of signals (Figure 5). DOSY NMR suggested that two species have the same size as **9** and **10** (Figure S23, S24). As mentioned above, molecular models suggested that, with the longer T3-3eg linker, both clockwise and counterclockwise *PP* tilted arrangements may form, possibly corresponding to the observed sets of signals.

Attempts to produce single crystals of **9-11** suitable for x-ray diffraction analysis were unsuccessful. Racemic crystallographic approaches have frequently been successful with helical structures,<sup>50-54</sup> and sequence **12**, the enantiomer of **9**, was synthesized for that purpose. The <sup>1</sup>H NMR spectrum of **12** was identical to that of **9** and

to that of the **9+12** racemic mixture (Figures S25-S27), indicating that **9** and **12** fold without interfering with one another. Unfortunately, no suitable crystals were produced from the racemic mixture either.

We next considered sequences **13-15**. These are analogues of **9-11**, respectively, in which handedness is controlled only at the N-terminal helix segment by a (1*S*)-camphanyl group. Sequences **13-15** can thus exist as *PP* or *PM* conformers but *a priori* not as *MM* or *MP* conformers. In **13-15**, the two chiral B monomers of **9-11** have been replaced by Q monomers. Although Q and B contribute similarly to helix curvature, small differences in helix shape and properties might also result from this change. The NMR spectrum of **14** showed the coexistence of numerous species (Figure 5). For this compound with a T3-3eg linker, releasing handedness control at the C-terminal helix allowed access to new unidentified conformers or aggregates. In the absence of a prevalent species, investigations were not pursued in this series. In contrast, the <sup>1</sup>H NMR spectra of **13** and **15** showed one dominant set of signals (Figure 5).

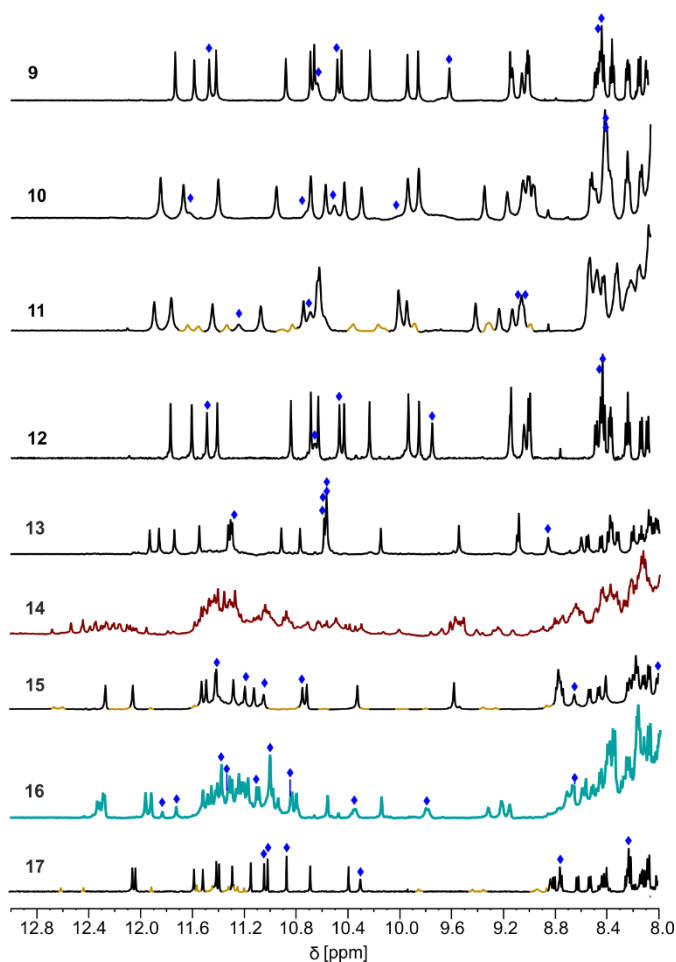


**Figure 5.** Part of the 500 MHz <sup>1</sup>H NMR spectra of sequences **9-17** at 2.3 mM in CDCl<sub>3</sub> at 25 °C showing the amide and hydrogen-bonded OH proton resonances. Signals assigned to OH protons are marked with a blue diamond. A few OH protons could not be unambiguously assigned due to signal overlap. Signals assigned to different aggregates are shown in a different color.

Band intensity in CD spectra confirmed that these species must be *PP* and not *PM* (Figure S28). Here, the handedness preference of the C-terminal helix is determined by its interaction with the N-terminal helix. DOSY NMR spectra indicated that they have the same size as **9-11** (Figures S29-S32). The assignment of OH resonances again suggested their involvement in hydrogen bonding (Figure S33, S34). The conformations of **13** and **15** in solution may thus be assigned to the same structures as the prevailing conformations of **9** and **11**, respectively (Figure 4). The fact that **15** seems better behaved than **11** (one clearly prevalent species vs two coexisting species) may result from the differences imparted by Q monomers in the former vs B monomers in the latter.<sup>55</sup>

In another attempt to obtain single crystals, sequences **16** and **17** were produced as achiral, nitro-terminated analogues of **13** and **15**, respectively. Nitro-terminated aromatic helices have frequently shown good crystallization abilities.<sup>38</sup> Sequences **16** and **17** can be *PP*, *MM*, *PM*, or *MP*. However, because of the preference of **13** and **15** for *PP* conformations, we expected **16** and **17** to exist as a racemic *PP/MM* mixture. The <sup>1</sup>H NMR of **17** is similar to that of **15** (Figures 5, S35-S37), supporting a similar behaviour in the absence of handedness control. Yet no suitable crystals were obtained to elucidate its structure unambiguously. In contrast, the NMR spectrum of **16** showed twice as many resonances as that of **13**, as if two monomeric species coexisted in equal proportions, or as if an aggregate containing four inequivalent helices had formed. A DOSY NMR spectrum of **16** mixed with its fully protected precursor showed that **16** has a smaller diffusion coefficient despite having lost the protecting groups (Figure S38). Furthermore, DOSY NMR showed that all protons of **16** belonged to entities of similar size. The only possibility for **16** to be larger than its precursor is to form some kind of discrete aggregate. The absence of aggregation for **13**, in which the handedness of the N-terminal helix is biased to *P*, suggests that the aggregate formed by **16** may not be produced from *PP* and *PM* conformers alone. It must involve *PP* and *MM* conformers, or *PM* and *MP* conformers, or all four, that is, combinations not accessible to **13**. The aggregate shows no sign of dissociation upon diluting down to 0.46 mM (Figure S39) and no significant change upon cooling to – 40 °C or heating to 40 °C (Figure S40). Multiple hydrogen-bonded OH signals could be identified (Figures 5, S41) but the full assignment is complicated by overlap due to a large number of resonances.

### **Solid state structure of 16 as a tetrameric eight-helix bundle**

Single crystals of **16** suitable for x-ray crystallographic analysis grew from a mixture of chloroform/toluene/acetonitrile and diffracted at 1.05 Å resolution, allowing for the elucidation of its solid state structure (Figures 6, 7a, S42-44). The structure revealed a tetramer composed of two *PP* conformers of **16** (which we named A and B) and two *MM* conformers of **16** (which we named A' and B'). With eight helices involved, the structure is larger and far more complex than any previously characterized abiotic foldamer. It admits a crystallographic centre of symmetry (Figure 6b).

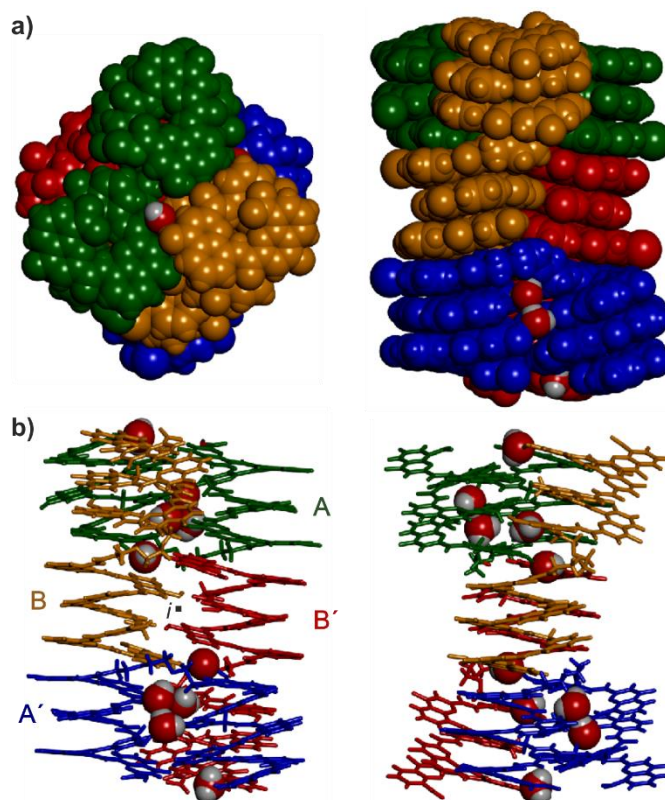


**Figure 6.** Structure of **164** in the solid state. a) Top view and side view of the tetramer shown in space-filling representation. The four molecules are shown in blue, red, gold and green. b) Side view and front view of the tetramer in tube representation. The same colors are used as in a). The inversion center is indicated by a black dot (*i*). Water molecules hydrogen bonded at helix-helix interfaces are shown in space-filling representation. Side chains and other included solvent molecules are omitted for clarity.

A' and B' are thus the inverted structures of A and B, respectively. The structure is thus consistent with the number of signals observed by  $^1\text{H}$  NMR spectroscopy (Figure 5). It is composed of three domains stacked on top of one another. Two peripheral domains consist of a parallel bundle of three helices composed of the two helices of A (respectively A') and the N-terminal helix of B (respectively the N-terminal helix of B'). The central domain, across the centre of inversion, is a head-to-tail *PM* parallel shifted helix bundle of two C-terminal helical segments of B and B'. The domains are held together by helix-to-helix hydrogen bonds involving mostly (but not only) hydroxy donors of X and Y residues and amide carbonyl acceptors. Remarkably, no less than six of these contacts are mediated by a bridging water molecule.

The three-helix bundle domains can only be remotely compared to the trimeric helix bundle that was previously characterized (Figures 7b, S42).<sup>34</sup> The latter was homochiral (*PPP* or *MMM*), with all three helices parallel and oriented head-to-head. We have previously shown that inverting both the handedness and the orientation of a helix within a parallel aggregate produces a similar arrangement of hydrogen bond donors and acceptors. One could thus imagine a parallel trimeric bundle in which two *P* helices would be oriented head-to-head and a third helix would be *M*-helical and have the opposite orientation. However, the three-helix bundles of the structure of **16** show yet another pattern: two helices are *P* and one *M* in one bundle (two *M*, one *P* in the other

bundle), but the two *P* helices (resp. *M*) are arranged head-to-tail. Besides, the three helices are not strictly parallel. One helix axis forms an angle with the two others. This helix is also shifted along the bundle axis, *i.e.* protruding a bit outwards (Figure 7a).

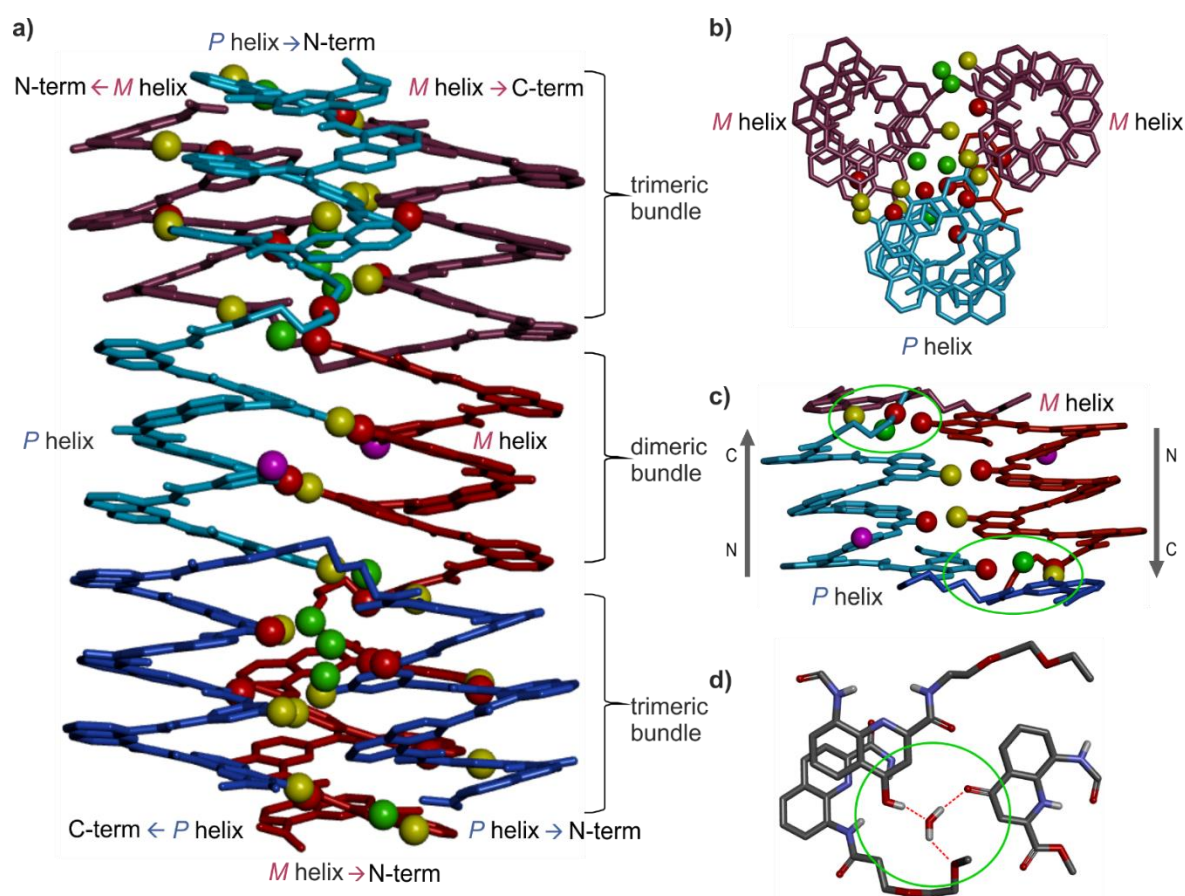


**Figure 7.** a) Side-view of the crystal structure of **16<sub>4</sub>** in tube representation indicating the three different domains. The four molecules are shown in brown (A), light blue (B) red (B') and dark blue (A'). The oxygen atoms in position 4 of X and Y units involved in hydrogen bonding are shown as yellow balls. Those not involved in hydrogen bonding are shown as purple balls. The oxygen atoms of amide carbonyl groups involved in hydrogen bonding are shown as red balls. Bridging water molecules are shown as green balls. Hydroxyl protons and carbonyl oxygen atoms of the hydrogen-bonding arrays are shown as yellow and red balls, respectively. Hydrogen atoms and side chains are not shown for clarity. b) Top view of a three-helix domain with the same representation as in a). c) Side view of the central two-helix domain with the same representation as in a). Arrows indicate the N->C orientation of the sequences. Green circles highlight areas of interest that are shown in d). d) Water molecule hydrogen bonded simultaneously to three different helices, including one T3-2eg linker and the carbonyl in position 4 of the C-terminal X unit of molecule B, found as its (1*H*)-4-quinolinone tautomer.

This arrangement results from the presence of molecules A within the bundle (respectively A' in the other bundle), which have two segments of the same handedness but are arranged head-to-tail since connected by the T3-2eg spacer. The outcome of this complex arrangement is that each three-helix bundle involves only three direct helix-to-helix hydrogen bonds, including the hydroxy group of a Y unit that serves both as a donor and acceptor to bind to the two other helices. Other contacts are mediated by five bridging water molecules per bundle. Some of the water bridges occur within one molecule of A (or A'), others between A and B



(respectively A' and B'). Two water molecules bridge simultaneously three helices (one is shown in Figure 7d). Bridging water molecules are common at the interface between biopolymers in water but much less so in organic solvents. We have before observed only one instance of a water molecule insertion in a helix-helix hydrogen-bonding interface in an organic solvent.<sup>35</sup> Bridging water molecules have also been reported in self-assembled calix[4]resorcinarene-based capsules.<sup>56</sup> Their occurrence within **16**, shows how they can give access to complex, hard to predict, interfaces in organic solvents.

The central two-helix domain in the middle of the structure is composed of the C-terminal helices of B and B'. B and B' thus have an extended conformation with one helix involved in the two-helix domain and the other involved in a three-helix domain, in contrast with A and A', which are back-folded on themselves and are entirely involved in a three-helix domain. The central part of the two helix domain is typical of a head-to-tail heterochiral (*PM*) parallel shifted dimer,<sup>38</sup> giving rise to two intermolecular hydrogen bonds (Figures 7c, S43). This arrangement leaves the hydroxy groups of two Y units not involved in hydrogen bonding, the only two in the entire structure (purple balls in Figure 7a,c). At the periphery of the two-helix domain, the C-terminal X units of B and B' are found as 4-(1*H*)-quinolinone tautomers instead of the usual 4-hydroxyquinoline (Figures 7d, S44). The quinolinone NH is involved in hydrogen bonds with the adjacent ester and amide carbonyl groups. The latter entails a 180° rotation about the NH-aryl bond, which results in the quinolinone being flipped away from the helix (Figure S44). This tautomer should, in principle, give rise to an additional correlation in the <sup>1</sup>H,<sup>15</sup>N-HSQC spectra, but the spectrum shows too much signal overlap to ascertain a clear assignment (Figure S41). However, we noted that the number of hydrogen-bonded OH signals identified in the NMR spectrum of **16** – ten (Figure 5) – matches the number of hydrogen-bonded OH groups in the crystal structure. The carbonyl in position 4 of the flipped 4-(1*H*)-quinolinone hydrogen bonds to a water molecule that simultaneously bridges monomers from three different helices (Figure 7d).

Overall the eight-helix bundle structure is held together by hydrogen bonds, notably those involving by B and B' molecules, which span across the trimeric and dimeric domains, by aromatic stacking at domain-domain interfaces, and by the bridging water molecules. While some of its structural features have been observed before, it is novel in several aspects. The structure may be termed a sort of pseudo-quaternary structure. It is indeed composed of multiple subunits but may perhaps not qualify as a true quaternary structure in that it is not composed of independent, self-assembled, tertiary folds.

## Conclusion

Using an approach that combined molecular modelling, the screening of three different T3 linkers, and selective handedness control in helix-linker-helix sequences, we have identified sequences that fold in discrete homochiral clockwise tilted arrangements in which helix-to-helix hydrogen bonds maintain the helices at an angle. This arrangement complements earlier work in which other linkers had been shown to promote helix-

turn-helix structures where helices were parallel. Combining both parallel and tilted arrangements in future design will allow for a significant enhancement of the complexity of the abiotic tertiary folds that can be produced.

In one instance, removing all handedness control, that is, allowing all helix segments to be *P* or *M* helical, led to the unexpected formation of a large (12.9 kDa) heterochiral aggregate. A crystal structure revealed an architecture of unprecedented complexity in the field of abiotic folding. The architecture consists of four molecules and a total of eight helices arranged in three distinct domains: two three-helix-bundle domains and one two-helix-bundle domain. The domains contain some previously reported hydrogen-bonded helix-helix arrangements as well as new ones. Several helix-to-helix hydrogen bonds were mediated by bridging water molecules. This object constitutes an important milestone as it gives a glimpse of the vastness of the chemical space available to abiotic foldamers. The field will undoubtedly keep developing through combinations of design by modelling on the one hand, and discovery on the other.

### **Author contributions**

FM synthesized new compounds. FM and LA performed solution studies. BW performed crystallographic studies. FM and VM performed modelling studies. All authors contributed to experiment design and interpretation. IH supervised the research. FM and IH wrote the manuscript. All authors proofread and improved the manuscript.

### **Conflicts of interest**

There are no conflicts to declare.

### **Acknowledgements**

This work was supported by the DFG (Excellence Cluster 114, CIPSM). D. Gill is gratefully acknowledged for contributing synthetic precursors and monomer synthesis. We also thank S. Wang, L. Wang and D. Bindl for monomer synthesis, C. Glas and C. Ober for assistance with NMR measurements, and B. Kauffmann for crystallographic data collection. This work has benefited from the facilities and expertise of the Biophysical and Structural Chemistry platform (BPCS) at IECB, CNRS UMS3033, Inserm US001, and Bordeaux University.

## Notes and references

† Throughout the manuscript, the term "parallel" refers to helical axes having a parallel orientation without prejudice of the head-to-head or head-to-tail relative arrangement of the oligoamide chains. The term "anti-parallel" is avoided.

‡ Slight hyper- and hypsochromic shifts are observed for **5** because of the larger number of contiguous pseudo-conjugated quinolinecarboxamide units (Figure S4).

§ Exchange between the various types of dimers is always slow on the <sup>1</sup>H NMR time scale. See references 34-37.

1. G. Guichard and I. Huc, *Chem. Commun.*, 2011, **47**, 5933.
2. S. H. Gellman, *Acc. Chem. Res.*, 1998, **31**, 173-180.
3. C. M. Goodman, S. Choi, S. Shandler and W. F. DeGrado, *Nat. Chem. Biol.*, 2007, **3**, 252-262.
4. R. V. Nair, K. N. Vijayadas, A. Roy and G. J. Sanjayan, *Eur. J. Org. Chem.*, 2014, **2014**, 7763-7780.
5. I. Saraogi and A. D. Hamilton, *Chem. Soc. Rev.*, 2009, **38**, 1726.
6. I. Huc, *Eur. J. Org. Chem.*, 2004, **2004**, 17-29.
7. D.-W. Zhang, X. Zhao, J.-L. Hou and Z.-T. Li, *Chem. Rev.*, 2012, **112**, 5271-5316.
8. C. W. Wood and D. N. Woolfson, *Protein Sci.*, 2018, **27**, 103-111.
9. F. Thomas, W. M. Dawson, E. J. M. Lang, A. J. Burton, G. J. Bartlett, G. G. Rhys, A. J. Mulholland and D. N. Woolfson, *ACS Synth. Biol.*, 2018, **7**, 1808-1816.
10. G. G. Rhys, J. A. Cross, W. M. Dawson, H. F. Thompson, S. Shanmugaratnam, N. J. Savery, M. P. Dodding, B. Höcker and D. N. Woolfson, *Nat. Chem. Biol.*, 2022, **18**, 999-1004.
11. A. J. Scott, A. Niitsu, H. T. Kratochvil, E. J. M. Lang, J. T. Sengel, W. M. Dawson, K. R. Mahendran, M. Mravic, A. R. Thomson, R. L. Brady, L. Liu, A. J. Mulholland, H. Bayley, W. F. DeGrado, M. I. Wallace and D. N. Woolfson, *Nat. Chem.*, 2021, **13**, 643-650.
12. M. J. Chalkley, S. I. Mann and W. F. DeGrado, *Nat. Rev. Chem.*, 2022, **6**, 31-50.
13. M. Mravic, J. L. Thomaston, M. Tucker, P. E. S. Lijun Liu and W. F. DeGrado, *Science*, 2019, **363**, 1418-1423.
14. F. Pirro, N. Schmidt, J. Lincoff, Z. X. Widel, N. F. Polizzi, L. Liu, M. J. Therien, M. Grabe, M. Chino, A. Lombardi and W. F. DeGrado, *Proc. Natl. Acad. Sci.*, 2020, **117**, 33246-33253.
15. T. Lebar, D. Lainšček, E. Merljak, J. Aupič and R. Jerala, *Nat. Chem. Biol.*, 2020, **16**, 513-519.
16. F. Lapenta, J. Aupič, M. Vezzoli, Ž. Strmšek, S. Da Vela, D. I. Svergun, J. M. Carazo, R. Melero and R. Jerala, *Nat. Commun.*, 2021, **12**.
17. F. Lapenta, J. Aupič, Ž. Strmšek and R. Jerala, *Chem. Soc. Rev.*, 2018, **47**, 3530-3542.
18. P. Kumar, N. G. Paterson, J. Clayden and D. N. Woolfson, *Nature*, 2022, **607**, 387-392.
19. W. S. Horne, J. L. Price, J. L. Keck and S. H. Gellman, *J. Am. Chem. Soc.*, 2007, **129**, 4178-4180.

20. E. J. Petersson, C. J. Craig, D. S. Daniels, J. X. Qiu and A. Schepartz, *J. Am. Chem. Soc.*, 2007, **129**, 5344-5345.
21. D. S. Daniels, E. J. Petersson, J. X. Qiu and A. Schepartz, *J. Am. Chem. Soc.*, 2007, **129**, 1532-1533.
22. G. W. Collie, K. Pulka-Ziach, C. M. Lombardo, J. Fremaux, F. Rosu, M. Decossas, L. Mauran, O. Lambert, V. Gabelica, C. D. Mackereth and G. Guichard, *Nat. Chem.*, 2015, **7**, 871-878.
23. G. W. Collie, R. Bailly, K. Pulka-Ziach, C. M. Lombardo, L. Mauran, N. Taib-Maamar, J. Dessolin, C. D. Mackereth and G. Guichard, *J. Am. Chem. Soc.*, 2017, **139**, 6128-6137.
24. H. Jiang, J.-M. Léger and I. Huc, *J. Am. Chem. Soc.*, 2003, **125**, 3448-3449.
25. T. Qi, V. Maurizot, H. Noguchi, T. Charoenraks, B. Kauffmann, M. Takafuji, H. Ihara and I. Huc, *Chem. Commun.*, 2012, **48**, 6337.
26. F. Devaux, X. Li, D. Sluysmans, V. Maurizot, E. Bakalis, F. Zerbetto, I. Huc and A.-S. Duwez, *Chem*, 2021, **7**, 1333-1346.
27. N. Delsuc, F. Godde, B. Kauffmann, J.-M. Léger and I. Huc, *J. Am. Chem. Soc.*, 2007, **129**, 11348-11349.
28. D. Sánchez-García, B. Kauffmann, T. Kawanami, H. Ihara, M. Takafuji, M.-H. Delville and I. Huc, *J. Am. Chem. Soc.*, 2009, **131**, 8642-8648.
29. M. Vallade, P. Sai Reddy, L. Fischer and I. Huc, *Eur. J. Org. Chem.*, 2018, **2018**, 5489-5498.
30. V. Maurizot, C. Dolain, Y. Leydet, J.-M. Léger, P. Guionneau and I. Huc, *J. Am. Chem. Soc.*, 2004, **126**, 10049-10052.
31. N. Delsuc, S. Massip, J.-M. Léger, B. Kauffmann and I. Huc, *J. Am. Chem. Soc.*, 2011, **133**, 3165-3172.
32. C. Dolain, J.-M. Léger, N. Delsuc, H. Gornitzka and I. Huc, *Proc. Natl. Acad. Sci.*, 2005, **102**, 16146-16151.
33. J. Graton, F. Besseau, A.-M. Brossard, E. Charpentier, A. Deroche and J.-Y. Le Questel, *J. Phys. Chem. A*, 2013, **117**, 13184-13193.
34. S. De, B. Chi, T. Granier, T. Qi, V. Maurizot and I. Huc, *Nat. Chem.*, 2018, **10**, 51-57.
35. D. Mazzier, S. De, B. Wicher, V. Maurizot and I. Huc, *Chem. Sci.*, 2019, **10**, 6984-6991.
36. D. Mazzier, S. De, B. Wicher, V. Maurizot and I. Huc, *Angew. Chem. Int. Ed.*, 2020, **59**, 1606-1610.
37. F. S. Menke, D. Mazzier, B. Wicher, L. Allmendinger, B. Kauffmann, V. Maurizot and I. Huc, *Org. Biomol. Chem.*, 2023, DOI: 10.1039/D10320B02109A.
38. F. S. Menke, B. Wicher, V. Maurizot and I. Huc, *Angew. Chem. Int. Ed.*, 2023, DOI: 10.1002/anie.202217325.
39. C. Dolain, J.-M. Léger, N. Delsuc, H. Gornitzka and I. Huc, *Proc. Natl. Acad. Sci.*, 2005, **102**, 16146-16151.
40. A. M. Kendhale, L. Poniman, Z. Dong, K. Laxmi-Reddy, B. Kauffmann, Y. Ferrand and I. Huc, *J. Org. Chem.*, 2011, **76**, 195-200.
41. D. Bindl, E. Heinemann, P. K. Mandal and I. Huc, *Chem. Commun.*, 2021, **57**, 5662-5665.

## 5.2 Supplementary Information

for:

An abiotic, tetrameric, eight-helix bundle

Friedericke S. Menke, Barbara Wicher, Lars Allmendinger, Victor Maurizot and Ivan Huc

5.2.1	List of Abbreviations	199
5.2.2	Supplementary figures	200
5.2.3	Supplementary methods	231
5.2.3.1	HRMS analyses	231
5.2.3.2	Molecular modeling	231
5.2.3.3	Nuclear magnetic resonance spectroscopy	231
5.2.3.4	CD studies	233
5.2.3.5	X-ray crystallography	233
5.2.4	Synthetic Schemes	237
5.2.4.1	Synthesis of sequences to test handedness-induction via chiral B-unit	237
5.2.4.2	Synthesis of helix-turn-helix-motif with a flexible linker and handedness-control in both helices via a chiral B-unit	238
5.2.4.3	Synthesis of helix-turn-helix-motif with a flexible linker and handedness-control in one helix	239
5.2.4.4	Synthesis of helix-turn-helix-motif with a flexible linker and without any handedness -control	240
5.2.5	Experimental Procedures	241
5.2.5.1	General methods	241
5.2.5.2	Solid phase synthesis general methods	241
5.2.5.2.1	Loading of the resin via HBTU-coupling	241
5.2.5.2.2	Estimation of the loading	241
5.2.5.2.3	Solid Phase Synthesis via in-situ-activation	242
5.2.5.2.4	Mini Cleavage	243
5.2.5.2.5	Full Cleavage	243
5.2.5.3	Synthesis of oligomers	243

5.2.5.3.1	Synthesis of sequences to test handedness-induction via chiral B-unit	243
5.2.5.3.2	Synthesis of sequences with a helix-turn-helix-motif and handedness-control in both helices	247
5.2.5.3.3	Synthesis of sequences with a helix-turn-helix-motif and handedness-control in one helix	253
5.2.5.3.4	Synthesis of achiral sequences with a helix-turn-helix-motif	257
4.2.6	References	261
4.2.7	NMR spectra of new compounds	262
4.2.7.1	Sequences to test handedness-induction via chiral B-unit	262
4.2.7.2	Sequences with a helix-turn-helix-motif and handedness-control in both helices	272
4.2.7.3	Sequences with a helix-turn-helix-motif and handedness-control in one helix	284
4.2.7.4	Achiral sequences with a helix-turn-helix-motif	293

### 5.2.1 List of Abbreviations

<b>CD</b>	circular dichroism
<b>DCM</b>	dichloromethane
<b>DIPEA</b>	<i>N,N</i> -diisopropylethylamine
<b>DMF</b>	<i>N,N</i> -dimethylformamide
<b>DOSY</b>	diffusion-ordered spectroscopy
<b>ESI</b>	electrospray ionization
<b>EtOAc</b>	ethylacetate
<b>eq</b>	equivalent
<b>Fmoc</b>	fluorenylmethoxycarbonyl
<b>HBTU</b>	Hexafluorophosphate Benzotriazole Tetramethyl Uronium
<b>hex</b>	hexane
<b>HFIP</b>	hexafluoroisopropanol
<b>HR-ESI</b>	high-resolution electrospray ionization
<b>HRMS</b>	high-resolution mass spectrometry
<b>HSQC</b>	heteronuclear single quantum correlation
<b>MeOH</b>	methanol
<b>min</b>	minutes
<b>MS</b>	mass spectrometry
<b>MW</b>	microwave
<b>NMR</b>	nuclear magnetic resonance
<b>r. t.</b>	room temperature
<b>SPS</b>	solid phase synthesis
<b>TFA</b>	trifluoroacetic acid
<b>THF</b>	tetrahydrofuran
<b>UV/Vis</b>	ultraviolet–visible

## 5.2.2 Supplementary figures

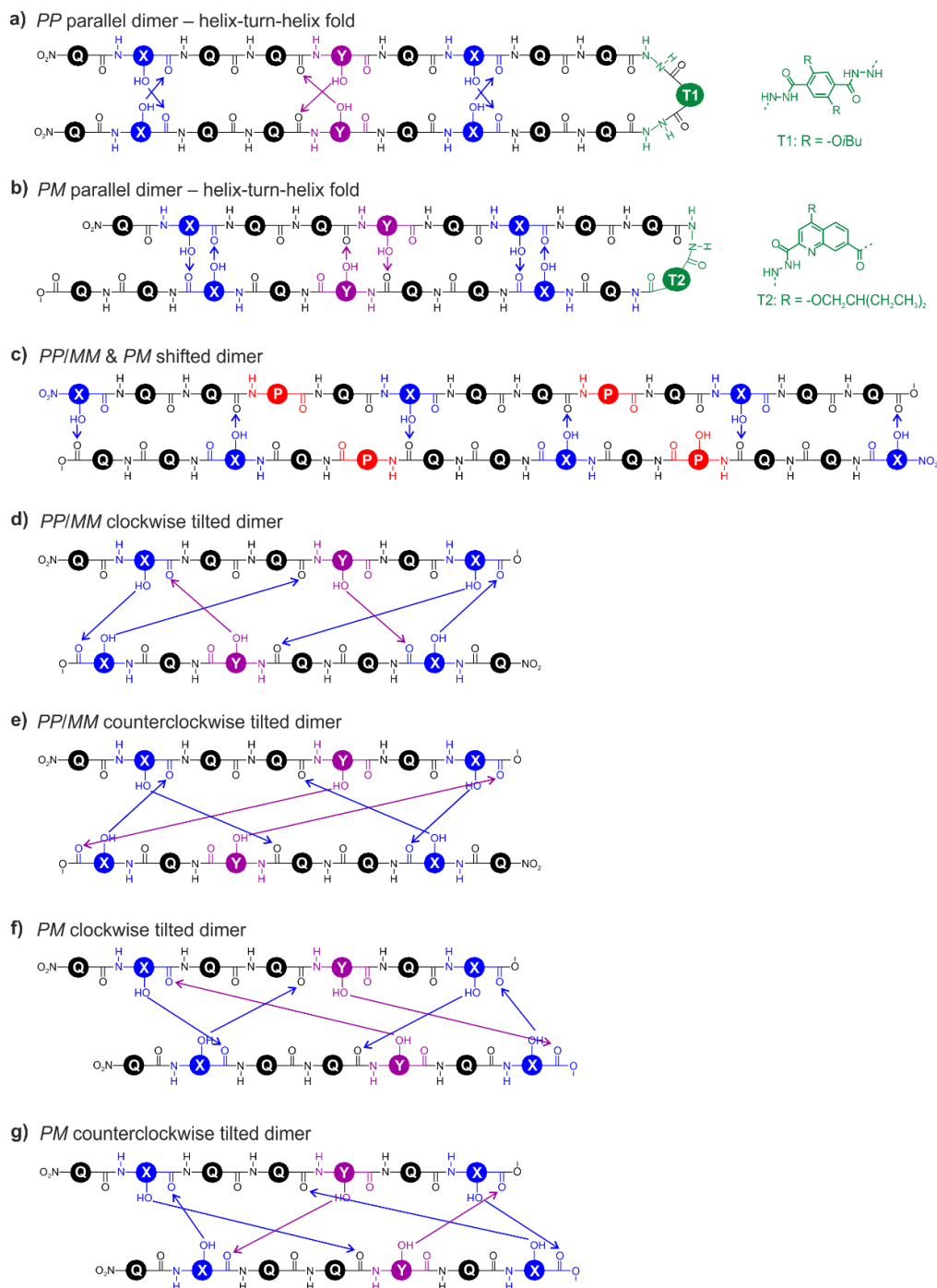


**Figure S1. Schematic representation of hydrogen-bonding interfaces of previously described and hypothetical self-organizations.** a) and b) Hydrogen bonding interfaces as characterized in a *PP/IMM* (a) and *PM* (b) parallel dimer, as observed in helix-turn-helix tertiary structures stabilized by a T1 or T2 turn unit, respectively.<sup>1-3</sup> c) Hydrogen bonding interface as observed in *PP/IMM* and *PM* shifted dimers.<sup>4</sup> d) and e) Hydrogen bonding interfaces observed in *PP/IMM* clockwise (d) and counterclockwise (e) tilted dimers.<sup>1</sup> f) and g) Hypothetical hydrogen bonding interfaces in *PM* clockwise (f) and counterclockwise (g) tilted dimers.



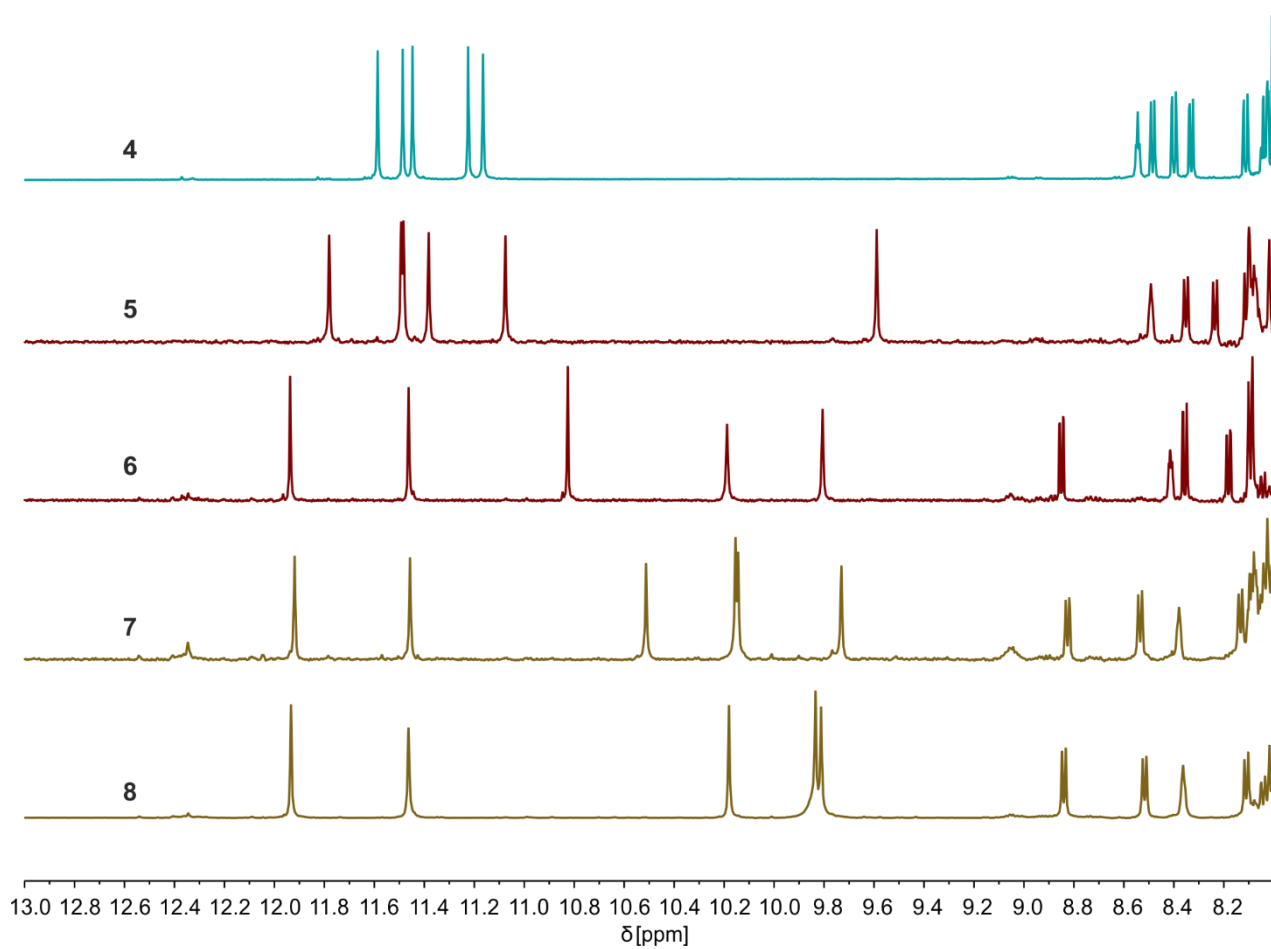


**Figure S2. Sequences 4-8 show one set of  $^1\text{H}$  NMR signals in  $\text{CDCl}_3$ .** Extracts of  $^1\text{H}$  NMR spectra (500 MHz, 25  $^\circ\text{C}$ ) of **4-8** in  $\text{CDCl}_3$  at 2.4 mM showing the amide region. Different color of the  $^1\text{H}$  NMR signals indicate the presence of a different level of handedness-control: Achiral sequences are marked in turquoise, sequences at which one unit controls handedness are marked in brown and sequences at which two units are inducing handedness control are marked in gold.

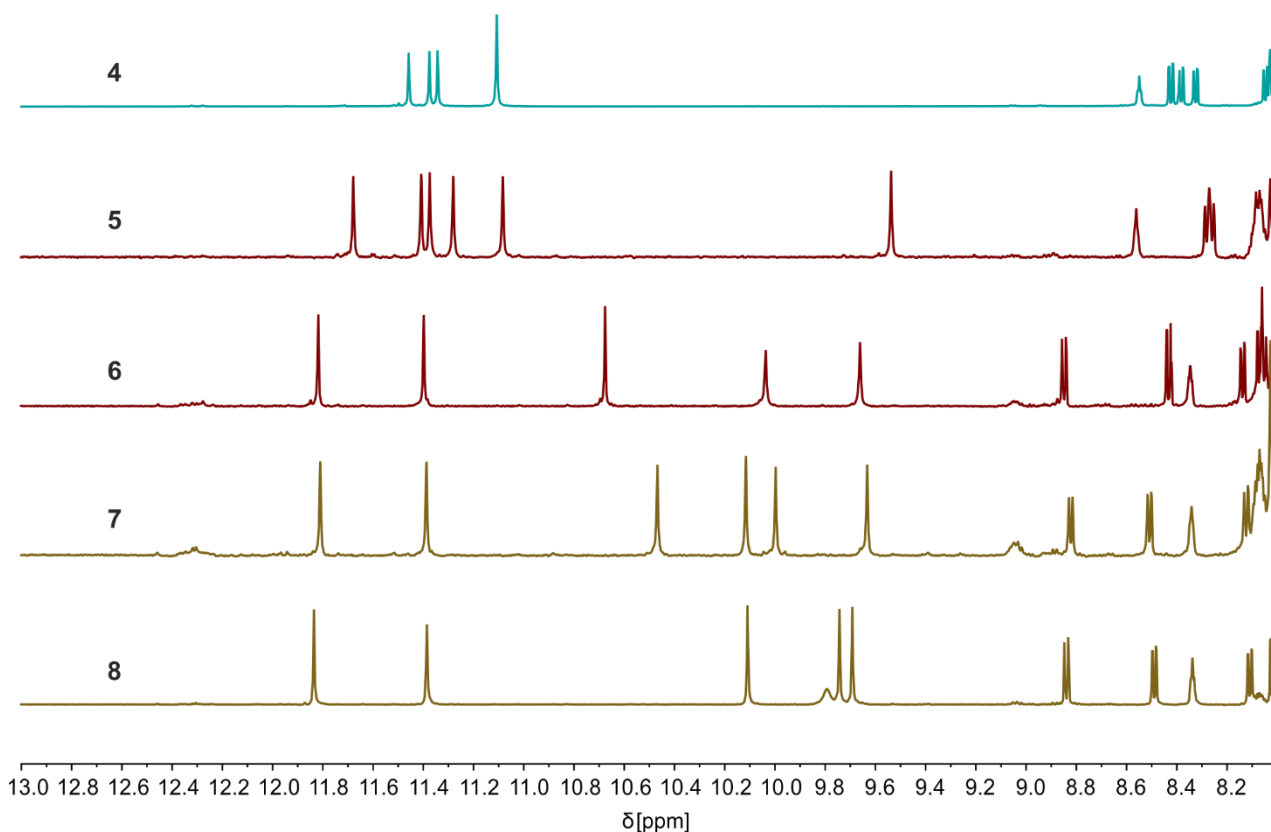


**Figure S3. Sequences 4-8 show one set of  $^1\text{H}$  NMR signals in  $\text{CD}_2\text{Cl}_2$ .** Extracts of  $^1\text{H}$  NMR spectra (500 MHz, 25 °C) of **4-8** in  $\text{CD}_2\text{Cl}_2$  at 2.4 mM showing the amide region. Different color of the  $^1\text{H}$  NMR signals indicate the presence of a different level of handedness-control: Achiral sequences are marked in turquoise, sequences at which one unit controls handedness are marked in brown and sequences at which two units are inducing handedness control are marked in gold.

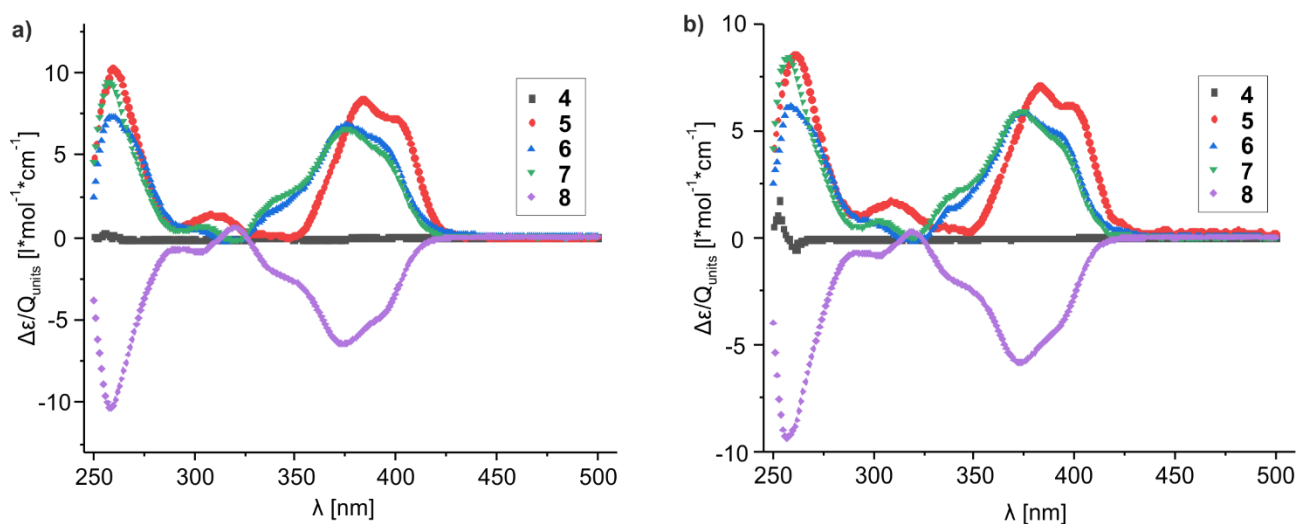


**Figure S4. The chiral B unit biases helix handedness quantitatively and overcomes the opposing effect of a camphanyl group.** CD spectra of **4-8** in  $\text{CHCl}_3$  (a) and  $\text{CH}_2\text{Cl}_2$  (b) between 250 and 500 nm at 25 °C. The molar extinction ( $\Delta\epsilon$ ) is normalized for the number of Q units for better comparability.

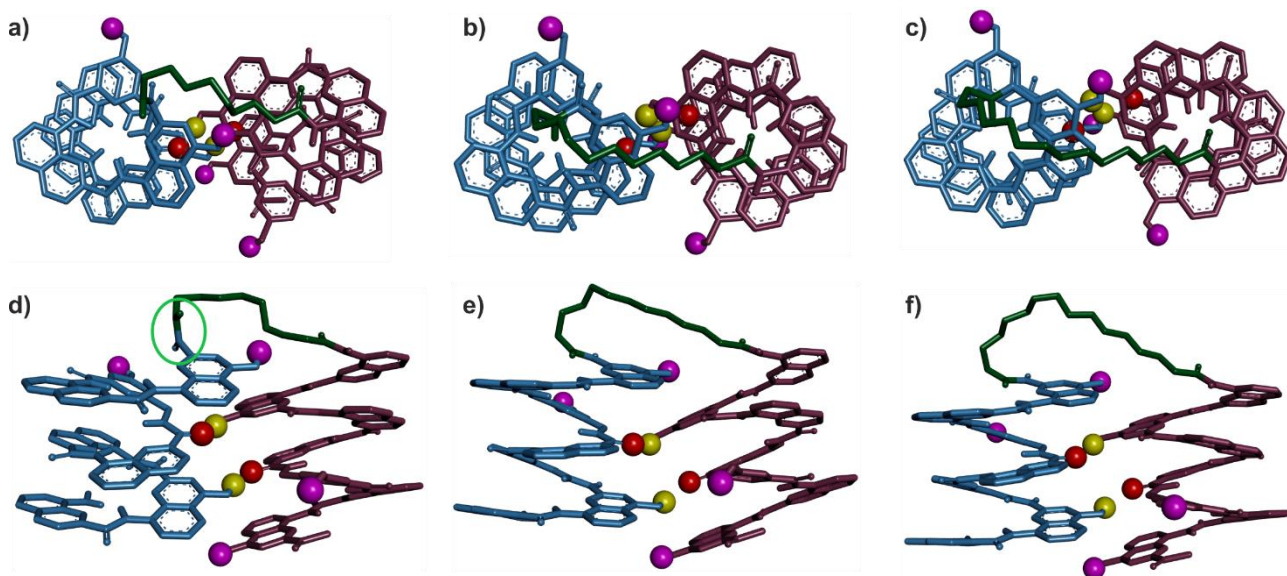


**Figure S5. Energy minimized models<sup>5</sup> of *PM* shifted dimers<sup>4</sup> connected by flexible linkers of different lengths, showing hydroxy groups not involved in hydrogen bonding.** Top view of a computational model<sup>5</sup> of a *PM* shifted dimer<sup>4</sup> containing a flexible linker unit with a flexible peg2 (a), peg3 (b) and peg4 (c) backbone, respectively. Side view of a computational model<sup>5</sup> of a *PM* shifted dimer<sup>4</sup> containing a flexible linker unit with a flexible peg2 (d), peg3 (e) and peg4 (f) backbone, respectively. Purple and blue helices represent *M*- and *P*-handedness, respectively. The hydroxyl protons and carbonyl oxygen atoms of the hydrogen-bonding arrays are shown as yellow and red balls. The flexible linker is shown in green. Hydrogen and other side-chains are omitted for clarity. The linker amide bond is turned out of the plane (marked in light green) in (d).

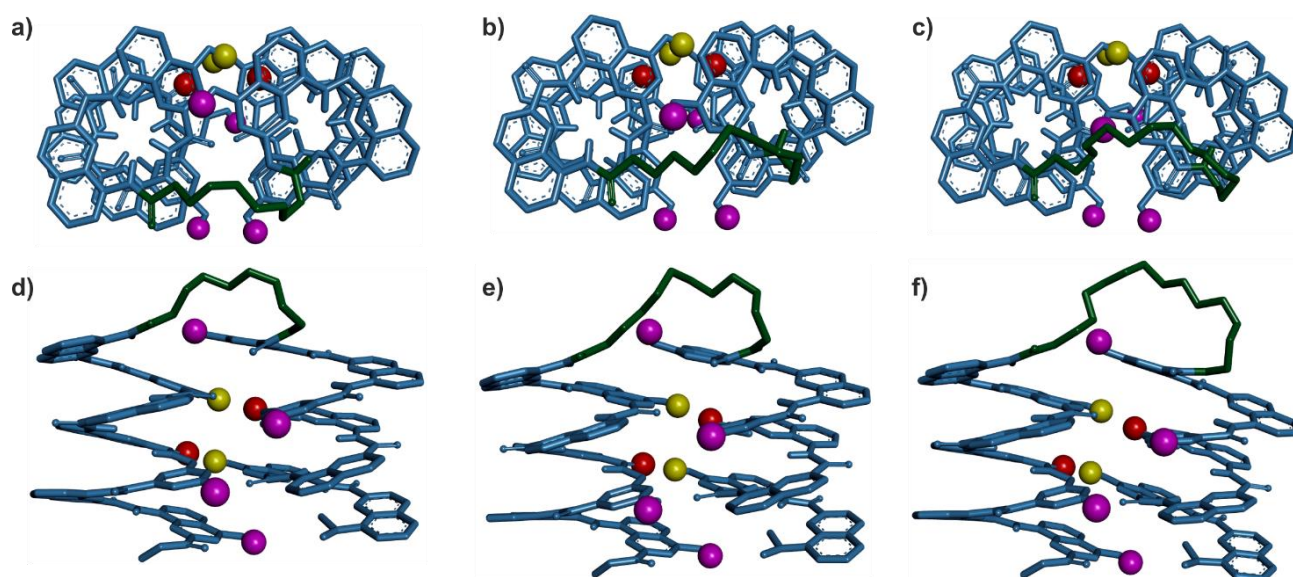


**Figure S6. Energy minimized models<sup>5</sup> of *PP* shifted dimers<sup>4</sup> connected by flexible linkers of different lengths, showing hydroxy groups not involved in hydrogen bonding.** Top view of a computational model<sup>5</sup> of a *PP* shifted dimer<sup>4</sup> containing a flexible linker unit with a flexible peg2 (a), peg3 (b) and peg4 (c) backbone, respectively. Side view of a computational model<sup>5</sup> of a *PP* shifted dimer<sup>4</sup> containing a flexible linker unit with a flexible peg2 (d), peg3 (e) and peg4 (f) backbone, respectively. The hydroxyl protons and carbonyl oxygen atoms of the hydrogen-bonding arrays are shown as yellow and red balls. Non-hydrogen-bonded hydroxyl groups are marked in brown. Blue helices represent *P*-handedness. The flexible linker is shown in dark green. Hydrogen and other side-chains are omitted for clarity.

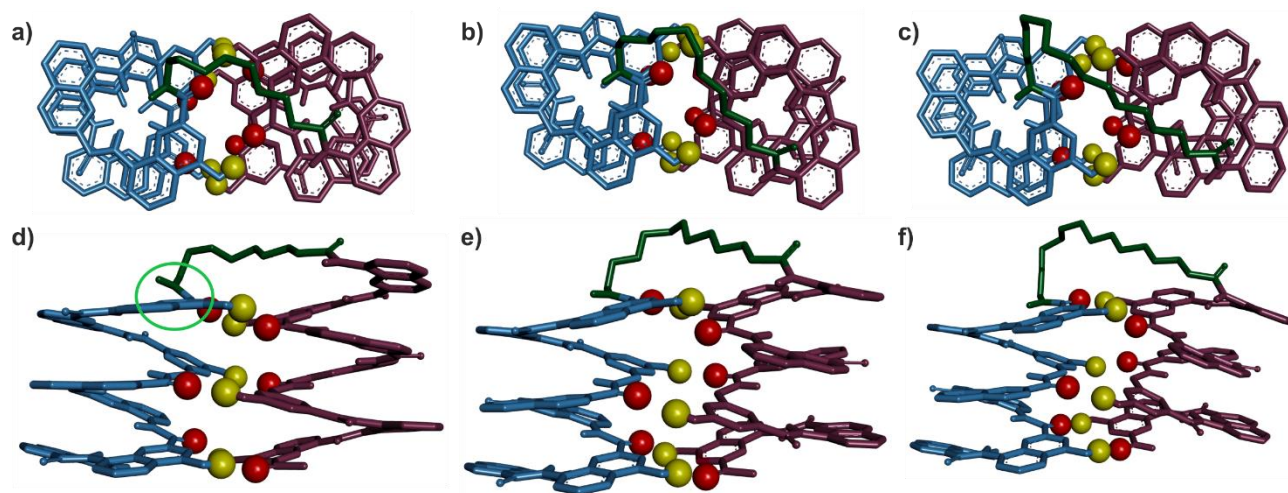


**Figure S7. Energy minimized models<sup>5</sup> of *PM* parallel dimers<sup>2</sup> connected by flexible linkers of different lengths. Only minor perturbations are observed.<sup>1,4</sup>** Top view of a computational model<sup>5</sup> of a *PM* parallel dimer<sup>2</sup> containing a flexible linker unit with a flexible peg2 (a), peg3 (b) and peg4 (c) backbone, respectively. Side view of a computational model<sup>5</sup> of a *PM* parallel dimer<sup>2</sup> containing a flexible linker unit with a flexible peg2 (d), peg3 (e) and peg4 (f) backbone, respectively. Purple and blue helices represent *M*- and *P*-handedness, respectively. The hydroxyl protons and carbonyl oxygen atoms of the hydrogen-bonding arrays are shown as yellow and red balls. The flexible linker is shown in green. Hydrogen and other side-chains are omitted for clarity. The linker amide bond is turned out of the plane (marked in light green) in (d).

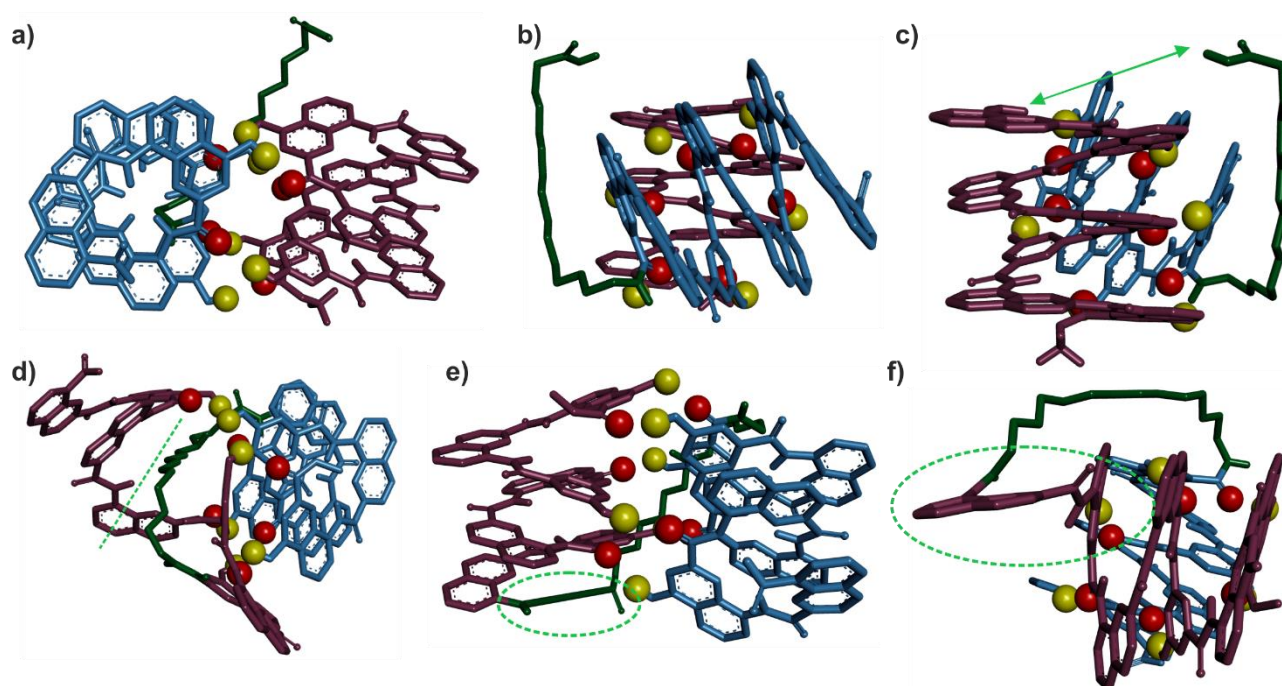


**Figure S8. Energy minimized models<sup>5</sup> of *PM* clockwise tilted dimers emphasizing the insufficient length of even the longest linker.** Top- (a), side- (b) and front-view (c) of a computational model<sup>5</sup> of a *PM* clockwise tilted dimer in respect to head-to-tail arrangement containing a flexible linker unit with a peg4-backbone. Here the flexible linker is only linked to one helix and not to the other. The great distance between the linker and the N-Terminus of the other not connected helix is marked by a green arrow in (c). This amplifies the unlikelihood of the formation of a *PM*-clockwise tilted dimer (with respect to head-to-head arrangement). Computational model<sup>5</sup> of a *PM*-clockwise tilted dimer (with respect to head-to-head arrangement) stabilized by a flexible linker with a peg4-backbone. Here the linker goes through the helix (d), part of the linker is stretched (e) or the helix-partially unfolds (f). The unlikely conformations are marked in green. The hydroxyl protons and carbonyl oxygen atoms of the hydrogen-bonding arrays are shown as yellow and red balls. Blue and purple helices represent *P*- and *M*-handedness, respectively. The flexible linker is shown in dark green. Hydrogens and other side-chains are omitted for clarity. This model has only been modelled in the case of a peg4-based linker.

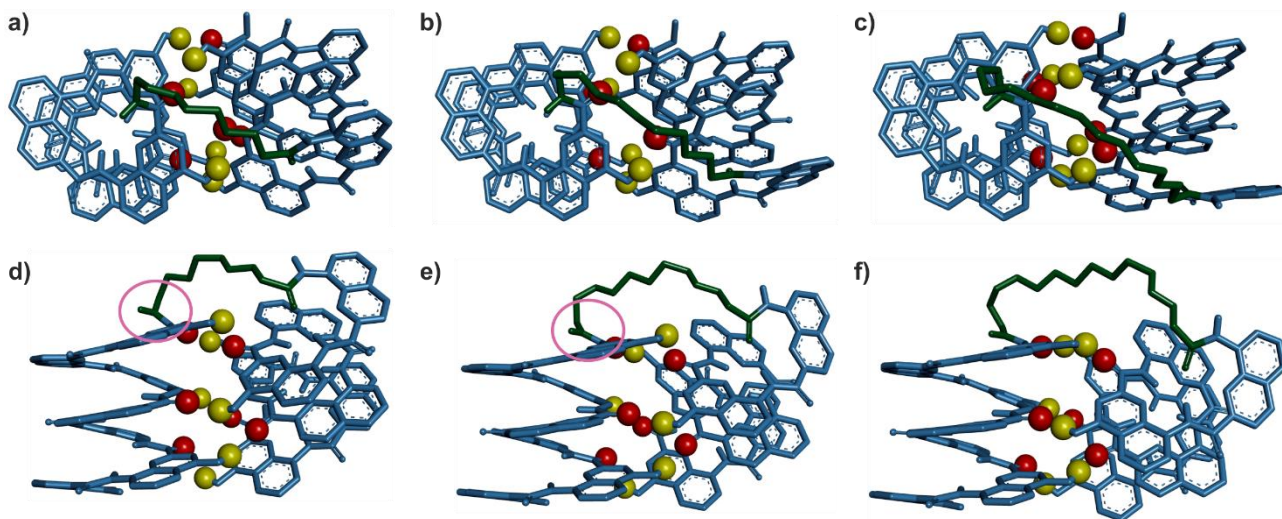


**Figure S9. Energy minimized models<sup>5</sup> of *PP* counterclockwise tilted dimers connected by flexible linkers of different lengths. T3-2eg and T3-3eg linkers perturb the conformation.** Top view of a computational model<sup>5</sup> of a *PP* counterclockwise tilted dimer with respect to head-to-head arrangement containing a flexible linker unit with a flexible peg2 (a), peg3 (b) and peg4 (c) backbone, respectively. Side view of a computational model<sup>5</sup> of a *PP* counterclockwise tilted dimer with respect to head-to-head containing a flexible linker unit with a flexible linker unit with a flexible peg2 (d), peg3 (e) and peg4 (f) backbone, respectively. The hydroxyl protons and carbonyl oxygen atoms of the hydrogen-bonding arrays are shown as yellow and red balls. Blue helices represent *P*-handedness, respectively. The flexible linker is shown in dark green. Hydrogens and other side-chains are omitted for clarity. The linker amide bond is turned out of the plane (marked in pink) in (d) and (e).

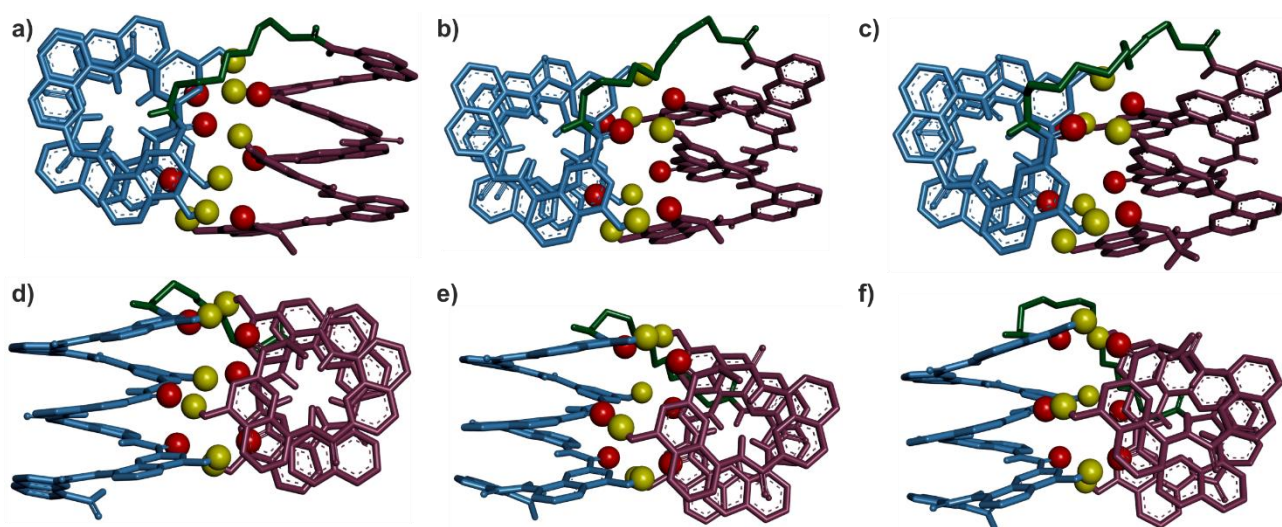


**Figure S10. Energy minimized models<sup>5</sup> of *PM* counterclockwise tilted dimer connected by flexible linkers of different lengths.<sup>6</sup>** Top view of a computational model<sup>5</sup> of a *PM* counterclockwise tilted dimer with respect to head-to-tail arrangement containing a flexible linker unit with a flexible peg2 (a), peg3 (b) and peg4 (c) backbone, respectively. Side view of a computational model<sup>5</sup> of a *PM* counterclockwise tilted dimer with respect to head-to-tail arrangement containing a flexible linker unit with a flexible peg2 (d), peg3 (e) and peg4 (f) backbone, respectively. The hydroxyl protons and carbonyl oxygen atoms of the hydrogen-bonding arrays are shown as yellow and red balls. Blue and purple helices represent *P*- and *M*-handedness, respectively. The flexible linker is shown in dark green. Hydrogens and other side-chains are omitted for clarity.



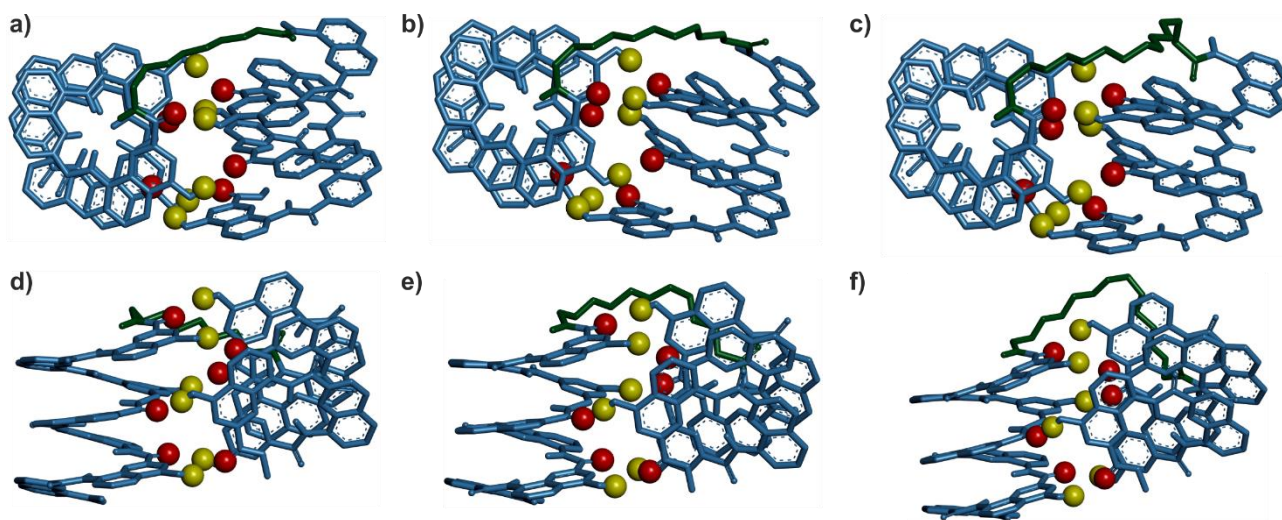


**Figure S11. Energy minimized models<sup>5</sup> of *PP* clockwise tilted dimer connected by flexible linkers of different lengths. All linkers seem compatible with the helix-helix arrangement.** Top view of a computational model<sup>5</sup> of a *PP* clockwise tilted dimer with respect to head to head containing a flexible linker unit with a flexible peg2 (a), peg3 (b) and peg4 (c) backbone, respectively. Side view of a computational model<sup>5</sup> of a *PP* clockwise tilted dimer with respect to head to head containing a flexible linker unit with a flexible peg2 (d), peg3 (e) and peg4 (f) backbone, respectively. The hydroxyl protons and carbonyl oxygen atoms of the hydrogen-bonding arrays are shown as yellow and red balls. Blue helices represent *P*-handedness, respectively. The flexible linker is shown in dark green. Hydrogens and other side-chains are omitted for clarity. Blue helices represent *P*-handedness, respectively.

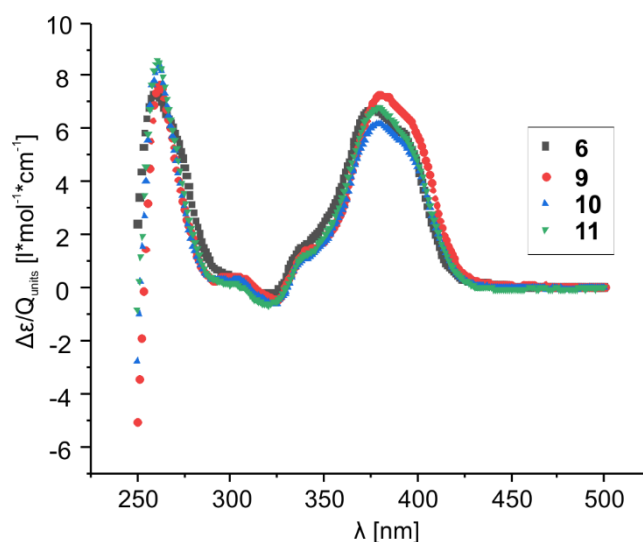


**Figure S12. Confirmation of the formation of a *P*-homochiral species in 9-11.** CD spectra of **6**, **9**, **10** and **11** in chloroform between 250 and 500 nm at 25 °C. The molar extinction ( $\Delta\epsilon$ ) is normalized for the number of Q units for better comparability.

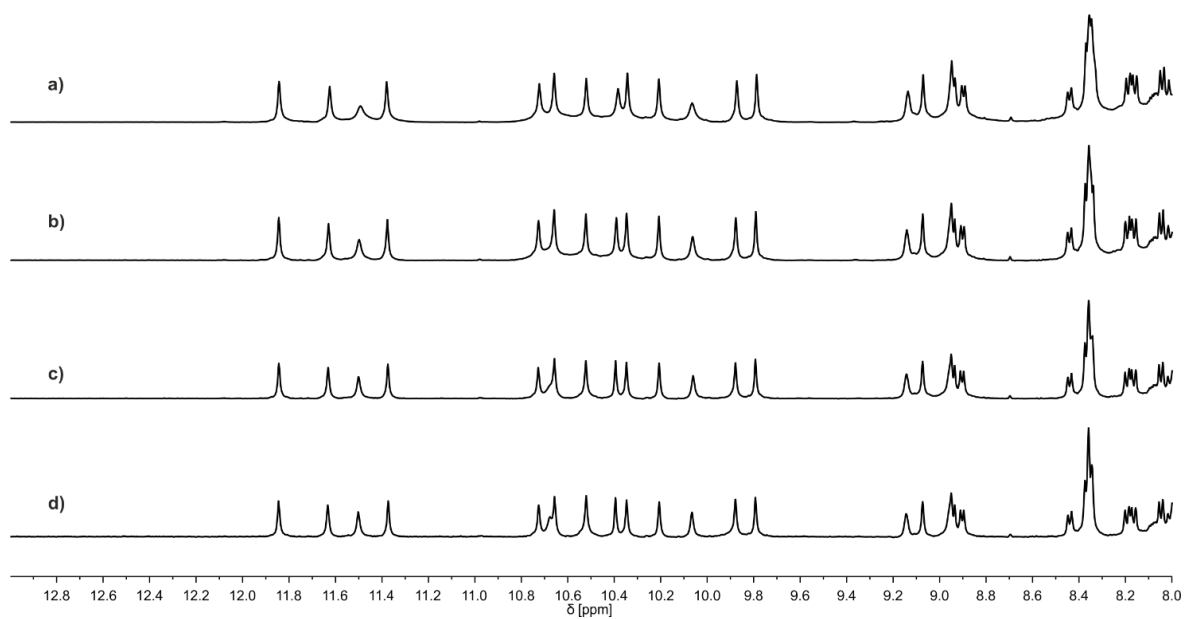


**Figure S13. A single species of **9** prevails over a range of concentrations.** Part of the  $^1\text{H}$  NMR spectra (500 MHz, 25 °C) in  $\text{CDCl}_3$  after 2 weeks showing amide resonances of **9** at 6.28 mM (a), 3.14 mM (b), 1.57 mM (c), and 0.79 mM (d), respectively.

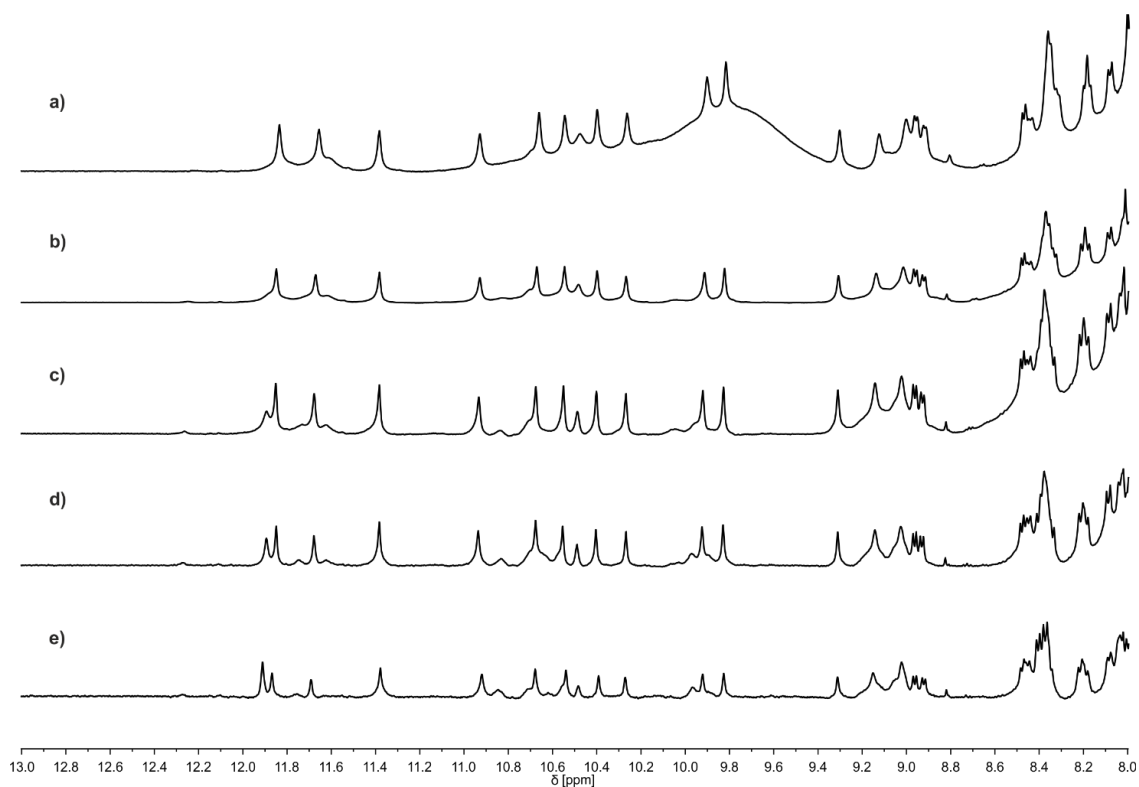


**Figure S14. A single species of **10** prevails over a range of concentrations.** Part of the  $^1\text{H}$  NMR spectra (500 MHz, 25 °C) in  $\text{CDCl}_3$  after 2 weeks showing amide resonances of **10** at 13.90 mM (a), 6.95 mM (b), 3.48 mM (c), 1.74 mM (d), and 0.87 mM (e), respectively.

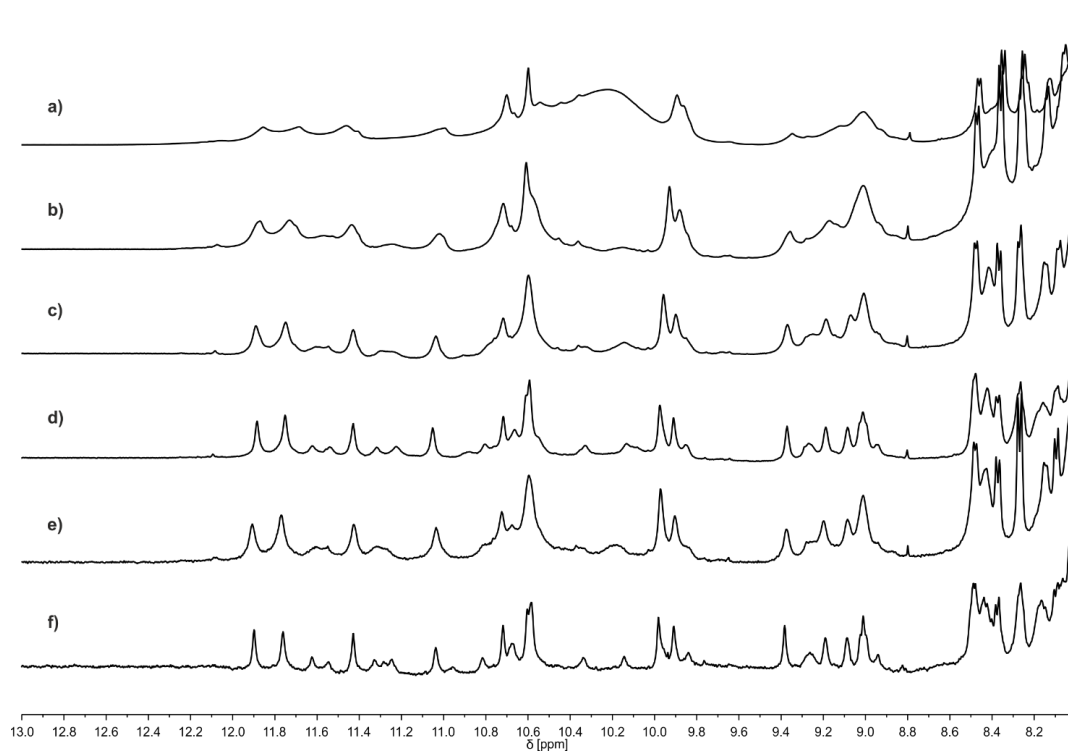


**Figure S15. A single species of **11** prevails over a range of concentrations.** Part of the  $^1\text{H}$  NMR spectra (500 MHz, 25 °C) in  $\text{CDCl}_3$  after 2 weeks showing amide resonances of **11** at 18.49 mM (a), 9.24 mM (b), 4.62 mM (c), 2.31 mM (d), 1.16 mM (e) and 0.58 mM (f), respectively.

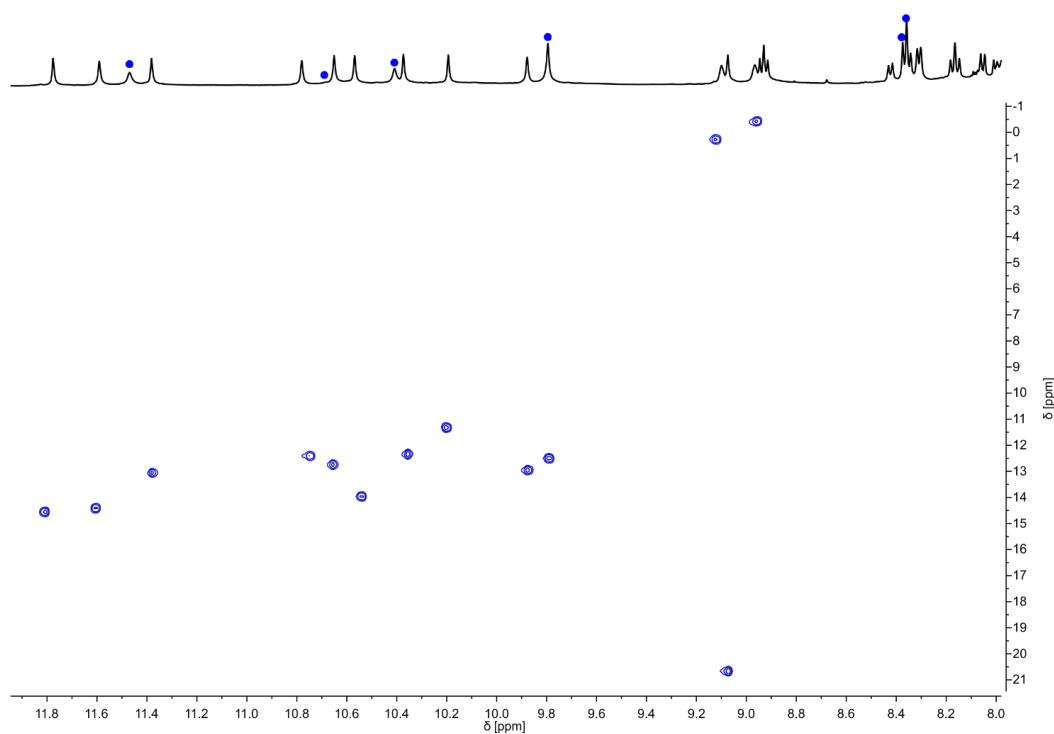


**Figure S16. Identification of hydrogen bonded OH signals of **9** in  $\text{CDCl}_3$ .** Part of the  $^1\text{H}, ^{15}\text{N}$ -HSQC NMR spectra (500 MHz,  $\text{CDCl}_3$ ) at 25 °C showing amide resonances of **9** at 6.28 mM and 2 weeks after pyridine-treatment. Only NH resonances correlate, blue dots indicate the signals of OH protons.

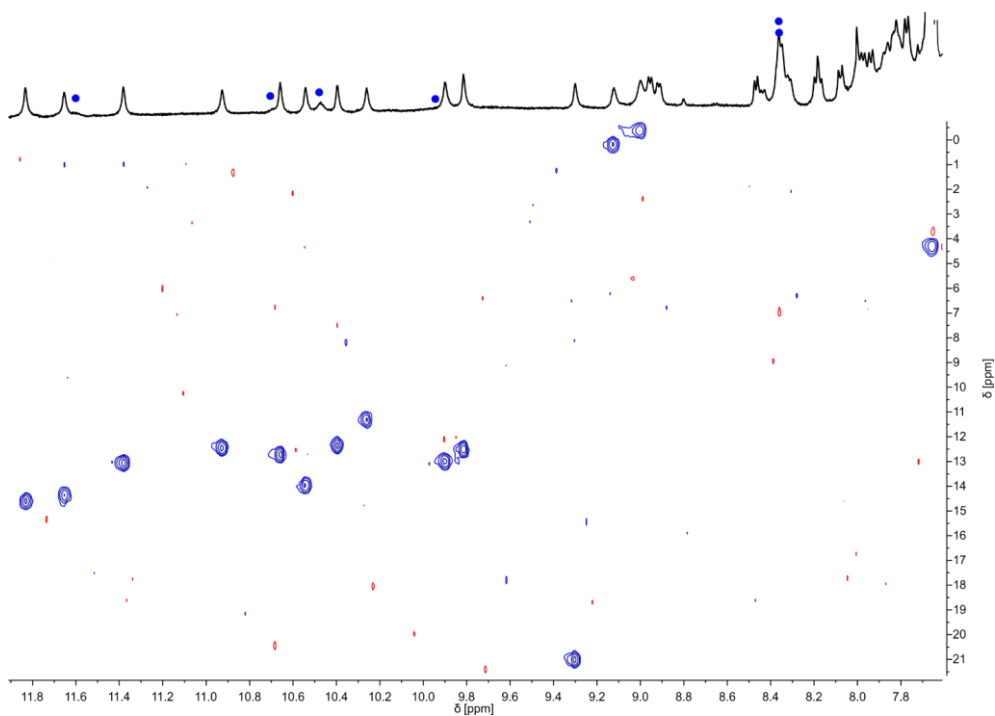


**Figure S17. Identification of hydrogen bonded OH signals of **10** in  $\text{CDCl}_3$ .** Part of the  $^1\text{H}$ ,  $^{15}\text{N}$ -HSQC NMR spectra (500 MHz,  $\text{CDCl}_3$ ) at 25 °C showing amide resonances of **10** at 13.90 mM and 2 weeks after pyridine-treatment. Only NH resonances correlate, blue dots indicate the signals of OH protons.

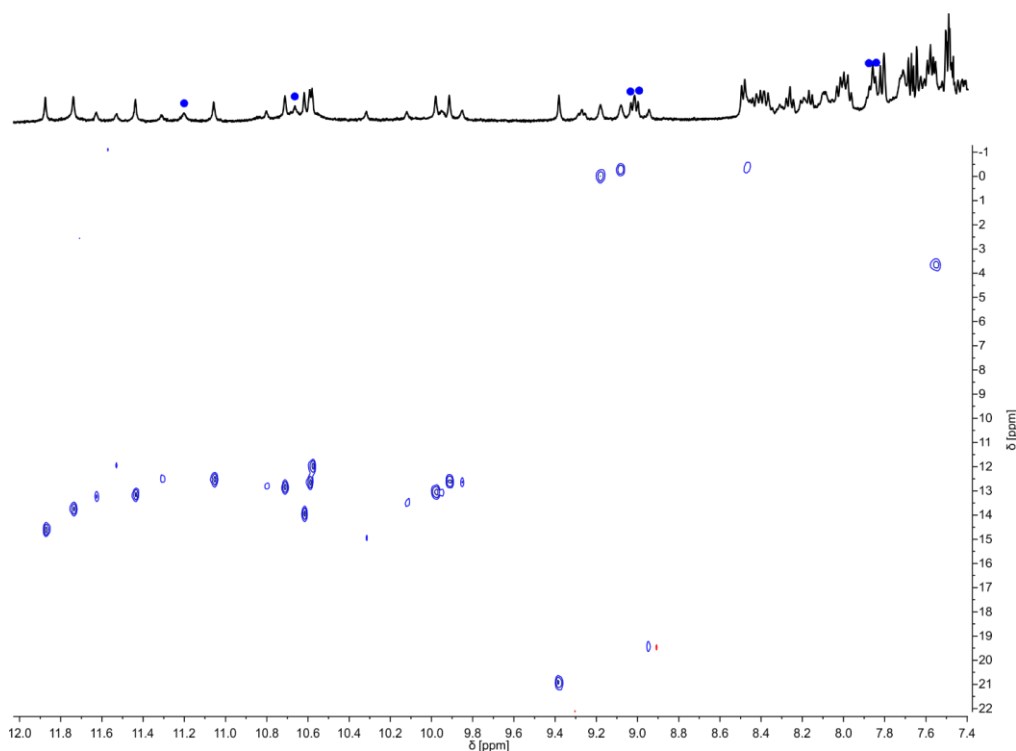


**Figure S18. Identification of hydrogen bonded OH signals of **11** in  $\text{CDCl}_3$ .** Part of the  $^1\text{H}$ ,  $^{15}\text{N}$ -HSQC NMR spectra (500 MHz,  $\text{CDCl}_3$ ) at 25 °C showing amide resonances of **11** at 2.31 mM and 2 weeks after pyridine-treatment. Only NH resonances correlate, blue dots indicate the signals of OH protons.

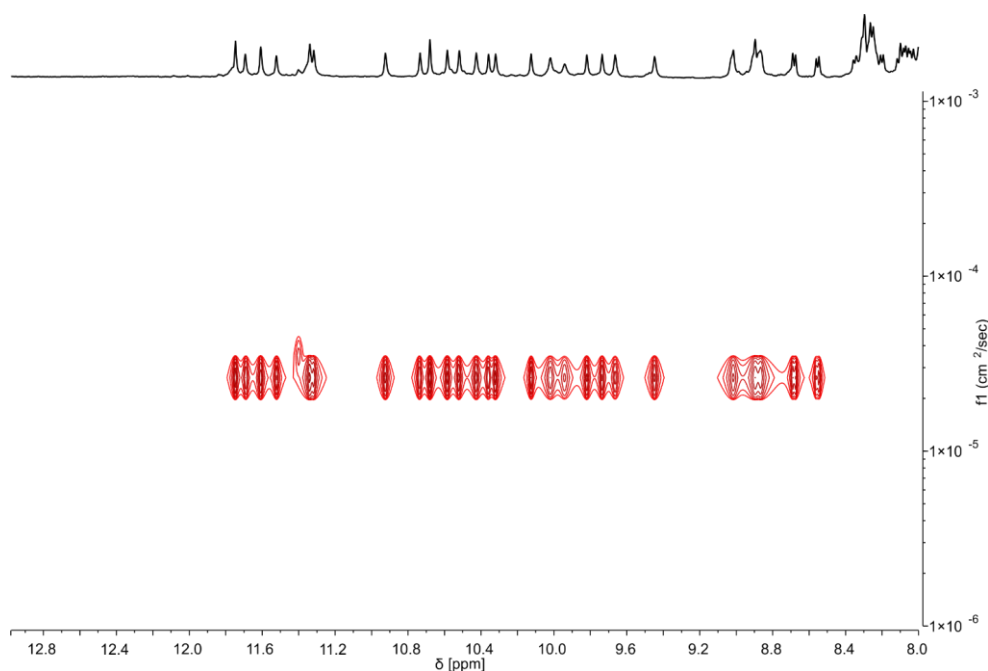


**Figure S19.** Compound **9** has the same hydrodynamic radius as its protected precursor, and is thus monomeric. Extract of  $^1\text{H}$  DOSY (500 MHz,  $\text{CDCl}_3$ ) at 25 °C of a 1 to 1 mixture of **9** and its protected precursor **24** each at 1.62 mM, and after 3 weeks showing amide resonances and hydrogen-bonded hydroxyl groups, respectively.  $\Delta = 115$  ms,  $\delta = 0.6$  ms. The extracted value of the diffusion coefficient of **9** and **24** is  $2.67 \times 10^{-5}$ , each.

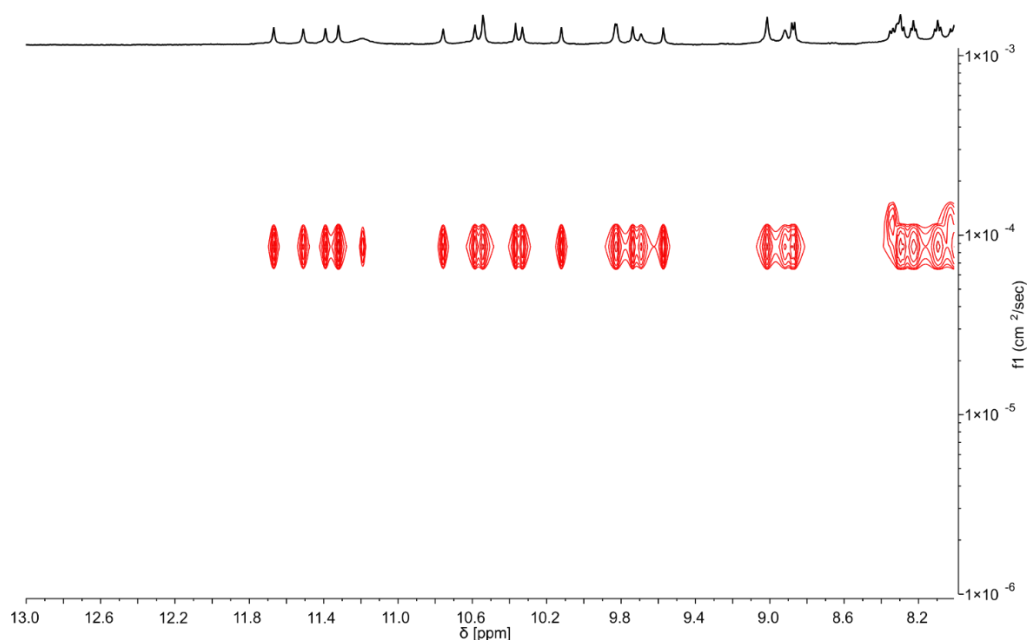


**Figure S20.** Compound **9** has a similar hydrodynamic radius to **10**, **11**, **13**, **15** and **17**. Extract of  $^1\text{H}$  DOSY (500 MHz,  $\text{CDCl}_3$ ) at 25 °C of **9** at 1.62 mM and after 2 weeks showing amide resonances and hydrogen-bonded hydroxyl groups, respectively.  $\Delta = 75$  ms,  $\delta = 0.6$  ms. The extracted value of the diffusion coefficient of **9** is  $8.62 \times 10^{-5}$ .

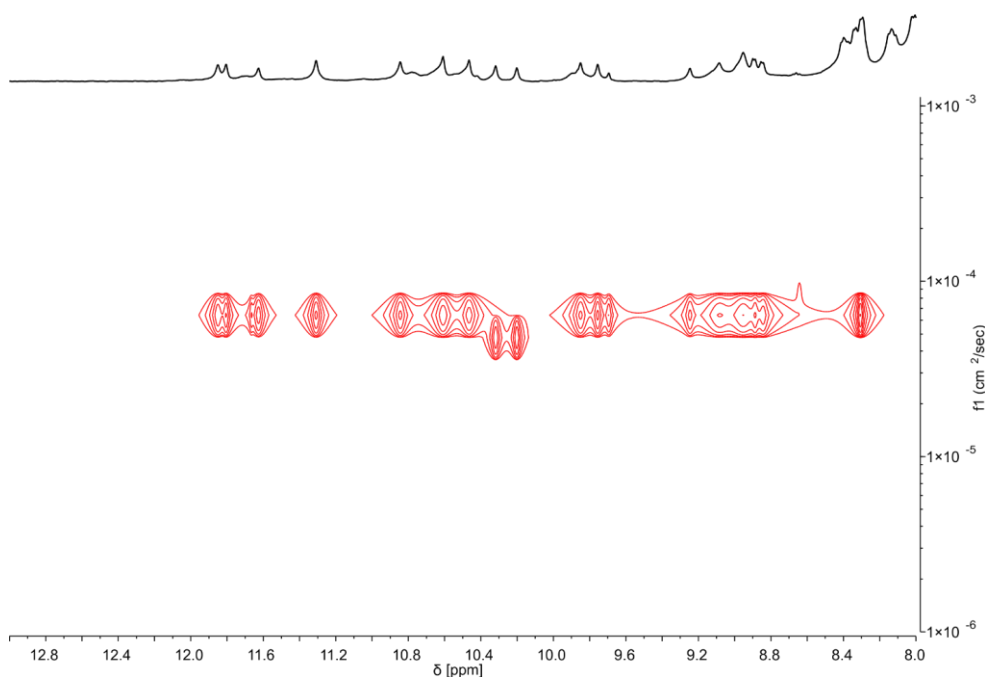


**Figure S21.** Compound **10** has a similar hydrodynamic radius to **9**, **11**, **13**, **15** and **17**. Extract of  $^1\text{H}$  DOSY (500 MHz,  $\text{CDCl}_3$ ) at 25 °C of **10** at 1.62 mM and after 2 weeks showing amide resonances and hydrogen-bonded hydroxyl groups, respectively.  $\Delta = 250$  ms,  $\delta = 0.6$  ms. The extracted value of the diffusion coefficient of **10** is  $6.40 \times 10^{-5}$ .

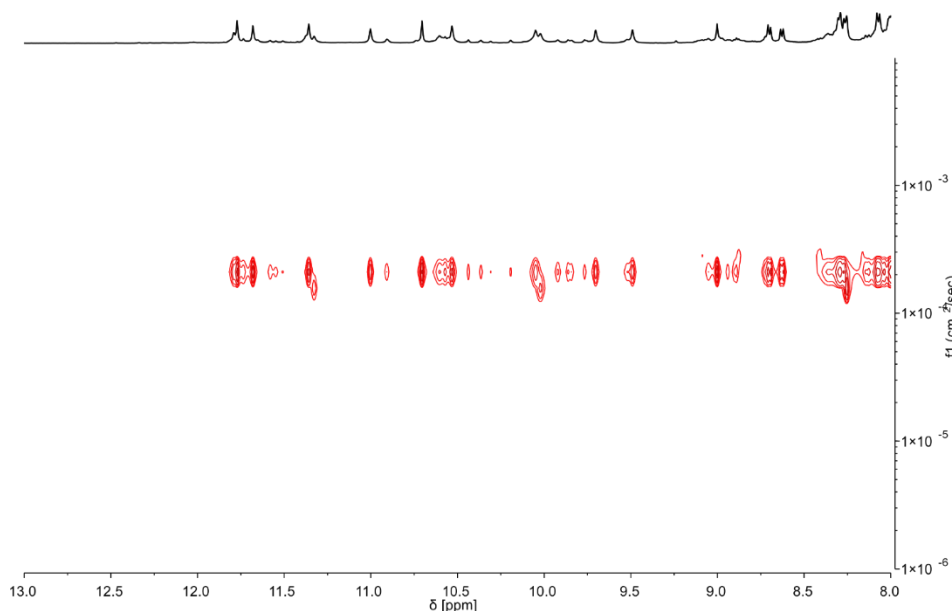


**Figure S22.** Compound **10** has the same hydrodynamic radius as its protected precursor, and is thus monomeric. Extract of  $^1\text{H}$  DOSY (500 MHz,  $\text{CDCl}_3$ ) at 25 °C of a 1 to 1 mixture of **10** and its protected precursor **26** at 1.39 mM, each and after 2 days showing amide resonances and hydrogen-bonded hydroxyl groups, respectively. Here signals corresponding to **10** are more broad.  $\Delta = 250$  ms,  $\delta = 0.6$  ms. The extracted value of the diffusion coefficient of **10** and **26** is  $2.10 \times 10^{-4}$ , each.

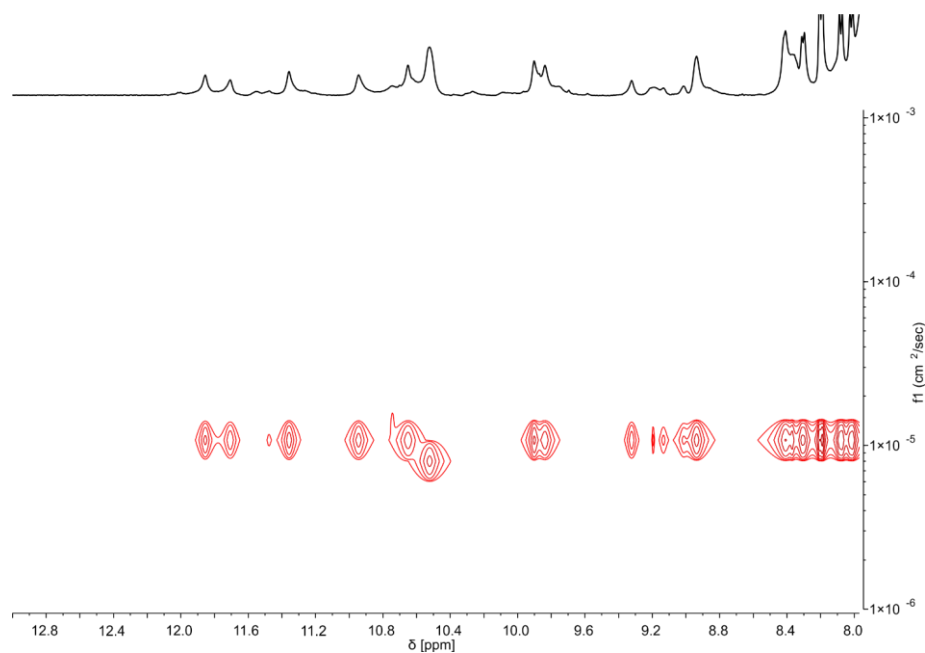


**Figure S23.** Compound **11** has a similar hydrodynamic radius to **9**, **10**, **13**, **15** and **17**, and is thus monomeric. Extract of  $^1\text{H}$  DOSY (400 MHz,  $\text{CDCl}_3$ ) at  $25\text{ }^\circ\text{C}$  of **11** at 1.39 mM and after 2 weeks showing amide resonances and hydrogen-bonded hydroxyl groups, respectively.  $\Delta = 200\text{ ms}$ ,  $\delta = 0.6\text{ ms}$ . The extracted value of the diffusion coefficient of **11** is  $1.08 \times 10^{-5}$ .

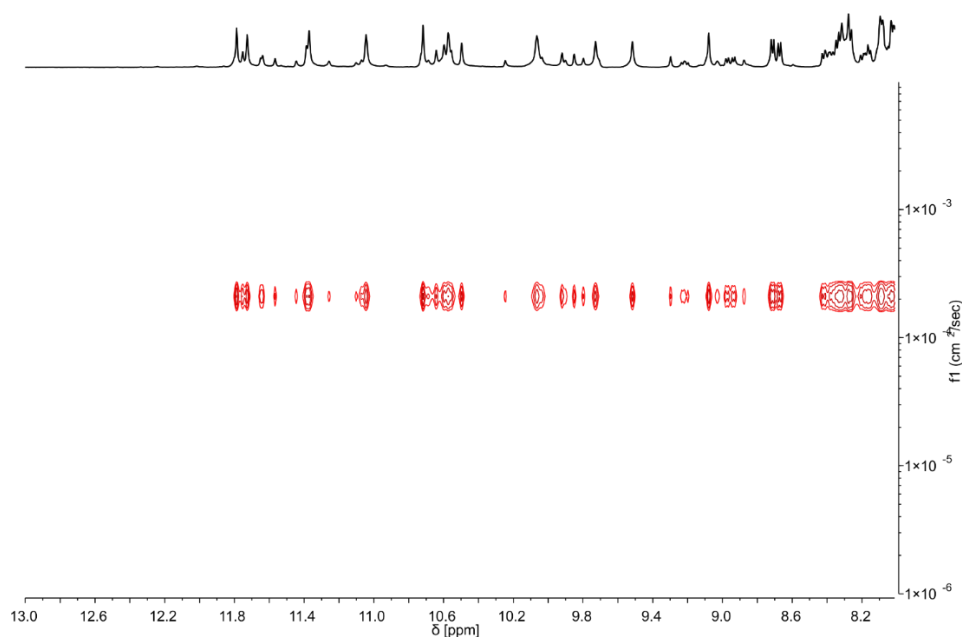


**Figure S24.** Compound **11** has the same hydrodynamic radius as its protected precursor, and is thus monomeric. Extract of  $^1\text{H}$  DOSY (500 MHz,  $\text{CDCl}_3$ ) at  $25\text{ }^\circ\text{C}$  of a 1 to 1 mixture of **11** and its protected precursor **28** at 1.39 mM, each and after 12 hours showing amide resonances and hydrogen-bonded hydroxyl groups, respectively. Here signals corresponding to **11** are more broad and a 2<sup>nd</sup> species is formed.  $\Delta = 200\text{ ms}$ ,  $\delta = 0.6\text{ ms}$ . The extracted value of the diffusion coefficient of **11** and **28** is  $2.10 \times 10^{-4}$ , each.

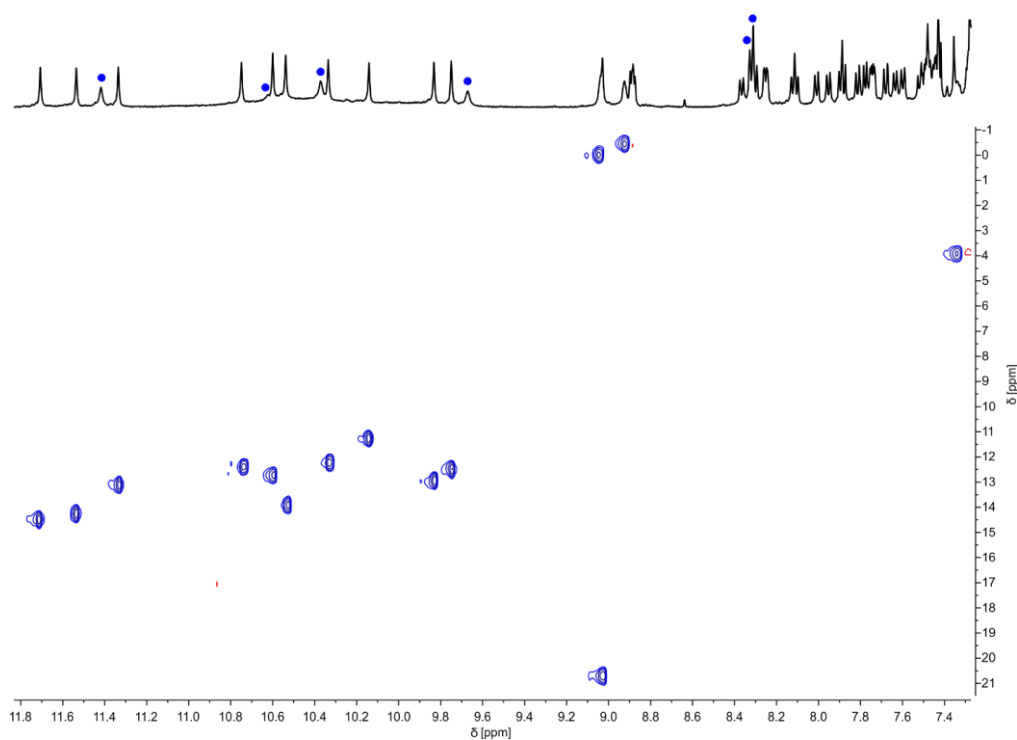


**Figure S25. Identification of hydrogen bonded OH signals of **12** in  $\text{CDCl}_3$ .** Part of the  $^1\text{H}, ^{15}\text{N}$ -HSQC NMR spectra (500 MHz,  $\text{CDCl}_3$ ) at 25 °C showing amide resonances of **12** at 15.04 mM and 2 weeks after pyridine-treatment. Only NH resonances correlate, blue dots indicate the signals of OH protons.

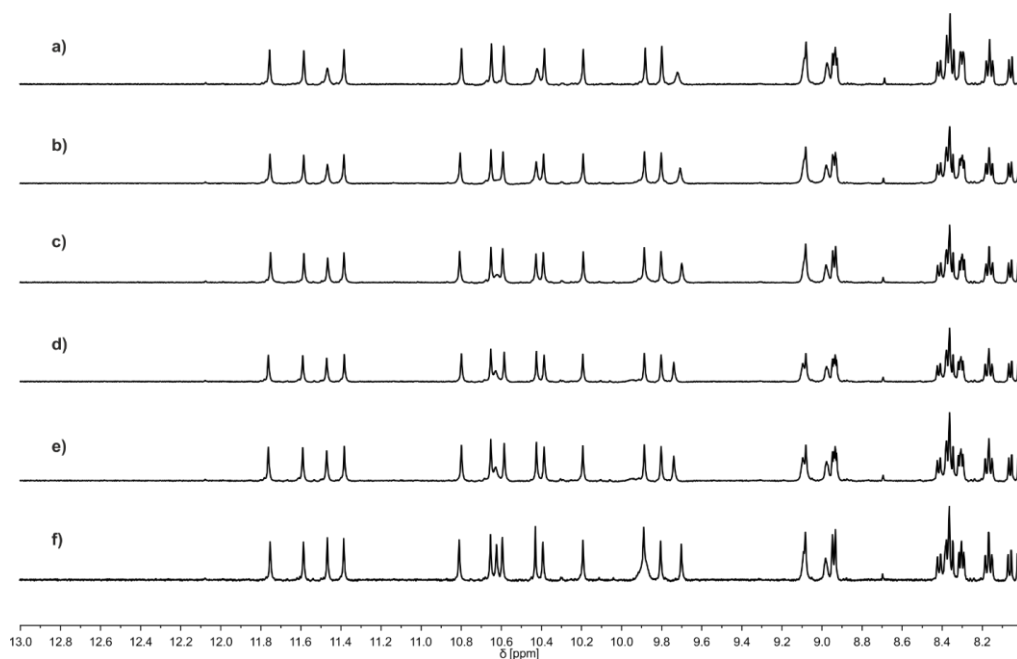


**Figure S26. The spectrum of **12** does not depend on concentration.** Part of the  $^1\text{H}$  NMR spectra (500 MHz, 25 °C) in  $\text{CDCl}_3$  after 2 weeks showing amide resonances of **12** at 15.04 mM (a), 7.52 mM (b), 3.76 mM (c), 1.88 mM (d), 0.94 mM (e) and 0.47 mM (f), respectively.



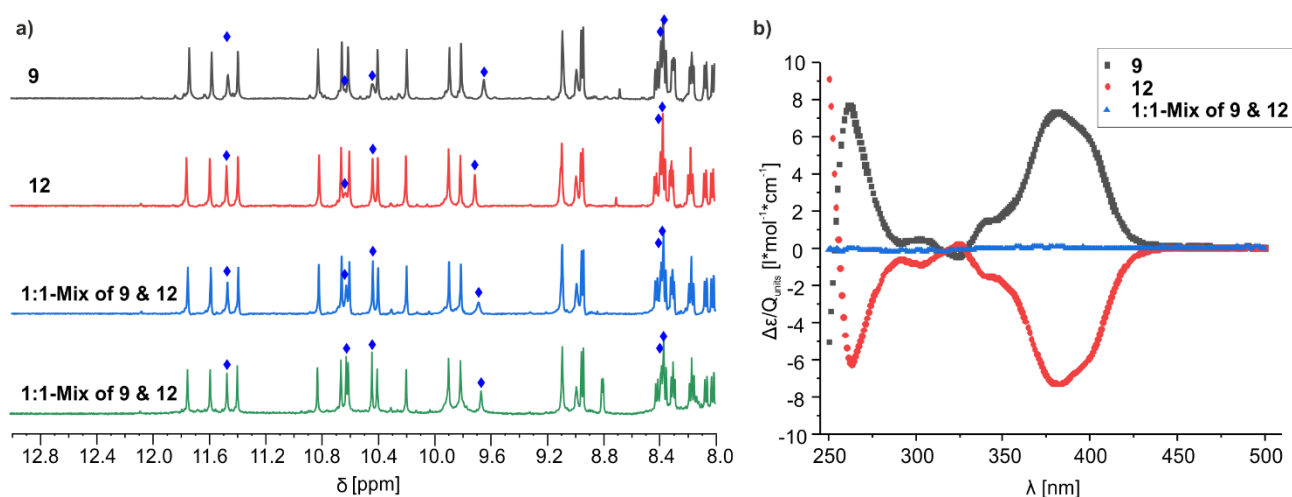


**Figure S27. Compound 9 and 12 form the enantiomeric species and fold without interfering with one another.** Extracts of  $^1\text{H}$  NMR spectra (500 MHz, 25  $^\circ\text{C}$ ) of **9**, **12** and a 1:1-mixture of **9** and **12** in  $\text{CDCl}_3$  at 2.3 mM (in total) each before (blue) and after disruption by pyridine (green) showing the amide region and hydrogen-bonded hydroxyl groups (a). CD spectra of **9**, **12** and a 1:1-mixture of **9** and **12** in  $\text{CHCl}_3$  before disruption by pyridine between 250 and 500 nm (b). The molar extinction ( $\Delta\epsilon$ ) is normalized for the number of Q units for better comparability.

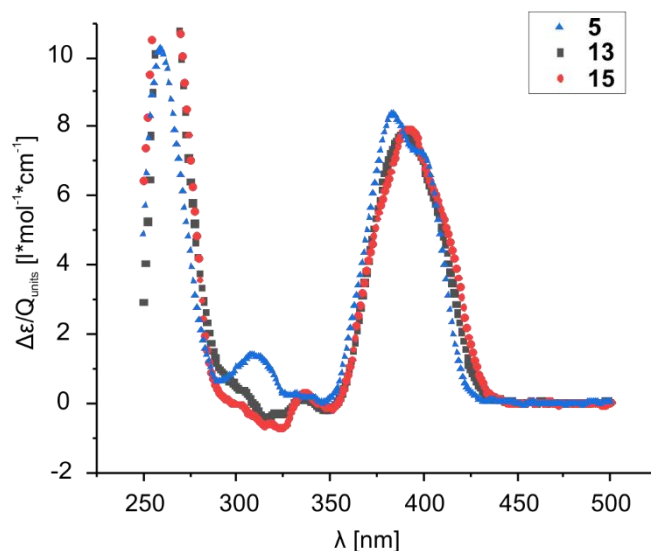


**Figure S28. Assignment of P-helicity in 13 and 15.** CD spectra of **5**, **13** and **15** in chloroform between 250 and 500 nm at 25  $^\circ\text{C}$ . The molar extinction ( $\Delta\epsilon$ ) is normalized for the number of Q units for better comparability.

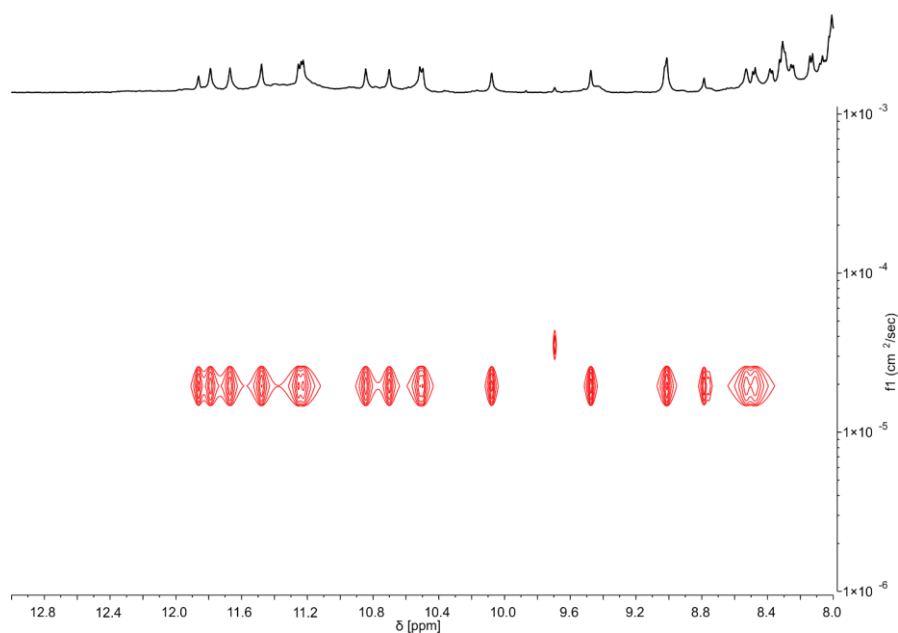


**Figure S29.** Compound **13** has a similar hydrodynamic radius to **9**, **10**, **11**, **15** and **17**, and is thus **monomeric**. Extract of  $^1\text{H}$  DOSY (400 MHz,  $\text{CDCl}_3$ ) at 25 °C of **13** at 1.62 mM and after 2 weeks showing amide resonances and hydrogen-bonded hydroxyl groups, respectively.  $\Delta = 275$  ms,  $\delta = 0.6$  ms. The extracted value of the diffusion coefficient of **13** is  $1.95 \times 10^{-5}$ .

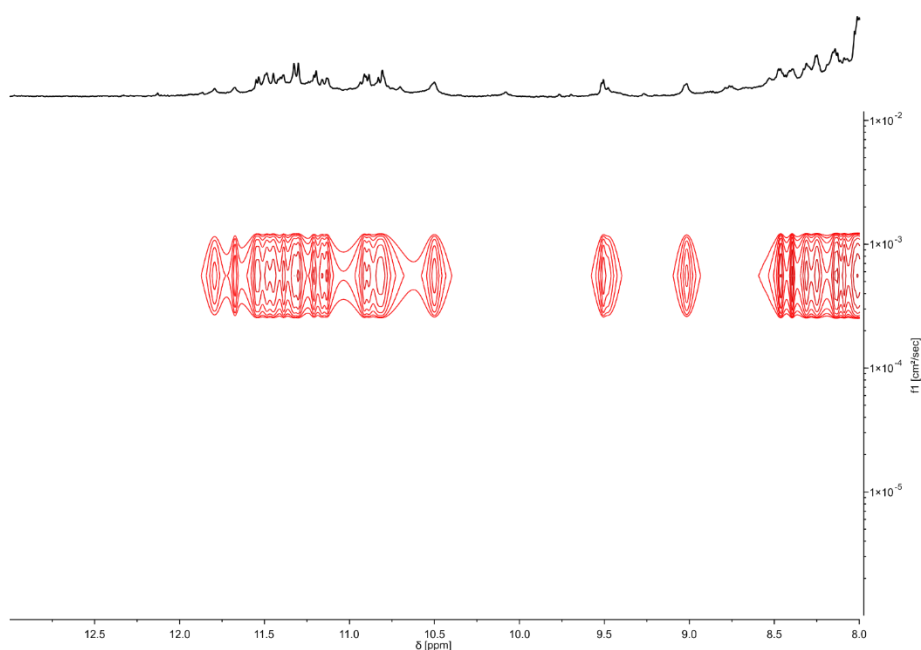


**Figure S30.** Compound **13** has the same hydrodynamic radius as its protected precursor, and is thus **monomeric**. Extract of  $^1\text{H}$  DOSY (500 MHz,  $\text{CDCl}_3$ ) at 25 °C of a 1 to 1 mixture of **13** and its protected precursor **32** at 0.74 mM, each and after 4 days showing amide resonances and hydrogen-bonded hydroxyl groups, respectively. Here some signals corresponding to **13** appear more broad.  $\Delta = 275$  ms,  $\delta = 0.6$  ms. The extracted value of the diffusion coefficient of **13** and **32** is  $5.56 \times 10^{-4}$ , each.

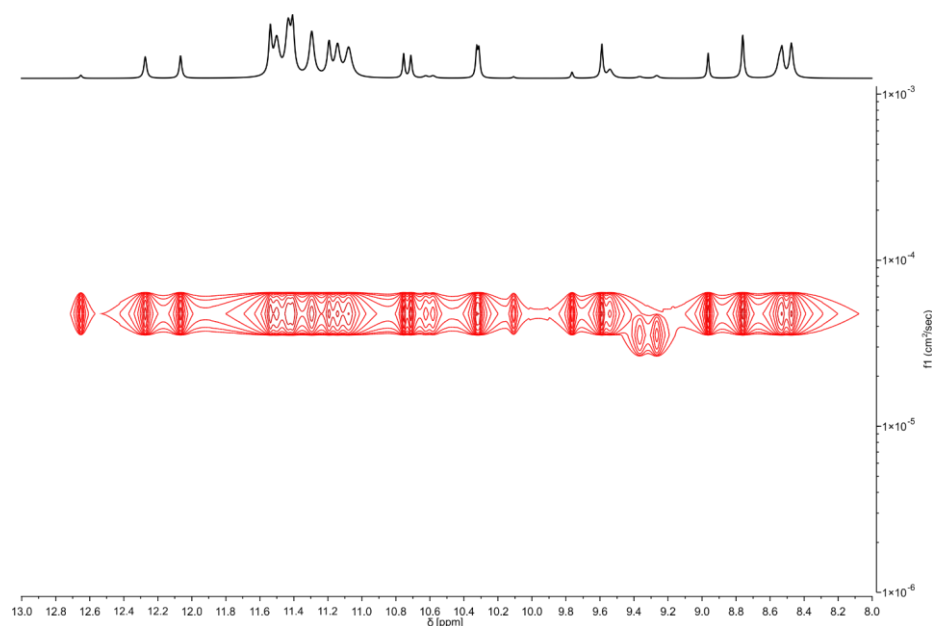


**Figure S31.** Compound **15** has a similar hydrodynamic radius to **9**, **10**, **11**, **13** and **17**, and is thus monomeric. Extract of  $^1\text{H}$  DOSY (500 MHz,  $\text{CDCl}_3$ ) at 25 °C of **15** at 1.62 mM and after 2 weeks showing amide resonances and hydrogen-bonded hydroxyl groups, respectively.  $\Delta = 100$  ms,  $\delta = 0.6$  ms. The extracted value of the diffusion coefficient of **15** is  $4.76 \times 10^{-5}$ .

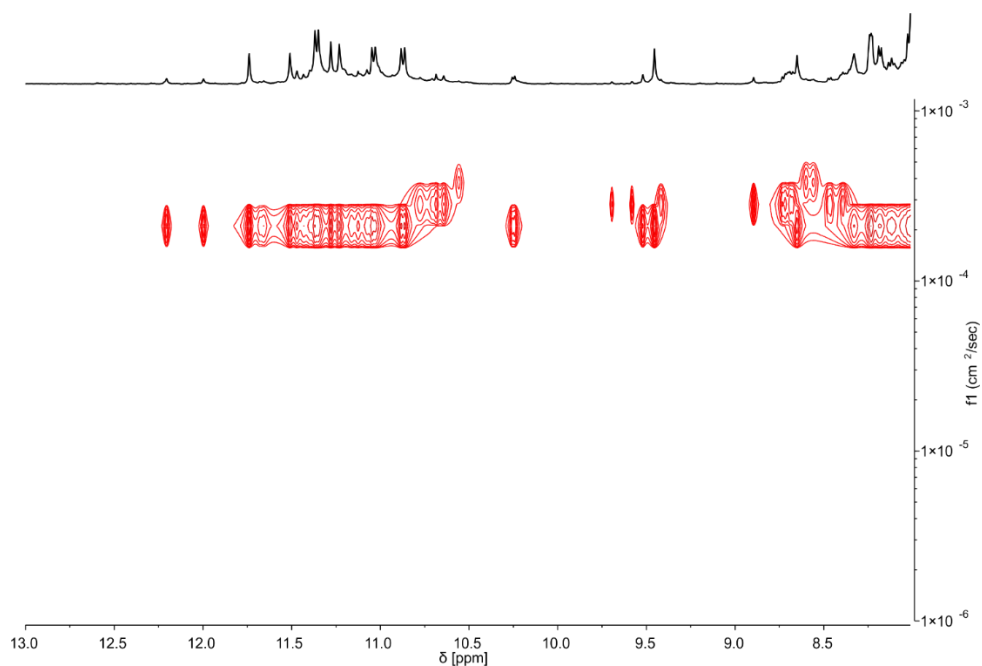


**Figure S32.** Compound **15** has the same hydrodynamic radius as its protected precursor, and is thus monomeric. Extract of  $^1\text{H}$  DOSY (500 MHz,  $\text{CDCl}_3$ ) at 25 °C of a 1 to 1 mixture of **15** and its protected precursor **36** at 0.4 mM and 1.39 mM, respectively and after 1 week showing amide resonances and hydrogen-bonded hydroxyl groups, respectively.  $\Delta = 275$  ms,  $\delta = 0.6$  ms. The extracted value of the diffusion coefficient of **15** and **36** is  $2.11 \times 10^{-4}$ , each.

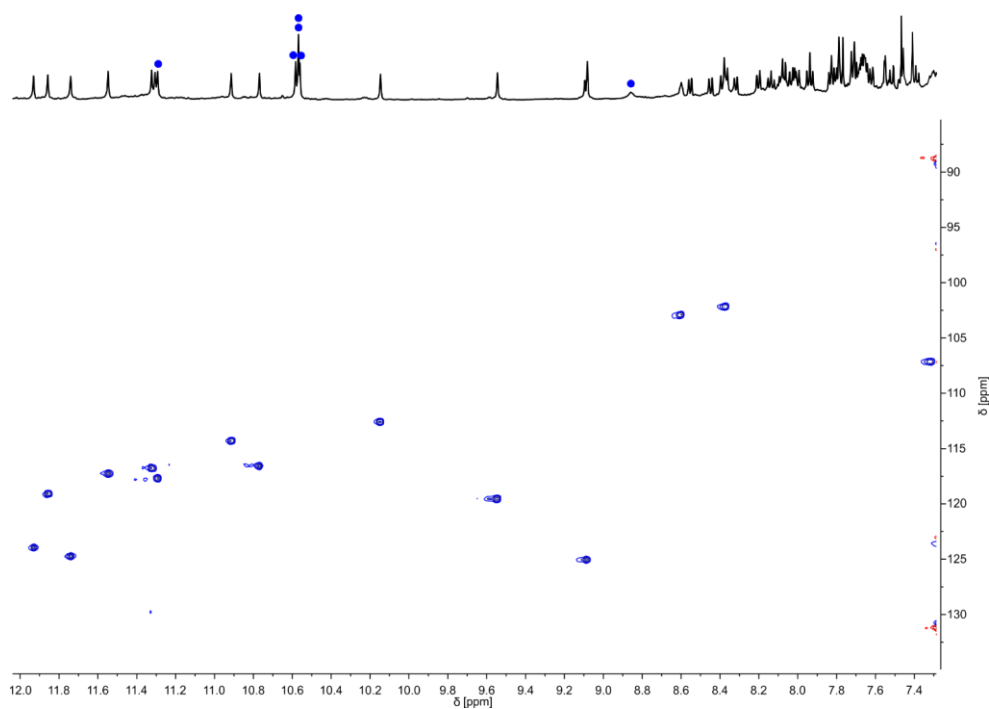


**Figure S33. Identification of hydrogen bonded OH signals of **13** in  $\text{CDCl}_3$ .** Part of the  $^1\text{H}, ^{15}\text{N}$ -HSQC NMR spectra (500 MHz,  $\text{CDCl}_3$ ) at 25 °C showing amide resonances of **13** at 7.73 mM and 2 weeks after pyridine-treatment. Only NH resonances correlate, blue dots indicate the signals of OH protons.

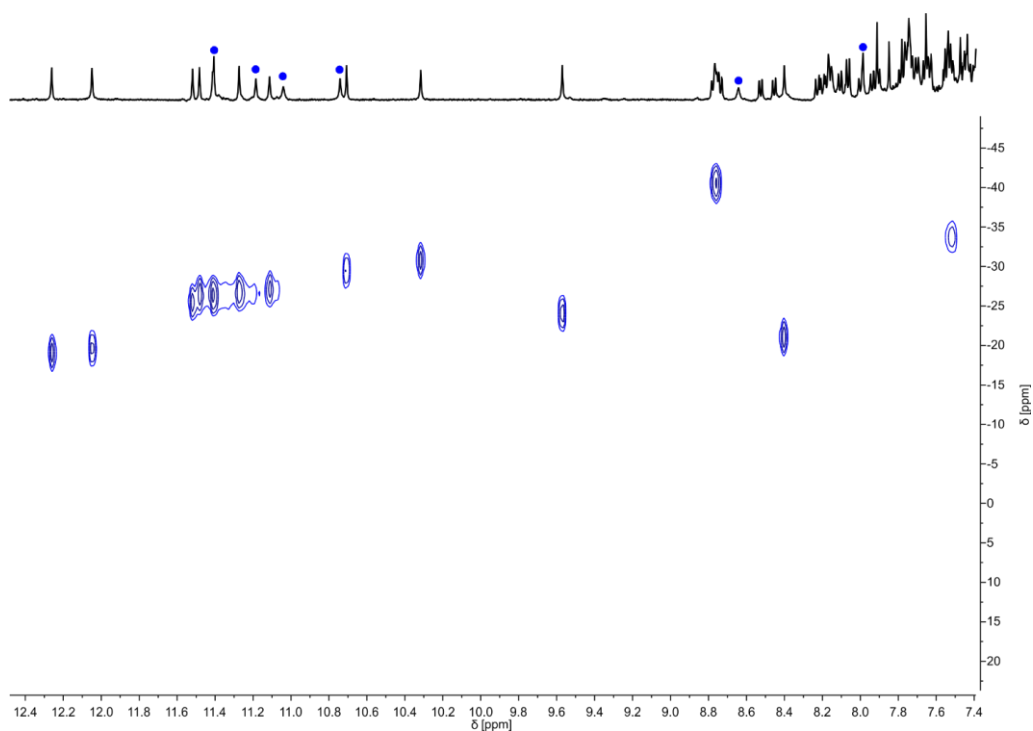


**Figure S34. Identification of hydrogen bonded OH signals of **15** in  $\text{CDCl}_3$ .** Part of the  $^1\text{H}, ^{15}\text{N}$ -HSQC NMR spectra (500 MHz,  $\text{CDCl}_3$ ) at 25 °C showing amide resonances of **15** at 9.0 mM and 2 weeks after pyridine-treatment. Only NH resonances correlate, blue dots indicate the signals of OH protons.

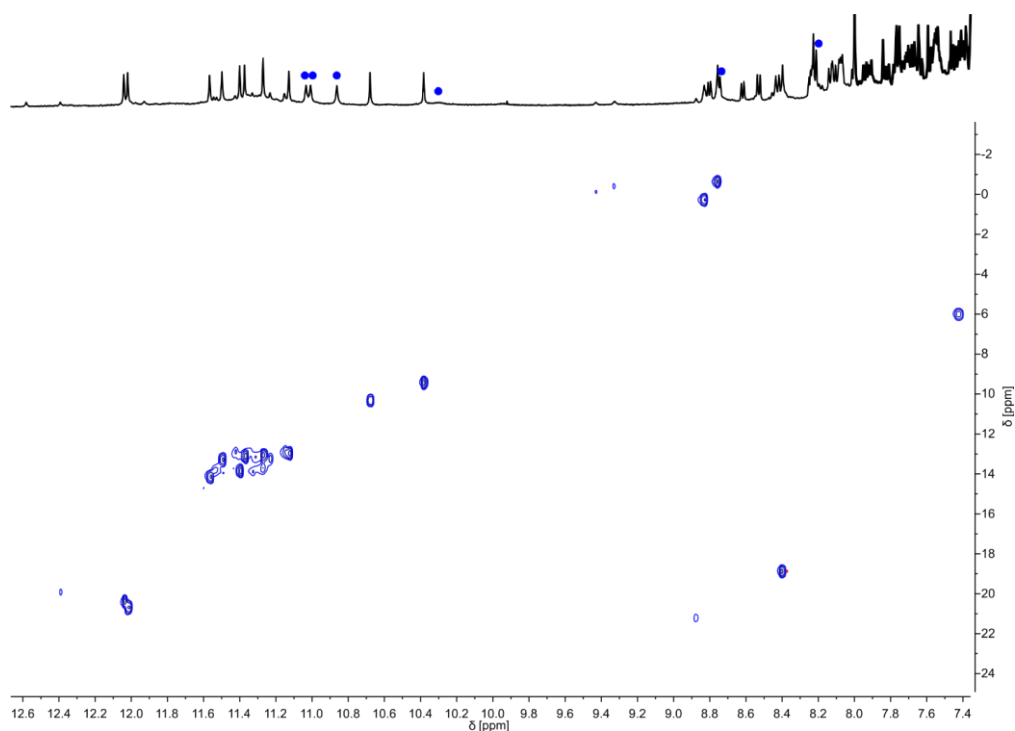


**Figure S35. Identification of hydrogen bonded OH signals of **17** in  $\text{CDCl}_3$ .** Part of the  $^1\text{H}, ^{15}\text{N}$ -HSQC NMR spectra (500 MHz,  $\text{CDCl}_3$ ) at 25 °C showing amide resonances of **17** at 7.73 mM and 2 weeks after pyridine-treatment. Only NH resonances correlate, blue dots indicate the signals of OH protons.

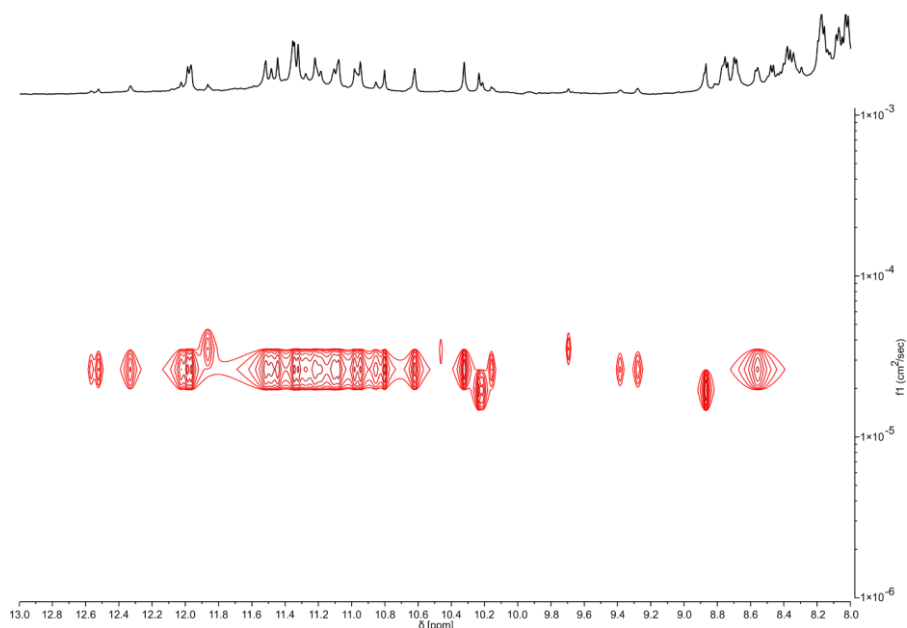


**Figure S36.** Compound **17** has a similar hydrodynamic radius to **9-11, 13 & 15**, and is thus monomeric. Extract of  $^1\text{H}$  DOSY (500 MHz,  $\text{CDCl}_3$ ) at  $25\text{ }^\circ\text{C}$  of **17** at 1.62 mM and after 2 weeks showing amide resonances and hydrogen-bonded hydroxyl groups, respectively.  $\Delta = 100\text{ ms}$ ,  $\delta = 1.0\text{ ms}$ . The extracted value of the diffusion coefficient of **17** is  $2.63 \times 10^{-5}$ .

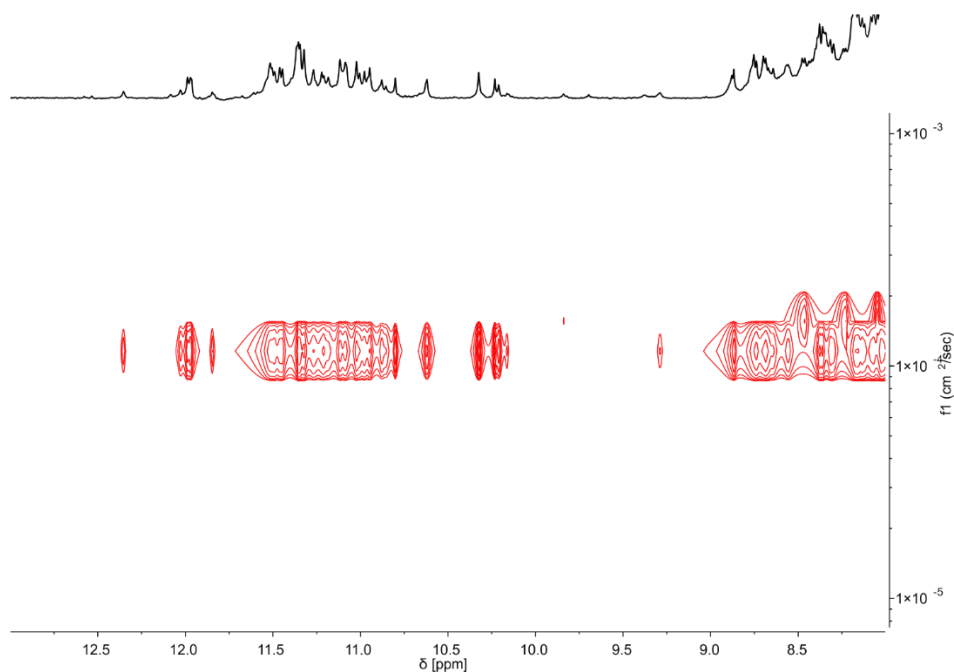


**Figure S37.** Compound **17** has the same hydrodynamic radius as its protected precursor, and is thus monomeric. Extract of  $^1\text{H}$  DOSY (500 MHz,  $\text{CDCl}_3$ ) at  $25\text{ }^\circ\text{C}$  of a 1 to 1 mixture of **17** and its protected precursor **40** at 0.45 mM, each and after 1 week showing amide resonances and hydrogen-bonded hydroxyl groups, respectively.  $\Delta = 110\text{ ms}$ ,  $\delta = 1.0\text{ ms}$ . The extracted value of the diffusion coefficient of **17** and **40** is  $1.16 \times 10^{-4}$ , each.

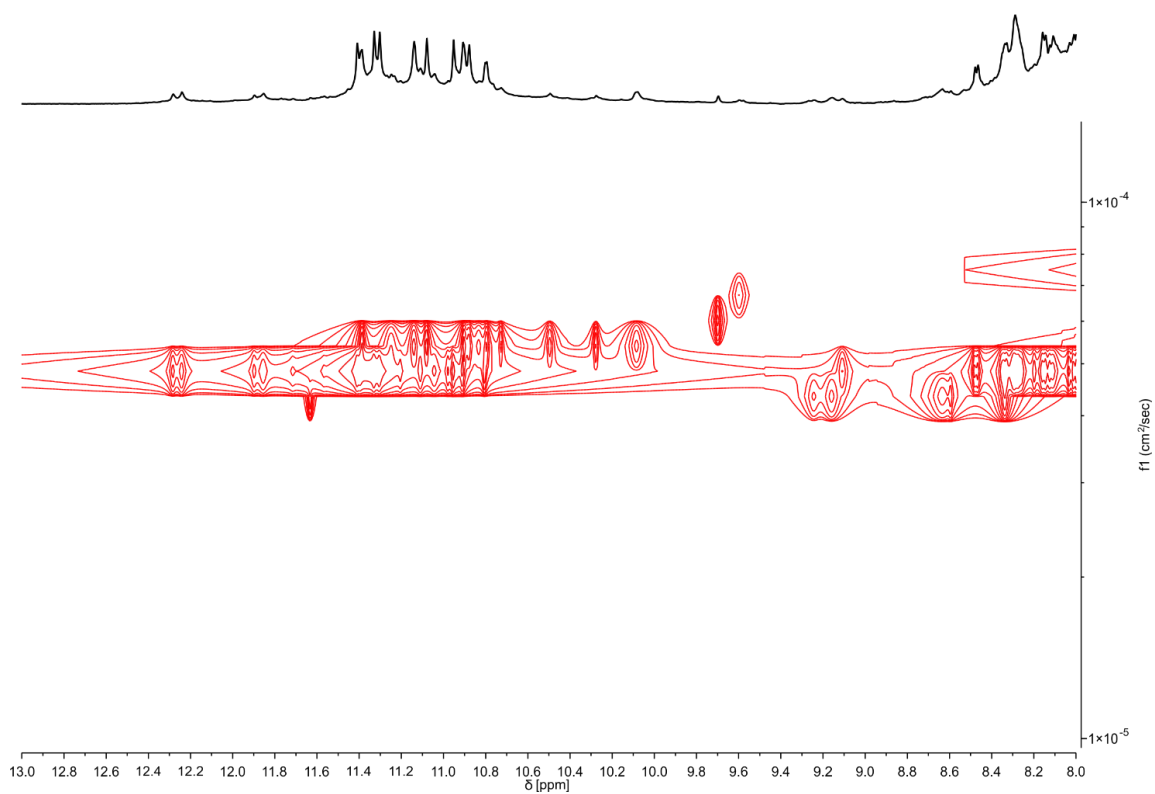


**Figure S38. Compound 16 has a different hydrodynamic radius from its protected precursor.** Extract of  $^1\text{H}$  DOSY (500 MHz,  $\text{CDCl}_3$ ) at 25 °C of a 1 to 1 mixture of **16** and its protected precursor **38** at 3.24 mM, respectively and after 3 weeks showing amide resonances and hydrogen-bonded hydroxyl groups, respectively.  $\Delta = 110$  ms,  $\delta = 1.0$  ms. The extracted value of the diffusion coefficient of **16** and **38** is  $4.81 \times 10^{-5}$  and  $5.32 \times 10^{-5}$ , respectively.

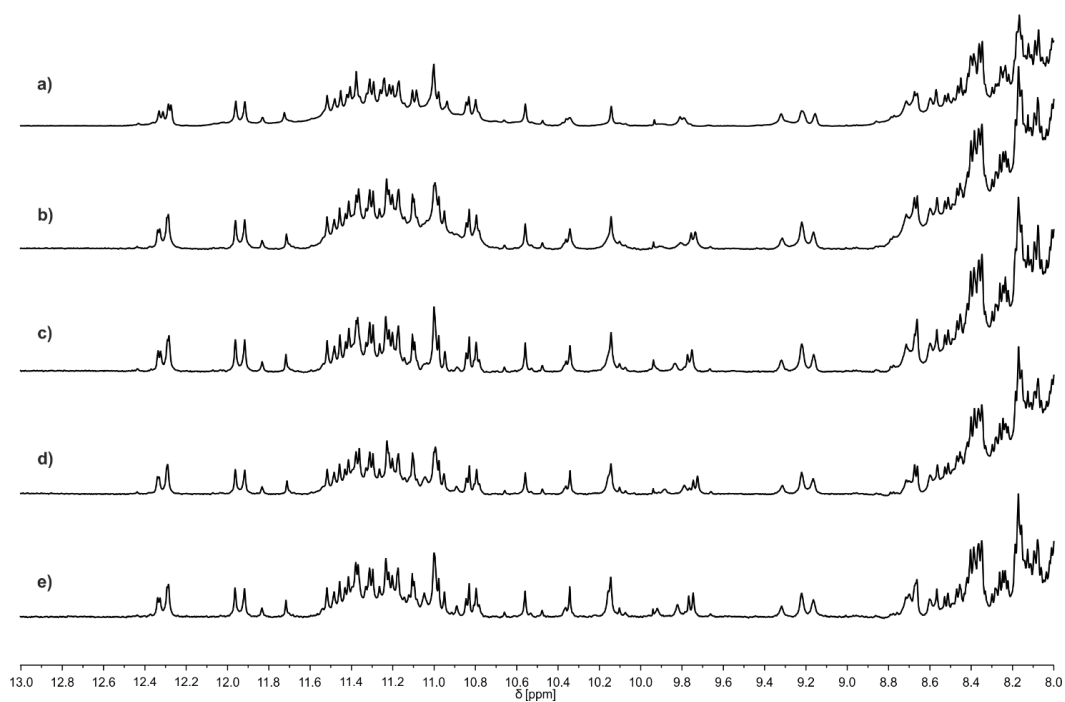


**Figure S39.** The spectrum of **16** does not depend on concentration. Part of the  $^1\text{H}$  NMR spectra (500 MHz, 25 °C) in  $\text{CDCl}_3$  after 2 weeks showing amide resonances of **16** at 7.41 mM (a), 3.70 mM (b), 1.85 mM (c), 0.93 mM (d) and 0.46 mM (e), respectively.

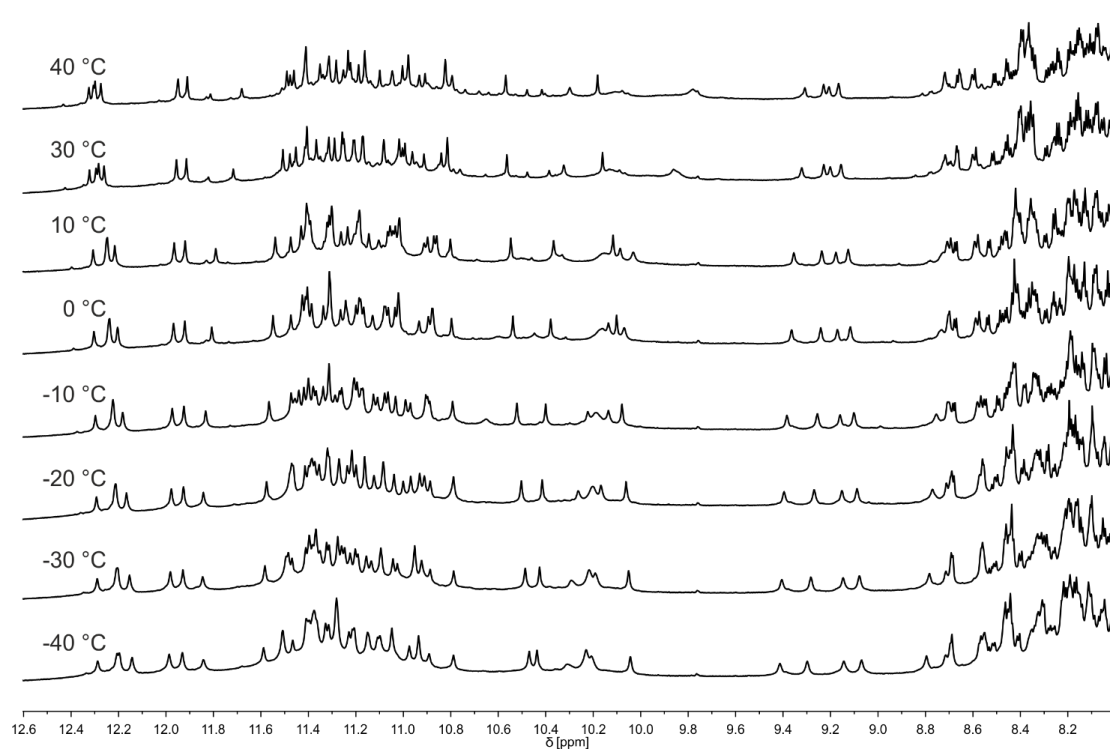


**Figure S40.** The aggregate formed by **16** is stable over a wide range of temperature. Part of the 800 MHz  $^1\text{H}$  NMR spectra of **16** (6.90 mM in  $\text{CDCl}_3$ ) showing the amide and hydroxy proton resonances at different temperatures. The corresponding temperatures are indicated at left.



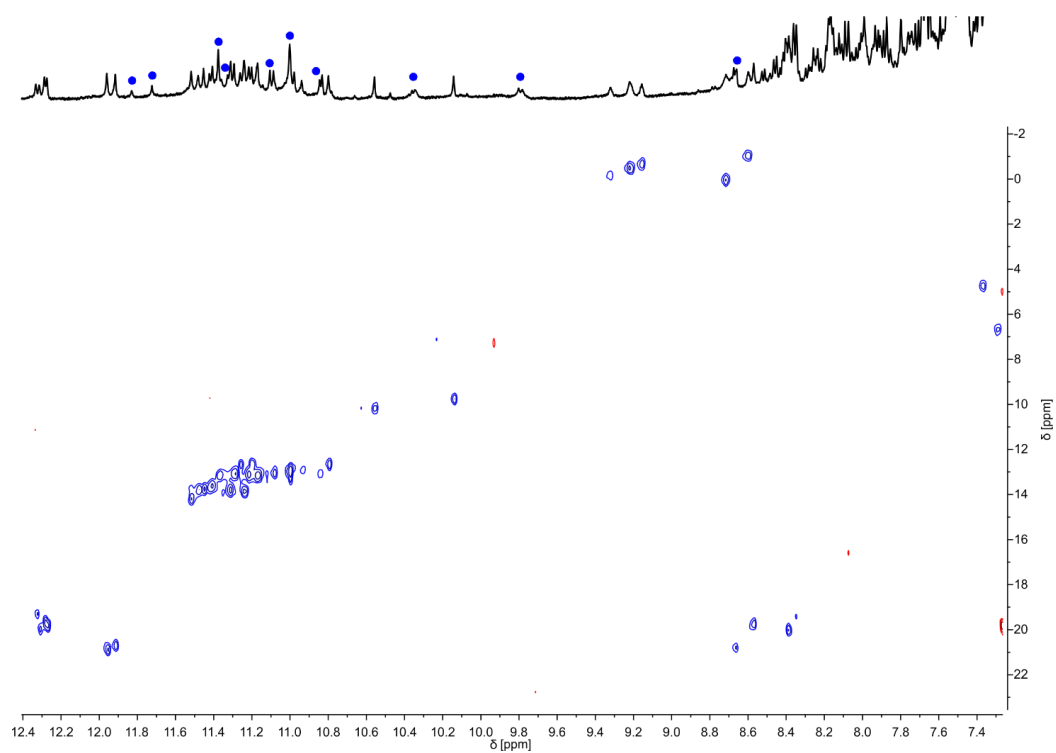


**Figure S41. Identification of hydrogen bonded OH signals of **16** in  $\text{CDCl}_3$ .** Part of the  $^1\text{H}, ^{15}\text{N}$ -HSQC NMR spectra (500 MHz,  $\text{CDCl}_3$ ) at 25 °C showing amide resonances of **16** at 7.73 mM after a two-week incubation. Only NH resonances correlate, blue dots indicate the signals of OH protons.

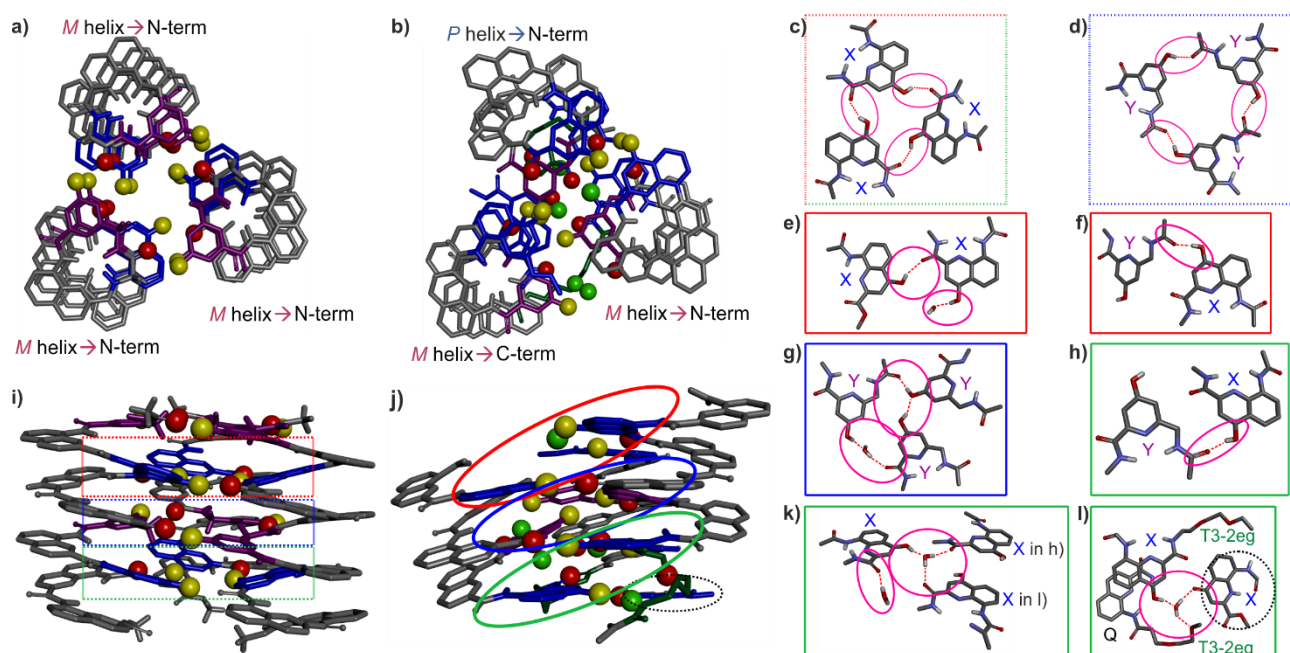


**Figure S42. Comparison of the previously described trimeric bundle<sup>1</sup> and the one found in the crystal structure of **16**.** Top- (a) and side-view (i) of crystal structure and hydrogen-bonding patterns (c & d) of a trimer of **2**.<sup>1</sup> Top- (b) and side-view (j) of crystal structure and hydrogen-bonding patterns (e-h, k, l) of the distorted trimeric hydrogen bonding interface of **16**. Hydrogen bonds found in the distorted trimer in **16** are marked with boxes in the corresponding color in j. Here hydrogen bonds at the same level as in the trimer of **2** are marked in the same color. Hydrogen bonds belonging to **2** are marked with boxes using dashed lines in the same colors. The X-unit belonging to helices of the dimeric hydrogen bonding interface is marked with a black circle in j & l. The hydroxy groups and carbonyl groups of the hydrogen-bonding arrays are shown as yellow and red balls, respectively. Water molecules are shown as green balls. X-units, Y-units and linker units are shown in blue, violet and green tubes, respectively. Included solvent molecules, hydrogens and other side-chains are omitted for clarity.

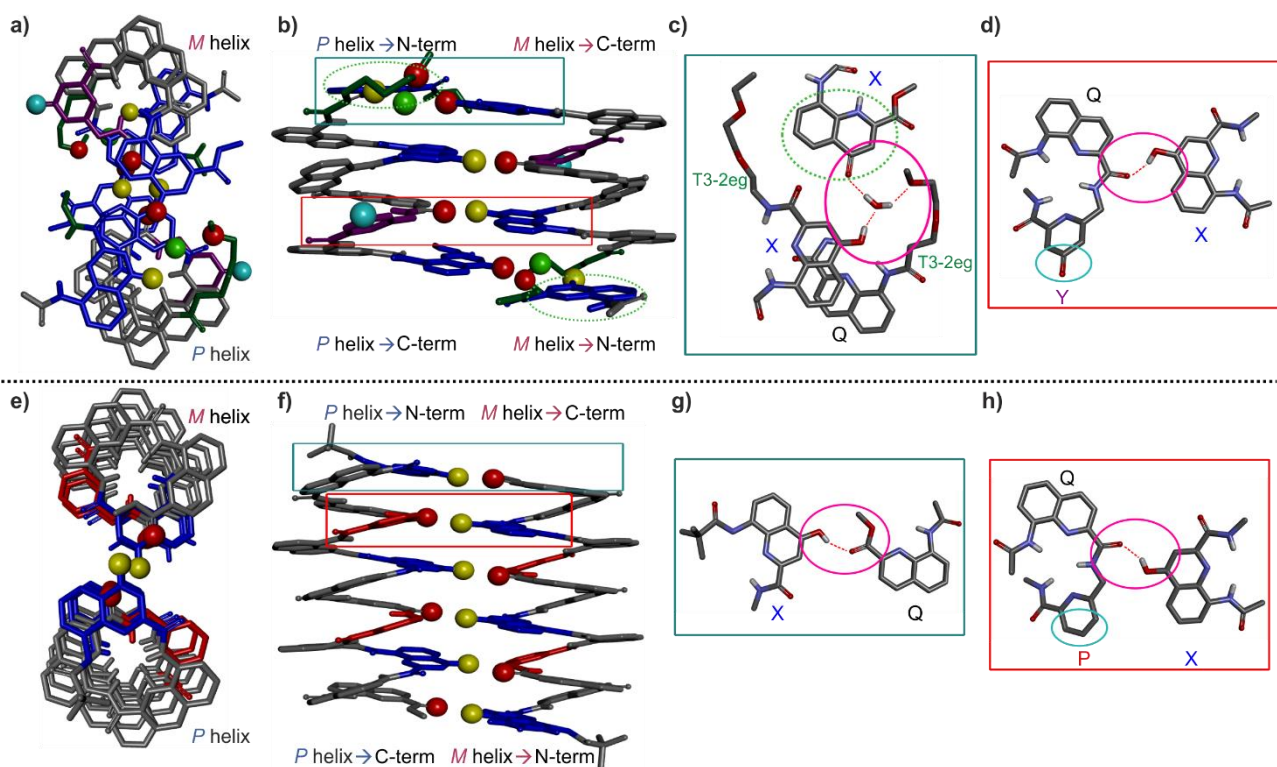


**Figure S43.** Comparison of the previously described dimeric bundle<sup>4</sup> and the one found in the crystal structure of **16**. Top- (a) and side-view (b) of crystal structure and hydrogen-bonding patterns (c & d) of the shifted head-to-tail PM dimeric hydrogen bonding interface of **16**. Top- (e) and side-view (f) of crystal structure and hydrogen-bonding patterns (g & h) of a shifted head-to-tail PM dimer of **3**.<sup>4</sup> The hydroxyl protons and carbonyl oxygen atoms of the hydrogen-bonding arrays are shown as yellow and red balls, respectively. Water molecules are shown as green balls. The X-units are shown in blue and the Y units in violet tubes. Included solvent molecules, hydrogens and other side-chains are omitted for clarity.

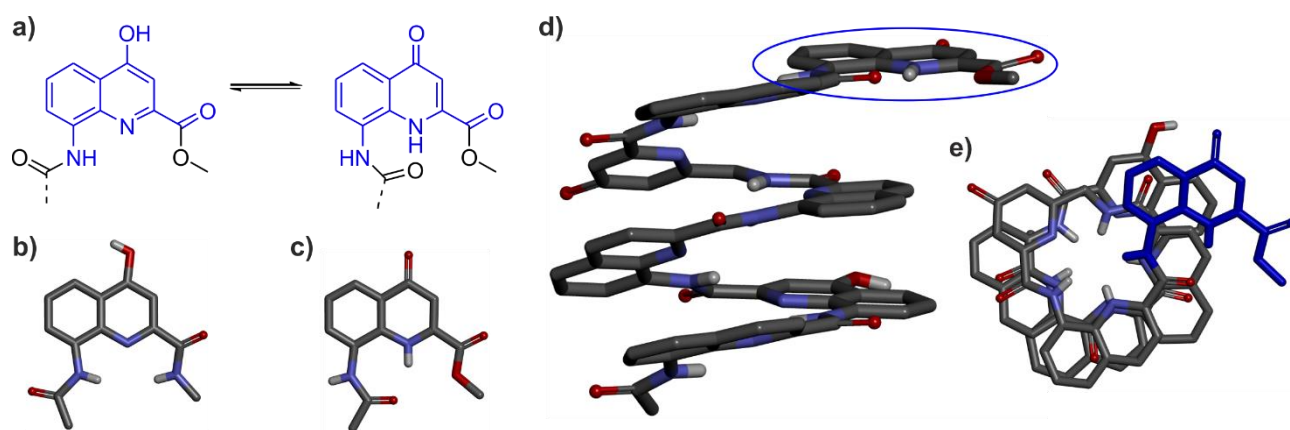


**Figure S44. A flipped X unit in its quinolinone tautomeric form was found in the structure of 16.** Quinoline-quinolinone-equilibrium of a C-terminal X-unit belonging to a B and B'-domain (a). Part of the crystal structure of 16 showing a X-quinoline unit (b) and a X-quinolinone unit (c). Side- (d) and top- (e) view of the C-terminal helix of a B and B'-domain. The flipped X-quinolinone unit is marked with a blue circle in (d) and shown in blue in (e). Side chains, hydrogen atoms and included solvent molecules are omitted for clarity.

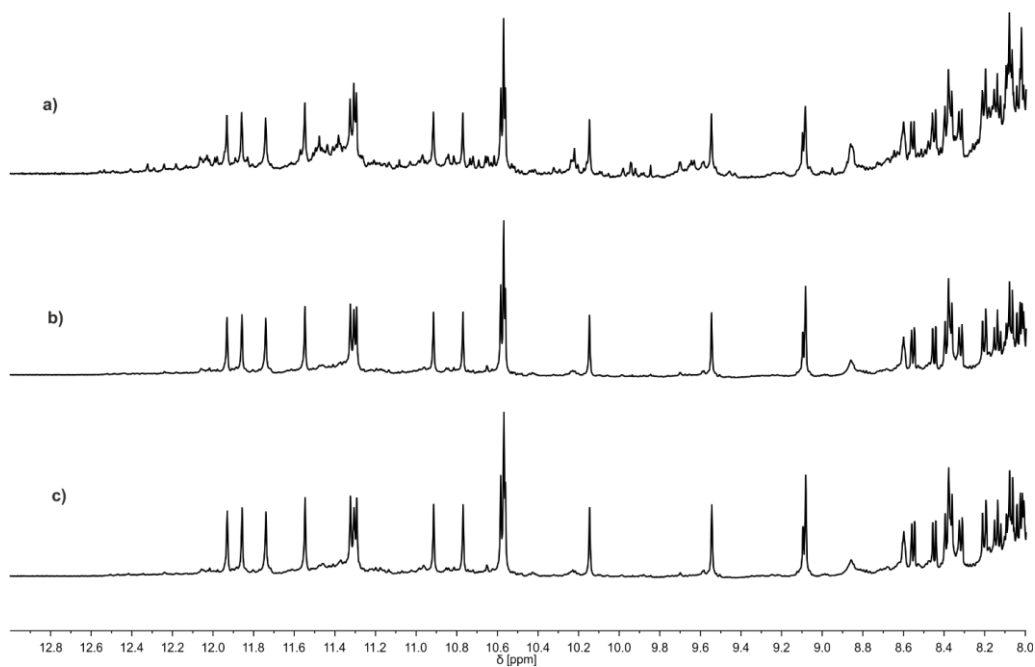


**Figure S45. Control experiment to verify that thermodynamic equilibrium is reached in spectra of **13**.** Part of the  $^1\text{H}$  NMR spectra (500 MHz, 25 °C) in  $\text{CDCl}_3$  at 5.8 mM showing amide resonances of **13** after 24 hours (a), 1 week (b) and 2 weeks (c), respectively.

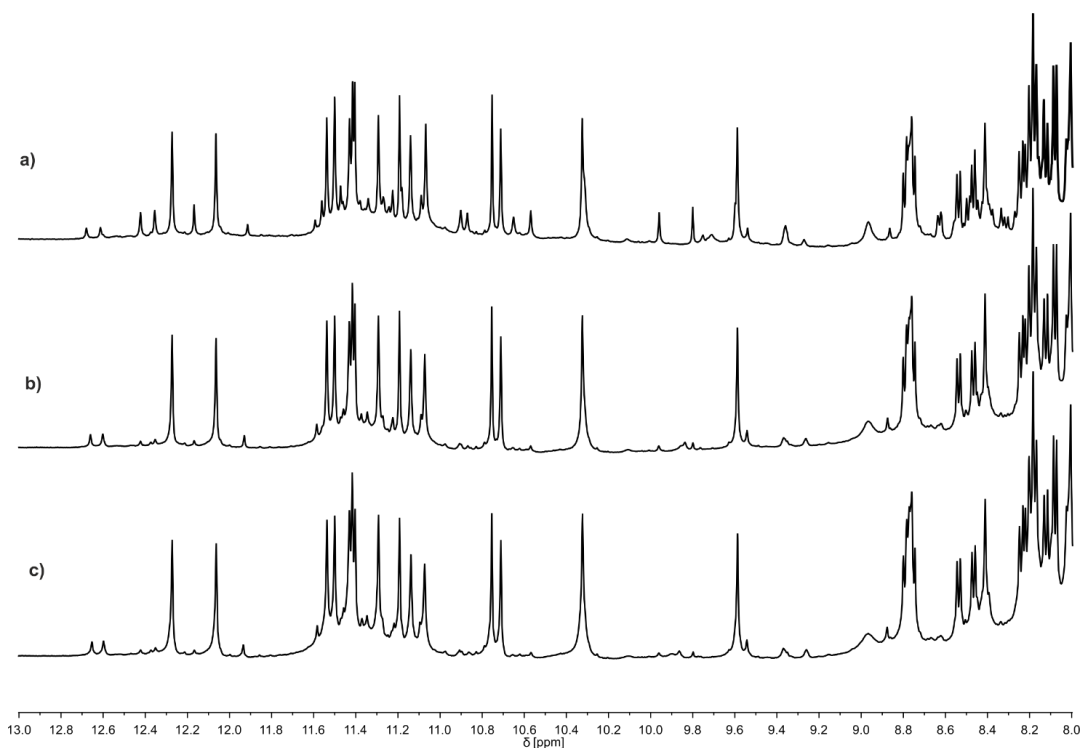


**Figure S46. Control experiment to verify that thermodynamic equilibrium is reached in spectra of **15**.** Part of the  $^1\text{H}$  NMR spectra (500 MHz, 25 °C) in  $\text{CDCl}_3$  at 7.5 mM showing amide resonances of **15** after 24 hours (a), 1 week (b) and 2 weeks (c), respectively.

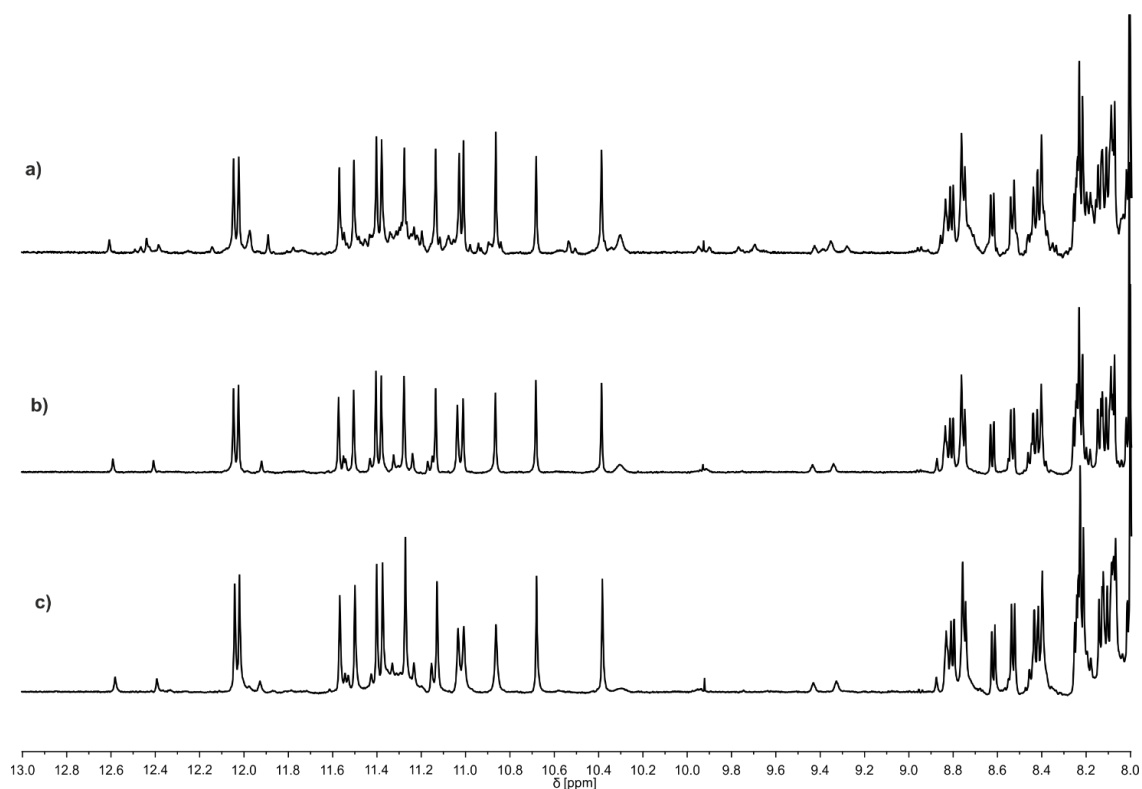


**Figure S47. Control experiment to verify that thermodynamic equilibrium is reached in spectra of **17**.** Part of the  $^1\text{H}$  NMR spectra (500 MHz, 25 °C) in  $\text{CDCl}_3$  at 7.5 mM showing amide resonances of **17** after 24 hours (a), 3 weeks (b) and 6 weeks (c), respectively.

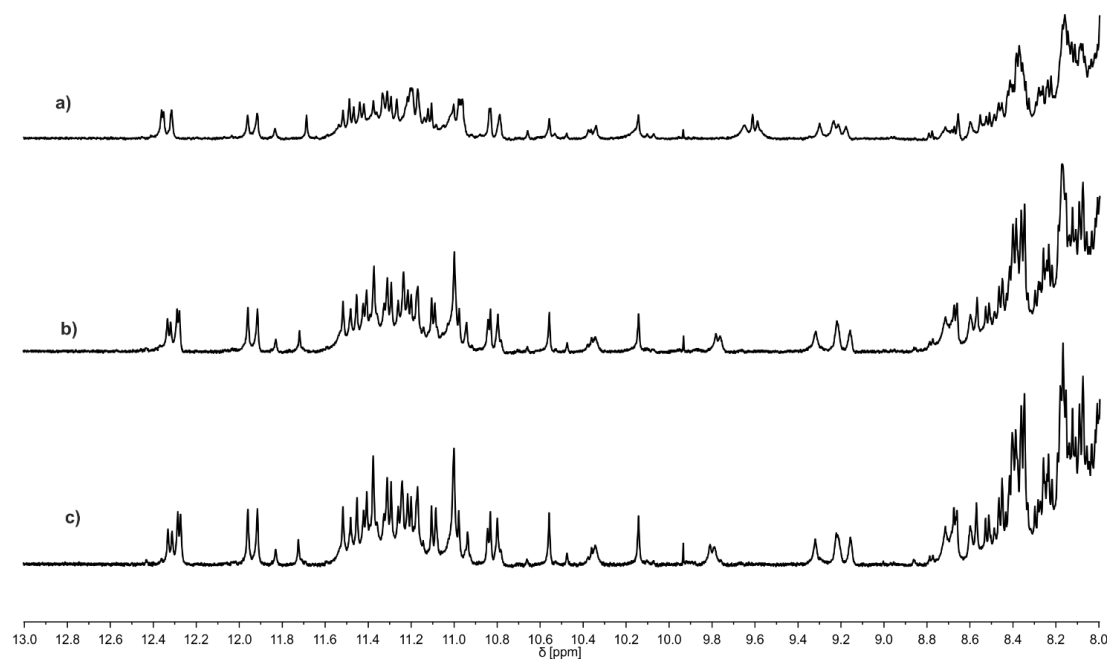


**Figure S48. Control experiment to verify that thermodynamic equilibrium is reached in spectra of **16**.** Part of the  $^1\text{H}$  NMR spectra (500 MHz, 25 °C) in  $\text{CDCl}_3$  at 7.5 mM showing amide resonances of **16** after 24 hours (a), 3 weeks (b) and 6 weeks (c), respectively.

## 5.2.3 Supplementary methods

### 5.2.3.1 HRMS analyses

HR-MS spectra were recorded on a Bruker microTOF II by direct infusion from acetonitrile in positive ionization mode. The instrument was calibrated in positive mode by direct infusion of a calibration solution (Agilent Technologies ESI-L Low Concentration Tuning Mix). The mass sample was prepared by adding 10  $\mu$ L of a solution of the sample in DCM (0.1 mg/mL) to 1 mL of a solution of 0.1% formic acid in acetonitrile.

### 5.2.3.2 Molecular modeling

Models were simulated by using Maestro version 11.5 (Schrödinger Inc.). Energy minimized structures were obtained using MacroModel energy minimization with the following parameters: force field: MMFFs; solvent: none; electrostatic treatment: constant dielectric; dielectric constant: 1.0; charges from: force field; cutoff: normal; Van der Waals: 7.0; electrostatic: 12.0; H-bond: 4.0; mini method: TNCG; maximum iterations: 2500; converge on: gradient; convergence threshold: 0.05; constraints: distances. As a starting point, the coordinates of previously described crystal structures CCDC entry # 1451494 (*PP* clockwise and counterclockwise tilted dimer),<sup>1</sup> CCDC entry # 2209187 (for models of *PP* shifted head-to-tail dimer),<sup>4</sup> CCDC entry # 1955168 (for models of *PM* parallel head-to-tail dimer),<sup>2</sup> CCDC entry # 2209189 (for models of *PM* shifted head-to-tail dimer),<sup>4</sup> were used. For models of the *PM* clockwise and counterclockwise tilted dimer the crystal structures CCDC entry # 1451494<sup>1</sup> and CCDC entry # 2209189<sup>4</sup> were combined. A single helix was first energy-minimized. In a second round, two helices were placed in a plausible arrangement, and distance constraints between plausible hydrogen-bonding partners were set on purpose to 2.5. While setting the constraints, it was important to match the hydroxy group to their correct hydrogen-bonding carbonyl partner. The energy-minimized model was fixed regarding possible unlikely conformations and energy-minimized again. Then all constraints were removed, and energy minimization was repeated. Typically, only minimal changes occurred at this stage. Then the connecting T3-linker was introduced, and the model again energy minimized without fixed distances. If no changes were observed another energy minimization with fixed distances has been run. If afterwards no changes were observed the structure was exported as a mol2-file.

### 5.2.3.3 Nuclear magnetic resonance spectroscopy

NMR spectra were recorded on different NMR spectrometers: (I) an Avance III HD NMR spectrometer 500 MHz (Bruker BioSpin) with CryoProbe™ Prodigy for <sup>1</sup>H NMR, <sup>1</sup>H,<sup>15</sup>N-HSQC, and DOSY spectra

of foldamers. (II) an Avance III HD NMR spectrometer 800 MHz with cryoprobe (Bruker BioSpin) for variable temperature measurements. Chemical shifts are described in part per million (ppm,  $\delta$ ) relative to the  $^1\text{H}$  residual signal of the deuterated solvent used. Meaning DMSO- $d_6$  ( $\delta$  2.50 ppm), pyridine- $d_5$  ( $\delta$  8.74 ppm),  $\text{CD}_2\text{Cl}_2$  ( $\delta$  5.32 ppm) and  $\text{CDCl}_3$  ( $\delta$  7.16 ppm).  $^1\text{H}$  NMR splitting patterns with observed first-order coupling are entitled as singlet (s), doublet (d), triplet (t), quartet (q), multiplet (m) or broad singlet (bs). Coupling constants ( $J$ ) are ported in Hertz.

Sample preparation and incubation times to reach equilibrium required attention. The required equilibration times of sequences **9-17** were estimated by equilibrating each sample in  $\text{CDCl}_3$  after complete disruption of the aggregates. Complete disruption was achieved by dissolving the sample in pyridine and then evaporating the solvent. Spectra were measured at different time intervals from 2h to 6 weeks until no further change was observed.

In the case of sequences **9-12** and **14**, equilibration times were generally fast (around 5 min). Samples were typically incubated for 2h, which gave a large margin. In the case of **13**, **15** and **17**, equilibration times are considerably longer, and incubation of two to three weeks is indicated (Figures S45-47). In the case of **16**, slight changes in regard to signal sharpening are observed over time (Figure S48).

$^1\text{H}$ ,  $^{15}\text{N}$ -HSQC spectra were recorded with a phase-sensitive pulse sequence with sensitivity enhancement using trim pulses in inept transfer (hsqcetgps2) from the Bruker pulse program library. Data acquisition was performed utilizing non-uniform sampling (NUS; NUS amount: 50% with an automatically created NUSList) yielding 1024 (F2) x 128 (F1) data points in Echo/Antiecho gradient selection mode. The recycling delay was 2.0 s and 64 transients per increment were applied at a sweep width of 2.5 kHz in F2 and 7 kHz in F1 resulting in an acquisition time of 0.1462 s. NUS processing was performed using the fully automated NUS processing tool provided by MestReNova. Zero filling in F1 has been used to yield a final matrix of 1K x 1K real points.

The DOSY spectra were recorded by applying a pulse sequence with stimulated echo using bipolar gradient pulses for diffusion from the Bruker pulse program library (stebpgp1s). The diffusion delay  $\Delta$  (big delta) and the diffusion gradient pulse length  $\delta$  (little delta) was set to values specified in the respective capture. The number of gradient steps were set to 32 with linear spacing starting from 2% reaching 95% of the full gradient strength in the final step. For each of the 32 gradient amplitudes, 256 transients of 65k complex data points were acquired. DOSY processing was performed with the DOSY processing tool from MestReNova (v.12.x64) employing the Peak Heights Fit algorithm including the autocorrect peak position with 32 points in diffusion dimension and a window of  $1.00 \cdot 10^{-6}$  to  $1.00 \cdot 10^{-2} \text{ cm}^2 \text{ s}^{-1}$ .



#### 5.2.3.4 CD studies

All CD spectra were recorded on a Jasco J-810 spectrometer with 10 mm quartz cuvette. The following parameters were used: wavelength range from 500 to 250 nm. Scan speed: 200 nm/min; accumulation: 3; response time: 1.0 s; bandwidth: 2; temperature: 25 °C; sensitivity: standard (100 mdeg); data pitch: 1 nm; nitrogen gas flow rate: 500 L/h. The sample solution was prepared in distilled chloroform or DCM filtered over alumina before use.  $\Delta\epsilon$  values (in  $\text{cm}^2\cdot\text{mmol}^{-1}$ ) were obtained by using the formula:  $\Delta\epsilon = m^\circ / (C \cdot l \cdot 32980)$  where  $m^\circ$  = CD value in millidegrees;  $l$  = cuvette pathlength in cm;  $C$  = sample concentration in mol/L. The CD spectra of all samples were carried out at 0.01 mM in chloroform and DCM. Thus, a solution of each in pyridine was prepared, and the same volume was taken, respectively. After the removal of the solvent, the samples were dissolved and incubated in chloroform or DCM.

#### 5.2.3.5 X-ray crystallography

X-ray diffraction experiments for **16** were performed at the IECB x-ray facility (CNRS UMS 3033, University of Bordeaux) with a Rigaku FRX rotating anode (2.9 kW) diffractometer.  $\text{CuK}\alpha$  radiation was monochromated with high flux Osmic Varimax HF mirrors for data collection. The x-ray source is equipped with a Pixel Hybrid Dectris Eiger 1M detector and partial chi goniometer (AFC11). The data were processed with CrysAlis PRO software<sup>7</sup> with a multiscan absorption correction. Crystal was kept at 100(2) K during data collection. The structure was solved with the ShelXT<sup>8</sup> structure solution program using a dual-space algorithm. Crystal model refinement was performed with ShelXL<sup>9</sup> package using Least Squares minimization implemented in Olex2<sup>10</sup>.

During refinement, anisotropic displacement parameters were used only for backbones. For two isobutoxy side chains, not all C atoms were found. The foldamer molecules' C- and N-bound hydrogen atoms were placed in an idealized position. H atoms of side chains were not localized. Hydrogen atoms of water molecules and OH groups of foldamer molecules were identified based on possible hydrogen bond interactions. All H atoms were refined in the riding-model approximation, with  $U_{\text{iso}}(\text{H}) = 1.2U_{\text{eq}}(\text{CH}, \text{CH}_2, \text{NH})$ ,  $U_{\text{iso}}(\text{H}) = 1.5U_{\text{eq}}(\text{OH}, \text{CH}_3)$ . EADP and DELU instructions were employed to model temperature parameters. The geometry of the molecules was improved with DFIX and AFIX commands.

The solvent masking procedure implemented in Olex2<sup>10</sup> was employed to remove severely disordered solvent molecules. The solvent radius was set to 1.2 Å, and the calculated total potential solvent-accessible void volume and electron counts per unit cell were 7644 Å<sup>3</sup> and 1939.

The final cif files were checked using IUCR's checkcif algorithm. Due to the characteristics of the crystal, i.e. large volume fractions of disordered solvent molecules, weak diffraction intensity, incompleteness of the data and moderate resolution, A - level and B - level alerts remain in the check

cif file. These alerts are inherent to the data and refinement procedures and do not reflect errors. They are explicitly listed below and have been divided into two groups. The first group illustrates the poor quality of the data and refinement statistics compared to that expected for small molecule structures from highly diffracting crystals. The second group is connected to decisions made during refinement and explained below.

**Group 1:**

THETM01\_ALERT\_3\_A The value of  $\sin(\theta_{\max})/\lambda$  is less than 0.550

Calculated  $\sin(\theta_{\max})/\lambda = 0.4762$

PLAT023\_ALERT\_3\_A Resolution (too) Low [ $\sin(\theta)/\lambda < 0.6$ ].. 0.48 Ang-1

PLAT084\_ALERT\_3\_A High wR2 Value (i.e.  $> 0.25$ ) ..... 0.48 Report

PLAT934\_ALERT\_3\_A Number of (Iobs-Icalc)/Sigma(W)  $> 10$  Outliers .. 77

CheckPLAT082\_ALERT\_2\_B High R1 Value ..... 0.16 Report

PLAT241\_ALERT\_2\_B High 'MainMol' Ueq as Compared to Neighbors

PLAT242\_ALERT\_2\_B Low 'MainMol' Ueq as Compared to Neighbors

**Group 2:**

PLAT201\_ALERT\_2\_A Isotropic non-H Atoms in Main Residue(s)

Not all atoms were refined with ADPs

PLAT315\_ALERT\_2\_B Singly Bonded Carbon Detected (H-atoms Missing)

Not all H-atoms were localized, but they were used in SFAC calculation

**Table S1.** Crystal data and refinement details

<b>Identification code</b>	<b>16</b>
<b>Chemical formula</b>	2(C <sub>17</sub> H <sub>15</sub> N <sub>2</sub> O <sub>3</sub> Se)·5(H <sub>2</sub> O)·4(C <sub>2</sub> H <sub>3</sub> N)·[+solvents]*
<b>Formula weight</b>	6704.71
<b>Crystal system</b>	Triclinic
<b>Space group</b>	P-1
<b>Unit cell dimensions (Å, °)</b>	a=27.1355 (6) α=67.428 (2) b=29.0697 (6) β=80.522 (2) c=33.4936 (7) γ=62.942 (2)
<b>Volume (Å<sup>3</sup>)</b>	21724.7 (9)
<b>Z</b>	2
<b>Density (calculated) (Mg m<sup>-3</sup>)</b>	1.02
<b>Absorption coefficient (mm<sup>-1</sup>)</b>	0.78
<b>Crystal size (mm)</b>	0.60 × 0.40 × 0.07
<b>Completeness</b>	99.5 (up to 47.24°)
<b>Reflections collected</b>	132507
<b>Reflections observed</b>	29171
<b>[I &gt; 2σ(I)]</b>	
<b>R<sub>int</sub></b>	0.028
<b>Data/parameters/restraints</b>	39094/3273/179
<b>Goodness-of-fit on F<sup>2</sup></b>	2.09
<b>Final R indices [I &gt; 2σ(I)]</b>	0.1552, 0.4553
<b>R indices (all data)</b>	0.1721, 0.4735
<b>Largest diff. peak and hole</b>	0.99, -0.82
<b>CCDC #</b>	2216678

Experiments were carried out at 100 K with Cu Kα radiation. Absorption was corrected by multi-scan

\* Solvent mask was used to remove severely disordered solvent molecules

**Table S2.** Intermolecular hydrogen bonds geometry in the crystal structure. Atom numbers are those of the cif file.

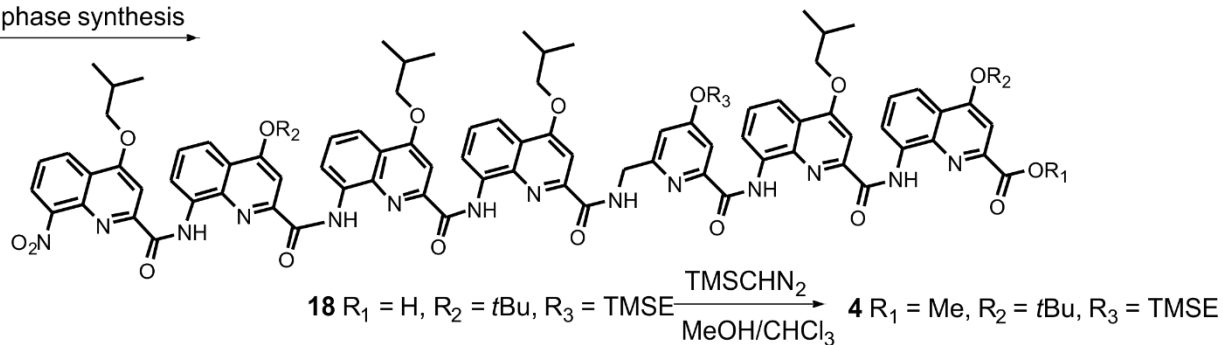
D—H...A	D—H	H...A	D...A	D—H...A
O1B-H1B...O4W	0.84	1.75	2.579 (7)	168
O5A-H5A...O1W <sup>i</sup>	0.84	1.77	2.587 (7)	160
O1W-H1WB...O3E	0.84	1.83	2.653 (7)	166
O1W-H1WA...O8F <sup>i</sup>	0.84	2.12	2.797 (7)	137
O1E-H1E...O14F	0.84	1.89	2.638 (9)	148
O4D-H4D...O14C	0.84	1.77	2.604 (9)	173
O4A-H4A...O4D	0.84	2.03	2.814 (8)	155
O4W-H4WA...O7F	0.84	1.92	2.740 (8)	164
O4W-H4WB...O7C	0.84	1.88	2.712 (8)	172
O5D-H5D...O4C	0.84	1.80	2.596 (11)	157
O3A-H3A...O4F	0.84	1.82	2.622 (9)	158
O2B-H2B...O3W	0.84	1.73	2.541 (13)	162
O2W-H2WA...O12C	0.84	1.90	2.743 (10)	178
O2W-H2WB...O8C	0.84	1.96	2.798 (10)	178
O3W-H3WA...O5C	0.84	2.04	2.864 (10)	165
O3W-H3WB...O2W	0.84	1.88	2.711 (11)	170
O3D-H3D...O5W	0.84	1.75	2.564 (16)	163
O5W-H5WB...O2C	0.84	1.94	2.773 (11)	174
O5W-H5WA...O2D <sup>ii</sup>	0.84	2.06	2.863 (14)	156

(i) 1-x, 2-y, 1-z; (ii) 1-x, 1-y, 2-z

## 5.2.4 Synthetic Scheme

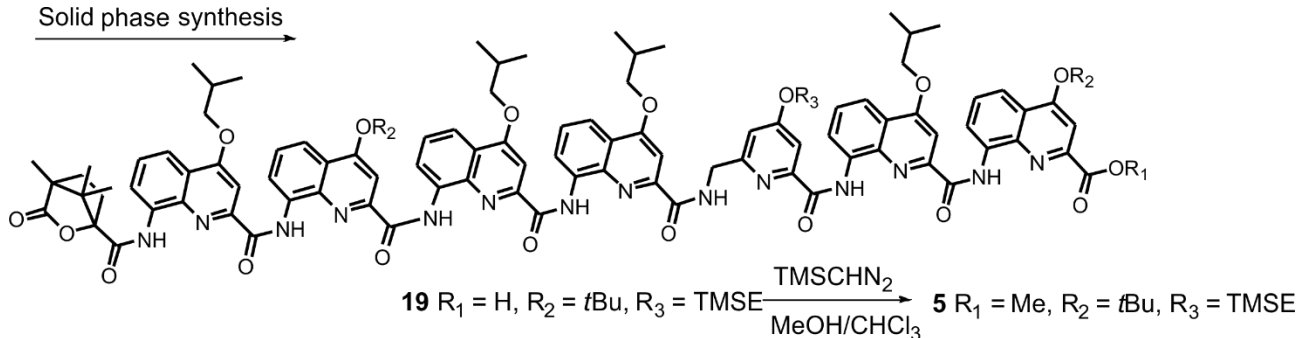
### 5.2.4.1 Synthesis of sequences to test handedness-induction via chiral B-unit

Solid phase synthesis



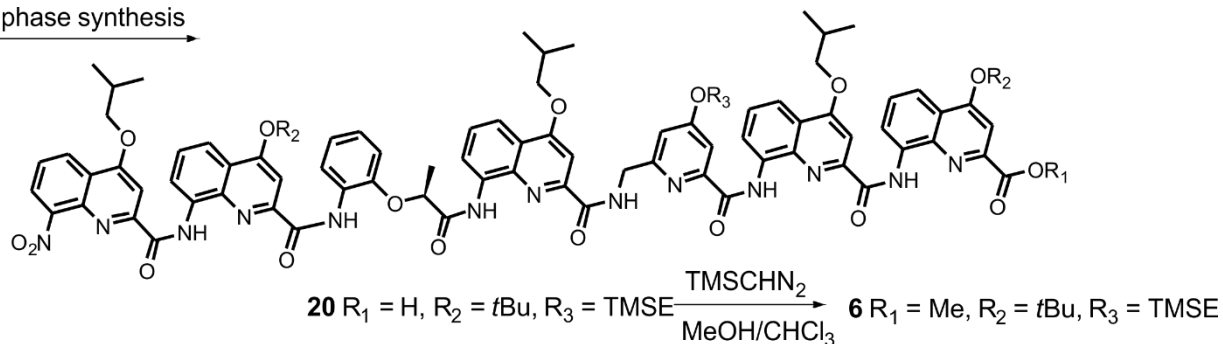
**Scheme 1.** Synthesis of **4**.

Solid phase synthesis

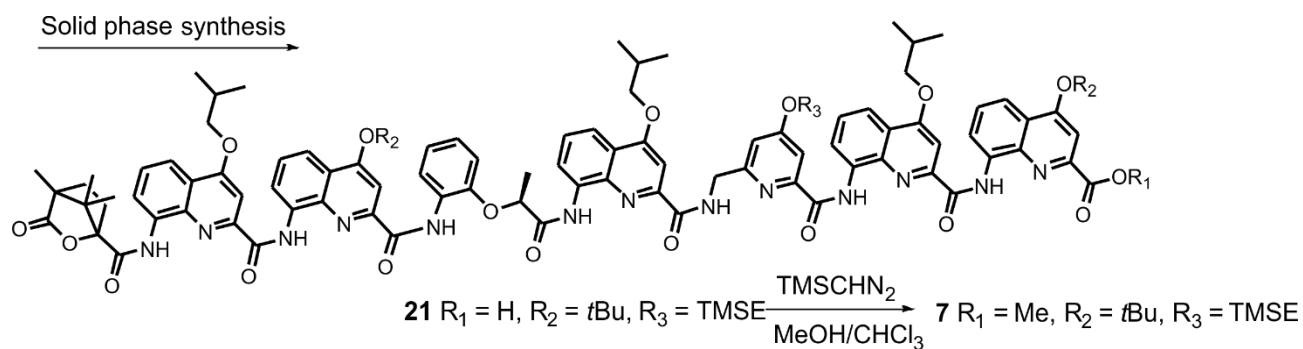


**Scheme 2.** Synthesis of **5**.

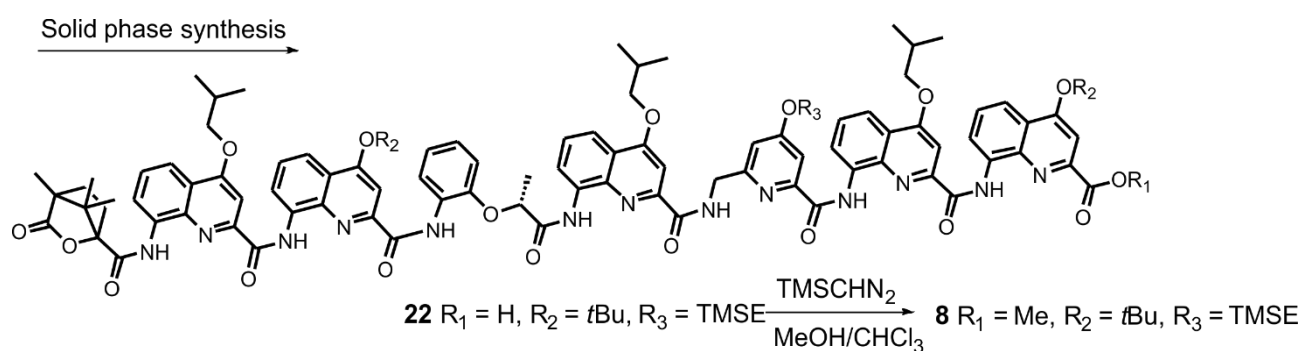
Solid phase synthesis



**Scheme 3.** Synthesis of **6**.

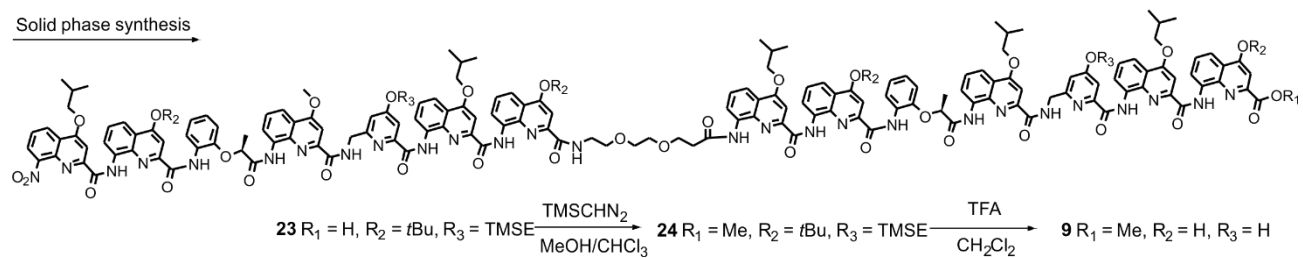


**Scheme 4.** Synthesis of **7**.

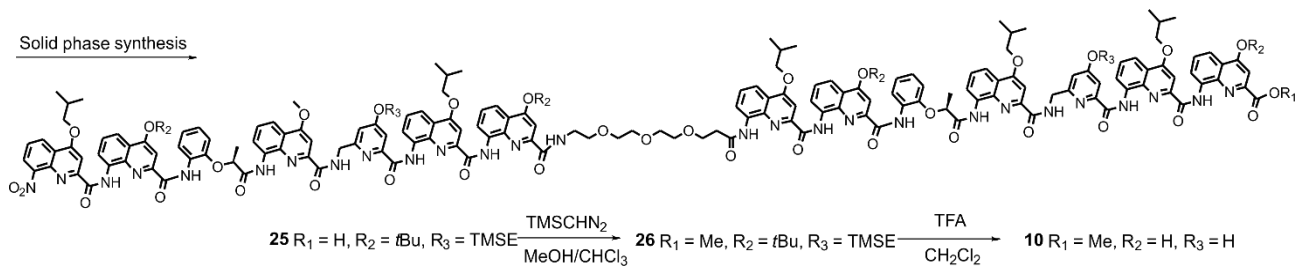


**Scheme 5.** Synthesis of **8**.

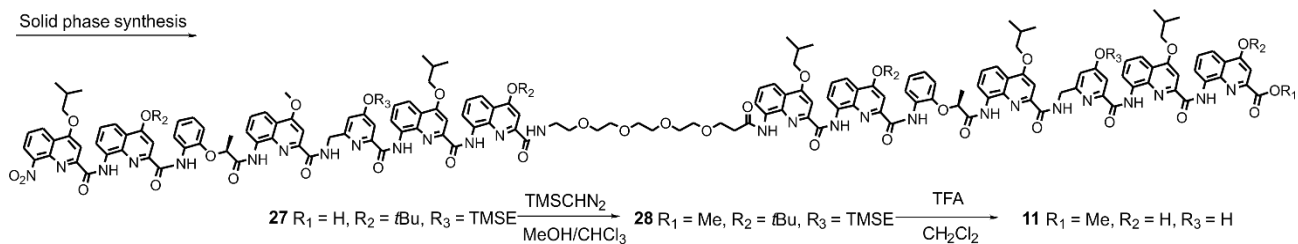
### 5.2.4.2 Synthesis of helix-turn-helix-motif with a flexible linker and handedness-control in both helices via a chiral B-unit



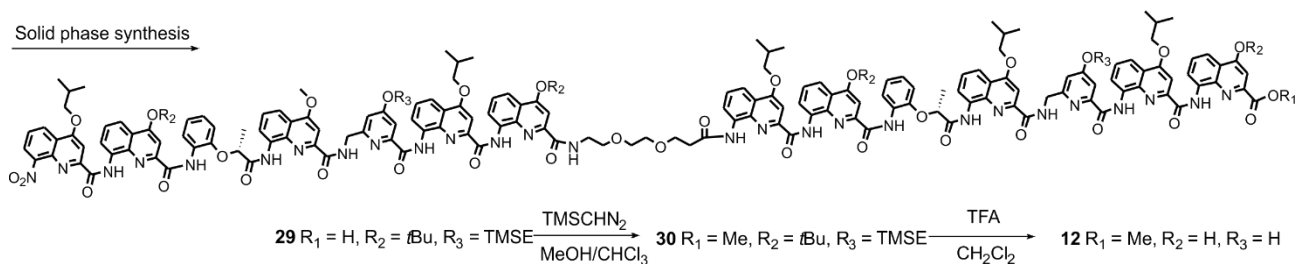
**Scheme 6.** Synthesis of **9**.



**Scheme 7.** Synthesis of **10**.

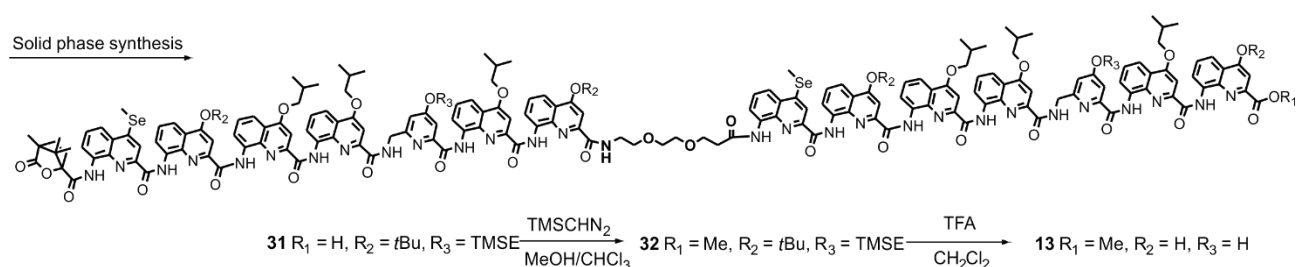


**Scheme 8.** Synthesis of **11**.

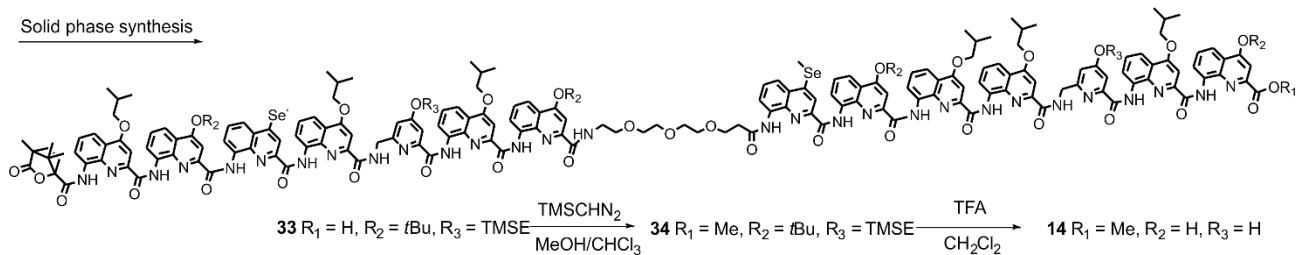


**Scheme 9.** Synthesis of **12**.

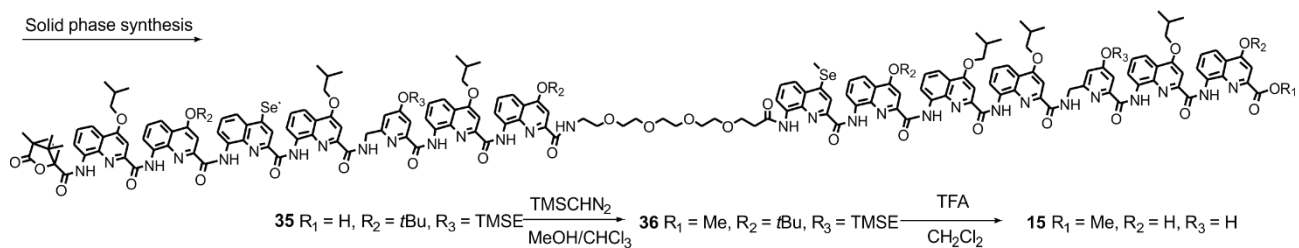
### 5.2.4.3 Synthesis of helix-turn-helix-motif with a flexible linker and handedness-control in one helix



**Scheme 10.** Synthesis of **13**.

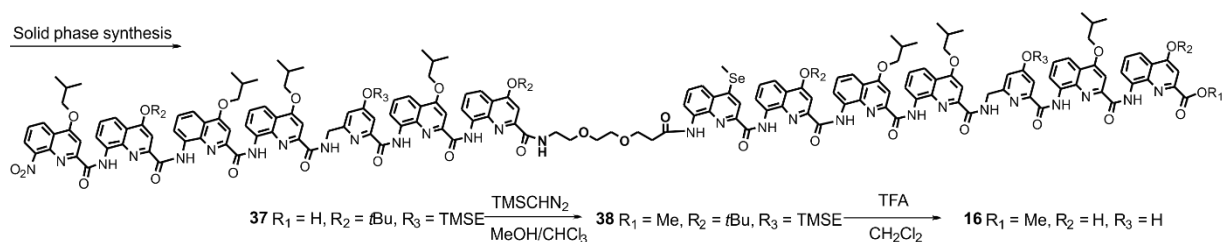


**Scheme 11.** Synthesis of **14**.

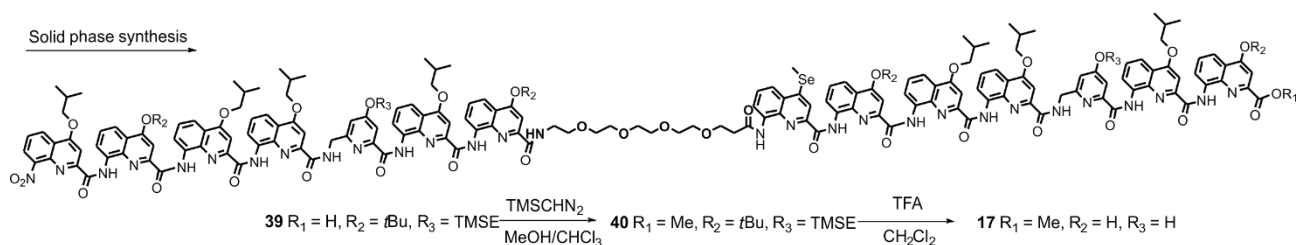


**Scheme 12.** Synthesis of **15**.

#### 5.2.4.4 Synthesis of helix-turn-helix-motif with a flexible linker and without any handedness-control



**Scheme 13.** Synthesis of **16**.



**Scheme 14.** Synthesis of **17**.



## 5.2.5 Experimental Procedures

### 5.2.5.1 General methods

Commercially available reagents were purchased from Sigma-Aldrich, Alfa-Aesar or TCI and were used without further purification unless otherwise specified. SASRIN resin (100-200 mesh, loading 0.7-1.0 mmol/g) was purchased from Bachem. Tetrahydrofuran (THF), dichloromethane (DCM) and toluene were dried over alumina columns (MBRAUN SPS-800 solvent purification system); diisopropylethylamine (DIPEA) was distilled over ninhydrin and then over potassium hydroxide (KOH); chloroform was distilled over calcium hydride (CaH<sub>2</sub>) prior to use. Solid phase synthesis (SPS) was performed manually under MW-irradiation on a CEM Discover (Liberty Bio) microwave oven using an open reaction vessel and an internal fibre optic probe for temperature control. High-resolution electrospray mass spectra were recorded on a Thermo Exactive orbitrap instrument.

### 5.2.5.2 Solid phase synthesis general methods

The monomers Fmoc-Q<sup>B</sup>-OH,<sup>11</sup> Fmoc-Q<sup>M</sup>-OH<sup>12</sup>, Fmoc-B<sup>R</sup>-OH<sup>13</sup>, Fmoc-X-OH<sup>4</sup> (X denotes tBu-protected X), and Fmoc-Y-OH<sup>3</sup> (Y denotes TMSE-protected Y) have been synthesized according to literature. The synthesis of Fmoc-Q<sup>S</sup>-OH and Fmoc-B<sup>S</sup>-OH will be published elsewhere.

#### 5.2.5.2.1 Loading of the resin via HBTU-coupling

SASRIN resin (800 mg, 100-200 mesh, loading 0.7-1.0 mmol/g) was swollen in DMF for 1 h, transferred to the microwave vessel and washed three times with dry DMF (purchased as 'extra-dry' solvent from Acros Organics). DIPEA (272  $\mu$ L, 2 eq.) was added to a mixture of X (471 mg; 0.7 eq.) and HBTU (456 mg, 1.5 eq.) in dry DMF (5 mL), then the mixture was added to the resin. The reaction mixture was subjected to treatment in the microwave (50 °C, 20 min, 25 W), then the resin was washed five times with DMF until the washing solution was colourless, then it was washed ten times with DCM. If the loading was sufficient, a capping was performed, otherwise, the resin re-loaded. Capping was performed by adding a mixture of DCM/pyridine/benzoyl chloride (v/v/v, 3:1:1), and the resin was left for 30 min, then it was rinsed 20x times with DCM.

#### 5.2.5.2.2 Estimation of the loading

After drying a small part of the resin under vacuum for 5 h, the loading of the resin was determined. To a small amount of resin (1-2 mg), a freshly prepared mixture of DMF/piperidine (v/v, 8:2, 3 mL) was added. The mixture was shaken and incubated for 5 min. Then the absorption was measured at 290 nm using a NanoDrop One Microvolume UV-Vis Spectrophotometer and a Hellma quartz glass cuvette 104

(path length 10 mm). Three replicates were measured, then the loading was calculated with the following equation:

$$\text{loading (in } \frac{\text{mmol}}{\text{g}}) = \frac{A_{290 \text{ nm}}}{1.65 \cdot m_{\text{resin}}(\text{in mg})} \quad (1)$$

### 5.2.5.2.3 Solid Phase Synthesis via in-situ-activation

After swelling of the SASRIN resin (800 mg, 100-200 mesh, loading 0.388 mmol/g, 0.310  $\mu\text{mol}$ ) in DMF for 1 h, the resin was transferred into the microwave vessel and washed three times with DMF. For deprotection, an 8:2 mixture of DMF/piperidine (6 mL) was added to the resin and nitrogen was bubbled through the suspension for 3 min. The solution was removed, the resin was washed five times with DMF, and an 8:2 mixture of DMF/piperidine (6 mL) was added again. After bubbling nitrogen through the suspension for 7 min, the resin was washed five times with DMF and five times with THF. For coupling, dry THF (4 mL) and 2,3,5-collidine (5 eq. with regards to the resin-loading) were added to the resin. A mixture of the monomer (2 eq. with regards to the resin-loading) and  $\text{PPh}_3$  (4 eq. with regards to the resin-loading) in dest. chloroform (4 mL) or dry NMP (4 mL) was prepared. All monomers except for Fmoc-P-OH were dissolved in dest. chloroform. Fmoc-P-OH was dissolved in dry NMP. After the addition of trichloroacetonitrile (4 eq. with regards to the resin-loading), this mixture was added to the resin. Then the reaction mixture was subjected to treatment in the microwave (50 °C, 5 min, 50 W) Then the resin was washed five times with dry THF, then dry THF (4 mL) and 2,3,5-collidine (5 eq. with regards to the resin-loading) were added to the resin. Again, a mixture of monomer (2 eq. with regards to the resin-loading) and  $\text{PPh}_3$  (4 eq. with regards to the resin-loading) in dest. chloroform (4 mL) or dry NMP (4 mL) with trichloroacetonitrile was prepared and added to the resin. The reaction mixture was again subjected to microwave vessel treatment (50 °C, 5 min, 25 W). After washing with DCM, THF, DMF and DCM, in that order, the resin was kept in a swollen state at 10 °C.

The sequence Fmoc-NH-Y-Q-X-OH needed to be deprotected by adding an 8:2 mixture of DMF/piperidine (6 mL) to the resin and subjecting it to MW treatment (50 °C, 5 min, 25 W). This step was repeated twice, and the in-situ coupling was then proceeded.

For installation of (1S)-camphanic amide, the resin (0.030 mmol) was Fmoc deprotected (20% piperidine in DMF, 1 x 3 min and 1 x 7 min), washed with DMF and dry THF, then a solution of DIPEA (31.1  $\mu\text{L}$ , 10 eq.) in dry THF (0.5 mL) was added to the resin. To this suspension a solution of (1S)-camphanic acid chloride (3 eq.) in dry THF (0.5 mL) was added, and rests on the reaction vessel was rinsed down with dry THF (0.5 mL). The reaction was carried out under MW irradiation (25 W) at 50°C for 5 min. The resin was washed briefly with dry THF, and the process was repeated. Successively the resin was washed with DMF and DCM.

#### 5.2.5.2.4 Mini Cleavage

To perform a mini cleavage, SASRIN resin (~5 mg) was swelled in DCM for 15 min, then HFIP [DCM (2.8 mL) and HFIP (1.2 mL)] were added, and the mixture was stirred at r. t. for 1 h. Then the solvent was evaporated.

#### 5.2.5.2.5 Full Cleavage

To perform the full cleavage, SASRIN resin (~50 mg) was swelled in DCM for 15 min, HFIP [DCM/HFIP, v/v, 1:1 (6 mL in total)] was added, and the mixture was stirred at r. t. for 12 h. Then the solvent was evaporated. The process was repeated until no more foldamer is left on the resin (up to three times).

### 5.2.5.3 Synthesis of oligomers

#### 5.2.5.3.1 Synthesis of sequences to test handedness-induction via chiral B-unit

**O<sub>2</sub>N-Q<sup>B</sup>XQ<sup>B</sup>Q<sup>B</sup>YQ<sup>B</sup>X-OH (18)** Compound **18** was synthesized using the SPS procedures reported in 0 on SASRIN resin loaded via HBTU-coupling described in 0 (scale: 78 μmol). After full cleavage and precipitation in ethyl acetate/n-Hex, the product was obtained as a yellow solid (61.13 mg, 45 %). <sup>1</sup>H NMR (500 MHz, CDCl<sub>3</sub>, 25 °C) δ [ppm] 11.61 (s, 1H), 11.26 (d, J = 4.0 Hz, 2H), 11.18 (s, 1H), 10.96 (s, 1H), 8.70 (d, J = 3.9 Hz, 1H), 8.50 – 8.47 (m, 1H), 8.40 (dd, J = 8.2, 1.5 Hz, 1H), 8.32 (dd, J = 7.5, 1.4 Hz, 1H), 8.12 (d, J = 1.3 Hz, 1H), 8.05 (dd, J = 10.1, 1.3 Hz, 2H), 8.03 – 7.97 (m, 3H), 7.86 – 7.82 (m, 1H), 7.77 (dd, J = 8.3, 1.3 Hz, 1H), 7.62 – 7.58 (m, 3H), 7.43 – 7.38 (m, 3H), 7.37 – 7.32 (m, 2H), 7.21 – 7.16 (m, 2H), 6.97 (d, J = 2.2 Hz, 1H), 6.73 (s, 1H), 6.60 (d, J = 2.2 Hz, 1H), 6.35 (s, 1H), 6.26 (s, 1H), 4.00 – 3.98 (m, 2H), 3.90 – 3.87 (m, 1H), 3.83 – 3.81 (m, 1H), 3.79 – 3.75 (m, 1H), 2.51 – 2.42 (m, 1H), 2.34 – 2.21 (m, 2H), 1.78 – 1.66 (m, 4H), 1.61 – 1.54 (m, 7H), 1.53 – 1.44 (m, 9H), 1.38 – 1.28 (m, 12H), 1.23 – 1.13 (m, 6H), 1.10 – 0.99 (m, 3H), 0.90 – 0.80 (m, 12H), 0.24 (s, 9H). MS calcd for C<sub>96</sub>H<sub>102</sub>N<sub>14</sub>NaO<sub>17</sub>Si [M+Na]<sup>+</sup> 1773.7209, found (HR-ESI) 1774.5839.

**O<sub>2</sub>N-Q<sup>B</sup>XQ<sup>B</sup>Q<sup>B</sup>YQ<sup>B</sup>X-OMe (4)** Compound **18** (61.13 mg, 35 μmol, 1 eq.) was dissolved in a mixture of dry Chloroform/MeOH 3:2 (5 mL) under N<sub>2</sub>. TMSCHN<sub>2</sub> (solut. 2 M in Hex, 42 μL, 0.07 mmol, 2 eq.) was added dropwise, and the solution was stirred at r.t. for 2 h. A few drops of acetic acid were added, and the solution was stirred for 5 min at r.t. Then the solution was diluted with DCM, washed with NaHCO<sub>3</sub>, dried MgSO<sub>4</sub>, filtered and concentrated. The product was obtained as a yellow solid (47.56 mg, 77 %). <sup>1</sup>H NMR (500 MHz, CDCl<sub>3</sub>, 25 °C) δ [ppm] 11.59 (s, 1H), 11.49 (s, 1H), 11.45 (s, 1H), 11.22 (s, 1H), 11.16 (s, 1H), 8.54 (t, J = 3.7 Hz, 1H), 8.49 (dd, J = 7.6, 1.3 Hz, 1H), 8.40 (dd, J = 8.2, 1.5 Hz, 1H), 8.33 (dd, J = 7.6, 1.4 Hz, 1H), 8.11 (dd, J = 8.2, 1.4 Hz, 1H), 8.05 – 7.99 (m, 3H), 7.84 (dd, J = 8.2, 1.2 Hz, 1H), 7.81 (s, 1H), 7.77 (ddd, J = 8.4, 2.3, 1.3 Hz, 2H), 7.64 (dd, J = 7.5, 1.4 Hz, 1H), 7.48 – 7.44 (m, 2H), 7.41 – 7.36 (m, 3H), 7.35 – 7.30 (m, 1H), 7.23 (dd, J = 8.2, 7.5 Hz, 1H), 7.19

– 7.14 (m, 2H), 6.89 (d,  $J = 2.3$  Hz, 1H), 6.70 (s, 1H), 6.56 (d,  $J = 2.4$  Hz, 1H), 6.38 (s, 1H), 6.27 (s, 1H), 4.29 – 4.20 (m, 2H), 4.16 (dd,  $J = 8.8, 6.2$  Hz, 1H), 4.06 (ddd,  $J = 8.7, 6.4, 4.9$  Hz, 2H), 4.00 (dd,  $J = 8.7, 7.3$  Hz, 1H), 3.91 – 3.77 (m, 5H), 3.39 – 3.36 (m, 1H), 3.15 (s, 3H), 2.51 – 2.35 (m, 4H), 2.33 – 2.25 (m, 2H), 2.19 – 2.14 (m, 1H), 2.05 – 1.98 (m, 1H), 1.72 (s, 6H), 1.61 (s, 8H), 1.35 – 1.24 (m, 10H), 1.23 – 1.16 (m, 12H), 0.90 – 0.80 (m, 3H), 0.23 (s, 9H). **MS** calcd for  $C_{97}H_{104}N_{14}NaO_{17}Si$   $[M+Na]^+$  1787.7365 found (HR-ESI) 1788.6438.

**(1S)-Camph-Q<sup>B</sup>XQ<sup>B</sup>YQ<sup>B</sup>X-OH (19)** Compound **19** was synthesized using the SPS procedures reported in 0 on SASRIN resin loaded via HBTU-coupling described in 0 (scale: 78  $\mu$ mol). After full cleavage and precipitation in EtOAc/*n*-Hex, the product was obtained as a yellow solid (60.79 mg, 41 %). **<sup>1</sup>H NMR** (500 MHz,  $CDCl_3$ , 25 °C)  $\delta$  [ppm] 11.81 (s, 1H), 11.41 (s, 1H), 11.25 (s, 1H), 11.09 (s, 1H), 10.99 (s, 1H), 9.57 (s, 1H), 8.57 (d,  $J = 3.8$  Hz, 1H), 8.36 (d,  $J = 7.4$  Hz, 1H), 8.24 (d,  $J = 7.4$  Hz, 1H), 8.13 (dd,  $J = 8.2, 1.3$  Hz, 1H), 8.01 – 7.92 (m, 2H), 7.87 (dd,  $J = 8.3, 1.3$  Hz, 1H), 7.83 – 7.77 (m, 3H), 7.74 (dd,  $J = 8.4, 1.3$  Hz, 1H), 7.69 – 7.66 (m, 1H), 7.62 – 7.58 (m, 2H), 7.48-7.44 (m, 4H), 7.40 – 7.33 (m, 2H), 7.16 – 7.11 (m, 2H), 7.10 – 7.03 (m, 2H), 6.81 (s, 1H), 6.61 (s, 1H), 6.10 (s, 1H), 4.29 – 4.11 (m, 3H), 4.03 – 3.93 (m, 4H), 3.90 – 3.81 (m, 3H), 3.77 – 3.71 (m, 2H), 2.48 – 2.41 (m, 3H), 2.36 – 2.30 (m, 3H), 2.27 – 2.24 (m, 3H), 1.74 – 1.67 (m, 9H), 1.62 – 1.55 (m, 10H), 1.38 – 1.28 (m, 10H), 1.11 – 0.99 (m, 12H), 0.91 – 0.79 (m, 3H), 0.66 (s, 3H), 0.61 (s, 3H), 0.23 (s, 9H), 0.16 (s, 3H). **MS** calcd for  $C_{106}H_{116}N_{14}NaO_{18}Si$   $[M+Na]^+$  1923.8254, found (HR-ESI) 1924.6668.

**(1S)-Camph-Q<sup>B</sup>XQ<sup>B</sup>YQ<sup>B</sup>X-OMe (5)** Compound **19** (60.79 mg, 32  $\mu$ mol, 1 eq.) was dissolved in a mixture of dry Chloroform/MeOH 3:2 (5 mL) under  $N_2$ . TMSCHN<sub>2</sub> (solut. 2 M in Hex, 39  $\mu$ L, 0.064 mmol, 2 eq.) was added dropwise, and the solution was stirred at r.t. for 2 h. A few drops of acetic acid were added, and the solution was stirred for 5 min at r.t. Then the solution was diluted with DCM, washed with  $NaHCO_3$ , dried  $MgSO_4$ , filtered and concentrated. The product was obtained as a yellow solid (77.55 mg, 70 %). **<sup>1</sup>H NMR** (500 MHz,  $CDCl_3$ , 25 °C)  $\delta$  [ppm] 11.78 (s, 1H), 11.49 (s, 1H), 11.48 (s, 1), 11.38 (s, 1H), 11.08 (s, 1H), 9.59 (s, 1H), 8.49 (s, 1H), 8.35 (d,  $J = 7.3$  Hz, 1H), 8.24 (d,  $J = 7.3$  Hz, 1H), 8.11 – 8.06 (m, 2H), 8.02 (s, 1H), 7.97 – 7.92 (m, 2H), 7.89 – 7.83 (m, 2H), 7.83 – 7.72 (m, 2H), 7.70 – 7.61 (m, 1H), 7.45 – 7.37 (m, 7H), 7.07 (d,  $J = 4.1$  Hz, 1H), 6.94 (d,  $J = 2.3$  Hz, 1H), 6.76 (s, 1H), 6.56 (s, 1H), 6.39 (s, 1H), 6.12 (s, 1H), 5.58 (s, 1H), 5.35 (s, 1H), 5.31 – 5.28 (m, 1H), 4.69 (s, 1H), 4.40 – 4.37 (m, 1H), 4.25-4.19 (m, 3H), 4.19 – 4.09 (m, 4H), 4.09 – 4.01 (m, 3H), 4.01 – 3.96 (m, 3H), 3.94 – 3.80 (m, 3H), 3.79 – 3.72 (m, 1H), 3.71 – 3.58 (m, 9H), 3.47 – 3.35 (m, 3H), 3.13 (s, 3H), 2.96 (s, 3H), 2.88 (s, 3H), 2.49 – 2.39 (m, 3H), 2.36 – 2.18 (m, 11H), 2.09-2.00 (m, 4H), 1.35 – 1.27 (m, 2H), 1.24 – 1.17 (m, 2H), 0.90 – 0.79 (m, 3H), 0.66 (s, 3H), 0.61 (s, 3H), 0.23 (s, 9H), -0.05 (s, 3H). **MS** calcd for  $C_{107}H_{118}N_{14}NaO_{18}Si$   $[M+Na]^+$  1937.8410 found (HR-ESI) 1938.7302.

**O<sub>2</sub>N-Q<sup>B</sup>XB<sup>S</sup>Q<sup>B</sup>YQ<sup>B</sup>X-OH (20)** Compound **20** was synthesized using the SPS procedures reported in 0 on SASRIN resin loaded via HBTU-coupling described in 0 (scale: 53  $\mu$ mol). After full cleavage and precipitation in EtOAc/*n*-Hex, the product was obtained as a yellow solid (46.96 mg, 53 %). **<sup>1</sup>H NMR**

(500 MHz, CDCl<sub>3</sub>, 25 °C)  $\delta$  [ppm] 11.72 (s, 1H), 10.98 (s, 1H), 10.85 (s, 1H), 10.23 (s, 1H), 9.82 (s, 1H), 8.86 (dd,  $J = 7.7, 1.3$  Hz, 1H), 8.57 (s, 1H), 8.37 (dd,  $J = 8.4, 1.4$  Hz, 1H), 8.26 – 8.23 (m, 1H), 8.08 – 8.01 (m, 1H), 7.91 – 7.84 (m, 2H), 7.82 – 7.73 (m, 2H), 7.63 – 7.56 (m, 2H), 7.57 – 7.51 (m, 3H), 7.51 – 7.43 (m, 3H), 7.37 – 7.27 (m, 2H), 7.14 – 7.10 (m, 2H), 6.87 – 6.84 (m, 1H), 6.66 – 6.60 (m, 2H), 6.52 (d,  $J = 7.9$  Hz, 1H), 6.48 (s, 1H), 6.44 (s, 1H), 5.58 (s, 1H), 4.29 – 4.16 (m, 5H), 4.16 – 4.10 (m, 3H), 4.09 – 4.03 (m, 3H), 4.00 – 3.98 (m, 1H), 3.90 – 3.78 (m, 5H), 2.37 – 2.31 (m, 3H), 2.28 – 2.25 (m, 2H), 1.73 – 1.63 (m, 3H), 1.62 – 1.54 (m, 3H), 1.53 – 1.45 (m, 3H), 1.42 – 1.30 (m, 8H), 1.22–1.10 (m, 5H), 1.10 – 1.02 (m, 5H), 0.96 – 0.91 (m, 3H), 0.91 – 0.76 (m, 3H), 0.21 (s, 9H). **MS** calcd for C<sub>91</sub>H<sub>97</sub>N<sub>13</sub>NaO<sub>17</sub>Si [M+Na]<sup>+</sup> 1694.6787, found (HR-ESI) 1695.5758.

**O<sub>2</sub>N-Q<sup>B</sup>X<sup>B</sup>S<sup>Q</sup>Y<sup>Q</sup>X-OMe (6)** Compound **20** (46.96 mg, 28  $\mu$ mol, 1 eq.) was dissolved in a mixture of dry Chloroform/MeOH 3:2 (5 mL) under N<sub>2</sub>. TMSCHN<sub>2</sub> (solut. 2 M in Hex, 34  $\mu$ L, 0.056 mmol, 2 eq.) was added dropwise, and the solution was stirred at r.t. for 2 h. A few drops of acetic acid were added, and the solution was stirred for 5 min at r.t. Then the solution was diluted with DCM, washed with NaHCO<sub>3</sub>, dried MgSO<sub>4</sub>, filtered and concentrated. The product was obtained as a yellow solid (38.23 mg, 81 %). **<sup>1</sup>H NMR** (500 MHz, CDCl<sub>3</sub>, 25 °C)  $\delta$  [ppm] 11.94 (s, 1H), 11.46 (s, 1H), 10.83 (s, 1H), 10.19 (s, 1H), 9.81 (s, 1H), 8.85 (dd,  $J = 7.6, 1.3$  Hz, 1H), 8.44 – 8.40 (m, 1H), 8.36 (dd,  $J = 8.4, 1.5$  Hz, 1H), 8.18 (dd,  $J = 7.6, 1.3$  Hz, 1H), 8.09 (dt,  $J = 7.6, 1.6$  Hz, 2H), 7.84 (dd,  $J = 8.3, 1.3$  Hz, 2H), 7.80 – 7.72 (m, 3H), 7.70 – 7.63 (m, 4H), 7.58 – 7.39 (m, 5H), 7.12 (t,  $J = 8.0$  Hz, 1H), 6.83 (td,  $J = 7.6, 1.7$  Hz, 1H), 6.62 (s, 1H), 6.58 (t,  $J = 7.2$  Hz, 1H), 6.52 (d,  $J = 6.4$  Hz, 2H), 6.39 (d,  $J = 2.4$  Hz, 1H), 4.26 – 4.18 (m, 4H), 4.11 – 3.99 (m, 4H), 3.92 (s, 1H), 3.87 (t,  $J = 7.9$  Hz, 1H), 3.83 – 3.76 (m, 2H), 3.75 – 3.64 (m, 1H), 3.50 (dd,  $J = 15.9, 8.3$  Hz, 2H), 3.39 (s, 3H), 2.51 – 2.42 (m, 1H), 2.40 – 2.20 (m, 2H), 2.05 – 1.99 (m, 1H), 1.75 – 1.67 (m, 4H), 1.39 – 1.27 (m, 8H), 1.21 – 1.15 (m, 12H), 0.90 – 0.78 (m, 3H), 0.22 (s, 9H), 0.19 (d,  $J = 6.6$  Hz, 3H), 0.12 (q,  $J = 3.4$  Hz, 3H), 0.07 (s, 3H). **MS** calcd for C<sub>92</sub>H<sub>99</sub>N<sub>13</sub>NaO<sub>17</sub>Si [M+Na]<sup>+</sup> 1708.6943 found (HR-ESI) 1709.5631.

**(1S)-Camph-Q<sup>B</sup>X<sup>B</sup>S<sup>Q</sup>Y<sup>Q</sup>X-OH (21)** Compound **21** was synthesized using the SPS procedures reported in 0 on SASRIN resin loaded via HBTU-coupling described in 0 (scale: 53  $\mu$ mol). After full cleavage and precipitation in EtOAc/*n*-Hex, the product was obtained as a yellow solid (42.48 mg, 44 %). **<sup>1</sup>H NMR** (500 MHz, CDCl<sub>3</sub>, 25 °C)  $\delta$  [ppm] 11.67 (s, 1H), 10.95 (s, 1H), 10.53 (s, 1H), 10.16 (s, 1H), 10.14 (s, 1H), 9.74 (s, 1H), 8.86 (dd,  $J = 7.5, 1.2$  Hz, 1H), 8.54 (dd,  $J = 7.6, 1.3$  Hz, 1H), 8.46 (s, 1H), 8.23 (dd,  $J = 7.6, 1.3$  Hz, 1H), 8.02 (td,  $J = 8.0, 1.5$  Hz, 3H), 7.89 – 7.84 (m, 3H), 7.66 – 7.59 (m, 3H), 7.58 – 7.52 (m, 3H), 7.40 – 7.29 (m, 4H), 7.14 – 7.10 (m, 2H), 6.70 (s, 1H), 6.55 (d,  $J = 7.8$  Hz, 1H), 6.50 (s, 1H), 6.43 (d,  $J = 2.3$  Hz, 1H), 6.40 (s, 1H), 4.27 – 4.16 (m, 4H), 4.08 – 4.01 (m, 2H), 3.91 – 3.80 (m, 6H), 3.71 – 3.62 (m, 2H), 3.10 (tt,  $J = 7.4, 3.7$  Hz, 2H), 2.74 – 2.68 (m, 1H), 2.51 – 2.44 (m, 1H), 2.38 – 2.21 (m, 10H), 2.03 – 1.98 (m, 2H), 1.73 – 1.52 (m, 5H), 1.50 – 1.37 (m, 4H), 1.37 – 1.26 (m, 8H), 1.22 – 1.12 (m, 8H), 1.09 – 0.99 (m, 8H), 0.67 (s, 3H), 0.46 (s, 3H), 0.21 (s, 9H). **MS** calcd for C<sub>101</sub>H<sub>111</sub>N<sub>13</sub>NaO<sub>18</sub>Si [M+Na]<sup>+</sup> 1844.7832, found (HR-ESI) 1845.6781.

**(1S)-Camph-Q<sup>B</sup>X<sup>B</sup>S<sup>Q</sup>Y<sup>Q</sup>X-OMe (7)** Compound **21** (42.48 mg, 23  $\mu$ mol, 1 eq.) was dissolved in a mixture of dry Chloroform/MeOH 3:2 (5 mL) under N<sub>2</sub>. TMSCHN<sub>2</sub> (solut. 2 M in Hex, 28  $\mu$ L, 0.046 mmol, 2 eq.) was added dropwise, and the solution was stirred at r.t. for 2 h. A few drops of acetic acid were added, and the solution was stirred for 5 min at r.t. Then the solution was diluted with DCM, washed with NaHCO<sub>3</sub>, dried MgSO<sub>4</sub>, filtered and concentrated. The product was obtained as a yellow solid (35.05 mg, 83 %). <sup>1</sup>H NMR (500 MHz, CDCl<sub>3</sub>, 25 °C)  $\delta$  [ppm] 11.92 (s, 1H), 11.46 (s, 1H), 10.51 (s, 1H), 10.15 (s, 1H), 10.14 (s, 1H), 9.73 (s, 1H), 8.84 – 8.81 (m, 1H), 8.54 (d, *J* = 7.6 Hz, 1H), 8.38 (s, 1H), 8.13 (d, *J* = 6.3 Hz, 1H), 8.09 – 7.93 (m, 2H), 7.90 – 7.80 (m, 2H), 7.79 – 7.71 (m, 2H), 7.71 – 7.61 (m, 3H), 7.61 – 7.52 (m, 1H), 7.52 – 7.42 (m, 1H), 7.35 (d, *J* = 26.7 Hz, 3H), 7.24 – 7.10 (m, 2H), 6.85 (t, *J* = 7.0 Hz, 1H), 6.64 (s, 1H), 6.52 (dd, *J* = 18.2, 8.2 Hz, 2H), 6.44 (s, 1H), 6.37 (s, 1H), 5.58 (s, 1H), 4.69 (s, 2H), 4.39 – 4.36 (m, 2H), 4.23 – 3.97 (m, 5H), 3.92 (s, 1H), 3.90 – 3.78 (m, 3H), 3.68 – 3.62 (m, 2H), 3.56 – 3.47 (m, 2H), 3.36 (s, 3H), 2.96 (s, 1H), 2.88 (s, 1H), 2.57 – 2.42 (m, 2H), 2.42 – 2.29 (m, 3H), 2.10 – 1.98 (m, 3H), 1.73 – 1.63 (m, 8H), 1.39 – 1.27 (m, 8H), 1.24 – 1.16 (m, 7H), 1.12 (s, 3H), 1.06 (s, 3H), 0.96 (s, 3H), 0.91 – 0.80 (m, 3H), 0.67 (s, 3H), 0.46 (s, 3H), 0.21 (s, 9H). MS calcd for C<sub>102</sub>H<sub>113</sub>N<sub>13</sub>NaO<sub>18</sub>Si [M+Na]<sup>+</sup> 1858.7988 found (HR-ESI) 1859.7043.

**(1S)-Camph-Q<sup>B</sup>X<sup>B</sup>R<sup>Q</sup>Y<sup>Q</sup>X-OH (22)** Compound **22** was synthesized using the SPS procedures reported in 0 on SASRIN resin loaded via HBTU-coupling described in 0 (scale: 53  $\mu$ mol). After full cleavage and precipitation in EtOAc/*n*-Hex, the product was obtained as a yellow solid (43.00 mg, 44 %). <sup>1</sup>H NMR (500 MHz, CDCl<sub>3</sub>, 25 °C)  $\delta$  [ppm] 11.99 (s, 1H), 11.30 (s, 1H), 10.30 (s, 1H), 9.12 (s, 1H), 9.06 (d, *J* = 7.6 Hz, 1H), 8.48 (d, *J* = 7.5 Hz, 1H), 8.13 (s, 1H), 8.05 – 8.01 (m, 2H), 7.98 (dd, *J* = 8.2, 1.2 Hz, 2H), 7.73 (t, *J* = 8.0 Hz, 1H), 7.63 – 7.54 (m, 5H), 7.49 – 7.46 (m, 3H), 7.36 (dd, *J* = 16.6, 8.6 Hz, 2H), 7.18 – 7.11 (m, 3H), 7.03 (s, 1H), 6.91 (d, *J* = 12.7 Hz, 1H), 6.88 (d, *J* = 6.9 Hz, 2H), 6.76 (d, *J* = 8.0 Hz, 1H), 6.69 (s, 1H), 6.62 – 6.58 (m, 1H), 6.39 (s, 1H), 4.72 (s, 1H), 4.64 (s, 1H), 4.53 – 4.48 (m, 1H), 4.28 – 4.09 (m, 4H), 3.99 – 3.87 (m, 3H), 3.84 – 3.72 (m, 4H), 2.41 – 2.30 (m, 9H), 2.30 – 2.24 (m, 4H), 2.06 – 1.98 (m, 11H), 1.61 – 1.52 (m, 6H), 1.50 – 1.44 (m, 6H), 1.44 – 1.32 (m, 7H), 1.19 – 0.98 (m, 6H), 0.98 – 0.76 (m, 6H), 0.19 (s, 9H). MS calcd for C<sub>101</sub>H<sub>111</sub>N<sub>13</sub>NaO<sub>18</sub>Si [M+Na]<sup>+</sup> 1844.7832, found (HR-ESI) 1845.6798.

**(1S)-Camph-Q<sup>B</sup>X<sup>B</sup>R<sup>Q</sup>Y<sup>Q</sup>X-OMe (8)** Compound **22** (43.00 mg, 23  $\mu$ mol, 1 eq.) was dissolved in a mixture of dry Chloroform/MeOH 3:2 (5 mL) under N<sub>2</sub>. TMSCHN<sub>2</sub> (solut. 2 M in Hex, 28  $\mu$ L, 0.046 mmol, 2 eq.) was added dropwise, and the solution was stirred at r.t. for 2 h. A few drops of acetic acid were added, and the solution was stirred for 5 min at r.t. Then the solution was diluted with DCM, washed with NaHCO<sub>3</sub>, dried MgSO<sub>4</sub>, filtered and concentrated. The product was obtained as a yellow solid (35.55 mg, 84 %). <sup>1</sup>H NMR (500 MHz, CDCl<sub>3</sub>, 25 °C)  $\delta$  [ppm] 11.93 (s, 1H), 11.46 (s, 1H), 10.18 (s, 1H), 9.83 (s, 1H), 9.81 (s, 2H), 8.84 (dd, *J* = 7.6, 1.3 Hz, 1H), 8.55 – 8.49 (m, 1H), 8.36 (t, *J* = 3.7 Hz, 1H), 8.11 (d, *J* = 6.4 Hz, 1H), 8.05 – 7.88 (m, 3H), 7.85 (dd, *J* = 8.5, 1.4 Hz, 1H), 7.81 (dd, *J* = 8.4, 1.4 Hz, 1H), 7.70 (dd, *J* = 8.4, 1.4 Hz, 1H), 7.66 (s, 1H), 7.56 (t, *J* = 7.9 Hz, 2H), 7.44 (td, *J* = 8.1, 4.2

Hz, 2H), 7.41 – 7.35 (m, 3H), 7.22 (s, 1H), 7.16 – 7.10 (m, 2H), 6.89 (td,  $J = 7.8, 1.7$  Hz, 1H), 6.70 (s, 1H), 6.59 (t,  $J = 7.8$  Hz, 1H), 6.51 (d,  $J = 7.6$  Hz, 1H), 6.40 (d,  $J = 2.7$  Hz, 2H), 4.30 – 3.96 (m, 5H), 3.94 – 3.79 (m, 2H), 3.59 – 3.48 (m, 1H), 3.38 (t,  $J = 7.1$  Hz, 1H), 3.34 (s, 3H), 2.52 – 2.19 (m, 6H), 1.61 – 1.55 (m, 11H), 1.36 – 1.31 (m, 6H), 1.28 – 1.19 (m, 19H), 0.88 (t,  $J = 6.9$  Hz, 3H), 0.73 (s, 3H), 0.43 (s, 3H), 0.21 (s, 9H), 0.07 (s, 3H), -0.06 – -0.12 (m, 3H). **MS** calcd for  $C_{102}H_{113}N_{13}NaO_{18}Si$   $[M+Na]^+$  1858.7988 found (HR-ESI) 1859.6670.

### 5.2.5.3.2 Synthesis of sequences with a helix-turn-helix-motif and handedness-control in both helices

**O<sub>2</sub>N-Q<sup>B</sup>X<sup>B</sup>S<sup>Q</sup>M<sup>Y</sup>Q<sup>B</sup>X-T3-2eg-Q<sup>B</sup>X<sup>B</sup>S<sup>Q</sup>B<sup>Y</sup>Q<sup>B</sup>X-OH (23)** Compound **23** was synthesized using the SPS procedures reported in 0 on SASRIN resin loaded via HBTU-coupling described in 0 (scale: 93  $\mu$ mol). The product was obtained after full cleavage and precipitation in EtOAc/*n*-Hex as a yellow solid (162.34 mg, 49 %). **<sup>1</sup>H NMR** (500 MHz, CD<sub>2</sub>Cl<sub>2</sub>, 25 °C)  $\delta$  [ppm] 11.57 (s, 1H), 11.46 (s, 1H), 10.88 (s, 1H), 10.84 (s, 1H), 10.62 (s, 1H), 10.31 (s, 1H), 9.98 (s, 1H), 9.83 (s, 1H), 9.59 (s, 1H), 9.32 (s, 1H), 8.97 (s, 1H), 8.63 (s, 1H), 8.59 – 8.54 (m, 1H), 8.39 (dd,  $J = 8.3, 1.4$  Hz, 1H), 8.31 – 8.19 (m, 1H), 8.12 – 7.92 (m, 5H), 7.92 – 7.73 (m, 7H), 7.71 – 7.49 (m, 6H), 7.48 – 7.32 (m, 13H), 7.32 – 7.20 (m, 6H), 7.15 (dq,  $J = 14.4, 6.7$  Hz, 3H), 7.03 – 6.99 (m, 2H), 6.96 (dd,  $J = 7.6, 3.5$  Hz, 1H), 6.75 (tt,  $J = 9.7, 4.7$  Hz, 2H), 6.54 (t,  $J = 7.2$  Hz, 1H), 6.46 (t,  $J = 7.6$  Hz, 1H), 6.41 (d,  $J = 4.4$  Hz, 2H), 6.36 – 6.33 (m, 1H), 6.25 (s, 1H), 4.27 – 4.17 (m, 6H), 4.14 (dd,  $J = 9.0, 7.2$  Hz, 4H), 3.96 – 3.91 (m, 2H), 3.72 – 3.62 (m, 6H), 3.50 – 3.42 (s, 2H), 2.71 – 2.65 (m, 1H), 2.65 – 2.55 (m, 2H), 2.45 – 2.29 (m, 7H), 1.66 (s, 9H), 1.61 (d,  $J = 3.27$  Hz, 18H), 1.52 (s, 9H), 1.34 – 1.22 (m, overlap with solvent residue of ethyl acetate), 1.21 – 1.11 (m, 39H), 0.21 (s, 9H), 0.19 (s, 9H) 0.04 (d,  $J = 5.9$  Hz, 3H), -0.25 (s, 3H). **MS** calcd for  $C_{186}H_{201}N_{27}NaO_{34}Si_2$   $[M+Na]^+$  3435.4260, found (HR-ESI) 3437.2217.

**O<sub>2</sub>N-Q<sup>B</sup>X<sup>B</sup>S<sup>Q</sup>M<sup>Y</sup>Q<sup>B</sup>X-T3-2eg-Q<sup>B</sup>X<sup>B</sup>S<sup>Q</sup>B<sup>Y</sup>Q<sup>B</sup>X-OMe (24)** Compound **23** (162.34 mg, 45.57  $\mu$ mol, 1 eq.) was dissolved in a mixture of dry Chloroform/MeOH 3:2 (5 mL) under N<sub>2</sub>. TMSCHN<sub>2</sub> (solut. 2 M in Hex, 26  $\mu$ L, 0.091 mmol, 2 eq.) was added dropwise, and the solution was stirred at r.t. for 2 h. A few drops of acetic acid were added, and the solution was stirred for 5 min at r.t. Then the solution was diluted with DCM, washed with NaHCO<sub>3</sub>, dried MgSO<sub>4</sub>, filtered and concentrated. The product was obtained as a yellow solid (151.57 mg, 93 %). **<sup>1</sup>H NMR** (500 MHz, CD<sub>2</sub>Cl<sub>2</sub>, 25 °C)  $\delta$  [ppm] 11.71 (s, 1H), 11.59 (s, 1H), 11.36 (s, 1H), 10.92 (s, 1H), 10.60 (s, 1H), 10.39 (s, 1H), 9.94 (s, 1H), 9.86 (s, 1H), 9.60 (s, 1H), 9.39 (s, 1H), 8.95 (s, 1H), 8.77 (dd,  $J = 7.6, 1.3$  Hz, 1H), 8.59 (dd,  $J = 7.5, 1.3$  Hz, 1H), 8.40 (dd,  $J = 8.4, 1.4$  Hz, 1H), 8.25 (q,  $J = 3.9$  Hz, 2H), 8.20 – 8.17 (m, 1H), 8.08 (dd,  $J = 7.5, 1.3$  Hz, 1H), 8.05 – 8.01 (m, 2H), 8.00 – 7.96 (m, 2H), 7.89 (dd,  $J = 8.0, 1.6$  Hz, 1H), 7.85 – 7.72 (m, 4H), 7.67 – 7.58 (m, 8H), 7.50 – 7.43 (m, 4H), 7.43 – 7.37 (m, 4H), 7.34 – 7.27 (m, 4H), 7.27 – 7.11 (m, 5H), 7.08 – 7.04 (m, 1H), 7.01 (d,  $J = 2.2$  Hz, 1H), 6.94 – 6.90 (m, 1H), 6.76 (qd,  $J = 7.8, 1.7$  Hz, 3H), 6.60 – 6.51 (m, 2H), 6.48 – 6.35 (m, 3H), 6.33 (dd,  $J = 6.3, 2.6$  Hz, 2H), 6.26 (d,  $J = 2.2$  Hz, 1H), 4.24 – 4.18

(m, 4H), 4.18 – 4.08 (m, 6H), 4.04 (s, 3H), 4.02 (d,  $J = 8.0$  Hz, 3H), 3.92 (d,  $J = 6.5$  Hz, 1H), 3.80 – 3.77 (m, 3H), 3.70 (dd,  $J = 6.6, 4.5$  Hz, 2H), 3.36 – 3.33 (m, 2H), 2.70 (dd,  $J = 7.1, 5.0$  Hz, 2H), 2.62 (dt,  $J = 9.9, 4.9$  Hz, 1H), 2.50 – 2.31 (m, 7H), 2.31 – 2.24 (m, 3H), 2.24 – 2.15 (m, 4H), 2.02 – 1.98 (m, 2H), 1.86 – 1.80 (m, 2H), 1.67 – 1.64 (m, 7H), 1.63 (s, 9H), 1.63 (s, 9H), 1.35 – 1.29 (m, 10H), 1.22 – 1.17 (m, 21H), 1.16 – 1.13 (m, 8H), 1.09 (d,  $J = 6.7$  Hz, 4H), 0.21 (s, 9H), 0.19 (s, 9H), 0.06 (d,  $J = 2.3$  Hz, 3H), -0.18 (d,  $J = 6.3$  Hz, 3H). **MS** calcd for  $C_{187}H_{203}N_{27}NaO_{34}Si_2$   $[M+Na]^+$  3449.4417 found (HR-ESI) 3451.1943.

**O<sub>2</sub>N-Q<sup>B</sup>XB<sup>S</sup>Q<sup>M</sup>YQ<sup>B</sup>X-T3-2eg-Q<sup>B</sup>XB<sup>S</sup>Q<sup>B</sup>YQ<sup>B</sup>X-OMe (9)** Compound **24** (24.25 mg, 6.78  $\mu$ mol) was treated with a 50 % solution of TFA in DCM (4 mL) at r.t. for 48 h. Then the solvent was removed under vacuum, obtaining the product as a yellow solid (21.37 mg, quant.). **<sup>1</sup>H NMR** (500 MHz, Pyridine-*d*<sub>5</sub>, 25 °C)  $\delta$  [ppm] 12.41 (s, 1H), 12.31 (s, 1H), 12.08 (s, 1H), 11.52 (s, 1H), 11.20 (s, 1H), 11.03 (s, 1H), 10.64 (s, 1H), 10.52 (s, 1H), 10.20 (s, 1H), 10.00 (s, 1H), 9.72 (s, 1H), 9.26 (dd,  $J = 7.6, 1.3$  Hz, 1H), 9.16 (dd,  $J = 7.5, 1.3$  Hz, 1H), 8.99 (t,  $J = 3.6$  Hz, 1H), 8.87 (dd,  $J = 7.5, 1.3$  Hz, 1H), 8.80 – 8.76 (m, 2H), 8.63 – 8.57 (m, 2H), 8.52 (dd,  $J = 7.6, 1.3$  Hz, 1H), 8.45 – 8.37 (m, 5H), 8.30 (ddd,  $J = 7.5, 3.0, 1.3$  Hz, 2H), 8.16 (ddd,  $J = 17.0, 8.0, 2.4$  Hz, 2H), 8.08 – 8.04 (m, 2H), 8.00 (dd,  $J = 8.1, 1.4$  Hz, 1H), 7.95 – 7.88 (m, 5H), 7.84 (d,  $J = 2.7$  Hz, 2H), 7.80 – 7.72 (m, 7H), 7.69 – 7.65 (m, 2H), 7.57 – 7.51 (m, 5H), 7.46 (t,  $J = 7.8$  Hz, 1H), 7.34 (dt,  $J = 22.5, 7.9$  Hz, 2H), 7.28 – 7.24 (m, 1H), 7.13 (s, 1H), 7.07 – 7.02 (m, 2H), 6.98 – 6.76 (m, 4H), 6.75 (d,  $J = 2.2$  Hz, 1H), 6.70 (d,  $J = 2.1$  Hz, 1H), 4.40 (q,  $J = 6.4$  Hz, 1H), 4.26 (dd,  $J = 8.4, 6.0$  Hz, 1H), 4.20 (s, 1H), 4.10 (s, 3H), 4.02 (dd,  $J = 8.9, 6.3$  Hz, 4H), 3.98 – 3.90 (m, 4H), 3.88 – 3.83 (m, 1H), 3.70 – 3.61 (m, 4H), 3.52 – 3.49 (m, 1H), 3.24 (ddd,  $J = 16.7, 11.4, 7.0$  Hz, 1H), 3.15 (dt,  $J = 9.6, 5.8$  Hz, 2H), 2.99 (td,  $J = 10.1, 9.5, 6.0$  Hz, 3H), 2.95 – 2.88 (m, 1H), 2.71 (dt,  $J = 10.3, 5.6$  Hz, 1H), 2.63 (dt,  $J = 10.4, 5.3$  Hz, 1H), 2.53 (dt,  $J = 13.5, 6.7$  Hz, 3H), 2.38 (dt,  $J = 15.6, 6.1$  Hz, 2H), 2.19 – 2.00 (m, 5H), 1.29 (d,  $J = 6.6$  Hz, 4H), 1.21 (d,  $J = 6.7$  Hz, 3H), 1.07 – 0.95 (m, 23H), 0.45 (d,  $J = 6.5$  Hz, 3H), 0.29 – 0.24 (m, 3H). **MS** calcd for  $C_{161}H_{147}N_{27}Na_2O_{34}$   $[M+2Na]^{2+}$  1524.0194, found (HR-ESI) 1524.3674.

**O<sub>2</sub>N-Q<sup>B</sup>XB<sup>S</sup>Q<sup>M</sup>YQ<sup>B</sup>X-T3-3eg-Q<sup>B</sup>XB<sup>S</sup>Q<sup>B</sup>YQ<sup>B</sup>X-OH (25)** Compound **25** was synthesized using the SPS procedures reported in 0 on SASRIN resin loaded via HBTU-coupling described in 0 (scale: 93  $\mu$ mol). The product was obtained after full cleavage and precipitation in EtOAc/*n*-Hex as a yellow solid (154.29 mg, 46 %). **<sup>1</sup>H NMR** (500 MHz, CD<sub>2</sub>Cl<sub>2</sub>, 25 °C)  $\delta$  [ppm] 11.67 (s, 1H), 11.57 (d,  $J = 8.6$  Hz, 1H), 11.03 (s, 1H), 10.91 (s, 1H), 10.63 (s, 1H), 10.51 (s, 1H), 9.97 (s, 1H), 9.64 (s, 1H), 9.46 (s, 1H), 9.09 (s, 1H), 8.77 (dd,  $J = 7.6, 1.3$  Hz, 1H), 8.68 (dd,  $J = 7.5, 1.3$  Hz, 1H), 8.41 (dd,  $J = 8.4, 1.4$  Hz, 1H), 8.33 – 8.24 (m, 3H), 8.19 – 8.15 (m, 1H), 8.10 – 8.03 (m, 3H), 8.03 – 7.95 (m, 3H), 7.93 – 7.90 (m, 1H), 7.87 – 7.75 (m, 3H), 7.72 – 7.61 (m, 9H), 7.52 – 7.35 (m, 10H), 7.34 – 7.26 (m, 3H), 7.25 – 7.13 (m, 3H), 7.12 – 7.08 (m, 2H), 6.80 (td,  $J = 7.8, 1.7$  Hz, 2H), 6.62 – 6.55 (m, 2H), 6.51 (q,  $J = 8.8, 8.2$  Hz, 3H), 6.46 – 6.41 (m, 2H), 6.40 – 6.31 (m, 3H), 4.28 – 4.16 (m, 9H), 4.14 – 3.98 (m, 16H), 3.98 – 3.90 (m, 2H), 3.84 – 3.78 (m, 4H), 3.77 – 3.68 (m, 3H), 3.56 – 3.45 (m, 2H), 3.17 – 3.04 (m, 2H), 2.71



-2.57 (m, 4H), 2.51 – 2.42 (m, 3H), 2.41 – 2.31 (m, 2H), 2.31 – 2.24 (m, 3H), 2.20 – 2.16 (m, 3H), 1.67 (s, 9H), 1.64 (s, 9H), 1.63 (s, 9H), 1.55 (s, 9H), 1.38 – 1.24 (m, 10H), 1.24 – 1.14 (m, 10H), 1.13 (d,  $J = 6.7$  Hz, 2H), 1.08 (d,  $J = 6.7$  Hz, 2H), 0.90 – 0.87 (m, 2H), 0.21 (s, 18H), 0.07 (t,  $J = 2.2$  Hz, 3H), -0.12 (d,  $J = 6.6$  Hz, 3H). **MS** calcd for  $C_{188}H_{205}N_{27}NaO_{35}Si_2$   $[M+Na]^+$  3479.4522, found (HR-ESI) 3479.1593.

**O<sub>2</sub>N-Q<sup>B</sup>X<sup>B</sup>S<sup>Q</sup>M<sup>Y</sup>Q<sup>B</sup>X-T3-3eg-Q<sup>B</sup>X<sup>B</sup>S<sup>Q</sup>B<sup>Y</sup>Q<sup>B</sup>X-OMe (26)** Compound **25** (154.29 mg, 42.78  $\mu$ mol, 1 eq.) was dissolved in a mixture of dry Chloroform/MeOH 3:2 (5 mL) under N<sub>2</sub>. TMSCHN<sub>2</sub> (solut. 2 M in Hex, 24.5  $\mu$ L, 0.086 mmol, 2 eq.) was added dropwise, and the solution was stirred at r.t. for 2 h. A few drops of acetic acid were added, and the solution was stirred for 5 min at r.t. Then the solution was diluted with DCM, washed with NaHCO<sub>3</sub>, dried MgSO<sub>4</sub>, filtered and concentrated. The product was obtained as a yellow solid (148.69 mg, 96 %). **<sup>1</sup>H NMR** (500 MHz, CD<sub>2</sub>Cl<sub>2</sub>, 25 °C)  $\delta$  [ppm] 11.74 (s, 1H), 11.68 (s, 1H), 11.38 (s, 1H), 11.03 (s, 1H), 10.62 (s, 1H), 10.51 (s, 1H), 9.97 (s, 1H), 9.94 (s, 1H), 9.65 (s, 1H), 9.44 (s, 1H), 9.08 (s, 1H), 8.82 – 8.78 (m, 1H), 8.68 (dd,  $J = 7.5, 1.2$  Hz, 1H), 8.41 (dd,  $J = 8.3, 1.4$  Hz, 2H), 8.34 – 8.28 (m, 3H), 8.12 – 7.94 (m, 10H), 7.89 – 7.75 (m, 4H), 7.72 – 7.61 (m, 6H), 7.59 – 7.29 (m, 9H), 7.27 – 7.05 (m, 7H), 6.81 – 6.76 (m, 3H), 6.58 (d,  $J = 8.0$  Hz, 3H), 6.51 – 6.41 (m, 3H), 6.40 – 6.33 (m, 2H), 6.32 (d,  $J = 2.2$  Hz, 1H), 4.23-4.17 (m, 4H), 4.14 – 4.02 (m, 3H), 3.98-3.94 (m, 1H), 3.82-3.78 (m, 3H), 3.75-3.68 (m, 3H), 3.36 – 3.34 (m, 2H), 3.34 (s, 3H), 3.16-3.08 (m, 2H), 3.06-3.02 (m, 1H), 2.98 (s, 1H), 2.89-2.85 (m, 1H), 2.84 – 2.78 (m, 2H), 2.71 – 2.60 (m, 2H), 2.51 – 2.33 (m, 4H), 2.32 – 2.22 (m, 3H), 2.18 – 2.15 (m, 2H), 2.04 – 1.97 (m, 1H), 1.90 – 1.84 (m, 1H), 1.64 (s, 18H), 1.63 (s, 9H), 1.58 (s, 9H), 1.36 – 1.31 (m, 4H), 1.23 – 1.15 (m, 24H), 1.13 (d,  $J = 6.8$  Hz, 4H), 1.09 – 1.07 (m, 4H), 0.90 – 0.81 (m, 2H), 0.24 – 0.22 (m, 4H), 0.21 (d,  $J = 1.2$  Hz, 18H), 0.09 – 0.06 (m, 3H), -0.12 (d,  $J = 6.6$  Hz, 3H). **MS** calcd for  $C_{189}H_{207}N_{27}NaO_{35}Si_2$   $[M+Na]^+$  3493.4679 found (HR-ESI) 3495.1820.

**O<sub>2</sub>N-Q<sup>B</sup>X<sup>B</sup>S<sup>Q</sup>M<sup>Y</sup>Q<sup>B</sup>X-T3-3eg-Q<sup>B</sup>X<sup>B</sup>S<sup>Q</sup>B<sup>Y</sup>Q<sup>B</sup>X-OMe (10)** Compound **26** (25.54 mg, 7.05  $\mu$ mol) was treated with a 50 % solution of TFA in DCM (3 mL) at r.t. for 48 h. Then the solvent was removed under vacuum, obtaining the product as a yellow solid (22.55 mg, quant.). **<sup>1</sup>H NMR** (500 MHz, Pyridine-*d*<sub>5</sub>, 25 °C)  $\delta$  [ppm] 12.43 (s, 1H), 12.36 (s, 1H), 12.09 (s, 1H), 11.60 (s, 1H), 11.21 (s, 1H), 11.12 (s, 1H), 10.66 (s, 1H), 10.59 (s, 1H), 10.23 (s, 1H), 10.03 (s, 1H), 9.86 (s, 1H), 9.30 – 9.26 (m, 1H), 9.23 – 9.20 (m, 1H), 9.02 (t,  $J = 3.7$  Hz, 1H), 8.96 (t,  $J = 3.8$  Hz, 1H), 8.88 (d,  $J = 7.4$  Hz, 1H), 8.82 (t,  $J = 6.8$  Hz, 1H), 8.63 – 8.55 (m, 3H), 8.50 – 8.41 (m, 3H), 8.35-8.29 (m, 3H), 8.16 (td,  $J = 8.5, 2.0$  Hz, 1H), 8.07 (dd,  $J = 8.5, 3.5$  Hz, 4H), 8.01 – 7.95 (m, 2H), 7.96 – 7.87 (m, 3H), 7.87 – 7.82 (m, 3H), 7.81 – 7.67 (m, 3H), 7.58 – 7.50 (m, 3H), 7.49 – 7.38 (m, 3H), 7.32 (td,  $J = 7.9, 3.6$  Hz, 3H), 7.08 – 7.04 (m, 3H), 7.03 – 6.93 (m, 3H), 6.92 – 6.84 (m, 3H), 6.84 – 6.77 (m, 3H), 6.75 (dd,  $J = 5.6, 2.1$  Hz, 3H), 4.44 – 4.40 (m, 1H), 4.30 – 4.26 (m, 1H), 4.25 – 4.20 (m, 1H), 4.12 (s, 3H), 4.09 – 4.00 (m, 3H), 3.99 – 3.95 (m, 3H), 3.95 – 3.85 (m, 3H), 3.84 – 3.80 (m, 1H), 3.75 – 3.62 (m, 2H), 3.54 – 3.49 (m, 5H), 3.43 – 3.38 (m, 1H), 3.33 – 3.27 (m, 1H), 3.19 – 3.15 (m, 2H), 3.15 – 3.09 (m, 3H), 2.98 – 2.95 (m, 2H), 2.83 – 2.67 (m, 2H),

2.62 – 2.56 (m, 2H), 2.55 – 2.53 (m, 1H), 2.50 (d,  $J = 5.9$  Hz, 1H), 2.44 – 2.36 (m, 2H), 2.17 – 2.02 (m, 6H), 1.31 (d,  $J = 6.5$  Hz, 4H), 1.23 (dd,  $J = 7.0, 4.2$  Hz, 4H), 1.16 (t,  $J = 7.3$  Hz, 1H), 1.09 – 0.94 (m, 18H), 0.46 (d,  $J = 6.4$  Hz, 3H), 0.31 (d,  $J = 7.3$  Hz, 3H). **MS** calcd for  $C_{163}H_{151}N_{27}NaO_{35}$   $[M+Na]^+$  3069.0758, found (HR-ESI) 3070.8337, calcd for  $C_{163}H_{151}N_{27}Na_2O_{35}$   $[M+2Na]^{2+}$  1546.0325, found (HR-ESI) 1546.4091.

**O<sub>2</sub>N-Q<sup>B</sup>X<sup>B</sup>S<sup>S</sup>Q<sup>M</sup>Y<sup>Q</sup>B<sup>X</sup>-T3-4eg-Q<sup>B</sup>X<sup>B</sup>S<sup>S</sup>Q<sup>B</sup>Y<sup>Q</sup>B<sup>X</sup>-OH (27)** Compound **27** was synthesized using the SPS procedures reported in 0 on SASRIN resin loaded via HBTU-coupling described in 0 (scale: 93  $\mu$ mol). The product was obtained after full cleavage and precipitation in EtOAc/*n*-Hex as a yellow solid (125.62 mg, 37%). **<sup>1</sup>H NMR** (500 MHz, CD<sub>2</sub>Cl<sub>2</sub>, 25 °C)  $\delta$  [ppm] 11.73 (s, 1H), 11.53 (s, 1H), 11.09 (s, 1H), 10.92 (s, 1H), 10.68 (s, 1H), 10.56 (s, 1H), 10.05 (s, 2H), 10.00 (s, 1H), 9.68 (s, 1H), 9.43 (s, 2H), 9.18 (s, 1H), 8.77 – 8.69 (m, 1H), 8.41 (td,  $J = 8.6, 2.7$  Hz, 1H), 8.38 – 8.30 (m, 2H), 8.12 – 7.97 (m, 6H), 7.94 (s, 1H), 7.89 – 7.73 (m, 7H), 7.69 – 7.55 (m, 6H), 7.53 – 7.38 (m, 9H), 7.34 (dd,  $J = 17.9, 9.9$  Hz, 3H), 7.29 – 7.13 (m, 4H), 7.10 (t,  $J = 7.9$  Hz, 1H), 6.84 – 6.77 (m, 2H), 6.60 (t,  $J = 7.7$  Hz, 2H), 6.54 – 6.46 (m, 3H), 6.45 – 6.36 (m, 3H), 6.34 (dd,  $J = 6.6, 1.8$  Hz, 2H), 4.28 – 4.18 (m, 8H), 4.00 (t,  $J = 6.8$  Hz, 1H), 3.81 (t,  $J = 7.6$  Hz, 1H), 3.77 – 3.69 (m, 5H), 3.29 – 3.24 (m, 1H), 3.20 – 3.13 (m, 1H), 3.03 – 2.95 (m, 1H), 2.70 – 2.65 (m, 1H), 2.62 – 2.53 (m, 2H), 2.45 – 2.32 (m, 4H), 2.28 – 2.18 (m, 1H), 1.78 – 1.71 (m, 1H), 1.69 (s, 9H), 1.64 (d,  $J = 3.2$  Hz, 18H), 1.60 (s, 9H), 1.53 – 1.50 (m, 1H), 1.46 – 1.33 (m, 4H), 1.23 – 1.09 (m, overlap with signals corresponding to ethyl acetate), 0.92 – 0.85 (m, overlap with signals corresponding to *n*-Hex.), 0.78 – 0.75 (m, 1H), 0.22 (s, 18H), 0.12 – 0.10 (m, 3H), -0.08 – -0.15 (m, 3H). **MS** calcd for  $C_{190}H_{209}N_{27}Na_2O_{36}Si_2$   $[M+2Na]^{2+}$  1773.2338, found (HR-ESI) 1774.1275.

**O<sub>2</sub>N-Q<sup>B</sup>X<sup>B</sup>S<sup>S</sup>Q<sup>M</sup>Y<sup>Q</sup>B<sup>X</sup>-T3-4eg-Q<sup>B</sup>X<sup>B</sup>S<sup>S</sup>Q<sup>B</sup>Y<sup>Q</sup>B<sup>X</sup>-OMe (28)** Compound **27** (125.62 mg, 34.41  $\mu$ mol, 1 eq.) was dissolved in a mixture of dry Chloroform/MeOH 3:2 (5 mL) under N<sub>2</sub>. TMSCHN<sub>2</sub> (solut. 2 M in Hex, 20  $\mu$ L, 0.069 mmol, 2 eq.) was added dropwise, and the solution was stirred at r.t. for 2 h. A few drops of acetic acid were added, and the solution was stirred for 5 min at r.t. Then the solution was diluted with DCM, washed with NaHCO<sub>3</sub>, dried MgSO<sub>4</sub>, filtered and concentrated. The product was obtained as a yellow solid (113.49 mg, 90 %). **<sup>1</sup>H NMR** (500 MHz, CD<sub>2</sub>Cl<sub>2</sub>, 25 °C)  $\delta$  [ppm] 11.76 (s, 1H), 11.72 (s, 1H), 11.39 (s, 1H), 11.08 (s, 1H), 10.64 (s, 1H), 10.56 (s, 1H), 9.99 (s, 1H), 9.69 – 9.65 (m, 1H), 9.46 (s, 1H), 8.81 (dd,  $J = 7.5, 1.2$  Hz, 1H), 8.73 (dd,  $J = 7.5, 1.2$  Hz, 1H), 8.42 (dd,  $J = 8.4, 1.4$  Hz, 1H), 8.37 (dd,  $J = 7.6, 1.3$  Hz, 1H), 8.31 (dt,  $J = 7.8, 3.7$  Hz, 2H), 8.13 – 8.11 (m, 2H), 8.07 (ddd,  $J = 7.6, 5.1, 1.5$  Hz, 2H), 8.04 – 7.98 (m, 3H), 7.86 (dt,  $J = 8.3, 1.1$  Hz, 2H), 7.85 – 7.81 (m, 2H), 7.79 – 7.74 (m, 2H), 7.71 – 7.63 (m, 5H), 7.60 – 7.52 (m, 2H), 7.51 – 7.40 (m, 12H), 7.32 (s, 3H), 7.26 – 7.11 (m, 6H), 6.81 (dtd,  $J = 9.7, 7.7, 1.6$  Hz, 2H), 6.59 (d,  $J = 4.2$  Hz, 2H), 6.54 (s, 1H), 6.53 – 6.44 (m, 2H), 6.37 (t,  $J = 1.8$  Hz, 2H), 6.34 (d,  $J = 2.2$  Hz, 1H), 4.25 – 4.18 (m, 6H), 4.13 – 4.08 (m, 2H), 4.08 – 4.04 (m, 4H), 4.06 – 4.01 (m, 1H), 3.99 (q,  $J = 6.4$  Hz, 1H), 3.85 – 3.77 (m, 4H), 3.77 – 3.71 (m, 2H), 3.34 (s, 3H), 3.30 – 3.25 (m, 2H), 3.18 – 3.13 (m, 2H), 3.01 – 2.92 (m, 3H), 2.88 – 2.83 (m, 2H),

2.75 – 2.66 (m, 5H), 2.61 – 2.54 (m, 3H), 2.48 – 2.42 (m, 1H), 2.42 – 2.25 (m, 7H), 2.23-2.19 (m, 1H), 2.09 – 2.05 (m, 1H), 1.96 (dt,  $J = 15.1, 5.0$  Hz, 1H), 1.65 – 1.63 (m, 24H), 1.37 – 1.26 (m, 14H), 1.24 – 1.13 (m, 28H), 1.10 (d,  $J = 6.7$  Hz, 2H), 0.23 – 0.22 (m, 1H), 0.22 (s, 18H), 0.14 – 0.11 (m, 1H), 0.10 – 0.08 (m, 3H), -0.09 (d,  $J = 6.5$  Hz, 3H). **MS** calcd for  $C_{191}H_{211}N_{27}NaO_{36}Si_2$   $[M+Na]^+$  3537.4941 found (HR-ESI) 3539.2315, calcd for  $C_{191}H_{211}N_{27}Na_2O_{36}Si_2$   $[M+2Na]^{2+}$  1780.2417 found (HR-ESI) 1781.0692.

**O<sub>2</sub>N-Q<sup>B</sup>XB<sup>S</sup>Q<sup>M</sup>YQ<sup>B</sup>X-T3-4eg-Q<sup>B</sup>XB<sup>S</sup>Q<sup>B</sup>YQ<sup>B</sup>X-OMe (11)** Compound **28** (34.30 mg, 9.36  $\mu$ mol) was treated with a 50 solution of TFA in DCM (2 mL) at r.t. for 48 h. Then the solvent was removed under vacuum, obtaining the product as a yellow solid (30.33 mg, quant.). **<sup>1</sup>H NMR** (500 MHz, Pyridine-*d*<sub>5</sub>, 25 °C)  $\delta$  [ppm] 12.44 (s, 1H), 12.39 (s, 1H), 12.11 (s, 1H), 11.63 (s, 1H), 11.22 (s, 1H), 11.16 (s, 1H), 10.67 (s, 1H), 10.62 (s, 1H), 10.25 (s, 1H), 10.05 (s, 1H), 9.90 (s, 1H), 9.31 – 9.23 (m, 2H), 9.04 (t,  $J = 3.8$  Hz, 1H), 8.98 (t,  $J = 3.7$  Hz, 1H), 8.91 – 8.88 (m, 1H), 8.85 (dt,  $J = 7.6, 1.6$  Hz, 2H), 8.61 (ddt,  $J = 7.7, 3.8, 2.0$  Hz, 3H), 8.52 (dd,  $J = 8.0, 1.6$  Hz, 1H), 8.46 – 8.41 (m, 3H), 8.36 – 8.32 (m, 3H), 8.17 – 8.15 (m, 1H), 8.12 – 8.06 (m, 3H), 8.00 (dd,  $J = 8.2, 1.3$  Hz, 1H), 7.95 – 7.89 (m, 5H), 7.89 – 7.83 (m, 3H), 7.80 – 7.69 (m, 7H), 7.57 – 7.50 (m, 2H), 7.50 – 7.41 (m, 4H), 7.35 (dd,  $J = 15.1, 7.7$  Hz, 3H), 7.19 (d,  $J = 9.5$  Hz, 2H), 7.08 (d,  $J = 7.1$  Hz, 2H), 7.01 – 6.79 (m, 3H), 6.79 – 6.76 (m, 2H), 4.46-4.42 (m, 1H), 4.31-4.28 (m, 1H), 4.25-4.22 (m, 1H), 4.13 (s, 3H), 4.10 – 4.01 (m, 3H), 4.00-3.96 (m, 1H), 3.95 – 3.87 (m, 3H), 3.77 – 3.72 (m, 2H), 3.68-3.64 (m, 3H), 3.56 (s, 3H), 3.55 – 3.46 (m, 3H), 3.29 – 3.16 (m, 4H), 3.16 – 3.09 (m, 3H), 3.07 – 3.02 (m, 2H), 3.02 – 2.89 (m, 3H), 2.89 – 2.83 (m, 2H), 2.76 – 2.71 (m, 2H), 2.63 – 2.55 (m, 1H), 2.43-2.38 (m, 1H), 2.19 – 2.01 (m, 2H), 1.31 (d,  $J = 6.7$  Hz, 4H), 1.23 (d,  $J = 6.8$  Hz, 4H), 1.16 (t,  $J = 7.3$  Hz, 1H), 1.09 – 0.97 (m, 30H), 0.48 (d,  $J = 6.1$  Hz, 3H), 0.33 (d,  $J = 6.6$  Hz, 3H). **MS** calcd for  $C_{165}H_{155}N_{27}NaO_{36}$   $[M+Na]^+$  3113.1020 found (HR-ESI) 3113.8610, calcd for  $C_{165}H_{155}N_{27}Na_2O_{36}$   $[M+2Na]^{2+}$  1568.0456 found (HR-ESI) 1568.4159.

**O<sub>2</sub>N-Q<sup>B</sup>XB<sup>R</sup>Q<sup>M</sup>YQ<sup>B</sup>X-T3-2eg-Q<sup>B</sup>XB<sup>R</sup>Q<sup>B</sup>YQ<sup>B</sup>X-OH (29)** Compound **29** was synthesized using the SPS procedures reported in 0 on SASRIN resin loaded via HBTU-coupling described in 0 (scale: 55  $\mu$ mol). After full cleavage, the product was obtained as a yellow solid (97.97 mg, 50 %). **<sup>1</sup>H NMR** (500 MHz, CDCl<sub>3</sub>, 25 °C)  $\delta$  [ppm] 11.68 (s, 1H), 11.58 (s, 1H), 10.99 (s, 1H), 10.89 (s, 1H), 10.75 (s, 1H), 10.52 (s, 1H), 10.09 (s, 1H), 10.05 (s, 1H), 9.73 (s, 1H), 9.53 (s, 1H), 9.40 (s, 3H), 8.98 (s, 1H), 8.77 (d,  $J = 7.6$  Hz, 1H), 8.62 (dd,  $J = 7.4, 1.2$  Hz, 1H), 8.36 – 8.21 (m, 6H), 8.13 – 7.98 (m, 6H), 7.93 – 7.84 (m, 2H), 7.84 – 7.72 (m, 3H), 7.72 – 7.58 (m, 7H), 7.58 – 7.51 (m, 4H), 7.50 – 7.40 (m, 6H), 7.40 – 7.31 (m, 4H), 7.19 (q,  $J = 7.9$  Hz, 1H), 7.12 (d,  $J = 8.0$  Hz, 1H), 7.09 – 7.00 (m, 3H), 6.73 (q,  $J = 7.0$  Hz, 2H), 6.56 – 6.34 (m, 4H), 6.27 (s, 1H), 4.26 – 4.09 (m, 6H), 4.04 – 3.92 (m, 2H), 3.84 – 3.74 (m, 3H), 3.69 – 3.64 (m, 3H), 3.15-3.10 (m, 7H), 2.83-2.81 (m, 2H), 2.70 – 2.64 (m, 1H), 2.61-2.56 (m, 1H), 2.46 – 2.41 (m, 1H), 2.41 – 2.32 (m, 10H), 2.32 – 2.21 (m, 8H), 2.05 – 1.99 (m, 5H), 1.92-1.88 (m, 14H), 1.73 – 1.65 (m, 14H), 1.66 – 1.55 (m, overlap with solvent residue of water), 1.20 – 1.09 (m, overlap with signals corresponding to HFIP), 1.07-1.06 (m, 4H), 0.19 (s, 9H), 0.17 (s, 9H), 0.14 (d,  $J =$

5.3 Hz, 3H), -0.09 (s, 3H). **MS** calcd for C<sub>186</sub>H<sub>201</sub>N<sub>27</sub>NaO<sub>34</sub>Si<sub>2</sub> [M+Na]<sup>+</sup> 3435.4260, found (HR-ESI) 3437.2217.

**O<sub>2</sub>N-Q<sup>B</sup>X<sup>B</sup>R<sup>Q</sup>M<sup>Y</sup>Q<sup>B</sup>X-T3-2eg-Q<sup>B</sup>X<sup>B</sup>R<sup>Q</sup>Y<sup>Q</sup>B<sup>X</sup>-OMe (30)** Compound **29** (31.03 mg, 8.71 μmol, 1 eq.) was dissolved in a mixture of dry Chloroform/MeOH 3:2 (5 mL) under N<sub>2</sub>. TMSCHN<sub>2</sub> (solut. 2 M in Hex, 5 μL, 0.017 mmol, 2 eq.) was added dropwise, and the solution was stirred at r.t. for 2 h. A few drops of acetic acid were added, and the solution was stirred for 5 min at r.t. Then the solution was diluted with DCM, washed with NaHCO<sub>3</sub>, dried MgSO<sub>4</sub>, filtered and concentrated. The product was obtained as a yellow solid (31.16 mg, quant.). **<sup>1</sup>H NMR** (500 MHz, CDCl<sub>3</sub>, 25 °C) δ [ppm] 11.82 (s, 1H), 11.68 (s, 1H), 11.41 (s, 1H), 10.99 (s, 1H), 10.75 (s, 1H), 10.50 (s, 1H), 10.09 (s, 1H), 10.02 (s, 1H), 9.74 (s, 1H), 9.52 (s, 1H), 8.96 (s, 1H), 8.75 (dd, *J* = 7.5, 1.2 Hz, 1H), 8.62 (dd, *J* = 7.5, 1.3 Hz, 1H), 8.34 – 8.26 (m, 4H), 8.13 – 8.08 (m, 2H), 8.06 – 7.99 (m, 3H), 7.90 – 7.86 (m, 1H), 7.82 – 7.72 (m, 5H), 7.70 – 7.59 (m, 6H), 7.55 (d, *J* = 1.3 Hz, 1H), 7.46 – 7.39 (m, 5H), 7.39 – 7.29 (m, 5H), 7.24 – 7.13 (m, 4H), 7.11 (t, *J* = 8.0 Hz, 2H), 7.03 (td, *J* = 12.5, 4.4 Hz, 4H), 6.75 – 6.69 (m, 2H), 6.54 (d, *J* = 7.1 Hz, 2H), 6.49 – 6.35 (m, 5H), 6.27 (dd, *J* = 12.2, 2.2 Hz, 2H), 4.19 – 4.15 (m, 3H), 4.07 – 4.00 (m, 3H), 3.99 – 3.93 (m, 2H), 3.84 – 3.77 (m, 1H), 3.75 – 3.72 (m, 2H), 3.67 – 3.65 (m, 2H), 3.34 (s, 3H), 3.05 – 2.97 (m, 1H), 2.82 – 2.80 (m, 2H), 2.68 – 2.64 (m, 1H), 2.60 – 2.54 (m, 1H), 2.47 – 2.40 (m, 3H), 2.36 – 2.18 (m, 4H), 2.18 – 2.12 (m, 3H), 2.11 – 2.07 (m, 2H), 1.90 – 1.85 (m, 1H), 1.80 – 1.77 (m, 1H), 1.58 – 1.56 (m, 22H), 1.35 – 1.22 (m, overlap with solvent residue of ethyl acetate), 1.19 – 1.09 (m, 22H), 1.06 (d, *J* = 6.7 Hz, 4H), 0.20 (s, 9H), 0.17 (s, 9H), 0.13 (d, *J* = 5.9 Hz, 3H), -0.10 (d, *J* = 5.3 Hz, 3H). **MS** calcd for C<sub>187</sub>H<sub>203</sub>N<sub>27</sub>NaO<sub>34</sub>Si<sub>2</sub> [M+Na]<sup>+</sup> 3449.4417 found (HR-ESI) 3451.1943.

**O<sub>2</sub>N-Q<sup>B</sup>X<sup>B</sup>R<sup>Q</sup>M<sup>Y</sup>Q<sup>B</sup>X-T3-2eg-Q<sup>B</sup>X<sup>B</sup>R<sup>Q</sup>Y<sup>Q</sup>B<sup>X</sup>-OMe (12)** Compound **30** (31.16 mg, 8.71 μmol) was treated with a 50 % solution of TFA in DCM (4 mL) at r.t. for 48 h. Then the solvent was removed under vacuum, obtaining the product as a yellow solid (27.46 mg, quant.). **<sup>1</sup>H NMR** (500 MHz, Pyridine-*d*<sub>5</sub>, 25 °C) δ [ppm] 12.41 (s, 1H), 12.31 (s, 1H), 12.08 (s, 1H), 11.52 (s, 1H), 11.20 (s, 1H), 11.03 (s, 1H), 10.64 (s, 1H), 10.52 (s, 1H), 10.20 (s, 1H), 10.00 (s, 1H), 9.72 (s, 1H), 9.26 (dd, *J* = 7.6, 1.3 Hz, 1H), 9.16 (dd, *J* = 7.5, 1.3 Hz, 1H), 8.99 (t, *J* = 3.6 Hz, 1H), 8.87 (dd, *J* = 7.5, 1.3 Hz, 1H), 8.80 – 8.76 (m, 2H), 8.63 – 8.57 (m, 2H), 8.52 (dd, *J* = 7.6, 1.3 Hz, 1H), 8.45 – 8.37 (m, 5H), 8.30 (ddd, *J* = 7.5, 3.0, 1.3 Hz, 2H), 8.16 (ddd, *J* = 17.0, 8.0, 2.4 Hz, 2H), 8.08 – 8.04 (m, 2H), 8.00 (dd, *J* = 8.1, 1.4 Hz, 1H), 7.95 – 7.88 (m, 5H), 7.84 (d, *J* = 2.7 Hz, 2H), 7.80 – 7.72 (m, 7H), 7.69 – 7.65 (m, 2H), 7.57 – 7.51 (m, 5H), 7.46 (t, *J* = 7.8 Hz, 1H), 7.34 (dt, *J* = 22.5, 7.9 Hz, 2H), 7.28 – 7.24 (m, 1H), 7.13 (s, 1H), 7.07 – 7.02 (m, 2H), 6.98 – 6.76 (m, 4H), 6.75 (d, *J* = 2.2 Hz, 1H), 6.70 (d, *J* = 2.1 Hz, 1H), 4.40 (q, *J* = 6.4 Hz, 1H), 4.26 (dd, *J* = 8.4, 6.0 Hz, 1H), 4.20 (s, 1H), 4.10 (s, 3H), 4.02 (dd, *J* = 8.9, 6.3 Hz, 4H), 3.98 – 3.90 (m, 4H), 3.88 – 3.83 (m, 1H), 3.70 – 3.61 (m, 4H), 3.52 – 3.49 (m, 1H), 3.24 (ddd, *J* = 16.7, 11.4, 7.0 Hz, 1H), 3.15 (dt, *J* = 9.6, 5.8 Hz, 2H), 2.99 (td, *J* = 10.1, 9.5, 6.0 Hz, 3H), 2.95 – 2.88 (m, 1H), 2.71 (dt, *J* = 10.3, 5.6 Hz, 1H), 2.63 (dt, *J* = 10.4, 5.3 Hz, 1H), 2.53 (dt, *J* = 13.5, 6.7 Hz, 3H), 2.38 (dt, *J* = 15.6, 6.1 Hz, 2H), 2.19 – 2.00 (m, 5H), 1.29 (d, *J* = 6.6 Hz, 4H), 1.21 (d, *J* = 6.7 Hz, 3H), 1.07 – 0.95

(m, 23H), 0.45 (d,  $J = 6.5$  Hz, 3H), 0.29 – 0.24 (m, 3H). **MS** calcd for  $C_{161}H_{147}N_{27}Na_2O_{34}$   $[M+2Na]^{2+}$  1524.0194, found (HR-ESI) 1524.3674.

### 7.2.5.3.3 Synthesis of sequences with a helix-turn-helix-motif and handedness-control in one helix

**(1S)-Camph-Q<sup>S</sup>XQ<sup>B</sup>Q<sup>B</sup>YQ<sup>B</sup>X-T3-2eg-Q<sup>S</sup>XQ<sup>B</sup>Q<sup>B</sup>YQ<sup>B</sup>X-OH (31)** Compound **31** was synthesized using the SPS procedures reported in 0 on SASRIN resin loaded via HBTU-coupling described in 0 (scale: 60  $\mu$ mol). After full cleavage and precipitation in EtOAc/*n*-Hex, the product was obtained as a yellow solid (112.00 mg, 49 %). **<sup>1</sup>H NMR** (500 MHz,  $CD_2Cl_2$ , 25 °C)  $\delta$  [ppm] 11.55 (dd,  $J = 8.3, 3.8$  Hz, 2H), 11.44 – 11.41 (m, 3H), 11.33 (s, 1H), 11.28 (s, 1H), 11.23 (s, 1H), 11.19 (d,  $J = 4.6$  Hz, 3H), 11.16 (d,  $J = 5.1$  Hz, 1H), 11.12 (d,  $J = 6.2$  Hz, 1H), 10.96 (dd,  $J = 10.8, 4.7$  Hz, 4H), 10.92 (s, 2H), 10.90 (d,  $J = 3.4$  Hz, 1H), 10.88 – 10.85 (m, 2H), 9.55 (s, 1H), 9.54 (s, 1H), 8.56 – 8.37 (m, 6H), 8.28 – 8.17 (m, 4H), 8.17 – 8.10 (m, 2H), 7.99 – 7.94 (m, 8H), 7.92 – 7.80 (m, 10H), 7.76 – 7.70 (m, 9H), 7.63 – 7.52 (m, 12H), 7.51 – 7.37 (m, 13H), 7.36 – 7.20 (m, 12H), 7.18 – 7.01 (m, 9H), 7.00 – 6.95 (m, 1H), 6.86 – 6.82 (m, 1H), 6.78 – 6.74 (m, 2H), 6.71 – 6.69 (m, 1H), 6.65 – 6.59 (m, 3H), 6.57 – 6.48 (m, 4H), 6.45 – 6.39 (m, 2H), 6.22 – 6.07 (m, 9H), 4.52 (p,  $J = 6.2$  Hz, 1H), 4.29 – 3.92 (m, overlap with signals corresponding to ethyl acetate), 3.90 – 3.66 (m, 24H), 3.29 (d,  $J = 16.1$  Hz, 4H), 2.64 – 2.59 (m, 10H), 2.49 – 2.37 (m, 15H), 1.68 – 1.54 (m, 128H), 1.34 – 1.20 (m, overlap with signal corresponding to ethyl acetate), 1.20 – 1.13 (m, 30H), 1.12 – 1.05 (m, 21H), 0.61 (d,  $J = 3.2$  Hz, 5H), 0.58 (d,  $J = 3.0$  Hz, 5H), 0.26 – 0.19 (m, 56H), 0.12 (d,  $J = 3.5$  Hz, 5H), 0.03 (s, 1H), 0.01 (s, 1H), (mixture of two diastereomers *PP* & *PM* and their ratio is 1:1, both are reported). **MS** calcd for  $C_{203}H_{219}N_{29}O_{33}Se_2Si_2$   $[M+Na]^+$  3829.4113 found (HR-ESI) 15360.

**(1S)-Camph-Q<sup>S</sup>XQ<sup>B</sup>Q<sup>B</sup>YQ<sup>B</sup>X-T3-2eg-Q<sup>S</sup>XQ<sup>B</sup>Q<sup>B</sup>YQ<sup>B</sup>X-OMe (32)** Compound **31** (112.00 mg, 29  $\mu$ mol, 1 eq.) was dissolved in a mixture of dry Chloroform/MeOH 3:2 (5 mL) under  $N_2$ . TMSCHN<sub>2</sub> (solut. 2 M in Hex, 17  $\mu$ L, 0.058 mmol, 2 eq.) was added dropwise, and the solution was stirred at r.t. for 2 h. A few drops of acetic acid were added, and the solution was stirred for 5 min at r.t. Then the solution was diluted with DCM, washed with  $NaHCO_3$ , dried  $MgSO_4$ , filtered and concentrated. The product was obtained as a yellow solid (77.55 mg, 70 %). **<sup>1</sup>H NMR** (500 MHz,  $CD_2Cl_2$ , 25 °C)  $\delta$  [ppm] 11.55 (dd,  $J = 8.5, 3.3$  Hz, 2H), 11.51 (s, 1H), 11.43 (s, 1H), 11.42 – 11.39 (m, 2H), 11.31 – 11.29 (m, 4H), 11.26 (s, 1H), 11.20 (t,  $J = 5.4$  Hz, 3H), 11.16 (d,  $J = 4.0$  Hz, 1H), 10.98 (d,  $J = 4.8$  Hz, 1H), 10.95 (d,  $J = 3.2$  Hz, 1H), 10.92 (s, 1H), 10.91-10.89 (m, 2H), 10.85 (s, 1H), 10.83 (s, 1H), 9.55 (s, 1H), 9.54 (s, 1H), 8.56 – 8.36 (m, 10H), 8.27 – 8.22 (m, 3H), 8.14 – 8.06 (m, 4H), 8.06 – 8.03 (m, 2H), 8.00 – 7.92 (m, 7H), 7.90 – 7.78 (m, 7H), 7.76 – 7.71 (m, 7H), 7.67 – 7.54 (m, 9H), 7.54 – 7.48 (m, 2H), 7.48 – 7.39 (m, 7H), 7.39 – 7.34 (m, 5H), 7.31 – 7.21 (m, 7H), 7.19 – 7.08 (m, 7H), 7.08 – 7.00 (m, 4H), 7.00 – 6.90 (m, 3H), 6.79 – 6.78 (m, 1H), 6.71 – 6.67 (m, 3H), 6.63 – 6.58 (m, 3H), 6.55 – 6.50 (m, 3H), 6.50 – 6.44 (m, 3H), 6.44 – 6.39 (m, 2H), 6.22 – 6.06 (m, 9H), 4.22 – 4.09 (m, 4H), 4.08 – 3.92 (m, 4H), 3.88 – 3.72 (m, 9H), 3.31 – 3.23 (m, 2H), 3.15 (s, 3H), 3.07 (s, 3H), 2.63 – 2.60 (m, 6H), 2.55 (s, 1H), 2.49

– 2.35 (m, 3H), 2.36 – 2.13 (m, 16H), 2.09 – 1.88 (m, 18H), 1.68 – 1.62 (m, 31H), 1.62 – 1.56 (m, 56H), 1.35 – 1.34 (m, 68H), 1.23 – 1.06 (m, 27H), 0.62 – 0.61 (m, 5H), 0.58 – 0.57 (m, 5H), 0.24 – 0.22 (m, 17H), 0.22 – 0.20 (m, 27H), 0.13 – 0.11 (m, 5H), (mixture of two diastereomers *PP* & *PM* and their ratio is 1:1, both are reported). **MS** calcd for C<sub>204</sub>H<sub>221</sub>N<sub>29</sub>NaO<sub>33</sub>Se<sub>2</sub>Si<sub>2</sub> [M+Na]<sup>+</sup> 3843.4268 found (HR-ESI) 3844.1257.

**(1S)-Camph-Q<sup>S</sup>XQ<sup>B</sup>Q<sup>B</sup>YQ<sup>B</sup>X-T3-2eg-Q<sup>S</sup>XQ<sup>B</sup>Q<sup>B</sup>YQ<sup>B</sup>X-OMe (13)** Compound **32** (15.76 mg, 4.13 μmol) was treated with a 50 % solution of TFA in DCM (4 mL) at r.t. for 48 h. Then the solvent was removed under vacuum, obtaining the product as a yellow solid (14.03 mg, quant.). **<sup>1</sup>H NMR** (500 MHz, Pyridine-*d*<sub>5</sub>, 25 °C) δ [ppm] 12.27 (s, 1H), 12.23 (s, 1H), 12.17 (s, 1H), 12.12 – 12.10 (m, 1H), 12.04 (d, *J* = 22.2 Hz, 1H), 11.91 (s, 1H), 11.88 (d, *J* = 11.5 Hz, 1H), 11.83 (s, 1H), 11.67 (d, *J* = 2.3 Hz, 1H), 11.55 – 11.49 (m, 1H), 11.48 – 11.42 (m, 1H), 10.10 (s, 1H), 9.18 (d, *J* = 11.3 Hz, 2H), 9.11 (dd, *J* = 11.7, 7.3 Hz, 1H), 9.03 (s, 1H), 8.68 – 8.61 (m, 3H), 8.60 – 8.53 (m, 1H), 8.49 (dd, *J* = 23.1, 7.4 Hz, 1H), 8.42 – 8.31 (m, 5H), 8.26 – 8.14 (m, 6H), 8.05 – 7.91 (m, 3H), 7.87 – 7.80 (m, 4H), 7.79 – 7.73 (m, 3H), 7.70 – 7.61 (m, 3H), 7.57 – 7.48 (m, 4H), 7.48 – 7.40 (m, 4H), 7.39 – 7.29 (m, 4H), 7.07 – 6.97 (m, 3H), 6.89 – 6.74 (m, 5H), 6.52 – 6.44 (m, 1H), 4.43 – 4.32 (m, 1H), 4.08 – 3.96 (m, 3H), 3.94 – 3.75 (m, 6H), 3.67 – 3.60 (m, 2H), 3.15 – 3.06 (m, 1H), 3.06 – 2.95 (m, 1H), 2.81 – 2.74 (m, 1H), 2.72 – 2.63 (m, 1H), 2.43 – 2.21 (m, 6H), 2.21 – 2.05 (m, 4H), 1.88 – 1.70 (m, 1H), 1.70 – 1.63 (m, 1H), 1.59 – 1.51 (m, 2H), 1.49 – 1.42 (m, 2H), 1.35 – 1.13 (m, 34H), 1.13 – 1.00 (m, 18H), 0.66 (s, 3H), 0.58 (s, 3H), 0.23 (s, 3H). **MS** calcd for C<sub>178</sub>H<sub>165</sub>N<sub>29</sub>NaO<sub>33</sub>Se<sub>2</sub> [M+Na]<sup>+</sup> 3419.0347, found (HR-ESI) 3419.7741.

**(1S)-Camph-Q<sup>B</sup>XQ<sup>S</sup>Q<sup>B</sup>YQ<sup>B</sup>X-T3-3eg-Q<sup>S</sup>XQ<sup>B</sup>Q<sup>B</sup>YQ<sup>B</sup>X-OH (33)** Compound **33** was synthesized using the SPS procedures reported in 0 on SASRIN resin loaded via HBTU-coupling described in 0 (scale: 32 μmol). After full cleavage and precipitation in DCM/MeOH, the product was obtained as a yellow solid (56.00 mg, 45 %). **<sup>1</sup>H NMR** (500 MHz, CDCl<sub>3</sub>, 25 °C) δ [ppm] 11.76 (s, 1H), 11.54 (s, 1H), 11.28 (s, 1H), 11.27 (s, 1H), 11.19 (d, *J* = 1.9 Hz, 1H), 11.15 (d, *J* = 3.3 Hz, 1H), 11.03 (t, *J* = 3.4 Hz, 2H), 10.91 – 10.88 (m, 2H), 9.46 (s, 1H), 8.63 (s, 1H), 8.41 (t, *J* = 3.7 Hz, 1H), 8.30 (q, *J* = 3.6 Hz, 1H), 8.23 – 8.19 (m, 2H), 8.14 – 8.09 (m, 1H), 8.03 – 7.95 (m, 4H), 7.91 (dp, *J* = 8.3, 1.3 Hz, 1H), 7.86 (dt, *J* = 7.6, 1.6 Hz, 1H), 7.85 – 7.79 (m, 2H), 7.79 – 7.72 (m, 3H), 7.71 – 7.64 (m, 7H), 7.60 – 7.49 (m, 6H), 7.44 – 7.28 (m, 8H), 7.21 – 7.16 (m, 2H), 7.11 – 6.99 (m, 5H), 6.86 – 6.78 (m, 2H), 6.68 – 6.61 (m, 2H), 6.50 – 6.40 (m, 3H), 6.30 – 6.26 (m, 2H), 6.05 (d, *J* = 3.7 Hz, 1H), 4.20 – 4.08 (m, 5H), 3.98 – 3.93 (m, 3H), 3.92 – 3.87 (m, 1H), 3.84 – 3.74 (m, 5H), 3.70 – 3.66 (m, 2H), 2.58 – 2.53 (m, 6H), 2.42 – 2.38 (m, 4H), 2.38 – 2.30 (m, 6H), 2.27 – 2.21 (m, 2H), 2.17 – 2.11 (m, 4H), 2.04 – 1.96 (m, 4H), 1.75 – 1.67 (m, 2H), 1.64 – 1.62 (m, 18H), 1.56 – 1.53 (m, 22H), 1.29 – 1.18 (m, 26H), 1.19 – 1.10 (m, 14H), 1.08 (dd, *J* = 6.7, 1.8 Hz, 3H), 1.04 (dd, *J* = 6.7, 1.5 Hz, 3H), 0.59 (s, 3H), 0.54 (s, 3H), 0.18 – 0.15 (m, 18H), 0.09 (s, 3H). **MS** calcd for C<sub>205</sub>H<sub>223</sub>N<sub>29</sub>NaO<sub>34</sub>Se<sub>2</sub>Si<sub>2</sub> [M+Na]<sup>+</sup> 3873.4373, found (HR-ESI) 3874.2232, calcd for C<sub>205</sub>H<sub>223</sub>KN<sub>29</sub>NaO<sub>34</sub>Se<sub>2</sub>Si<sub>2</sub> [M+Na+K]<sup>2+</sup> 1959.7003, found (HR-ESI) 1959.0897.

**(1S)-Camph-Q<sup>B</sup>XQ<sup>S</sup>Q<sup>B</sup>YQ<sup>B</sup>X-T3-3eg-Q<sup>S</sup>XQ<sup>B</sup>Q<sup>B</sup>YQ<sup>B</sup>X-OMe (34)** Compound **33** (56.00 mg, 14.5  $\mu$ mol, 1 eq.) was dissolved in a mixture of dry Chloroform/MeOH 3:2 (5 mL) under N<sub>2</sub>. TMSCHN<sub>2</sub> (solut. 2 M in Hex, 8.5  $\mu$ L, 0.029 mmol, 2 eq.) was added dropwise, and the solution was stirred at r.t. for 2 h. A few drops of acetic acid were added, and the solution was stirred for 5 min at r.t. Then the solution was diluted with DCM, washed with NaHCO<sub>3</sub>, dried MgSO<sub>4</sub>, filtered and concentrated. The product was obtained as a yellow solid (52 mg, 87 %). <sup>1</sup>H NMR (500 MHz, CDCl<sub>3</sub>, 25 °C)  $\delta$  [ppm] 11.79 (s, 1H), 11.54 (s, 1H), 11.42 (s, 1H), 11.40 (s, 1H), 11.33 (s, 1H), 11.25 (s, 1H), 11.07 (d,  $J$  = 4.7 Hz, 1H), 11.05 (s, 1H), 10.93 (d,  $J$  = 1.9 Hz, 1H), 10.90 (d,  $J$  = 1.6 Hz, 1H), 9.51 (d,  $J$  = 1.6 Hz, 1H), 8.65 (d,  $J$  = 1.8 Hz, 1H), 8.38 (t,  $J$  = 3.7 Hz, 1H), 8.27 (dtd,  $J$  = 8.7, 4.5, 1.6 Hz, 3H), 8.24 (dt,  $J$  = 7.6, 1.2 Hz, 1H), 8.09 – 8.04 (m, 2H), 8.04 – 7.99 (m, 1H), 7.97 (dt,  $J$  = 8.3, 1.1 Hz, 1H), 7.92 (ddd,  $J$  = 7.6, 3.4, 1.3 Hz, 1H), 7.85 (td,  $J$  = 7.8, 1.3 Hz, 2H), 7.79 (ddt,  $J$  = 7.8, 5.1, 1.5 Hz, 2H), 7.76 – 7.66 (m, 6H), 7.65 – 7.60 (m, 3H), 7.59 – 7.53 (m, 2H), 7.47 – 7.42 (m, 2H), 7.40 (dt,  $J$  = 5.9, 2.5 Hz, 2H), 7.39 – 7.34 (m, 4H), 7.33 – 7.29 (m, 2H), 7.23 – 7.18 (m, 2H), 7.13 – 7.07 (m, 4H), 7.06 – 6.99 (m, 3H), 6.90 (t,  $J$  = 2.2 Hz, 1H), 6.88 (dd,  $J$  = 3.6, 2.2 Hz, 1H), 6.74 (s, 1H), 6.69 (d,  $J$  = 4.4 Hz, 1H), 6.50 (t,  $J$  = 2.7 Hz, 1H), 6.48 (d,  $J$  = 2.2 Hz, 1H), 6.44 (d,  $J$  = 10.0 Hz, 1H), 6.34 (s, 1H), 6.32 (s, 1H), 6.10 (d,  $J$  = 3.4 Hz, 1H), 4.23 – 4.13 (m, 4H), 4.03 – 3.94 (m, 3H), 3.94 – 3.87 (m, 2H), 3.86 – 3.78 (m, 3H), 3.74 – 3.69 (m, 3H), 3.46 – 3.39 (m, 1H), 3.35 (dt,  $J$  = 16.8, 3.9 Hz, 1H), 3.10 (s, 3H), 3.08 – 2.96 (m, 4H), 2.72 – 2.65 (m, 2H), 2.63 – 2.60 (m, 2H), 2.58 (s, 3H), 2.46 – 2.27 (m, 13H), 2.22 – 2.18 (m, 3H), 2.10 – 1.98 (m, 6H), 1.83 – 1.72 (m, 5H), 1.72 – 1.69 (m, 3H), 1.69 – 1.64 (m, 13H), 1.60 – 1.55 (m, 20H), 1.33 – 1.21 (m, 16H), 1.21 – 1.15 (m, 14H), 1.12 (dd,  $J$  = 6.7, 1.5 Hz, 4H), 1.07 (d,  $J$  = 6.7 Hz, 4H), 0.63 (s, 3H), 0.59 (s, 3H), 0.23 – 0.19 (m, 18H), 0.13 (s, 3H). MS calcd for C<sub>206</sub>H<sub>225</sub>N<sub>29</sub>NaO<sub>34</sub>Se<sub>2</sub>Si<sub>2</sub> [M+Na]<sup>+</sup> 3887.4530 found (HR-ESI) 3888.1566, calcd for C<sub>206</sub>H<sub>225</sub>N<sub>29</sub>Na<sub>2</sub>O<sub>34</sub>Se<sub>2</sub>Si<sub>2</sub> [M+2Na]<sup>2+</sup> 1955.2211 found (HR-ESI) 1955.5673.

**(1S)-Camph-Q<sup>B</sup>XQ<sup>S</sup>Q<sup>B</sup>YQ<sup>B</sup>X-T3-3eg-Q<sup>S</sup>XQ<sup>B</sup>Q<sup>B</sup>YQ<sup>B</sup>X-OMe (14)** Compound **34** (5.66 mg, 1.46  $\mu$ mol) was treated with a 50 % solution of TFA in DCM (4 mL) at r.t. for 48 h. Then the solvent was removed under vacuum, obtaining the product as a yellow solid (5.04 mg, quant.). <sup>1</sup>H NMR (500 MHz, Pyridine-*d*<sub>5</sub>, 25 °C)  $\delta$  [ppm] 12.39 (s, 1H), 12.20 (s, 1H), 12.10 (s, 1H), 12.06 (s, 1H), 12.00 (s, 1H), 11.87 (d,  $J$  = 2.3 Hz, 1H), 11.65 (d,  $J$  = 2.7 Hz, 1H), 11.62 (s, 1H), 11.59 (d,  $J$  = 5.7 Hz, 1H), 11.53 (d,  $J$  = 5.1 Hz, 1H), 10.05 (s, 1H), 9.28 (d,  $J$  = 4.4 Hz, 1H), 9.15 (d,  $J$  = 4.6 Hz, 1H), 9.03 (s, 1H), 8.92 – 8.77 (m, 2H), 8.70 (s, 2H), 8.59 (ddd,  $J$  = 12.6, 8.4, 6.6 Hz, 2H), 8.44 – 8.37 (m, 7H), 8.35 – 8.28 (m, 4H), 8.24 (ddd,  $J$  = 7.6, 3.2, 1.3 Hz, 1H), 8.17 (ddd,  $J$  = 9.6, 6.9, 5.5 Hz, 4H), 8.11 (s, 1H), 8.09 – 8.03 (m, 3H), 8.00 (dt,  $J$  = 8.2, 1.4 Hz, 1H), 7.90 (d,  $J$  = 8.3 Hz, 2H), 7.85 (d,  $J$  = 2.2 Hz, 1H), 7.80 (ddd,  $J$  = 12.2, 6.6, 3.7 Hz, 2H), 7.77 – 7.72 (m, 3H), 7.72 – 7.67 (m, 2H), 7.56 – 7.50 (m, 3H), 7.46 (td,  $J$  = 7.9, 3.7 Hz, 1H), 7.40 – 7.31 (m, 2H), 7.31 – 7.25 (m, 2H), 7.02 (s, 1H), 6.97 (d,  $J$  = 5.4 Hz, 1H), 6.91 – 6.84 (m, 2H), 6.82 (d,  $J$  = 5.0 Hz, 1H), 6.80 (d,  $J$  = 2.4 Hz, 1H), 6.54 (d,  $J$  = 3.0 Hz, 1H), 4.31 – 4.26 (m, 1H), 4.16 (s, 1H), 3.93 – 3.77 (m, 6H), 3.67 – 3.58 (m, 3H), 3.39 – 3.33 (m, 2H), 3.32 (s, 3H), 3.25 – 3.20 (m, 2H), 3.00 (t,  $J$  = 6.1 Hz, 1H), 2.95 (t,  $J$  = 6.1 Hz, 1H), 2.88 – 2.84 (m, 2H), 2.72 – 2.65 (m,

4H), 2.62 – 2.57 (m, 4H), 2.55 – 2.52 (m, 3H), 2.46 – 2.27 (m, 3H), 2.24 – 2.15 (m, 4H), 2.11 – 2.06 (m, 2H), 1.90 – 1.69 (m, 2H), 1.16 – 1.01 (m, 44H), 0.68 (s, 3H), 0.59 (s, 3H), 0.24 (s, 3H). **MS** calcd for  $C_{180}H_{169}N_{29}NaO_{34}Se_2$   $[M+Na]^+$  3463.0609, found (HR-ESI) 3463.9677, calcd for  $C_{180}H_{169}N_{29}Na_2O_{34}Se_2$   $[M+2Na]^{2+}$  1743.0251, found (HR-ESI) 1743.5069.

**(1S)-Camph-Q<sup>B</sup>XQ<sup>S</sup>Q<sup>B</sup>YQ<sup>B</sup>X-T3-4eg-Q<sup>S</sup>XQ<sup>B</sup>Q<sup>B</sup>YQ<sup>B</sup>X-OH (35)** Compound **35** was synthesized using the SPS procedures reported in 0 on SASRIN resin loaded via HBTU-coupling described in 0 (scale: 32  $\mu$ mol). After full cleavage and precipitation in DCM/MeOH, the product was obtained as a yellow solid (53.00 mg, 42 %). **<sup>1</sup>H NMR** (500 MHz,  $CDCl_3$ , 25 °C)  $\delta$  [ppm] 11.81 (s, 1H), 11.59 (s, 1H), 11.35 (s, 1H), 11.30 (s, 1H), 11.17 (s, 1H), 11.11 (s, 2H), 10.96 – 10.91 (m, 3H), 9.52 (s, 1H), 8.72 (s, 1H), 8.42 (s, 1H), 8.37 (s, 1H), 8.33 – 8.29 (m, 2H), 8.29 – 8.25 (m, 1H), 8.06 (d,  $J = 7.5$  Hz, 1H), 8.00 (dd,  $J = 8.3, 1.3$  Hz, 1H), 7.93 (d,  $J = 7.7$  Hz, 2H), 7.92 – 7.87 (m, 3H), 7.84 – 7.79 (m, 4H), 7.77 – 7.69 (m, 4H), 7.67 – 7.61 (m, 4H), 7.61 – 7.54 (m, 4H), 7.44 – 7.38 (m, 4H), 7.36 – 7.32 (m, 3H), 7.30 (d,  $J = 3.3$  Hz, 3H), 7.24 – 7.22 (m, 2H), 7.16 – 7.05 (m, 2H), 7.04 (d,  $J = 6.0$  Hz, 3H), 6.90 (s, 1H), 6.81 (s, 1H), 6.72 (s, 1H), 6.57 (d,  $J = 2.2$  Hz, 1H), 6.50 (d,  $J = 2.1$  Hz, 1H), 6.48 (d,  $J = 2.5$  Hz, 1H), 6.35 (s, 1H), 6.31 (s, 1H), 6.08 (d,  $J = 1.2$  Hz, 1H), 4.27 – 4.14 (m, 3H), 4.01 – 3.97 (m, 2H), 3.94 – 3.91 (m, 2H), 3.90 – 3.81 (m, 2H), 3.78 – 3.73 (m, 2H), 3.73 – 3.64 (m, 2H), 3.45 – 3.40 (m, 2H), 3.18 – 3.03 (m, 2H), 2.86 – 2.77 (m, 2H), 2.72 – 2.65 (m, 2H), 2.64 – 2.56 (m, 2H), 2.54 – 2.51 (m, 2H), 2.47 – 2.34 (m, 6H), 2.32 – 2.20 (m, 2H), 2.04 – 1.99 (m, 4H), 1.87 – 1.81 (m, 2H), 1.81 – 1.73 (m, 4H), 1.70 – 1.56 (m, 8H), 1.65 (s, 8H), 1.63 (s, 8H), 1.59 – 1.57 (m, 8H), 1.52 – 1.45 (m, 10H), 1.20 – 1.13 (m, 34H), 1.12 – 1.03 (m, 11H), 0.64 (s, 3H), 0.59 (s, 3H), 0.23 – 0.17 (m, 19H), 0.19 (s, 3H), 0.14 (s, 3H). **MS** calcd for  $C_{207}H_{227}N_{29}NaO_{35}Se_2Si_2$   $[M+Na]^+$  3917.4636, found (HR-ESI) 3918.1596.

**(1S)-Camph-Q<sup>B</sup>XQ<sup>S</sup>Q<sup>B</sup>YQ<sup>B</sup>X-T3-4eg-Q<sup>S</sup>XQ<sup>B</sup>Q<sup>B</sup>YQ<sup>B</sup>X-OMe (36)** Compound **35** (53.00 mg, 13.6  $\mu$ mol, 1 eq.) was dissolved in a mixture of dry Chloroform/MeOH 3:2 (5 mL) under  $N_2$ . TMSCHN<sub>2</sub> (solut. 2 M in Hex, 16.5  $\mu$ L, 0.027 mmol, 2 eq.) was added dropwise, and the solution was stirred at r.t. for 2 h. A few drops of acetic acid were added, and the solution was stirred for 5 min at r.t. Then the solution was diluted with DCM, washed with  $NaHCO_3$ , dried  $MgSO_4$ , filtered and concentrated. The product was obtained as a yellow solid (77.55 mg, 70 %). **<sup>1</sup>H NMR** (500 MHz,  $CDCl_3$ , 25 °C)  $\delta$  [ppm] 11.82 (s, 1H), 11.59 (s, 1H), 11.45 (s, 1H), 11.43 (s, 1H), 11.36 (s, 1H), 11.31 (s, 1H), 11.12 (s, 1H), 11.10 (s, 1H), 10.97 (s, 1H), 10.95 (s, 1H), 9.53 (s, 1H), 8.73 (s, 1H), 8.43 (s, 1H), 8.35 – 8.29 (m, 3H), 8.26 (d,  $J = 7.6$  Hz, 1H), 8.10 – 8.05 (m, 4H), 8.00 (dd,  $J = 8.3, 1.4$  Hz, 1H), 7.95 (dt,  $J = 7.6, 1.4$  Hz, 1H), 7.87 (ddt,  $J = 9.9, 7.5, 1.5$  Hz, 2H), 7.80 (ddd,  $J = 7.0, 5.6, 1.5$  Hz, 2H), 7.77 – 7.70 (m, 8H), 7.69 – 7.61 (m, 2H), 7.58 – 7.53 (m, 2H), 7.48 – 7.38 (m, 2H), 7.37 (d,  $J = 5.0$  Hz, 1H), 7.34 – 7.30 (m, 3H), 7.30 – 7.27 (m, 2H), 7.22 (td,  $J = 7.8, 2.4$  Hz, 2H), 7.15 – 7.08 (m, 3H), 7.08 – 7.05 (m, 3H), 6.91 (t,  $J = 2.1$  Hz, 2H), 6.75 (s, 1H), 6.73 (s, 1H), 6.61 (s, 1H), 6.52 (d,  $J = 7.9, 2.3$  Hz, 2H), 6.47 (d,  $J = 2.3$  Hz, 1H), 6.36 (s, 1H), 6.35 (s, 1H), 6.13 (d,  $J = 1.8$  Hz, 1H), 4.25 – 4.09 (m, 7H), 4.06 – 3.93 (m, 6H), 3.91 – 3.83 (m, 5H), 3.82 – 3.71 (m, 4H), 3.11 (s, 3H), 2.71 – 2.59 (m, 6H), 2.54 – 2.50 (m, 2H), 2.44 – 2.35



(m, 7H), 2.26 – 2.19 (m, 5H), 2.09 – 1.95 (m, 7H), 1.69 (d,  $J = 1.8$  Hz, 8H), 1.65 (s, 8H), 1.59 (s, 8H), 1.58 (d,  $J = 2.0$  Hz, 8H), 1.36 – 1.28 (m, 31H), 1.23 – 1.04 (m, 24H), 0.64 (s, 3H), 0.59 (s, 3H), 0.23 (d,  $J = 1.2$  Hz, 7H), 0.21 (s, 8H), 0.14 (s, 3H). **MS** calcd for  $C_{208}H_{229}N_{29}NaO_{35}Se_2Si_2$   $[M+Na]^+$  3931.4792 found (HR-ESI) 3932.1708.

**(1S)-Camph-Q<sup>B</sup>XQ<sup>S</sup>Q<sup>B</sup>YQ<sup>B</sup>X-T3-4eg-Q<sup>S</sup>XQ<sup>B</sup>Q<sup>B</sup>YQ<sup>B</sup>X-OMe (15)** Compound **36** (5.88 mg, 1.50  $\mu$ mol) was treated with a 50 % solution of TFA in DCM (4 mL) at r.t. for 48 h. Then the solvent was removed under vacuum, obtaining the product as a yellow solid (5.24 mg, quant.). **<sup>1</sup>H NMR** (500 MHz, Pyridine-*d*<sub>5</sub>, 25 °C)  $\delta$  [ppm] 12.16 (s, 1H), 11.99 (s, 1H), 11.86 (s, 1H), 11.83 (s, 1H), 11.77 (s, 1H), 11.66 (s, 1H), 11.42 (s, 1H), 11.40 (s, 1H), 11.38 (s, 1H), 11.33 (s, 1H), 9.81 (s, 1H), 9.09 (s, 1H), 8.92 (s, 1H), 8.80 (s, 1H), 8.64 – 8.58 (m, 2H), 8.38 (dd,  $J = 22.5, 7.5$  Hz, 2H), 8.21 – 8.14 (m, 5H), 8.10 (td,  $J = 7.8, 1.6$  Hz, 2H), 8.05 (dd,  $J = 7.5, 1.3$  Hz, 1H), 8.02 – 7.99 (m, 1H), 7.95 (d,  $J = 8.1$  Hz, 3H), 7.86 – 7.79 (m, 3H), 7.71 – 7.66 (m, 3H), 7.63 (d,  $J = 2.9$  Hz, 1H), 7.61 – 7.54 (m, 3H), 7.55 – 7.49 (m, 3H), 7.49 – 7.45 (m, 1H), 7.45 (s, 1H), 7.37 (s, 2H), 7.32 – 7.25 (m, 3H), 7.24 – 7.19 (m, 2H), 7.17 (d,  $J = 7.8$  Hz, 1H), 7.15 – 7.10 (m, 3H), 7.06 (t,  $J = 7.7$  Hz, 3H), 6.82 – 6.76 (m, 3H), 6.69 – 6.57 (m, 3H), 6.31 (s, 1H), 4.08 – 4.02 (m, 1H), 3.92 (t,  $J = 7.4$  Hz, 1H), 3.88 – 3.81 (m, 3H), 3.68 – 3.61 (m, 7H), 3.61 – 3.54 (m, 4H), 3.48 – 3.41 (m, 2H), 3.39 – 3.33 (m, 3H), 3.09 (s, 3H), 2.87 – 2.82 (m, 1H), 2.78 – 2.75 (m, 2H), 2.69 – 2.59 (m, 5H), 2.58 – 2.55 (m, 3H), 2.55 – 2.45 (m, 6H), 2.42 – 2.35 (m, 2H), 2.31 – 2.25 (m, 3H), 2.26 – 2.20 (m, 3H), 2.19 (d,  $J = 3.6$  Hz, 4H), 2.17 – 2.10 (m, 2H), 2.10 – 2.02 (m, 2H), 1.95 (dd,  $J = 13.5, 7.0$  Hz, 4H), 1.89 – 1.82 (m, 1H), 1.63 – 1.55 (m, 1H), 1.36 – 1.30 (m, 3H), 1.13 – 0.96 (m, 18H), 0.96 – 0.85 (m, 8H), 0.44 (s, 3H), 0.35 (s, 3H), 0.00 (s, 3H). **MS** calcd for  $C_{182}H_{173}N_{29}NaO_{35}Se_2$   $[M+Na]^+$  3507.0872, found (HR-ESI) 3506.9803, calcd for  $C_{182}H_{173}KN_{29}NaO_{35}Se_2$   $[M+Na+K]^{2+}$  1773.0252, found (HR-ESI) 1773.5141.

#### 7.2.5.3.4 Synthesis of achiral sequences with a helix-turn-helix-motif

**O<sub>2</sub>N-Q<sup>B</sup>XQ<sup>B</sup>Q<sup>B</sup>YQ<sup>B</sup>X-T3-2eg-Q<sup>S</sup>XQ<sup>B</sup>Q<sup>B</sup>YQ<sup>B</sup>X-OH (37)** Compound **37** was synthesized using the SPS procedures reported in 0 on SASRIN resin loaded via HBTU-coupling described in 0 (scale: 31  $\mu$ mol). After full cleavage, the product was obtained as a yellow solid (96.00 mg, 85 %). **<sup>1</sup>H NMR** (500 MHz, CD<sub>2</sub>Cl<sub>2</sub>, 25 °C)  $\delta$  [ppm] 11.42 (d,  $J = 5.2$  Hz, 2H), 11.35 (d,  $J = 4.2$  Hz, 2H), 11.13 – 11.11 (m, 4H), 11.04 (s, 1H), 11.03 (s, 1H), 11.00 (s, 1H), 10.99 (s, 1H), 10.93 (s, 1H), 10.91 (s, 1H), 10.88 (d,  $J = 2.3$  Hz, 3H), 10.87 (s, 2H), 10.86 (s, 1H), 10.85 (s, 1H), 10.80 (s, 1H), 8.53 (s, 1H), 8.46 (s, 1H), 8.43 (d,  $J = 3.7$  Hz, 2H), 8.37 (ddd,  $J = 8.2, 4.0, 1.7$  Hz, 5H), 8.31 (d,  $J = 7.7$  Hz, 2H), 8.22 (dd,  $J = 8.2, 6.9$  Hz, 3H), 8.14 (dd,  $J = 11.3, 7.3$  Hz, 2H), 8.02 (d,  $J = 8.4$  Hz, 2H), 7.98 – 7.85 (m, 7H), 7.79 (d,  $J = 1.3$  Hz, 1H), 7.74 (dd,  $J = 12.3, 7.3$  Hz, 7H), 7.70 – 7.67 (m, 2H), 7.65 – 7.58 (m, 11H), 7.47 – 7.39 (m, 12H), 7.39 – 7.27 (m, 8H), 7.27 – 7.22 (m, 6H), 7.19 – 7.12 (m, 6H), 7.09 – 7.01 (m, 4H), 6.97 (t,  $J = 8.0$  Hz, 1H), 6.76 – 6.74 (m, 3H), 6.67 – 6.63 (m, 4H), 6.61 (dd,  $J = 4.8, 2.2$  Hz, 3H), 6.49 (d,  $J = 13.7$  Hz, 4H), 6.41 (d,  $J = 9.2$  Hz, 2H), 6.18 – 6.12 (m, 8H), 6.08 (s, 1H), 4.23 – 4.09 (m, 10H), 4.03 – 3.98

(m, 10H), 3.87 – 3.79 (m, 9H), 3.80 – 3.71 (m, 7H), 2.61 – 2.54 (m, 14H), 2.41 – 2.36 (m, 11H), 2.37 – 2.29 (m, 6H), 2.29 – 2.25 (m, 3H), 2.21 – 2.16 (m, 5H), 2.05 – 1.98 (m, 13H), 1.73 – 1.68 (m, 44H), 1.67 – 1.62 (m, 31H), 1.59 – 1.54 (m, 41H), 1.40 – 1.35 (m, 23H), 1.15 – 1.04 (m, 13H), 0.22 (d,  $J = 1.6$  Hz, 37H), 0.20 (s, 19H), (mixture of two diastereomers *PP* and *PM* and their ratio is 1:1, both are reported). **MS** calcd for  $C_{196}H_{211}N_{29}NaO_{33}SeSi_2 [M+Na]^+$  3657.4320, found (HR-ESI) 3659.2401.

**O<sub>2</sub>N-Q<sup>B</sup>XQ<sup>B</sup>Q<sup>B</sup>YQ<sup>B</sup>X-T3-2eg-Q<sup>S</sup>XQ<sup>B</sup>Q<sup>B</sup>YQ<sup>B</sup>X-OMe (38)** Compound **37** (96.00 mg, 26  $\mu$ mol, 1 eq.) was dissolved in a mixture of dry Chloroform/MeOH 3:2 (5 mL) under N<sub>2</sub>. TMSCHN<sub>2</sub> (solut. 2 M in Hex, 15  $\mu$ L, 0.052 mmol, 2 eq.) was added dropwise, and the solution was stirred at r.t. for 2 h. A few drops of acetic acid were added, and the solution was stirred for 5 min at r.t. Then the solution was diluted with DCM, washed with NaHCO<sub>3</sub>, dried MgSO<sub>4</sub>, filtered and concentrated. The product was obtained after precipitation in EtOAc/*n*-Hex as a yellow solid (38.89 mg, 41 %). **<sup>1</sup>H NMR** (500 MHz, CDCl<sub>3</sub>, 25 °C)  $\delta$  [ppm] 11.48 (s, 1H), 11.47 (s, 1H), 11.46 (s, 1H), 11.40 (s, 2H), 11.37 (s, 2H), 11.21 (s, 1H), 11.20 (s, 1H), 11.15 (d,  $J = 1.6$  Hz, 2H), 11.02 (s, 2H), 10.98 (s, 1H), 10.97 (s, 1H), 10.95 (s, 2H), 10.88 (s, 1H), 10.87 (s, 1H), 8.54 (d,  $J = 7.5$  Hz, 2H), 8.41 (ddd,  $J = 7.6, 4.3, 1.3$  Hz, 2H), 8.38 – 8.33 (m, 6H), 8.22 (dt,  $J = 7.7, 1.3$  Hz, 3H), 8.18 (dd,  $J = 7.5, 1.3$  Hz, 2H), 7.98 (ddd,  $J = 7.5, 2.9, 1.3$  Hz, 5H), 7.95 – 7.89 (m, 4H), 7.91 – 7.87 (m, 4H), 7.86 – 7.80 (m, 4H), 7.78 (ddt,  $J = 8.1, 2.9, 1.3$  Hz, 4H), 7.76 – 7.64 (m, 4H), 7.64 – 7.58 (m, 4H), 7.38 (dd,  $J = 8.1, 2.2$  Hz, 7H), 7.34 (ddd,  $J = 7.6, 6.3, 2.3$  Hz, 5H), 7.32 – 7.27 (m, 5H), 7.22 – 7.15 (m, 7H), 7.15 – 7.09 (m, 4H), 7.07 – 7.01 (m, 4H), 7.00 – 6.95 (m, 5H), 6.92 – 6.89 (m, 2H), 6.87 (dd,  $J = 6.8, 2.3$  Hz, 4H), 6.84 (d,  $J = 3.5$  Hz, 2H), 6.73 – 6.69 (m, 5H), 6.58 (t,  $J = 9.2$  Hz, 3H), 6.48 – 6.43 (m, 4H), 6.33 – 6.28 (m, 4H), 6.14 (d,  $J = 13.2$  Hz, 3H), 6.07 (d,  $J = 9.0$  Hz, 2H), 4.23 – 4.06 (m, 10H), 4.06 – 3.94 (m, 8H), 3.91 – 3.75 (m, 12H), 3.76 – 3.64 (m, 10H), 3.35 – 3.25 (m, 6H), 3.13 – 3.08 (m, 4H), 3.09 (s, 3H), 3.08 (s, 3H), 2.86 – 2.81 (m, 2H), 2.65 – 2.60 (m, 4H), 2.59 – 2.55 (m, 6H), 2.53 (s, 3H), 2.44 – 2.28 (m, 26H), 2.27 (s, 9H), 2.09 – 1.98 (m, 2H), 1.85 – 1.70 (m, 18H), 1.69 – 1.67 (m, 18H), 1.65 (s, 9H), 1.57 (s, 9H), 1.56 – 1.55 (m, 18H), 1.54 (s, 9H), 1.22 – 1.13 (m, 47H), 1.13 – 1.04 (m, 24H), 0.22 (s, 9H), 0.20 – 0.19 (m, 27H), (mixture of two diastereomers *PP* and *PM* and their ratio is 1:1, both are reported). **MS** calcd for  $C_{197}H_{213}N_{29}Na_2O_{33}SeSi_2 [M+2Na]^{2+}$  1847.2184 found (HR-ESI) 1847.5735.

**O<sub>2</sub>N-Q<sup>B</sup>XQ<sup>B</sup>Q<sup>B</sup>YQ<sup>B</sup>X-T3-2eg-Q<sup>S</sup>XQ<sup>B</sup>Q<sup>B</sup>YQ<sup>B</sup>X-OMe (16)** Compound **16** (16.22 mg, 4.45  $\mu$ mol) was treated with a 50 % solution of TFA in DCM (4 mL) at r.t. for 48 h. Then the solvent was removed under vacuum, obtaining the product as a yellow solid (14.58 mg, quant.). **<sup>1</sup>H NMR** (500 MHz, Pyridine-*d*<sub>5</sub>, 25 °C)  $\delta$  [ppm] 12.23 (s, 3H), 12.12 (d,  $J = 4.0$  Hz, 2H), 12.07 (s, 3H), 12.02 (s, 2H), 11.85 (s, 2H), 11.75 (s, 1H), 11.74 (s, 1H), 11.71 (s, 1H), 11.70 (s, 1H), 11.60 (s, 1H), 11.58 (s, 1H), 11.52 (s, 1H), 11.47 (s, 1H), 11.45 (s, 1H), 11.42 (s, 1H), 9.13 (d,  $J = 16.5$  Hz, 3H), 9.09 (s, 2H), 9.08 – 9.05 (m, 2H), 8.92 – 8.88 (m, 4H), 8.83 (d,  $J = 7.5$  Hz, 4H), 8.71 – 8.65 (m, 4H), 8.65 – 8.59 (m, 4H), 8.54 – 8.50 (m, 2H), 8.43 – 8.30 (m, 10H), 8.17 – 8.09 (m, 7H), 8.07 – 8.01 (m, 7H), 7.99 – 7.90 (m, 8H), 7.84 – 7.76 (m, 8H), 7.76 – 7.64 (m, 9H), 7.48 – 7.42 (m, 8H), 7.39 – 7.35 (m, 4H), 7.33 – 7.29 (m, 4H), 7.05 (s,

1H), 7.00 (d,  $J = 4.1$  Hz, 3H), 6.94 (s, 1H), 6.89 (s, 1H), 6.87 (s, 1H), 6.85 – 6.83 (m, 3H), 6.79 (d,  $J = 2.2$  Hz, 1H), 6.77 – 6.74 (m, 3H), 6.53 – 6.49 (m, 4H), 4.27 – 4.22 (m, 2H), 4.18 – 4.10 (m, 8H), 4.08 – 4.00 (m, 7H), 3.96 – 3.72 (m, 11H), 3.66 – 3.56 (m, 5H), 3.33 – 3.29 (m, 3H), 3.31 (s, 3H), 3.30 (s, 3H), 3.11 – 3.00 (m, 1H), 2.99 – 2.92 (m, 1H), 2.80 – 2.72 (m, 2H), 2.71 – 2.63 (m, 5H), 2.55 – 2.44 (m, 6H), 2.43 – 2.31 (m, 10H), 2.31 – 2.17 (m, 8H), 2.13 – 2.05 (m, 6H), 1.30 – 1.14 (m, 53H), 1.14 – 0.99 (m, 38H), (mixture of two diastereomers *PP* and *PM* and their ratio is 1:1, both are reported). **MS** calcd for  $C_{171}H_{157}N_{29}NaO_{33}Se$   $[M+Na]^+$  3247.0556, found (HR-ESI) 3247.9970, calcd for  $C_{171}H_{158}N_{29}NaO_{33}Se$   $[M+H+Na]^{2+}$  1624.0314, found (HR-ESI) 1624.4006.

**O<sub>2</sub>N-Q<sup>B</sup>X<sup>B</sup>Q<sup>B</sup>Y<sup>B</sup>X-T3-4eg-Q<sup>S</sup>X<sup>B</sup>Q<sup>B</sup>Y<sup>B</sup>X-OH (39)** Compound **39** was synthesized using the SPS procedures reported in 0 on SASRIN resin loaded via HBTU-coupling described in 0 (scale: 21 μmol). After full cleavage, the product was obtained as a yellow solid (32.05 mg, 41 %). **<sup>1</sup>H NMR** (500 MHz, CDCl<sub>3</sub>, 25 °C) δ [ppm] 11.59 (s, 1H), 11.53 (s, 1H), 11.34 (s, 1H), 11.19 (s, 1H), 11.16 (s, 1H), 11.10 (s, 1H), 11.09 (s, 1H), 11.07 (s, 1H), 10.96 (s, 1H), 10.94 (s, 1H), 8.71 (s, 1H), 8.47 – 8.43 (m, 2H), 8.40 (d,  $J = 4.1$  Hz, 1H), 8.37 (d,  $J = 1.5$  Hz, 1H), 8.32 (d,  $J = 7.4$  Hz, 1H), 8.26 (dd,  $J = 7.6$ , 1.3 Hz, 1H), 8.19 (dd,  $J = 7.7$ , 1.3 Hz, 1H), 8.01 – 95 (m, 3H), 7.91 – 7.85 (m, 2H), 7.83 – 7.72 (m, 3H), 7.72 – 7.62 (m, 4H), 7.62 – 7.54 (m, 5H), 7.49 – 7.36 (m, 8H), 7.36 – 7.28 (m, 5H), 7.23 – 7.15 (m, 4H), 7.15 – 7.02 (m, 4H), 6.81 (s, 2H), 6.66 (s, 1H), 6.57 (d,  $J = 2.3$  Hz, 1H), 6.51 (d,  $J = 2.2$  Hz, 1H), 6.35 (s, 1H), 6.30 (s, 1H), 6.21 (s, 1H), 6.07 (s, 1H), 4.27 – 4.10 (m, 4H), 4.06 – 3.96 (m, 4H), 3.94 – 3.90 (m, 1H), 3.86 – 3.78 (m, 4H), 3.77 – 3.66 (m, 2H), 3.46 – 3.36 (m, 1H), 3.34 – 3.30 (m, 1H), 3.17 – 3.05 (m, 3H), 2.86 – 2.83 (m, 3H), 2.83 – 2.79 (m, 2H), 2.66 – 2.63 (m, 1H), 2.63 – 2.56 (m, 3H), 2.55 – 2.50 (m, 2H), 2.45 – 2.40 (m, 3H), 2.41 – 2.34 (m, 3H), 2.33 – 2.29 (m, 1H), 2.27 – 2.25 (m, 3H), 2.25 – 2.19 (m, 1H), 2.05 – 1.98 (m, 2H), 1.91 – 1.86 (m, 3H), 1.78 – 1.67 (m, 18H), 1.65 – 1.61 (m, 15H), 1.59 – 1.57 (m, 18H), 1.54 – 1.44 (m, 10H), 1.21 – 1.03 (m, 20H), 0.24 – 0.22 (m, 26H). **MS** calcd for  $C_{200}H_{219}N_{29}NaO_{35}SeSi_2$   $[M+Na]^+$  3745.4844, found (HR-ESI) 3747.2139.

**O<sub>2</sub>N-Q<sup>B</sup>X<sup>B</sup>Q<sup>B</sup>Y<sup>B</sup>X-T3-4eg-Q<sup>S</sup>X<sup>B</sup>Q<sup>B</sup>Y<sup>B</sup>X-OMe (40)** Compound **39** (32.00 mg, 8.61 μmol, 1 eq.) was dissolved in a mixture of dry Chloroform/MeOH 3:2 (5 mL) under N<sub>2</sub>. TMSCHN<sub>2</sub> (solut. 2 M in Hex, 5 μL, 0.017 mmol, 2 eq.) was added dropwise, and the solution was stirred at r.t. for 2 h. A few drops of acetic acid were added, and the solution was stirred for 5 min at r.t. Then the solution was diluted with DCM, washed with NaHCO<sub>3</sub>, dried MgSO<sub>4</sub>, filtered and concentrated. The product was obtained as a yellow solid (32.17 mg, quant.). **<sup>1</sup>H NMR** (500 MHz, CDCl<sub>3</sub>, 25 °C) δ [ppm] 11.57 (s, 1H), 11.53 (s, 1H), 11.43 (s, 1H), 11.41 (s, 1H), 11.34 (s, 1H), 11.18 (s, 1H), 11.09 (s, 2H), 11.07 (s, 1H), 10.94 (s, 1H), 8.71 (s, 1H), 8.45 (d,  $J = 7.4$  Hz, 1H), 8.42 (s, 1H), 8.38 (d,  $J = 8.5$  Hz, 2H), 8.30 (d,  $J = 7.2$  Hz, 1H), 8.27 – 8.18 (m, 2H), 8.19 (d,  $J = 7.4$  Hz, 2H), 8.10 – 7.94 (m, 5H), 7.91 – 7.87 (m, 2H), 7.81 – 7.71 (m, 5H), 7.71 – 7.62 (m, 2H), 7.57 – 7.46 (m, 6H), 7.47 – 7.30 (m, 5H), 7.17 – 7.11 (m, 4H), 7.09 – 7.06 (m, 2H), 6.92 (s, 2H), 6.82 (s, 2H), 6.74 (s, 2H), 6.67 (s, 2H), 6.51 (s, 1H), 6.34 (s, 2H), 6.33 (s, 1H), 6.19 (s, 1H), 6.11 (s, 1H), 4.24 – 4.16 (m, 4H), 4.16 – 4.10 (m, 4H), 4.08 – 3.97 (m, 5H), 4.06

– 3.96 (m, 9H), 3.55 – 3.47 (m, 8H), 3.40 – 3.37 (m, 8H), 3.10 (s, 3H), 2.64 – 2.51 (m, 14H), 2.39 – 2.25 (m, 19H), 2.05 – 1.98 (m, 9H), 1.72 – 1.54 (m, 21H), 1.20 – 1.02 (m, 34H), 0.24 – 0.22 (m, 18). **MS** calcd for C<sub>201</sub>H<sub>221</sub>N<sub>29</sub>NaO<sub>35</sub>SeSi<sub>2</sub> [M+Na]<sup>+</sup> 3759.5001 found (HR-ESI) 3759.2182.

**O<sub>2</sub>N-Q<sup>B</sup>XQ<sup>B</sup>Q<sup>B</sup>YQ<sup>B</sup>X-T3-4eg-Q<sup>S</sup>XQ<sup>B</sup>Q<sup>B</sup>YQ<sup>B</sup>X-OMe (17)** Compound **40** (30.00 mg, 8.03 μmol) was treated with a 50 % solution of TFA in DCM (4 mL) at r.t. for 48 h. Then the solvent was removed under vacuum, obtaining the product as a yellow solid (26.59 mg, quant.). **<sup>1</sup>H NMR** (500 MHz, Pyridine-*d*<sub>5</sub>, 25 °C) δ [ppm]

12.27 (s, 1H), 12.23 (s, 1H), 12.10 (s, 1H), 12.06 (s, 1H), 11.96 (s, 1H), 11.77 (s, 1H), 11.75 (s, 1H), 11.66 (s, 1H), 11.60 (s, 1H), 11.56 (s, 1H), 9.31 (s, 1H), 9.18 – 9.14 (m, 1H), 9.13 (t, *J* = 3.4 Hz, 1H), 8.95 – 8.91 (m, 1H), 8.87 – 8.82 (m, 2H), 8.71 – 8.68 (m, 2H), 8.62 (d, *J* = 8.2 Hz, 1H), 8.54 (dd, *J* = 7.5, 1.4 Hz, 1H), 8.44 (s, 1H), 8.43 – 8.37 (m, 3H), 8.37 – 8.32 (m, 2H), 8.20 – 8.16 (m, 4H), 8.14 (d, *J* = 7.4 Hz, 1H), 8.07 – 8.01 (m, 3H), 7.98 (s, 1H), 7.93 – 7.90 (m, 1H), 7.85 (d, *J* = 3.0 Hz, 2H), 7.79 – 7.72 (m, 4H), 7.71 (d, *J* = 6.0 Hz, 2H), 7.49 – 7.37 (m, 8H), 7.37 – 7.31 (m, 3H), 7.31 – 7.26 (m, 2H), 7.09 – 7.05 (m, 1H), 7.02 (s, 1H), 6.97 (s, 1H), 6.89 (s, 1H), 6.84 – 6.80 (m, 2H), 6.57 (s, 1H), 6.55 (s, 1H), 4.27 – 4.25 (m, 1H), 4.18 – 4.15 (m, 1H), 4.11 – 4.07 (m, 2H), 3.98 – 3.90 (m, 2H), 3.90 – 3.83 (m, 3H), 3.79 – 3.76 (m, 3H), 3.64 – 3.58 (m, 3H), 3.49 – 3.42 (m, 3H), 3.33 (s, 3H), 3.07 – 3.04 (m, 3H), 3.03 – 2.98 (m, 2H), 2.90 – 2.83 (m, 3H), 2.80 – 2.79 (m, 3H), 2.75 – 2.69 (m, 3H), 2.63 – 2.57 (m, 2H), 2.52 (d, *J* = 6.8 Hz, 4H), 2.41 – 2.36 (m, 3H), 2.35 – 2.27 (m, 3H), 2.23 – 2.19 (m, 2H), 2.18 – 2.07 (m, 3H), 1.67 – 1.61 (m, 2H), 1.69 – 1.62 (m, 2H), 1.14 – 1.10 (m, 16H), 1.09 – 1.02 (m, 22H), **MS** calcd for C<sub>175</sub>H<sub>165</sub>N<sub>29</sub>NaO<sub>35</sub>Se [M+Na]<sup>+</sup> 3335.1080, found (HR-ESI) 3334.8369.

## 5.2.6 References

1. S. De, B. Chi, T. Granier, T. Qi, V. Maurizot and I. Huc, *Nat. Chem.*, 2018, **10**, 51-57.
2. D. Mazzier, S. De, B. Wicher, V. Maurizot and I. Huc, *Angew. Chem. Int. Ed.*, 2020, **59**, 1606-1610.
3. D. Mazzier, S. De, B. Wicher, V. Maurizot and I. Huc, *Chem. Sci.*, 2019, **10**, 6984-6991.
4. F. S. Menke, B. Wicher, V. Maurizot and I. Huc, *Angew. Chem. Int. Ed.*, 2023, accepted.
5. *Maestro*, Schrödinger, LLC, New York, NY, 2021.
6. K.-J. Liu and J. L. Parsons, *Macromolecules*, 1969, **2**, 529-533.
7. Rigaku-Oxford-Diffraction, *CrysAlisPro Software System, Version 171.41*, 2020, Rigaku Corporation: Wrocław, Poland.
8. G. M. Sheldrick, *Acta Cryst.*, 2015, **A71**, 3-8.
9. G. M. Sheldrick, *Acta Cryst.*, 2015, **C71**, 3-8.
10. O. V. Dolomanov, L. J. Bourhis, R. J. Gildea, J. A. K. Howard and H. Puschmann, *J. Appl. Cryst.*, 2009, **42**, 339-341.
11. B. Baptiste, C. Douat-Casassus, K. Laxmi-Reddy, F. Godde and I. Huc, *J. Org. Chem.*, 2010, **75**, 7175-7185.
12. J. Buratto, C. Colombo, M. Stupfel, S. J. Dawson, C. Dolain, B. Langlois D'Estaintot, L. Fischer, T. Granier, M. Laguerre, B. Gallois and I. Huc, *Angew. Chem. Int. Ed.*, 2014, **126**, 902-906.
13. D. Bindl, E. Heinemann, P. K. Mandal and I. Huc, *Chem. Commun.*, 2021, **57**, 5662-5665.

## 5.2.7 NMR spectra of new compounds

### 5.2.7.1 Sequences to test handedness-induction via chiral B-unit

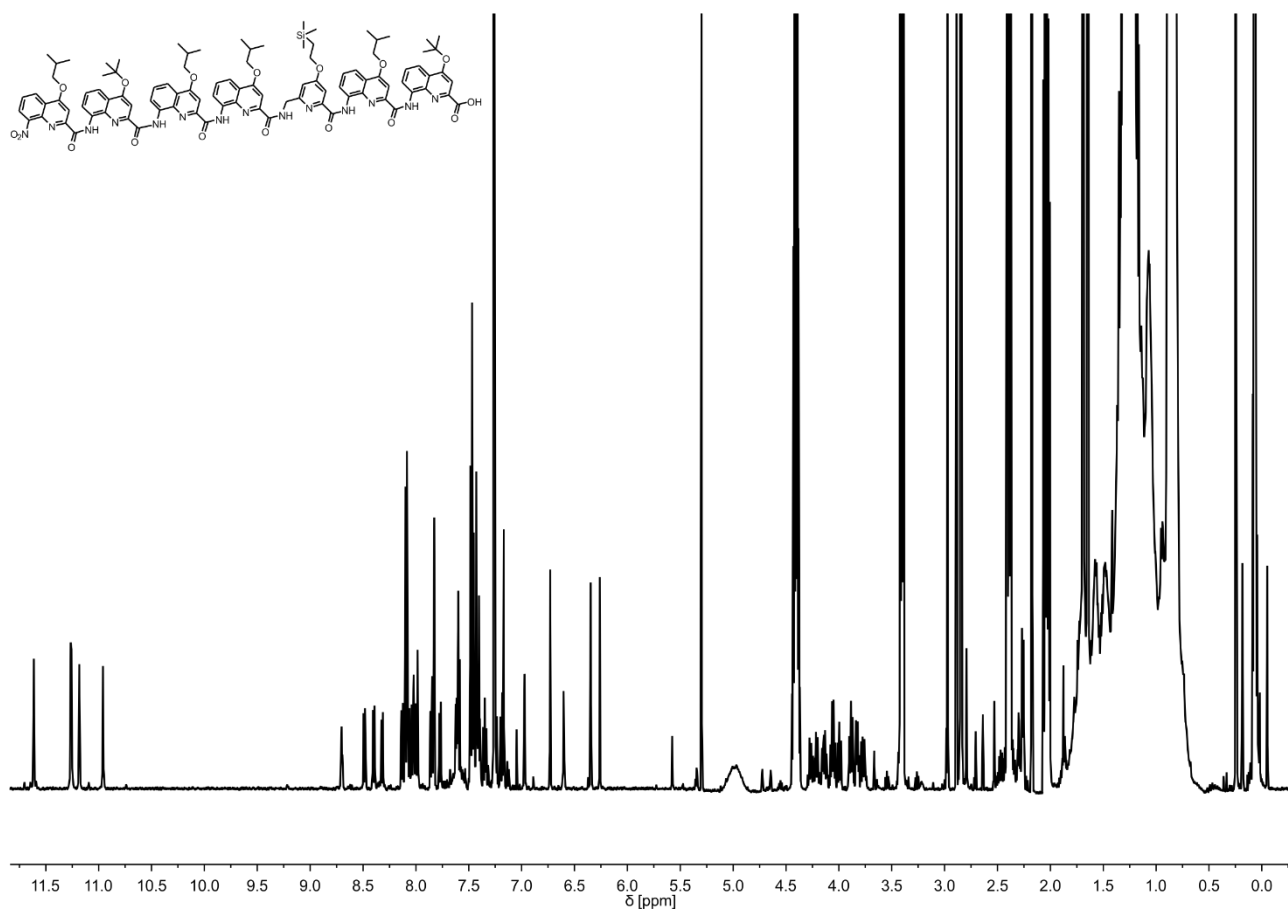


**Figure S49.** <sup>1</sup>H NMR spectrum (500 MHz, CDCl<sub>3</sub>) of **18**.

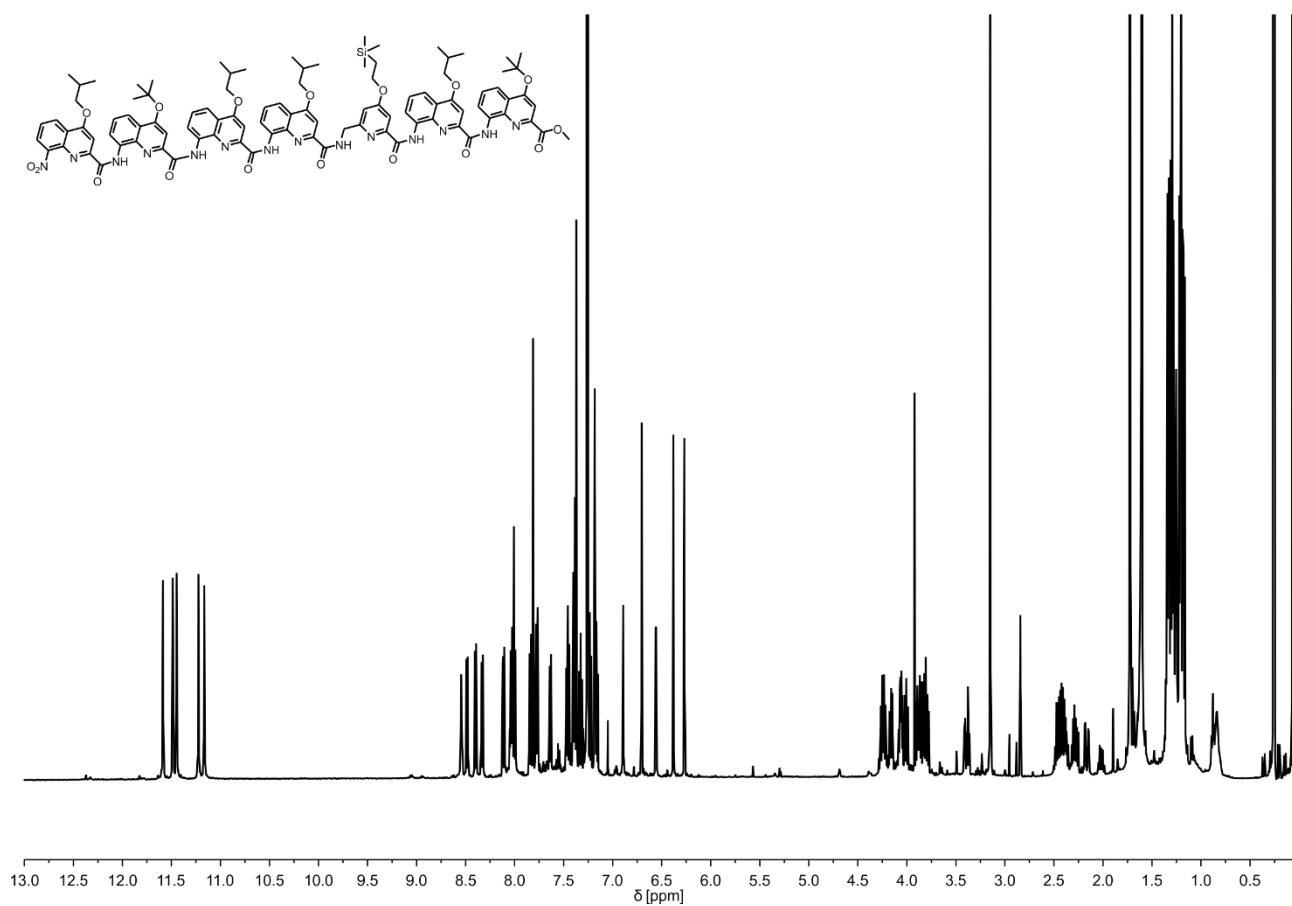


**Figure S50.** <sup>1</sup>H NMR spectrum (500 MHz, CDCl<sub>3</sub>) of **4**.

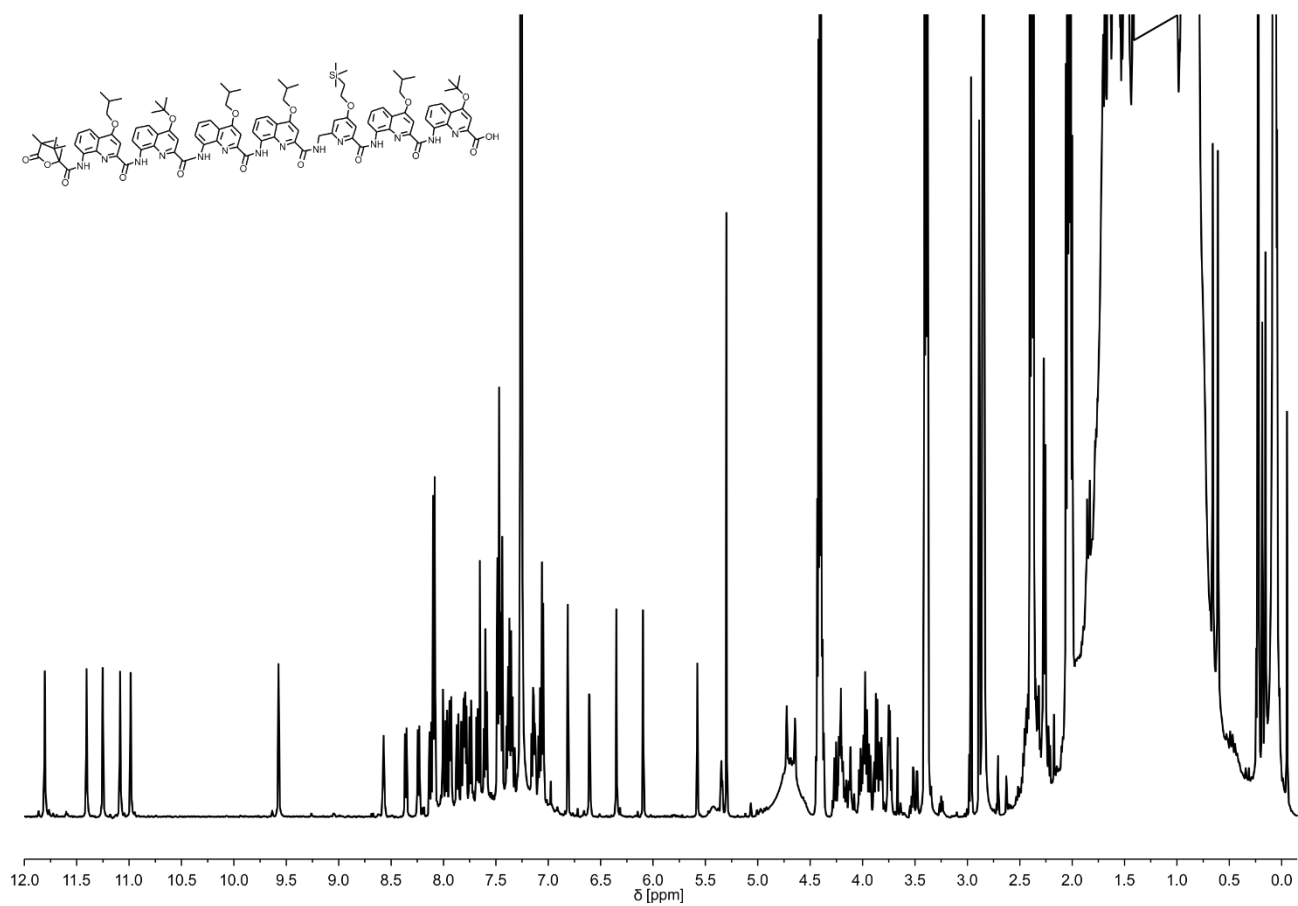


**Figure S51.** <sup>1</sup>H NMR spectrum (500 MHz, CDCl<sub>3</sub>) of **19**.



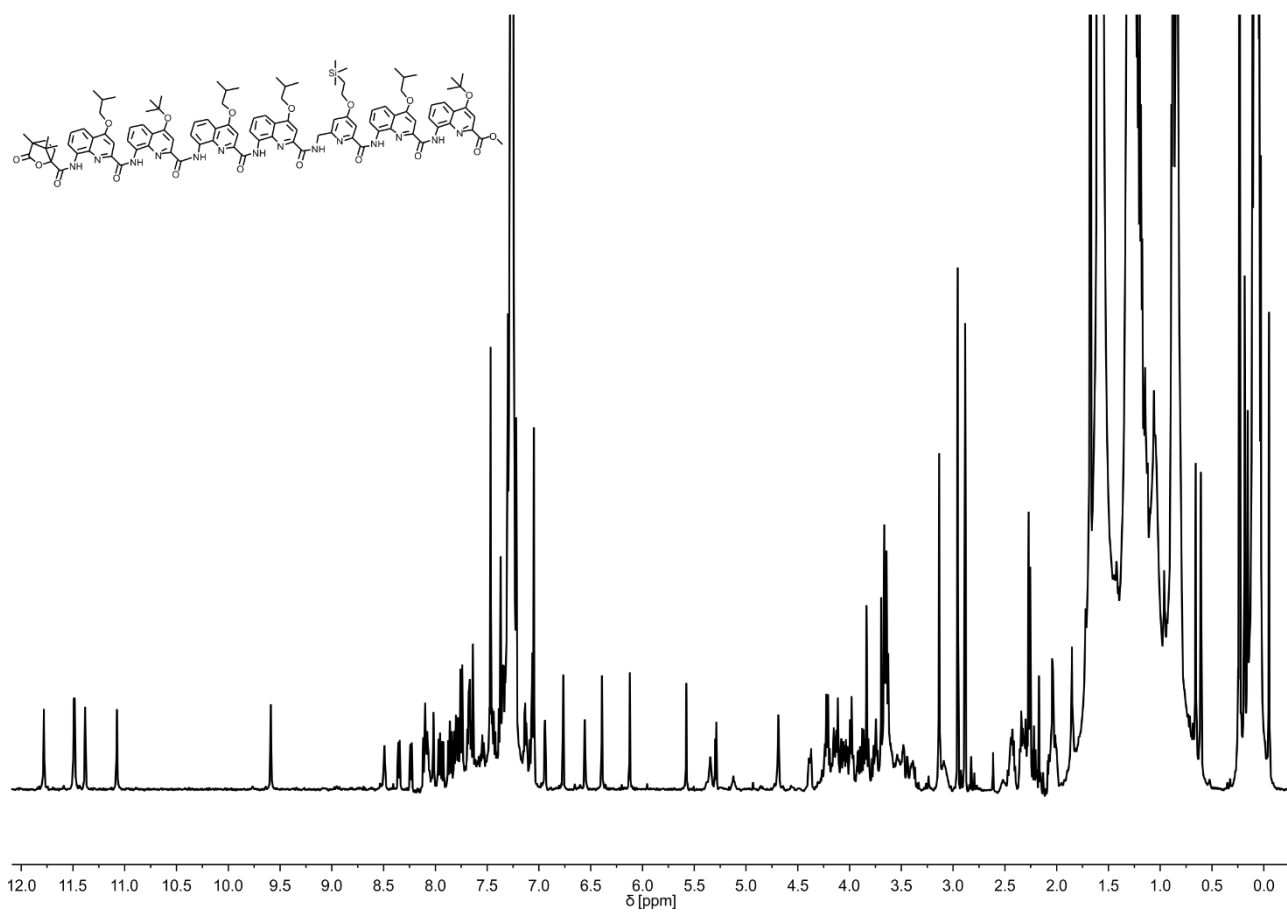


**Figure S52.** <sup>1</sup>H NMR spectrum (500 MHz, CDCl<sub>3</sub>) of **5**.

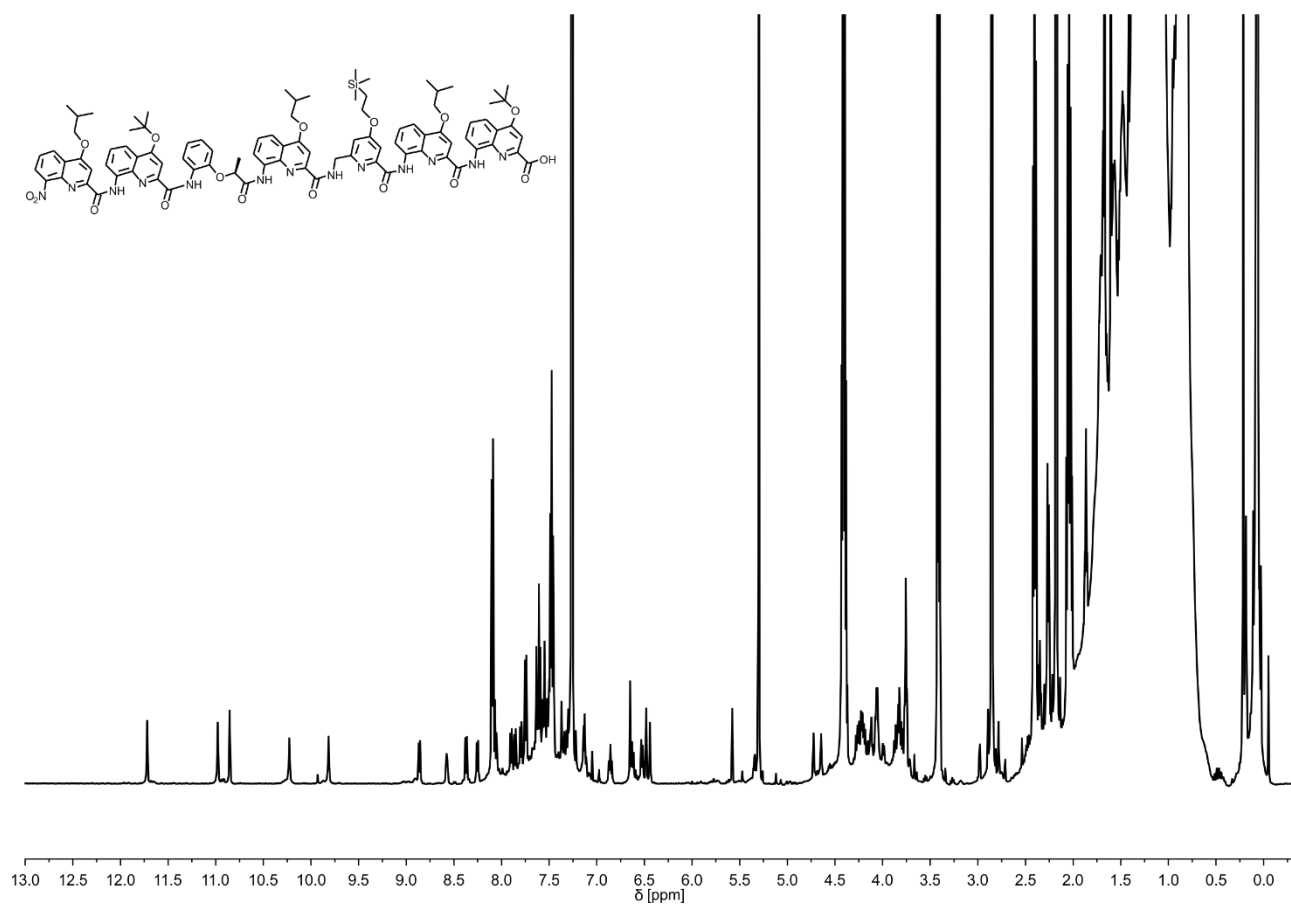


**Figure S53.**  $^1\text{H}$  NMR spectrum (500 MHz,  $\text{CDCl}_3$ ) of **20**.

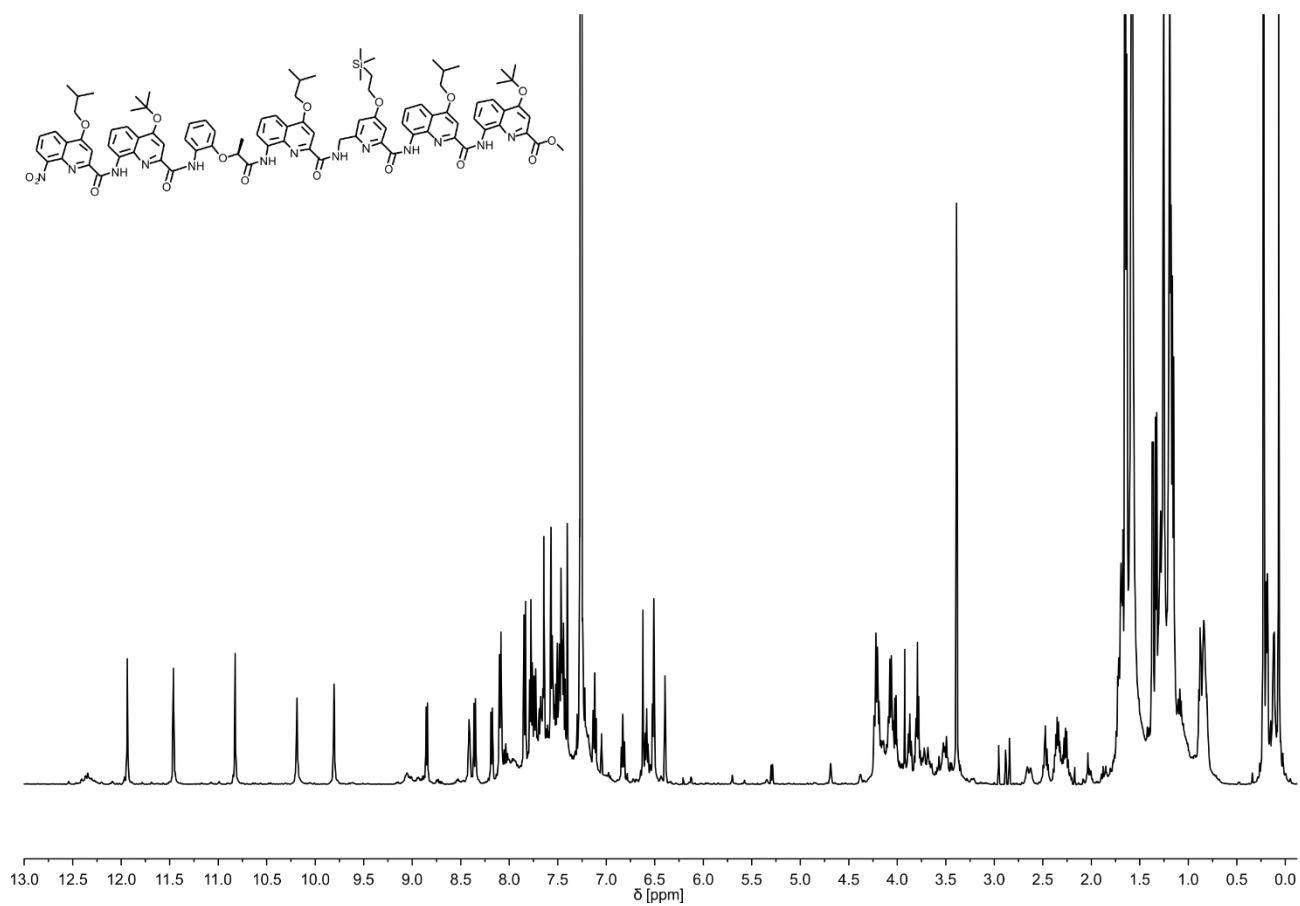


**Figure S54.** <sup>1</sup>H NMR spectrum (500 MHz, CDCl<sub>3</sub>) of **6**.

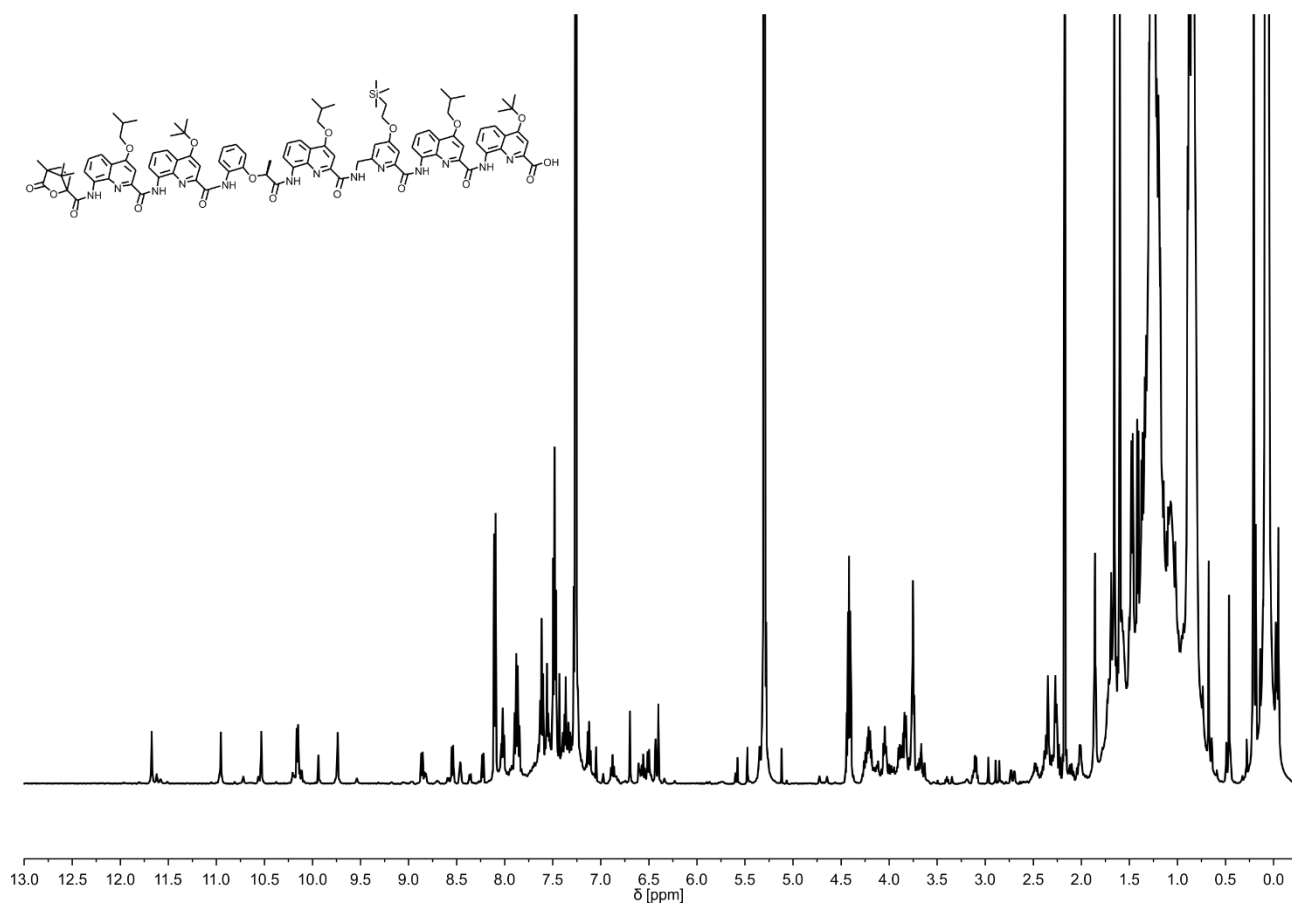


**Figure S55.** <sup>1</sup>H NMR spectrum (500 MHz, CDCl<sub>3</sub>) of **21**.

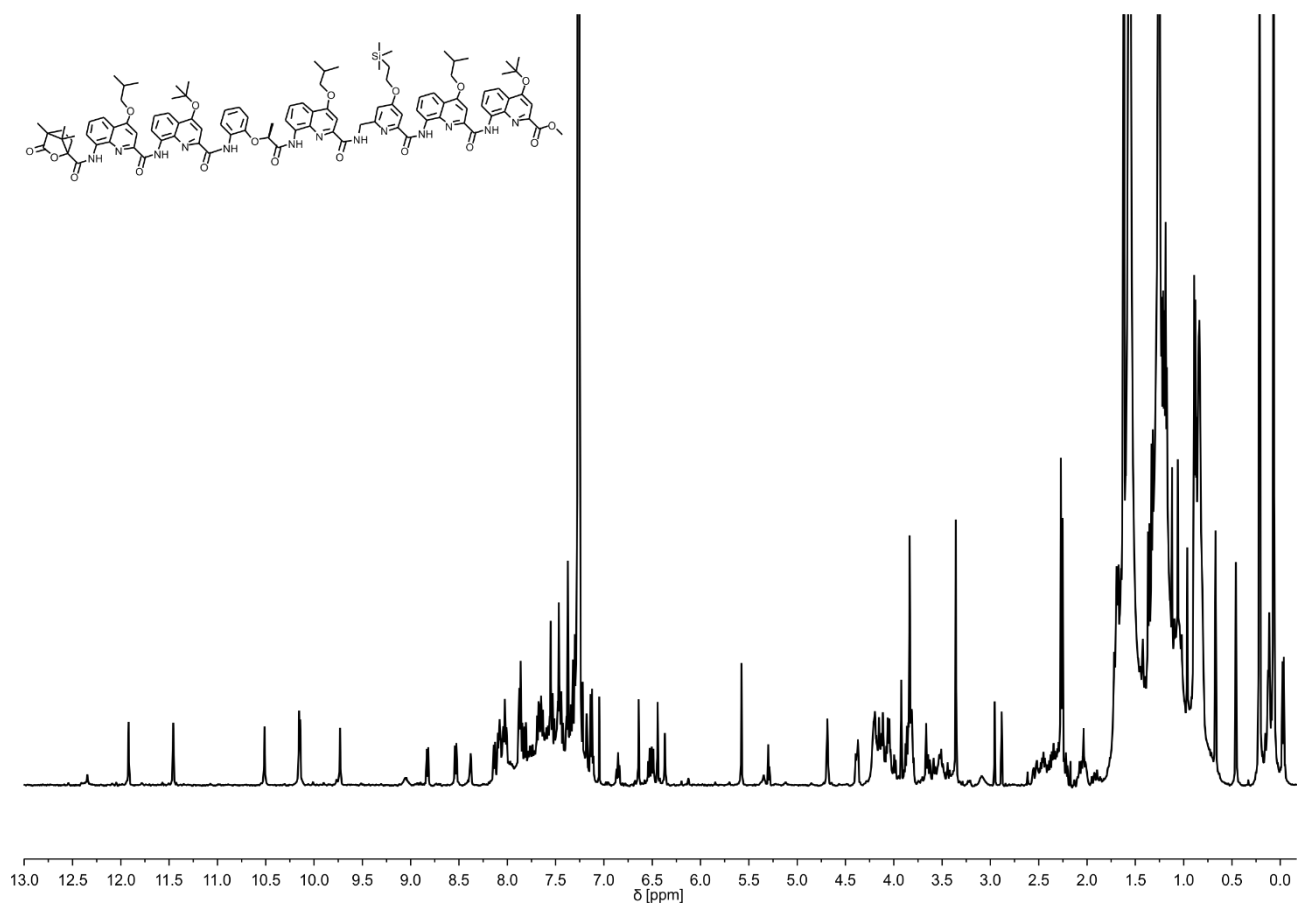


**Figure S56.** <sup>1</sup>H NMR spectrum (500 MHz, CDCl<sub>3</sub>) of 7.

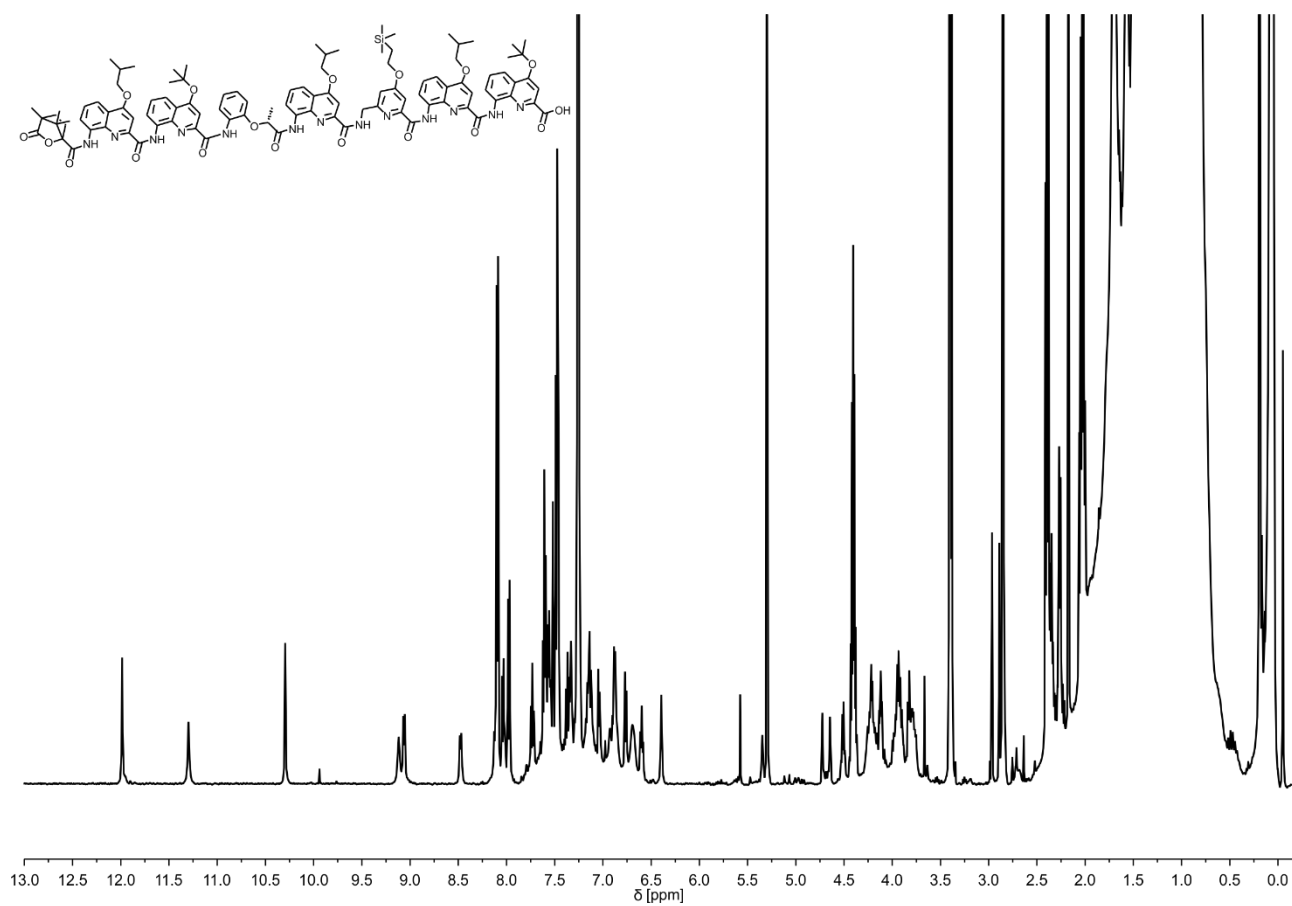


**Figure S57.** <sup>1</sup>H NMR spectrum (500 MHz, CDCl<sub>3</sub>) of **22**.

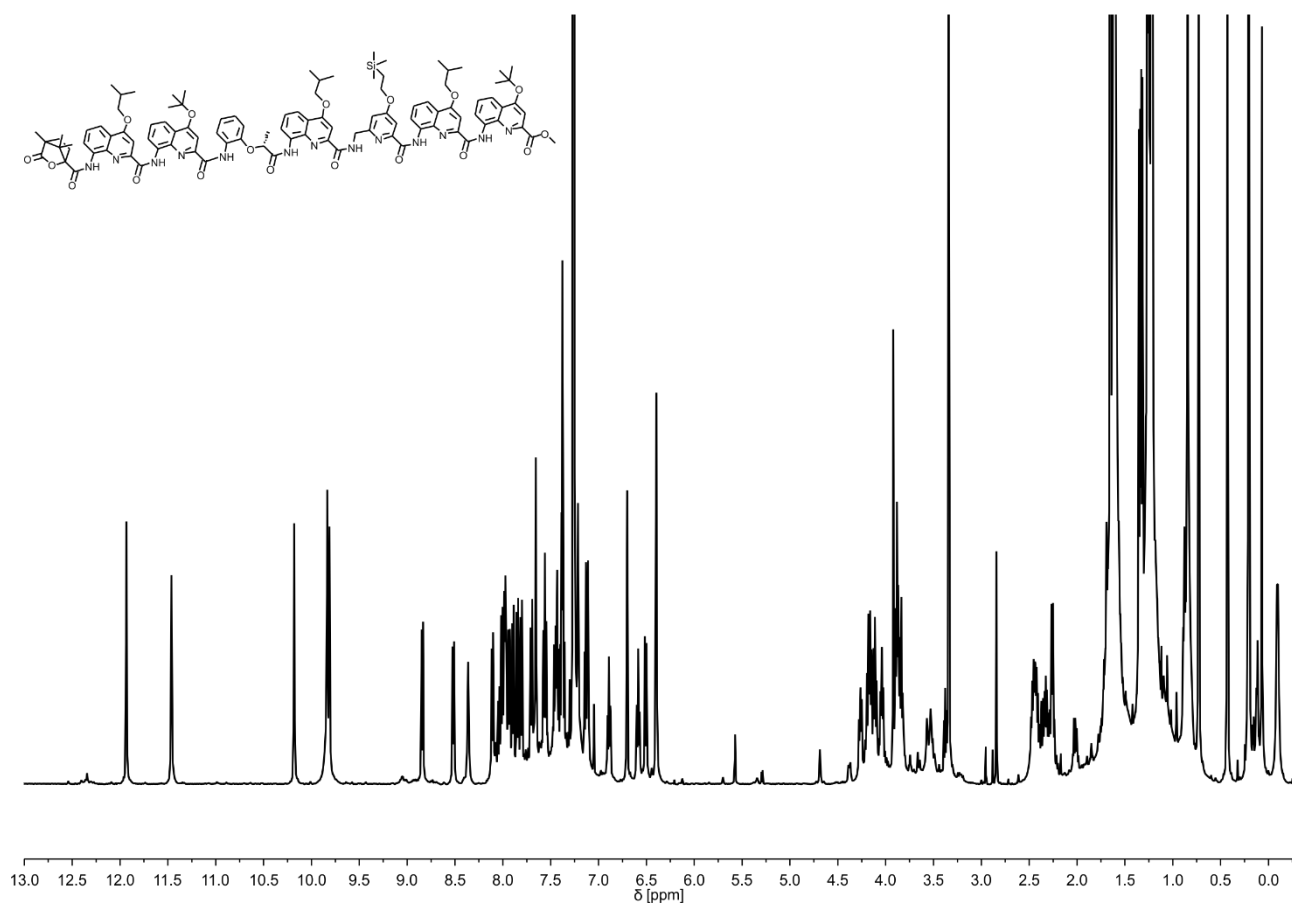


**Figure S58.**  $^1\text{H}$  NMR spectrum (500 MHz,  $\text{CDCl}_3$ ) of **8**.

### 5.2.7.2 Sequences with a helix-turn-helix-motif and handedness-control in both helices

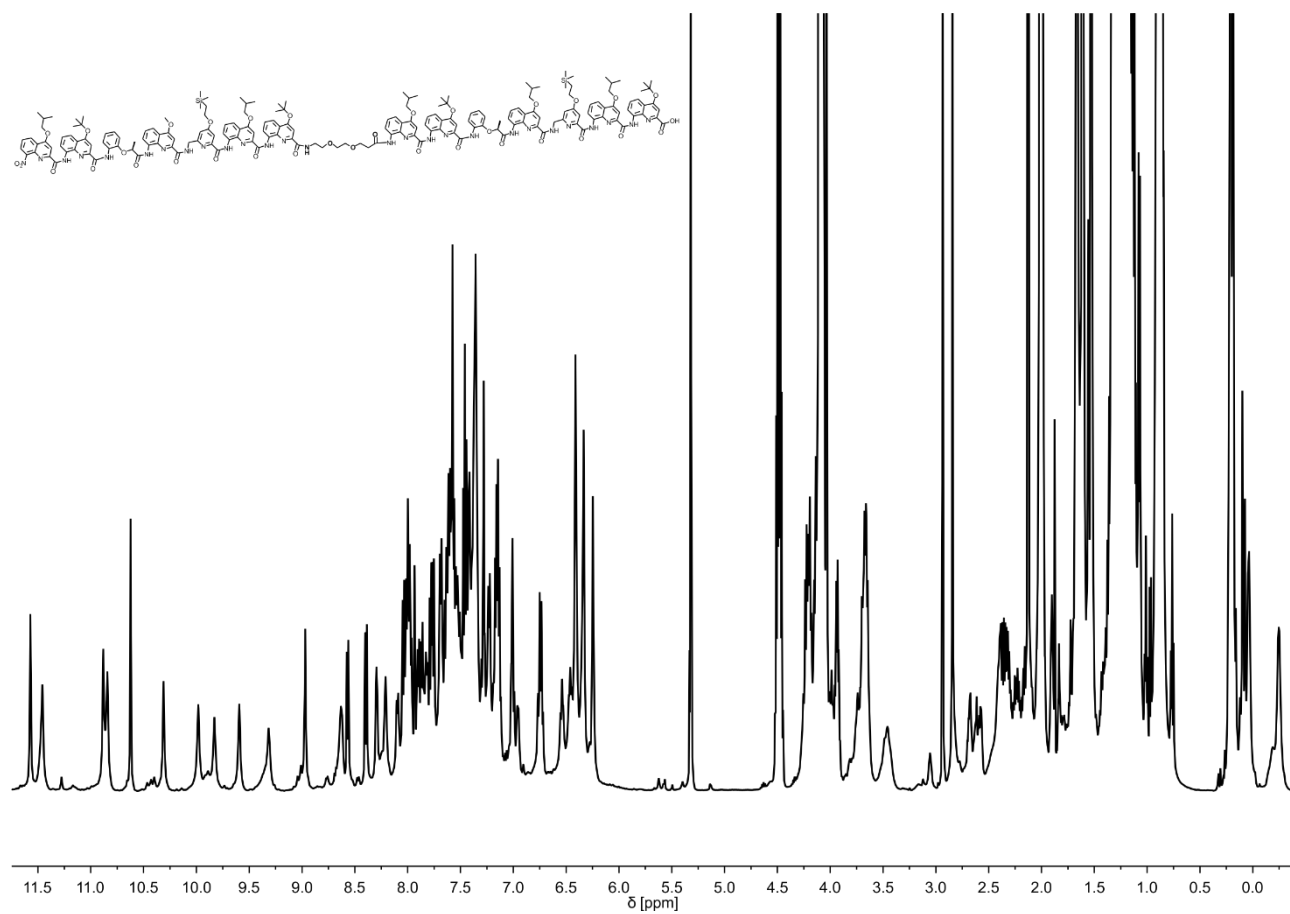


**Figure S59.** <sup>1</sup>H NMR spectrum (500 MHz, CD<sub>2</sub>Cl<sub>2</sub>) of **23**.



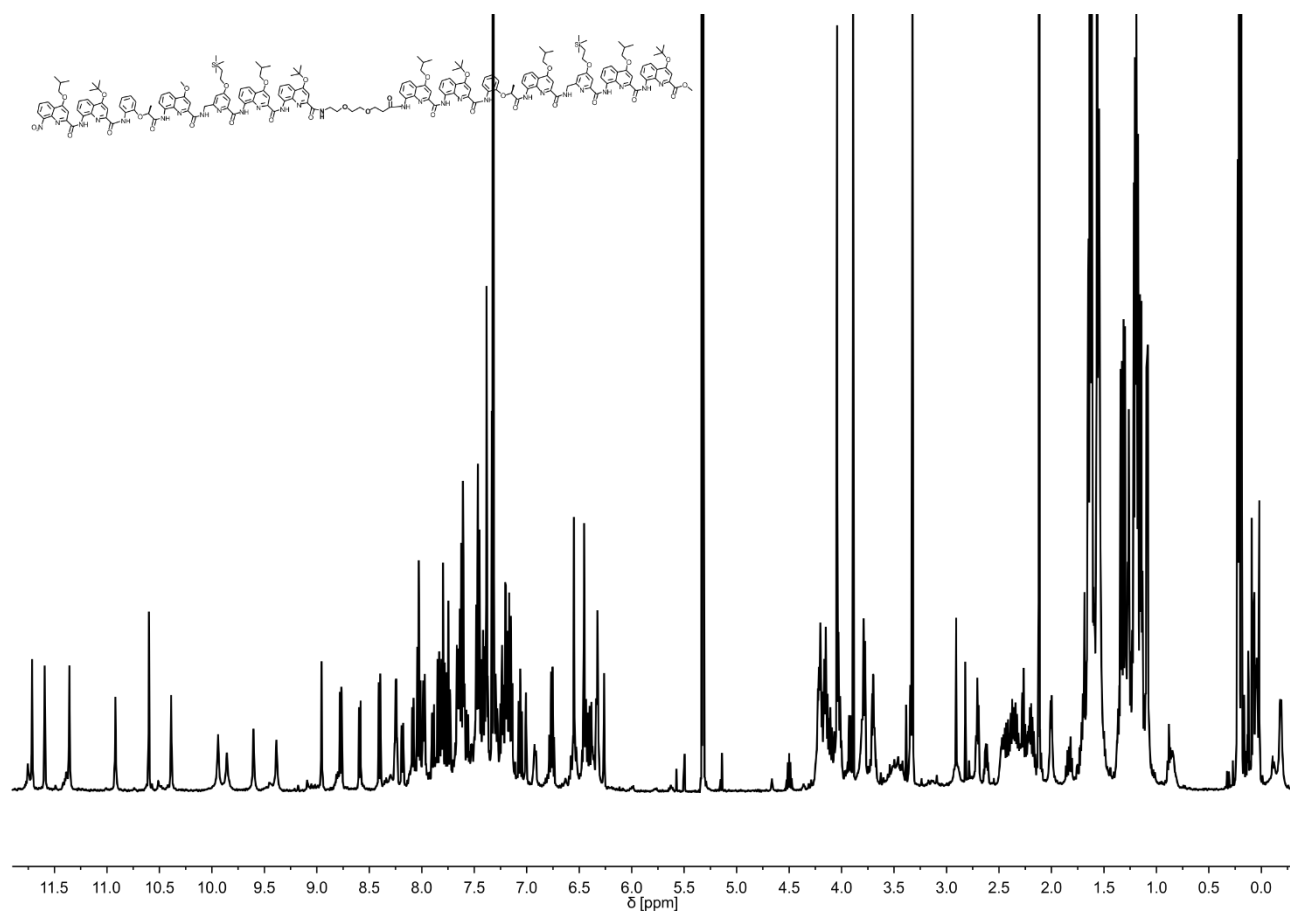


**Figure S60.**  $^1\text{H}$  NMR spectrum (500 MHz,  $\text{CD}_2\text{Cl}_2$ ) of **24**.

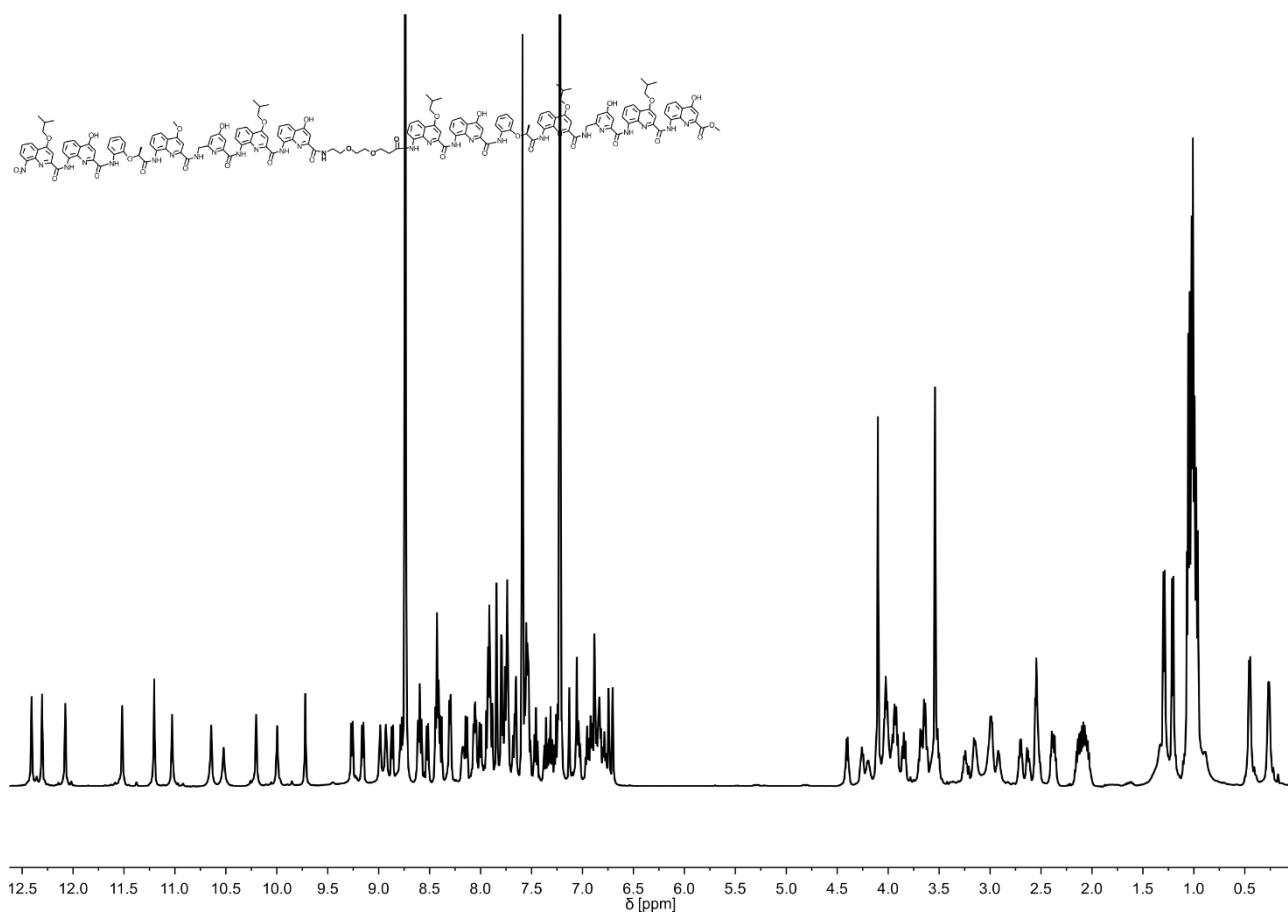


**Figure S61.** <sup>1</sup>H NMR spectrum (500 MHz, Pyridine-*d*<sub>5</sub>) of **9**.

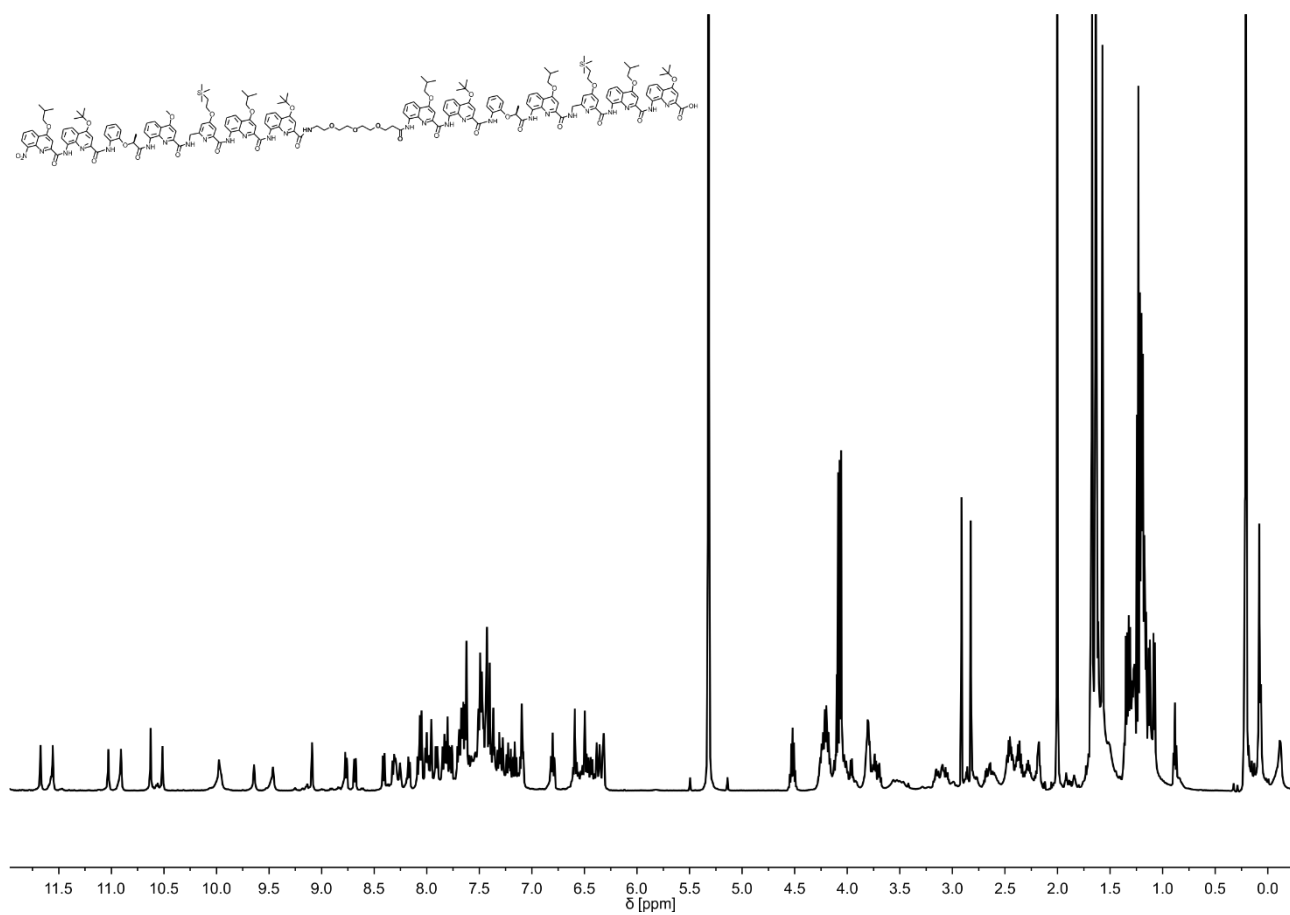


**Figure S62.** <sup>1</sup>H NMR spectrum (500 MHz, CD<sub>2</sub>Cl<sub>2</sub>) of **25**.

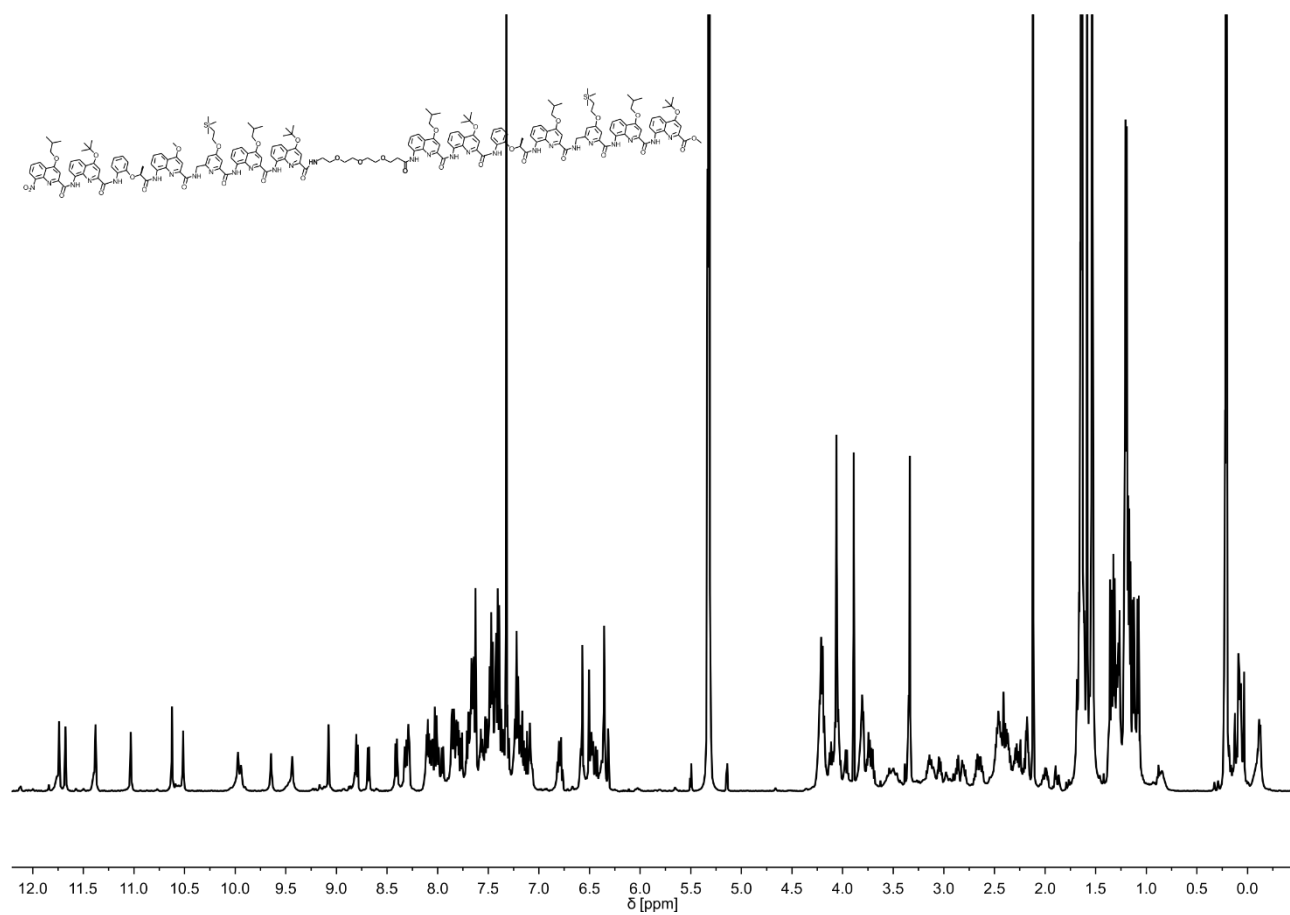


**Figure S63.** <sup>1</sup>H NMR spectrum (500 MHz, CD<sub>2</sub>Cl<sub>2</sub>) of **26**.

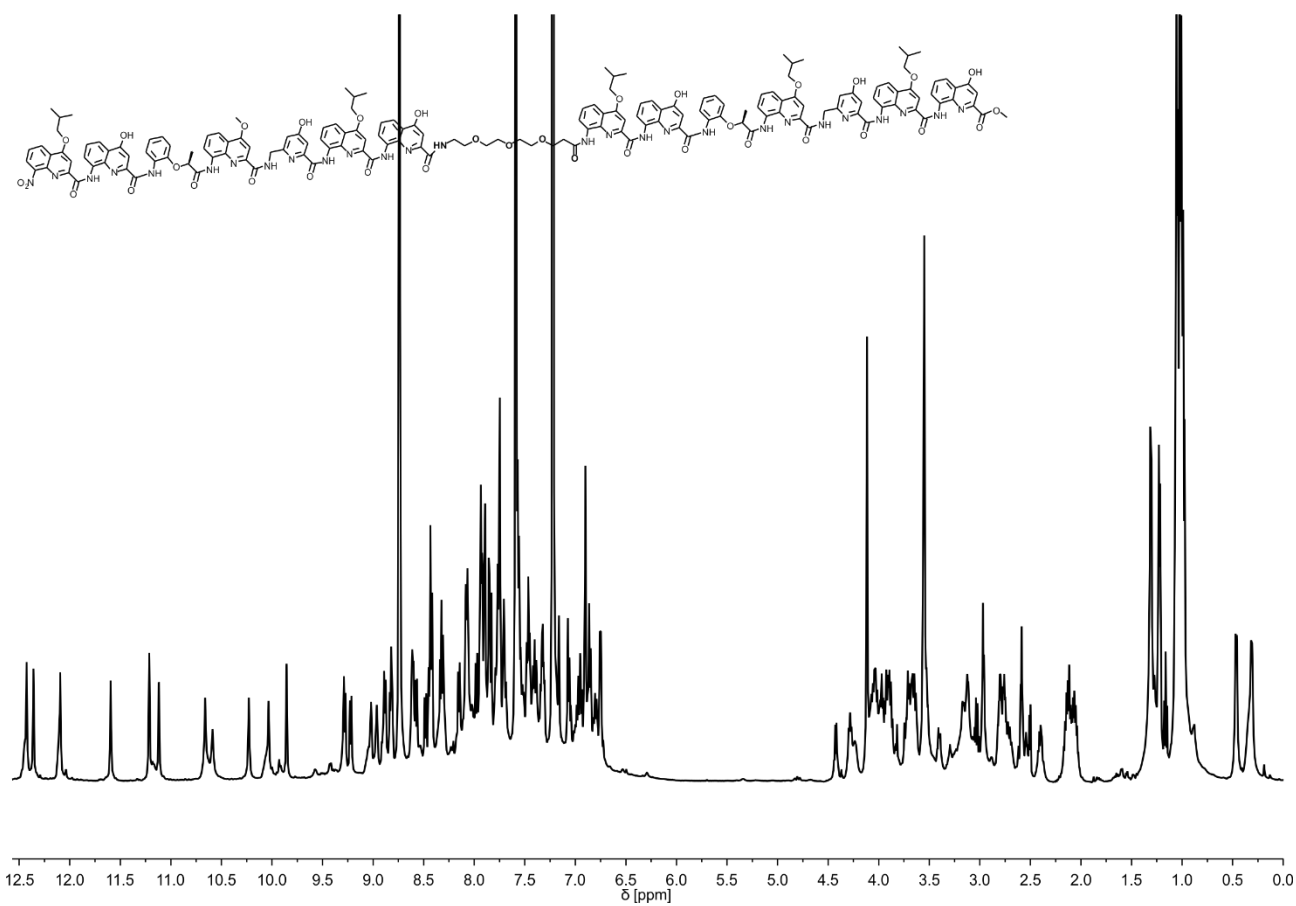


**Figure S64.**  $^1\text{H}$  NMR spectrum (500 MHz, Pyridine- $d_5$ ) of **10**.

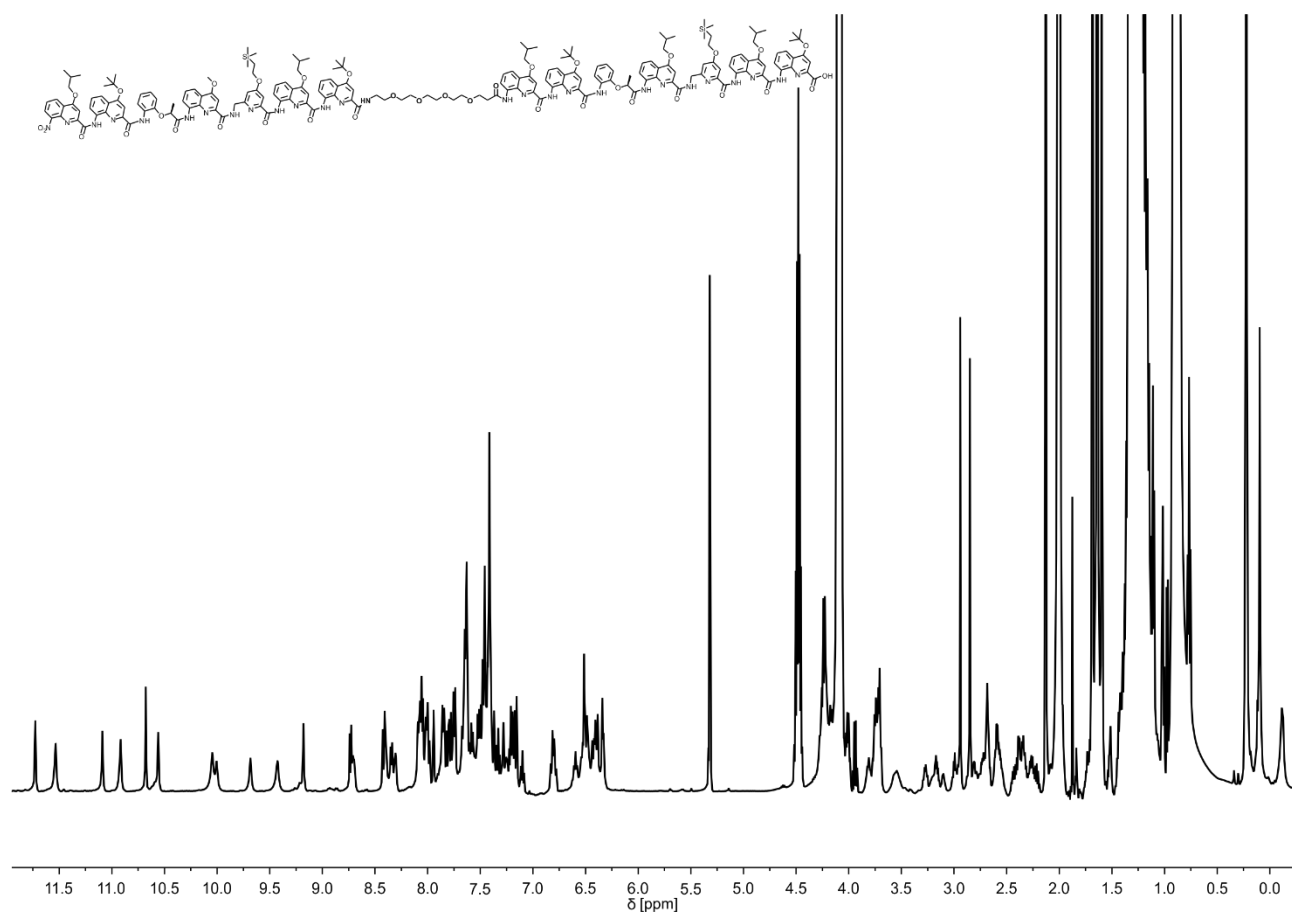


**Figure S65.** <sup>1</sup>H NMR spectrum (500 MHz, CD<sub>2</sub>Cl<sub>2</sub>) of **27**.

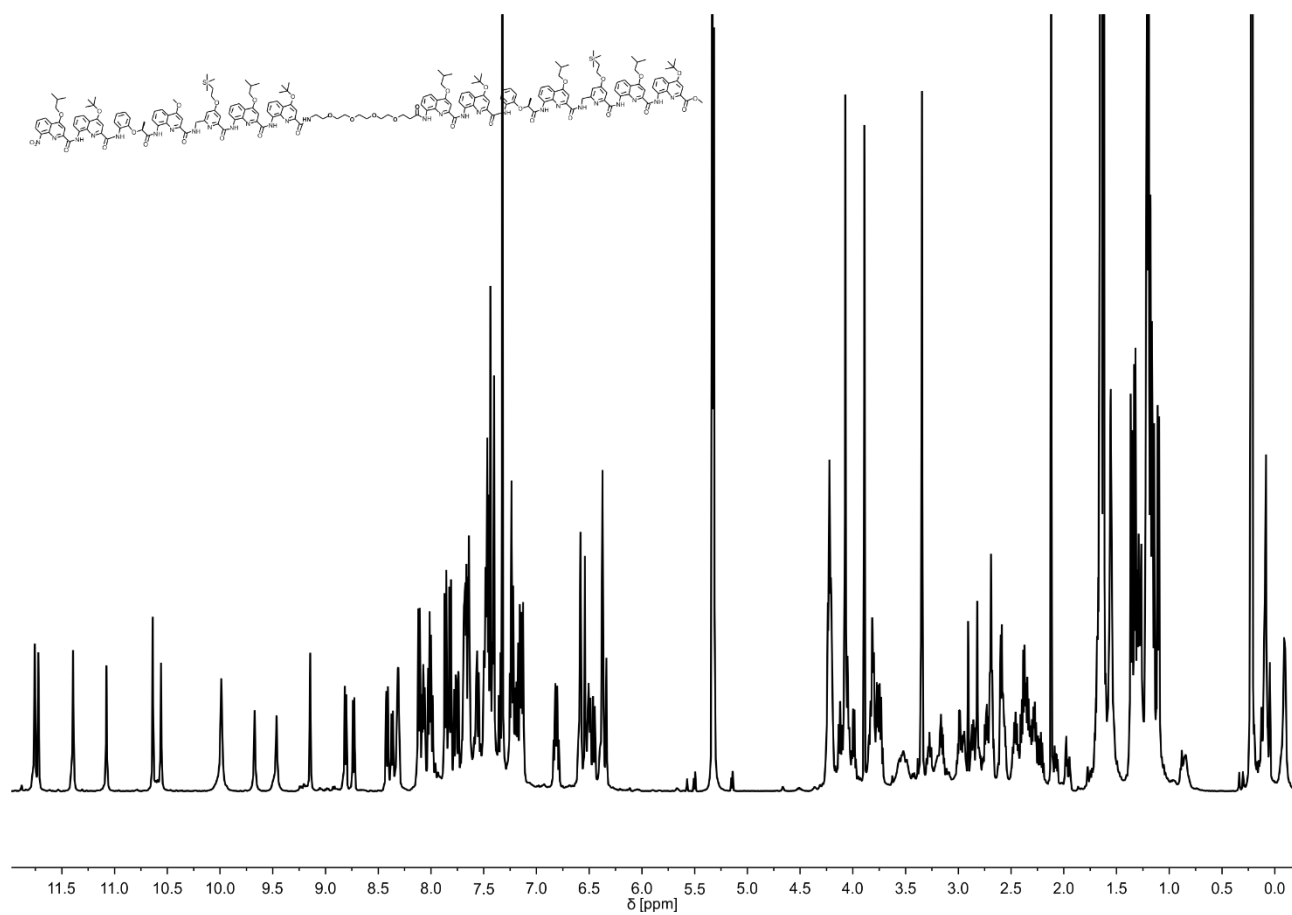


**Figure S66.** <sup>1</sup>H NMR spectrum (500 MHz, CD<sub>2</sub>Cl<sub>2</sub>) of **28**.

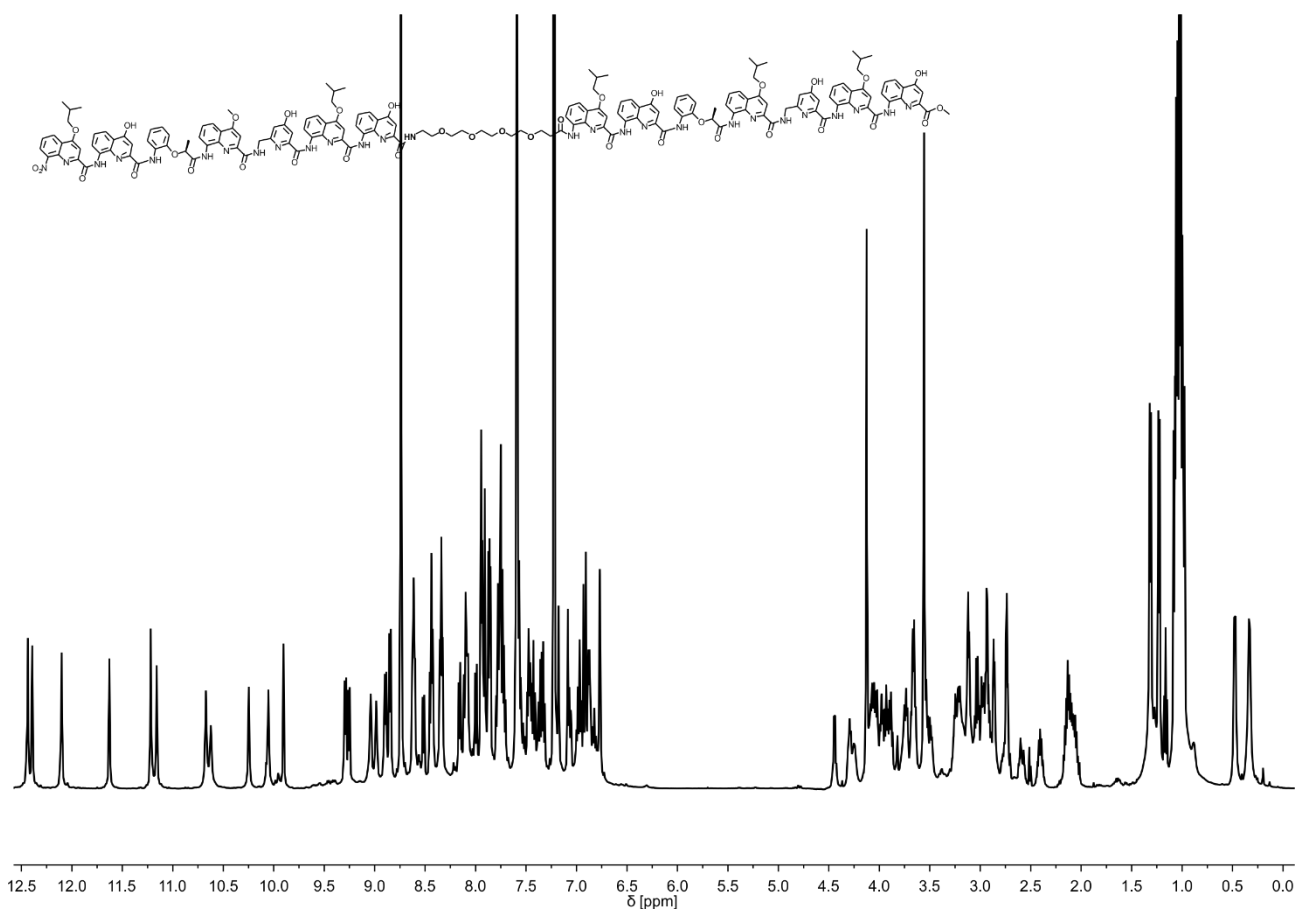


**Figure S67.** <sup>1</sup>H NMR spectrum (500 MHz, Pyridine-*d*<sub>5</sub>) of **11**.



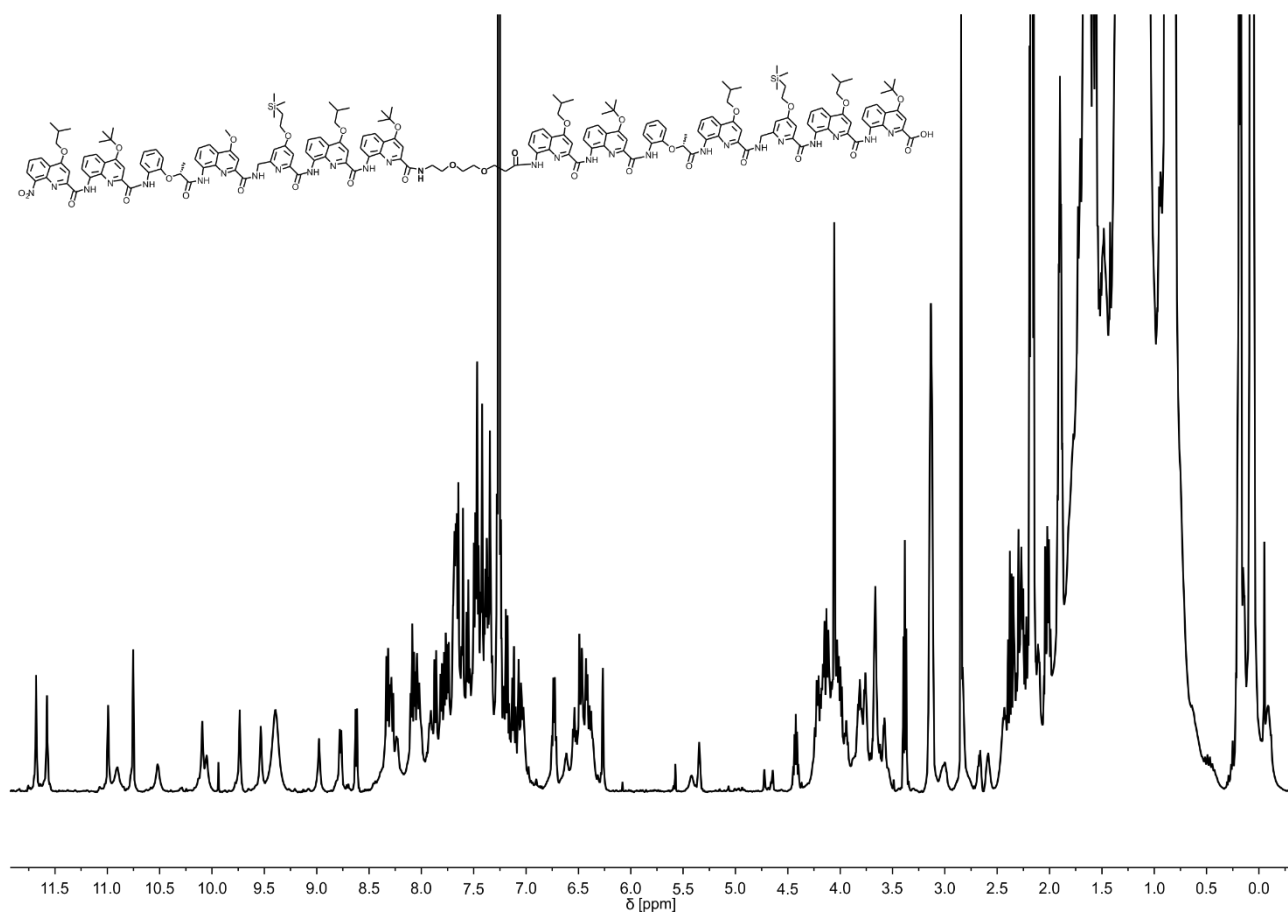


**Figure S68.**  $^1\text{H}$  NMR spectrum (500 MHz,  $\text{CDCl}_3$ ) of **29**.

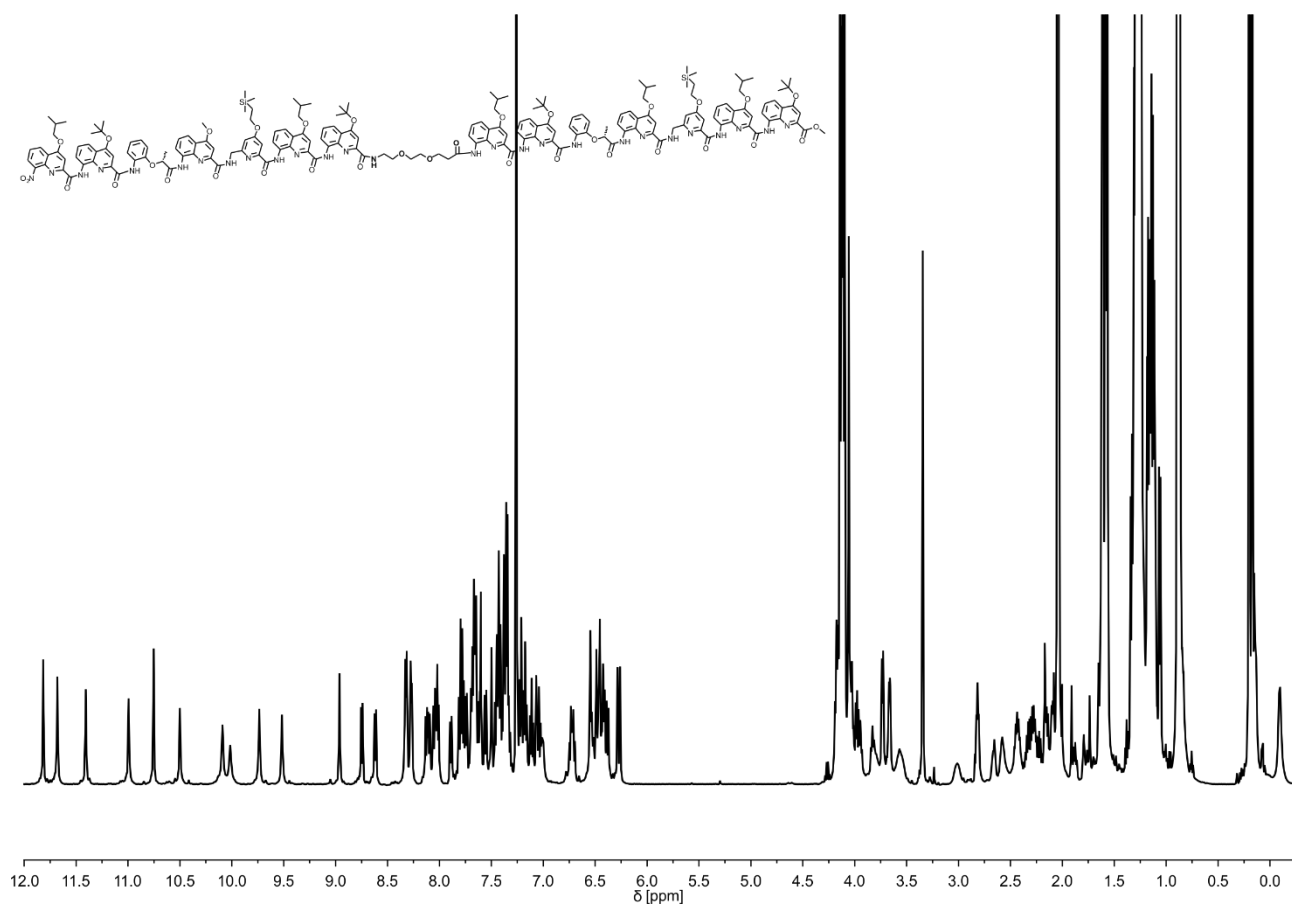


**Figure S69.** <sup>1</sup>H NMR spectrum (500 MHz, CDCl<sub>3</sub>) of **30**.

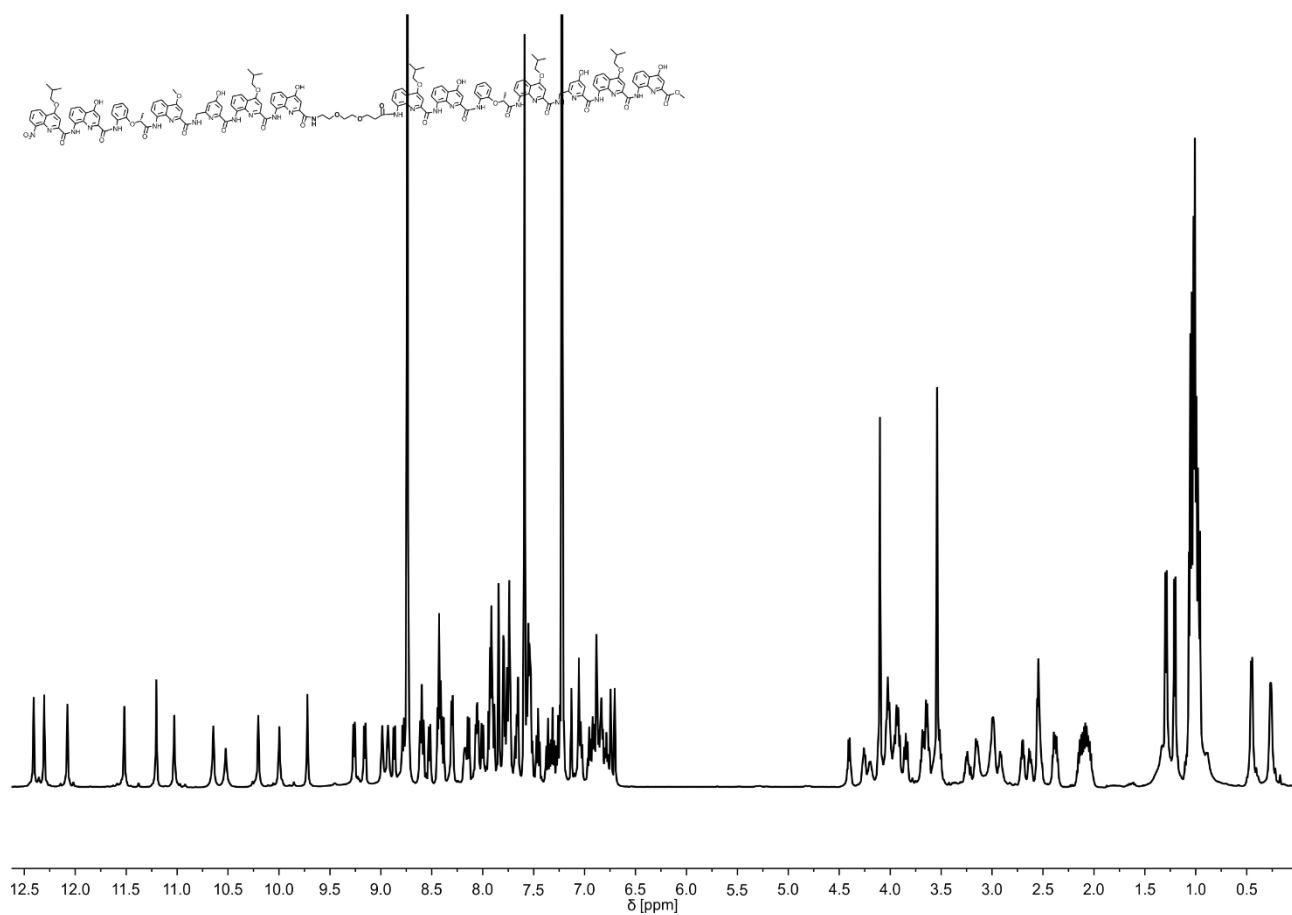


**Figure S70.** <sup>1</sup>H NMR spectrum (500 MHz, Pyridine-*d*<sub>5</sub>) of **12**.

### 5.2.7.3 Sequences with a helix-turn-helix-motif and handedness-control in one helix

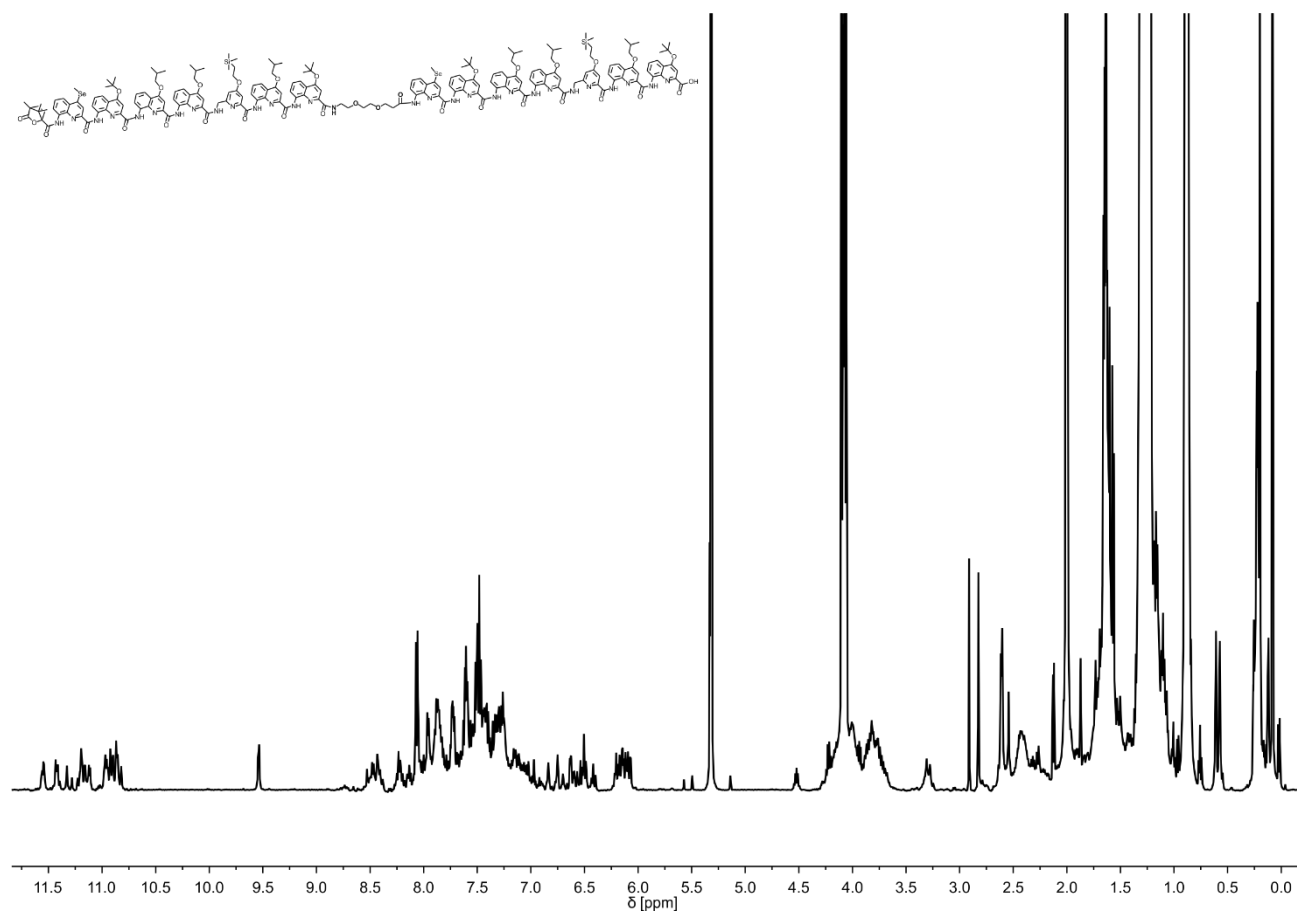


**Figure S71.** <sup>1</sup>H NMR spectrum (500 MHz, CD<sub>2</sub>Cl<sub>2</sub>) of **31**.

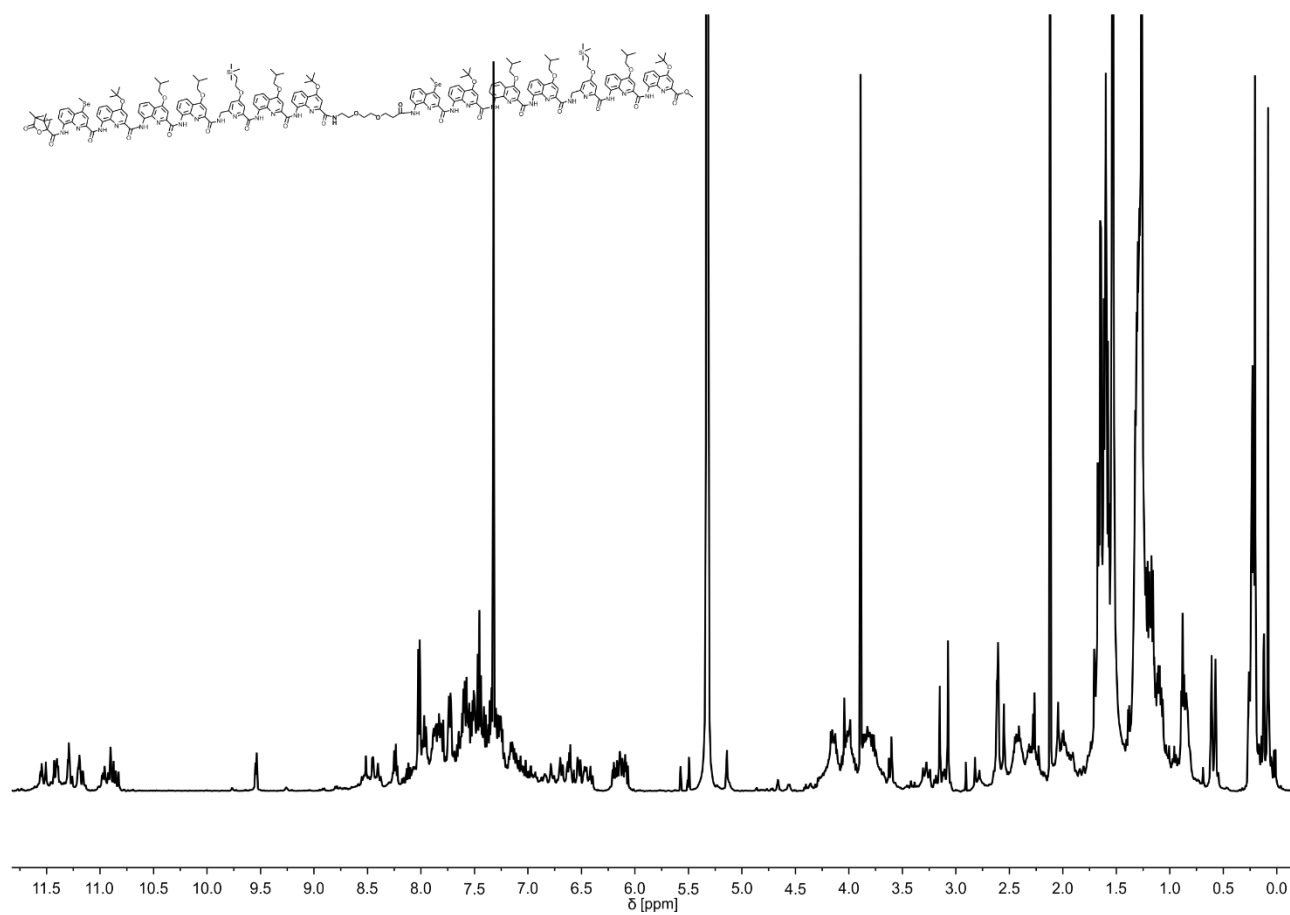


**Figure S72.** <sup>1</sup>H NMR spectrum (500 MHz, CD<sub>2</sub>Cl<sub>2</sub>) of **32**.

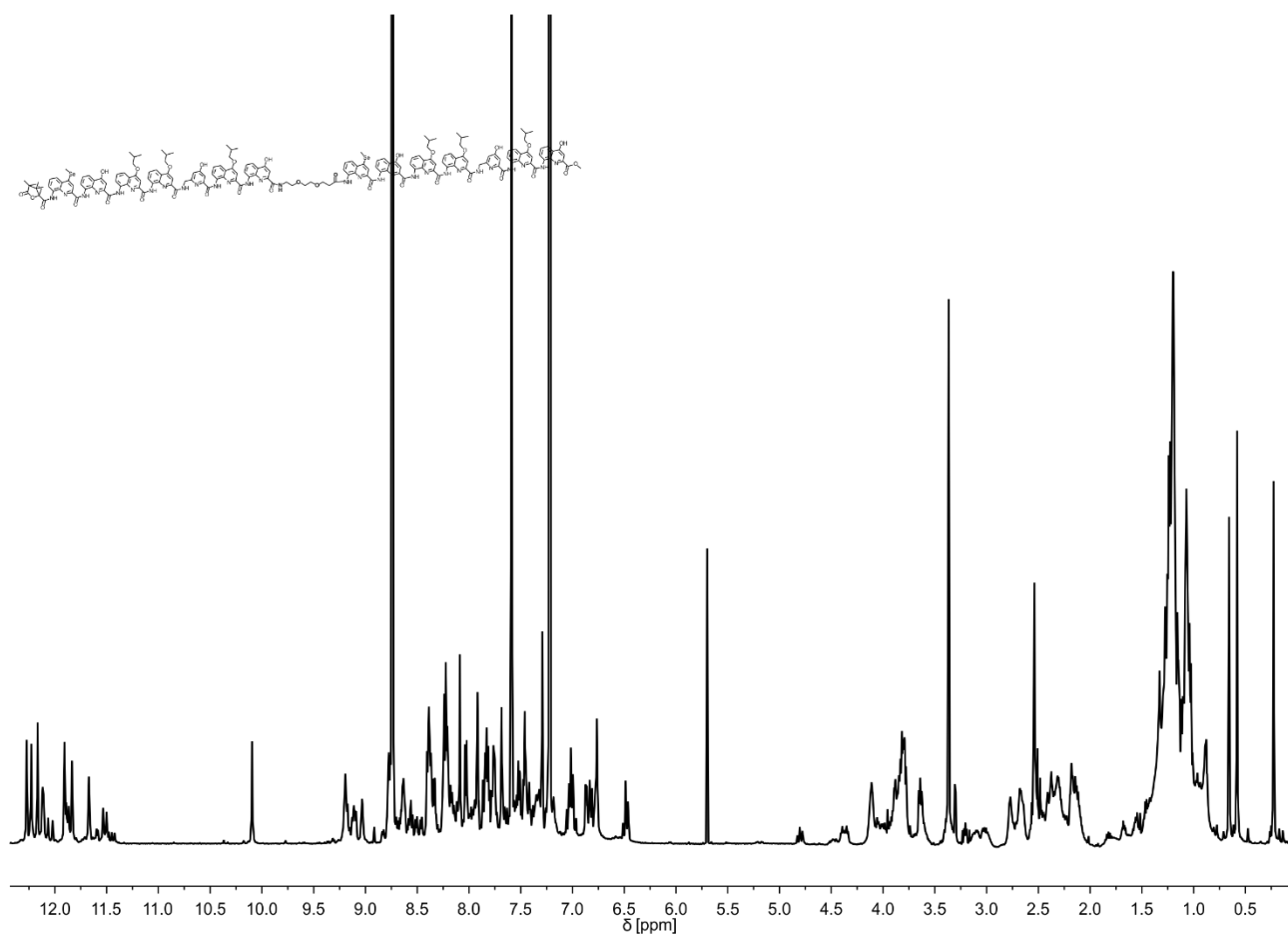


**Figure S73.** <sup>1</sup>H NMR spectrum (500 MHz, Pyridine-*d*<sub>5</sub>) of **13**.

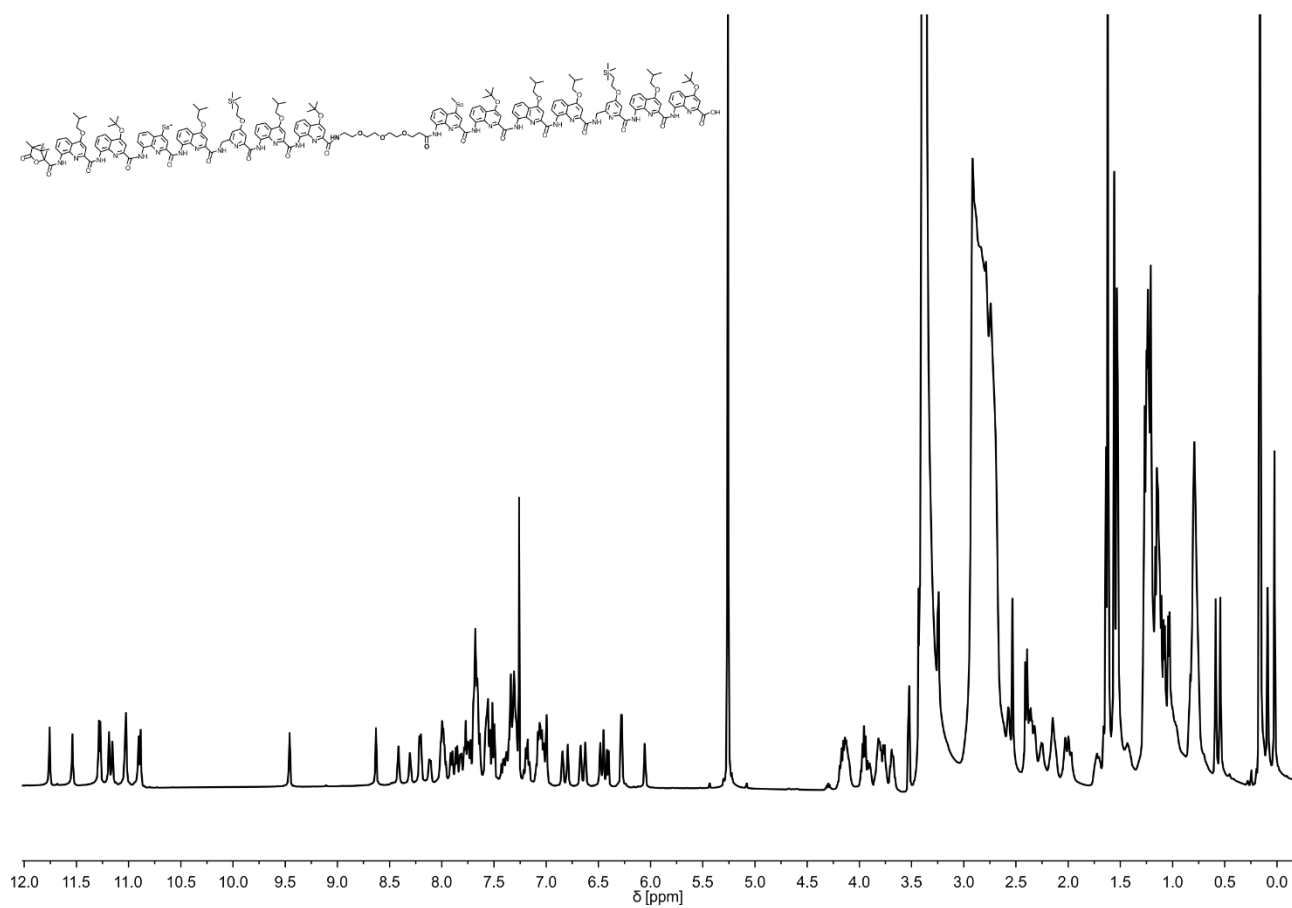


**Figure S74.** <sup>1</sup>H NMR spectrum (500 MHz, CDCl<sub>3</sub>) of **33**.

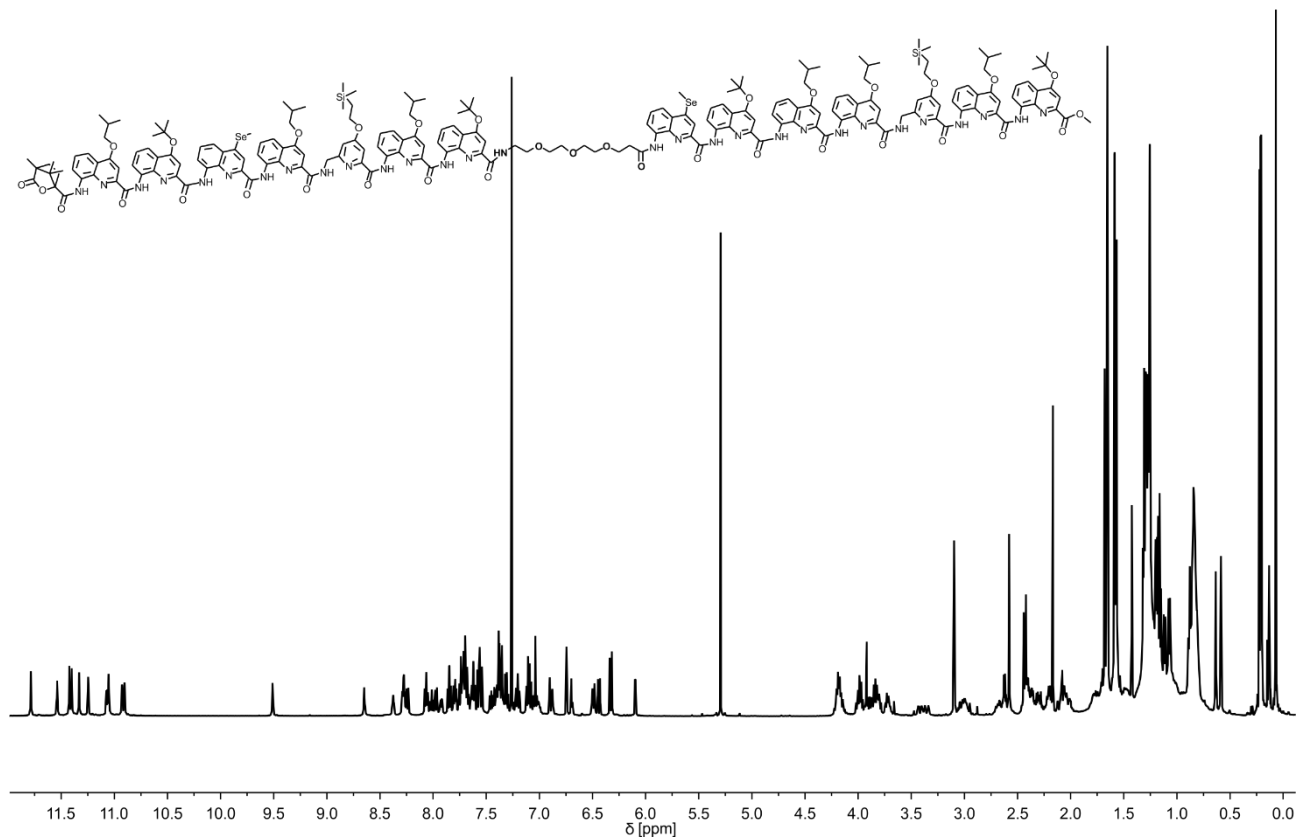


**Figure S75.** <sup>1</sup>H NMR spectrum (500 MHz, CDCl<sub>3</sub>) of **34**.



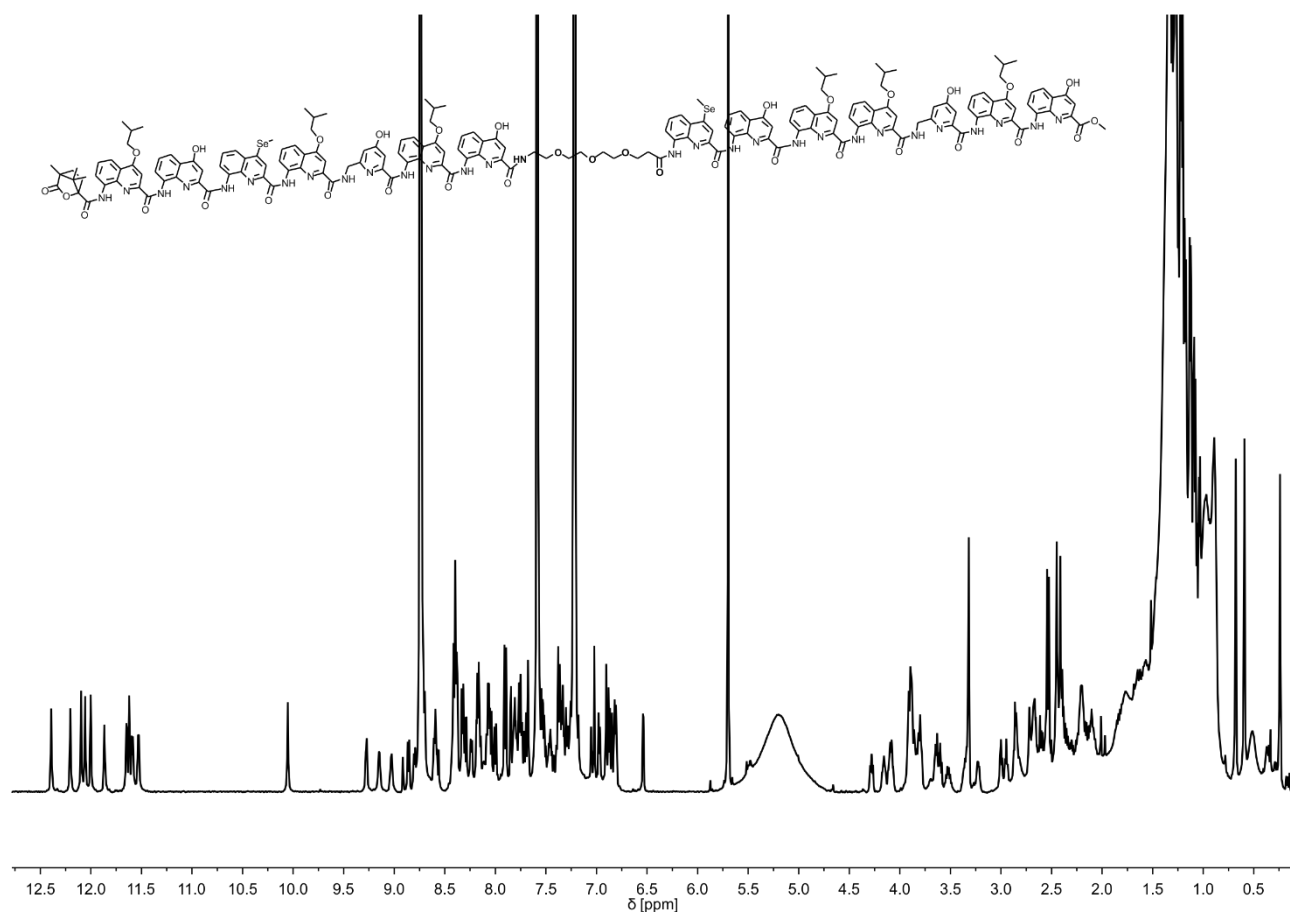


**Figure S76.**  $^1\text{H}$  NMR spectrum (500 MHz,  $\text{Pyridine-}d_5$ ) of **14**.

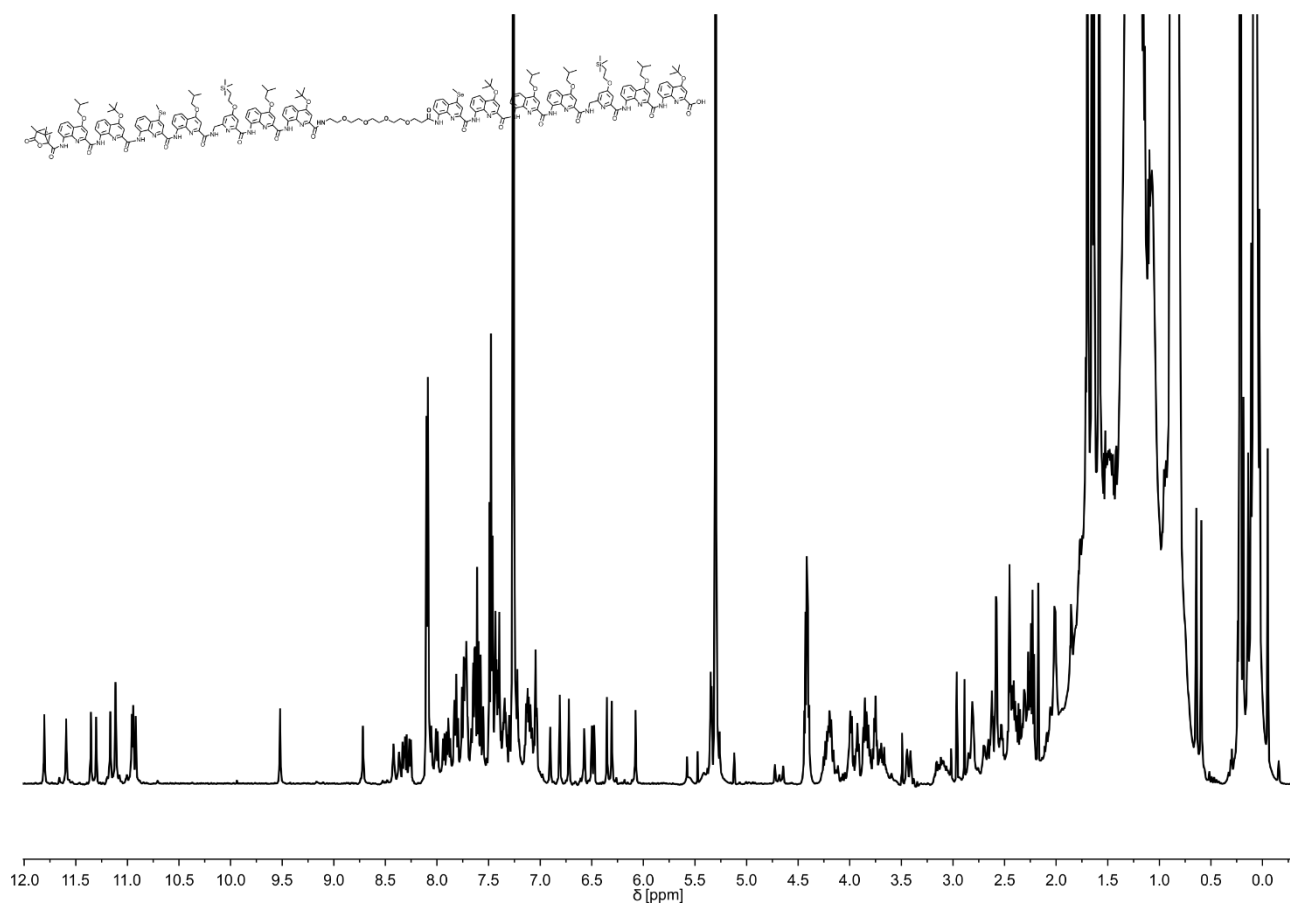


**Figure S77.** <sup>1</sup>H NMR spectrum (500 MHz, CDCl<sub>3</sub>) of 35.

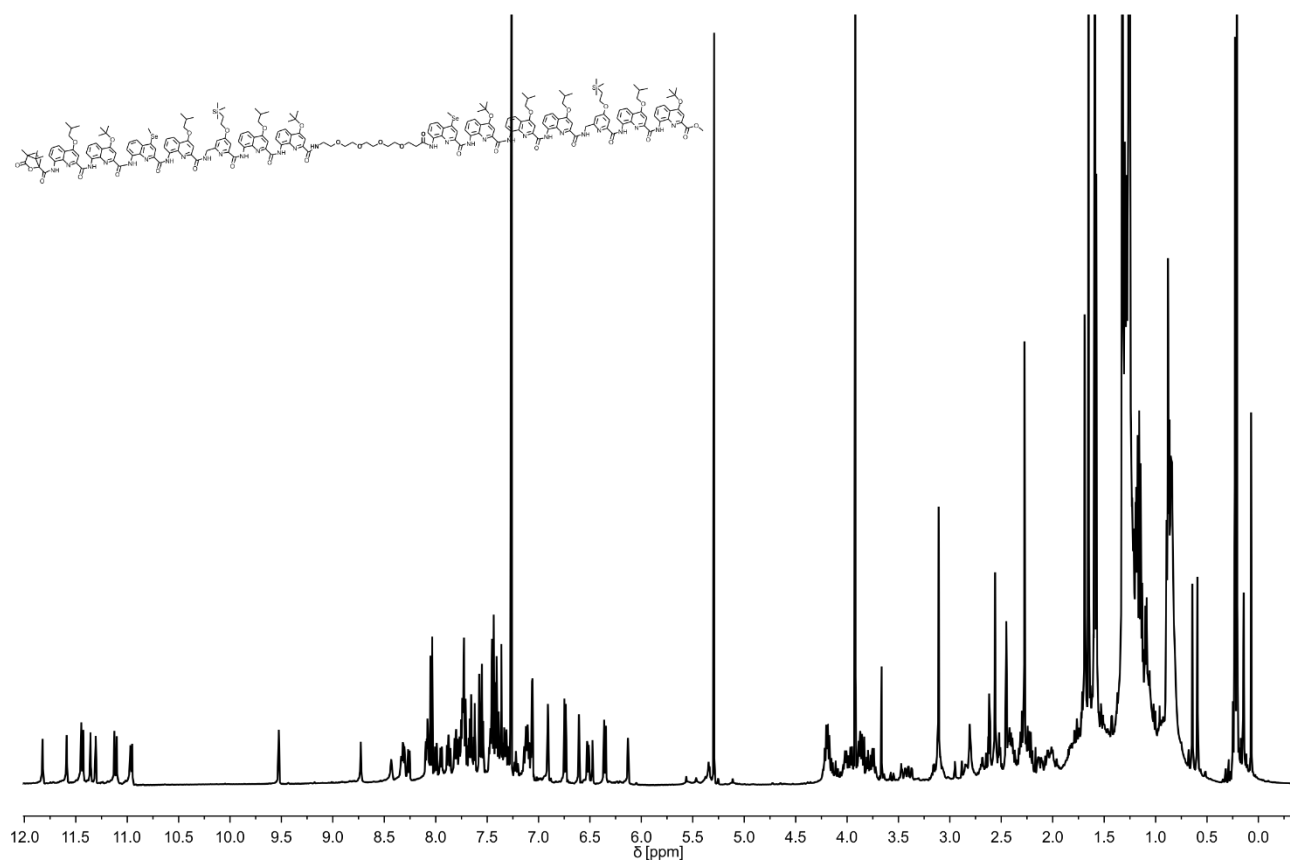


**Figure S78.** <sup>1</sup>H NMR spectrum (500 MHz, CDCl<sub>3</sub>) of **36**.

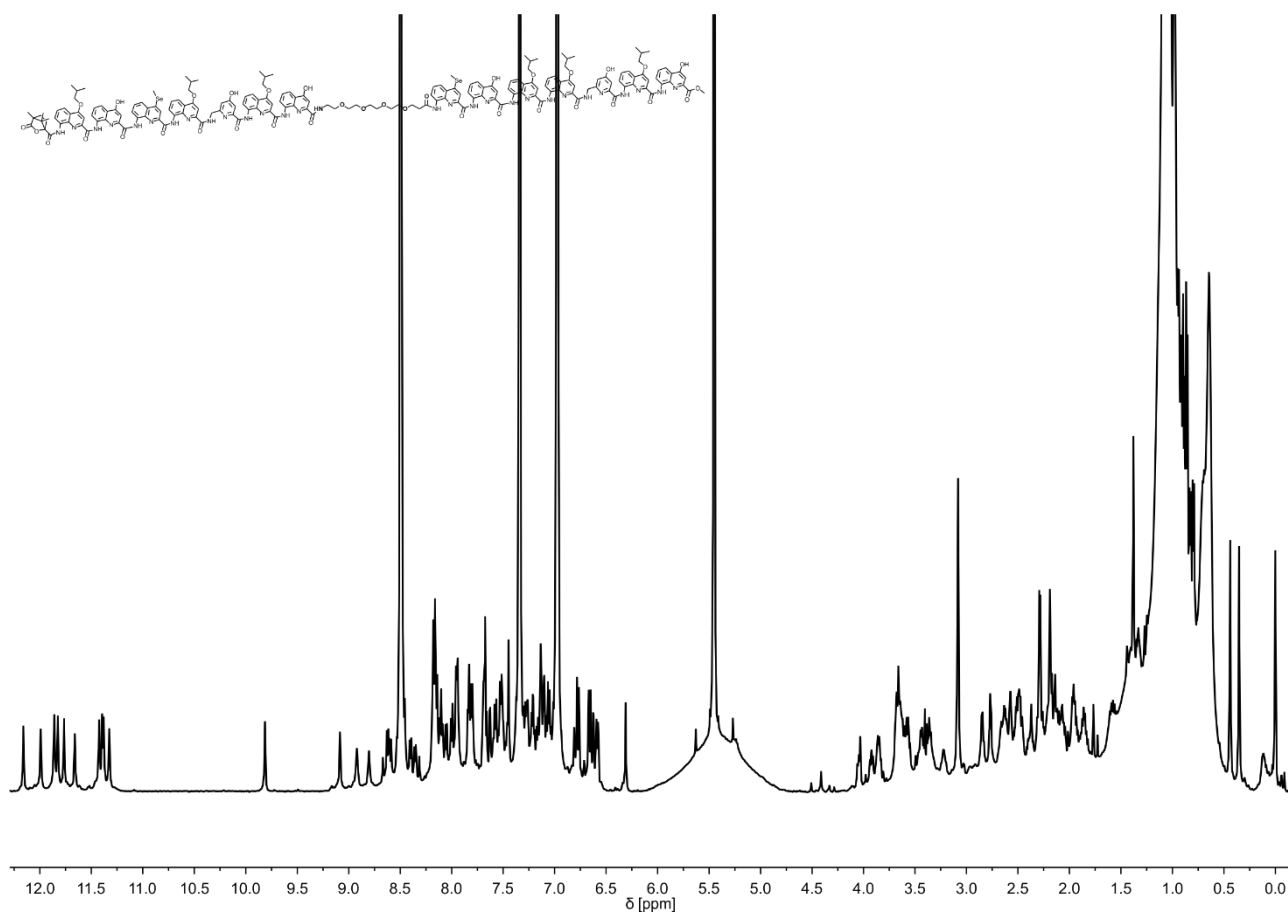


**Figure S79.** <sup>1</sup>H NMR spectrum (500 MHz, Pyridine-*d*<sub>5</sub>) of **15**.

### 5.2.7.4 Achiral sequences with a helix-turn-helix-motif

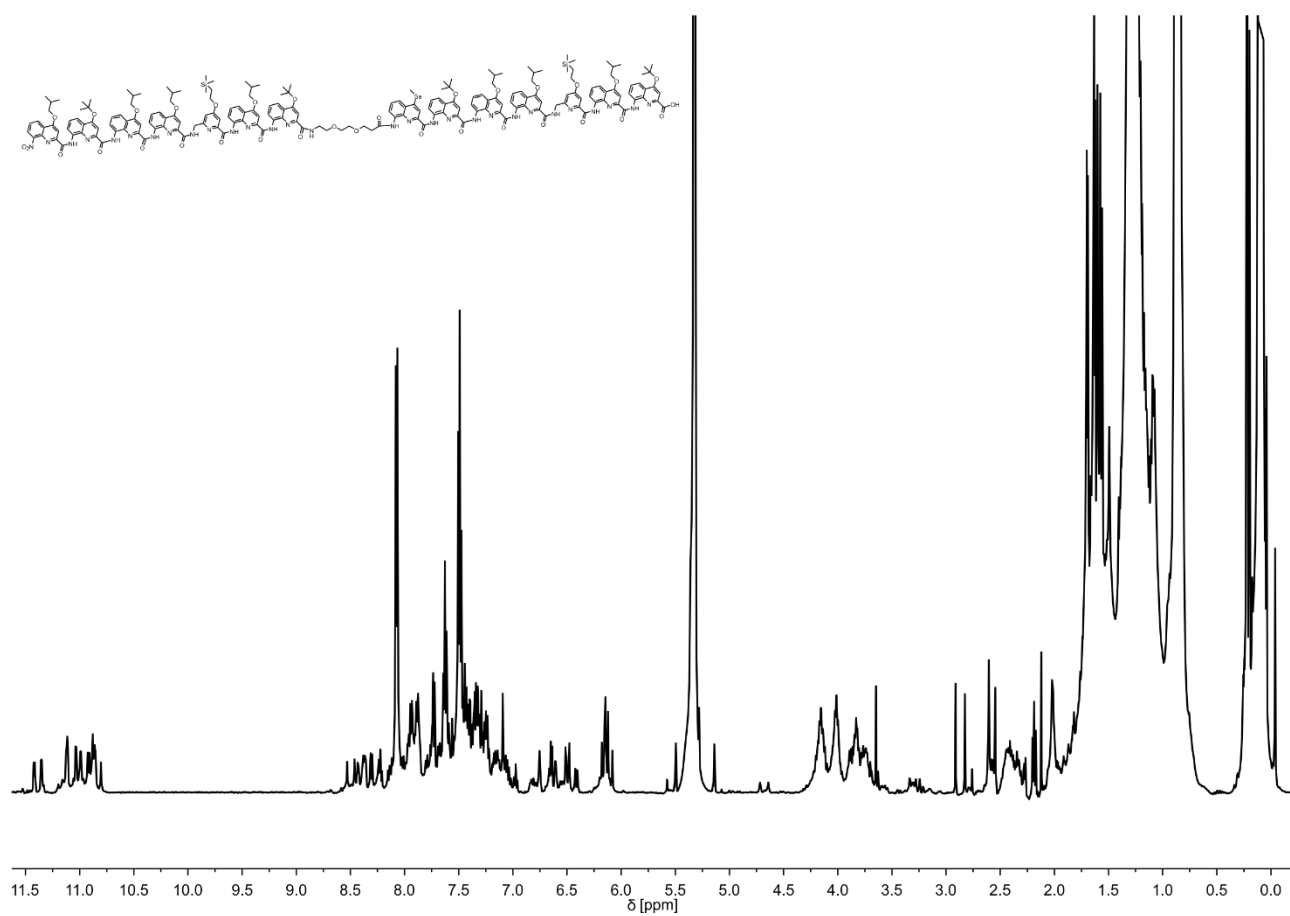


**Figure S80.** <sup>1</sup>H NMR spectrum (500 MHz, CD<sub>2</sub>Cl<sub>2</sub>) of **37**.

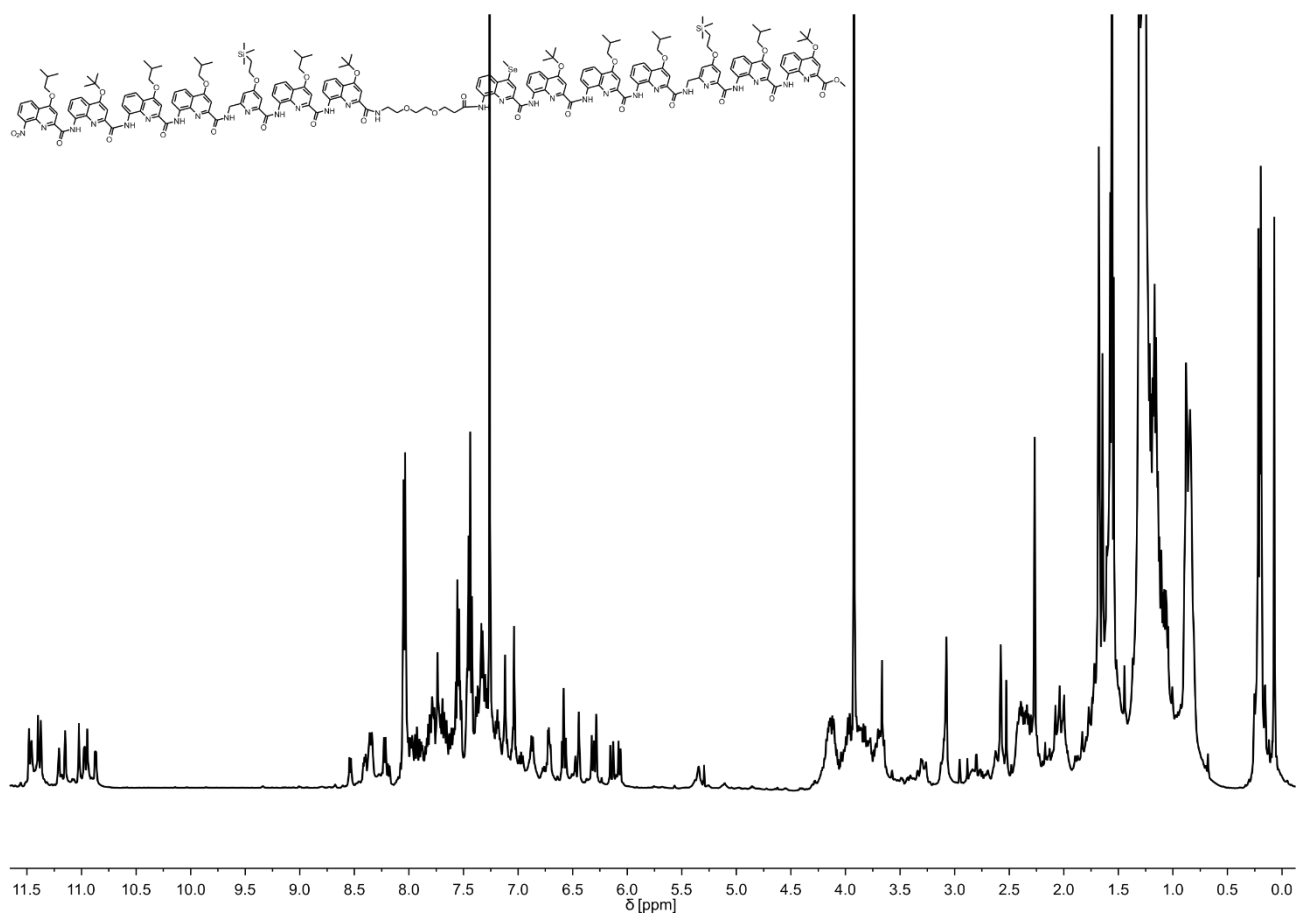


**Figure S81.** <sup>1</sup>H NMR spectrum (500 MHz, CDCl<sub>3</sub>) of **38**.

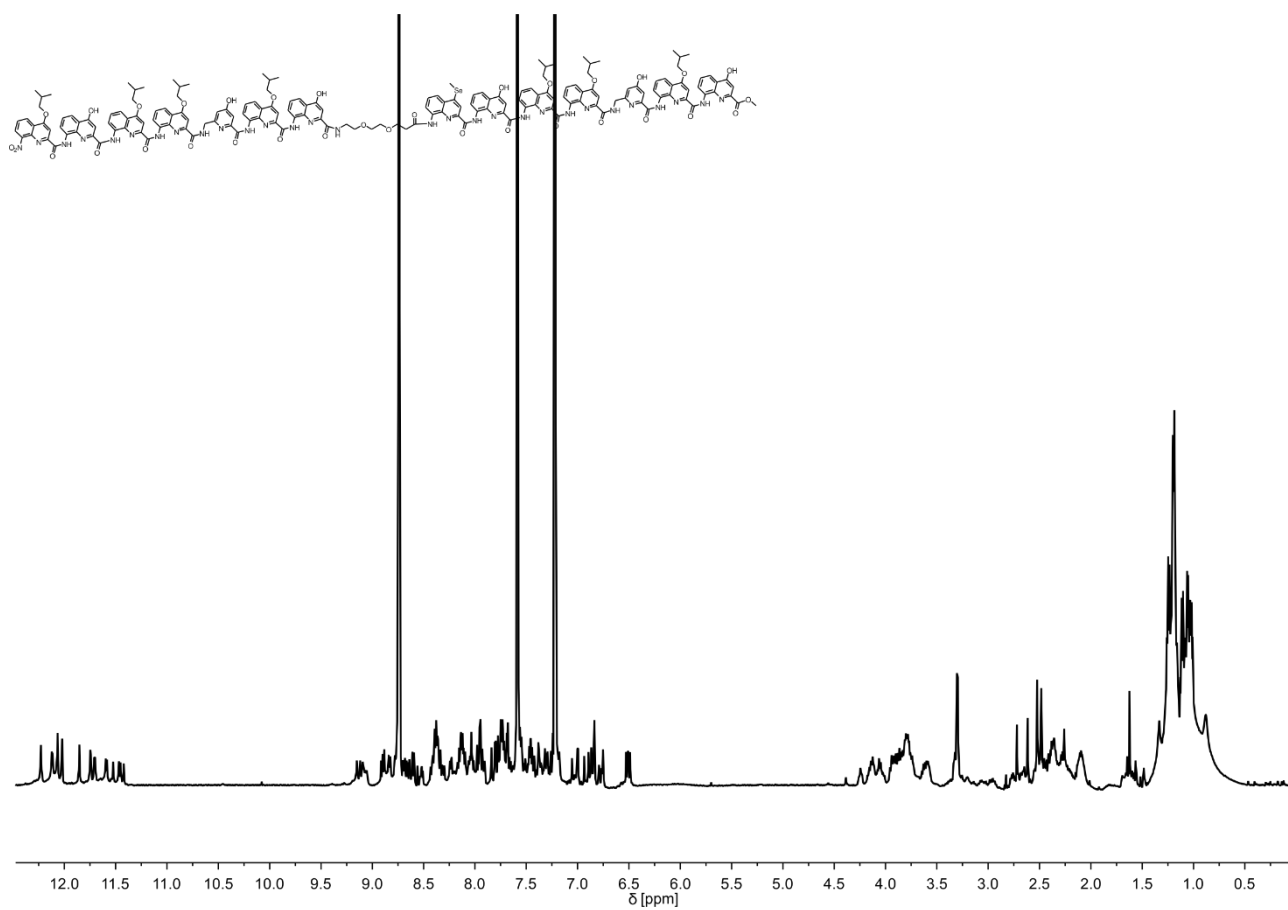


**Figure S82.** <sup>1</sup>H NMR spectrum (500 MHz, Pyridine-*d*<sub>5</sub>) of **16**.

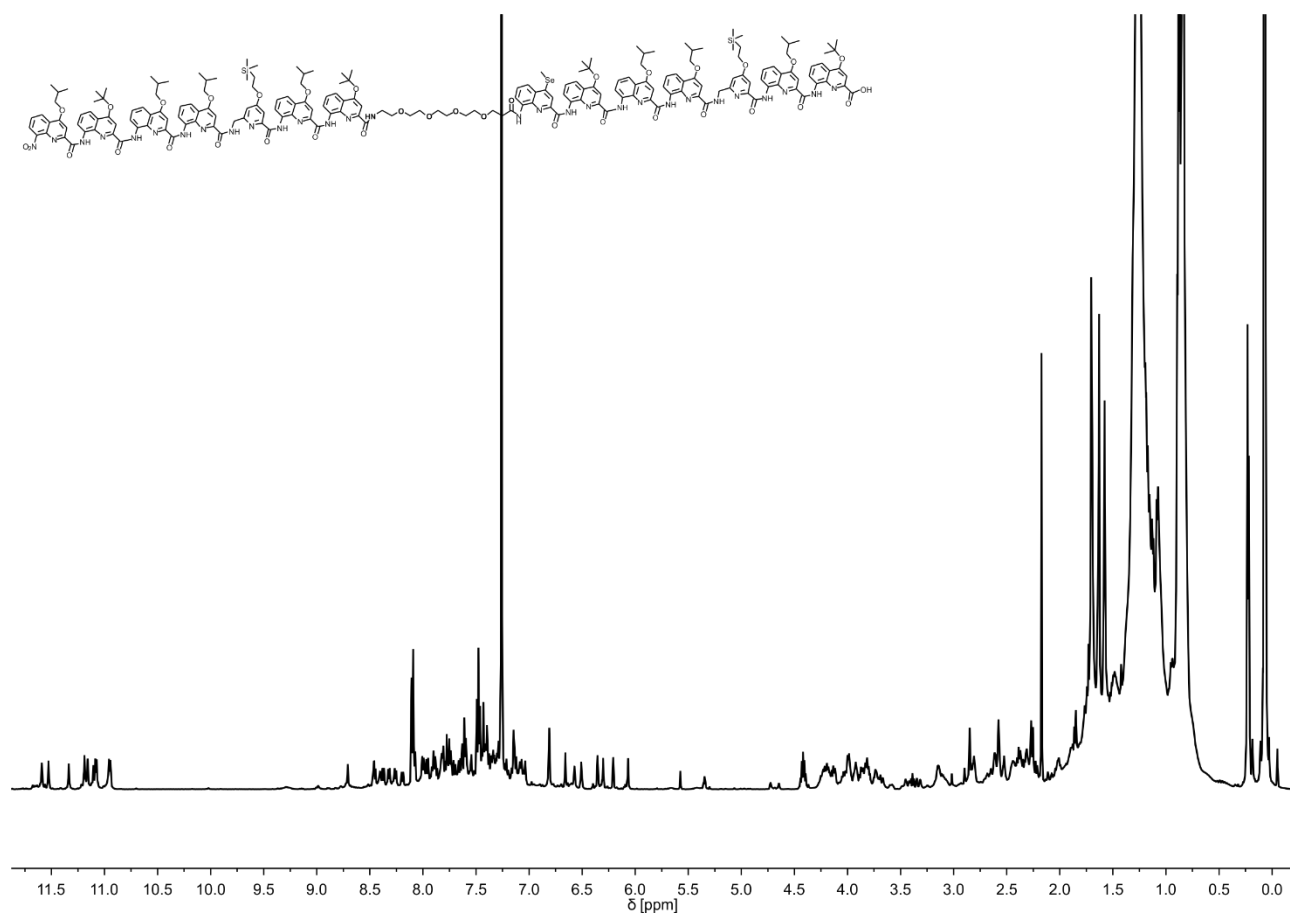


**Figure S83.** <sup>1</sup>H NMR spectrum (500 MHz, CDCl<sub>3</sub>) of **39**.



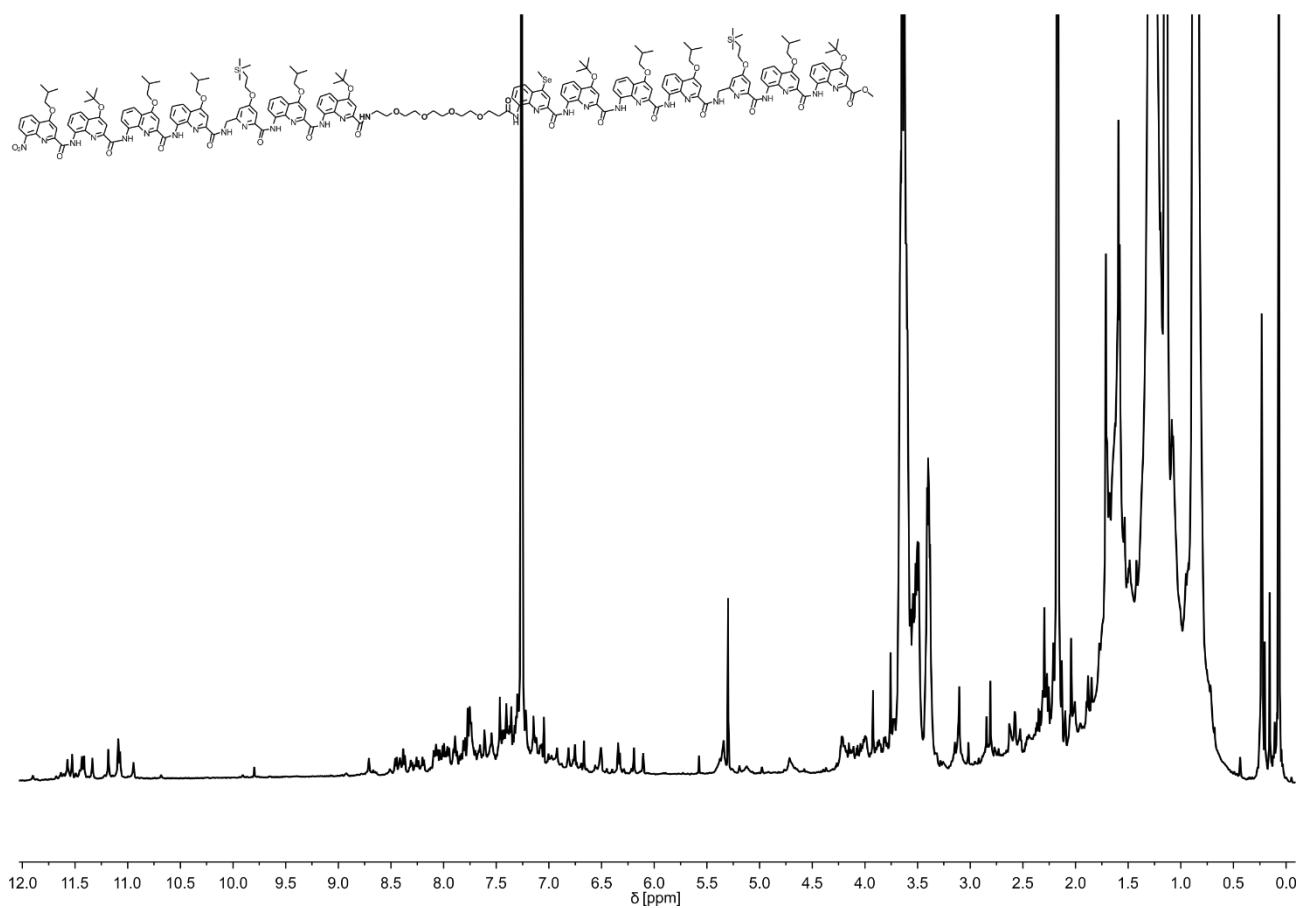


**Figure S84.** <sup>1</sup>H NMR spectrum (500 MHz, CDCl<sub>3</sub>) of **40**.

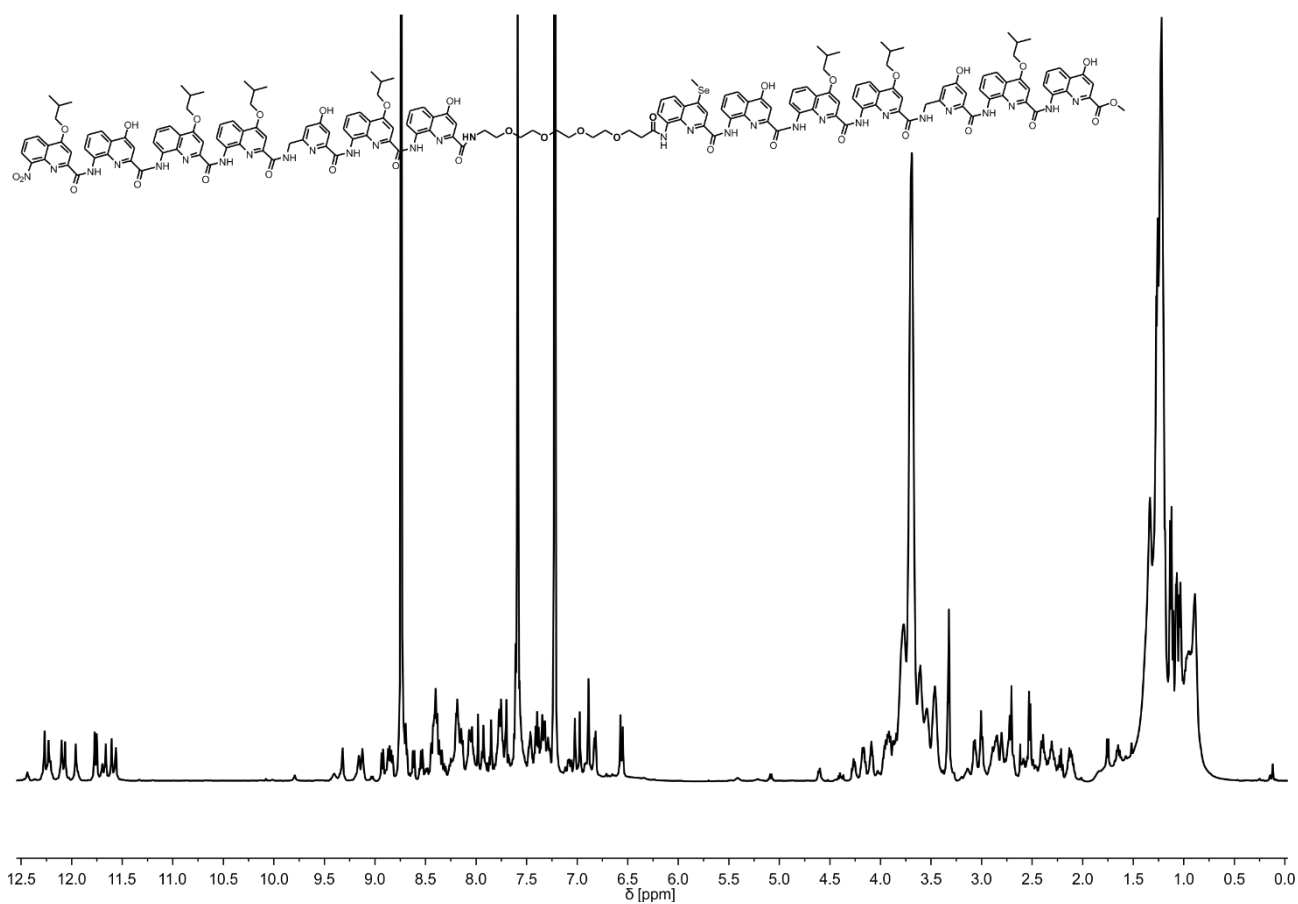


**Figure S85.**  $^1\text{H}$  NMR spectrum (500 MHz,  $\text{Pyridine-}d_5$ ) of **17**.

## 6 Summary and Perspective

In nature the function of macromolecules such as proteins is determined by their shape and structure, which is the result of various kinds of interactions controlling their self-organization.<sup>1-6</sup> Small mutations can alter a protein's make-up and have a significant impact on its self-organization and functionality. To access functions not yet seen in nature the field of abiotic foldamers has been developed. Foldamers are an emerging class of molecules inspired by natural biopolymers, that also have the ability to fold into well-defined three-dimensional structures.<sup>7</sup> As their name suggests, *abiotic* foldamers consist of units absent from natural environments yet they fold into conformationally ordered states, stabilized by noncovalent interactions.<sup>8</sup> In contrast to the random mutations occurring in nature, substitutions and alterations in the primary structure of the synthetic foldamers can be made with intent, allowing for an accurate prediction of their structure and functionality. In this thesis, work regarding abiotic folding focused on oligomers mainly consisting of aromatic  $\delta$ -amino acids. The handling of such foldamers, especially in media different from water, will enable us to access and develop new functions unimaginable in nature. The function of natural biopolymers mostly emerges at the tertiary and quaternary structure level.<sup>3-6</sup> The same is to be expected for *abiotic* foldamers. In order to predictably design foldamers on such complex structural levels, however, the intricacies of basic structures must be fully understood first. The pioneering steps towards this goal have been made in the Ivan Huc group. Here, the tertiary structure of a foldamer based on an aromatic oligo amide helix-turn-helix motif and its stabilizing hydrogen bonds have been predicted successfully by accurate computational modelling.<sup>9</sup> In these models the formation of a parallel PP dimer was stabilized by a rigid turn unit.<sup>9, 10</sup> Here, it is assumed that the more intermolecular hydrogen bonds had formed the more stable is the tertiary fold. Furthermore, it was thought that to stabilize the tertiary fold of a parallel PP dimer all hydrogen bonds formed matter equally. However, in this thesis it is shown that, by systematic removal of certain hydrogen bonds, some hydrogen bonds stabilize the tertiary fold more than others.

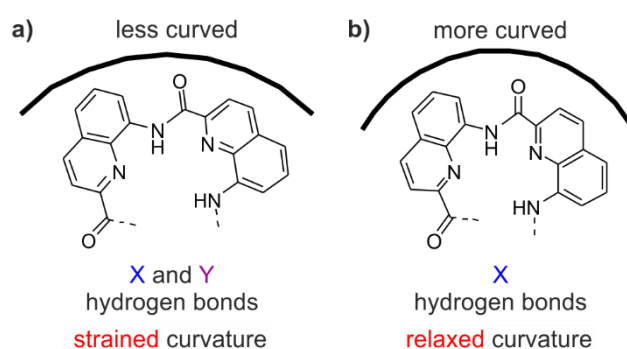


**Figure 6.1.** Helix curvature in a tertiary fold stabilized by X and Y hydrogen bonds (a) and stabilized by only X hydrogen bonds (b), respectively.<sup>11</sup>

A closer look revealed that the formation of superfluous hydrogen bonds could cause a destabilizing change of the helix curvature within the secondary fold of homochiral head-to-head parallel dimers

(Figure 6.1). This also highlighted the influence a tertiary fold can have on its underlying secondary fold. Formation of a stable tertiary structure can enforce a twisting strain on its secondary fold. Similar circumstances can be found in proteins<sup>12, 13</sup>, especially in publications related to enzymatic activity.<sup>14-20</sup> All in all, the found twisting strain is a promising sign of a protein imitation and might lead to further steps towards its utilization. At the very least, the occurrence of a twisting strain in a secondary fold should no longer be neglected when designing stabilizing linkers for other aggregational modes.

Furthermore, this discovery shed light on previous observations regarding self-assembly. Self-assemblies between helices in which no hydroxyl groups have been replaced by protons happened to be less predictable than tertiary structures stabilized by a rigid turn unit. Such a foldamer produced several thermodynamically and kinetically stable dimeric and trimeric homochiral bundles with structures distinct from the desired helix-turn-helix motif. This behavior could not be definitively explained and was suspected to be related to an unforeseen orientation of their hydrogen bonds.<sup>9</sup> However, re-investigation of the crystal structures of these self-assemblies, showed that a conformation which did not disturb the secondary structure was formed in both cases. It was further assumed, that the linked helices in a tertiary structure were sterically prohibited to form an energetically optimal aggregate and thus would not form a parallel PP dimer during a self-assembly.<sup>11</sup> In the third chapter of this thesis it is shown how foldamer designs can be manipulated to promote the formation of new dimeric hydrogen bonding interfaces during a self-assembly (Figure 6.2).

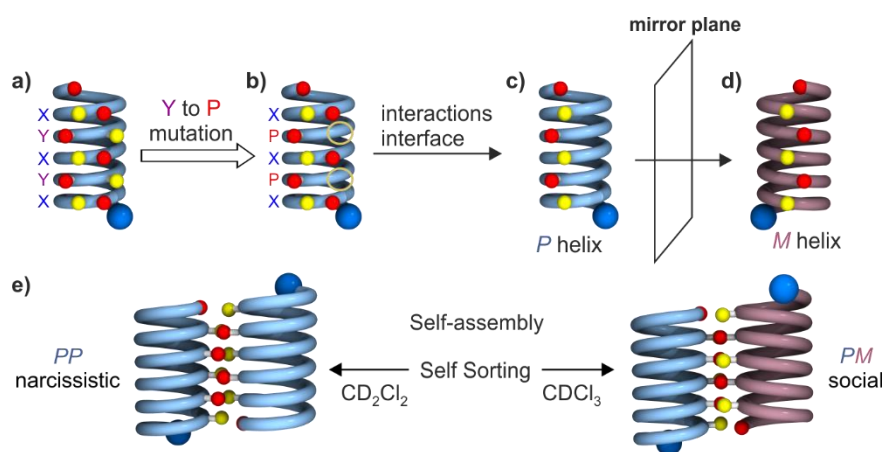


**Figure 6.2.** Front view of a single helix before (a) and after (a) precise point removal of hydroxyl groups. Front view of a single helix depicting the interaction interface of a P-helix (b) and a M-Helix (d). Self-sorting behaviour of single helices in chlorinated solvents (e).<sup>21</sup>

Precise removal of hydroxyl groups on one side of the helix, thusly introducing one linear array of hydrogen bond donors destabilized tilted dimer and trimer aggregates (Figure 6.2a&c). Instead formation of shifted *PM*- and *PP/MM*-dimers have been observed as a result of these adjustments within which hydrogen bonds formed in one linear array.<sup>21</sup> This is in contrast to tape-like or flat rigid structures presented in other contexts.<sup>22-25</sup> Furthermore, formation of hetero- or homochiral dimers can be influenced by the choice of a chlorinated solvent or by imposing absolute handedness control, thereby

inhibiting *PM* aggregates (Figure 6.2e). In conclusion, the chlorinated solvent-dependent self-assembly behavior exemplifies a remarkable case of social or narcissistic chiral self-sorting. In nature, specific self-sorting behaviors have been known to occur in support of important biological processes.<sup>26, 27</sup> The reasons why similar chlorinated solvents may give rise to such large effects has to be further investigated, however. Understanding this aspect of self-assembly would undoubtedly be vital for designing predictable foldamers with protein-like functionality. The research on self-assemblies with a reduced number of hydrogen bond donors showed the formation of very stable and predictable aggregates. Information gained from the new dimeric hydrogen-bonding interfaces explored in chapter four might be used for other kinds of self-assemblies and could even be implemented in the design of quaternary structures.

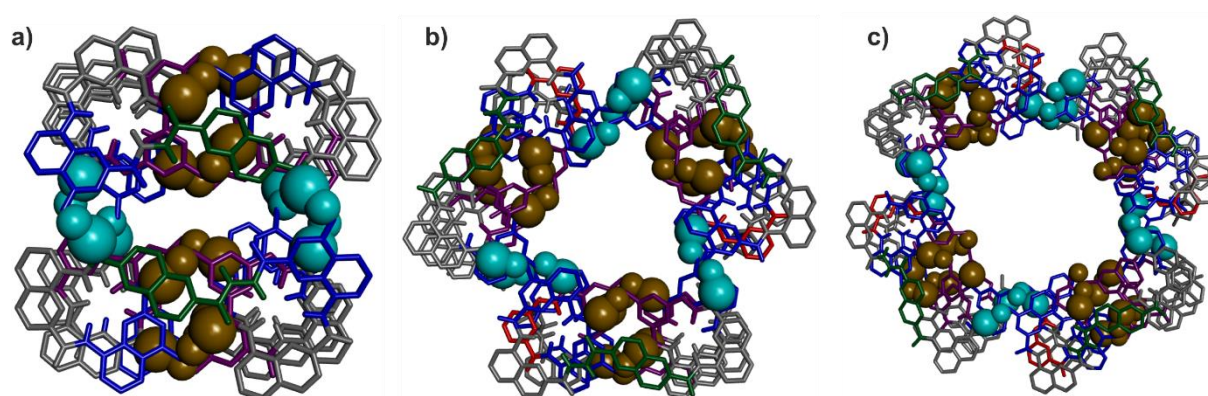


**Figure 6.3.** Top view of a computational model of a quaternary dimer (a), trimer (b) and tetramer (c). Intramolecular and intermolecular hydrogen bonds are shown as gold and turquoise balls, respectively. The X units are shown in blue, the Y units in violet, the P units in red and turn units in green tubes. Side-chains are omitted for clarity.

In the design of such quaternary structures hydroxyl groups are introduced to the outer surface of a basic tertiary structure. A parallel *PM* dimer stabilized by a rigid turn unit is stabilized by intramolecular hydrogen bonds and could serve as the basis for such a design.<sup>28</sup> Theoretically, these modified tertiary structures are able to form intermolecular hydrogen bonds to one another and form a quaternary structure in the process. Work on this subject is currently conducted in our laboratory by Shuhe Wang (Figure 6.3).

As of yet the successful synthesis of a quaternary structure has not been reported. In chapter five, of this work, however, the formation of a complex, abiotic, tetrameric, eight-helix bundle, has been discovered. This structure was obtained while investigating how the formation of a non-parallel tilted dimer could be stabilized by a flexible turn unit. The single helices used in this endeavor had previously formed tilted dimers when unhindered in their aggregation. However, the flexible linkers used in this project allowed for the formation of a macro aggregate to occur, whose complexity is unprecedented in the field of abiotic folding.

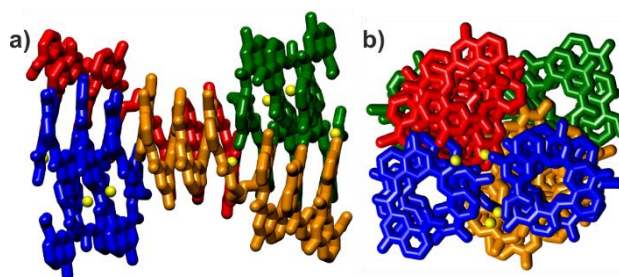


**Figure 6.4.** Side (a) and top (b) view of an abiotic, tetrameric, eight-helix bundle abiotic eight helix bundle in the solid state. The four molecules are shown in blue, red, gold and green. Molecules in a closed conformation are shown in red and golden. Molecules in an open conformation are shown in green and blue. Water molecules are shown as yellow balls. Side chains and other included solvent molecules are omitted for clarity.<sup>29</sup>

This large heterochiral aggregate (12.9 kDa) consists of four secondary structures and a total of eight helices arranged in three distinct domains; two three-helix bundle domains and one two-helix-bundle domain. Thus, three hydrogen bonding interfaces are formed within the aggregate in total (Figure 6.4a, c, d). One of these hydrogen bonding interfaces resembled the previously reported head-to-tail shifted *PM* dimer<sup>21</sup> (Figure 6.4c). The other two identical interfaces formed a distorted trimer (Figure 6.4d).<sup>29</sup> This hydrogen bonding interface variant was new and most closely resembled a homochiral head-to-head-to-head parallel trimer.<sup>9</sup> The newly found distorted head-to-head-to-tail parallel trimer was different in regards to parallelism (helices were head-to-head-to-tail parallel), handedness of the helices (one out of three helices had a different handedness) and its hydrogen bonding interface. Here many water molecules bridging hydrogen bonds were observed (Figure 6.4). Additionally, the dimeric and distorted trimeric hydrogen bonding interface interacted with one another in two ways: a shared secondary structure and overlapping hydrogen bonds (Figure 6.4a, b&e). Furthermore, two distinct conformations of the secondary structures are observed; a closed (A and A' in Figure 6.4a) and an open (B and B' in Figure 6.4a). In summary, four secondary structures interacted with one another via inter- and intra-molecular hydrogen bonds within this macro aggregate, which displayed a high level of symmetry, incorporating the same set of interactions multiple times.<sup>13</sup> Both symmetry<sup>13</sup> as well as water-bridging<sup>30</sup> have been observed in protein folding processes and appear to be integral to the understanding of foldamer design. Knowledge gained from the new distorted trimeric hydrogen-bonding interface within the abiotic, tetrameric, eight-helix bundle could be useful for other projects, such as the design of stable trimeric aggregates. In conclusion, the discovery of this complex structure provided possible insights into future designs and predictions of more diverse and sophisticated self-organizations. Hypothetically, the synthesis of an alternative aggregate involving eight helices could be explored. An alternating pattern of head-to-tail parallel *PM* helices linked by rigid turn units<sup>28</sup> could potentially become a sub-unit in the design of tubular macromolecules. Here four parallel *PM* dimers could be combined to one octo-helical abiotic tertiary structure consisting of 72 units (Figure 6.5a-c).

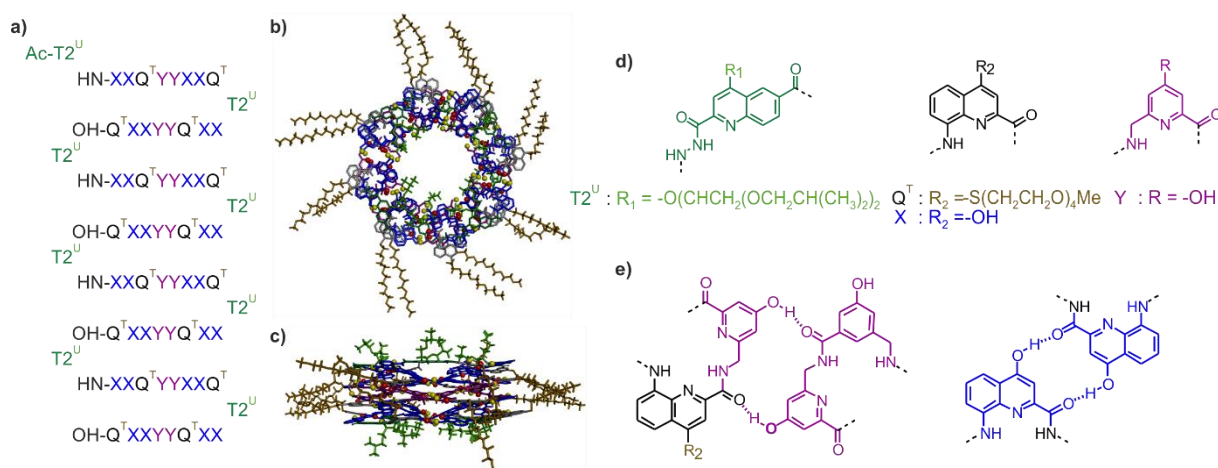


**Figure 6.5.** a) Oligoamide foldamer sequence. Ac- abbreviates acetyl. Top- (b) and side-view (c) of computational model of a tertiary octa-helical macromolecule.<sup>31</sup> d) Structures of units  $T2^U$ ,  $Q^T$ , X and Y, amino acid monomers. e) Hydrogen-bonding patterns involving X and Y units.

In such a hypothetical structure three types of hydrogen bonds would be necessary. In one type the hydroxyl group of the X-Units would bind to the carbonyl function of the neighboring helix' X-unit (Figure 6.5e) and the hydroxyl group of the Y-units would either bind to the carbonyl function of the Q-units of the neighboring helix or the carbonyl function of the Y-unit of the neighboring helix (Figure 6.5e). In the past long oligomers consisting of 96 quinoline units with isobutoxy side-chains (25.7 kDa) have shown decreased solubility.<sup>32</sup> Thus, to avoid solubility issues in case of this 72-mer, more solubilizing side-chains, such as a tetraethylene glycol sidechain should be introduced to the Q-units (Figure 6.5d). To hamper aromatic stacking, a bulky side-chain pointing out of the flat aromatic surface should be introduced to the rigid linker as well (Figure 6.5c&d).

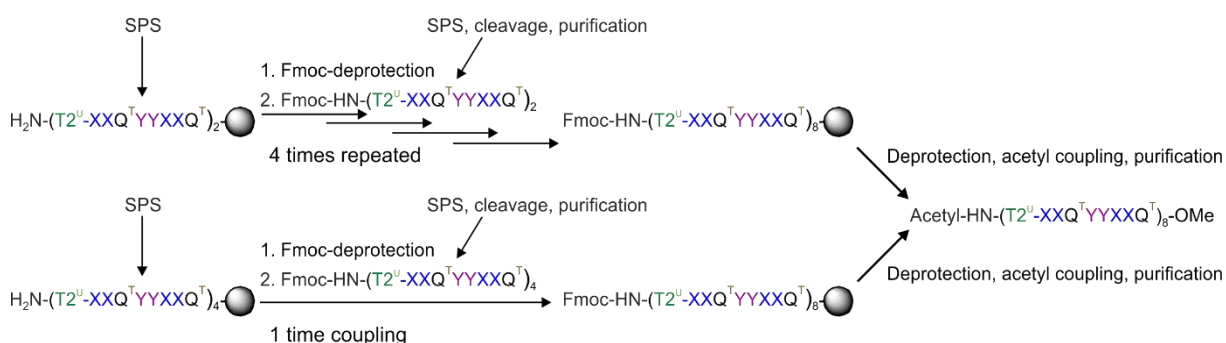


**Figure 6.6.** Scheme of potential synthesis routes of an abiotic octo-helical tertiary bundle via solidphase fragment-condensation.

The successful synthesis of such a macro molecule would require a very clean and high yielding synthetic protocol. After all, this macro molecule would consist of 72 units, which would have to be coupled in 72 individual coupling steps. Such a long synthesis route is greatly volatile. To simplify synthesis fragment condensation might be used. In this process, four dimers or two tetramers could be synthesized via solid phase synthesis on a large scale, purified and coupled to one another (Figure 6.6). Here solid phase synthesis of the final fragment should be performed on an HMBA resin, which should

induce esterification upon cleavage. In general, a synthetic scheme including fragment condensation would also require monomer synthesis on a larger scale. Such a task has been completed in our laboratory, yielding up to 60 g of Q<sup>T</sup> and X monomer each and 17 g of T2<sup>U</sup> monomer (see Supplementary Information, chapter 7). Solid phase supported fragment condensation has previously been used to synthesize the largest abiotic tertiary structure so far. This structure consists of four helices connected by rigid turn units.<sup>28</sup> However, fragment condensation on solid phase synthesis warrants further optimization.

The synthesis of such a symmetrical, highly ordered macromolecule would necessitate the enforcement of parallel helices. Since natural biopolymers rarely contain exclusively parallel assemblies<sup>33</sup>, the linker design for stabilizing tilted dimer formations should be further explored to gain access to more complex composites. Work regarding this project is currently conducted in our laboratory by Shuhe Wang.



## 6.1 References for Chapter 6

1. H.-D. Jakubke and H. Jeschkeit, *Aminosäuren, Peptide, Proteine*, Verlag Chemie, Weinheim, 1982.
2. H. Rehm and T. Letzel, *Der Experimentator: Proteinbiochemie/Proteomics.*, Spektrum Akademischer Verlag, Heidelberg, 2009.
3. D.-W. Zhang, X. Zhao, J.-L. Hou and Z.-T. Li, *Chem. Rev.*, 2012, **112**, 5271-5316.
4. T. Hu, A. L. Connor, D. P. Miller, X. Wang, Q. Pei, R. Liu, L. He, C. Zheng, E. Zurek, Z.-L. Lu and B. Gong, *Org. Lett.*, 2017, **19**, 2666-2669.
5. C. Li, Y.-Y. Zhu, H.-P. Yi, C.-Z. Li, X.-K. Jiang, Z.-T. Li and Y.-H. Yu, *Chem. Eur. J.*, 2007, **13**, 9990-9998.
6. Z.-T. Li, J.-L. Hou and C. Li, *Acc. Chem. Res.*, 2008, **41**, 1343-1353.
7. S. H. Gellman, *Acc. Chem. Res.*, 1998, **31**, 173-180.
8. C. Dolain, A. Grélard, M. Laguerre, H. Jiang, V. Maurizot and I. Huc, *Chem. Eur. J.*, 2005, **11**, 6135-6144.
9. S. De, B. Chi, T. Granier, T. Qi, V. Maurizot and I. Huc, *Nat. Chem.*, 2018, **10**, 51-57.
10. D. Mazzier, S. De, B. Wicher, V. Maurizot and I. Huc, *Chem. Sci.*, 2019, **10**, 6984-6991.
11. F. S. Menke, D. Mazzier, B. Wicher, L. Allmendinger, B. Kauffmann, V. Maurizot and I. Huc, *Org. Biomol. Chem.*, 2023, accepted.
12. D. U. Ferreira, J. A. Hegler, E. A. Komives and P. G. Wolynes, *Proc. Natl. Acad. Sci. U.S.A.*, 2007, **104**, 19819-19824.
13. D. U. Ferreira, E. A. Komives and P. G. Wolynes, *Q. Rev. Biophys.*, 2014, **47**, 285-363.
14. J.-P. Changeux, *Nat. Rev. Mol. Cell Biol.*, 2013.
15. Y. Gambin, A. Schug, E. A. Lemke, J. J. Lavinder, A. C. M. Ferreon, T. J. Magliery, J. N. Onuchic and A. A. Deniz, *Proc. Natl. Acad. Sci.*, 2009, **106**, 10153-10158.
16. D. U. Ferreira and E. A. Komives, *Biochemistry*, 2010, **49**, 1560-1567.
17. A. Dixit and G. M. Verkhivker, *PLoS ONE*, 2011, **6**, c26071.
18. B. K. Shoichet, W. A. Baase, R. Kuroki and B. W. Matthews, *Proc. Natl. Acad. Sci. U.S.A.*, 1995, **92**, 452-456.
19. E. M. Meiering, L. Serrano and A. R. Fersht, *J. Mol. Biol.*, 1992, **225**, 585-589.
20. N. Tokuriki and D. S. Tawfik, *Curr. Opin. Struct. Biol.*, 2009, **19**, 596-604.
21. F. S. Menke, B. Wicher, V. Maurizot and I. Huc, *Angew. Chem. Int. Ed.*
22. B. Gong, *Acc. Chem. Res.*, 2012, **45**, 2077-2087.
23. D. A. Leigh, C. C. Robertson, A. M. Z. Slawin and P. I. T. Thomson, *J. Am. Chem. Soc.*, 2013, **135**, 9939-9943.
24. J. Liu, Y. Wang, G. Lei, J. Peng, Y. Huang, Y. Cao, M. Xie, X. Pu and Z. Lu, *J. Mater. Chem.*, 2009, **19**, 7753.

25. P. Troselj, P. Bolgar, P. Ballester and C. A. Hunter, *J. Am. Chem. Soc.*, 2021, **143**, 8669-8678.
26. H. Jędrzejewska and A. Szumna, *Chem. Rev.*, 2017, **117**, 4863-4899.
27. T. Koga, M. Matsuoka and N. Higashi, *J. Am. Chem. Soc.*, 2005, **127**, 17596-17597.
28. D. Mazzier, S. De, B. Wicher, V. Maurizot and I. Huc, *Angew. Chem. Int. Ed.*, 2020, **59**, 1606-1610.
29. F. S. Menke, B. Wicher, L. Allmendinger, V. Maurizot and I. Huc, *Chem. Sci.*
30. G. A. Papoian and P. G. Wolynes, *Biopolymers*, 2003, **68**, 333-349.
31. *Maestro*, Schrödinger, LLC, New York, NY, 2021.
32. X. Li, T. Qi, K. Srinivas, S. Massip, V. Maurizot and I. Huc, *Org. Lett.*, 2016, **18**, 1044-1047.
33. P. D. Sun, C. E. Foster and J. C. Boyington, *Curr. Protoc. Protein Sci.*, 2004, **35**.

## 7 Supplementary Information (non-published)

for:

Perspective: Synthesis of octa-helical tertiary abiotic structure

Friedericke S. Menke, Daniela Mazzier, Victor Maurizot and Ivan Huc

7.1	List of Abbreviations	308
7.2	Supplementary methods	309
	7.2.1 Nuclear magnetic resonance spectroscopy	309
7.3	Synthetic Scheme	310
	7.3.1 Synthesis of small units	310
7.4	Experimental Procedures	311
	7.4.1 General methods	311
	7.4.2 Synthesis of small units	311
7.5	References	316
7.6	$^1\text{H}$ and $^{13}\text{C}$ NMR spectra of new compounds	317

## 7.1 List of Abbreviations

<b>DCM</b>	dichloromethane
<b>DIPEA</b>	<i>N,N</i> -diisopropylethylamine
<b>DMF</b>	<i>N,N</i> -dimethylformamide
<b>DMSO</b>	dimethyl sulfoxide
<b>DIAD</b>	Diisopropylazodicarboxylat
<b>ESI</b>	electrospray ionization
<b>Fmoc</b>	fluorenylmethoxycarbonyl
<b>HBTU</b>	Hexafluorophosphate Benzotriazole Tetramethyl Uronium
<b>HPLC</b>	high performance liquid chromatography
<b>HRMS</b>	high resolution mass spectrometry
<b>MS</b>	mass spectrometry
<b>MW</b>	molecular weight
<b>NMP</b>	<i>N</i> -Methyl-2-pyrrolidone
<b>NMR</b>	nuclear magnetic resonance
<b>RP</b>	reversed phase
<b>TFA</b>	trifluoroacetic acid
<b>THF</b>	tetrahydrofuran
<b>TLC</b>	thin layer chromatography
<b>UV/Vis</b>	ultraviolet–visible

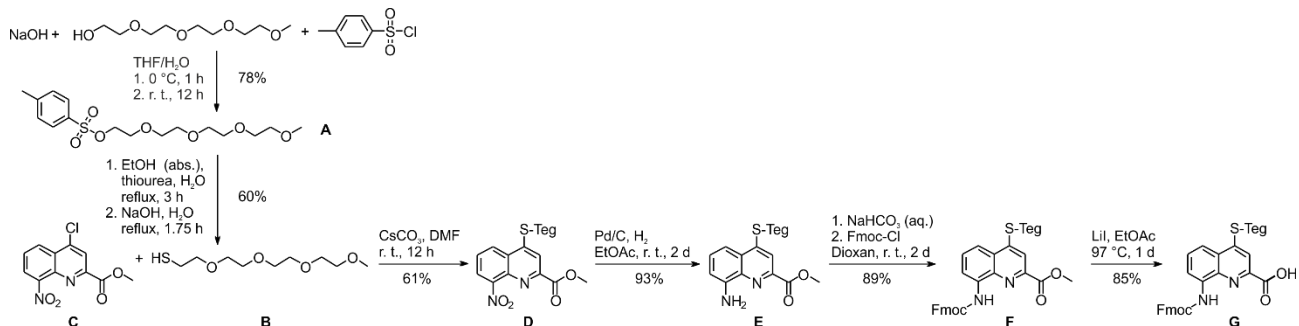
## 7. 2 Supplementary methods

### 7.2.1 Nuclear magnetic resonance spectroscopy

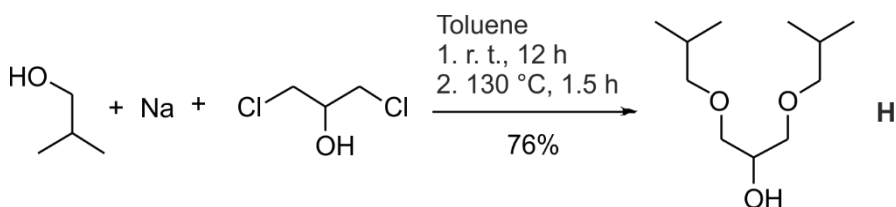
NMR spectra were recorded on different NMR spectrometers: (I) an Avance III HD NMR spectrometer 400 MHz (Bruker BioSpin) and (II) an Avance III HD NMR spectrometer 500 MHz (Bruker BioSpin) with CryoProbe™ Prodigy. Chemical shifts are described in part per million (ppm,  $\delta$ ) relative to the  $^1\text{H}$  residual signal of the deuterated solvent used. Meaning DMSO- $d_6$  ( $\delta$  2.50 ppm) and  $\text{CDCl}_3$  ( $\delta$  7.16 ppm).  $^1\text{H}$  NMR splitting patterns with observed first-order coupling are entitled as singlet (s), doublet (d), triplet (t), quartet (q), multiplet (m) or broad singlet (bs). Coupling constants ( $J$ ) are ported in Hertz.

## 7.3 Synthetic Scheme

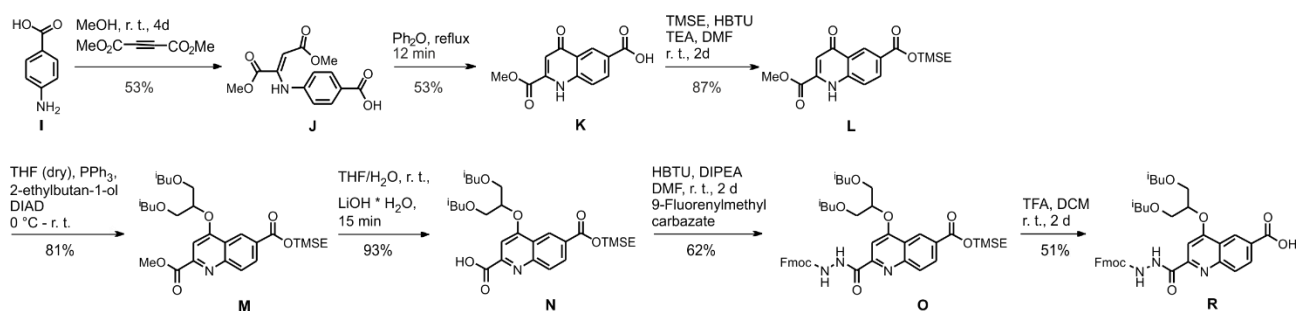
### 7.3.1 Synthesis of small units



Scheme 7.1. Synthesis of **G**.



Scheme 7.2. Synthesis of **H**.



Scheme 7.3. Synthesis of **R**.

## 7.4 Experimental Procedures

### 7.4.1 General methods

Commercially available reagents were purchased from Sigma-Aldrich, Alfa-Aesar or TCI and were used without further purification unless otherwise specified. Tetrahydrofuran (THF), dichloromethane (DCM) and toluene were dried over alumina columns (MBRAUN SPS-800 solvent purification system); diisopropylethylamine (DIPEA) was distilled over ninhydrin and then over potassium hydroxide (KOH); chloroform was distilled over calcium hydride (CaH<sub>2</sub>) prior to use. Reactions were monitored by thin layer chromatography (TLC) on Merck silica gel 60-F254 plates and observed under UV light. Column chromatography purifications were carried out on Merck GEDURAN Si60 (40-63 μm). Analytical RP-HPLC analyses were performed on an Ultimate 3000 HPLC System (ThermoFisher Scientific) using a C18 column (4.6 x 100 mm, 5 μm, ThermoFisher Scientific). The mobile phase was composed of H<sub>2</sub>O (solvent A) and CH<sub>3</sub>CN (solvent B). High-resolution electrospray mass spectra were recorded on a Thermo Exactive orbitrap instrument.

### 7.4.2 Synthesis of small units

Methyl-4-chloro-8-nitroquinoline-2-carboxylate has been provided by D. Gill. Final Fmoc-protected amino acid had to have a purity of ≥ 97%. The monomer Fmoc-Y-OH<sup>1</sup> (Y denotes TMSE-protected Y) has been synthesized according to literature.

**13-tosyl-2,5,8,11-tetraoxatridecane (A).** To a solution of diethylene monomethyl alcohol (25.32 g, 122 mmol, 1.0 eq.) in dry THF (30 mL) was added a solution of NaOH (8.90 g, 0.3 mol, 2.5 eq.) in H<sub>2</sub>O (30 mL). The mixture was cooled to 0 °C internal temperature, then a solution of *p*-toluenesulfonylchloride (23.23 g, 0.158 mol, 1.3 eq.) was added dropwise while keeping the internal temperature at 4-10 °C. After complete addition the reaction mixture was allowed to warm to r. t. and for 12 h. Before being extracted with Et<sub>2</sub>O (50 mL) five times. The combined organic layers were washed with H<sub>2</sub>O until the aqueous phase was neutral. Then the organic layer was dried over Na<sub>2</sub>SO<sub>4</sub>, filtered and the solvent removed under reduced pressure without heating. The product was obtained as a colorless oil that solidifies over time (34.30 g, 94.76 mmol, 78 %). <sup>1</sup>H NMR (500 MHz, CDCl<sub>3</sub>) δ [ppm] 7.82 – 7.78 (m, 2H), 7.36 – 7.33 (m, 2H), 4.18 – 4.14 (m, 2H), 3.71 – 3.68 (m, 2H), 3.65 – 3.62 (m, 6H), 3.58 (s, 4H), 3.56 – 3.53 (m, 2H), 3.37 (s, 3H), 2.45 (s, 3H). The obtained data largely matches the literature values, thus indicating the presence of the desired product.<sup>2</sup>

**2,5,8,11-tetraoxatridecane-13-thiol (B).** To a solution of **A** (34.30 g, 94.76 mmol, 1.0 eq.) in ethanol (56.0 mL) was added a solution of thiourea (7.24 g, 94.76 mmol, 1.0 eq.) in H<sub>2</sub>O (39 mL). The reaction mixture was refluxed for 3 h at 94 °C oil bath temperature, after which a solution of NaOH (4.25 g, 106 mmol, 1.1 eq.) in H<sub>2</sub>O (28.0 mL) was added and the reaction mixture was heated to reflux at 97 °C oil bath temperature for 1.75 h. After cooling down to r. t., the crude was acidified with HCl (conc.), extracted with DCM and dried

over MgSO<sub>4</sub>. The residue was purified via distillation at 163 °C oil bath under 10<sup>-2</sup> mbar of pressure to afford the product as a colorless oil (24.462 g, 60 %). <sup>1</sup>H NMR (500 MHz, CDCl<sub>3</sub>) δ [ppm] 3.67 – 3.60 (m, 12H), 3.57 – 3.53 (m, 2H), 3.38 (s, 3H), 2.72 – 2.66 (m, 2H), 1.59 (t, *J* = 8.2 Hz, 1H). The obtained data largely matches the literature values, thus indicating the presence of the desired product.<sup>2</sup>

**Methyl 4-((2,5,8,11-tetraoxatridecan-13-yl)thio)-8-nitroquinoline-2-carboxylate (D).** Methyl-4-chloro-8-nitroquinoline-2-carboxylate (**C**) (55.0 g, 0.206 mol, 1.0 eq.) and CsCO<sub>3</sub> (100.84 g, 0.31 mol, 1.5 eq.) were dissolved in dry DMF (2 L) under N<sub>2</sub> atmosphere. Compound **B** (43.61 g, 0.194 mol, 0.94 eq., 39.60 mL) was then added and the suspension was stirred overnight at r. t. under N<sub>2</sub> atmosphere. The reaction mixture was then filtered over a small pad of silica and washed with EtOAc until the filtrate came off colourless. Some colour remained on the pad, which is assumed to be by-product. The solvent was removed under reduced pressure and the residue was purified via column chromatography on silica gel with cyclohexane/EtOAc (8:2) as eluent. After evaporation at 50 °C water bath the product was obtained as a yellow solid (55.63 g, 0.122 mol, 61%). <sup>1</sup>H-NMR (500 MHz, CDCl<sub>3</sub>) δ [ppm] 8.38 (dd, *J* = 8.5, 1.2 Hz, 1H), 8.12 (s, 1H), 8.07 (dd, *J* = 7.5, 1.4 Hz, 1H), 7.69 (dd, *J* = 8.5, 7.5 Hz, 1H), 4.03 (s, 3H), 3.90 (t, *J* = 6.2 Hz, 2H), 3.71 – 3.62 (m, 10H), 3.54 – 3.52 (m, 2H), 3.45 (t, *J* = 6.2 Hz, 2H), 3.36 (s, 3H). The obtained data largely matches the literature values, thus indicating the presence of the desired product.<sup>3</sup>

**Methyl 4-((2,5,8,11-tetraoxatridecan-13-yl)thio)-8-(((9H-fluoren-9-yl)-methoxy)-carbonyl)-amino-quinoline-2-carboxylate (F).** Compound **D** (55.63 g, 0.122 mol, 1.0 eq) was suspended in EtOAc (806 mL) and N<sub>2</sub> was bubbled through for 5 min. After addition of the Pd/C-catalyst (8.35 g, 15wt%), vacuum was pulled shortly prior to establishing H<sub>2</sub> atmosphere. The suspension was stirred for 2 d under H<sub>2</sub> atmosphere, then the mixture was filtered over a pad of celite, the residue was washed with EtOAc until the yellow filtrate remained colorless. Some brown color remained on the pad which is assumed to be by-product. The filtrate was evaporated and removed in vacuo at 50 °C water bath to afford the intermediate **E** as a yellow solid (48.47 g, 0.114 mol, 93%). <sup>1</sup>H-NMR (500 MHz, CDCl<sub>3</sub>) [ppm] 7.96 (s, 1H), 7.40 – 7.38 (m, 2H), 6.93 (dd, *J* = 5.6, 3.1 Hz, 1H), 5.19 (s, 2H), 4.02 (s, 3H), 3.85 (t, *J* = 6.6 Hz, 2H), 3.70 – 3.61 (m, 11H), 3.54 – 3.50 (m, 2H), 3.37 (d, *J* = 10.4 Hz, 1H), 3.35 (s, 3H). This compound was used without further purification. Compound **E** (48.47 g, 0.114 mol, 1.0 eq.) was dissolved in dioxane (344 mL), then a solution of NaHCO<sub>3</sub> (47.90 g, 0.570 mol, 5.0 eq.) in H<sub>2</sub>O (479 mL, 10wt%-solution) was added and the reaction mixture was cooled down to 0 °C. At this temperature a solution of Fmoc-chloride (38.35 g, 0.148 mol, 1.3 eq.) in dioxane (121 mL) was added dropwise over the course of an hour. After complete addition, the reaction mixture was stirred for 1 h at 0 °C, followed by 2 d at r.t.. The reaction mixture was brought to pH 3-4 using a 20% HCl-solution in H<sub>2</sub>O. The precipitate was filtered off, dissolved in DCM, the water-phase separated and the organic layer dried over MgSO<sub>4</sub>. The solvent was then removed under reduced pressure at 50 °C water bath to afford the product as a brown solid (65.7 g, 0.102 mol, 89%). <sup>1</sup>H NMR (500 MHz, CDCl<sub>3</sub>) δ [ppm] 9.37 (s, 1H), 8.46 (s, 1H), 8.03 (s, 1H), 7.79 – 7.74 (m, 3H), 7.72 – 7.69 (m, 2H), 7.62 – 7.56 (m, 1H), 7.42 (tt, *J* = 7.5, 0.9 Hz, 2H), 7.34 (td, *J* = 7.5, 1.2 Hz, 2H), 4.55 (d, *J* = 6.9 Hz, 2H), 4.39 (t, *J* = 7.3 Hz, 1H), 4.08 (s, 3H), 3.88 (t, *J* = 6.5 Hz, 2H),



3.71 – 3.61 (m, 10H), 3.55 – 3.51 (m, 2H), 3.41 (t,  $J = 6.5$  Hz, 2H), 3.36 (s, 3H).  $^{13}\text{C}$  NMR (126 MHz,  $\text{CDCl}_3$ )  $\delta$  [ppm] 171.29, 165.59, 153.29, 149.71, 144.46, 143.81, 141.31, 136.45, 135.92, 129.16, 127.78, 127.14, 127.09, 125.20, 120.02, 116.32, 115.79, 115.72, 71.90, 70.66, 70.63, 70.59, 70.56, 70.50, 68.80, 67.41, 60.35, 58.99, 52.98, 47.06, 31.11, 14.18. MS calcd for  $\text{C}_{35}\text{H}_{39}\text{N}_2\text{O}_8\text{S}$   $[\text{M}+\text{H}]^+$  647.2422, found (HR-ESI) 647.2418.

**4-((2,5,8,11-tetraoxatridecan-13-yl)thio)-8-(((9H-fluoren-9-yl)methoxy)carbonyl)amino)quinoline-2-carboxylic acid (G).** Compound **F** (40 g, 0.062 mol, 1.0 eq.) was dissolved in EtOAc (544 mL) and three times degassed with  $\text{N}_2$ . The mixture was heated to 97 °C and LiI (50 g, 0.36 mol, 5.0 eq.) was added in portions. The reaction mixture refluxed for 1 d, then allowed to cool down to r. t. prior to recovering the precipitate via filtration. The solid was dissolved in DCM, washed once with a  $\text{Na}_2\text{S}_2\text{O}_3$  (5% in  $\text{H}_2\text{O}$ ), twice with a solution of citric acid (5% in  $\text{H}_2\text{O}$ ), and finally once with  $\text{H}_2\text{O}$ . The organic layer was then dried over  $\text{Na}_2\text{SO}_4$  and, after filtration, the solvent was removed under reduced pressure at 50 °C water bath. The residue was crystallized Et<sub>2</sub>O to afford the product as a yellow solid (33.34 g, 0.053 mol, 85%) with a purity of 97%. This reaction has been performed twice in parallel.  $^1\text{H}$  NMR (500 MHz,  $\text{CDCl}_3$ )  $\delta$  [ppm] 9.16 (s, 1H), 8.58 – 8.31 (m, 1H), 8.16 (s, 1H), 7.78 (dd,  $J = 8.0, 5.3$  Hz, 4H), 7.65 (d,  $J = 7.5$  Hz, 2H), 7.56 (s, 1H), 7.43 – 7.38 (m, 2H), 7.31 (tt,  $J = 7.5, 1.0$  Hz, 2H), 4.38 (t,  $J = 6.3$  Hz, 1H), 3.87 (t,  $J = 6.2$  Hz, 2H), 3.69 – 3.56 (m, 11H), 3.55 – 3.52 (m, 3H), 3.40 (t,  $J = 6.0$  Hz, 2H), 3.37 (s, 3H). The obtained data largely matches the literature values, thus indicating the presence of the desired product. A residue of DCM could be detected. ).<sup>3</sup>

**1,3-diisobutoxypropan-2-ol (H).** To a solution of 2-methyl-1-propanol (250 mL, 2.70 mol, 20.0 eq.) in toluene (250 mL) was added sodium (10.40 g, 0.435 mol, 3.3 eq.) in portions under  $\text{N}_2$  atmosphere. After complete consumption of the sodium 1,3-dichloropropan-2-ol (13 mL, 0.132 mol, 1.0 eq.) was added and the mixture refluxed at 130 °C in an oil bath for 1.5 hours. The reaction mixture was treated with  $\text{H}_2\text{O}$  and extracted with Et<sub>2</sub>O. The combined organic layers were dried over  $\text{MgSO}_4$ , and the solvent removed under reduced pressure at 50 °C water bath. The residue was purified via distillation at 140 °C oil bath under 1 mbar of pressure to afford the product as a colorless oil (21.73 g, 0.100 mol, 76%)  $^1\text{H}$  NMR (500 MHz,  $\text{CDCl}_3$ )  $\delta$  [ppm] 3.95 (tt,  $J = 6.1, 4.7$  Hz, 1H), 3.51 – 3.42 (m, 4H), 3.24 – 3.21 (m, 4H), 1.87 (dp,  $J = 13.3, 6.6$  Hz, 2H), 0.92 – 0.88 (m, 12H). The obtained data largely matches the literature values, thus indicating the presence of the desired product.<sup>4</sup>

**(Z)-4-((1,4-dimethoxy-1,4-dioxobut-2-en-2-yl)amino)benzoic acid (J).** 4-amino benzoic acid (**I**) (53.08 g, 387 mmol, 1.0 eq.) was dissolved in MeOH (531 mL) under  $\text{N}_2$ . Then dimethyl acetylene dicarboxylate (48 mL, 387 mmol, 1.0 eq.) was added and the solution stirred at r.t. for 4 days. The solid obtained was collected by filtration, washed with MeOH and dried under vacuum. The compound was obtained as a light yellow solid (57.27 g, 53% yield).  $^1\text{H}$  NMR (500 MHz,  $\text{CDCl}_3$ )  $\delta$  [ppm] 9.74 (s, 1H), 8.02 – 7.99 (m, 2H), 6.89 – 6.86 (m, 2H), 5.56 (s, 1H), 3.76 (s, 3H), 3.75 (s, 3H). The obtained data largely matches the literature values, thus indicating the presence of the desired product.<sup>5</sup>

**2-(methoxycarbonyl)-4-oxo-1,4-dihydroquinoline-6-carboxylic acid (K).** Diphenyl ether (500 mL) was heated until its boiling point, then compound **J** (56.74 g, 203 mmol) was added. The reaction mixture was

boiled for 12 min. After cooling to r.t., cyclohexane was added and the precipitate filtered. The solid was washed thoroughly with cyclohexane and diethyl ether. After drying under vacuum, the compound was obtained as a brownish solid (47.00 g, 95% yield). <sup>1</sup>H NMR (500 MHz, DMSO-*d*<sub>6</sub>) δ [ppm] 13.11 (s, 1H), 12.31 (s, 1H), 8.66 (d, *J* = 2.0 Hz, 1H), 8.18 (dd, *J* = 8.8, 2.1 Hz, 1H), 8.00 (d, *J* = 8.9 Hz, 1H), 6.69 (s, 1H), 3.98 (s, 3H). The obtained data largely matches the literature values, thus indicating the presence of the desired product.<sup>5</sup>

**2-methyl 6-(2-(trimethylsilyl)ethyl) 4-oxo-1,4-dihydroquinoline-2,6-dicarboxylate (L).** Compound **K** (46.00 g, 0.186 mol, 1 eq.) and HBTU (72.00 g, 0.186 mol, 1.0 eq.) were dissolved in dry DMF (627 mL) under N<sub>2</sub> atmosphere. 2-(Trimethylsilyl)ethanol (41 mL, 0.279 mol, 1.5 eq.) and Et<sub>3</sub>N (53 mL, 0.373 mol, 2.0 eq.) were added and the reaction mixture was stirred at r.t. for 2 d. The precipitate was filtered and washed thoroughly with CH<sub>3</sub>CN and MeOH. After drying under vacuum, the compound was obtained as a white solid (56.27 g, 87% yield). <sup>1</sup>H NMR (400 MHz, DMSO-*d*<sub>6</sub>) δ [ppm] 12.34 (s, 1H), 8.68 (d, *J* = 2.1 Hz, 1H), 8.18 (dd, *J* = 8.8, 2.1 Hz, 1H), 8.02 (d, *J* = 8.8 Hz, 1H), 6.70 (s, 1H), 4.45 – 4.38 (m, 2H), 3.97 (s, 3H), 1.17 – 1.09 (m, 2H), 0.07 (s, 9H). The obtained data largely matches the literature values, thus indicating the presence of the desired product.<sup>5</sup>

**2-methyl 6-(2-(trimethylsilyl)ethyl) 4-((1,3-diisobutoxypropan-2-yl)oxy)quinoline-2,6-dicarboxylate (M).** Compound **L** (37.35 g, 0.108 mol, 1.0 eq.) and Ph<sub>3</sub>P (33.87 g, 0.129 mol, 1.2 eq.) were dissolved in dry THF (760 mL) under nitrogen atmosphere. Then 1,3-diisobutoxypropan-2-ol (**H**) (25.85 g, 0.118 mol, 1.1 eq.) was added and the reaction mixture was cooled to 0 °C. After 20 minutes DIAD (23.24 mL, 0.118 mol, 1.1 eq.) was slowly added dropwise. The reaction mixture was allowed to come to room temperature and stirred overnight under N<sub>2</sub> atmosphere. The solvent was removed by vacuum and the residue was triturated in hexane and filtrated. Triphenylphosphine oxide was precipitated as white solid and was filtered under vacuum. The residue was purified by column chromatography on silica gel with DCM/MeOH as eluent (300:0.6). The product was obtained as a yellow solid (46.66 g, 0.087 mol, 81%). <sup>1</sup>H-NMR (500 MHz, CDCl<sub>3</sub>) δ [ppm] 8.96 (d, *J* = 1.9 Hz, 1H), 8.30 (dt, *J* = 8.9, 1.6 Hz, 1H), 8.22 (dd, *J* = 8.9, 1.5 Hz, 1H), 7.81 (d, *J* = 1.1 Hz, 1H), 4.50 – 4.43 (m, 2H), 4.05 (t, *J* = 1.1 Hz, 3H), 3.83 – 3.76 (m, 4H), 3.49 – 3.40 (m, 1H), 3.29 – 3.18 (m, 4H), 1.88 – 1.77 (m, 2H), 1.19 – 1.11 (m, 2H), 0.91 – 0.80 (m, 12H), 0.09 (d, *J* = 1.4 Hz, 9H). <sup>13</sup>C NMR (126 MHz, CDCl<sub>3</sub>) δ [ppm] 166.28, 165.98, 163.62, 150.93, 150.67, 130.45, 130.03, 129.27, 125.31, 122.16, 103.07, 78.77, 78.48, 78.18, 72.05, 70.26, 63.78, 53.41, 28.48, 28.43, 19.38, 19.30, 19.27, 17.55, -1.30. MS calcd for C<sub>28</sub>H<sub>44</sub>NO<sub>7</sub>Si [M+H]<sup>+</sup> 534.2882, found (HR-ESI) .534.2881.

**4-((1,3-diisobutoxypropan-2-yl)oxy)-6-((2-(trimethylsilyl)ethoxy)carbonyl)quinoline-2-carboxylic acid (N).** Compound **M** (46.66 g, 0.087 mol, 1.0 eq.) was dissolved in a mixture of THF/H<sub>2</sub>O ((3:1), 410 ml/137ml) and LiOH·H<sub>2</sub>O (4.03 g, 0.096 mol, 1.1 eq.) was added. The reaction mixture was stirred at room temperature for 15 minutes. The solution was neutralized with citric acid (5% in H<sub>2</sub>O) until the pH was slightly acidic (pH-value: 3). The solvents were removed by vacuum and the precipitated solid was recovered by filtration and washed thoroughly with H<sub>2</sub>O. After drying under vacuum the product was obtained as a light yellow solid

(42.04 g, 0.081 mol, 93%). **<sup>1</sup>H-NMR** (500 MHz, CDCl<sub>3</sub>) δ [ppm] 9.01 (d, *J* = 1.9 Hz, 1H), 8.40 (dd, *J* = 8.8, 2.0 Hz, 1H), 8.27 (d, *J* = 8.8 Hz, 1H), 7.93 (s, 1H), 5.71 (s, 1H), 5.11 (p, *J* = 5.2 Hz, 1H), 4.58 – 4.45 (m, 2H), 3.82 (d, *J* = 5.1 Hz, 4H), 3.47 (qd, *J* = 9.7, 5.4 Hz, 1H), 3.25 (qd, *J* = 9.0, 6.6 Hz, 4H), 1.83 (th, *J* = 13.3, 6.7 Hz, 2H), 1.34 – 1.15 (m, 2H), 0.94 – 0.78 (m, 12H), 0.12 (s, 9H). **<sup>13</sup>C NMR** (126 MHz, CDCl<sub>3</sub>) δ [ppm] 165.97, 165.75, 163.76, 150.00, 147.65, 131.34, 129.88, 128.23, 125.68, 122.31, 101.49, 78.88, 78.82, 78.54, 72.08, 70.11, 69.62, 64.11, 28.50, 19.42, 19.33, 19.31, 17.59, -1.25. **MS** calcd for C<sub>27</sub>H<sub>42</sub>NO<sub>7</sub>Si [M+H]<sup>+</sup> 520.2725, found (HR-ESI) 520.27725.

**2-(trimethylsilyl)ethyl 2-(2-(((9H-fluoren-9-yl)methoxy)carbonyl)hydrazine-1-carbonyl)-4-((1,3-diisobutoxy-propan-2-yl)oxy)quinoline-6-carboxylate (O)**. Compound N (42.04 g, 0.080 mol, 1.0 eq.) and HBTU (30.72 g, 0.080 mol, 1.0 eq.) were dissolved in dry DMF (270 mL) under N<sub>2</sub> atmosphere. After addition of 9-Fluorenylmethyl carbazate (30.90 g, 0.120 mol, 1.5 eq.) and DIPEA (28 mL, 0.160 mol, 2.0 eq.), the solution was stirred at r.t. for 2 d. After removing the solvent under vacuum, the crude was purified by flash chromatography. The polarity of the eluent (cyclohexane/EtOAc) was gradually increased from a ration of 8:2 to 7:3 and finally 1:1 with acetic acid. The last fraction was collected with DCM and acetic acid as eluent. After removing the solvent under vacuum, the product was obtained as a yellow solid (38.16 g, 0.05 mol, 62%). **<sup>1</sup>H NMR** (500 MHz, DMSO-*d*<sub>6</sub>) δ [ppm] 10.95 (s, 1H), 10.68 (s, 1H), 9.55 (s, 1H), 8.87 (s, 1H), 8.15 (dd, *J* = 15.7, 8.8 Hz, 1H), 7.93 – 7.90 (m, 2H), 7.89 – 7.86 (m, 2H), 7.86 – 7.82 (m, 2H), 7.80 (d, *J* = 7.0 Hz, 2H), 7.77 (s, 1H), 5.24 – 5.15 (m, 2H), 4.46 (t, *J* = 7.8 Hz, 2H), 4.40 (d, *J* = 7.0 Hz, 2H), 3.25 – 3.23 (m, 3H), 3.21 – 3.18 (m, 3H), 3.16 – 3.13 (m, 1H), 1.78 – 1.68 (m, 5H), 0.78-0.74 (m, 12H), 0.09 (d, *J* = 1.5 Hz, 9H). (mixture of two conformers, only the major peaks are reported). **<sup>13</sup>C NMR** (126 MHz, DMSO-*d*<sub>6</sub>) δ [ppm] 170.40, 165.22, 163.57, 163.18, 155.97, 152.82, 149.46, 143.68, 142.73, 140.78, 139.42, 137.43, 129.71, 128.91, 128.15, 127.71, 127.27, 127.14, 125.32, 124.47, 121.37, 121.31, 120.16, 120.02, 109.72, 101.01, 77.96, 77.56, 77.41, 72.37, 69.51, 68.72, 66.22, 63.28, 59.74, 46.52, 28.05, 27.83, 26.32, 20.74, 19.20, 19.00, 18.97, 16.83, 14.07, -1.38. **MS** calcd for C<sub>42</sub>H<sub>54</sub>N<sub>3</sub>O<sub>8</sub>Si [M+H]<sup>+</sup> 756.3675, found (HR-ESI) 756.3676.

**2-(2-(((9H-fluoren-9-yl)methoxy)carbonyl)hydrazine-1-carbonyl)-4-((1,3-diisobutoxypropan-2-yl)-oxy)-quinoline-6-carboxylic acid (R)**. Compound O (38.20 g, 0.05 mol) was treated with a solution of TFA (50% in DCM, 260 mL) at r. t. under stirring for 2 d. The solvent was removed under vacuum, the residue was triturated in Et<sub>2</sub>O, filtered and dried. The compound was obtained as a white solid (17.40 g, 0.026 mol, 51% yield). **<sup>1</sup>H NMR** (500 MHz, DMSO-*d*<sub>6</sub>) δ [ppm] δ 13.35 (s, 1H), 10.68 (s, 1H), 9.55 (s, 1H), 8.98 – 8.81 (m, 1H), 8.36 – 8.26 (m, 1H), 8.15 (dd, *J* = 35.5, 8.8 Hz, 1H), 7.98 – 7.58 (m, 3H), 7.36 (tt, *J* = 45.9, 7.5 Hz, 4H), 7.02 (t, *J* = 7.6 Hz, 1H), 5.17 (p, *J* = 4.9 Hz, 1H), 4.41 (d, *J* = 7.1 Hz, 2H), 4.31 (t, *J* = 7.0 Hz, 1H), 3.78 (d, *J* = 4.7, 6H), 3.25 (dd, *J* = 9.3, 6.5 Hz, 3H), 3.19 (dd, *J* = 9.2, 6.5 Hz, 3H), 1.73 (dq, *J* = 14.1, 7.5, 7.1 Hz, 3H), 0.77 – 0.75 (m, 7H). (mixture of two conformers, only the major peaks are reported). **<sup>13</sup>C NMR** (126 MHz, DMSO-*d*<sub>6</sub>) δ 166.77, 163.62, 163.19, 155.99, 152.62, 143.69, 140.79, 130.06, 129.52, 129.04, 127.73, 127.57, 127.16, 126.83, 125.49, 125.33, 124.65, 121.31, 120.18, 119.99, 100.90, 77.96, 77.58, 69.51, 66.23, 46.53, 27.82, 18.99. **MS** calcd for C<sub>37</sub>H<sub>40</sub>N<sub>3</sub>O<sub>8</sub> [M-H]<sup>-</sup> 654.2821, found (HR-ESI) 654.2822.

## 7.5 References for chapter 7

1. D. Mazzier, S. De, B. Wicher, V. Maurizot and I. Huc, *Chem. Sci.*, 2019, **10**, 6984-6991.
2. A. W. Snow and E. E. Foos, *Synthesis*, 2003, **2003**, 0509-0512.
3. C. Tsiamantas, S. J. Dawson and I. Huc, *C. R. Chimie* **19**, 2016, 132-142.
4. A. C. Denis Beltrami, Mansour Haddad, Hugo Laureano, Hamid Mokhtari, Bruno Courtaud, Sylvain Jugé & Gérard Cote, *Taylor & Francis Online*, 2013, **48**, 480-486.
5. D. Mazzier, S. De, B. Wicher, V. Maurizot and I. Huc, *Angew. Chem. Int. Ed.*, 2020, **59**, 1606-1610.

## 7.6 $^1\text{H}$ and $^{13}\text{C}$ NMR spectra of new compounds

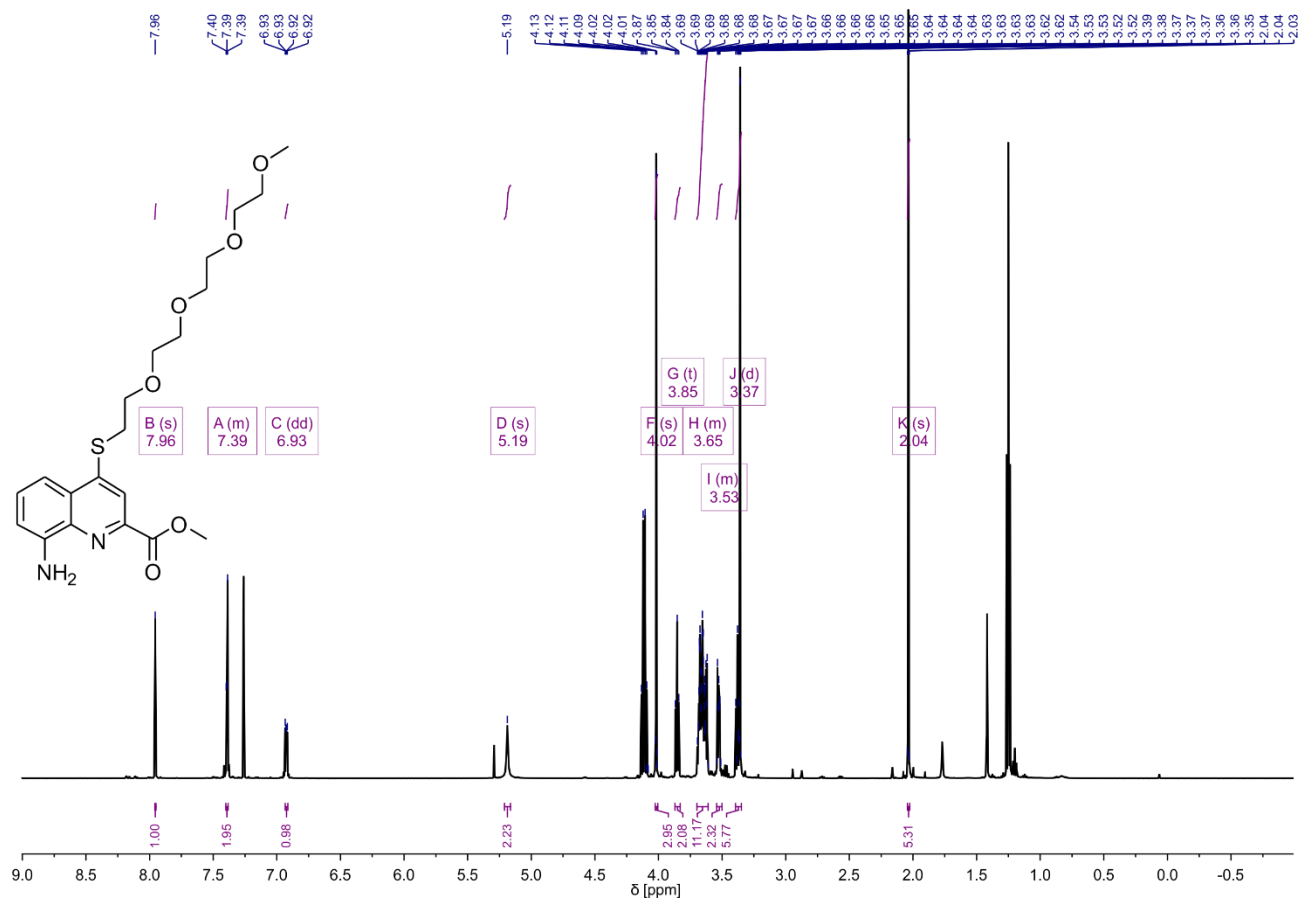


**Figure S7.1.**  $^1\text{H}$  NMR spectrum (500 MHz,  $\text{CDCl}_3$ ) of **E**.

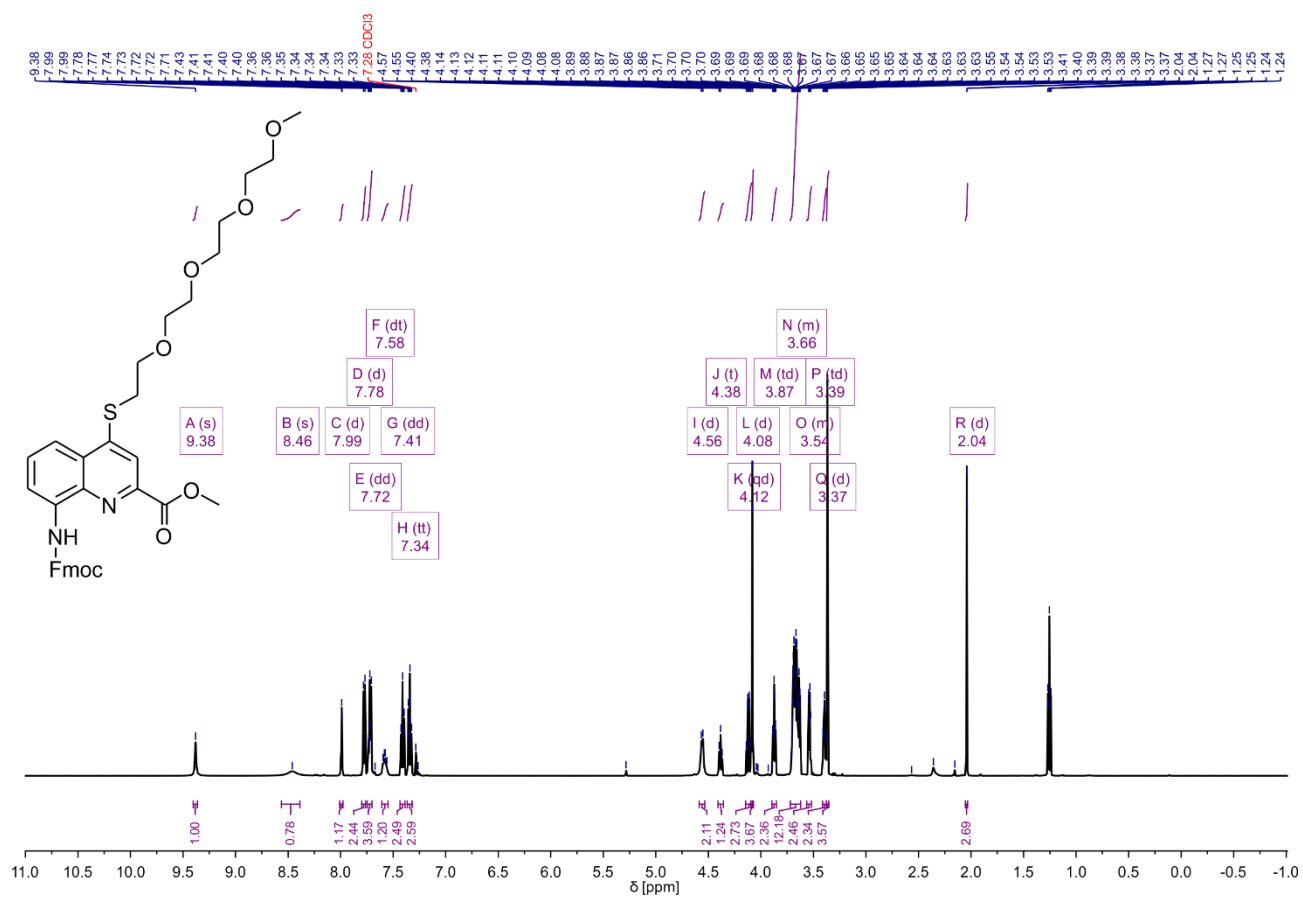
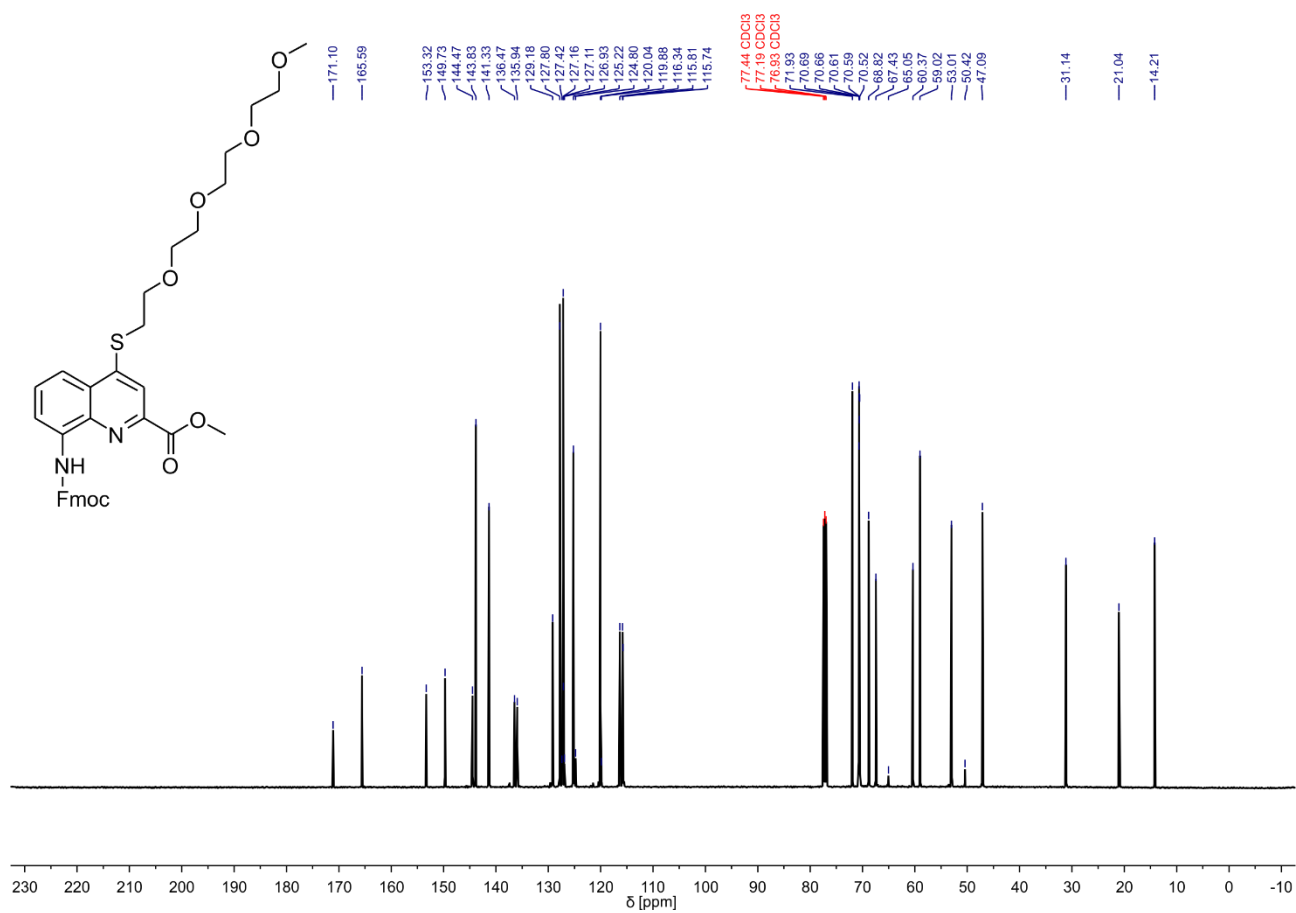
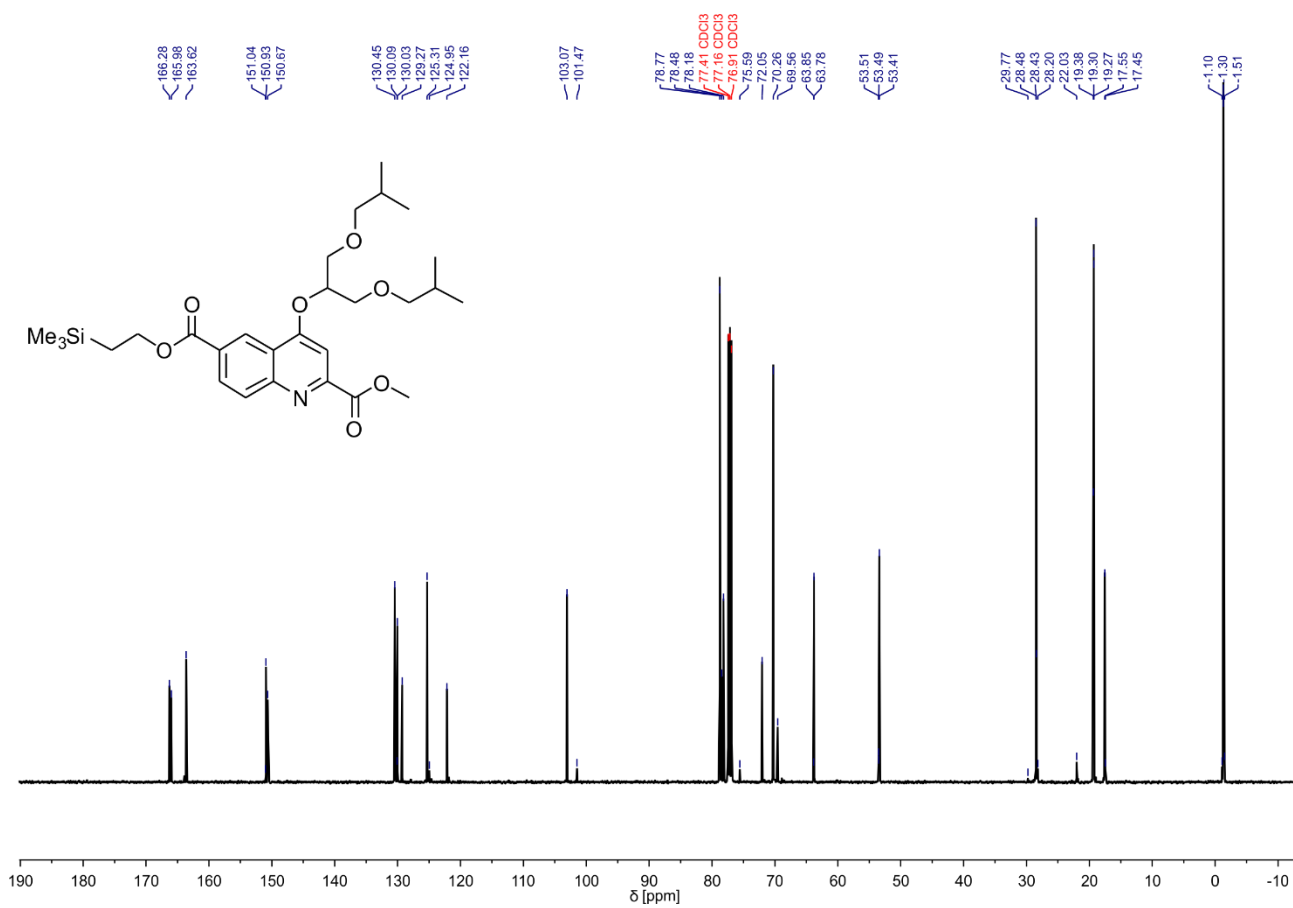


Figure S7.2. <sup>1</sup>H NMR spectrum (500 MHz, CDCl<sub>3</sub>) of F.



**Figure S7.3.**  $^{13}\text{C}$  NMR spectrum (126 MHz,  $\text{CDCl}_3$ ) of **F**.



**Figure S7.4.**  $^1\text{H}$  NMR spectrum (500 MHz,  $\text{CDCl}_3$ ) of M.



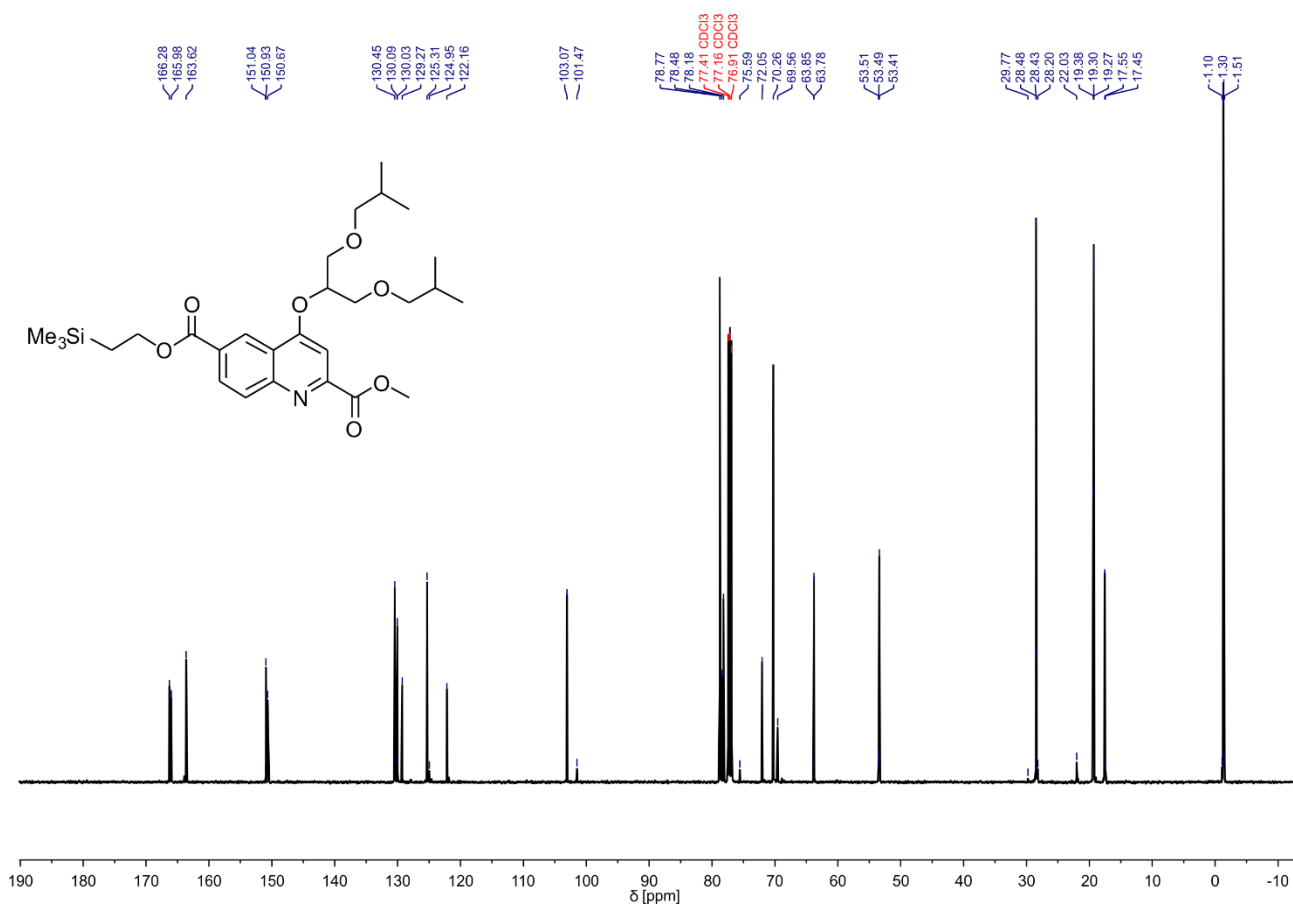


**Figure S7.5.**  $^{13}\text{C}$  NMR spectrum (126 MHz,  $\text{CDCl}_3$ ) of M.

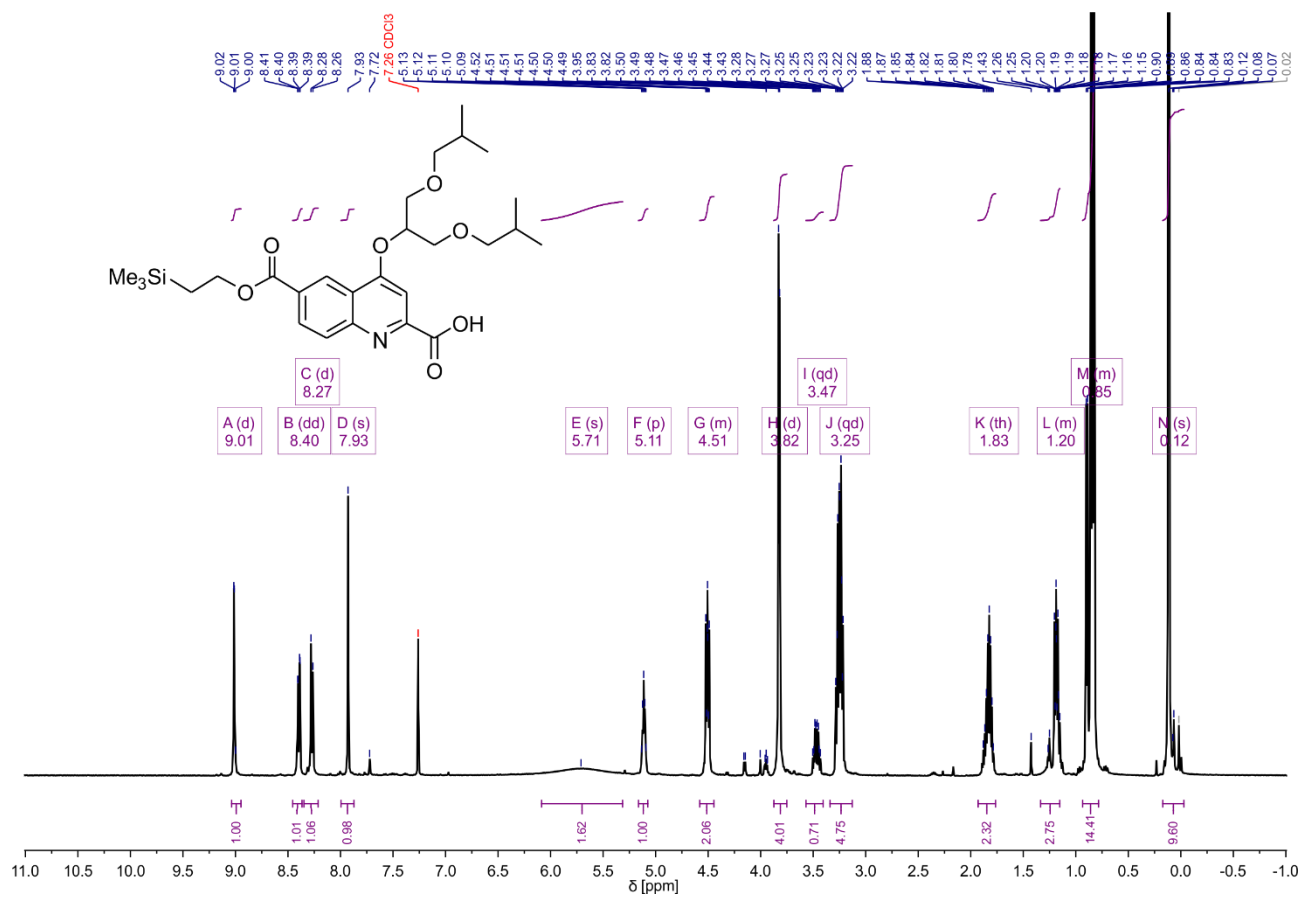
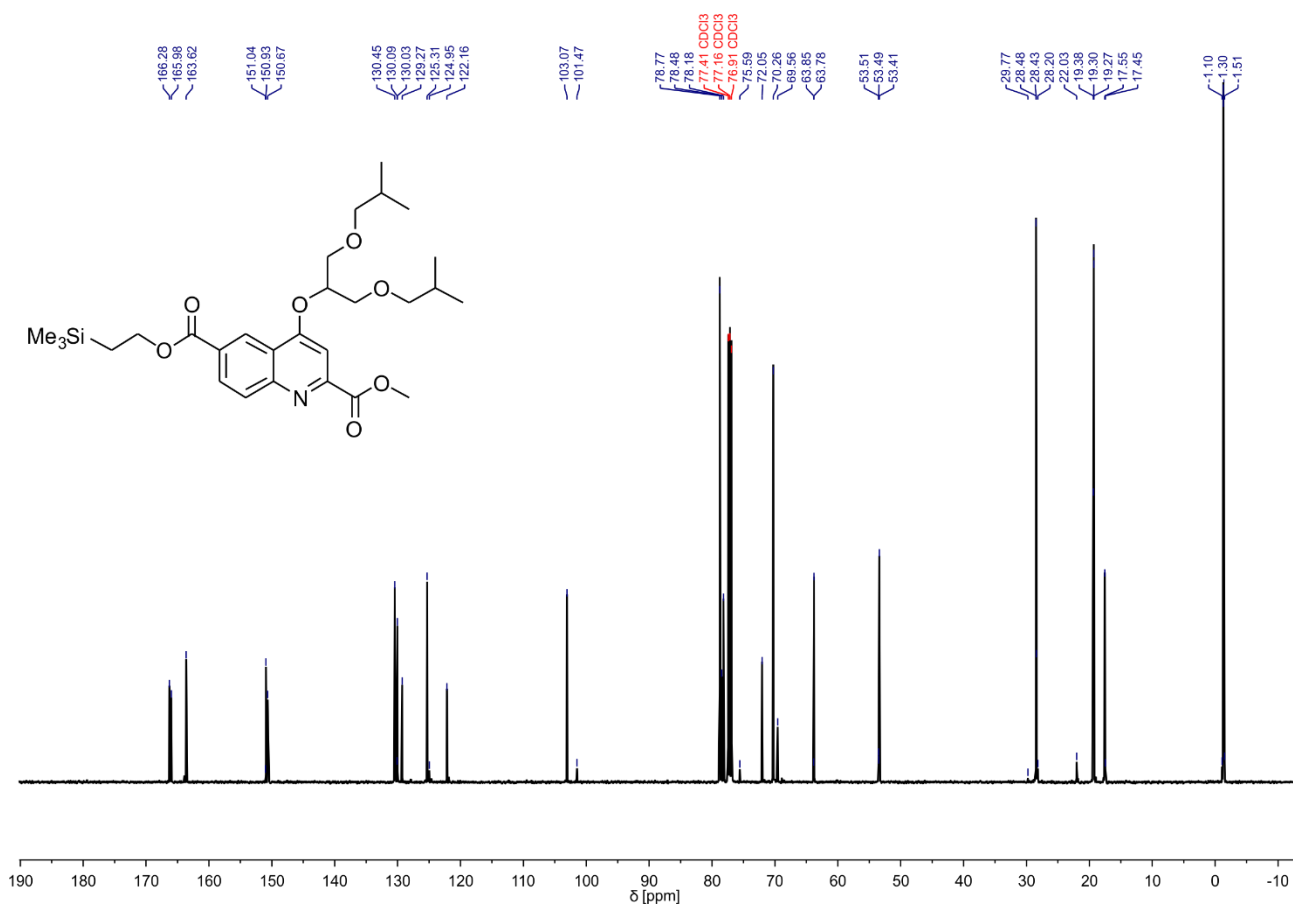


Figure S7.6. <sup>1</sup>H NMR spectrum (500 MHz, CDCl<sub>3</sub>) of N.



**Figure S7.7.**  $^{13}\text{C}$  NMR spectrum (126 MHz,  $\text{CDCl}_3$ ) of N.

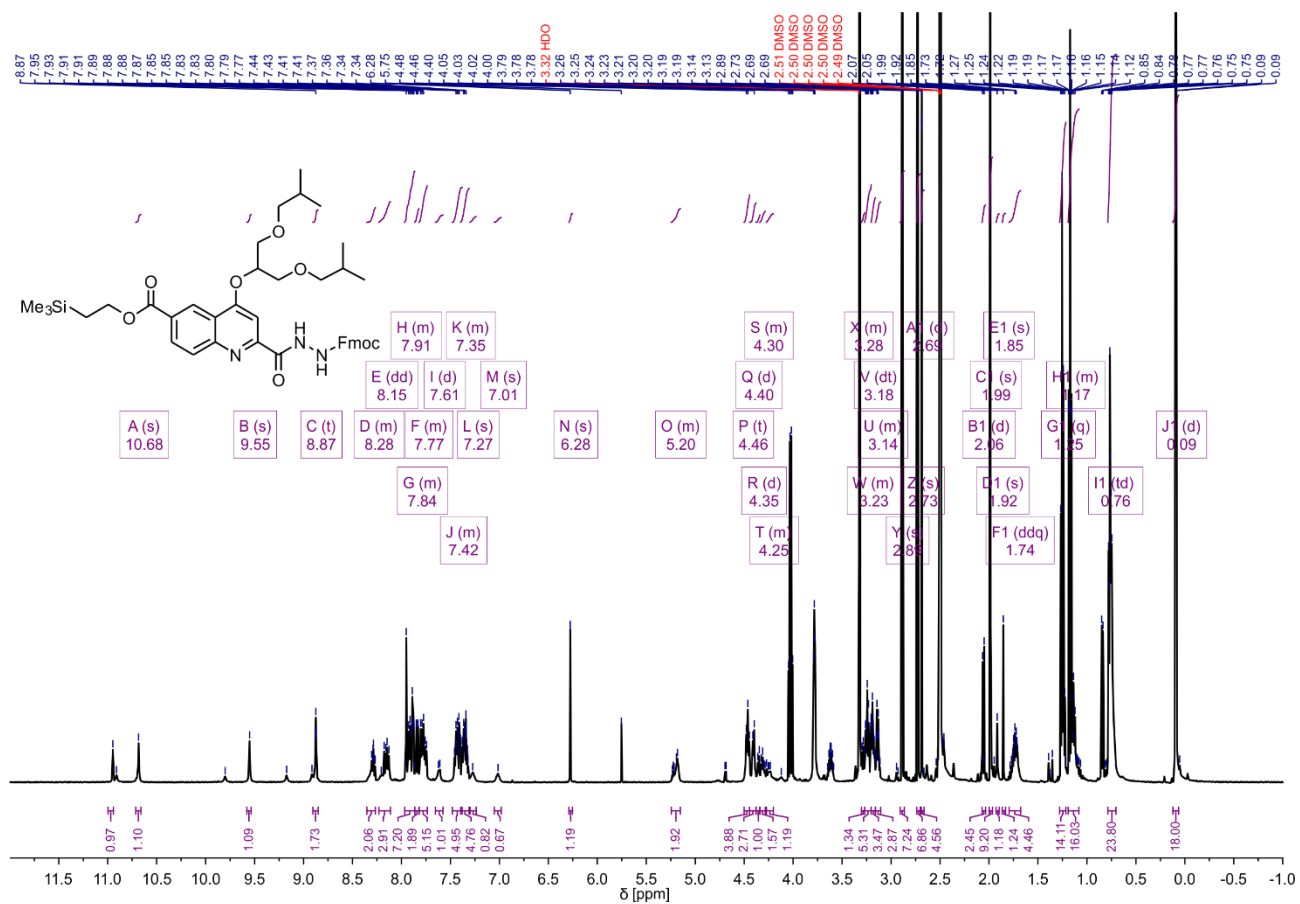
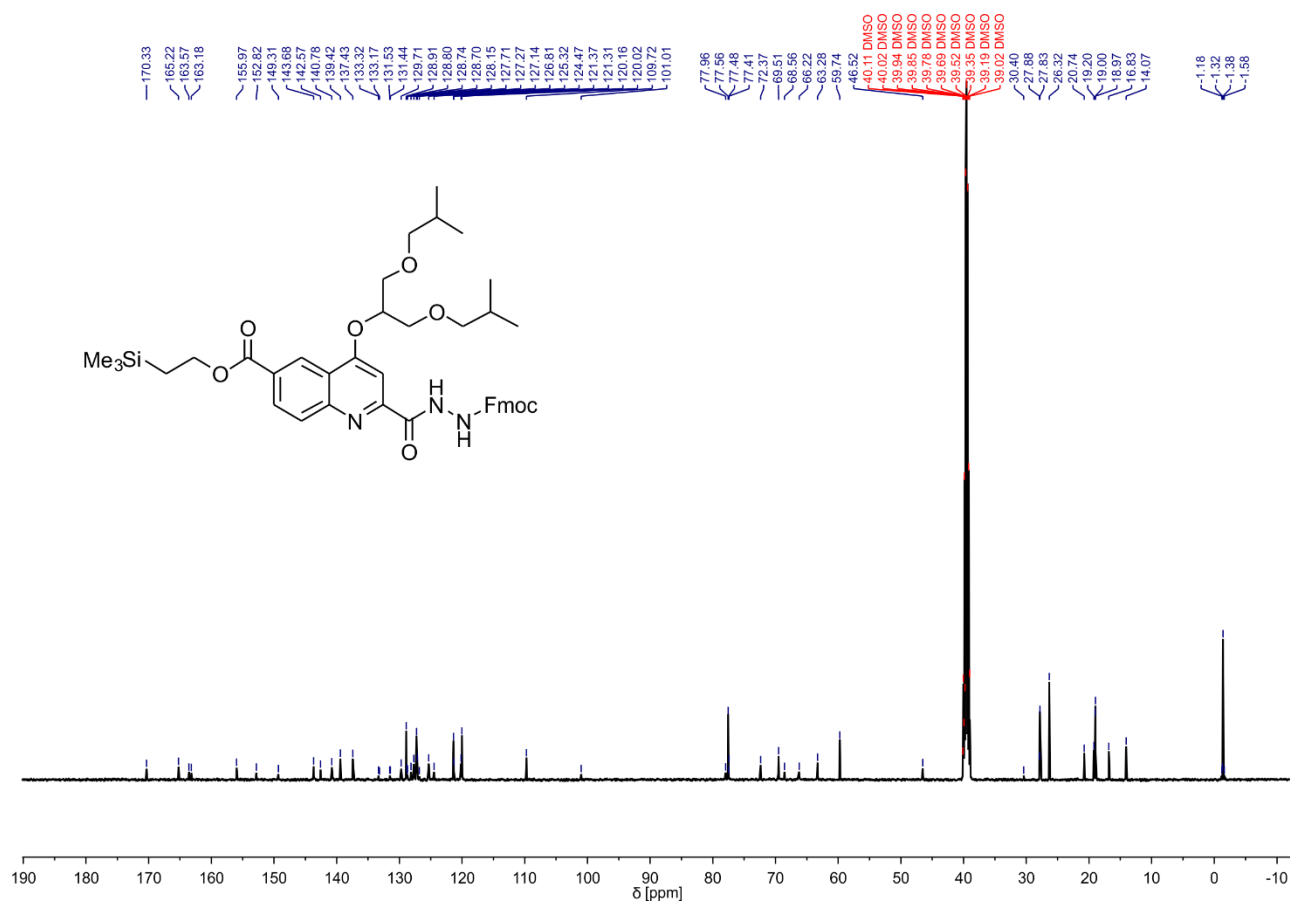
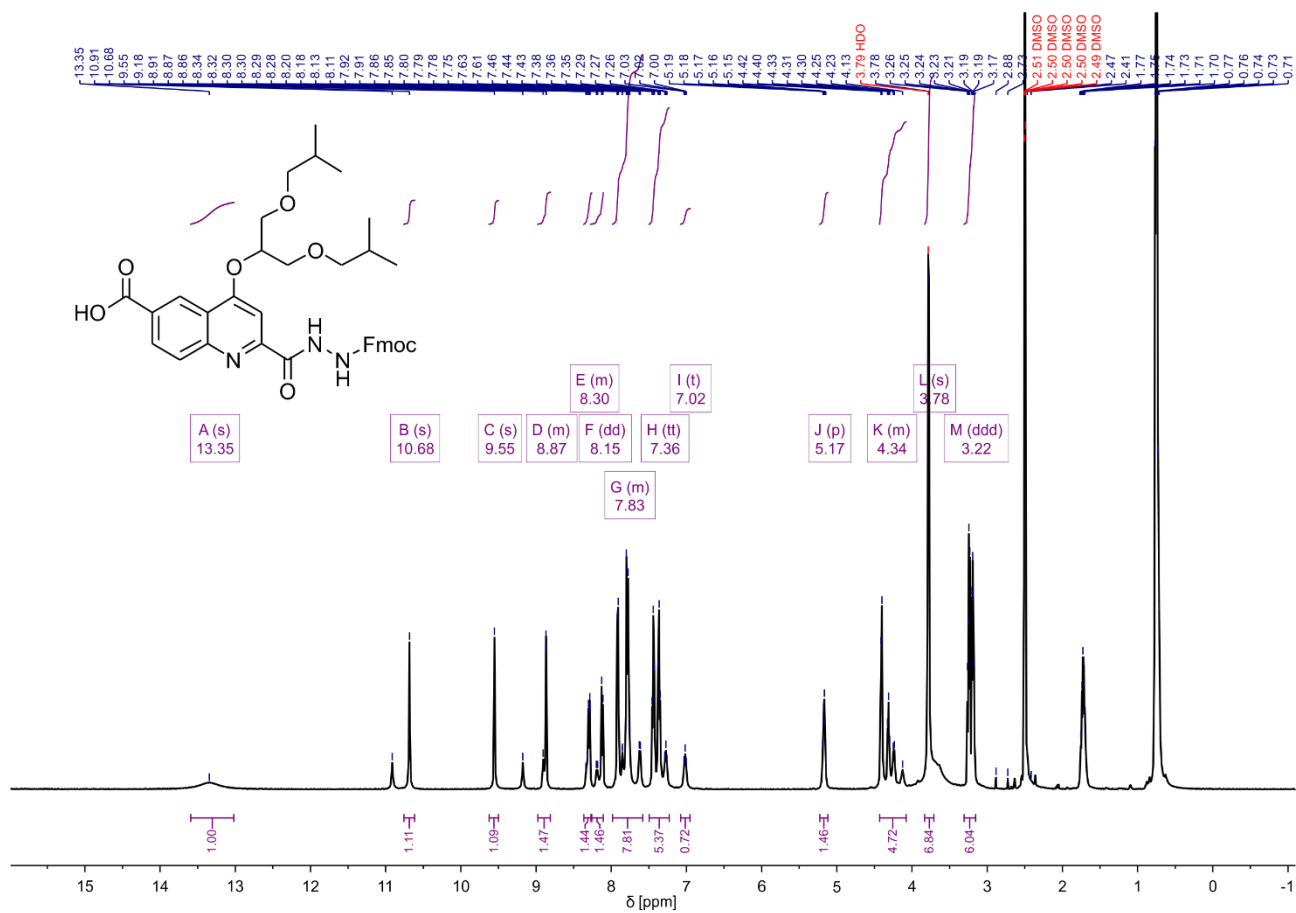


Figure S7.8. <sup>1</sup>H NMR spectrum (500 MHz, DMSO-*d*<sub>6</sub>) of O.



**Figure S7.9.** <sup>13</sup>C NMR spectrum (126 MHz, DMSO-*d*<sub>6</sub>) of O.



**Figure S7.10.** <sup>1</sup>H NMR spectrum (500 MHz, DMSO-*d*<sub>6</sub>) of **R**.

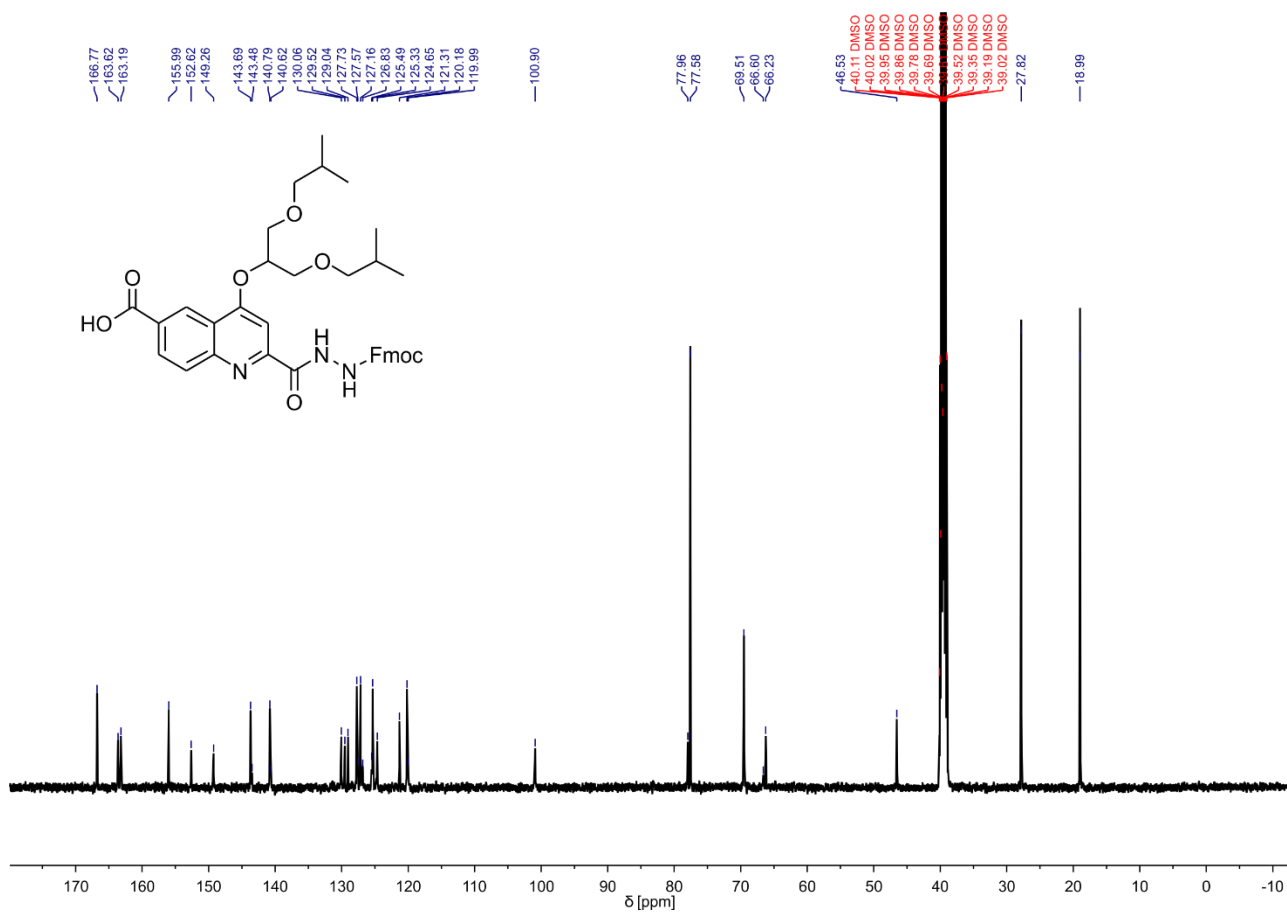


**Figure S7.11.**  $^{13}\text{C}$  NMR spectrum (126 MHz,  $\text{DMSO-}d_6$ ) of **R**.

## 8 Acknowledgements

I thank Professor Ivan Huc for his supervision. He always gave me helpful advice and guidance throughout my research.

I am also grateful to all the members of the group for creating a collaborative working environment. I was always able to count on their support and teamwork. Special thanks goes to Daniela Mazzier who supervised me in the beginning of my PhD. I thank Victor Maurizot for his continuous help and advice, especially with crystal growth and experimental design. Barbara Wicher, who showed immense motivation and provided invaluable help with X-ray analysis. I also thank Lars Allmendinger for his tremendous commitment in his involvement with NMR measurements and data interpretation. This work would not have been possible without them. I am grateful to Daniel Bindl, Sebastian Dengler, Daniel Gill, Florian Sanchez and Niklas Böcher for their support. I thank my lab members Lizeth Bodero Padilla, Alexandru Grozavu, Florian Sanchez, Shuhe Wang and Arundhati Roy for not only creating a supportive work environment but also giving good scientific guidance. I am also thankful to Mathieu Denis and Daniel Gill for synthetic help. I am grateful to Ivan R. B. Alonso for his help with technical issues and HPLC-measurments. I also thank Johannes Sigl for his help with Maestro.

I thank my friends and family, who have supported me throughout my whole path up to this point. In particular, I am grateful for my parents and siblings Elisabeth H. and Jan-Michael Menke who always supported, helped and motivated me throughout my studies. Likewise, I am grateful to Eva Späh, Ryan Howard, Daniel Gill, Alexandre Desaintjean and Torben Kälber who all helped enhancing my thesis writing. Here I am especially thankful to Torben Kälber, for he has put tremendous efforts into improving my thesis.